REPORT DOCUMENTATION PAGE		FORM APPROVED OMB No. 0704-0188

1. AGENCY USE ONLY (Leave blank)	2. REPORT DATE June 1998	3. REPORT TYPE AND DATES COVERED

4. TITLE AND SUBTITLE OF REPORT
One-Success Random Access Without Feedback for a Bounded Number of Active Stations

5. FUNDING NUMBERS
DAAH 04-95-1-0246

6. AUTHOR(S)
Philippe P. Bruneteau

7. PERFORMING ORGANIZATION NAME(S) AND ADDRESS(ES)
Coordinated Science Laboratory
University of Illinois
1308 W. Main Street
Urbana, IL 61801

8. PERFORMING ORGANIZATION REPORT NUMBER:
UILU-ENG-98-2214

9. SPONSORING/MONITORING AGENCY NAME(S) AND ADDRESS(ES)
U.S. Army Research Office
P. O. Box 12211
Research Triangle Park, NC 27709-2211

10. SPONSORING/MONITORING AGENCY REPORT NUMBER:
33988-EL-FRI

11. SUPPLEMENTARY NOTES:
The views, opinions and/or findings contained in this report are those of the author and should not be construed as an official Dept. of the Army position, policy or decision, unless so designated by other documentation.

12a. DISTRIBUTION AVAILABILITY STATEMENT
Approved for public release; distribution unlimited.

12b. DISTRIBUTION CODE

13. ABSTRACT (Maximum 200 words)

We consider a random multi-access system, where T active stations among M stations contend for transmission over a common medium in L minislots. Each active station transmits in a subset of these minislots, the subsets chosen by the stations being mutually independent. A success is said to occur if during at least one minislot there is a single transmission; otherwise, a failure occurs. We seek transmission policies which minimize the probability of failure. We investigate a transmission strategy which is suitable if the number of active stations T is unknown but bounded by some number T_0. We derive performance bounds for the strategy and suggest particular choices of parameters for the strategy for given values of L and T_0.

19990621109

14. SUBJECT TERMS
Random access, synchronization, spread-spectrum modulation

15. NUMBER OF PAGES: 42

16. PRICE CODE

17. SECURITY CLASSIFICATION OF REPORT: UNCLASSIFIED	18. SECURITY CLASSIFICATION OF THIS PAGE UNCLASSIFIED	19. SECURITY CLASSIFICATION OF ABSTRACT UNCLASSIFIED	20. LIMITATION OF ABSTRACT UL

STANDARD FORM 298 (REV 2-89)

ONRCHI COMPUTER V 1.0 11/94 DTIC QUALITY INSPECTED 4

ACKNOWLEDGMENTS

First of all, I would like to thank my advisor, Professor Bruce Hajek, for his guidance and advice throughout my studies in the University of Illinois.

I also would like to express my acknowledgment to all the members of my family in France for their support and encouragement despite the distance.

TABLE OF CONTENTS

LIST OF TABLES

LIST OF FIGURES

CHAPTER 1

INTRODUCTION

1.1 One-Success Random Access without Feedback

The random multiaccess system that we designate here by *one-success random access without feedback* can be presented as follows: suppose that T active stations among M stations contend for transmission over a common medium in L time slots (also called *minislots*). Each active station transmits in a subset of these minislots (the subsets chosen by the stations being mutually independent). Success occurs if, during at least one minislot, there is a single transmission; otherwise, a failure occurs. We seek transmission policies that minimize the probability of failure. This problem was formulated in [1].

Some comments on this model are in order as presented in [1]. First, the stations do not receive any feedback during the L minislots. Second, it does not matter how many stations transmit in slots without a conflict (that problem is addressed in [2]), as long as there is at least one. As a matter of fact, this discussion about *one-success random access without feedback* systems is motivated by the difficulty of transmitter synchronization in a code-division multiple access system (in which each large data packet transmission is preceeded by L minislots); during those minislots, the transmitters attempt to notify the receiver which code is being used for the transmission that immediately follows. Since no more than one of the packets that follow can be received (or "captured"), there is little reason to be concerned whether more than one packet has been captured.

Throughout this thesis, we assume $M = \infty$, which means that the T stations independently select sets of slots in which to transmit, each using the same probability. It models the situation in which T active stations are chosen from a very large finite population.

1.2   Some Simple Transmission Strategies

The first simple transmission policy one can think of is the following: each active station transmits in each slot with probability a. In this case, the probability of failure is given by:

$$P_F = [1 - aT(1 - a)^{T-1}]^L$$

Figure 1.1 illustrates that the minimum over a of the probability of failure is achieved for $a = \frac{1}{T}$. But the point is that this transmission policy is optimal only for that particular value of T and therefore is inappropriate when T is unknown.
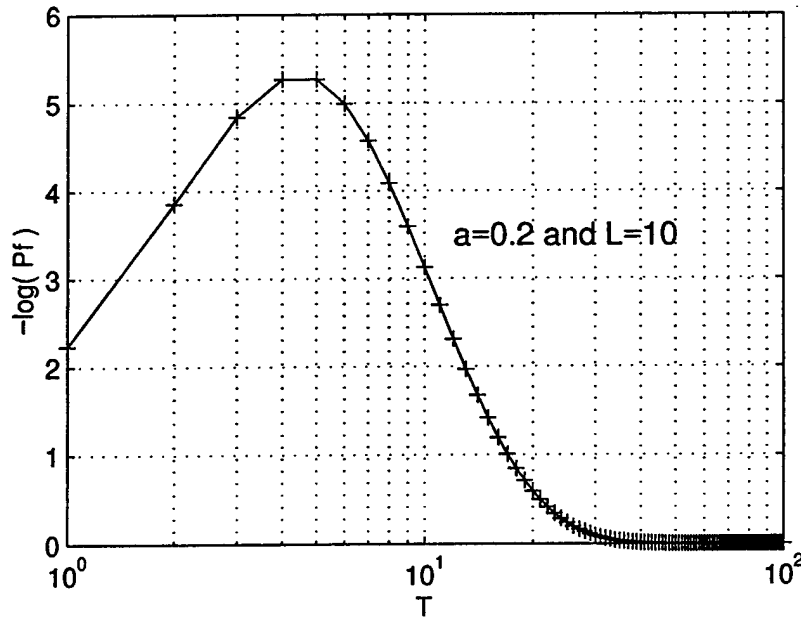
Figure 1.1 Probability of failure when each active station transmits in each minislot with probability $1/a$

Other simple policies exist (and have been simulated in [1]), but the same last remark applies. Hence we need to consider a more specific transmission policy that would be suitable over a range of values of T. This is the focus of this thesis, as described in more detail in the next section.

1.3 Proposed Transmission Strategy for Unknown and Bounded Number T of Active Stations

In the remainder of this thesis, we assume that the number of active stations T is unknown and that it is bounded by some positive integer T_0: $1 \leq T \leq T_0$. Within this framework we define $\tilde{P}_F$ such that:

$$\forall T_0, \forall \mathbf{a}, \quad \tilde{P}_F(T_0, \mathbf{a}) \hat{=} \max_{1 \leq T \leq T_0} P_F(T, \mathbf{a}) \tag{1.1}$$

where $\mathbf{a}$ is the transmission policy (common to all T active stations). We want to find the transmission policy $\mathbf{a}$ that minimizes $\tilde{P}_F(T_0, \mathbf{a})$.

Here is a transmission strategy to handle this case [1]: an active station transmits in each slot, transmitting in slot i with probability a_i, where $a_1 \geq a_2 \geq \ldots \geq a_L$ are the parameters of the policy. For that policy,

$$P_F(T, \mathbf{a}) = \prod_{i=1}^{L} [1 - T a_i (1 - a_i)^{T-1}] \tag{1.2}$$

since

1. the probability that there is a success in slot i is $P_{S_i} = T a_i (1 - a_i)^{T-1}$,

2. the probability that there is a failure in slot i is $P_{F_i} = 1 - P_{S_i}$, and

3. the resulting probability of failure is the probability that there is a failure for each one of the slots: $P_F = \prod_{i=1}^{L} P_{F_i}$.

In the next chapter, we investigate this transmission strategy by using a Poisson approximation for the probability of failure and give the corresponding optimal policy.

CHAPTER 2

OPTIMIZATION WHEN USING A POISSON APPROXIMATION

We investigate here the transmission strategy proposed in the previous section (for a number of active stations T which is only known to satisfy $1 \leq T \leq T_0$). We first derive a Poisson approximation for the probability of failure, present a simple choice of $\mathbf{a}$ motivated by the approximation, and give a lower bound to the probability of failure. Then, we proceed to an optimization of $\mathbf{a}$ based on the approximate expression of the probability of failure. We finally compare the results with those obtained without using an approximation.

2.1 Poisson Approximation of the Probability of Failure

Recall that we want to find the transmission policy $\mathbf{a}$ that minimizes $\tilde{P}_F(T_0, \mathbf{a})$, or equivalently that maximizes $\min_{1 \leq T \leq T_0} \{-log P_F(T, \mathbf{a})\}$.

Now for any policy $\mathbf{a}$,

$$
\begin{aligned}
-log P_F(T, \mathbf{a}) &= -log \prod_{i=1}^{L} [1 - T a_i (1 - a_i)^{T-1}] \\
&= \sum_{i=1}^{L} -log[1 - T a_i (1 - a_i)^{T-1}]
\end{aligned}
$$

4

$$= \sum_{i=1}^{L} \phi(T, a_i) \qquad (2.1)$$

where

$$\phi(T, a_i) = -log[1 - Ta_i(1 - a_i)^{T-1}]$$

Let $T_{a_i} = \frac{1}{a_i}$ for $1 \le i \le L$. Note that a_i is the optimal transmission probability for a single slot for T_{a_i} stations. Then, using a Poisson approximation (or equivalently $1 - a \approx \exp(-a)$ and $T - 1 \approx T$),

$$\begin{aligned}
\phi(T, a_i) &= -log[1 - \frac{T}{T_{a_i}}(1 - \frac{1}{T_{a_i}})^{T-1}] \\
&\approx -log[1 - \frac{T}{T_{a_i}} \cdot e^{-\frac{T}{T_{a_i}}}] \\
&\approx \phi(logT - logT_{a_i}) \qquad (2.2)
\end{aligned}$$

where $\phi(u) \doteq -log[1 - e^{u-e^u}]$ is shown in Figure 2.1.

Note that the functions $logT \longmapsto \phi(logT - logT_{a_i})$ are the same for all i, up to translation. Hence, in view of Equation (2.1), we can graphically represent $-logP_F(T, \mathbf{a})$ by superimposing the curves for the different i and taking the sum for each value of $logT$.

We are now able to make a first conjecture on the transmission probability distribution.

2.2 First Conjecture on the Transmission Probability Distribution

2.2.1 Transmission probability distribution

Recall that we want to maximize $\min_{1 \le T \le T_0}\{-logP_F(T, \mathbf{a})\}$ over $\mathbf{a}$. Under the Poisson approximation, this quantity becomes:

$$\min_{1 \le T \le T_0}\{-logP_F(T, \mathbf{a})\} = \min_{log1 \le logT \le logT_0}\{\sum_{i=1}^{L} \phi(logT - logT_{a_i})\} \quad (2.3)$$

$\phi(u) = -\log(1 - \exp(u - \exp(u)))$
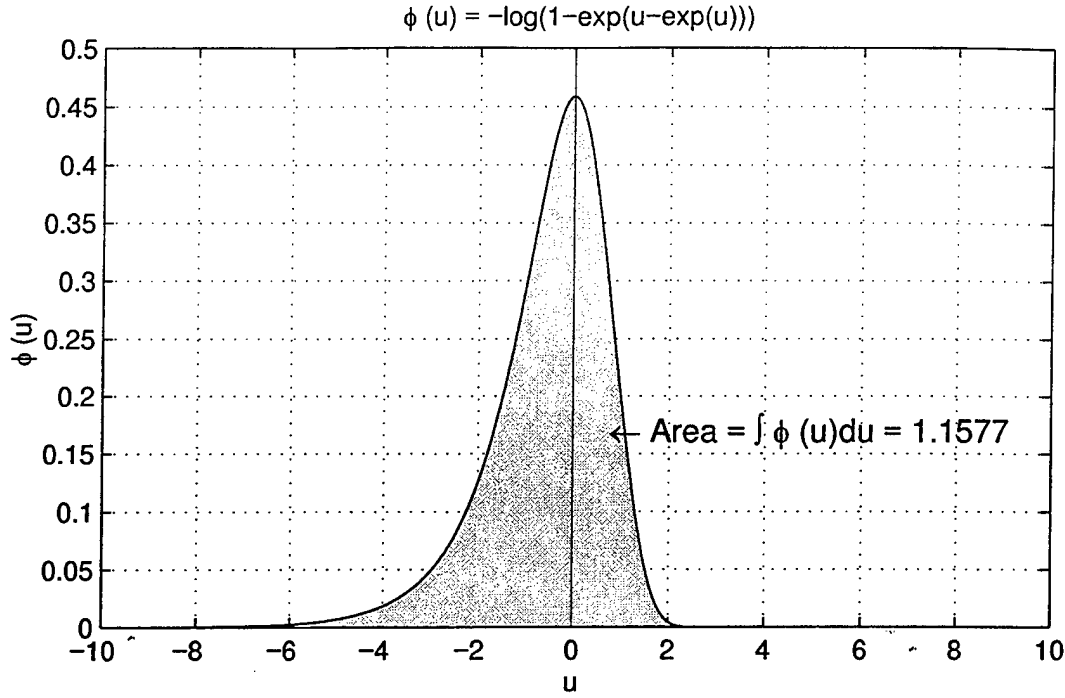
Figure 2.1 Plot of the function $\phi(u) = -log[1 - e^{u - e^u}]$

We can then conjecture that, as a first approximation, $\{logT_{a_i}\}_{1 \leq i \leq L}$ should be equally spaced over $[log1; logT_0]$, or equivalently that, for some $(A, B) \in \Re^{*2}$,

$$\forall i / 1 \leq i \leq L, \quad a_i = A \cdot B^i$$

The upper part of Figure 2.2 shows the plot of $\{T_{a_i}\}_{1 \leq i \leq L}$ when taking T_{a_1} to be 1 and T_{a_L} to be T_0, so that the range over which $-logP_F(T, \mathbf{a})$ takes high values covers $[1; T_0]$. The lower part of this figure shows both the sample ϕ functions and the resulting approximate probability of failure, obtained by summation. We primarily focus on the values taken by $-logP_F(T, \mathbf{a})$ when T varies over $[1; T_0]$ and would like to maximize the minimum over this reference interval.

Some comments are in order: we note that $-logP_F(T, \mathbf{a})$ first rapidly increases when T is in the vicinity of 1, and then slightly decreases before stalling when T passes over T_0. This can be easily understood when one considers that the curves of the ϕ functions

6
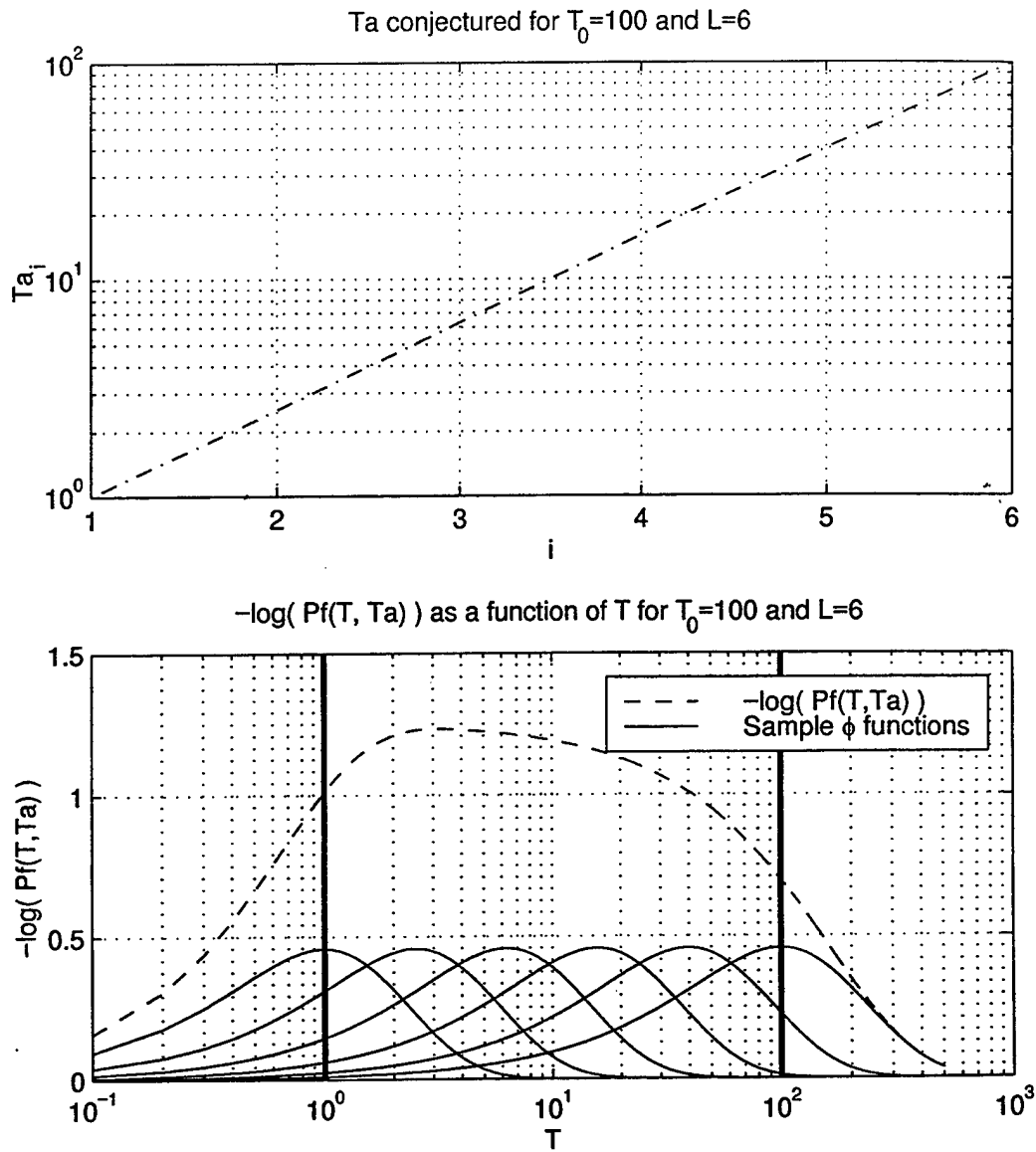
Figure 2.2 First conjecture about the transmission probability distribution and corresponding probability of failure

are summed to produce $-logP_F(T, \mathbf{a})$. Consequently, one improvement of the previous conjecture about the optimal transmission probability distribution would consist in increasing the number of T_{a_i} with values near the borders of the interval $[1; T_0]$.

Note that one might also want to extend the values of the T_{a_i} beyond T_0 in order to avoid the observed stall of $-logP_F(T, \mathbf{a})$ in the vicinity of T_0. Yet this would result in a less efficient use of our resources since T cannot be greater than T_0. Put another way, we do not want $-logP_F(T, \mathbf{a})$ to take big values outside of the reference interval $[1; T_0]$.

In Section 2.2.3, we will give another approximate expression for $-logP_F(T, \mathbf{a})$, but whose validity is restricted to the use of the first conjectured transmission probability distribution.

2.2.2 Comparison with the exact calculus

This section is motivated by the fact that the approximate expression for $-logP_F(T, \mathbf{a})$ using the Poisson approximation cannot be considered a bound to the exact expression. Figure 2.3, in which we use the transmission probability distribution conjectured in Section 2.2.1, shows that the results between the exact and the approximate calculus are very close when T is large enough. Furthermore, $-logP_F(T, \mathbf{a})$ tends to be underestimated (so P_F is overestimated) by the approximation when T is close to 1.

2.2.3 Other approximate expression for $-logP_F(T, \mathbf{a})$

Under the assumptions that $\Delta \log T_{a_i} = cst$ and that L is large enough (typically greater than 20), it can be shown that, by using Riemann's approximation (c.f. Appendix A)

$$-logP_F(T, \mathbf{a}) \approx \frac{L}{logT_{a_L} - logT_{a_1}} \cdot \int_{logT - \frac{(L-1) \cdot logT_{a_L} + logT_{a_1}}{L}}^{logT + \frac{logT_{a_L} - (L+1) \cdot logT_{a_1}}{L}} \phi(u) \, du \qquad (2.4)$$

Since $\int_{-\infty}^{\infty} \phi(u) \, du = 1.1577$, this leads to the particular following upper bound on $-logP_F(T, \mathbf{a})$:

$$\forall T, \forall \mathbf{a}, \quad -logP_F(T, \mathbf{a}) \leq \frac{1.1577 \cdot L}{logT_{a_L} - logT_{a_1}}$$

8
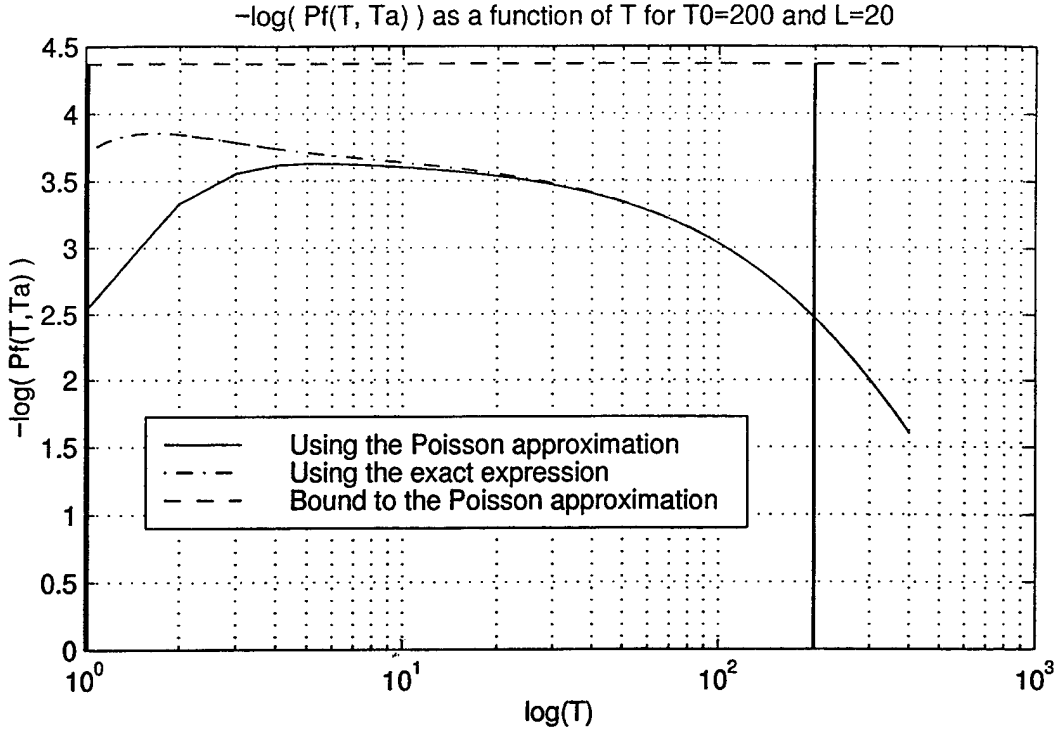
Figure 2.3 Comparison approximate/exact calculus

Figure 2.4 shows a comparison between the results for $-logP_F(T, \mathbf{a})$ when using either a summation or an integration for the approximate expression. In this plot, $L = 50$; one should keep in mind that the discrepancy becomes more significant when L is lower.

2.3 Upper Bound to $-logP_F(T, \mathbf{a})$

It might be useful to have a lower bound to P_F, or equivalently an upper bound to $-logP_F(T, \mathbf{a})$, which could serve as a target for the optimization we want to do. Without making any further assumption on the transmission probability distribution, we know that $\min_{1 \leq T \leq T_0}\{-logP_F(T, \mathbf{a})\}$ is lower than the average of $-logP_F(T, \mathbf{a})$ over the interval $[1, T_0]$. Moreover, $-logP_F(T, \mathbf{a})$ can be considered the sum of translated samples of the positive function ϕ, which enables us to write the following inequalities:

9
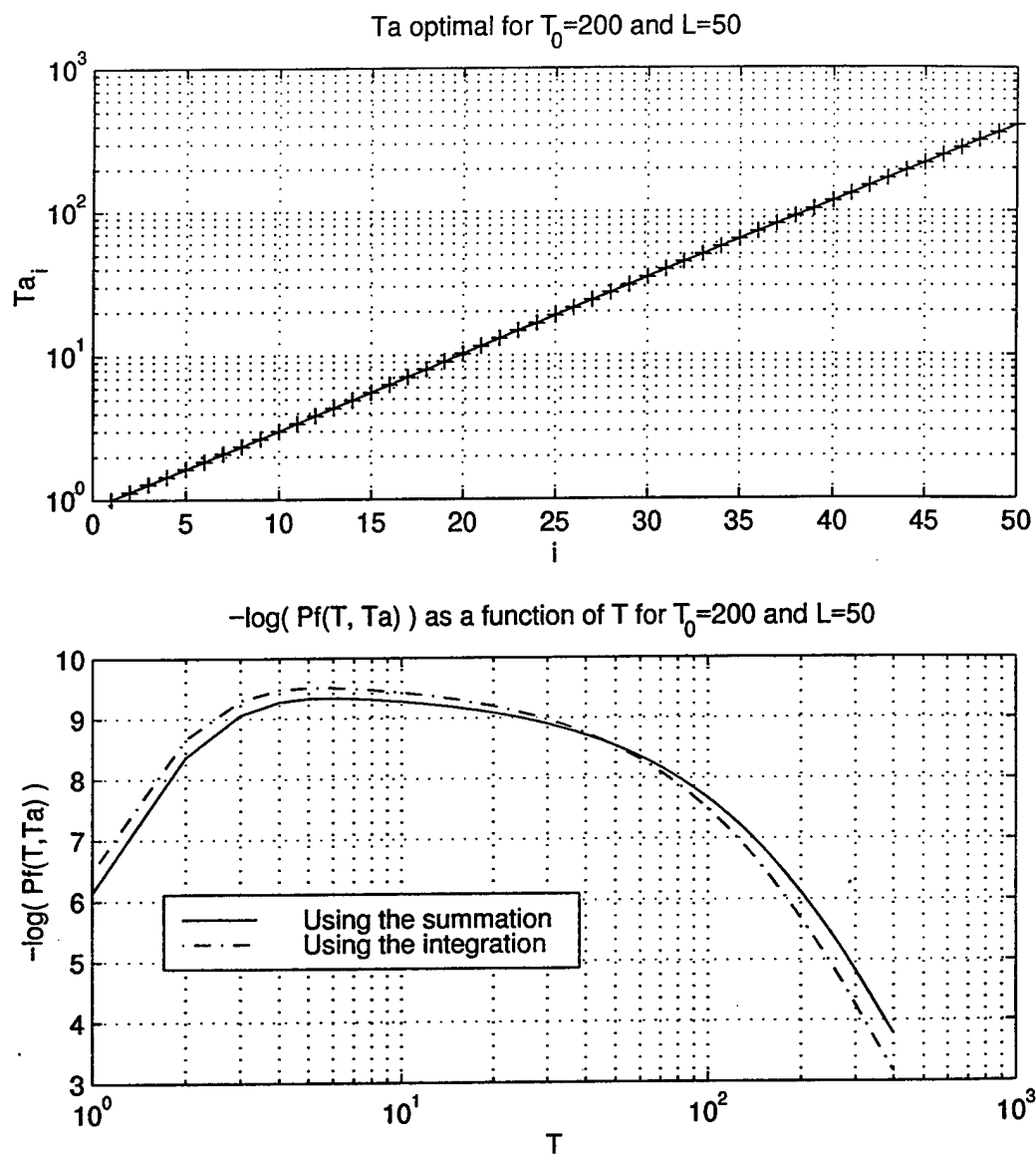
Figure 2.4 Plot of $-log P_F(T, \mathbf{a})$ when using Riemann's approximation, for equi-spaced $\log T_{a_i}$

10

$$\forall \mathbf{a}, \quad \min_{1 \le T \le T_0} \{-logP_F(T,\mathbf{a})\} \quad \le \quad Avg_{1 \le T \le T_0}(-logP_F(T,\mathbf{a}))$$

$$\le \quad \frac{\text{Area under } (-logP_F)}{\text{Interval length}}$$

$$< \quad \frac{L \times (\text{Area under } \phi)}{\text{Interval length}}$$

$$< \quad \frac{L \times \int_{-\infty}^{\infty} \phi(u) \, du}{logT_0 - log1}$$

So

$$\forall \mathbf{a}, \quad \min_{1 \le T \le T_0} \{-logP_F(T,\mathbf{a})\} < \frac{L}{logT_0} \cdot \int_{-\infty}^{\infty} \phi(u) \, du = \frac{1.1577 \times L}{logT_0} \qquad (2.5)$$
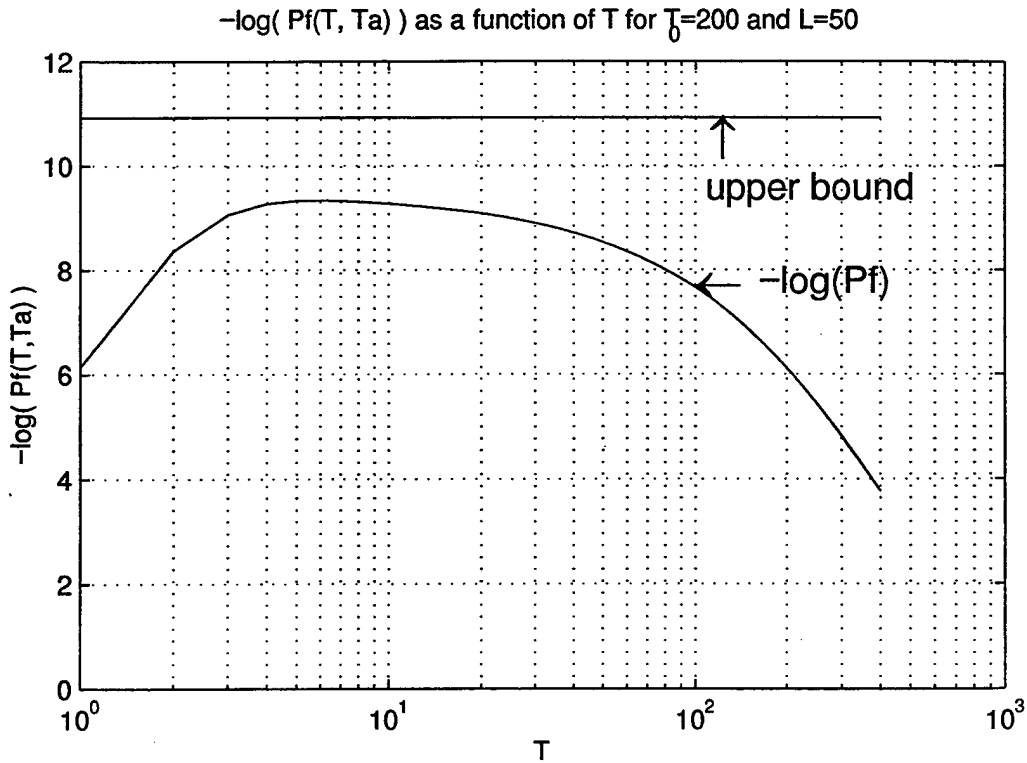
Figure 2.5 Upper bound to $-logP_F(T,\mathbf{a})$

11

As shown in Figure 2.5, the bound we have just given is quite loose. This is because, on one hand, $-logP_F(T, \mathbf{a})$ is not constant over $[1, T_0]$ and that, on the other hand, the samples of the ϕ function take some significant values when T is close but lower than 1 (in theory) or when T is close but greater than T_0. However, one might expect the bound to be a bit tighter with the optimal transmission probability distribution; note that, ideally, we would like $-logP_F(T, \mathbf{a})$ to have a rectangular shape (zero outside of $[1; T_0]$ and equal to the upper bound inside the interval).

2.4 Optimization of the Transmission Probability Distribution

As far as now, we used equi-spaced parameters for the transmission policy a. But, as illustrated in Figure 2.2, $-logP_F(T, \mathbf{a})$ prematurely stalls when T gets close to either 1 or T_0. One can then guess that more samples of the ϕ function need be centered near the borders of $[1; T_0]$. We chose here to perform an optimization of those policy parameters. Because using the exact expression of the transmission probability distribution to be optimized would be much too time consuming, we performed the optimization on the Poisson approximation of $-logP_F(T, \mathbf{a})$ by using the Matlab *minimax* function (local method). Figure 2.6 shows the optimal policy found for T_0=50 and L=10, along with the corresponding failure probability $-logP_F(T, \mathbf{a})$.

In the curve of the optimal policy, we observe that $1 < T_{a_1}$ and $T_{a_L} < T_0$. Moreover, T_{a_i} is at first constant (indeed it slightly increases), then $logT_{a_i}$ linearly increases, and finally T_{a_i} once again becomes roughly constant. Similarly, in the curve of the resulting probability of failure, the presence of a local maximum near each end of the interval $[1; T_0]$ reflects the need to prevent $-logP_F(T, \mathbf{a})$ from stalling at the borders of this interval, which can be easily understood when one considers both the shape of the ϕ function (see Figure 2.1) and what happened with the first conjectured policy (equi-spaced parameters, see Figure 2.2). This causes the transmission probability distribution to accumulate more
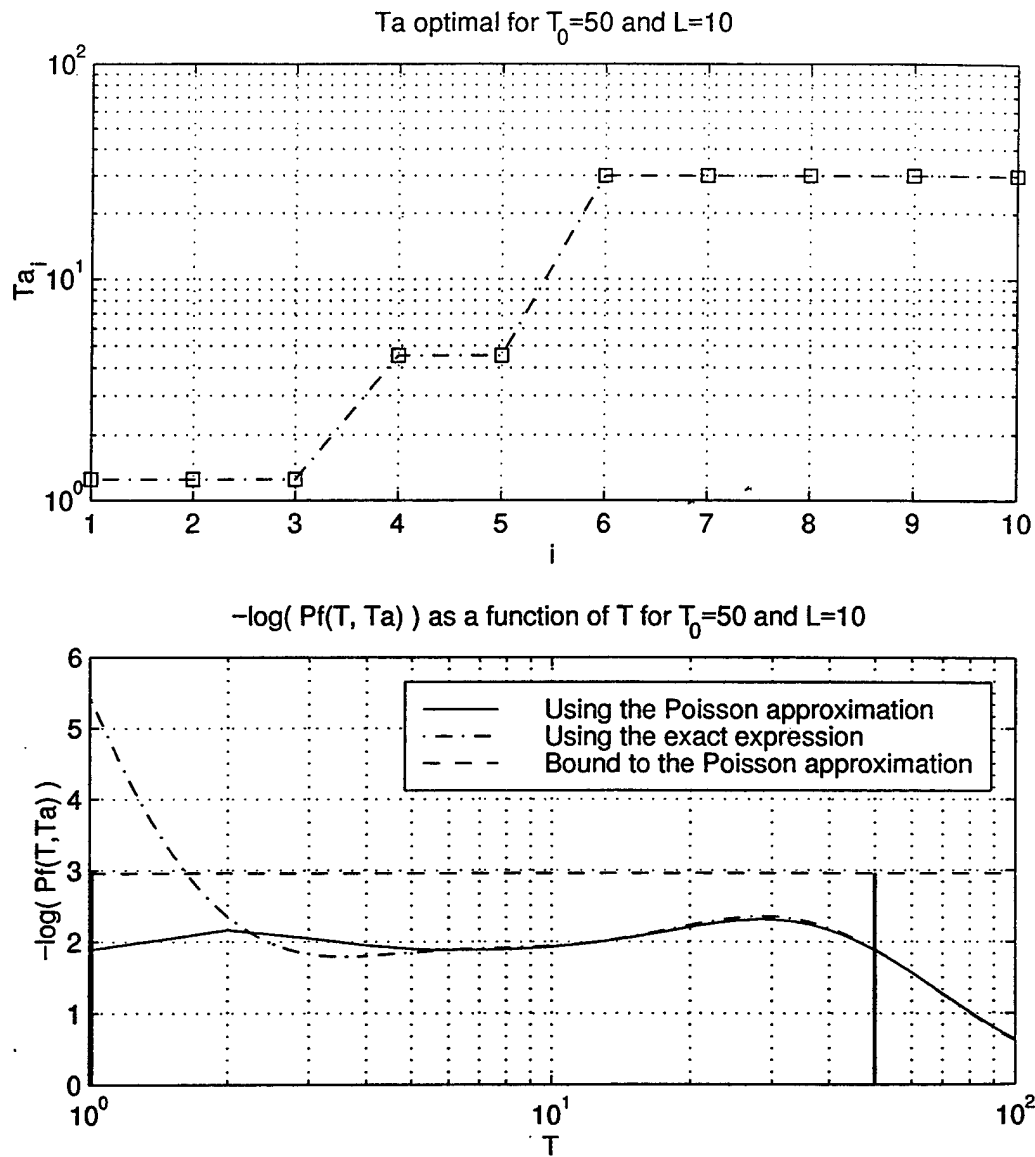
Figure 2.6 Optimal transmission policy and probability of failure for $T_0=50$ and $L=10$

T_{a_i} samples near the endpoints of the interval. Moreover, preventing $-logP_F(T, \mathbf{a})$ from stalling requires a larger number of T_{a_i} samples with values closer to T_0 than to 1. As a consequence, since the interval edges require the greatest care, these are also points where the minimum of $-logP_F(T, \mathbf{a})$ over $[1; T_0]$ is reached:

$$\tilde{P}_F(T_0, \mathbf{a}) = P_F\big|_{T=1} = P_F\big|_{T=T_0} \tag{2.6}$$

Between the local maxima near the endpoints, the curve of $-logP_F(T, \mathbf{a})$ is not much larger than the minimum. Note that the performed optimization yields one (or more as shown later) intermediate flat portion(s) in the curve of the transmission probability distribution; this may cause the resulting $-logP_F(T, \mathbf{a})$ to fluctuate slightly over its minimum value, though one might think it could be avoided.

2.4.1 Optimization for different values of L (T_0 being fixed)

Figures 2.7 through 2.11 show optimal policies and their resulting probability of failure for L taking values between 3 and 30, when T_0 has been fixed to 50.

As far as the transmission probability distribution is concerned, we can see that for a small value of L, such as $L = 3$ in Figure 2.7, we almost have a linear increase for $logT_{a_i}$, such that all the $[1; T_0]$ interval is covered, with $log(T_{a_2})$ being closer to $log(T_{a_3})$ than from $log(T_{a_1})$ in order to prevent the stall of the probability of failure at $T = T_0$ (see previous explanations at the beginning of Section 2.3 for more details).

Let's now take a look at what happens when L gets larger. As indicated for $L = 6$ (c.f. figure 2.8), several samples of T_{a_i} are first accumulated close to T_0 because of the potential stall of the probability of failure at T_0, which, as mentioned above, is the most significant problem that we have to face. Then, several samples of T_{a_i} are accumulated near 1 as seen in Figure 2.9. When L gets even larger (Figures 2.10 and 2.11), the optimal transmission policies that were found tend to converge towards a stairstep function, the interstep widths being geometrically distributed. Note that for $T_0 = 50$, we get three distinct steps in the curve of the limit optimal transmission policy, although this number

Figure 2.7 Optimal transmission policy and probability of failure for T_0=50 and L=3

Figure 2.8 Optimal transmission policy and probability of failure for $T_0=50$ and $L=6$
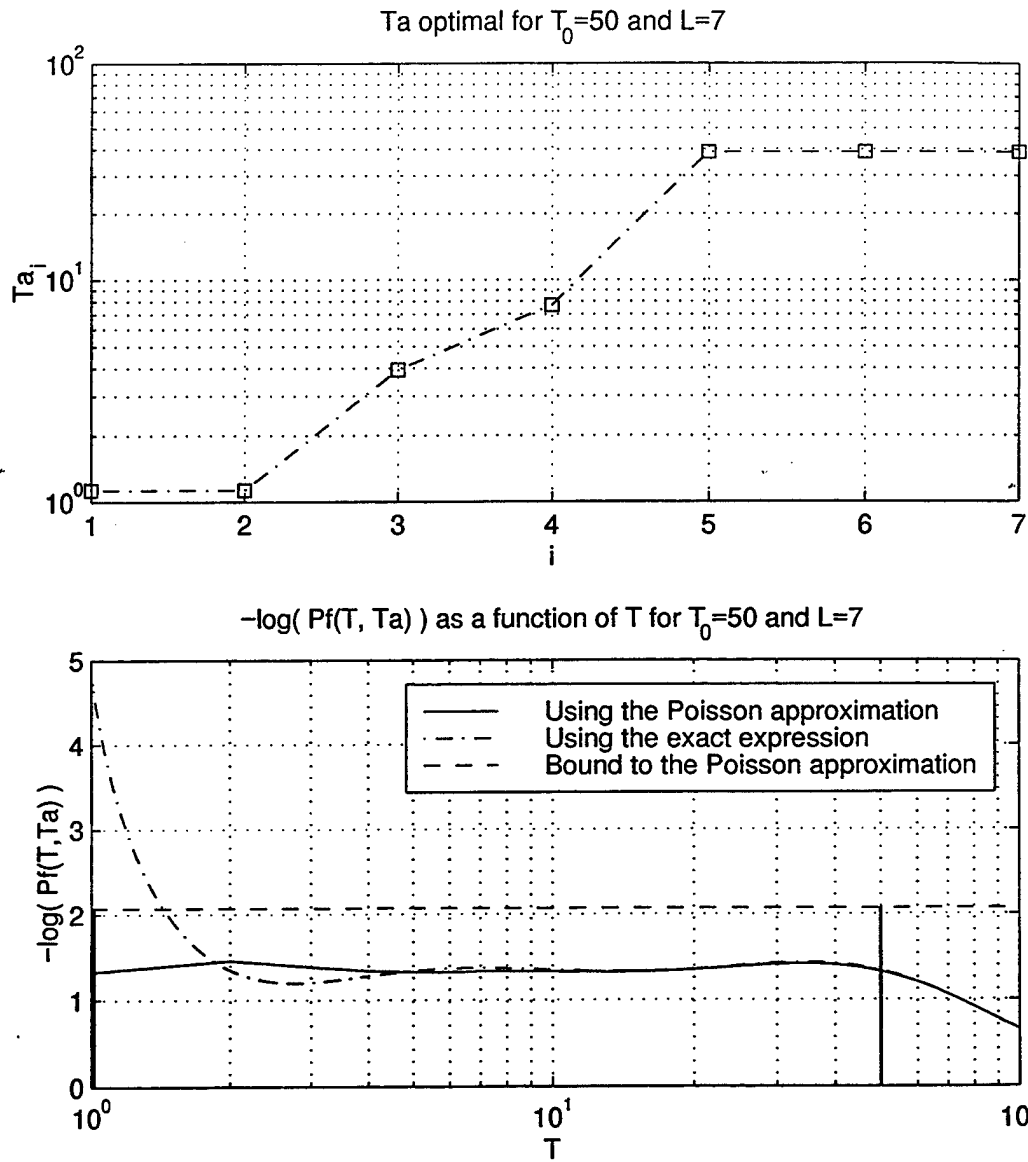
Figure 2.9 Optimal transmission policy and probability of failure for T_0=50 and L=7
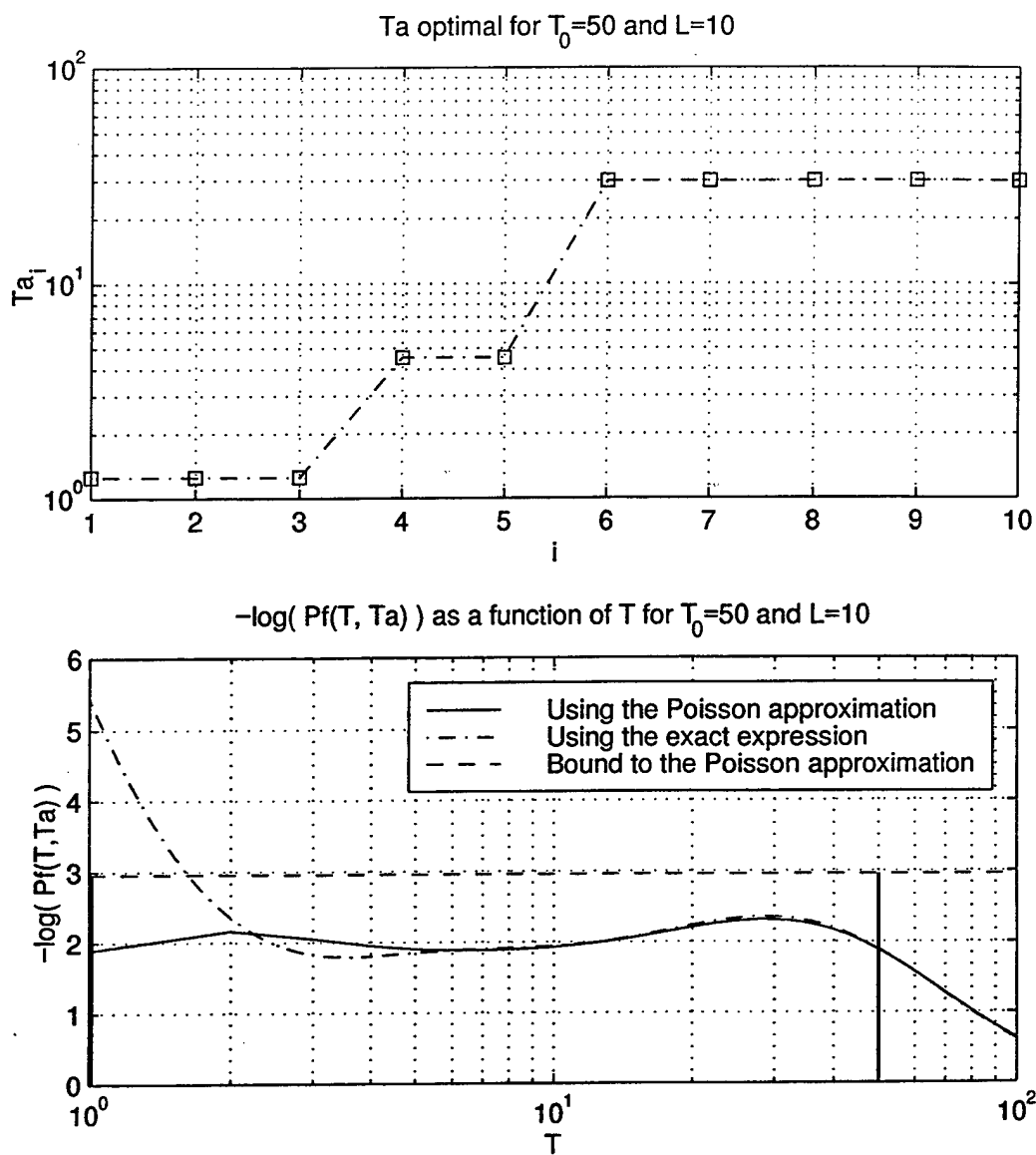
Figure 2.10 Optimal transmission policy and probability of failure for $T_0=50$ and $L=10$

18
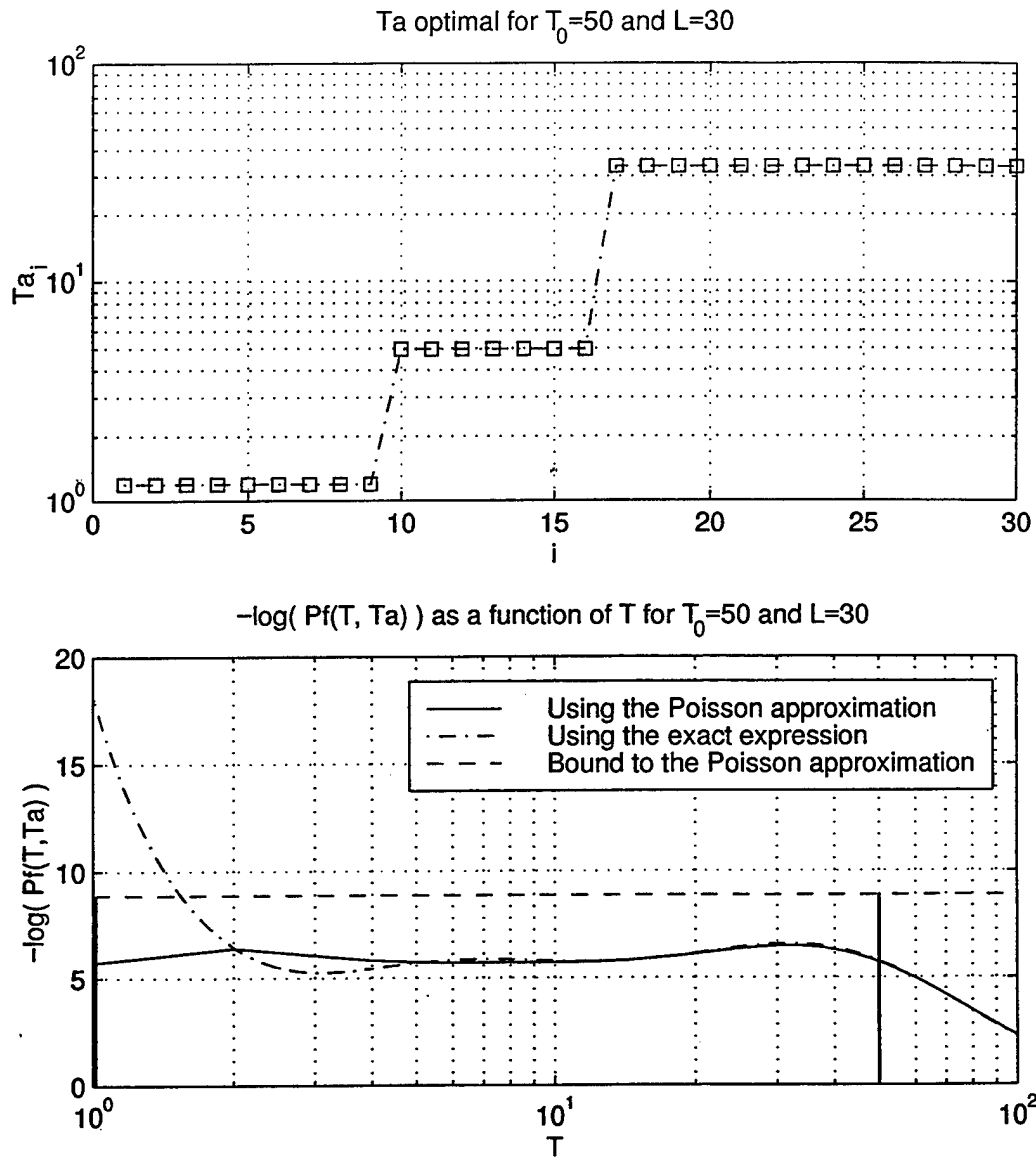
Figure 2.11 Optimal transmission policy and probability of failure for $T_0=50$ and $L=30$

19

can vary, depending on the value of T_0 and assuming that L is large enough to let these steps appear, as we shall see in the next subsection.

As far as the resulting probability of failure is concerned, we can note that, when L doubles (from $T = 3$ to $T = 6$ for instance), then $-log\tilde{P}_F(T_0, \mathbf{a})$ also roughly doubles, i.e., $-log[\tilde{P}_F(T_0, \mathbf{a})]^{\frac{1}{L}}$, which features the average probability of failure per slot, roughly stays the same. Hence, increasing L proportionally increases $-log\tilde{P}_F(T_0, \mathbf{a})$, but brings no improvement to the efficiency of the system over the number of minislots L.

2.4.2 Optimization for different values of T_0 (L being fixed)

Figures 2.12 through 2.15 show optimal policies and their corresponding resulting probability of failure for T_0 taking values between 26 and 2000, whereas L has been fixed to 10.

When T_0 is not too large compared to L, then the optimal transmission policy has a stairstep shape, whose interstep widths are roughly geometrically distributed. The number of steps depends on the value of T_0 because the previous widths are limited in size, due to the limited width of the interval over which the ϕ function takes some significant positive values.

When T_0 becomes very large with respect to L, then the transmission policy tends to have an initial step, a geometric increase and then a final step. The length of these steps is proportional to $\frac{L}{logT_0}$ and thus tends to zero when T_0 goes to infinity, while at the same time, the fraction of the interval over which there is a linear increase approaches to 1 (see Appendix B for more details about these subinterval lengths).

From Figures 2.12 and 2.13, we can deduce that the width between consecutive steps in the curve of the transmission probability disribution is bounded by

$$1.283 = \frac{1}{2} \cdot 2.566 < (\Delta logT_{a_i})_i \leq 2.566 \tag{2.7}$$

Moreover, we typically have

$$T_{a_1} \approx 1$$

and

$$T_{a_L} \approx \frac{2}{3} \cdot T_0$$

This enables us to make some recommendations, which is the purpose of the next chapter.
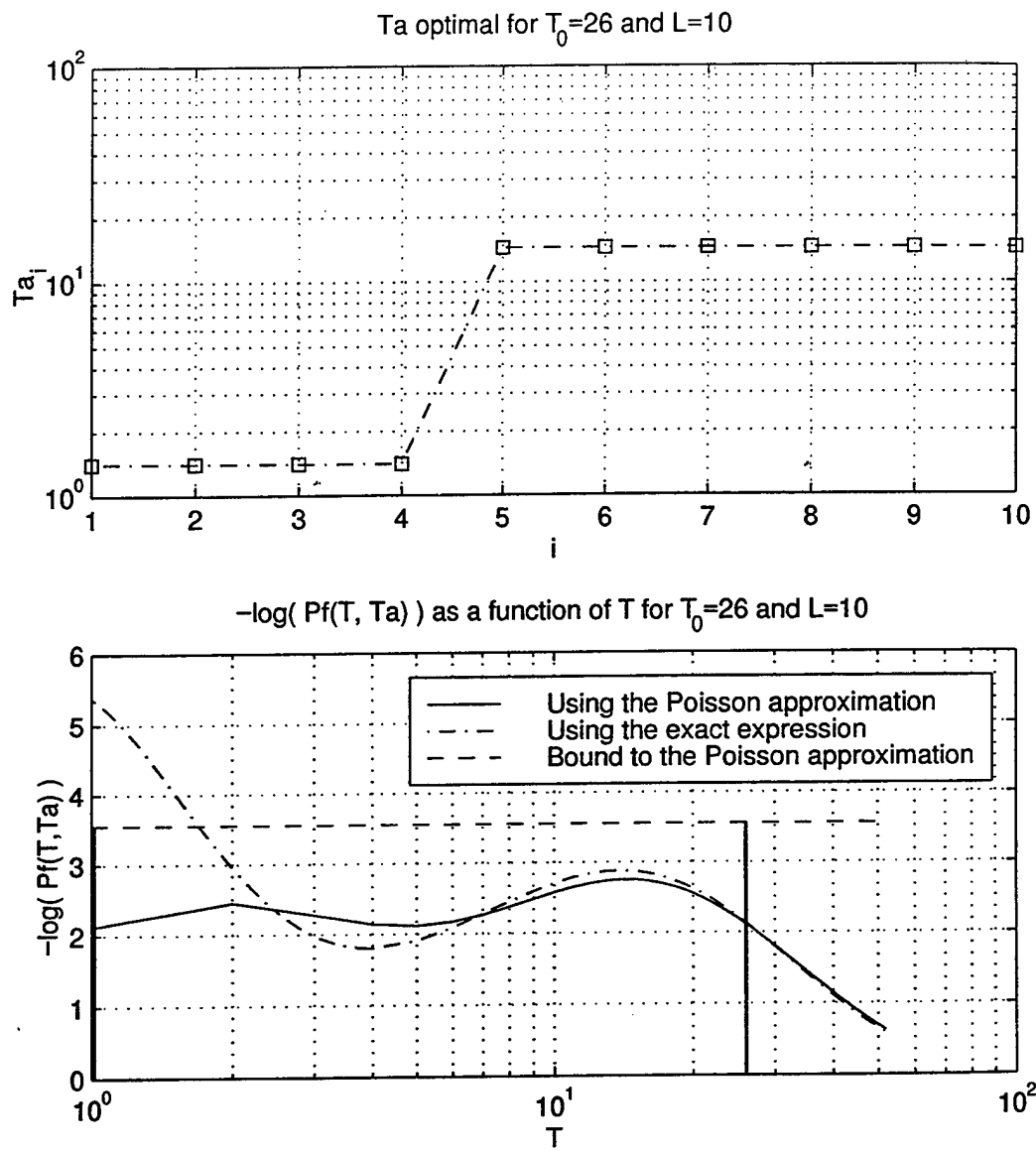
Figure 2.12 Optimal transmission policy and probability of failure for T_0=26 and L=10
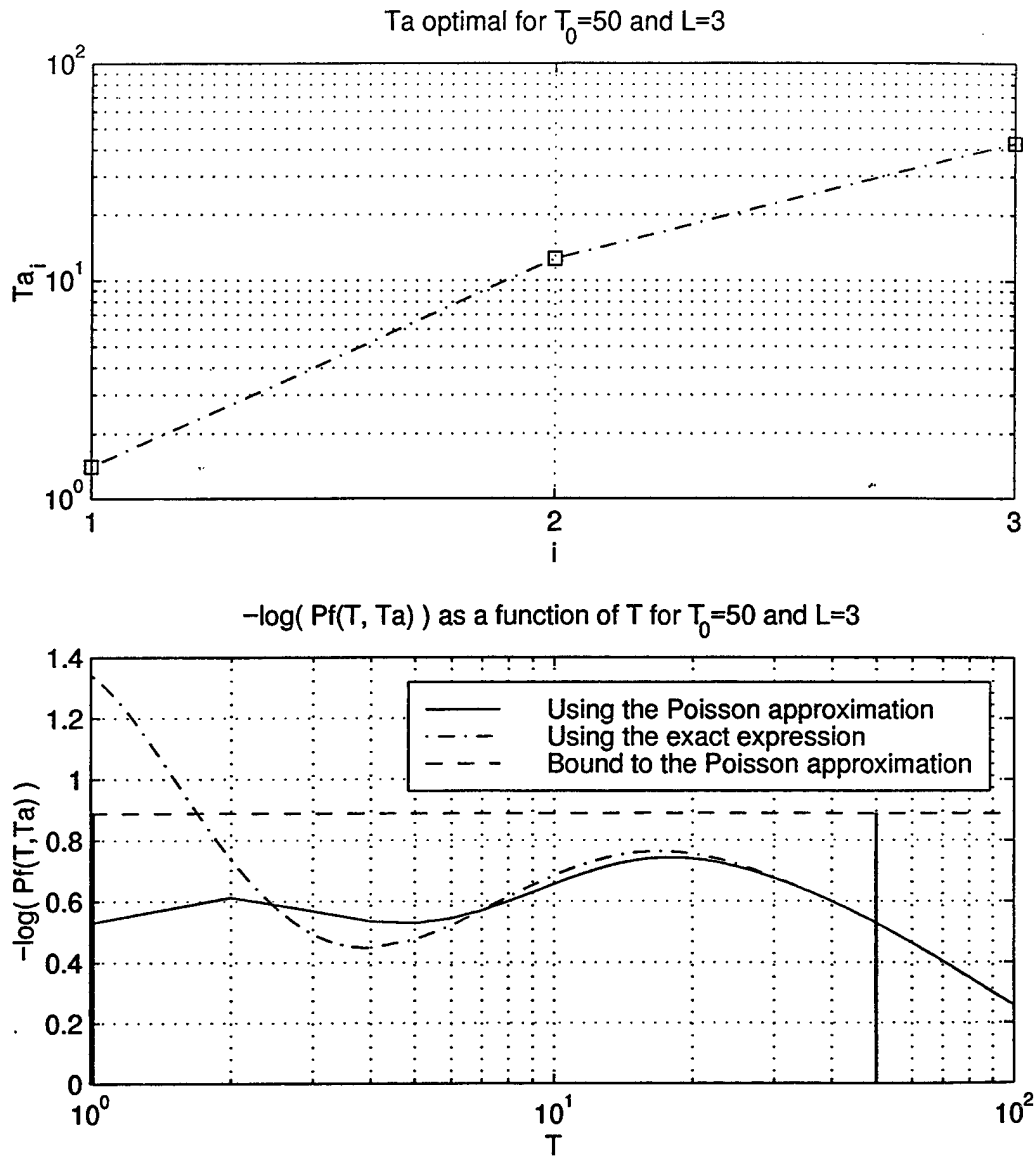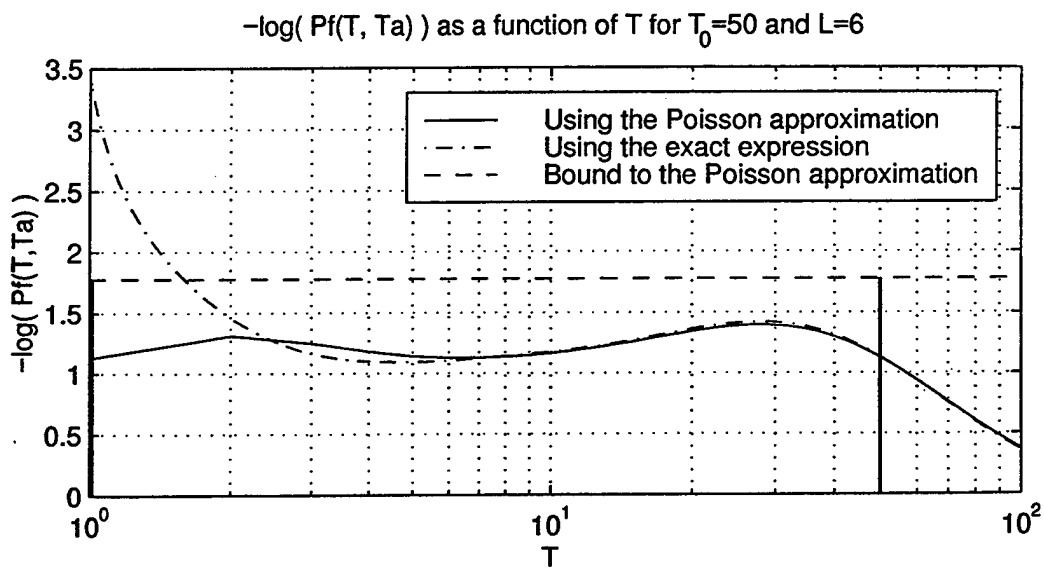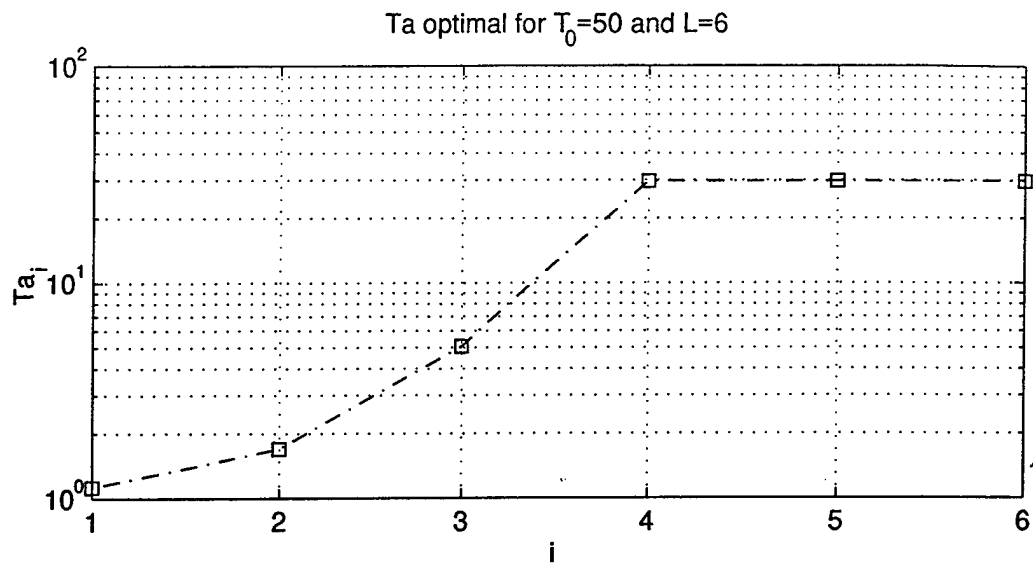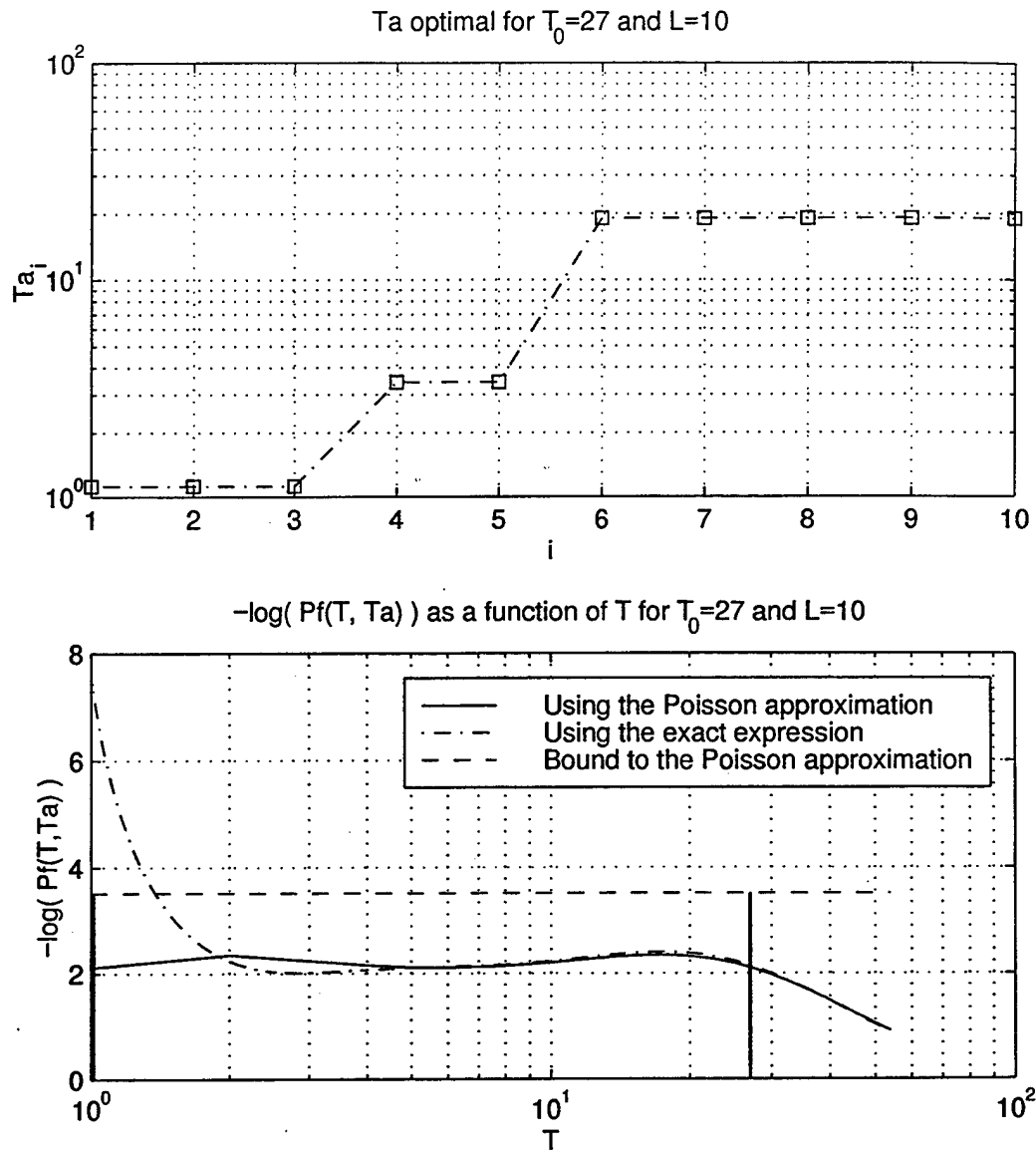
Figure 2.13 Optimal transmission policy and probability of failure for $T_0=27$ and $L=10$
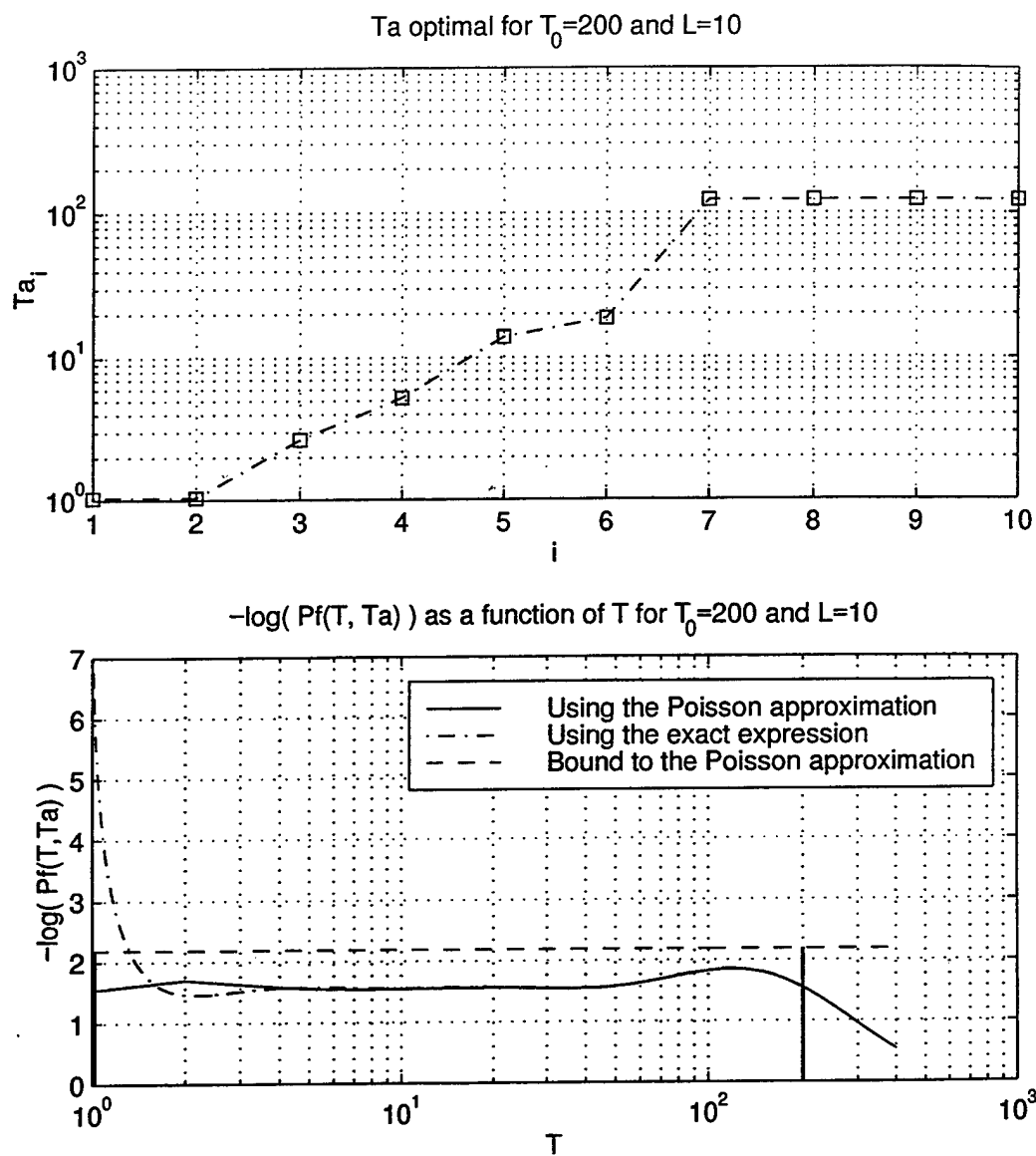
Figure 2.14 Optimal transmission policy and probability of failure for $T_0=200$ and $L=10$
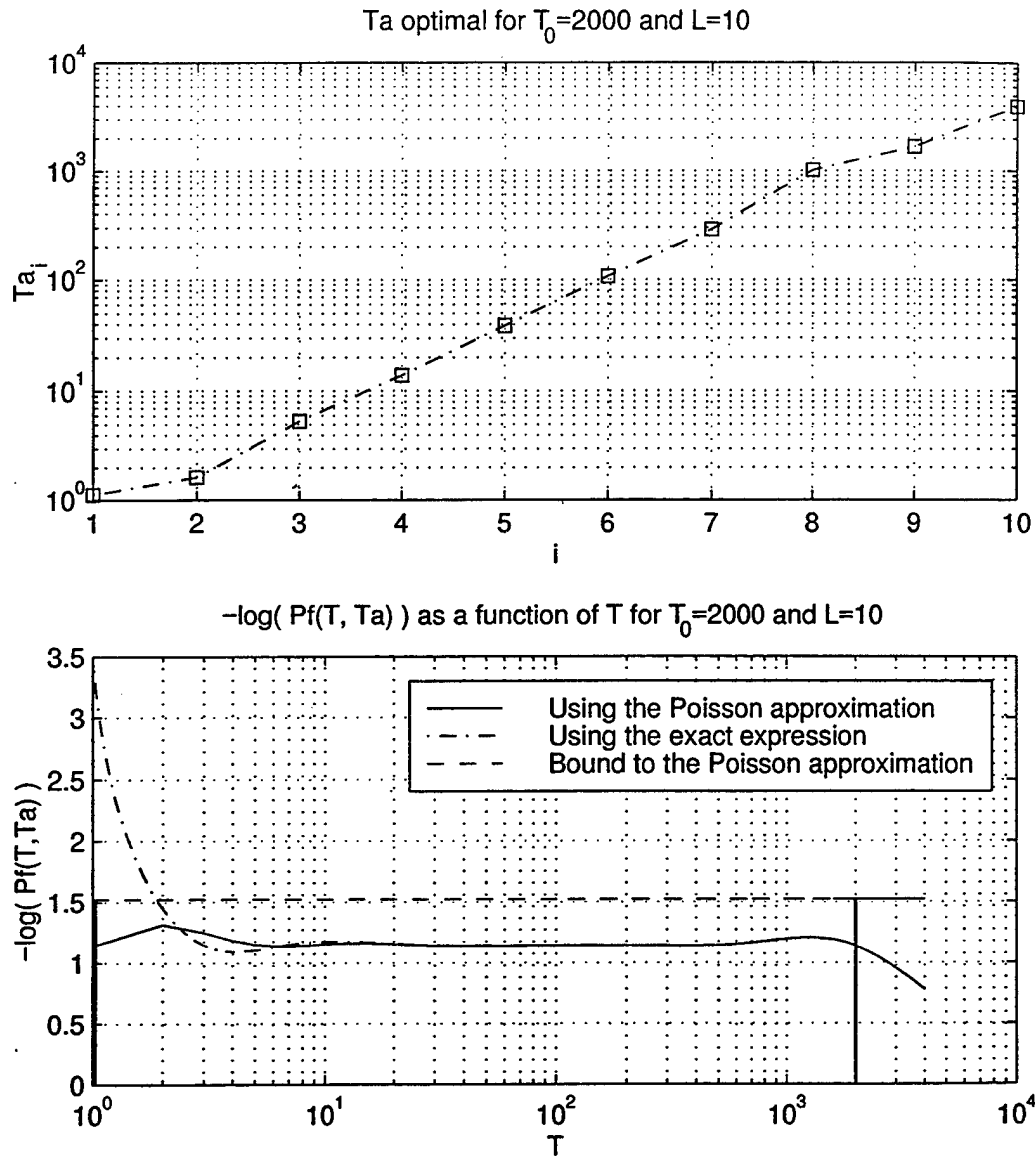
Figure 2.15 Optimal transmission policy and probability of failure for $T_0=2000$ and $L=10$

CHAPTER 3

RECOMMENDED TRANSMISSION POLICY

PARAMETERS

3.1 Parameters of the Transmission Policy

Based on the previous study and simulations, Figure 3.1 depicts the typical transmission probability distribution that we would recommend for some given values of T_0 and L.

For the use of L minislots and a number of active stations bounded by T_0, we propose to take a distribution for $-log T_{a_i}$ with an initial step, at value $log(2.3)$ (whose length should be the nearest integer to $\frac{L}{2+0.4 \cdot log T_0}$) and a final step at value $log(\frac{2}{3} \cdot T_0)$ (whose length should be the greatest integer below $\frac{1.5 \cdot L}{2+0.4 \cdot log T_0}$). Note that these interval lengths are slightly different from those given as an approximation in Appendix B in order to better fit to the simulation results.

Between these two end steps, the distribution of $-log T_{a_i}$ should be composed of N intermediate steps, roughly equally spaced and of the same length, where

$$N = \lfloor \frac{1}{2.2} \cdot (\log(\frac{2}{3} \cdot T_0) - log(2.3)) \rfloor$$

If $N = 0$, then $-log T_{a_i}$ should linearly increase between the two end steps. Note that the value of N comes from a relation analog to Equation (2.7), which was derived for

$\log(T_{a_i})$

$\log(\frac{2}{3}T_0)$

$\dfrac{\log(0.29*T_0)}{1.1*(\text{NbStep-1})}$

$\log(2.3)$

1     $\dfrac{L}{2 + 0.4*\log(T_0)}$ $L*(1 - \dfrac{1.5}{2 + 0.4*\log(T_0)})$ L   i
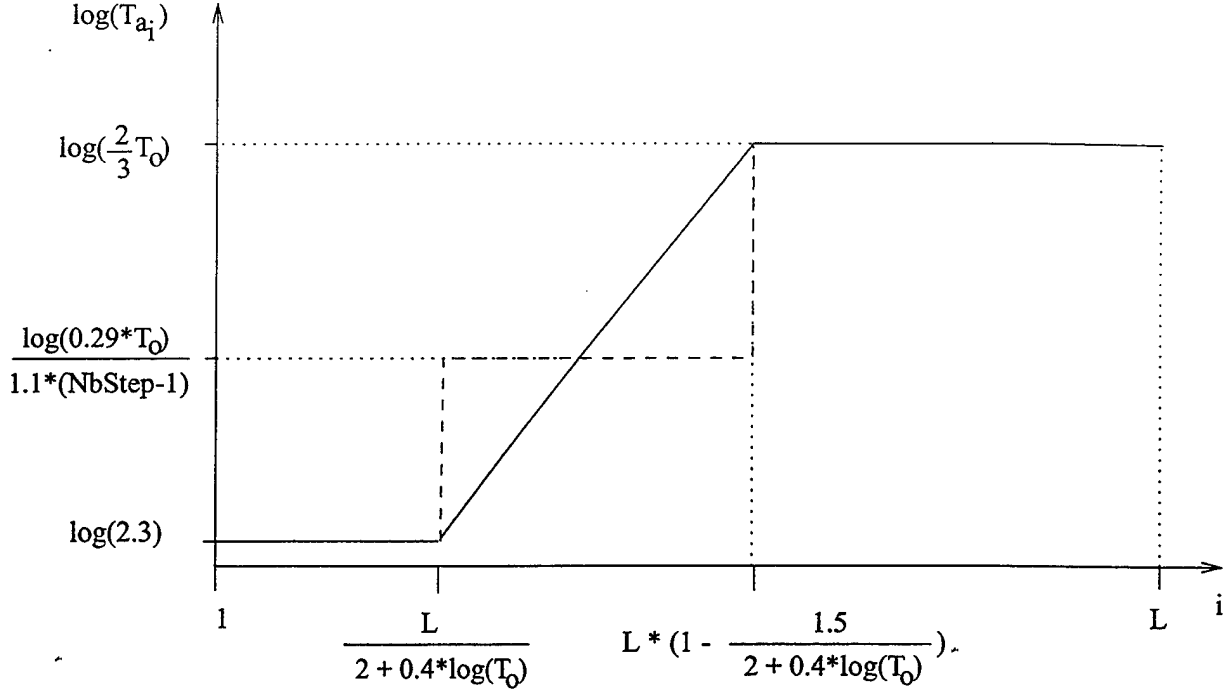
Figure 3.1 Recommended transmission probability distribution

the Poisson approximation of the probability of failure. Numerically, we get $N = 0$ for $1 \leq T_0 < 32$, $N = 1$ for $32 \leq T_0 < 281$ and so on.

3.2 Performance Comparison

We now focus on the results gained for $-logP_F(T, \mathbf{a})$ and $\tilde{P}_F(T_0, \mathbf{a})$, when using the exact expression of $-logP_F(T, \mathbf{a})$ (Equation (2.1)) for the evaluation of the probability of failure. As illustrated in Figure 3.2, the recommended policy parameters of the previous section sometimes lead to better results than the ones we would gain by using the "optimized" parameters of the previous chapter. This is because the previous optimization was only performed on the approximate expression of $-logP_F(T, \mathbf{a})$, due to computing-time considerations; consequently, the recommended parameters reflect that some minor modification of those parameters can somewhat improve the system efficiency.

27
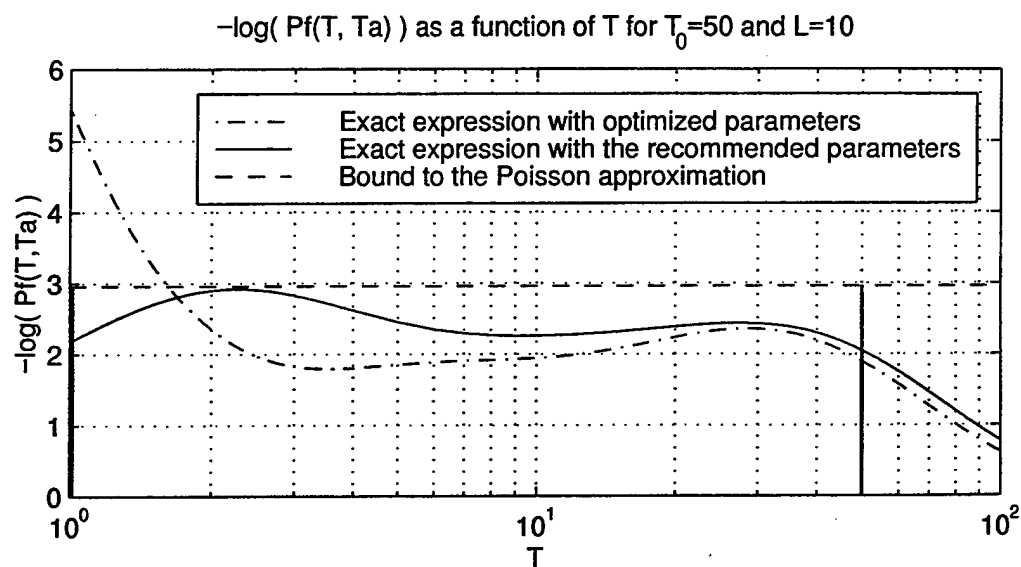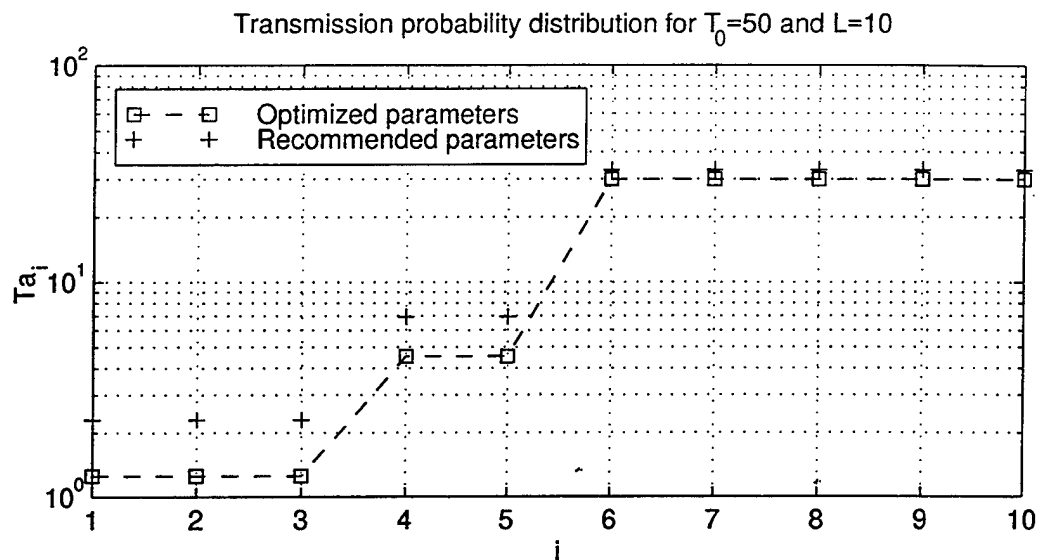
Figure 3.2 Performance comparison for $T_0=50$ and $L=10$

Tables 3.1 through 3.4 list, for different values of T_0, the resulting $-log(\tilde{P}_F(T_0, \mathbf{a})^{\frac{1}{L}})$. For each value of T_0, we successively compute $-log(\tilde{P}_F(T_0, \mathbf{a})^{\frac{1}{L}})$ first by using the exact expression for the probability of failure along with the previously gained optimized parameters (which, in fact, are only optimal for the Poisson approximate expression of $-logP_F(T, \mathbf{a})$), then by using the exact expression along with the recommended parameters, and by using the predicted value of P_F based on an approximation (Equation (B.3)):

$$-\log \tilde{P}_F(T_0, \mathbf{a}) \approx \frac{L \cdot A}{\log T_0 + \frac{A}{M} \cdot (\gamma + 1)}$$

where $M = 0.4587$, $A = 1.1577$ and $\gamma = 1.5$. We finally give the corresponding results for the upper bound when using the Poisson approximation.

Table 3.1 $\tilde{P}_F(T_0, \mathbf{a})$ for optimized/recommended parameters when $L = 3$

T_0	$-log(\tilde{P}_F(T_0, \mathbf{a})^{\frac{1}{L}})$		Prediction based on an approximation	Upper bound to the Poisson approximation
	Gained by using the exact expression along with the optimized parameters	recommended parameters		
10	0.1982	0.2911	0.1344	0.5028
20	0.1016	0.2435	0.1244	0.3864
30	0.1483	0.2254	0.1192	0.3404
40	0.1485	0.1923	0.1158	0.3138
50	0.1430	0.1642	0.1133	0.2959
70	0.1340	0.1293	0.1096	0.2725
100	0.1040	0.0990	0.1061	0.2514
200	0.0818	0.0576	0.0997	0.2185

Table 3.2 $\tilde{P}_F(T_0, \mathbf{a})$ for optimized/recommended parameters when $L = 6$

T_0	$-log(\tilde{P}_F(T_0, \mathbf{a})^{\frac{1}{L}})$			
	Gained by using the exact expression along with the optimized parameters	recommended parameters	Prediction based on an approximation	Upper bound to the Poisson approximation
10	0.1982	0.2911	0.1344	0.5028
20	0.2092	0.2212	0.1244	0.3864
30	0.1915	0.2128	0.1192	0.3404
40	0.1885	0.2060	0.1158	0.3138
50	0.1819	0.2049	0.1133	0.2959
70	0.1742	0.1847	0.1096	0.2725
100	0.1638	0.1604	0.1061	0.2514
200	0.1370	0.1264	0.0997	0.2185

Table 3.3 $\tilde{P}_F(T_0, \mathbf{a})$ for optimized/recommended parameters when $L = 10$

T_0	$-log(\tilde{P}_F(T_0, \mathbf{a})^{\frac{1}{L}})$			
	Gained by using the exact expression along with the optimized parameters	recommended parameters	Prediction based on an approximation	Upper bound to the Poisson approximation
10	0.1864	0.2815	0.1344	0.5028
20	0.1884	0.2283	0.1244	0.3864
30	0.1976	0.2202	0.1192	0.3404
40	0.1897	0.2062	0.1158	0.3138
50	0.1797	0.2050	0.1133	0.2959
70	0.1710	0.1996	0.1096	0.2725
100	0.1540	0.1628	0.1061	0.2514
200	0.1447	0.1501	0.0997	0.2185

Table 3.4 $\tilde{P}_F(T_0, \mathbf{a})$ for optimized/recommended parameters when $L = 15$

T_0	$-log(\tilde{P}_F(T_0, \mathbf{a})^{\frac{1}{L}})$			
	Gained by using the exact expression along with the optimized parameters	recommended parameters	Prediction based on an approximation	Upper bound to the Poisson approximation
10	0.1864	0.2612	0.1344	0.5028
20	0.2087	0.2351	0.1244	0.3864
30	0.1913	0.2160	0.1192	0.3404
40	0.1839	0.1930	0.1158	0.3138
50	0.1675	0.1916	0.1133	0.2959
70	0.1640	0.1904	0.1096	0.2725
100	0.1564	0.1628	0.1061	0.2514
200	0.1481	0.1461	0.0997	0.2185

CHAPTER 4

CONCLUSIONS

This thesis investigated a transmission policy for the case of an unknown but bounded number of active stations in a random multiple-access system without feedback. In particular, we came out with a description of the transmission policy parameters that roughly optimize the system efficiency for some given values of L, the number of access minislots, and of T_0, the maximum number of active stations. Finally we gave some results for the probability of failure with the use of those recommended parameters.

Future work might include finding an optimization method that can directly and efficiently produce the optimal parameters from the exact expression of the probability of failure. Also, the origin of the values found for the different steps of the transmission probability distribution would be worth to be investigated. Finally, further work should be done to find any existing more efficient transmission policy.

APPENDIX A

EVALUATION OF THE PROBABILITY OF FAILURE WHEN USING RIEMANN'S APPROXIMATION

Recall that Riemann's approximation can be written as follows:

$$\int_a^b f(t)\, dt = \lim_{n \to \infty} \frac{b-a}{n} \cdot \sum_{i=0}^{n-1} f(a + i \cdot \frac{b-a}{n})$$

$$= \lim_{n \to \infty} \frac{b-a}{n} \cdot \sum_{i=1}^{n} f(b - i \cdot \frac{b-a}{n}) \tag{A.1}$$

and that the probability of failure satisfies, under the Poisson approximation assumption

$$\forall T, \forall \mathbf{a}, \quad -log P_F(T, \mathbf{a}) = \sum_{i=1}^{L} \phi(T, a_i)$$

$$= \sum_{i=1}^{L} \phi(log T - log T_{a_i}) \tag{A.2}$$

where

$$\forall u, \quad \phi(u) = -log[1 - e^{u - e^u}]$$

Let $\quad \begin{cases} t = log T \\ t_i = log T_{a_i} \quad (1 \leq i \leq L) \end{cases}$

Assumption 1: $\Delta log T_{a_i} = cst$, or equivalently, $t_i = t_1 + (i-1) \cdot \frac{t_L - t_1}{L}$.

Then Equation (A.2) becomes:

$$-log P_F(T, \mathbf{a}) = \sum_{i=1}^{L} \phi(t - t_i) = \sum_{i=1}^{L} \phi(t - i \cdot \frac{t_L - t_1}{L} + \frac{t_L - t_1}{L} - t_1)$$

Let $\Psi/\forall u$, $\Psi(u) = \phi(u + \frac{t_L - (L+1) \cdot t_1}{L})$

.Then

$$
\begin{aligned}
-log P_F(T, \mathbf{a}) &= \sum_{i=1}^{L} \Psi(t - i \cdot \frac{t_L - t_1}{L}) \\
&= \frac{L}{t_L - t_1} \cdot \frac{t_L - t_1}{L} \cdot \sum_{i=1}^{L} \Psi(t - i \cdot \frac{t_L - t_1}{L}) \qquad \text{(A.3)}
\end{aligned}
$$

Assumption 2: L is large enough

Applying Riemann's formula to Equation (A.3) yields the following approximation:

$$
\begin{aligned}
-log P_F(T, \mathbf{a}) &\approx \frac{L}{t_L - t_1} \cdot \int_{t-(t_L - t_1)}^{t} \Psi(x)\, dx \\
&\approx \frac{L}{t_L - t_1} \cdot \int_{t-(t_L - t_1)}^{t} \phi(x + \frac{t_L - (L-1) \cdot t_1}{L})\, dx \\
&\approx \frac{L}{t_L - t_1} \cdot \int_{t - \frac{(L-1) \cdot t_L + t_1}{L}}^{t + \frac{t_L - (L+1) \cdot t_1}{L}} \phi(u)\, du, \quad where \quad u = x + \frac{t_L - (L+1) \cdot t_1}{L}
\end{aligned}
$$

Thus,

$$
\forall T, \forall \mathbf{a}, \quad -log P_F(T, \mathbf{a}) \approx \frac{L}{log T_{a_L} - log T_{a_1}} \cdot \int_{log T - \frac{(L-1) \cdot log T_{a_L} + log T_{a_1}}{L}}^{log T + \frac{log T_{a_L} - (L+1) \cdot log T_{a_1}}{L}} \phi(u)\, du \qquad \text{(A.4)}
$$

APPENDIX B

EVALUATION OF SUBINTERVAL LENGTHS IN THE TRANSMISSION PROBABILITY DISTRIBUTION

We assume that T_0 is large with respect to L. In this case, the transmission probability distribution curve has an initial step, then a linear increase and finally another step, which is larger than the first one. We can therefore consider that a of the L ϕ functions that are summed to produce $\log P_F$ are centered close to $logT = 0$, that b of them are equally spaced (geometric increase) over $[1; logT_0]$ and that c of them are centered close to $logT_0$, such that $L = a + b + c$.

Let $A = 1.1577$ denote the area under a sample ϕ function and $M = 0.4587$ be the maximum value of this function. Let h_a, h_b, and h_c, respectively, denote the values of $-logP_F(T, \mathbf{a})$ at $logT = 0$, $logT = \frac{1}{2} \cdot logT_0$, and $logT = logT_0$. These three quantities should be equal for an optimized transmission probability distribution, as shown in Section 2.3 (recall that, ideally, we would like the curve of $-logP_F(T, \mathbf{a})$ versus $logT$ to be rectangular, i.e., $-logP_F(T, \mathbf{a})$ should be some positive constant inside $[1; T_0]$ this and zero otherwise). Due to the particular shape of the ϕ function, this first implies that $c = \gamma \cdot a$, where $\gamma > 1$.

Now, by approximation,

$$\begin{cases} h_a \approx a \cdot M \\ h_b \approx A \cdot \frac{b}{logT_0} \end{cases}$$

So

$$\begin{cases} h_a = h_b \\ L = a + b + c \end{cases} \Rightarrow \begin{cases} a \cdot M = A \cdot \frac{b}{logT_0} \\ L = a + b + \gamma \cdot a \end{cases} \Rightarrow \begin{cases} b = \frac{M \cdot logT_0}{A} a \\ L = a \cdot (1 + \frac{M \cdot logT_0}{A} + \gamma) \end{cases}$$

Hence

$$\begin{cases} a = \frac{L}{1 + \frac{M \cdot logT_0}{A} + \gamma} \\ b = \frac{L \cdot M \cdot logT_0}{A + M \cdot logT_0 + \gamma \cdot A} \\ c = \frac{\gamma \cdot L}{1 + \frac{M \cdot logT_0}{A} + \gamma} \end{cases} \tag{B.1}$$

In particular, $M = 0.4587$, $A = 1.1577$ and $\gamma = 1.5$ yield

$$\begin{cases} a = \frac{L}{2.5 + 0.3962 \cdot logT_0} \\ b = \frac{0.3962 \cdot L \cdot logT_0}{2.5 + 0.3962 \cdot logT_0} \\ c = \frac{1.5 \cdot L}{2.5 + 0.3962 \cdot logT_0} \end{cases}$$

From Equation (B.1), we can note that the fraction $\frac{a}{L}$ of sample ϕ functions that are centered close to $T = 1$ does not depend on L. The same remark applies for $\frac{b}{L}$ and $\frac{c}{L}$. Moreover, $T_0 \rightarrow \infty$ yields:

$$\begin{cases} a \propto \frac{L}{logT_0} \rightarrow 0^+ \\ b \rightarrow L^- \\ c \propto \frac{L}{logT_0} \rightarrow 0^+ \end{cases} \tag{B.2}$$

Thus, when T_0 becomes very large, the transmission probability distribution curve tends to have only a linear increase over $[1; T_0]$, as examplified in section 2.4.2.

Finally we can derive an approximate expression for $-\log \tilde{P}_F(T_0, \mathbf{a})$ as follows:

$$-log\tilde{P}_F(T_0, \mathbf{a}) \approx h_a \approx a \cdot M \approx \frac{L \cdot M}{1 + \frac{M \cdot logT_0}{A} + \gamma} \approx \frac{L \cdot A}{logT_0 + \frac{A}{M} \cdot (\gamma + 1)} \tag{B.3}$$

and note that for $T_0 >> 1$, $-log\tilde{P}_F(T_0, \mathbf{a}) \approx \frac{L \cdot A}{logT_0}$, which is the upper bound to the Poisson approximation of $-logP_F(T, \mathbf{a})$ that we have derived in Section 2.3.

REFERENCES

[1] B. Hajek, N. B. Likhanonv, and B. S. Tsybakov, "One-success random access without feedback," 1993. Preprint.

[2] B. Hajek, N. B. Likhanonv, and B. S. Tsybakov, "On the delay in a multiple access system with large propagation delay," *IEEE Trans. Inf. Theory*, vol. 40, pp. 1158 – 1166, July 1994.

Channel Carrying: A Novel Handoff Scheme for Mobile Cellular Networks

Junyi Li   Ness B. Shroff   Edwin K.P. Chong

Abstract—

We present a new scheme that addresses the call handoff problem in mobile cellular networks. Efficiently solving the handoff problem is important for guaranteeing Quality of Service (QoS) to already admitted calls in the network. Our scheme is based on a new approach called *channel carrying*: when a mobile user moves from one cell to another, *under certain mobility conditions*, the user is allowed to *carry* its current channel into the new cell. We propose a new channel assignment scheme to ensure that this movement of channels will not lead to any extra co-channel interference or channel locking. In our scheme, the mobility of channels relies entirely on *localized information*, and no global coordination is required. Therefore, the scheme is simple and easy to implement. We further develop a hybrid channel carrying scheme that allows us to maximize performance under various constraints.

We provide numerical results comparing our scheme with the traditional channel reservation and borrowing types of techniques. We find that our scheme outperforms the reservation scheme over a broad range of traffic parameters. Our scheme also outperforms the channel borrowing scheme under high loads.

Keywords: Channel Borrowing, Dynamic Channel Allocation, Modified Fixed Channel Allocation, Channel Reservation.

I. Introduction

The increasing demand for mobile services has generated worldwide interest in wireless communication networks. Coupled with this interest comes the consumer expectation that the wireless systems provide comparable quality of service to their wired counterparts. Studies have shown that one of the most important user concerns is that service not be cut off during an ongoing call. We address this concern by proposing a new scheme to achieve efficient call handoffs in wireless cellular networks.

The use of cellular systems has been a very popular means of enhancing the capacity of wireless communication networks. In such a system, the service area is divided into cells, and *channels* are reused among those cells. Here a channel is referred to as the unit of wireless spectrum needed to serve a single user. For example, in a TDMA/FDMA system, a time-slot or carrier frequency can be considered as a channel. Channels that are used in one cell cannot be used in other cells that are closer than the *minimum reuse distance*. Handoff occurs when a mobile subscriber moves from one cell to another. A handoff call may be blocked if there is no free channel in the new cell.

Since blocking a handoff call is less desirable than blocking a new call, specific schemes have been developed to prioritize handoff calls. Two prioritization schemes have been commonly studied in the literature [14]. They are:

• *Channel reservation scheme:* In this type of scheme, a number of channels are reserved solely for the use of handoff, allowing both handoff and new calls to compete for the remaining channels [4], [8], [11]. Specifically, in each cell a threshold is set, and if the number of channels currently being used in the cell is below that threshold, both new and handoff calls are accepted. However, if the number of channels being used exceeds this threshold, an incoming new call is blocked and only handoff calls are admitted.

• *Queueing scheme:* In this type of scheme handoff requests are queued, and may later be admitted into the network in case a channel frees up [10].

The above two schemes can also be integrated together to improve the handoff blocking probability and the overall channel utilization. The scheme we propose in this paper is also readily integrated with the queueing schemes. Therefore, we shall concentrate on comparing our scheme only with the reservation scheme.

Our method for treating the handoff problem stems from the following simple idea. A user requesting a handoff always occupies a channel in its current cell. Therefore, if that channel could be *carried* into the new cell, the handoff request would not be blocked. When we say a channel is "carried" into a new cell, we mean that the mobile user continues to use this channel, but now communicates with the base-station in the new cell. From a practical point of view channel carrying is not difficult to achieve. For example, in an FDMA based system, suppose a user requesting handoff to some cell A communicates over a frequency band x that cell A is not allowed to use. Now, if normal handoff is not possible, the user (or its current base-station) could signal cell A giving it permission to communicate with it over channel x.[1] In a similar way, channels can be carried in TDMA systems.

Note that when a channel is carried into another cell, it shortens the reuse distance and may violate the minimum reuse distance requirement [6], [14]. To solve this problem, we propose a new channel assignment method that allows channels to be carried into a neighboring cell without violating the minimum reuse distance requirement. Furthermore, with an *a priori* agreement on channel movement, channel coordination can be achieved locally. This helps to

---

[1] We note that additional hardware equipment is required to implement channel carrying, since the base-station in cell A has to transmit/receive not only on channels initially assigned to cell A, but also on channels that would be carried into cell A.
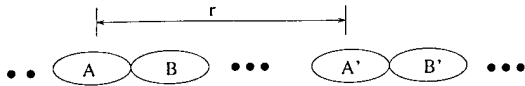
Fig. 1.   Linear Cellular System
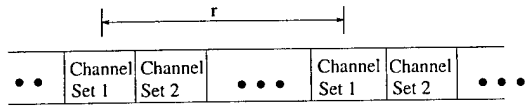
Fig. 2. r−Channel Assignment

significantly simplify the implementation. The new handoff scheme proposed in this paper is called *channel carrying*.

We first describe how the channels are assigned for the channel carrying scheme in a linear cellular (1-D) model, and then present our basic handoff algorithm. The linear cellular model is important since it is a good representation of a highway-type scenario. In addition, it also facilitates easy understanding of the basic concepts of the algorithm. We analyze our algorithm for the 1-D case and show that it provides substantially lower new call blocking and handoff call blocking probabilities than the channel reservation scheme. We then introduce a refinement of our channel carrying scheme, called the *hybrid channel carrying scheme*, which provides a useful design parameter that can be varied to satisfy various QoS constraints. We illustrate how to extend the channel carrying scheme to the planar (2-D) hexagonal model. We also provide numerical results that show that our scheme significantly outperforms the channel reservation technique over a large range of parameters.

II. Channel Assignment

For simplicity, we first describe our channel carrying scheme using a *linear cellular system* model. Later, in Section VI, we will briefly describe how to extend our channel carrying scheme to the 2-D cellular system.

In the linear cellular system, cells (or base stations) are arranged in a linear configuration, as shown in Figure 1. Let N denote the total number of distinct channels that are available in the cellular system. Two cells can use the same set of channels as long as they are at least r cells apart.[2] This distance r is called the *minimum reuse factor*. In the conventional fixed channel assignment scheme, channels are assigned such that the same channels are reused exactly r cells apart, as shown in Figure 2. Therefore, the total number of distinct channels available for each cell is N/r. We refer to this channel assignment as *r-channel assignment.*

In our channel carrying scheme, we alleviate blocking due to handoff by allowing calls to "carry" channels from one cell to another. The author in [5] considered a similar idea of channel borrowing for prioritizing handoffs using r-channel assignment. However, when using r-channel assignment, a call that carries a channel to an adjacent cell may violate the minimum reuse distance requirement. For

[2]Here we assume a minimum reuse distance-based fixed rule in cellular planning. In reality, however, dynamic reuse based on instantaneous interference measurement is also possible.
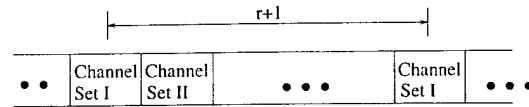
Fig. 3. $(r+1)$-Channel Assignment
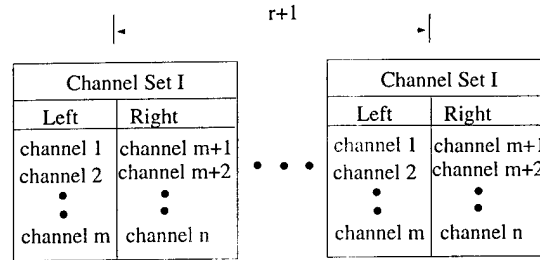
Fig. 4.   Channel Division used in $(r+1)$-Channel Assignment

example, in Figure 1, cells A and A' use the same set of channels. Suppose a call in cell A uses a channel y, and carries it to cell B. Now, if a user arrives in cell A' and uses channel y, then the two y channels are only a distance of $r-1$ cells apart, thus violating the minimum reuse distance requirement. One way to overcome this problem is to have global coordination algorithms that use *channel locking* [6] to ensure that such situations do not occur. For example, in Figure 1, knowing that channel y has been carried from cell A to cell B, we do not allow channel y to be used in cell A'. However, such schemes require excessive exchange of channel usage among remote cells, and channel locking could also degrade reuse efficiency [6].

To ensure that the minimum reuse distance requirement is not violated, we use an $(r+1)$-*channel assignment* scheme. In other words, the same channels are reused exactly $r+1$ cells apart, as shown in Figure 3. In this case, the total number of distinct channels available for each cell is $N/(r+1)$. To ensure that the same channels do not get closer than r cells apart (due to channel carrying), we restrict the channel movement in the following way. Each channel is allowed to be carried in only one direction, left or right. This restriction thus divides the channels assigned to each cell into two types. Further, as shown in Figure 4, exactly the same division is used in cells that are a distance $r+1$ apart. Using this $(r+1)$-channel assignment scheme, and the channel carrying algorithm described in the next section, we ensure that there is no co-channel interference due to channel movement, while avoiding the need for global coordination.

III. Handoff Algorithm

A. Algorithm Description

To describe our handoff algorithm, we first focus our attention on a particular (arbitrary) cell, which we call the *local cell*. The adjacent cells to the left and right of the local cell are called *foreign cells*. The channels that have been assigned to the local cell are called *local channels*, and are divided into two types: *local-left* (LL) and *local-right* (LR) channels, as shown in Figure 4. An LL (LR) channel is one

that can be carried to the left (right) cell during handoff. In other words, an LL (LR) channel can be used by a call in the local cell as well as in the foreign cell to the left (right). A channel from a foreign cell that is being used in the local cell is called a *foreign channel*. Foreign channels from the left cell are called *foreign-left* (FL) channels and foreign channels from the right cell are called *foreign-right* (FR) channels.

The protocol to handle new call arrivals and handoff requests from a foreign cell is straightforward. When a new call arrives, we check if there are any idle (unused) local channels. If there are, the new call is accepted and assigned the idle channel; otherwise, the call is rejected (blocked). When a handoff call request is received from a foreign (left or right) cell, we check if there are any idle local channels available. If there are, the handoff call is accepted and assigned the idle channel; otherwise, the foreign cell is notified that there are no idle local channels.

The main part of the protocol is to handle a handoff request to a foreign cell, which we describe next. Explicit details of the protocol can be found in [7]. For simplicity, suppose a user U in the local cell wants to move to the *left* foreign cell. The handoff operation is attempted in the following order:

1. If user U is currently using a foreign-left (FL) channel, then it simply carries it back to the left cell; otherwise, step 2 is initiated.
2. We send a handoff request to the left foreign cell. The foreign cell then executes the procedure described earlier. If the handoff is accepted, user U moves to the left cell and releases its own channel; if not, step 3 is initiated.
3. If user U is currently using a local-left (LL) channel, then it carries it to the left cell; otherwise, step 4 is initiated.
4. We check if there is an idle LL channel currently in the local cell. If so, U releases its own channel, grabs the idle LL channel, and carries it to the left cell; otherwise step 4 is initiated.
5. We check if there is an FL channel being used by some other user V in the local cell. If so, user U exchanges its channel with user V and then executes step 1 above; if not, we perform step 6.
6. We check if there is an LL channel being used by some other user W in the local cell. If so, user U exchanges its channel with user W, and executes step 3 above.
7. If all the above conditions do not hold, then the handoff cannot be accomplished. Normally, this would result in the handoff call being blocked.

A similar procedure would be applied if a user in the local cell wanted to move to the right foreign cell.

B. Salient Features of the Handoff Algorithm

The following are some of the significant features of our algorithm. Again, for simplicity, we focus only on handoff from the local cell to the *left* foreign cell.

• An important feature of our algorithm is that no global coordination is necessary, thus facilitating implementation. At the same time, the algorithm ensures that there is no co-channel interference due to channel movement. The major computational effort in the local cell includes signaling with the left foreign cells, channel swapping, and a simple table look-up. We will investigate the complexity of our protocol later in Section V-B.2 by estimating the expected number of times that intercellular signaling is sent and the number of times that channel swapping occurs for each call arrival.

• In our algorithm, handoff calls have access to a larger portion of the system capacity than new incoming calls. To see this, note that a new call is blocked if and only if there is no idle (local) channel in the local cell. On the other hand, a handoff request to the (left) foreign cell is *blocked if and only if all the left-local (LL) channels are being used in the foreign cell.* This occurrence is relatively rare because it requires that all three of the following conditions are simultaneously true:

1. All the channels in the left foreign cell are being used.
2. All the FL channels are being used by users in the left foreign cell.
3. All the LL channels have been previously carried to the left foreign cell.

It is therefore apparent that in our channel carrying scheme, handoff call requests are favored over new call requests. At the same time, we do not require channels to be reserved *a priori* for handoff calls. This helps increase the efficiency of our scheme compared to reservation schemes, as demonstrated in Sections IV-B, V-B, and VI-B.

IV. Performance Analysis using the Two-Cell Model

A. Markov Chain Model for the Channel Carrying and Reservation Schemes

In this section we develop a Markov chain model to analyze the performance of our handoff algorithm. The QoS measures that we are interested in are:

• P_{bN}, the steady state probability of blocking a new call; and

• P_{bH}, the steady state probability of blocking a handoff call.

The system that we are interested in modeling is the linear cellular system shown in Figure 5(a). The traffic is assumed to be symmetrically distributed over all the cells; the new call arrival rate at every cell is λ_n. The handoff rate between cells is assumed to be directly proportional to the number of users in that cell, so if a cell has i users the handoff rate to its neighboring cell is $i\lambda_H$, as shown in Figure 5(a). Here the value $1/\lambda_H$ is defined as the expected time between the time-instant when a user enters a cell and the time-instant when it departs the same cell (given that this users' call does not terminate before departure).

The analysis of this entire system is computationally infeasible. Therefore, the performance analysis of call handoff schemes in wireless systems is typically done by focusing on a single cell, which results in a one-dimensional Markov chain [8]. However, the one-cell model does not accurately capture the essence of our algorithm. For example, suppose that a user in the local cell wants to move to the left foreign cell. Whether or not it carries a channel during
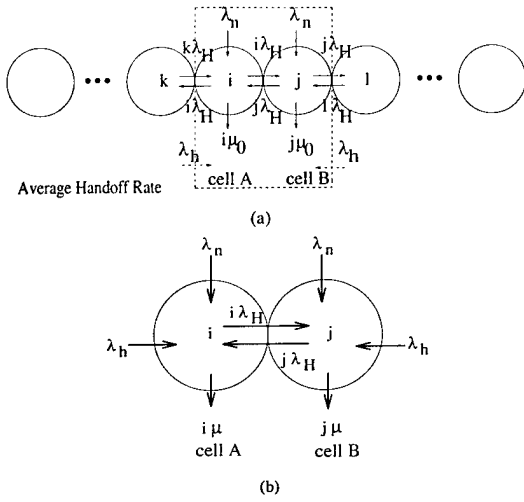
Fig. 5. (a) Linear Cellular system with various traffic parameters. (b) Two-Cell model with the corresponding traffic parameters.

handoff depends not only on the availability of FL and LL channels in the local cell but also on whether there is an idle channel in the left foreign cell. Hence, the availability of channels in adjacent cells is coupled.

To alleviate difficulties with a one-cell model, we consider a two-cell model, as shown in Figure 5(b). We assume that in each cell A and B, new call requests arrive according to Poisson processes with rate λ_n. The time it takes for each call in a cell to request a handoff to the other cell is assumed to be exponentially distributed with mean $1/\lambda_H$. Call handoffs arrive from outside the two-cell subsystem according to a Poisson process with rate λ_h. The time until a call terminates is assumed to be exponentially distributed with mean $1/\mu_0$. Therefore the time until a call leaves the two-cell system (either due to handoff or call termination) is exponentially distributed with mean $1/\mu = 1/(\mu_0 + \lambda_H)$. Now, assuming that all of the above operations (new arrival, call handoff request, and call termination) are independent, we can analyze our two-cell system using a Markov Chain.

Recall that the total number of local channels in each cell is $M = N/(r+1)$. To further simplify the model, we assume that the total number of local channels, M, is divided into an equal number, $m = M/2$, of local left (LL) and local right (LR) channels.

In our Markov chain model, we let $N_A \in \{0, \ldots, M\}$ and $N_B \in \{0, \ldots, M\}$ represent the number of idle local channels in cell A and cell B, respectively. Next, let $N_{B \to A} \in \{-\frac{M}{2}, \ldots, 0, \ldots, \frac{M}{2}\}$ be defined as follows. If $N_{B \to A} \geq 0$, it denotes the number of foreign channels from cell B that are being used in cell A. On the other hand, if $N_{B \to A} \leq 0$, it denotes the number of foreign channels from cell A that are being used in cell B. Hence, $N_{B \to A}(t)$ can take values from $-\frac{M}{2}$ to $\frac{M}{2}$. The triple $(N_A, N_B, N_{B \to A})$ represents the state of the Markov chain. Although there are three components in each state, the state transition diagram of the Markov chain can be represented in a planar fashion. To see this, recall that a foreign channel will

move into a cell only when there is no idle local channel in that cell. Also, whenever service is terminated, the foreign channel within the local cell will be returned immediately. Thus, if we neglect the additional time it would take to return or carry a channel, it follows that

$$N_{B \to A} > 0 \quad \Rightarrow \quad N_A = 0$$
$$N_{B \to A} < 0 \quad \Rightarrow \quad N_B = 0.$$

The above equations help restrict one degree of freedom thereby resulting in a planar or two-dimensional Markov chain. The state transition diagram of this Markov chain can be found in our technical report [7]. Let $P_{i,j,k} = P\{N_A = i, N_B = j, N_{B \to A} = k\}$ denote the steady state probability of the state $\{N_A = i, N_B = j, N_{B \to A} = k\}$. We obtain these probabilities by exploiting the above mentioned symmetry and by applying standard numerical Markov chain techniques.

Now observe Figures 5(a) and 5(b) again. In Figure 5(b) we focus only on cells A and B of Figure 5(a). Let the cells to the right of cell B and to the left of cell A be called *external cells*. The handoff rate λ_h in the two-cell model of Figure 5(a) is actually the average of the state dependent handoff rate from their neighboring external cells. Averaging over all the states, λ_h is given by

$$\lambda_h = \sum_{i=0}^{M} (M-i)\lambda_H \sum_{j=0}^{M} \sum_{k=-m}^{m} P_{i,j,k}, \tag{1}$$

where $m = M/2$. Since λ_h depends on $P_{i,j,k}$, we iteratively solve the Markov chain. The iteration procedure is made to terminate when *both* the absolute and relative errors are less than 10^{-3}.

Having determined $P_{i,j,k}$, we calculate P_{bN}, the steady state probability of blocking a new call, and P_{bH}, the steady state probability of blocking a handoff call by summing over the appropriate states. Specifically,

$$P_{bN} = \sum_{k=0}^{m} \sum_{j=0}^{M-k} P_{0,j,k}$$

$$P_{bH} = \sum_{j=0}^{M-m-1} P_{0,j,m},$$

where $m = M/2$, as before.

Similarly, we can develop a Markov chain model to analyze the system performance using the traditional channel reservation scheme. As in the channel carrying scheme, we focus on the two-cell model shown in Figure 5. The parameters λ_h, λ_n, λ_H, and μ are defined as before. Since no channel movement is allowed, the pair (N_A, N_B), $N_A \in \{0, \ldots, M'\}$, $N_B \in \{0, \ldots, M'\}$, suffices to characterize the state of the two-cell system. Here, $M' = N/r$ is the total number of distinct channels available to each cell, and N_A (N_B) is the total number of idle channels in cell A (cell B). Once again, for space considerations, we do not include the detailed Markov chain model for the channel reservation scheme (details are shown in [7]).

It is instructive to intuitively compare the channel carrying and reservation schemes. There are two main differences. First, because of the r-channel assignment, the number of local channels in each cell is M' in the reservation scheme instead of M in the carrying scheme, where $M' = N/r$. The difference d is given by

$$d \triangleq M' - M = \frac{N}{r(r+1)},$$

which is the cost we pay for channel mobility. Clearly, when the reuse factor r is large, this difference is marginal. Second, because of channel reservation, new calls have to be blocked when the number of occupied local channels exceeds a threshold K in the channel reservation scheme. The arrival rate is then reduced from $\lambda_n + \lambda_h$ to λ_h, which is a disadvantage of the reservation scheme compared to the channel carrying scheme. Therefore, when we set $K = M$, the number of channels accessible by new arrivals is roughly the same for the channel carrying and reservation schemes, since if the number of occupied local channels in a cell reaches K (or M), any new call in the reservation (or carrying) scheme is now blocked. Thus, the new call blocking probabilities would be close for both schemes in the case. On the other hand, in the reservation scheme, there are $M' - K$ channels dedicated for the use of handoff calls, while in the carrying scheme, although there are no channels dedicated for handoff calls, the maximum number of channels that can be carried into a single cell is M $(= \frac{N}{r+1})$ which is larger than $M' - K$ $(= \frac{N}{r(r+1)})$. Hence, by appropriately taking advantage of the stochastic traffic fluctuation in the different cells, we expect that channel carrying would be more effective in serving handoff calls.

B. Numerical Examples

In this section, we provide numerical results, based on analysis and simulation, to compare the performance of the channel carrying scheme and the reservation scheme.

To obtain the analytical results we use the two-cell model of Figure 5(b). We then obtain values for the new call blocking probability P_{bN} and the handoff blocking probability P_{bH} under various traffic parameters, using the analytical method outlined in Section IV-A.

In addition to computing the performance measures using our Markov chain model, we also simulate the system under the carrying and reservation schemes. Our simulation consists of a 120-cell linear cellular system. The boundary cells on the two sides are then connected to each other to avoid the "edge" effect at the boundaries. We assume a Poisson arrival process with rate λ_n for new calls in each cell, and exponentially distributed call termination times with mean $1/\mu_0$. The time duration between the arrival of a user at a cell and the instant of a handoff request is exponentially distributed with mean λ_H. Handoff requests are directed to each of the adjacent cells with equal probability. The above processes are assumed independent. Since we are interested in the performance of a typical cell, the statistics are averaged over all cells. Each simulation
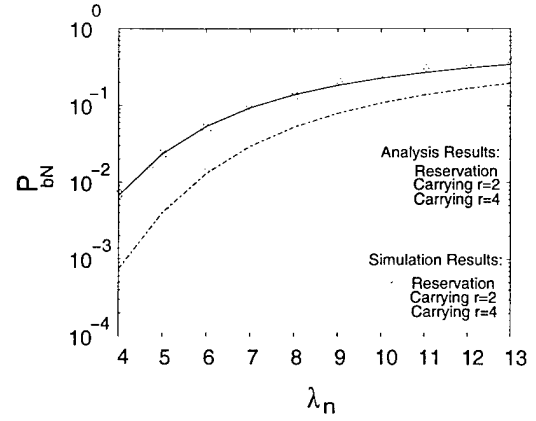
Fig. 6. Plot of P_{bN} versus λ_n. The parameters used in this figure are $N/r = 15$, $K = 10$, $\lambda_H = 1$, $\mu_0 = 1$.
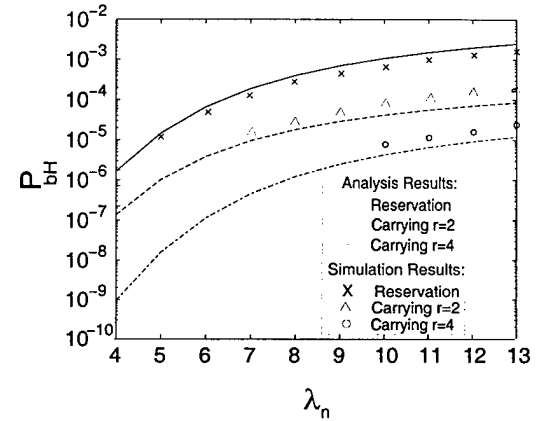
Fig. 7. Plot of P_{bH} versus λ_n. The parameters used in this figure are $N/r = 15$, $K = 10$, $\lambda_H = 1$, $\mu_0 = 1$.

run is started with no users present in the system and is terminated after 10^7 discrete events have occurred. The initialization effects can be ignored since we have simulated such a large number of iterations. Moreover, the simulation results shown in this paper are valid for up to 95% confidence intervals.[3]

In Figure 6 we plot P_{bN}, and in Figure 7 we plot P_{bH} for both the channel carrying and the reservation scheme under different traffic loads λ_n, ranging from 4 calls to 13 calls per unit time. The call handoff rate is $\lambda_H = 1$ call per unit time, and the call termination rate is $\mu_0 = 1$ call per unit time.

For the channel carrying case, two values for the reuse distance are considered: $r = 2$, the minimum possible reuse distance, and $r = 4$, a more typical value for the reuse distance. Further, in both figures, we have $M' = N/r = 15$; hence, $N = 30$ when $r = 2$, and $N = 60$ when $r = 4$.

Note, that in the channel reservation scheme, for a given arrival rate, we can vary the threshold K to give us different values of P_{bN} and P_{bH}. We find that if we choose

---

[3]For the simulation results plotted in this paper, the confidence intervals are so narrow that we do not explicitly show them in the figures. For example, in Figure 6, the confidence intervals for each point are narrower than the height of each circle or triangle shown.

$K = M = N/(r+1)$, then the values of P_{bN} for the reservation scheme are close to those of the carrying scheme. For $r = 2$, we choose $K = M = 10$, and we can observe in Figure 6 that the new call blocking probability (P_{bN}) curves for the reservation and carrying schemes are in fact very close. However, for the same parameters, the call handoff blocking probability (P_{bH}) as shown in Figure 7 is at least about one order of magnitude lower in the carrying scheme than in the reservation scheme. When the value of the reuse distance is increased to $r = 4$, and we set $K = 10$, the carrying scheme significantly outperforms the reservation scheme in terms of both P_{bN} and P_{bH}. This result can be observed in Figure 6, where the P_{bN} curve in the carrying case is up to one order of magnitude lower than in the reservation scheme, and in Figure 7, where the P_{bH} curve in the carrying scheme is up to three orders of magnitude lower than in the reservation scheme. The reason the carrying scheme provides a lower P_{bN} curve for $r = 4$ is that $M = 12 > K$, in this case. However, if we choose $K = M$, then, although the P_{bN} curves will be closer, the difference in the P_{bH} curves will be even larger.

We next develop a hybrid channel carrying scheme which can be used to maximize performance, under various constraints, by allowing us to vary the number of channels that can be carried.

V. HYBRID CHANNEL CARRYING SCHEME

A. Description

In the numerical examples of the previous section, we observe that the channel carrying scheme results in a large difference between the values of P_{bH} and P_{bN}. In particular, when the load is high, the value of P_{bN} is much higher than that of P_{bH}. For example, for $\lambda_n = 13$ and $r = 4$, the value of P_{bH} is only about 10^{-5} while that of P_{bN} is greater than 10^{-1}. This observation suggests that our channel carrying scheme excessively favors handoff requests over new calls and could, under certain scenarios (e.g., when λ_h/μ_0 is very small), perform even worse than the channel reservation scheme. The authors in [2] have also studied a hybrid type of idea to address similar channel assignment problems. We next present our hybrid scheme that allows trading off potential handoff blocking for availability of idle channels for new calls.

Recall that in the $(r+1)$-channel assignment scheme, the number of channels assigned to each cell is $M = N/(r+1)$, and every channel can be carried either to the left or to the right. On the other hand, in the r-channel assignment scheme, the number of channels assigned to each cell is N/r, but none of the channels can be carried to foreign cells. In our hybrid scheme, we divide the total number of channels N into two distinct groups of size N_1 and N_2, such that

$$N = N_1 + N_2.$$

The N_1 channels are assigned according to the r-channel assignment scheme, and cannot be carried to foreign cells. The N_2 channels, however, are assigned according to the $(r+1)$-channel assignment scheme, and can be carried ei-ther to the left or to the right, just as in the previous channel carrying scheme. Therefore, in the hybrid scheme, each cell is assigned

$$M_h = \frac{N_1}{r} + \frac{N_2}{r+1}$$

channels, where the two terms in the sum corresponds to the two groups of channels. As before, the $N_2/(r+1)$ *movable* channels are themselves divided into two types: left and right.

The hybrid scheme above defines a family of channel assignments that encompasses both the pure r- and $(r+1)$-channel assignment schemes. Specifically, $N_1 = 0$ corresponds to the $(r+1)$-channel assignment scheme, while $N_2 = 0$ leads to the r-channel assignment scheme. The N_2 channels allow us to trade off the ability to carry (and hence avoid handoff blocking) with a reduced number of channels available to each cell. In particular, the number of channels that we sacrifice in using $(r+1)$-channel assignment instead of r-channels assignment is

$$d_h = \frac{N_2}{r} - \frac{N_2}{r+1} = \frac{1}{r}\left(\frac{N_2}{r+1}\right).$$

The parameter d_h serves as a design parameter that we can adjust to balance the requirements of the performance measures P_{bN} and P_{bH}, analogous to the threshold parameter K in the channel reservation scheme. The larger the value of d_h in the hybrid scheme, the more we favor handoff calls because there are more movable channels. Hence, as d_h increases, we expect P_{bH} to decrease and P_{bN} to increase. A similar observation holds for the design parameter K in the reservation scheme. Also note that, as in the original channel carrying case, for a fixed number of channels N_2 that are allowed to move, the price we pay for the $(r+1)$-channel assignment scheme (in terms of d_h) decreases with increasing r.

In the next section we provide numerical (both simulations and analysis) results comparing the carrying scheme with the reservation scheme for various performance measures.

B. Numerical Examples

For the purpose of analytical evaluation, we adopt the two-cell model and make the same assumptions here as we did in Section IV-B. The resulting Markov chain has exactly the same structure as before, the only difference being that we substitute $m_h = \frac{N_2}{2(r+1)}$ in place of m. We can then solve for the steady state probabilities in the Markov chains for the hybrid and reservation schemes, and compute P_{bH} and P_{bN} as before. Also, as in Section IV-B, for our simulation study we use a 120 cell linear cellular system and we plot the results together with those obtained from our Markov chain model.

B.1 Utilization versus λ_n

From the point of view of a network provider, a useful parameter of interest is the *normalized channel utilization*,

Fig. 8. Plot of optimal γ versus λ_n for the problem defined in Equation (3). The parameters used in this figure are: $N/r = 15$, $\lambda_H = 1$, $\mu_0 = 1$, $H_{max} = 10^{-4}$.

Fig. 9. Plot of optimal γ versus λ_n for the problem defined in Equation (3), for various values of r. The parameters used in this figure are: $N/r = 30$, $\lambda_H = 1$, $\mu_0 = 1$, $H_{max} = 10^{-4}$.

γ , defined as

$$\gamma = \frac{\text{average number of users in one cell}}{\text{total number of available channels in one cell}}, \quad (2)$$

where the total number of available channels in one cell is $M' = N/r$. The parameter γ is directly related to the revenue of a cellular network because it incorporates both new and handoff calls. To compute γ for the hybrid scheme we use the equation

$$\gamma = \frac{1}{M'} \sum_{i=0}^{M_h} \sum_{j=0}^{M_h} \sum_{k=-m_h}^{m_h} \frac{1}{2}[(M_h - i) + (M_h - j)]P_{i,j,k}$$

and for the reservation scheme,

$$\gamma = \frac{1}{M'} \sum_{i=0}^{M'} \sum_{j=0}^{M'} \frac{1}{2}[(M' - i) + (M' - j)]P_{i,j},$$

where $P_{i,j}$ are the state transition probabilities in the corresponding Markov chain, using the two-cell model, for the reservation scheme [7].

To plot the values of γ under varying loads for the hybrid scheme, we define the optimization problem

$$\begin{array}{ll} \underset{d_h}{\text{maximize}} & \gamma \\ \text{subject to} & P_{bH} \leq H_{max}. \quad (3) \end{array}$$

Once again, we define a similar optimization problem for the reservation scheme by replacing the decision variable d_h by K.

In Figure 8 we plot values of γ under varying λ_n. The parameters used for this figure are: $\lambda_H = 1$, $\mu_0 = 1$, $M' = 15$, $H_{max} = 10^{-4}$. The hybrid scheme achieves uniformly higher values of γ under various loads. The difference between the hybrid and reservation schemes is most apparent at high loads. At such loads, a low value of K is required in the reservation scheme to maintain the QoS constraint on P_{bH}, thus resulting in a low value of γ. On the other hand, due to the mobility of channels

in the hybrid scheme, the sacrifice in the number of local channels to maintain the QoS constraint on P_{bH} is not as great. When $r = 4$, the channel utilization for the channel carrying scheme at high loads is over 50% more than the reservation scheme. Further, this advantage will be even more significant as r increases. An interesting observation made in Figure 8 is that γ does not monotonically increase with λ_n. The reason is that the tuning parameter K for the reservation scheme and d_h for the carrying scheme can take on only discrete values. For example, for a particular value of K and λ_n, the maximum utilization (γ) may be achieved at a blocking probability P_{bH} which is much less than the constraint 10^{-4}. Then, when we increase λ_n, this constraint is still met without K being changed, and therefore the utilization γ is increased. However, eventually when λ_n is large enough, K will have to be decremented to satisfy the constraint, thus resulting in a lowered capacity for new calls and a drop in the utilization.

To study the effect of changing the value of r, in Figure 9 we plot the optimal values of γ versus λ_n for various values of r: 4, 8, and ∞. The traffic parameters we use here are: $M' = 30$, $\lambda_H = 1$, $\mu_0 = 1$. The constraint is $H_{max} = 10^{-4}$. For comparison, we also include a plot for the reservation scheme in Figure 9. Note that, as expected, the channel utilization is highest when $r = \infty$, in which case the optimal value of d_h is 0. We observe that even for moderate values of r (e.g., $r = 8$), the utilization levels achieved are close to the maximum value (achieved with $r = \infty$), while the utilization levels achieved by the reservation scheme are significantly lower.

B.2 Protocol Complexity

In this section, we investigate the protocol complexity of the channel carrying scheme. Recall from the algorithm description in Section III that the complexity associated with channel carrying mainly includes signaling between neighboring cells and channel swapping within a local cell. For illustration, we consider the optimum hybrid channel carrying schemes obtained under varying λ_n in Figure 8, and quantitatively estimate, via simulations, the number of

intercellular signals that are transmitted and the number of times channel swapping occurs.

We first estimate the expected number of times that intercellular signals are sent to serve a mobile user over the duration of its call. We do this by dividing the total number of handoff requests that have been submitted in the simulation to the total number of call arrivals. Here we count all handoff request signals, including those that are not granted. We find that the expected number of handoff requests per call arrival does not exceed 0.3 in all the cases shown in Figure 8.

We then estimate the expected number of times that channel swapping is needed to serve a mobile user during the duration of the entire call. This can be done by dividing the total number of times that channel swapping is observed in the simulation to the total number of call arrivals. We find that the maximum number of times channel swapping is needed per call arrival is less than 0.1 for the hybrid carrying schemes in Figure 8. These results suggest that the overhead required to implement the channel carrying scheme is not significant.

B.3 Comparison with Channel Borrowing Scheme

The channel carrying scheme reduces the handoff blocking probability by allowing channel mobility. Thus, it can be viewed as a simple dynamic channel assignment scheme. The most attractive feature of the channel carrying scheme is its simplicity compared with most dynamic channel assignment schemes which adopt more complex coordination or power control. The channel borrowing scheme [13] is representative of another relatively simple dynamic channel assignment scheme. We next compare the performance and complexity of these two schemes.

To treat the call handoff problem, we modify the channel borrowing scheme as follows. Consider again the linear cellular system in Figure 1. Suppose that the fixed channel assignment scheme is employed and each cell is assigned N/r channels, which are called the *permanent channels* of that cell. Similar to the channel reservation scheme, a threshold K_b is set in each cell to protect handoff calls—new calls can be accepted only if (1) the number of channels currently used in the cell is below that threshold; and (2) there is an idle channel available in the cell. The channel borrowing mechanism is used to further prioritize handoff calls. In particular, suppose a call, using a permanent channel of cell A, moves from cell A to cell B, and there is no idle channel currently available in cell B.[4] Instead of blocking this handoff request, cell B attempts to borrow a permanent channel from its neighbors (cells A and C). A channel can be borrowed from cell A to cell B, only if (1) it is not locked in cell A; and (2) it is not being used in cell A' (recall that cells A' and A are assigned the same set of permanent channels). Once a channel is borrowed from cell A to cell B, the same channel is locked in cell A', i.e., it cannot be used in cell A' or lent to any neighbor of cell

A'. A similar operation can be applied when borrowing a channel from cell C. Note that channel locking potentially degrades reuse efficiency.

Compared with the channel carrying scheme, the above channel borrowing scheme involves more complexity. To borrow channels from cell A, cell B has to communicate with both cells A and A' to determine the usage and locking status of *all* permanent channels in those cells. Clearly, this intercellular signaling overhead in the channel borrowing scheme is more significant than that required in the channel carrying scheme. Also, since cells B and A' are not adjacent, communication between both cells could experience large latency, which is undesirable when responding to handoff requests. However, we note that the channel borrowing scheme does not adopt channel division as in the carrying scheme (see Figure 4). Thus, the channel borrowing scheme would require less channel swapping.[5]

We next compare the performance of the channel carrying, borrowing, and reservation schemes for the optimization problem (3). The decision variable for the channel borrowing scheme is K_b, which is similar to K in the reservation scheme. For the sake of comparison, we investigate the performance of the channel borrowing scheme only via simulation. In Figure 10 we plot the optimal channel utilization γ versus varying λ_n for the three handoff schemes. The parameters used for this figure are the same as for Figure 8. In this figure, we simply replot the simulation results for the channel carrying and reservation schemes from Figure 8, and compare them with those obtained by the channel borrowing scheme. We observe that when the traffic load is light, the performance of all three schemes is virtually the same. When the load is increased slightly, the channel borrowing scheme allows a higher utilization than the carrying scheme. However, as the load is further increased, the channel utilization for the borrowing scheme drops. This is because channel locking degrades the reuse efficiency. To favor *one* current handoff request, the channel borrowing scheme may block *two* other potential handoff requests in the future. This adverse effect becomes more severe when the traffic load is high. The observation agrees with a common concern about the channel borrowing scheme that it would even perform worse than the fixed channel assignment scheme at a high traffic load [6].

B.4 Relative invariance of the performance measures P_{bN} and P_{bH} over a large range of λ_H

In all the above numerical examples, we use the same value of λ_H, i.e., $\lambda_H = 1$. We now investigate the effect of varying λ_H on performance measures. Intuitively, it is obvious that when the handoff rate is very small compared to the new call arrival rate and service rate, handoff calls rarely occur, and thus the handoff blocking probability is small. On the other hand, when users move from cell to cell very rapidly, λ_H tends to infinity. It can be shown that

---

[4] If cell A is currently holding a channel previously borrowed from cell B, then we swap channels and allow the handoff call to take that borrowed channel back to cell B.

[5] If we allow more intercellular coordination overhead, the channel carrying scheme also does not require channel division, and would have less channel swapping and better system performance.
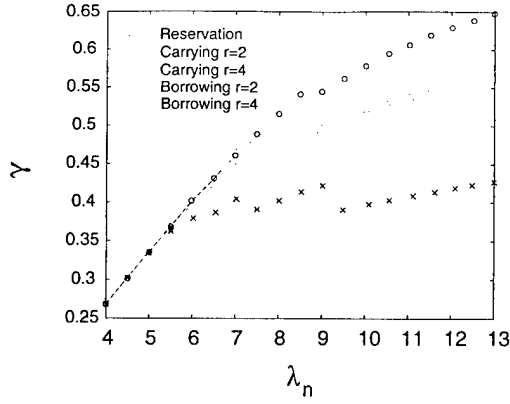
Fig. 10. Simulation comparsion of optimal γ versus λ_n with the channel carrying, borrowing, and reservation sche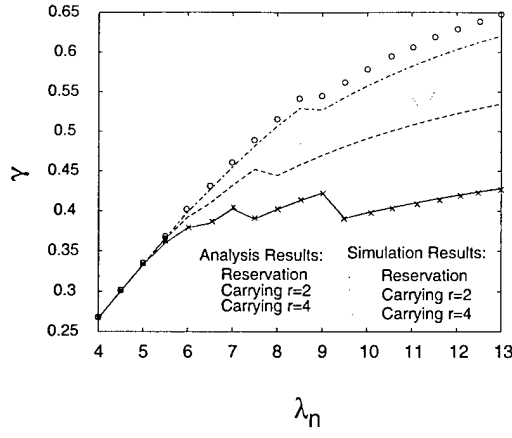mes for the problem defined in Equation (3). The parameters used in this figure are: $N/r = 15$, $\lambda_H = 1$, $\mu_0 = 1$, $H_{max} = 10^{-4}$.
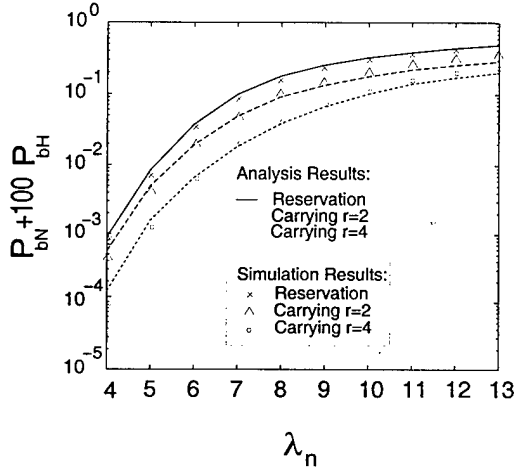
Fig. 11. Plots of ϕ versus λ_n. The parameters used in this figure are $N/r = 15$, $\lambda_H = 1$, and $\mu_0 = 1$

the handoff blocking probability also tends to zero in this case (see [12]). But, we observe that for a broad range of values of λ_H (say, from 1 to 10), the performance measures P_{bN} and P_{bH} are not sensitive to changes in λ_H.

For illustration, in Figure 12, we plot P_{bN} and P_{bH} versus λ_H for both the reservation and carrying schemes with $r = 2$ and $r = 4$. We can see that the P_{bN} curve in Figure 12 is quite flat over a wide range of λ_H. Further, the relative variation of the P_{bH} curve in Figures 12 is small for medium values of λ_H, while P_{bH} decreases dramatically at either end of small or large λ_H. Based on these observations, we use $\lambda_H = 1$ in all the above numerical comparisons and expect that the conclusions and observations made there can be extended to traffic conditions with other values of λ_H.

B.5 Correlated/Nonuniform Traffic

So far, we have considered a commonly used traffic model for the cellular network, where the new call arrival processes for different cells are assumed to be uniform and independent. However, in a real cellular system, traffic could
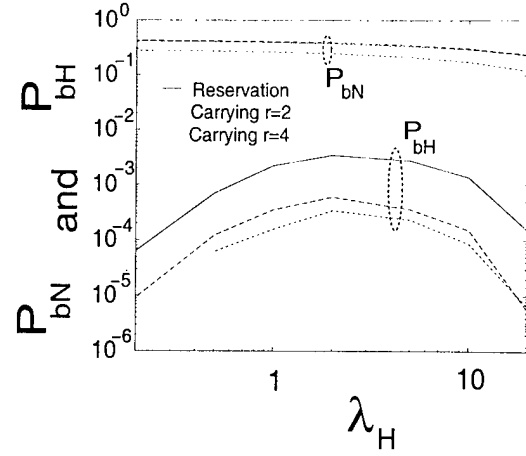
Fig. 12. Plots of P_{bN} and P_{bH} versus λ_H. The parameters used in this figure are $N/r = 15$, $K = 10$, $M = 10$ for $r = 2$ and $M = 13$ for $r = 4$, $\lambda_n = 15$, $\mu_0 = 1$.
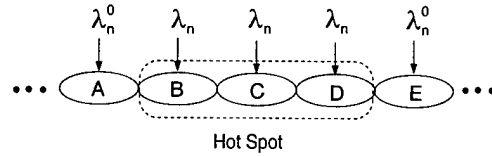
Fig. 13. Roaming Hot Spot Traffic Model

be correlated among cells. For example, if a cell is experiencing a high traffic load, it is likely that its neighboring cells also experience a high traffic load. The earlier traffic model does capture this effect to a certain extent. For example, recall that the handoff rate between two neighboring cells is assumed to be directly proportional to the number of users in the handoff originating cell. Thus, a cell with a large number of users has a high outgoing handoff rate, and will eventually increase the traffic load in its neighboring cells. However, we note that our model does not reflect the correlation among new call arrivals.

To investigate the performance of the channel carrying scheme with the correlated/nonuniform traffic effect, in this section we consider a *roaming hot spot* model, as shown in Figure 13. Again, we assume that new calls arrive according to a Poisson process in each cell. However, the arrival rates in all the cells are not assumed to be the same anymore. Specifically, the new call arrival rate is equal to λ_n^0 in each cell in the network, except at a hot spot which covers three contiguous cells. The new call arrival rate in a cell covered by a hot spot is equal to λ_n, where $\lambda_n \geq \lambda_n^0$. We allow the hot spot to roam in the system. For example, in Figure 13, the hot spot covers cells B, C, and D. After an exponentially distributed random duration with mean $1/\beta$, the hot spot moves leftward (or rightward, with equal probability) and covers cells A, B, and C (or cells C, D, and E, respectively). This process is repeated.

This roaming hot spot model simulates the transient nonuniform effect in cellular traffic. Since the hot-spot roams, a cell whose neighboring cell is in the hot spot will, with high probability, soon experience the high new ar-
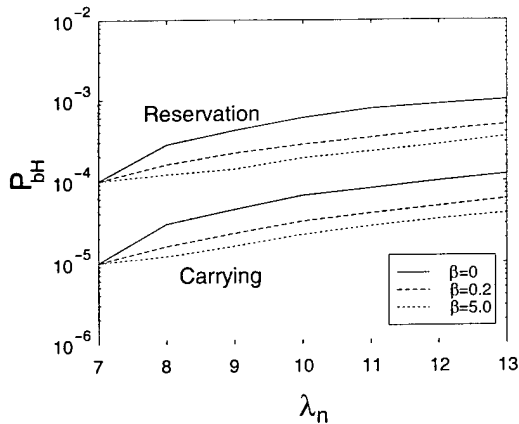
Fig. 14. Plot of P_{bH} in the middle cell of the hot spot versus λ_n. The parameters used in this figure are $r = 2$, $N/r = 15$, $K = 10$, $N_2 = N$, $\lambda_H = 1$, $\lambda_n^0 = 7$, $\mu_0 = 1$.

Fig. 15. Plot of average P_{bH} in the system with a hot spot versus λ_n. The parameters used in this figure are $r = 2$, $N/r = 15$, $K = 10$, $N_2 = N$, $\lambda_H = 1$, $\lambda_n^0 = 7$, $\mu_0 = 1$.

rival rate. Further, the traffic load in the middle cell of the hot spot is highly correlated with both its neighboring cells, since they are always under heavy traffic load condition simultaneously. In this way, we capture the traffic correlation among cells.

Note that because of the nonuniform traffic load, the performance varies for different cells, and it would be hard to define an appropriate optimization problem for the entire system as we did before. To emphasize the hot spot effect and simplify the performance comparison between the channel carrying and reservation schemes, we next focus on the statistics in the middle cell of the hot spot, and plot the simulation result of handoff blocking probability under varying load conditions.[6] Specifically, we fix $r = 2$, $\mu_0 = 1$, $\lambda_H = 1$, $\lambda_n^0 = 7$, and $N/r = 15$. In the reservation scheme, we set $K = 10$. In the carrying scheme, we simply set $N_2 = N$. Similar to Figure 6, we find from our simulation results that in this case, the average new call blocking probabilities for the channel carrying and reservation schemes are very close when $r = 2$. Thus, we only compare the handoff blocking probabilities. In Figure 14, we plot P_{bH} in the middle cell of the hot spot versus varying λ_n. In Figure 15, we plot the average P_{bH} of all the cells. Here we consider three cases for β ($\beta = 5.0$, $\beta = 0.2$, and $\beta = 0$). The case $\beta = 5.0$ indicates that the hot spot is moving rapidly, while the case $\beta = 0.2$ indicates that the hot spot is moving very slowly and $\beta = 0$ represents the case of a stationary hot spot. Similar to our earlier observation, we find that the channel carrying scheme outperforms the reservation scheme significantly in the roaming hot spot traffic model. It is also interesting to note that when the hot spot moves quickly, the performance curves are quite flat, because the hot spot effect can indeed be smoothed out effectively. However, when the hot spot moves slowly, the congestion at the hot spot accumulates and increases the handoff blocking probability.

[6]Note that since the hot spot moves, in our simulation, we track the location of the middle cell at the hot spot, and record the associated statistics.
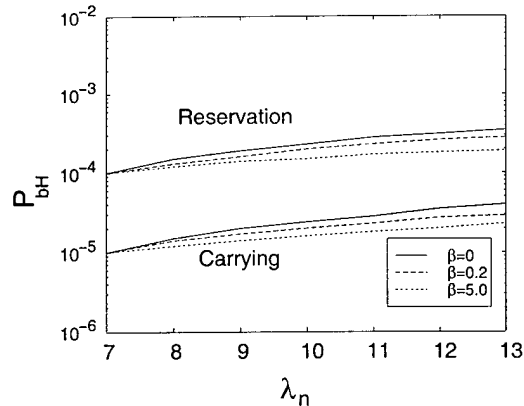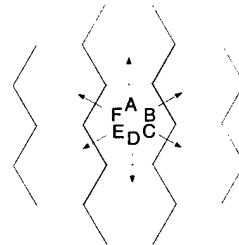
Fig. 16. In a hexagonal cell the movable channels are divided into six different groups, where channels from each group can be carried into a particular (immediate) neighboring cell.

VI. AN EXTENSION TO THE PLANAR (2-D) CASE

The linear (1-D) case described in the previous sections is important in its own right. For example, it is useful for modeling handoff scenarios on highways and rural areas. However, to handle cellular systems in metropolitan environments, we need to extend our carrying scheme to the 2-D case.

A. Channel Assignment

In the planar or 2-D case, the cellular configuration is usually assumed to be hexagonal. This means that the entire area of interest is covered with equal sized hexagonal cells. Here, the *minimum reuse distance* D is the minimum physical distance between the centers of two cells using the same channel set. As in the linear case, the minimum reuse factor R is the minimum number of distinct channel sets necessary to cover the entire area, subject to co-channel interference constraints. In this case R can be directly determined from D by

$$R = (1/3)(D/\rho)^2, \qquad (4)$$

where ρ is the radius of a single cell. The reuse factor R can only take on integer values as generated by the sequence $(i + j)^2 - ij$, with i and j being integers.

To allow for channel carrying in this type of system, we need to assign channels in a similar way to the $(r + 1)$-channel assignment scheme in the linear case. The main
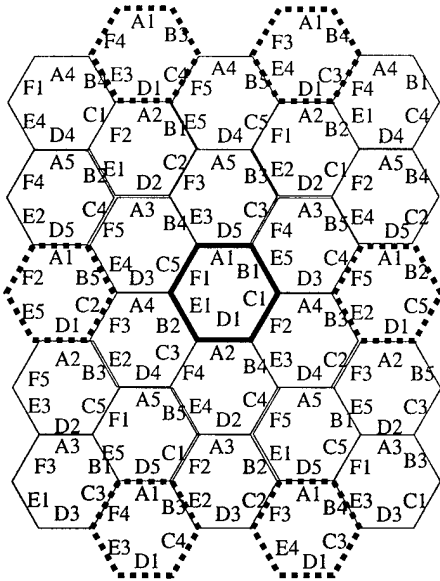
Fig. 17. Channel assigment to allow carrying for $R = 3$.

difference in this case is that users can issue handoff requests to six different neighboring cells, instead of just two. Therefore, we partition our movable channels into six different groups (or sets), where each group of movable channels can be carried into a particular neighboring cell (or "direction"), as shown in Figure 16. For example, channels belonging to channel-set A can be carried to the immediate neighboring cell in the "north" direction, channels belonging to channel-set B can be carried to the immediate neighboring cell in the "north-east" direction, etc. Instead of describing the details of the channel assignment scheme as we did in the 1-D case, we will simply illustrate the basic idea with an example using Figure 17.

In Figure 17, we show how channels can be assigned to allow carrying for the $R = 3$ case. To ensure that the co-channel interference constraints are not violated when channel carrying occurs, we cannot use the minimum reuse factor R, but must instead use a larger reuse factor $\bar{R}$. In this case the minimum reuse factor is $R = 3$, but we need to use an increased reuse factor of $\bar{R} = 5$ to allow for carrying. In Figure 17, channel sets in each cell are denoted by a capital letter followed by a subscript, e.g., A_1. The capital letter denotes the "direction" in which a channel in that set can be carried according to the designation in Figure 16 (e.g., channels belonging to A_1 can be moved in the "north" direction, since channels belonging to set A in Figure 16 can be moved in the north direction). The subscripts are used to distinguish channel sets between cells. Let us now focus on the cell in Figure 17 whose boundary is highlighted with dark solid lines, and call it the *local cell*. Further, let us concentrate on how channels belonging to A_1 in the local cell can be carried. Note that the neighboring cells of the local cell *that use the same channel-set* A_1 have their boundaries highlighted by dark dashed lines. Now, in the local cell, if a channel in A_1 is carried to its immediate neighbor (this can only be its neighbor in the

north direction, as per our scheme), the assignment ensures that there is no extra co-channel interference. In fact, the distance[7] between the immediate neighbor to the north of the local cell (in which a channel from set A_1 has been carried), and the closest neighboring cells that use channel-set A_1 (these are the shaded cells to the north-west and north-east of the local cell) is 6ρ. Also, from Equation (4), $D = 6\rho$ (when $R = 3$), so this distance corresponds to the shortest reuse distance possible without additional co-channel interference. Similarly, by picking other channel sets in the local cell (and their corresponding neighboring cells) one can see that the channel assignment shown will allow carrying without requiring dynamic global coordination or power control techniques.

We next provide some numerical examples to illustrate the performance of the carrying technique for the 2-D case.

B. Numerical Examples

The typical values of the minimum reuse factor when ignoring *shadowing fading* are $R = 7$ and $R = 12$ [1]. However, when shadowing fading is taken into account, the value of the minimum reuse factor R is between 43 and 61 for high transmission quality, and between 13 and 16 for low transmission quality [3]. We next provide numerical examples for $R = 12, 19, 27$. As will be shown in the examples, our performance improvement over reservation increases with larger values of R. The analysis of the carrying scheme in the 2-D case using Markov chain techniques results in a state explosion problem. Therefore, we will provide only simulation results in our examples. For the simulations, we used a 36-cell configuration, with each cell having 6 adjacent neighboring cells. To avoid problems at the boundaries of the 36-cell configuration, the cells on the boundary of one side of the configuration are connected to the cells on the boundary of the other side, as done in [6].

As before, $M' = N/R$ denotes the number of channels in each cell using the reservation scheme. For the carrying scheme this number will be reduced to M. Now, λ_H denotes the handoff rate of each user in a cell to any of the six adjacent neighboring cells, λ_n denotes the new call arrival rate in a cell, $1/\mu_0$ denotes the mean time until a call terminates. As mentioned in the linear case, the hybrid carrying scheme allows us to trade off potential handoff blocking for availability of idle channels for new calls and is the appropriate scheme to be used for comparison. Therefore, in all of our examples we will compare the reservation scheme with the hybrid version of the carrying scheme for the 2-D case.

In Figure 18, we plot the utilization γ (defined by Equation (2)) versus the new call arrival rate in the optimization problem given by Equation (3). The hybrid scheme achieves uniformly higher values of γ under various loads. For $R = 27$, the channel utilization for the channel carrying scheme at high loads is about 18% more than in the reservation scheme. Note, once again, that for low values

---

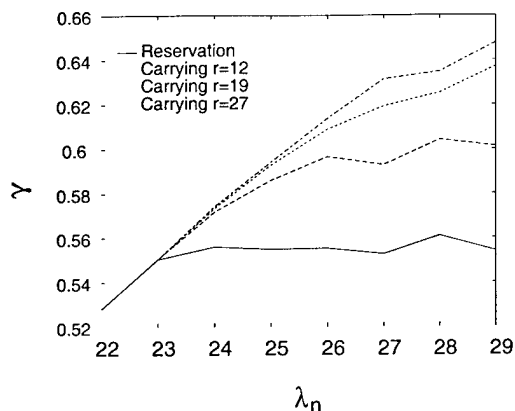[7] Distances are always measured between the centers of two cells.

Fig. 18. Plot of optimal γ versus λ_n for the problem defined in Equation (3). Six directional mobility is assumed. The parameters used in this figure are: $M' = 40$, $\lambda_H = 10$, $\mu_0 = 1$, $H_{max} = 10^{-4}$.

of the traffic load, there is virtually no difference in the performance of the schemes.

Let us now try and relate the performance of our scheme in the linear and 2-D case. If one were to observe the topology of the 2-D case for $R = 27$, it roughly corresponds to $r = 5$ in the linear case. However, the performance gains even for $r = 4$ in the linear case are better than the corresponding gains for $R = 27$ in the 2-D case. The main reason is the need to divide the movable channels into six distinct groups as opposed to only two, in the linear case. This means that the number of movable channels in each direction in the 2-D case is much fewer than in the linear case. However, in many real situations, mobile users move only in four directions instead of six. If such is the case for the system of interest, we may divide up the movable channels into four, rather than six, distinct groups for the carrying scheme, which will help increase the gain in utilization.

VII. Conclusions

We have presented a novel channel carrying scheme to address the problem of handoffs in mobile cellular systems. Our basic idea is to allow mobile users to carry their current channels into new cells under certain conditions. In order to avoid co-channel interference, due to channel movement, we develop the $(r + 1)$-channel assignment scheme for linear cellular networks. This affords us channel mobility at the expense of some capacity. An attractive feature of the channel carrying scheme is that it does not require complex power control techniques or global channel coordination, which simplifies its implementation.

We develop a two-cell model to analyze our channel carrying scheme and the traditional channel reservation technique for the linear cellular system. We find that for the linear case, even when considering the minimum possible reuse factor $r = 2$, the channel carrying scheme outperforms the reservation technique. We then propose a refinement to the channel carrying scheme, called the hybrid scheme, which provides a useful design parameter d_h that

allows us to optimize various parameters of interest. We again find that our scheme uniformly and significantly improves the system performance, in some cases resulting in over 50% better network utilization than the channel reservation scheme in the linear case. We also illustrate how the channel carrying scheme can be extended to the 2-D case. We then provide examples comparing it with the reservation scheme for the classical hexagonal cell configuration. We show that our scheme outperforms the channel reservation scheme over a wide range of parameters.

In most cases, we have assumed Poisson new call arrivals that are uncorrelated from cell to cell, and symmetrical and memoryless handoff directions. However, traffic in a real cellular system could be quite different. To investigate the effect of uncorrelated and nonuniform traffic, we developed a simple hot spot model and compared the channel carrying scheme with the reservation scheme under this model. We find that the channel carrying scheme still outperforms the reservation scheme in this case. For future work it would be interesting to model user mobility (roaming patterns) based on observations of actual systems. In this case, the performance improvement of the channel carrying scheme could be quite different from that reported in this paper. If the traffic were to exhibit strong deterministic correlation between neighboring cells, it may be more difficult to take advantage of channel carrying, and more complex dynamic channel allocation schemes (such as the maximal packing scheme [9]) may be warranted. In these cases it would be interesting to analytically quantify the trade-offs between complexity and performance going from the carrying scheme to the more dynamic and complicated channel allocation schemes.

References

[1] M.-L. Cheng and J.-I. Chuang, "Performance evaluation of distributed measurement-based dynamic channel assignment in local wireless communications," *IEEE Journal On Selected Areas In Communications*, vol. 14, pp. 698–710, May 1996.

[2] D. Cox and D. Reudink, "Increasing channel occupancy in large-scale mobile radio sysyems: dynamic channel reassignment," *IEEE Transactions on Vehicle Technology*, vol. 22, pp. 218–222, 1973.

[3] A. Şafak, "Optimal channel reuse in cellular radio systems with multiple correlated log-normal interferers," *IEEE Transactions on Vehicle Technology*, vol. 43, no. 2, pp. 304–312, 1994.

[4] D. Hong and S. Rappaport, "Traffic model and performance analysis for cellular mobile radio telephone systems with prioritized and non-prioritized handoff procedures," *IEEE Transactions on Vehicle Technology*, vol. 35, pp. 77–92, 1986.

[5] N. Jain, *Cell design in a cellular system using guard channels, call queuing and channel borrowing*. Virginia Polytechnic Institute and State University, Blacksburg, Virginia: Ph.D. dissertation, 1993.

[6] H. Jiang and S. Rappaport, "CBWL: A new channel assignment and sharing method for cellular communication systems," *IEEE Transactions on Vehicle Technology*, vol. 43, pp. 313–322, May 1994.

[7] J. Li, N. B. Shroff, and E. K. P. Chong, "Channel Carrying: A Novel Handoff Scheme for Mobile Cellular Networks," *Technical Report, School of Electrical and Computer Engineering, Purdue University, West Lafayette, Indiana*, 1997.

[8] S. Oh and D. Tcha, "Prioritized channel assignment in a cellular radio networks," *IEEE Transactions On Communications*, vol. 40, pp. 1259–1269, 1992.

[9] K. OKada and F. Kubota, "On dynamic channel assignment

in cellular mobile radio systems," in *Proc.IEEE Int'l.Symp. on Circuits and Systems*, pp. 938–941, 1991.

[10] C. Purzynski and S. Rappaport, "Multiple call handoff problem with queued handoffs and mixed platform types," *IEE Proceedings.-Communications*, vol. 142, pp. 31–39, 1995.

[11] R. Ramjee, R. Nagarajan, and D. Towsley, "On optimal call admission control in cellular networks," in *Proc. IEEE INFOCOM*, pp. 43–50, 1996.

[12] M. Sidi and D. Starobinski, "New call blocking versus handoff blocking in cellular networks," in *Proc. IEEE INFOCOM*, pp. 35–42, 1996.

[13] R. Singh, S. Elnoubi, and C. Gupta, "A new frequency channel assignment algorithm in high capacity mobile communications systems," *IEEE Transactions on Vehicle Technology*, vol. 31, 1982.

[14] S. Tekinay and B. Jabbari, "Handover and channel assignment in mobile cellular networks," *IEEE Communications Magazine*, pp. 42–46, November 1991.

Emmons Terman Award in 1998. He is a Senior Member of IEEE, and is chairman of the IEEE Control Systems Society Technical Committee on Control Theory and the Working Group on Discrete Event Systems. He has served on the editorial board of the IEEE Transactions on Automatic Control, and on various conference committees. His current interests are in communication networks and optimization methods. He spent a sabbatical at Bell Laboratories, Holmdel, in the fall of 1998. He coauthored a recent book, An Introduction to Optimization, Wiley-Interscience, 1996.

Junyi Li (S'97, M'98) received the B.S. degree and M.S.E.E. degrees from Shanghai Jiao Tong University, in China. His M.S. thesis "Intelligent Predictive Control" was awarded the prize *1991 Best Science and Technology Papers of Shanghai Young Scholars Under the Age of 35*. From 1991 to 1994, he was an assistant professor in the Department of Automatic Control at Shanghai Jiao Tong University. In 1998, he received a PhD degree in Electrical and Computer Engineering from Purdue University, and has been working in Digital Communications Research at Bell Labs, Lucent Technologies, Holmdel, NJ since Feb. 1998.

Ness B. Shroff (S'90, M'94) received the B.S. degree in from the University of Southern California, the M.S.E. degree from the University of Pennsylvania, and the M.Phil and Ph.D. degrees from Columbia University. He is currently an Assistant Professor in the School of Electrical and Computer Engineering at Purdue University. During his doctoral study Dr. Shroff worked at AT&T Bell Labs (1991) and Bell Communications Research (1992), on problems involving fault management in telephone networks. His current research interests are in High Speed Broadband and Wireless Communication networks. He is especially interested in studying issues related to Performance Modeling and Analysis, Routing, Network Management, Scheduling, and Control in such networks. Dr. Shroff has received research and equipment grants to conduct fundamental work in broadband and wireless networks, and source coding from the National Science Foundation, AT&T, Hewlett Packard, Intel, LG Electronics, and the Purdue Research Foundation. He received the NSF CAREER award from the National Science Foundation in 1996. Dr. Shroff has served on the technical program committees of various conferences and on NSF review panels. He is the Program Chair for the 14th Annual IEEE Computer Communications Workshop (CCW) to be held in October 1999.

Edwin K.P. Chong (S'86, M'91, SM'96) joined the School of Electrical and Computer Engineering at Purdue University in 1991, where he is currently an Associate Professor. He received the B.E.(Hons.) degree with First Class Honors from the University of Adelaide, South Australia, in 1987; and the M.A. and Ph.D. degrees in 1989 and 1991, respectively, both from Princeton University, where he held an IBM Fellowship. He received the NSF CAREER Award in 1995 and the ASEE Frederick

Channel Carrying: A Novel Handoff Scheme
for Mobile Cellular Networks *

Junyi Li   Ness B. Shroff[†]   Edwin K.P. Chong

School of Electrical and Computer Engineering
Purdue University, West Lafayette, IN 47907, U.S.A.
E-mail: {junyi, shroff, echong}@ecn.purdue.edu

Abstract

We present a new scheme that addresses the call handoff problem in mobile cellular networks. Efficiently solving the handoff problem is important for guaranteeing Quality of Service (QoS) to already admitted calls in the network. Our scheme is based on a new concept called *channel carrying*: when a mobile user moves from one cell to another, *under certain mobility conditions*, the user is allowed to *carry* its current channel. We propose a new channel assignment scheme to ensure that this movement of channels will not lead to any extra co-channel interference or channel locking. *In our scheme, the mobility of channels relies entirely on localized information, and no global coordination is required.* Therefore, the scheme is simple and easy to implement. We further develop a hybrid channel carrying scheme that allows us to maximize performance under various constraints.

We provide numerical results comparing our scheme with the traditional channel reservation types of techniques. We find that our scheme outperforms the reservation scheme over a broad range of traffic parameters.

1 Introduction

The use of cellular systems is a popular means for enhancing the capacity of wireless communication networks. In such a system, the service area is divided into cells, and *channels* are reused among those cells. A channel can be thought of as a generic network resource; for example, a frequency band in FDMA, a time-slot in TDMA, or a specific spread spectrum code in CDMA. This definition is consistent with that in [4]. Channels that are used in one cell cannot be used in other cells that are closer than the *minimum reuse distance*. Handoff occurs when a mobile subscriber moves from one cell to another. A handoff call may be blocked if there is no free channel in the new cell. However, studies have shown that blocking a handoff

call is less desirable than blocking a new call. Therefore, specific schemes have been developed to prioritize handoff calls. Two prioritization schemes have been commonly studied in the literature [1]. They are:

(i) *Channel reservation schemes*: In this type of schemes, a number of channels are reserved solely for the use of handoff, allowing both handoff and new calls to compete for the remaining channels [5]. Specifically, in each cell a threshold is set, and if the number of channels currently used in the cell is below that threshold, both new and handoff calls are accepted. However, if the number of channels used exceeds this threshold, an incoming new call is blocked and only handoff calls are admitted.

(ii) *Queueing schemes*: In this type of schemes handoff requests are queued, and may be later admitted into the network in case channels free up [2].

The above two schemes can also be integrated together to improve the handoff blocking probability and the overall channel utilization. The scheme we propose in this paper is also readily integrated with the queueing schemes. Therefore, we compare our scheme only with the reservation scheme.

Our method for treating the handoff problem stems from the following simple idea. A user requesting a handoff always occupies a channel in its current cell. *Therefore, if that channel could be carried into the new cell, the handoff request would not be blocked.* From a practical point of view this is not difficult to achieve. For example, in an FDMA based system, suppose a user requesting handoff to some cell A communicates over a frequency band x that cell A is not allowed to use. Now, if normal handoff is not possible the user (or its current base-station) could signal cell A giving it permission to communicate over channel x with it. In a similar way, channels can be carried in CDMA and TDMA systems.

However, when a channel is allowed to move into another cell, it shortens the reuse distance and may violate the minimum reuse distance requirement [1, 3]. To solve this problem, we propose a new channel assignment method that allows channels to be "carried" into a neighboring cell. Furthermore, with an *a priori* agreement on channel movement, channel coordination can be achieved locally. This helps to significantly
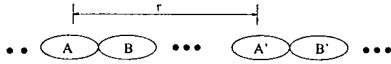
Figure 1: Linear Cellular System
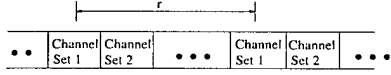
Figure 2: r−Channel Assignment

Figure 3: $(r + 1)$-Channel Assignment

Figure 4: Channel Division in the $(r + 1)$-Channel Assignment Scheme

simplify the implementation. The new handoff scheme proposed in this paper is called *channel carrying*.

We next describe how the channels are assigned for the channel carrying scheme, and then present our basic handoff algorithm.

2 Channel Assignment

For simplicity, we describe our channel carrying scheme using a *linear cellular system* model. In this system, cells (or base stations) are arranged in a linear configuration, as shown in Figure 1. Let N denote the total number of distinct channels that are available in the cellular system. Two cells can use the same set of channels as long as they are at least r cells apart. This distance r is called the *minimum reuse distance* or *reuse factor*. In the conventional fixed channel assignment scheme, the channels are assigned such that the same channels are reused exactly r cells apart, as shown in Figure 2. Therefore, the total number of distinct channels available to each cell is N/r. We refer to this channel assignment as *r-channel assignment*.

In our channel carrying scheme, we alleviate blocking due to handoff by allowing calls to "carry" channels from one cell to another. However, using r-channel assignment, a call that carries a channel to an adjacent cell may violate the minimum reuse distance requirement. For example, in Figure 1, cells A and A' use the same set of channels. Suppose a call in cell A uses a channel y, and carries it to cell B. Now, if a user arrives in cell A' and uses channel y, then the two y channels are only a distance of $r - 1$ cells apart, thus violating the minimum reuse distance requirement. One way to overcome this problem is to have global coordination algorithms that use *channel locking* [3] to ensure that such situations do not occur. However, such schemes are computationally expensive and therefore difficult to implement [3]. Moreover, channel locking also degrades efficiency.

To ensure that the minimum reuse distance requirement is not violated, we use an $(r + 1)$-*channel assignment* scheme. In other words, the same channels are reused exactly $r + 1$ cells apart, as shown in Figure 3. In this case, the total number of distinct channels available to each cell is $N/(r + 1)$. To ensure that the same channels do not get closer than r cells apart (due to channel carrying), we restrict channel movement in the following way. Each channel is allowed to be carried in only one direction, left or right. This restriction thus divides the channels assigned to each

cell into two types. Further, as shown in Figure 4, exactly the same division is used in cells that are a distance $r + 1$ apart. Using this $(r + 1)$-channel assignment scheme, and the channel carrying algorithm described in the next section, we ensure that there is no co-channel interference due to channel movement, while avoiding the need for global coordination.

3 Handoff Algorithm
3.1 Algorithm Description

To describe our handoff algorithm, we first focus our attention on a particular (arbitrary) cell, which we call the *local cell*. The adjacent cells to the left and right of the local cell are called *foreign cells*. The channels that have been assigned to the local cell are called *local channels*, and are divided into two types: *local-left* (LL) and *local-right* (LR) channels as shown in Figure 4. An LL (LR) channel is one that can be carried to the left (right) cell during handoff. In other words, an LL (LR) channel can be used by a call in the local cell as well as in the foreign cell to the left (right). A channel from a foreign cell that is being used in the local cell is called a *foreign channel*. Foreign channels from the left cell are called *foreign-left* (FL) channels and foreign channels from the right cell are called *foreign-right* (FR) channels.

Our algorithm can be described in five main parts, corresponding to five different possible scenarios: *arrival of a new call, handoff from a foreign cell, handoff to a foreign cell, termination of a call,* and when *a local channel becomes idle.*

3.1.1 Arrival of a new call

When a new call arrives, we check if there are any idle (unused) local channels. If there are, the new call is accepted and assigned the idle channel; otherwise, the call is rejected (blocked).

3.1.2 Handoff request from a foreign cell

When a handoff call request is received from a foreign (left or right) cell, we check if there are any idle lo-

cal channels available. If there are, the handoff call is accepted and assigned the idle channel; otherwise, the foreign cell is notified that there are no idle local channels.

3.1.3 Handoff to a foreign cell

For simplicity, suppose a user U in the local cell wants to move to the *left* foreign cell. The handoff operation is attempted according to the following order:

1. If user U is currently using a foreign-left (FL) channel, then it simply carries it back to the left cell; otherwise, step 2 is initiated.

2. We check if there is an FL channel being used by some other user V in the local cell. If so, user U exchanges its channel with user V and then executes step 1 above; if not, we perform step 3.

3. We send a handoff request to the left foreign cell. The foreign cell then executes the procedure in Section 3.1.2. If the handoff is accepted, user U moves to the left cell and releases its own channel; if not, step 4 is initiated.

4. If user U is currently using a local-left (LL) channel, then it carries it to the left cell; otherwise, step 5 is initiated.

5. We check if there is an idle LL channel currently in the local cell. If so, U releases its own channel, grabs the idle LL channel, and carries it to the left cell; otherwise step 6 is initiated.

6. We check if there is an LL channel being used by some other user W in the local cell. If so, user U exchanges its channel with user W, and executes step 4 above.

7. If all the above conditions do not hold, then the handoff cannot be accomplished. Normally, this would result in the handoff call being blocked.

A similar procedure would be applied if a user in the local cell wanted to move to the right foreign cell.

3.1.4 Termination of a call

When a call U is terminated (either due to the normal end of the call, or due to handoff blocking), we first check if the channel being used by U is a foreign channel. If so, we release the foreign channel and return it to its originally assigned cell. Otherwise, U is using a local channel—the call is then terminated and the channel becomes idle.

3.1.5 Local channel becomes idle

This scenario arises in the following situations:

1. Termination of a call in the local cell.

2. Handoff from the local cell to a foreign cell without carrying.

3. Return of an idle local channel from a foreign cell (when a local channel is released in the foreign cell and returned to the local cell).

When a local channel becomes newly idle, we check if there is a user V using a foreign channel in the local cell. If so, user V is assigned the newly idle local channel, and the foreign channel is released and returned to its originally assigned cell.

3.2 Salient Features of the Algorithm

The following are some of the significant features of our algorithm. Again, for simplicity, we focus only on handoff from the local cell to the *left* foreign cell.

(i) An important feature of our algorithm is that no global coordination is necessary, thus facilitating implementation. At the same time, the algorithm ensures that there is no co-channel interference due to channel movement.

(ii) In our algorithm, handoff calls have access to a larger portion of the system capacity than new incoming calls. To see this, note that a new call is blocked if and only if there is no idle (local) channel in the local cell. On the other hand, a handoff request to the (left) foreign cell is *blocked if and only if all the left-local (LL) channels are being used in the foreign cell.* This occurrence is relatively rare because it requires that all three of the following conditions are simultaneously true:

(a) All the FL channels are being used by users in the left foreign cell.

(b) All the channels in the left foreign cell are being used.

(c) All the LL channels have been previously carried to the left foreign cell.

It is therefore apparent that in our channel carrying scheme, handoff call requests are favored over new call requests. Meanwhile, we do not require channels to be reserved *a priori* for handoff calls. This helps increase the efficiency of our scheme compared to reservation schemes, as demonstrated in Sections 4.3 and 5.2.

(iii) In our algorithm, we prefer to use local channels whenever possible. We refer to this policy as a *return-as-soon-as-possible* policy. For example, whenever a channel becomes idle, we always return the foreign channel (if any) instead of keeping that idle channel waiting for a potential call in the local cell. The policy serves to protect potential handoff calls, because the accumulation of foreign channels may block further handoff requests from the foreign cell.

4 Performance Analysis

4.1 Channel Carrying Scheme

In this section we develop a Markov chain model to analyze the performance of our handoff algorithm. The QoS measures that we are interested in are:

- P_{bN}, the steady state probability of blocking a new call; and
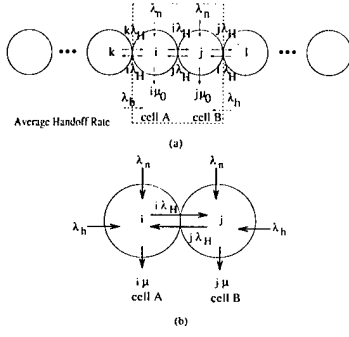
Figure 5: (a) Linear Cellular system with various traffic parameters. (b) Two-Cell model with the corresponding traffic parameters.

- P_{bH}, the steady state probability of blocking a handoff call.

The system that we are interested in modeling is the linear cellular system shown in Figure 5(a). The traffic is assumed to be symmetrically distributed over all the cells, for example, the new call arrival rate at every cell is λ_n. The handoff rates between cells is assumed to be directly proportional to the number of users in that cell, so if a cell has i users the handoff rate to its neighboring cell is $i\lambda_H$, as shown in Figure 5(a). Analysis of this entire system is computationally infeasible. Therefore, the performance analysis of call handoff schemes in wireless systems is typically done by focusing on a single cell which results in a one dimensional Markov chain. However, the one-cell model does not accurately capture the essence of our algorithm. For example, suppose that a user in the local cell wants to move to the left foreign cell. Whether or not it carries a channel during handoff depends not only on the availability of FL and LL channels in the local cell but also on whether there is an idle channel in the left foreign cell. Hence, the availability of channels in adjacent cells is coupled.

To alleviate difficulties with a one-cell model we consider a two-cell model, as shown in Figure 5(b). We assume that in each cell A and B, new call requests arrive according to Poisson processes with rate λ_n. The time it takes for each call in a cell to request a handoff to the other cell is assumed to be exponentially distributed with mean $1/\lambda_H$. Call handoffs arrive from outside the two-cell subsystem according to a Poisson process with rate λ_h. The time until a call terminates is assumed to be exponentially distributed with mean $1/\mu_0$. Therefore the time until a call leaves the two-cell system (either due to handoff or call termination) is exponentially distributed with mean $1/\mu = 1/(\mu_0 + \lambda_H)$. Now, assuming that all of the above mentioned processes (new arrival, call handoff request, and call termination) are mutually independent, we can analyze our two-cell system using a Markov Chain.

Recall that the total number of local channels in each cell is $M = N/(r + 1)$. To further simplify the
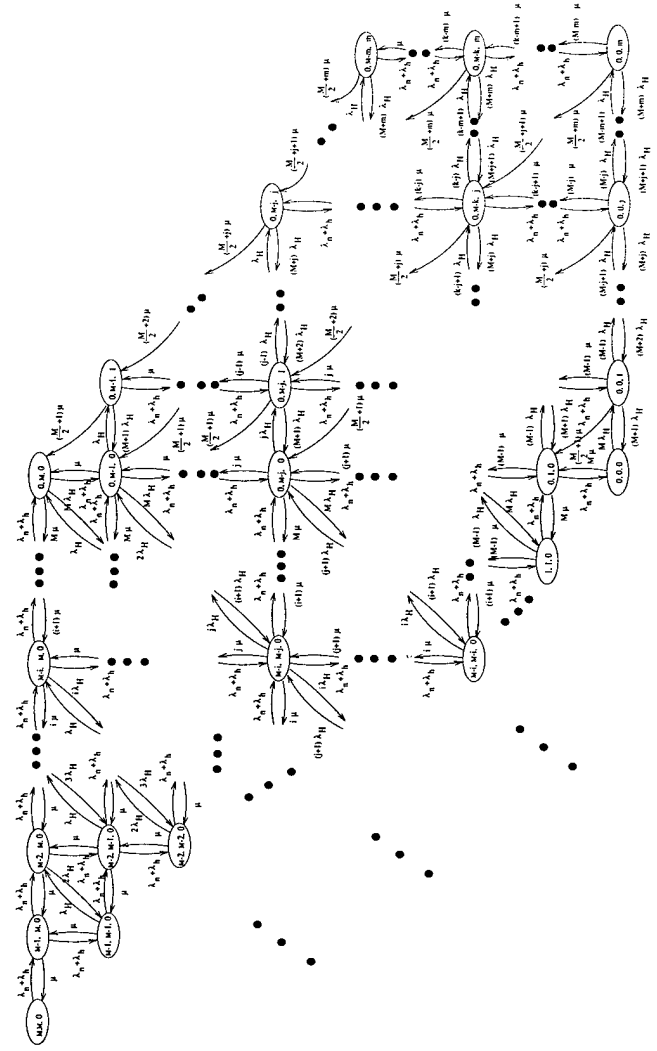
Figure 6: Markov Chain for the Channel Carrying Scheme using the Two-Cell model. Note that $m = M/2$, and $M = N/(r + 1)$.

model, we assume that the total number of local channels, M, is divided into an equal number, $m = M/2$, of local left (LL) and local right (LR) channels.

Our Markov chain model is shown in Figure 6. To describe the model, let $N_A \in \{0, \ldots, M\}$ and $N_B \in \{0, \ldots, M\}$ represent the number of idle local channels in cell A and cell B, respectively. Next, let $N_{B \to A} \in \{-\frac{M}{2}, \ldots, 0, \ldots, \frac{M}{2}\}$ represent the following. If $N_{B \to A} \geq 0$, it denotes the number of foreign channels from cell B that are being used in cell A. On the other hand, if $N_{B \to A} \leq 0$, it denotes the number of foreign channels from cell A that are being used in cell B. Hence, $N_{B \to A}(t)$ can take values from $-\frac{M}{2}$ to $\frac{M}{2}$. The triple $(N_A, N_B, N_{B \to A})$ represents the state of the Markov chain. Although there are three components in each state, the state transi-

tion diagram of the Markov chain can be represented in a planar fashion. To see this, recall that a foreign channel will move into a cell only when there is no idle local channel in that cell. Also, whenever service is terminated, the foreign channel within the local cell will be returned immediately. Thus, if we neglect the additional time it would take to return or carry a channel, it follows that $N_{B \to A} > 0 \Rightarrow N_A = 0$, and $N_{B \to A} < 0 \Rightarrow N_B = 0$. These equations help restrict one degree of freedom thereby resulting in the planar or two-dimensional Markov chain shown in Figure 6.

Note that, because of the symmetric nature of the Markov chain, i.e., $P\{N_A = i, N_B = j, N_{B \to A} = k\} = P\{N_A = j, N_B = i, N_{B \to A} = -k\}$, only half of the Markov chain is shown in the figure. Let $P_{i,j,k} = P\{N_A = i, N_B = j, N_{B \to A} = k\}$ denote the steady state probability of the state $\{N_A = i, N_B = j, N_{B \to A} = k\}$. We obtain these probabilities by exploiting the above mentioned symmetry and by applying standard numerical Markov chain techniques.

Now observe Figures 5(a) and 5(b) again. In Figure 5(b) we have focussed only on cells A and B of Figure 5(a). Let the cells to the right of cell B and to the left of cell A be called *external cells*. The handoff rate λ_h in the two-cell model of Figure 5(a) is actually the average of the state dependent handoff rate from their neighboring external cells. Averaging over all the states, λ_h is given by

$$\lambda_h = \sum_{i=0}^{M}(M-i)\lambda_H \sum_{j=0}^{M}\sum_{k=-m}^{m} P_{i,j,k}, \qquad (1)$$

where $m = M/2$. Since λ_h depends on $P_{i,j,k}$, we iteratively solve the Markov chain. Having determined $P_{i,j,k}$, we calculate P_{bN}, and P_{bH} as follows:

$$P_{bN} = \sum_{k=0}^{m}\sum_{j=0}^{M-k} P_{0,j,k}; \quad P_{bH} = \sum_{j=0}^{M-m-1} P_{0,j,m}, \qquad (2)$$

4.2 Channel Reservation Scheme

In this section we develop a Markov chain model, shown in Figure 7, to analyze the system performance using the traditional channel reservation scheme. As in the channel carrying scheme, we focus on the two-cell model shown in Figure 5. The parameters λ_h, λ_n, λ_H, and μ are defined as before. Since no channel movement is allowed, the pair (N_A, N_B), $N_A \in \{0, \ldots, M'\}$, $N_B \in \{0, \ldots, M'\}$, suffices to characterize the state of the two-cell system. Here, $M' = N/r$ is the total number of distinct channels available to each cell, and N_A (N_B) is the total number of idle channels in cell A (cell B). The resulting Markov chain is shown in Figure 7. Again, because of the symmetric nature of the Markov chain, i.e., $P\{N_A = i, N_B = j\} = P\{N_A = j, N_B = i\}$, only half of the Markov chain is shown in Figure 7. Let $P_{ij} \stackrel{\Delta}{=} P\{N_A = i, N_B = j\}$ denote the steady state probability of the state $\{N_A = i, N_B = j\}$. Then, as in the channel carrying scheme, λ_h, the average external handoff arrival rate, is given by:
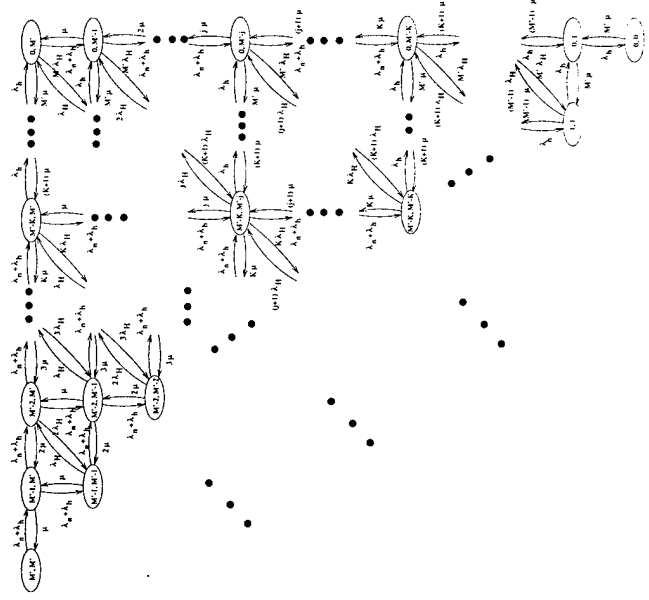
Figure 7: Markov Chain for the Channel Reservation Scheme using the Two-Cell model. Note: $M' = N/r$.

$$\lambda_h = \sum_{i=0}^{M'}(M'-i)\lambda_H \sum_{j=0}^{M'} P_{i,j}. \qquad (3)$$

Since λ_h depends on $P_{i,j}$, we iteratively solve the Markov chain in Figure 7. Now P_{bN} and P_{bH} are given by

$$P_{bN} = \sum_{i=0}^{M'-K}\sum_{j=0}^{M'} P_{i,j}; \quad P_{bH} = \sum_{j=0}^{M'} P_{0,j} \qquad (4)$$

It is instructive to compare the state transition diagrams in Figures 6 and 7. The number of local channels in each cell is $M' = N/r$ in the reservation scheme (Figure 6) instead of $M = N/(r+1)$ in the carrying scheme (Figure 7). The difference is $d = M' - M = \frac{N}{r(r+1)}$, which is the cost we pay for channel mobility. Clearly, when the reuse factor r is large, this difference is marginal. Also, because of channel reservation, new calls have to be blocked when the number of occupied local channels exceeds a threshold K in Figure 7. Then, the arrival rate is reduced from $\lambda_n + \lambda_h$ to λ_h, which is a disadvantage of the reservation scheme compared to the channel carrying scheme.

4.3 Numerical Results

In this section, we provide numerical results to compare the performance of the channel carrying scheme and the reservation scheme.

We use our Markov chain model for computing the performance measures P_{bN} and P_{bH} and also simulate the system under the carrying and reservation schemes. Our simulation consists of a 120 cell linear
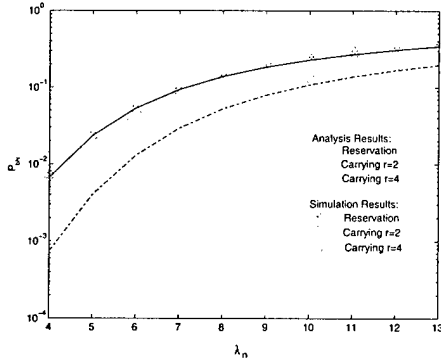
Figure 8: Plot of P_{bN} versus λ_n.
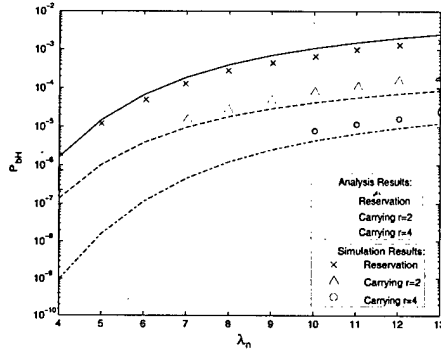
Figure 9: Plot of P_{bH} versus λ_n.

cellular system, such as the one shown in Figure 5(a). Since we are interested in the performance of a typical cell, the statistics are averaged over all cells. Throughout the paper, we find that the simulation and analytical results match quite well, which indicates that the two-cell model works well in characterizing the behavior of the algorithm in a linear cellular system.

In Figure 8 we plot P_{bN}, and in Figure 9, we plot P_{bH} for both the channel carrying and the reservation scheme under different traffic loads λ_n, ranging from 4 calls to 13 calls per unit time. The call handoff rate is $\lambda_H = 1$ call per unit time, and the call termination rate is $\mu_0 = 1$ call per unit time.

For the channel carrying case, two values for the reuse distance are considered: $r = 2$, the minimum possible reuse distance, and $r = 4$, a more typical value for the reuse distance. Further, in both figures, $M' = N/r = 15$; hence, $N = 30$ when $r = 2$, and $N = 60$ when $r = 4$.

Note, that in the channel reservation scheme, for a given arrival rate, we can vary the threshold K to give us different values of P_{bN} and P_{bH}. We find that if we choose $K = M = N/(r + 1)$, then the values of P_{bN} for the reservation scheme are close to those for the carrying scheme. The reason for this is that if the number of occupied local channels in a cell reaches K (or M), any new call in the reservation (or carrying, respectively) scheme is now blocked. For $r = 2$, we

choose $K = M = 10$, and we can observe in Figure 8 that the new call blocking probability (P_{bN}) curves for the reservation and carrying schemes are in fact very close. However, for the same parameters, the call handoff blocking probability (P_{bH}) as shown in Figure 9 is at least about one order of magnitude lower in the carrying scheme than in the reservation scheme. When the value of the reuse distance is increased to $r = 4$, and we set $K = 10$, the carrying scheme significantly outperforms the reservation scheme in terms of both P_{bN} and P_{bH}. This result can be observed in Figure 8, where the P_{bN} curve in the carrying case is up to one order of magnitude lower than in the reservation scheme, and in Figure 9, where the P_{bH} curve in the carrying scheme is up to three orders of magnitude lower than in the reservation scheme.

We next develop a hybrid channel carrying scheme which attempts to maximize performance, under various constraints, by allowing us to vary the number of channels that can be carried.

5 Hybrid Channel Carrying Scheme

5.1 Description

In the numerical examples of the previous section, we observe that the channel carrying scheme results in a large difference between the values of P_{bH} and P_{bN}. In particular, when the load is high, the value of P_{bN} is much higher than that of P_{bH}. For example, for $\lambda_n = 13$ and $r = 4$, the value of P_{bH} is only about 10^{-5} while that of P_{bN} is greater than 10^{-1}. This observation suggests that our channel carrying scheme excessively favors handoff requests over new calls. We next present a hybrid scheme that allows trading off potential handoff blocking for availability of idle channels for new calls.

Recall that in the $(r + 1)$-channel assignment scheme, the number of channels assigned to each cell is $M = N/(r + 1)$, and every channel can be carried either to the left or to the right. On the other hand, in the r-channel assignment scheme, the number of channels assigned to each cell is N/r, but none of the channels can be carried to foreign cells. In our hybrid scheme, we divide the total number of channels N into two distinct groups of size N_1 and N_2, such that $N = N_1 + N_2$. The N_1 channels are assigned according to the r-channel assignment scheme, and cannot be carried to foreign channels. The N_2 channels, however, are assigned according to the $(r+1)$-channel assignment scheme, and can be carried either to the left or to the right, just as in the previous channel carrying scheme. Therefore, in the hybrid scheme, each cell is assigned

$$M_{hybrid} = \frac{N_1}{r} + \frac{N_2}{r + 1} \qquad (5)$$

channels, where the two terms in the sum corresponds to the two groups of channels. As before, the $N_2/(r + 1)$ channels of the second type are themselves divided into two types: left and right.

The hybrid scheme above defines a family of channel assignments that encompasses both the pure r-

and $(r + 1)$-channel assignment schemes. Specifically, $N_1 = 0$ corresponds to the $(r + 1)$-channel assignment scheme, while $N_2 = 0$ leads to the r-channel assignment scheme. The N_2 channels allow us to trade off the ability to carry (and hence avoid handoff blocking) with a reduced number of channels available to each cell. In particular, the number of channels that we sacrifice in using $(r+1)$-channel assignment instead of r-channels assignment is

$$d_{hybrid} = \frac{N_2}{r} - \frac{N_2}{r+1} = \frac{1}{r}\left(\frac{N_2}{r+1}\right). \quad (6)$$

Thus, d_{hybrid} serves as a design parameter that we can adjust to balance the requirements of the performance measures P_{bN} and P_{bH}, analogous to the threshold parameter K in the channel reservation scheme. The larger the value of d_{hybrid} in the hybrid scheme, the more we favor handoff calls because there are more movable channels. Hence, as d_{hybrid} increases, we expect P_{bH} to decrease and P_{bN} to increase. A similar observation holds for the design parameter K in the reservation scheme. Also note that, as in the original channel carrying case, for a fixed number of channels N_2 that are allowed to move, the price we pay for the $(r+1)$-channel assignment scheme (in terms of d_{hybrid}) decreases with increasing r.

5.2 Numerical Results

For the purpose of performance evaluation, we adopt the two-cell model and make the same assumptions here as we did in Section 4.3. The resulting Markov chain has exactly the same structure as in Figure 6, the only difference being that we substitute $m_{hybrid} = \frac{N_2}{2(r+1)}$ in place of m. We can then solve for the steady state probabilities in the Markov chains for the hybrid and reservation schemes, and compute P_{bH} and P_{bN} as before. Also, as in Section 4.3, for our simulations we use a 120-cell linear cellular system.

We now provide plots of P_{bN} under varying load conditions for the hybrid and reservation schemes. The performance measures depend on the parameters d_{hybrid} and K in the hybrid and reservation schemes, respectively. To meaningfully compare our hybrid scheme with the reservation scheme, we determine the optimal values of P_{bN} for the two schemes, given a constraint on P_{bH}. Therefore, in the hybrid scheme, to appropriately choose d_{hybrid}, we consider the following optimization problem:

$$\underset{d_{hybrid}}{\text{minimize}} \quad P_{bN}, \quad \text{subject to} \quad P_{bH} \leq H_{max}, \quad (7)$$

where H_{max} denotes a prespecified maximum level for P_{bH}. A similar optimization problem can be defined for the reservation scheme, where the decision variable d_{hybrid} above is replaced with the threshold parameter K. For a fair comparison of our hybrid scheme with the reservation scheme, we calculate the optimal values of P_{bN} for the two schemes, given the same H_{max}. The optimal values can be computed numerically using the Markov chains in Figures 6 and 7. Figure 10
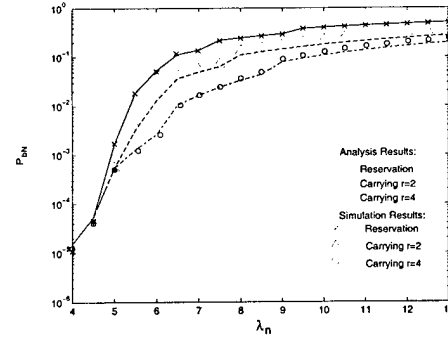
Figure 10: Plot of optimal P_{bN} versus λ_n for the problem defined in Equation (7).
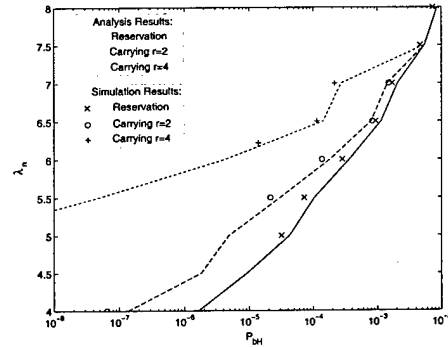
Figure 11: Plot of optimal λ_n versus P_{bH} for the problem defined in Equation (8).

shows plots of the optimal values of P_{bN} for the reservation and hybrid schemes under varying λ_n. For this figure we have used the following parameters: $\lambda_H = 1$, $\mu_0 = 1$, $M' = 15$. Therefore, $N = 30$ for $r = 2$, and $N = 60$ for $r = 4$. For the constraint on P_{bH}, we used $H_{max} = 10^{-4}$, a typically desirable constraint for the handoff blocking probability. We can see that the hybrid scheme achieves uniformly lower values of P_{bN} than the reservation scheme. As expected, increasing the value of r further decreases P_{bN} in the channel carrying case.

Next, in Figure 11, we plot a graph in which we compare the maximum new call arrival rate λ_n that can be admitted by the carrying scheme and the reservation scheme for various handoff blocking probabilities P_{bH}. More precisely we define the following optimization problem for the channel carrying scheme:

$$\underset{d_{hybrid}}{\text{maximize}} \quad \lambda_n,$$

$$\text{subject to} \quad P_{bN} \leq N_{max}, \quad P_{bH} = H. \quad (8)$$

Here the constraint H for P_{bH} is varied between 10^{-8} and 10^{-2} and the corresponding maximum value of λ_n is obtained. A similar optimization problem is defined for the reservation scheme by replacing d_{hybrid} by K. In Figure 11 we plot the optimal values of λ_n versus
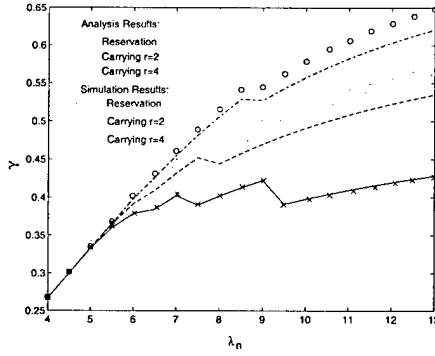
Figure 12: Plot of optimal γ versus λ_n for the problem defined in Equation (9).

P_{bH} for the reservation scheme and the channel carrying scheme with $r = 2$ and $r = 4$. For this figure we use the following parameters: $\lambda_H = 1$, $\mu_0 = 1$, $M' = 15$, $N_{max} = 10^{-2}$. From Figure 11 one can observe that the hybrid carrying scheme allows a higher new call rate than the reservation scheme over all values of P_{bH}. For large values of P_{bH} all the schemes perform essentially the same since it corresponds to the case when no carrying is necessary in the hybrid case ($N_2 = 0$) and no reservation is necessary ($K = N/r$) in the reservation scheme. However, for a typical value of $P_{bH} = 10^{-4}$, the hybrid scheme with $r = 4$ can admit approximately 20% more calls into the network than the reservation scheme. As is shown in the figure, for lower handoff probability constraints, this difference is even larger.

From a network provider's point of view, a more useful parameter of interest is the *normalized channel utilization*, γ , defined as

$$\gamma \triangleq \frac{\text{average number of users in one cell}}{\text{total number of available channels in one cell}},$$

where the total number of available channels in one cell is $M' = N/r$. The parameter γ is directly related to the revenue of a cellular network because it incorporates both new and handoff calls.

To plot the values of γ under varying loads for the hybrid scheme, we define the optimization problem

$$\underset{d_{hybrid}}{\text{maximize}} \quad \gamma, \quad \text{subject to} \quad P_{bH} \leq H_{max}. \quad (9)$$

Once again, we define a similar optimization problem for the reservation scheme by replacing the decision variable d_{hybrid} by K. In Figure 12 we plot values of γ under varying λ_n. The parameters used for this figure are: $\lambda_H = 1$, $\mu_0 = 1$, $M' = 15$, $H_{max} = 10^{-4}$. The hybrid scheme achieves uniformly higher values of γ under various loads. The difference between the hybrid and reservation schemes is most apparent at high loads. At such loads, a low value of K is required in the reservation scheme to maintain the QoS constraint on P_{bH}, thus resulting in a low value of γ.

On the other hand, due to the mobility of channels in the hybrid scheme, the sacrifice in the number of local channels to maintain the QoS constraint on P_{bH} is not as great. When $r = 4$, the channel utilization for the channel carrying scheme at high loads is over 50% more than the reservation scheme. Further, this advantage will be even more significant as r increases.

6 Conclusion

We have presented a novel channel carrying scheme to address the problem of handoffs in mobile cellular systems. Our basic idea is to allow mobile users to carry their current channels into new cells under certain conditions. We use the $(r+1)$-channel assignment scheme to avoid co-channel interference due to channel movement. This affords us channel mobility at the expense of some capacity. An attractive feature of the channel carrying scheme is that it does not require complex power control techniques or global channel coordination, which simplifies its implementation.

We develop a two-cell model to analyze our channel carrying scheme and the traditional channel reservation technique. We find through numerical results that even in the case of the minimum possible reuse distance, $r = 2$, the channel carrying scheme outperforms the reservation technique.

We further consider a refinement to the channel carrying scheme, which provides a useful design parameter that allows us to optimize various parameters of interest. We again find that our scheme scheme uniformly and significantly improves the system performance, in some cases resulting in over 50% better network utilization than the channel reservation scheme.

References

[1] S. Tekinay and B. Jabbari, "Handover and channel assignment in mobile cellular networks," *IEEE Communications Magazine*, vol.29, pp.42–46, Nov. 1991.

[2] G.N. Senarath and D.H. Everitt, "Performance of handover priority and queueing systems under different handover request strategies for microcellular mobile communications systems," *Proc. IEEE Veh. Technol. Conf.*, pp.897–901, 1995.

[3] H. Jiang and S.S. Rappaport, "CBWL: a new channel assignment and sharing method for cellular communication systems," *IEEE Trans. Veh. Technol.*, vol.VT-43, pp.313–322, May 1994.

[4] E.D. Re, R. Fantacci and G. Giambene, "Handover and dynamic channel allocation techniques in mobile cellular networks," *IEEE Trans. Veh. Technol.*, vol.VT-44, pp.229-237, May 1995.

[5] R. Ramjee, R. Nagarajan and D. Towsley, "On optimal call admission control in cellular networks," *Proc. INFOCOM.*, pp43–50, March 1996.

The Study of A Channel Sharing Scheme in Wireless Cellular Networks including Handoffs [1]

Junyi Li   Ness B. Shroff[2]   Edwin K.P. Chong

School of Electrical and Computer Engineering
Purdue University
West Lafayette, IN 47907, U.S.A.
E-mail: {junyi, shroff, echong}@ecn.purdue.edu

Abstract—Enhancing system capacity while maintaining quality of service is an important issue in wireless cellular networks. In this paper, we present a localized channel sharing scheme to address this problem. Our basic idea is to allow channels to be shared between adjacent cells at the expense of a smaller initial allocation of channels per cell. We show that this tradeoff results in a better utilization of network resources. An important feature of our sharing scheme is that channel management is localized between adjacent cells, and no global coordination or optimization is required, thus making it suitable for implementation. The sharing scheme can also facilitate handoff processing. We provide numerical results comparing our scheme with the channel reservation technique, and find a significant performance improvement over a wide range of traffic parameters and a variety of quality of service requirements.

I. INTRODUCTION

Worldwide focus on wireless networking research has intensified in recent years. Compared to its wired counterpart, wireless spectrum is a much more scarce resource. Thus, enhancing system capacity is of great importance in wireless networks. The use of cellular technology is a common means to this end. In a cellular system, the service area is divided into cells, and the wireless spectrum is reused among those cells. We refer to the unit of wireless spectrum needed to serve a single user as a *channel*.[1] We adopt the usual assumption that channels used in one cell cannot be used in other cells that are closer than the *minimum reuse distance*. A significant body of research has been conducted on efficiently allocating channels to individual cells under this minimum reuse distance constraint [3], [7]. There are, in general, two types of channel allocation schemes: Fixed Channel Allocation (FCA) and Dynamic Channel Allocation (DCA).

The use of cellular technology also gives rise to new quality of service (QoS) related problems; e.g., those related to hand-

offs. A handoff occurs when a mobile user moves from one cell to another. A handoff call is blocked if there is no free channel available in the new cell. The probability of blocking a handoff call is an important QoS measure that needs to be considered in wireless networks. In fact, since blocking a handoff call is less desirable than blocking a new call, specific schemes have to be developed to prioritize handoff calls. The channel reservation scheme is a common prioritization method used in FCA systems [1], [6]. Specifically, in each cell a threshold is set, and if the number of channels currently used in the cell is below that threshold, both new and handoff calls are accepted. However, if the number of channels used exceeds this threshold, an incoming new call is blocked and only handoff calls are admitted.

In this paper, we propose a novel channel sharing scheme to improve system capacity and QoS in wireless cellular networks. We have briefly introduced the idea of channel sharing in [5], without considering handoffs. In this paper we present a more comprehensive study taking into account handoffs, and the performance gains associated with it. The basic idea in our channel sharing scheme is to allow channels to be shared between adjacent cells; i.e., channels can be used by any user in either cell, without coordinating with other cells for the use of the same channels. In this way, channel management can be localized within adjacent cells. Further, to avoid global optimization, we propose a new fixed channel assignment scheme that attempts to keep the co-channel reuse distance as close as possible while allowing channel sharing. The sharing scheme can also facilitate handoff processing. Moreover, channels are assigned in such a way that each base-station is responsible to transmit over only a portion of the entire channel set, compared with the case in DCA where each base-station may have to transmit over any channel. Therefore, the physical implementation complexity of our channel sharing scheme is significantly simplified. The above salient features are especially attractive to micro-cellular networks, where handoff occurs more frequently, and, on the other hand, base-station equipment may

[2]Please address all correspondence to this author, Tel. +1 765 494 3471, Fax. +1 765 494 3358.

[1]Here, we consider circuit-switched applications, such as voice communications, where the bandwidth requirement for each connection is fixed.
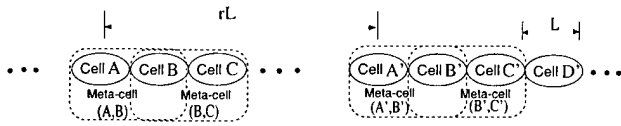
Fig. 1. Cells and meta-cells in the linear cellular system.

be inexpensive and not expected to carry out full hardware and software functionality.

Here, it should be emphasized that the concept of sharing or borrowing channels *per se* is not new [2], [3], [7]. However, what is new in our scheme is that channels can be shared without the need for global coordination or dynamic power control.

II. META-CELLS AND CHANNEL SHARING

Consider a set of cells in a cellular system. Each cell contains a base station, which communicates with mobile users in that cell. Associated with the cellular system is a set of channels, which are to be allocated to the cells. In each cell, an individual channel can be used by only one mobile user in the cell for communication with the base station. The same channel can be reused in two different cells as long as they (the cells) satisfy a *minimum reuse distance requirement*. To elaborate, we assume that we are given a distance measure d, where $d(X, Y)$ is the distance between cells X and Y. We are also given a parameter Δ that represents the *minimum reuse distance*. Two cells X and Y are said to satisfy the minimum reuse distance requirement if $d(X, Y) \geq \Delta$.

In the conventional scheme for fixed channel assignment, each channel is assigned to cells that are exactly a distance Δ apart, as shown in Figure 1 where $\Delta = rL$. Consequently, a maximum number of channels are assigned to each cell while still satisfying the minimum reuse distance requirement. We refer to this scheme as *tightest fixed channel assignment*.

In cellular systems using the tightest fixed channel assignment scheme, calls in a cell can only use those channels assigned to that cell. Call blocking results if such a channel is not available. For example, if a call arrives at cell B in Figure 1, where all channels are already being used, then this new call is blocked. Channel borrowing is one way to reduce call blocking. Specifically, if at the time the call arrives at cell B, cell A has some idle channels, then cell B may borrow one of the idle channels to serve the new call. To achieve this, however, we need to coordinate the use of channels in the co-channel cells of cell A. For example, to avoid violating the minimum reuse distance requirement, channels that are borrowed by cell B, cannot be used in cell A'. Such a global channel coordination is computationally expensive and therefore difficult to implement, and further channel utilization may be decreased at high traffic loads [2].

In our scheme, we attempt to alleviate call blocking by sharing channels between neighboring cells, while localizing the channel coordination. To facilitate the description of our scheme, we first introduce some terminology. A *meta-cell* is a fixed collection of neighboring cells (typically a pair of two adjacent cells). For example, Figure 1 shows a family of meta-cells in a linear cellular system, each comprising a pair of two adjacent cells. Each meta-cell is designated by a pair (X, Y), where X and Y are individual cells called the *component cells* of that meta-cell. For example, in Figure 1, cells A and B are components of meta-cell (A, B). As before, we assume that we have a distance measure for meta-cells (e.g., based on the distance measure d between cells).

The main idea of our channel assignment scheme is to allocate channels to meta-cells in such a way that a maximum number of channels can be assigned to each meta-cell while any two meta-cells assigned the same channels satisfy the minimum reuse distance requirement, i.e., the distance measure, now with respect to two meta-cells, is no shorter than Δ. Our channel assignment scheme, done at the meta-cell level, is different from the usual channel assignment scheme which is done at the cell level. In particular, channels are assigned not to individual cells but to meta-cells. A user in a given cell can use any channel that is assigned to a meta-cell for which the given cell belongs, with the usual proviso that only one user can use a given channel within a given meta-cell at a given instance. We next point out two fundamental advantages:

(i) First, the sharing of resources between cells leads to more efficient utilization of the resources. In particular, if a new user arrives at a cell and a channel is not being used in a neighboring cell, the user can use that channel (as long as the neighboring cell belongs to the same meta-cell). This feature potentially reduces the probability of blocking a new call.

(ii) Second, when a user moves from one cell to another, under certain circumstances it may not be necessary to assign another channel to the user. Specifically, if a user in a given cell moves to a neighboring cell which is part of the same meta-cell, and the user is using a channel that is assigned to that meta-cell, the user can move to the neighboring cell without any risk of handoff blocking. Moreover, the processing of the handoff can also be simplified because the user continues its service by using the same channel during handoff. Furthermore, if we model and predict the mobility of a particular user, we can reduce the incidence of handoff blocking by reassigning (if necessary) to the user a channel that can be shared with the next destination cell. The benefit comes from the fact that the time available to do this processing is the time a user spends in a given cell – potentially much longer than the time available to conventionally process a handoff call, typically only when a user is at the boundary between two cells. This feature is important for cellular systems with small-sized cells, such as micro-cellular systems.

The proposed channel sharing scheme differs from conventional channel borrowing. By using the meta-cell based channel assignment as described in Section III, channel sharing can be completely localized within a meta-cell, i.e., we do not require any channel locking or power control technique which is essential in channel borrowing schemes. Note that relative to the usual fixed channel assignment scheme, in our sharing scheme we need to coordinate between cells in a meta-cell. However, since meta-cells consist only of neighboring cells, the scheme should be easy to implement.

We next briefly describe the protocol to exploit the sharing feature of our scheme. The detailed protocol design can be found in [4]. For the sake of description, we focus our attention on a particular (arbitrary) cell, which is referred to as the *local cell*. Recall that each cell is always covered by several overlapping meta-cells, called the *covering meta-cells* of that cell. We call channels that are assigned to the covering meta-cells of the local cell the *accessible channels*, since users in the local cell may have access to those channels. At any given instance, each accessible channel can be used in only either the local cell or one of the adjacent cells. Those channels that can be used by the local cell are called *enabled channels*.

When a call arrives, it can be accepted if there is an idle enabled channel in the local cell. Otherwise, we attempt to obtain a channel from some sharing cell, as follows. We first look up all accessible channels currently not enabled in the local cell, and get a list of the sharing cells associated with those channels. We then choose one of those sharing cells on that list, and send it a *sharing request*. The sharing cell, upon receiving the sharing request, then executes the procedure described below. If the sharing request is granted, we accept the arriving call by assigning the idle channel specified by the sharing cell. If the request is denied, we proceed to send another sharing request to one of the remaining sharing cells on the list. The process is continued until the sharing request is accepted, or denied by all sharing cells on the list, in which case the call is rejected (blocked).

When a sharing request is received from a sharing cell, we first check whether there is any idle enabled channel, associated with that sharing cell. If so, we grant the sharing request. Otherwise, we attempt to obtain such an idle channel by *swapping channels*: if there is any idle enabled channel in the local cell, we first find another enabled channel associated with the sharing cell, and then swap those two channels so that we can grant the sharing request. If there is no idle enabled channel in the local cell, the sharing request is rejected.

III. META-CELL BASED CHANNEL ASSIGNMENT

In this section, we illustrate the meta-cell based channel assignment scheme for a 2-D cellular system. In the planar or 2-D case, the cellular configuration is usually assumed to be hexagonal. This means that the entire area of interest is covered with equal-sized hexagonal cells. The distance $d(X, Y)$ between two cells X and Y is traditionally defined as the distance between their centers. Let N denote the total number of distinct channels available in this hexagonal cellular system. In the tightest fixed channel assignment scheme, co-channel cells (i.e., cells that are assigned the same set of channels) are exactly a distance of Δ, the minimum reuse distance, apart. Consequently, each cell is assigned N/R channels, where R is the minimum reuse factor and can be determined from Δ by $R = (1/3)(\Delta/\rho)^2$, with ρ being the radius of a single cell. In general, the minimum reuse factor R can be represented by $R = p^2 + pq + q^2$, where p and q are nonnegative integers satisfying $p + q \geq 2$. Without loss of generality, we assume that $q \geq p$ in the following.

As in the linear case, a meta-cell here consists of two adjacent neighboring cells. To allow for channel sharing, we assign channels to meta-cells under the minimum reuse distance constraint in terms of meta-cells. Again, the main idea of our channel assignment scheme is to deploy co-channel meta-cells (i.e., meta-cells that are assigned the same set of channels) as close as possible to maximize channel reuse efficiency. In the remainder of this section, we describe this channel assignment scheme in detail.

Consider an arbitrary cell A_0 in the hexagonal cellular system as shown in Figure 2, and establish a set of coordinates i-j originating at the center of cell A_0, where the two axes form a $60°$ angle, and the unit distance along the axes is $\sqrt{3}\rho$. Then, the minimum reuse distance Δ is equal to R coordinate units in this set of coordinates. The center of any hexagon Z can be designated by a pair of coordinates (i_Z, j_Z), with i_Z and j_Z integers. Let B_0, C_0, D_0, E_0, F_0, and G_0 denote six hexagons with centers at the coordinates (p, q), $(-q, p+q)$, $(-p-q, p)$, $(-p, -q)$, $(q, -p-q)$, and $(p+q, -p)$, respectively, (see Figure 2). Note that their distance to cell A_0 (centered at $(0, 0)$) are equal and given by $p^2 + pq + q^2 = R$ units. In the tightest fixed channel assignment scheme, cells B_0, C_0, D_0, E_0, F_0, and G_0 are assigned the same set of channels as cell A_0.

Let A_1 be the adjacent right neighboring cell of A_0 along the i-axis as shown in Figure 2, i.e., $(i_{A_1}, j_{A_1}) = (i_{A_0} + 1, j_{A_0}) = (1, 0)$. We next focus on meta-cell (A_0, A_1) as the *reference meta-cell*. Note that in the 2-D case, meta-cells may have three distinct orientations[2], and each meta-cell may have six neighboring co-channel meta-cells. Consequently, there are an infinite number of different ways to deploy co-channel meta-cells, including irregular (non-repetitive) deployment patterns. For the sake of simplicity and regularity, in the following we re-

---

[2]The orientation of a meta-cell is the directional relationship between its two component cells.

Fig. 2. Configuration of co-channel meta-cells in the case of $p + 1 \geq p$.

Fig. 3. Partition of channels in local cell (for 2-D case).
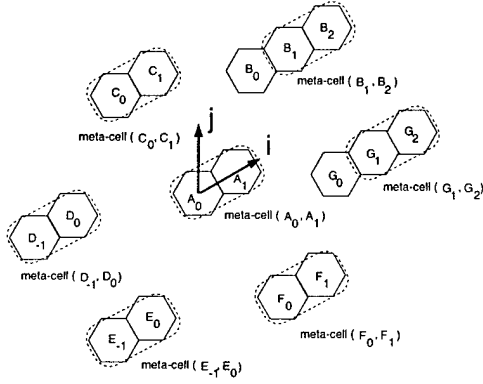
strict ourselves to deployment methods in which all co-channel meta-cells are of the same orientation. In other words, for any co-channel meta-cell of (A_0, A_1) of interest, two components are adjacent along the i-axis. Therefore, we can identify any co-channel meta-cell of reference meta-cell (A_0, A_1) by its left component[3].

It turns out that for different values of p and q, we need different methods to deploy co-channel meta-cells of reference meta-cell (A_0, A_1), depending on whether $p + 1 \geq q$. For simplicity, we assume that $p + 1 \geq q$ (the case where $p + 1 < q$ is considered in the appendix). The values of R within this category may be $3, 7, 12, 19$, etc. It can be shown that in this case, as illustrated in Figure 2, the meta-cells whose left components are respectively B_1, C_0, D_{-1}, E_{-1}, F_0 and G_1, can be deployed as co-channel meta-cells of reference meta-cell (A_0, A_1), where the centers of cells B_1, D_{-1}, E_{-1} and G_1 are given respectively as follows: $(i_{B_1}, j_{B_1}) = (p + 1, q)$, $(i_{D_{-1}}, j_{D_{-1}}) = (-p - q - 1, p)$, $(i_{E_{-1}}, j_{E_{-1}}) = (-p - 1, -q)$, and $(i_{G_1}, j_{G_1}) = (p + q + 1, -p)$. Some important observations of the above co-channel meta-cell deployment are made in the appendix.

IV. REFINEMENTS

In the previous section, we presented the basic channel sharing scheme. To make our scheme practically useful, we next discuss two refinements.

A. Combined Scheme

It is instructive to compare the effective channel capacity using our sharing scheme and the tightest fixed channel assignment scheme. In our scheme, the maximum possible channel capacity of each cell is clearly just the total number of distinct accessible channels for each cell. As we pointed out above, in an individual cell, the number of accessible channels in our

[3]The left component cell in a meta-cell is the component cell which is positioned in the left side along the i-axis.
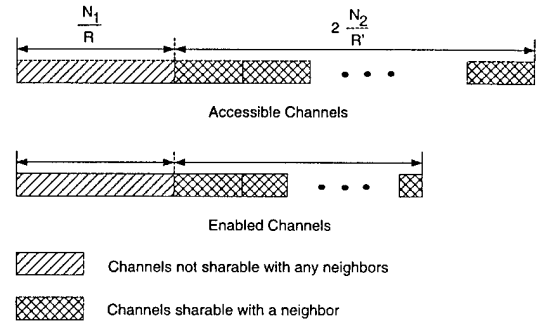
scheme is generally larger than that of the fixed scheme. Note that, however, this number is an upper bound of the effective channel capacity since it assumes that the statistical sharing advantage can be fully exploited. On the other hand, if we totally ignore the statistical sharing advantage, then we may obtain a lower bound for the channel capacity. To be specific, we equally distribute channels that are assigned to each meta-cell into two component cells, and then count the total number of distinct channels now available for each cell. Hence, the effective channel capacity using our sharing scheme is bounded by these two extreme scenarios, and depends on the extent to which the statistical sharing advantage is actually obtained.

Next, we present a combined scheme that attempts to maximize the effective channel capacity for each cell. Specifically, we divide all the N channels into two distinct groups of size N_1 and N_2 such that $N = N_1 + N_2$. The first group of N_1 channels is assigned to cells using the tightest fixed channel assignment scheme, and thus cannot be shared between adjacent cells. The remaining group of N_2 channels, however, is assigned to meta-cells according to our channel sharing assignment scheme, and can be shared within meta-cells, the same as in the previous sections.

Varying N_2 allows us to maximize the effective channel capacity. Specifically, the parameter N_2 enables us to trade off the potential advantage from statistical sharing with a reduction in the average number of channels for each cell. The larger the value of N_2 in the combined scheme, the more gain we expect from statistical sharing, but at the same time the more price we pay by reducing the average number of channels for each cell.

Figure 3 illustrates the partitioning of accessible channels in a cell into the two groups described above. The number of accessible channels in each of these groups is N_1/R and $2N_2/R'$, respectively (in the 2-D case). Note that the number of enabled channels in the first (N_1/R) group is fixed, whereas the number of enabled channels in the second group can vary between 0 and $2N_2/R'$.
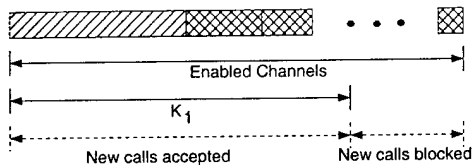
Fig. 4. K_1 threshold scheme.

B. Threshold Handoff Scheme

In our basic channel sharing scheme, we do not distinguish between new and handoff call arrivals. However, studies have shown that one of the most important user concerns is that service not be cut off during an on-going call. Therefore, blocking a handoff arrival is even less desirable than blocking a new arrival.

The *threshold* scheme is a popular way to prioritize handoff calls. Specifically, a number of channels can be reserved solely for the use of handoff, allowing both handoff and new calls to compete for the remaining channels. To prioritize handoff calls in our channel sharing scheme, we apply the following two threshold schemes. Note that the threshold restrictions apply only to new call requests.

K_1 threshold

The first part of our threshold scheme is the same as the channel reservation scheme. Specifically, a new call arriving at a cell will be blocked if the number of current users in that cell exceeds a threshold K_1, with $K_1 \leq \frac{N_1}{R} + \frac{2N_2}{R'}$ in the 2-D case. The threshold K_1 is set to avoid overall excessive use of accessible channels by new calls. For example, in some scenarios, accessible channels may be accumulated in one cell because of channel movement. In this case, it is desirable to limit excessive access to those channels by new calls, waiting instead for potential sharing requests from sharing cells. Note that the K_1 threshold takes effect only if the number of enabled channels is greater than K_1 (otherwise, we apply another threshold, K_2, described in the next section).

Figure 4 provides an illustration of the K_1 threshold scheme. In the figure, we assume that the number of enabled channels is greater than K_1. As illustrated, if the number of channels being used does not exceed K_1, then new calls are accepted; otherwise, they are blocked.

Note that to achieve a given quality of service requirement for handoff, the threshold K_1 in our scheme may be generally chosen higher than the threshold used in the channel reservation scheme, because now handoff requests have access to more channel capacity due to sharing. In other words, we need to reserve fewer channels *a priori* for handoff calls. This helps increase the efficiency of our handoff scheme compared to the conventional reservation scheme, as will be demonstrated in Section V.
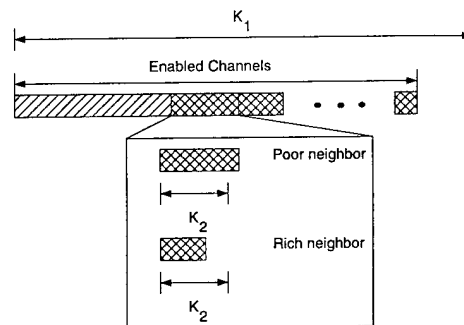
Fig. 5. K_2 threshold scheme.

K_2 threshold

If the new call is not blocked by the first part of the threshold scheme, it is accepted if there are idle channels in the cell. Otherwise, if there are no idle channels (i.e., the number of enabled channels is less than or equal to K_1), we then attempt to obtain an accessible channel from sharing cells. The second part of the threshold scheme is now applied to limit the sharing accessibility associated with individual sharing cells. Specifically, we first set the value of a second threshold K_2, where $K_2 \leq \frac{N_2}{R'}$ in the 2-D case. Then, we send out sharing requests only to the adjacent cells that have fewer than K_2 sharable channels currently being used in the local cell. In this way we prevent new calls from excessively using up sharable channels associated with any particular sharing cell, and thus prioritize potential handoffs from that sharing cell.

Figure 5 illustrates the K_2 threshold scheme. Note that the number of enabled channels here is not more than K_1 (for otherwise the K_2 threshold does not take effect). In the figure, we use the term *rich neighbor* to denote a neighboring cell that has fewer than K_2 sharable channels *in the local cell*. If the neighboring cell has more than or equal to K_2 channels *in the local cell*, we use the term *poor neighbor*. In other words, we send out sharing requests for new calls only to rich neighbors.

V. NUMERICAL RESULTS

In this section, we compare, via simulation, the performance of our sharing scheme with handoff prioritization and the channel reservation scheme based on the tightest fixed channel assignment. Here, we distinguish between the blocking of new and handoff calls. The QoS measures we are interested in this case are: P_{bN}, the blocking probability of new calls, and P_{bH}, the blocking probability of handoff calls.

Our simulation model for the the 2-D cellular system consists of 36 cells, with each cell having six adjacent cells. The cells on the boundary of one side of the configuration are connected to the cells on the boundary of the other side. The call traffic is assumed to be symmetrically distributed over all the cells. Calls are assumed to arrive at each cell according to a

Poisson process with rate λ_n. The time until a call terminates is assumed to be exponentially distributed with mean $1/\mu$. The time a user spends in a cell before making a handoff request to go to another cell is assumed to be exponentially distributed with mean $1/\lambda_H$. In our simulation model, users in a cell may direct a handoff request to each of the adjacent cells with equal probability. Since we are interested in the performance of a typical cell, the statistics obtained are averaged over all cells. To systematically compare our handoff scheme with the channel reservation scheme, we next investigate three design problems.

P_{bN} versus λ_n

Here we provide plots of P_{bN} under varying load conditions for the sharing and reservation schemes. The performance measures depend on the parameters N_2, K_1, and K_2 in the sharing scheme, and the parameter K in the reservation scheme. To meaningfully compare our combined scheme with the reservation scheme, we determine the optimal values of P_{bN} for the two schemes, given a constraint on P_{bH}. Therefore, in the sharing scheme, to appropriately choose N_2, K_1, and K_2, we consider the following optimization problem:

$$\underset{N_2,K_1,K_2}{\text{minimize}} \quad P_{bN}$$
$$\text{subject to} \quad P_{bH} \le H_{max} \tag{1}$$

where H_{max} denotes a prespecified maximum level for P_{bH}. A similar optimization problem can be defined for the reservation scheme, where the decision variable is now replaced with the threshold parameter K. For a fair comparison of our sharing scheme with the reservation scheme, we calculate the optimal values of P_{bN} for the two schemes, given the same H_{max}.

Figure 6 shows plots of the optimal values of P_{bN} for the reservation and sharing schemes under varying λ_n. For this figure we use the following parameters: $\lambda_H = 5$, $\mu = 1$, $N/R = 15$, (for example $N = 45$ when $R = 3$). The call handoff blocking probability P_{bH} is constrained by $H_{max} = 10^{-4}$, a typical value. Figure 6 shows that the combined sharing scheme achieves uniformly lower values of P_{bN} than the reservation scheme. We also notice that at low traffic load, there is virtually no new call blocking for the sharing scheme.

λ_n versus P_{bH}

In this experiment, we compare the maximum new call arrival rate λ_n that can be admitted by the sharing and the reservation schemes for various handoff blocking probabilities P_{bH}. More precisely, we define the following optimization problem for the channel sharing scheme:

$$\underset{N_2,K_1,K_2,\lambda_n}{\text{maximize}} \quad \lambda_n$$
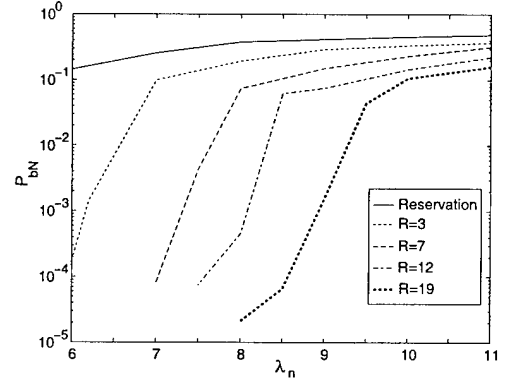
Fig. 6. Plot of optimal P_{bN} versus λ_n for the problem defined in Equation (1). The parameters used in this plot are: $N/R = 15$, $\lambda_H = 5$, $\mu = 1$, $H_{max} = 10^{-4}$.
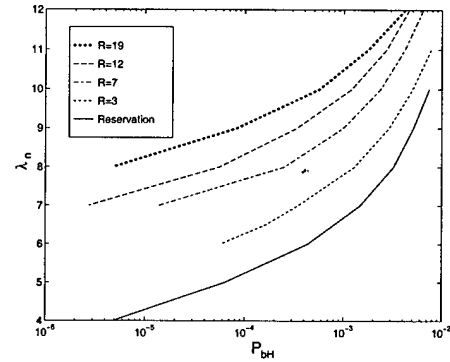
Fig. 7. Plot of optimal λ_n versus P_{bH} for the problem defined in Equation (2). The parameters in this figure are: $N/R = 15$, $\lambda_H = 5$, $\mu = 1$, $N_{max} = 10^{-2}$.

$$\text{subject to} \quad P_{bN} \le N_{max} \tag{2}$$
$$P_{bH} = H$$

Here, the constraint H for P_{bH} is varied between 10^{-6} and 10^{-2} and the corresponding maximum value of λ_n is obtained. Again, a similar optimization problem is defined for the reservation scheme by replacing N_2, K_1, and K_2 by K. In Figure 7, we plot the optimal values of λ_n versus P_{bH} for our sharing scheme and the reservation scheme scheme with $R = 3$, 7, 12, and 19. For this figure we use the following parameters: $\lambda_H = 5$, $\mu = 1$, $N/R = 15$, $N_{max} = 10^{-2}$. We observe that our sharing scheme allows a higher new call rate than the reservation scheme over all values of P_{bH}. For a typical value of $P_{bH} = 10^{-4}$, our sharing scheme with $R = 19$ can admit approximately 64% more calls into the network than the reservation scheme. As is also shown in the figure, for lower handoff probability constraints, this difference is even larger. Improving the admissible arrival rate results in increased revenue for the network provider.
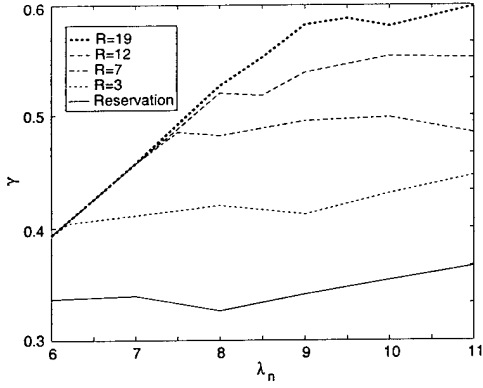
Fig. 8. Plot of optimal γ versus λ_n for the problem defined in Equation (3). The parameters used in this figure are: $N/R = 15, \lambda_H = 5, \mu = 1, H_{max} = 10^{-4}$.

Utilization versus λ_n

From the point of view of a network provider, a useful parameter of interest is the *normalized channel utilization*, γ , defined as

$$\gamma = \frac{\text{average number of users in one cell}}{\text{total number of available channels in one cell}},$$

where the total number of available channels in one cell is N/R. The parameter γ is directly related to the revenue of a cellular network because it incorporates both new and handoff calls.

To plot the values of γ under varying loads for the sharing scheme, we define the optimization problem

$$\begin{array}{ll} \underset{N_2, K_1, K_2}{\text{maximize}} & \gamma \\ \text{subject to} & P_{bH} \leq H_{max}. \end{array} \qquad (3)$$

Once again, we define a similar optimization problem for the reservation scheme by replacing the decision variable by K.

In Figure 8, we plot values of γ under varying λ_n. The parameters used for this figure are: $\lambda_H = 5, \mu = 1, N/R = 15, H_{max} = 10^{-4}$. The sharing scheme achieves uniformly higher values of γ under various loads. The difference between the combined and reservation schemes is most apparent at high loads. At such loads, a low value of K is required in the reservation scheme to maintain the QoS constraint on P_{bH}, thus resulting in a low value of γ. On the other hand, due to the channel sharing, the threshold to maintain the QoS constraint on P_{bH} is not as low. When $R = 19$, the channel utilization for the channel sharing scheme at high loads is over 64% more than the reservation scheme.

VI. CONCLUSION

We have presented a novel channel sharing scheme to improve system capacity and QoS in wireless cellular systems.

Our basic idea is to allow channels to be shared between adjacent cells without co-channel coordination with other cells. For this purpose, we introduce the concept of meta-cells to facilitate localized channel management. Further, to maximize channel reuse efficiency, we develop a channel assignment method based on the distance measure between meta-cells. In general, our channel sharing scheme leads to channel access in a statistical multiplexed fashion, but at the expense of some nominal capacity. An attractive feature of the channel sharing scheme is that it does not require complex power control techniques, global channel coordination, or on-line optimization, which simplifies its implementation.

To make our channel sharing scheme practically useful, we then propose two important refinements, which provide useful design parameters to maximize system performance under various QoS constraints. We numerically compare our channel sharing scheme with the channel reservation scheme. Simulation results show that our scheme significantly improves system capacity over a large range of traffic conditions and a variety of QoS requirements, in some cases resulting in over 60% better network utilization than the channel reservation scheme in the 2-D hexagonal system.

APPENDIX

APPENDIX

I. CHANNEL ASSIGNMENT SCHEME FOR THE 2-D CASE

A. Observations on the case of $p + 1 \geq q$

The following are some important observations of the co-channel meta-cell deployment for the case of $p + 1 \geq q$ in the 2-D hexagonal configuration.

• The distance measure between any neighboring meta-cells in this co-channel meta-cell deployment is exactly equal to the minimum reuse distance R units. In this way, we deploy co-channel meta-cells as close as possible and maximize channel reuse efficiency while allowing channel sharing.

• Comparing with the deployment of co-channel cells in the tightest fixed channel assignment scheme, we note that the left components of the co-channel meta-cells of reference meta-cell (A_0, A_1) can be readily generated by starting from cells $B_0, C_0, D_0, E_0, F_0, G_0$, and then keeping C_0, F_0, but substituting B_0, G_0 respectively by their immediate right, and D_0, E_0 respectively by their immediate left neighboring cells, all along the i-axis (see Figure 2).

B. Channel reuse factor for the case of $p + 1 \geq q$

We next determine the channel reuse factor for the co-channel meta-cell deployment method for the case of $p + 1 \geq q$ in the 2-D hexagonal configuration. Recall that in the tightest fixed channel assignment scheme, each cell is assigned N/R channels. For comparison, we now calculate the number of

distinct channels that a single meta-cell can be assigned using the channel assignment scheme described in Section II. Note that in the 2-D hexagonal cellular system, there are three types of meta-cell orientations. For simplicity, we equally divide the total N distinct channels into three groups, each assigned to meta-cells with one particular orientation. In other words, all meta-cells with the same orientation, say along the i-axis, will reuse $N/3$ distinct channels. Let the number of distinct sets of co-channel meta-cells with the same orientation to be R'. Then each meta-cell may be assigned $(N/3)/R'$ distinct channels. In fact, we claim that using the above meta-cell deployment method, R' is given by

$$R' = R + p + q. \tag{4}$$

For example, when $R = 3, 7, 12, 19$, the corresponding R' is given by $R' = 5, 10, 16, 24$.

To show that Equation (4) holds, we note that R', the number of distinct sets of co-channel meta-cells with the same orientation, is given by the number of cells whose centers lie in the parallelogram $A_0 B_1 G_1 F_0$[4] excluding the edges $B_1 G_1$ and $F_0 G_1$ (see Figure 2). Further, by symmetry, R' can be reduced to the ratio of the area of the parallelogram $A_0 B_1 G_1 F_0$ to the area of a single cell. The area of a single cell is simply given by $\frac{3\sqrt{3}}{2}\rho^2$. With some tedious manipulations, we obtain the area of the parallelogram $A_0 B_1 G_1 F_0$ as $\frac{3\sqrt{3}}{2}(p^2 + pq + q^2 + p + q)\rho^2$. Hence, Equation (4) follows.

C. The case of $p + 1 < q$

We now describe the channel assignment scheme in the case where $p + 1 < q$. Within this category, the values of R may be $4, 9, 13, 16$, etc. To deploy co-channel meta-cells as close as possible in this case, in general we need to compare the channel reuse efficiency for various deployment possibilities. Specifically, obtaining a tight co-channel meta-cell deployment of reference meta-cell (A_0, A_1) can be effectively reduced to finding another two cells, denoted as X_1, X_2, such that:

(i) meta-cells (A_0, A_1), (X_1, Y_1), and (X_2, Y_2) do not violate the minimum reuse distance requirement, where Y_1 and Y_2 denote the right adjacent cells along the i-axis of X_1 and X_2 respectively; and

(ii) the area of the triangle[5] $A_0 X_1 X_2$ is minimized.

Once we have determined cells X_1 and X_2, the left components of the remaining neighboring co-channel meta-cells of reference meta-cell (A_0, A_1) can be easily derived by symmetry.

A computer program has been developed to compare various possible choices of X_1 and X_2. We find that for $R < 100$
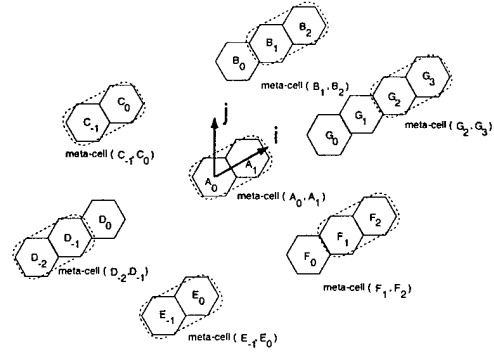
Fig. 9. Configuration of co-channel meta-cells in the case of $p + 1 < q$.

(a realistic range of R values), it would take less than two minutes to enumerate all possibilities and yield the tightest co-channel meta-cell deployment. Note that in a real-world application, channel assignment can be done off-line. Therefore, it would not be difficult to determine the tightest deployment by using computer enumeration. An interesting observation in our numerical results is that in most of the cases, the tightest deployment can be obtained from one of the following two $\{X_1, X_2\}$ choices: X_1 and X_2 center at $(p + 1, q)$ and $(p + q + 2, -p)$ respectively (shown in Figure 9) or at $(p, q + 1)$ and $(p + q + 1, -p + 1)$, respectively. Therefore, in most cases, we may even simply compare the areas of the triangle $A_0 X_1 X_2$ corresponding to those two $\{X_1, X_2\}$ choices, to compute a tight co-channel meta-cell deployment method.

REFERENCES

[1] D. Hong and S. Rappaport, "Traffic model and performance analysis for cellular mobile radio telephone systems with prioritized and non-prioritized handoff procedures," *IEEE Transactions on Vehicle Technology*, vol. 35, pp. 77–92, 1986.

[2] H. Jiang and S. Rappaport, "CBWL: A new channel assignment and sharing method for cellular communication systems," *IEEE Transactions on Vehicle Technology*, vol. 43, pp. 313–322, May 1994.

[3] I. Katzela and M. Naghshineh, "Channel assignment schemes for cellular mobile telecommunication systems: a comprehensive survey," *IEEE Personal Communications Magazine*, pp. 10–31, June 1996.

[4] J. Li, *Intercellular coordination schemes for improving spectrum utilization in wireless cellular networks*. Purdue University, West Lafayette, Indiana: Ph.D. dissertation, 1998.

[5] J. Li, N. Shroff, and E. Chong, "A Channel Sharing Scheme to Improve System Capacity and Quality of Service in Wireless Cellular Networks," in *Proceedings of the Third IEEE Symposium on Computers and Communications (ISCC'98)*, (Athens, Greece), pp. 700–704, 1998.

[6] R. Ramjee, R. Nagarajan, and D. Towsley, "On optimal call admission control in cellular networks," in *Proc. IEEE INFOCOM*, pp. 43–50, 1996.

[7] S. Tekinay and B. Jabbari, "Handover and channel assignment in mobile cellular networks," *IEEE Communications Magazine*, pp. 42–46, November 1991.

---

[4] A parallelogram $ABCD$ is defined by the centers of the four cells A, B, C, and D.

[5] A triangle ABC is defined by the centers of the three cells A, B, and C.

A New Localized Channel Sharing Scheme for Cellular Networks *

Junyi Li[a] Ness B. Shroff[b] Edwin K. P. Chong[c]

[a] *Room 4F-531*
101 Crawfords Corner Road Holmdel
NJ 07733-3030, USA
E-mail: junyi@dnrc.bell-labs.com

[b] *School of Electrical and Computer Engineering*
Purdue University
West Lafayette, IN 47907, USA
E-mail: shroff@ecn.purdue.edu

[c] *School of Electrical and Computer Engineering*
Purdue University
West Lafayette, IN 47907, USA
E-mail: echong@ecn.purdue.edu

Enhancing system capacity while maintaining quality of service is an important issue in wireless cellular networks. In this paper, we present a new localized channel sharing scheme to address this problem. Our basic idea is to allow channels to be shared between adjacent cells. We further propose a fixed channel assignment scheme to maximize channel reuse efficiency while allowing channel sharing. We show that our sharing scheme can also facilitate handoff processing. An important feature of our sharing scheme is that channel management is localized between adjacent cells, and no global coordination or optimization is required, thus making it suitable for implementation.

We provide simulation results comparing our scheme with the conventional channel assignment and handoff techniques. We find that our scheme improves system capacity over a broad range of traffic parameters and a variety of quality of service requirements.

Keywords: Cellular, channel sharing, channel borrowing, dynamic channel allocation, local control.

1. Introduction

Worldwide focus on wireless networking research has intensified in recent years. Compared to its wired counterpart, wireless spectrum is a much more scarce resource. Thus, enhancing system capacity is of great importance in wireless networks. The use of cellular technology is a common means to this end. In a cellular system, the service area is divided into cells, and the wireless spectrum is reused among those cells. We refer to the unit of wireless spectrum needed to serve a single user as a *channel*. For example, in a TDMA system, a

time-slot is viewed as a channel. We consider circuit-switched applications, such as voice communications, where the bandwidth requirement for each connection is fixed.

We adopt the usual assumption that channels used in one cell cannot be used in other cells that are closer than the *minimum reuse distance*. A significant body of research has been conducted on efficiently allocating channels to individual cells under this minimum reuse distance constraint [12,21]. There are, in general, two types of channel allocation schemes:

1. *Fixed Channel Allocation (FCA)*: Channels are allocated permanently to each cell for its exclusive use. Users in a cell can be served only by channels belonging to that cell. To maximize reuse efficiency, the same set of channels is reused in cells exactly a

minimum reuse distance apart [14,22]. An attractive feature of FCA lies in its simple implementation, compared to the dynamic channel allocation schemes, described next.

2. *Dynamic Channel Allocation (DCA)*: Channels are not tied to a fixed cell, but allocated dynamically upon each call request. DCA is expected to improve system capacity over FCA by exploiting the traffic fluctuation in different cells. However, in general, implementation complexity is also increased. Specifically, to avoid violating the minimum reuse distance constraint, coordination of channel use within the required reuse distance is necessary. Further, to maximize reuse efficiency, global optimization is typically required. Channel coordination and optimization can be done in a centralized [4,5,24,25] or decentralized fashion [1,2,6,8,13,18], which results in various tradeoffs between performance and complexity.

The use of cellular technology also gives rise to new quality of service (QoS) related problems; i.e., those related to handoffs. A handoff occurs when a mobile user moves from one cell to another. A handoff call is blocked if there is no free channel available in the new cell. The probability of blocking a handoff call is an important QoS measure that needs to be considered in wireless networks. In fact, since blocking a handoff call is less desirable than blocking a new call, specific schemes have to be developed to prioritize handoff calls. The channel reservation scheme is a common prioritization method used in FCA systems [7,17,19,20,23]. Specifically, in each cell a threshold is set, and if the number of channels currently used in the cell is below that threshold, both new and handoff calls are accepted. However, if the number of channels used exceeds this threshold, an incoming new call is blocked and only handoff calls are admitted.

In this paper, we propose a novel localized channel sharing (LCS) scheme to improve system capacity and QoS in wireless cellular networks. While the LCS scheme is motivated by our previous work in [15], it is more general, overcomes the drawbacks of the previous work, and provides significantly better performance. The basic idea in our LCS scheme is to allow channels to be shared between adjacent cells; i.e., channels can be used by any user in either cell, without coordinating with other cells for the use of the same channels. In this way, channel management can be localized within adjacent cells. Further, to avoid global optimization, we propose a new fixed channel assignment scheme that attempts to keep the co-channel reuse distance as close as possible while allowing channel sharing. We show that the LCS scheme can also facilitate handoff processing. Moreover, channels are assigned in such a way that each base-station is responsible to transmit over only a portion of the entire channel set, compared with the case in DCA where each base-station may have to transmit over any channel. Therefore, the physical implementation complexity of the LCS scheme is significantly simplified. The above salient features are especially attractive in micro-cellular networks, where handoff occurs more frequently, and, on the other hand, base-station equipment may be inexpensive and not expected to carry out full hardware and software functionality.

We first describe the main idea of the LCS scheme and channel assignment technique in Section 2.1, and then illustrate our scheme by considering two commonly used cellular configurations: linear (Section 2.2) and 2-D hexagonal (Section 2.3). In Section 3, we present in detail a protocol to implement the LCS scheme. To make the scheme practically useful, we then introduce two refinements in Section 4, which provide useful design parameters to maximize performance under various QoS constraints. Simulation results in Section 5 show that our scheme significantly outperforms the FCA and the reservation handoff scheme over a large range of traffic conditions and a variety of QoS requirements. We also quantitatively analyze the implementation complexity associated with the LCS scheme.

2. Localized Channel Sharing Assignment Scheme

2.1. Meta-cells

Consider a set of cells in a cellular system. Each cell contains a base station, which communicates with mobile users in that cell. Associated with the cellular system is a set of channels, which are to be allocated to the cells. In each cell, an individual channel can be used by only one mobile user in the cell for communication with the base station. The same channel can be reused in two different cells as long as they (the cells) satisfy a *minimum reuse distance requirement*. To elaborate, we assume that we are given a distance measure d, where

$d(X, Y)$ is the distance between cells X and Y. We are also given a parameter Δ that represents the *minimum reuse distance*. Two cells X and Y are said to satisfy the minimum reuse distance requirement if $d(X, Y) \geq \Delta$.

In the conventional scheme for fixed channel assignment, each channel is assigned to cells that are exactly a distance Δ apart. Consequently, a maximum number of channels are assigned to each cell while still satisfying the minimum reuse distance requirement. We refer to this scheme as *tightest fixed channel assignment*. To illustrate the scheme, consider a simple linear cellular system, as shown in Figure 1. In the figure, each cell is allocated a particular subset of channels, and the same channel set is allocated to cells that are exactly a distance of Δ apart.

In cellular systems using the tightest fixed channel assignment scheme, calls in a cell can only use those channels assigned to that cell. Call blocking results if such a channel is not available. For example, if a call arrives at cell B in Figure 1, where all channels are already being used, then this new call is blocked. Channel borrowing is one way to reduce call blocking. Specifically, if at the time the call arrives at cell B, cell A has some idle channels, then cell B may borrow one of the idle channels to serve the new call. To achieve this, however, we need to coordinate the use of channels in the co-channel cells of cell A. For example, to avoid violating the minimum reuse distance requirement, channels that are borrowed by cell B cannot be used in cell A'. Such a global channel coordination is computationally expensive and therefore difficult to implement, and further channel utilization may be decreased at high traffic loads [9].

In our scheme, we attempt to alleviate call blocking by sharing channels between neighboring cells, while localizing the channel coordination. To facilitate the description of our scheme, we first introduce some terminology. A *meta-cell* is a fixed collection of neighboring cells (typically a pair of two adjacent cells). For example, Figure 1 shows a family of meta-cells in a linear cellular system, each comprising a pair of two adjacent cells. Each meta-cell is designated by a pair (X, Y), where X and Y are individual cells called the *component cells* of that meta-cell. For example, in Figure 1, cells A and B are components of meta-cell (A, B). As before, we assume that we have a distance measure for meta-cells (e.g., based on the distance measure d be-

tween cells).

The main idea of our channel assignment scheme is to allocate channels to meta-cells in such a way that a maximum number of channels can be assigned to each meta-cell while any two meta-cells assigned the same channels satisfy the minimum reuse distance requirement, i.e., the distance measure, now with respect to two meta-cells, is no shorter than Δ. For example, Figure 2 (described in more detail later) depicts the channel assignment scheme for the two meta-cell groups in the linear cellular system illustrated previously.

Our channel assignment scheme, done at the meta-cell level, is different from the usual channel assignment scheme which is done at the cell level. In particular, channels are assigned not to individual cells but to meta-cells. A user in a given cell can use any channel that is assigned to a meta-cell to which the given cell belongs, with the usual proviso that only one user can use a given channel within a given meta-cell at a given instance.

Our channel allocation scheme allows channels to be shared between neighboring cells (namely, cells belonging to the same meta-cell). We point out two fundamental advantages:

1. First, the sharing of resources between cells leads to more efficient utilization of the resources. In particular, if a new user arrives at a cell and a channel is not being used in a neighboring cell, the user can use that channel (as long as the neighboring cell belongs to the same meta-cell). This feature potentially reduces the probability of blocking a new call.

2. Second, when a user moves from one cell to another, under certain circumstances it may not be necessary to assign another channel to the user. Specifically, if a user in a given cell moves to a neighboring cell which is part of the same meta-cell, and the user is using a channel that is assigned to that meta-cell, the user can move to the neighboring cell without any risk of handoff blocking. This feature potentially reduces the probability of blocking a handoff call.

Note that relative to the usual fixed channel assignment scheme, in the LCS scheme we need to coordinate between cells in a meta-cell. However, since meta-cells

consist only of neighboring cells, the scheme should be easy to implement.

The idea of sharing channels among users in adjacent cells has also been explored in [3,11], where the authors proposed to exploit the overlapping coverage of adjacent base-stations naturally arising in many cellular systems, and to allow users in overlapping areas to access channels of two base-stations. However, the performance improvement is limited by the physical area of overlapping coverage and the amount of instantaneous traffic in that area. The LCS scheme proposed in this paper creates logical overlapping coverage (meta-cell), and allocates the channels in such a way that all users in a cell can access channels assigned to the meta-cells covering that cell. Thus, it does not rely on a particular physical overlapping coverage in a given system.

Note that if no channels are available for a new call in the meta-cells in which the given call belongs, it may still be possible to satisfy the channel request, provided there is *some* channel available elsewhere. To see how this can be done, consider the linear cellular configuration shown in Figure 1. Suppose a channel is requested at cell A and no channel is available in meta-cell (A, B), but a channel is available in meta-cell (B, C). A user in cell B using a channel assigned to meta-cell (A, B) could then exchange its channel for the unused channel assigned to meta-cell (B, C), thus freeing up its channel, which can then be used to satisfy the channel request at cell A. If, instead, a channel is not available in meta-cell (B, C) but in some other meta-cell further along, a string of exchanges similar to the above can be made to eventually free up a channel in meta-cell (A, B) needed to serve the channel request. Of course, some limit will need to be placed in practice on the maximum number of exchanges allowed to serve any given channel request to limit the complexity of the scheme. Throughout this paper, unless otherwise specified, we assume that such exchanges are not allowed (i.e., for simplicity, we assume that if channels are not available for a cell in the meta cells in which the request occurs, the call is blocked).

In the following, we illustrate our channel assignment scheme for two typical cellular systems: linear and 2-D hexagonal. We develop methods to deploy meta-cells assigned the same channels as tightly as possible, while not violating the minimum reuse distance requirement. We then present a protocol to implement the channel assignment scheme, which maximally exploits the advantages of our framework. We then compare the performance of our scheme with the tightest fixed channel assignment scheme.

2.2. Linear Case

Consider again Figure 1. For this simple linear cellular system, the distance measure $d(X, Y)$ between two cells X and Y is typically given as $d(X, Y) = |c_X - c_Y|$, where c_X and c_Y denote the positions of the centers of cells X and Y, respectively. Suppose that the minimum reuse distance is $\Delta = rL$, where L is the width of a single cell and r is an integer. Cells that are assigned the same set of channels are called *co-channel cells*. Therefore, in the tightest fixed channel assignment scheme, co-channel cells are exactly r cells apart. For example, in Figure 1, cells A and A' are co-channel cells. Let N denote the total number of distinct channels that are available in this linear cellular system. Thus, the total number of distinct channels available for each cell is N/r. The integer r is called the *reuse factor*, being the ratio of the total number of channels in the system to the number of channels allowed to be used in a single cell.

To assign channels to meta-cells, we next define the *distance measure* $d((X, Y), (X', Y'))$ between two meta-cells (X, Y) and (X', Y'). Recall that in our scheme, when a channel is assigned to a meta-cell, it can be used by a mobile user in any cell belonging to that meta-cell. Thus, we have to ensure that the distance measure between any component cells of two meta-cells assigned the same set of channels complies with the minimum reuse distance requirement. Consequently, we define $d((X, Y), (X', Y'))$ as the minimum of the distance measures between the component cells of meta-cells $(X, Y), (X'Y')$, i.e.,

$$d((X, Y), (X', Y')) =$$
$$\min\{d(X, X'), d(X, Y'), d(Y, X'), d(Y, Y')\}. \quad (2.1)$$

For example, in Figure 1, the distance measure between meta-cells (A, B) and (A', B') is given by $(r-1)L$, which is the distance between cells B and A'.

We call meta-cells that are assigned the same set of channels *co-channel meta-cells*. To allocate a maximum number of channels to each meta-cell, co-channel meta-cells have to be deployed as close as possible to maximize channel reuse efficiency. Therefore, we assign the same set of channels to meta-cells that are exactly

the minimum reuse distance apart, i.e., rL in this case. For example, in Figure 2, meta-cells (A, B) and (B', C') are assigned the same set of channels (i.e., they are co-channel meta-cells). Consider a particular channel in this set. Now, when the channel is used simultaneously in meta-cells (A, B) and (B', C'), the shortest possible reuse distance is between cells B and B', which is exactly the minimum reuse distance rL. Thus, the same channel can be independently used in cell A or B and cell B' or C'.

It is easy to show that, using our scheme, each meta-cell is assigned $N/(r + 1)$ distinct channels. In other words, the reuse factor of our channel assignment scheme is

$$r' = r + 1. \tag{2.2}$$

This reuse factor is the same as that of the channel assignment scheme in [15].

The linear case described above is important in its own right. For example, it accurately models cellular configuration on highways and rural areas. However, to handle cellular systems in more metropolitan-type environments, we next discuss our channel assignment in the planar case.

2.3. Planar (2-D) Case

In the planar or 2-D case, the cellular configuration is usually assumed to be hexagonal. This means that the entire area of interest is covered with equal-sized hexagonal cells, as shown in Figure 3. As in the linear case, the distance $d(X, Y)$ between two cells X and Y is typically defined as the distance between their centers. Let N denote the total number of distinct channels available in this hexagonal cellular system. In the tightest fixed channel assignment scheme, co-channel cells are exactly a distance of Δ, the minimum reuse distance, apart. Consequently, each cell is assigned N/R channels, where R is the minimum reuse factor. It has been shown in [22] that R can be determined from Δ by $R = (1/3)(\Delta/\rho)^2$, where ρ is the radius of a single cell. In general, the minimum reuse factor R can be represented by

$$R = p^2 + pq + q^2, \tag{2.3}$$

where p and q are nonnegative integers satisfying $p+q \geq 2$. Without loss of generality, we assume that $q \geq p$ in the following.

As in the linear case, a meta-cell here consists of two adjacent neighboring cells. To allow for channel sharing, we assign channels to meta-cells, as in the linear case, under the minimum reuse distance constraint in terms of meta-cells. For our purpose, the distance measure between two meta-cells is defined in the same way as in Equation (2.1). Again, the main idea of our channel assignment scheme is to deploy co-channel meta-cells as close as possible, under the minimum reuse distance constraint, to maximize channel reuse efficiency. In the remainder of this section, we describe this channel assignment scheme in detail.

Consider an arbitrary cell A_0 in the hexagonal cellular system as shown in Figure 4, and establish a set of coordinates i-j originating at the center of cell A_0, where the two axes form a 60° angle, and the unit distance along the axes is $\sqrt{3}\rho$. Then, the minimum reuse distance Δ is equal to R coordinate units in this set of coordinates. The center of any hexagon Z can be designated by a pair of coordinates (i_Z, j_Z), with i_Z and j_Z integers. Let B_0, C_0, D_0, E_0, F_0, and G_0 denote six hexagons with centers at the coordinates (p, q), $(-q, p + q)$, $(-p - q, p)$, $(-p, -q)$, $(q, -p - q)$, and $(p + q, -p)$, respectively (see Figure 4). Note that their distance to cell A_0 (centered at $(0, 0)$) are equal and given by $p^2 + pq + q^2 = R$ units. In the tightest fixed channel assignment scheme, cells B_0, C_0, D_0, E_0, F_0, and G_0 are assigned the same set of channels as cell A_0.

Let A_1 be the adjacent right neighboring cell of A_0 along the i-axis as shown in Figure 4, i.e., $(i_{A_1}, j_{A_1}) = (i_{A_0} + 1, j_{A_0}) = (1, 0)$. We next focus on meta-cell (A_0, A_1) as the *reference meta-cell*. Note that in the 2-D case, meta-cells may have three distinct orientations (the orientation of a meta-cell is the directional relationship between its two component cells). Each meta-cell may have six neighboring co-channel meta-cells. Consequently, there are many different ways to deploy co-channel meta-cells, including irregular (non-repetitive) deployment patterns. For the sake of simplicity and regularity, in the following we restrict ourselves to deployment methods in which all co-channel meta-cells are of the same orientation. In other words, for any co-channel meta-cell of (A_0, A_1) of interest, two components are adjacent along the i-axis. Therefore, we can identify any co-channel meta-cell of reference meta-cell (A_0, A_1) by its left component (the component cell that

is positioned in the left side along the i-axis).

It turns out that for different values of p and q, we need different methods to deploy co-channel meta-cells of reference meta-cell (A_0, A_1), depending on whether $p+1 \geq q$. For simplicity, we assume that $p+1 \geq q$. (The case where $p + 1 < q$ is more involved and is therefore omitted in the interest of space; we refer to our technical report for the details [16]). The values of R within this category are $3, 7, 12, 19$, etc. It can be shown that in this case, as illustrated in Figure 5, the meta-cells whose left components are respectively B_1, C_0, D_{-1}, E_{-1}, F_0, and G_1, can be deployed as co-channel meta-cells of reference meta-cell (A_0, A_1), where the centers of cells B_1, D_{-1}, E_{-1}, and G_1 are given respectively as follows: $(i_{B_1}, j_{B_1}) = (p + 1, q)$, $(i_{D_{-1}}, j_{D_{-1}}) = (-p - q - 1, p)$, $(i_{E_{-1}}, j_{E_{-1}}) = (-p - 1, -q)$, and $(i_{G_1}, j_{G_1}) = (p + q + 1, -p)$. Furthermore, we have shown that when assigning channels according to this co-channel meta-cell deployment, the channel reuse factor is

$$R' = R + p + q. \tag{2.4}$$

The detailed proofs and further discussions are provided in [16].

3. Channel Sharing Protocol

In the previous section, we described our channel assignment scheme, in which channels are assigned to meta-cells instead of cells. Channels assigned to a meta-cell can be shared by any of its component cells. We next develop a channel sharing protocol to exploit this sharing feature of our scheme. Specifically, whenever a new call arrives at a given cell, the protocol determines whether or not the call can be accommodated, and which channel is to be used to serve the call. Here we do not distinguish between new and handoff call requests. We will explicitly address the handoff problem later in Section 4.2.

3.1. Protocol Description

To describe our channel sharing protocol, we focus our attention on a particular (arbitrary) cell, which we call the *local cell*. Recall from the previous section that using our channel assignment scheme, each cell in the cellular network is always covered by several overlapping meta-cells, called the *covering meta-cells* of that cell. For example, in the linear case, each cell is covered by two meta-cells, while in the 2-D case with a hexagonal configuration, each cell is covered by six meta-cells. We call channels that are assigned to the covering meta-cells of the local cell the *accessible channels*, since users in the local cell may have access to those channels. The entity that manages those accessible channels is called the *channel controller*, which resides in the base-station of the local cell. The channel controller only needs to exchange channel usage information with channel controllers of adjacent cells, as will be described in this section. This exchange of information can be done in a variety of ways, such as via an out-of-band signaling channel (or a wired channel) that connects the base-stations of the local cell and its adjacent cells.

In our channel assignment scheme, each accessible channel is shared between the local cell and one of its adjacent cells. Therefore, for each channel at any given instance, either the local cell or one of the adjacent cells can use the channel. In other words, at any given instance, not all the accessible channels can be used by the local cell. Those channels that can be used by the local cell are called *enabled channels*. To coordinate the use of accessible channels between the local cell and the corresponding sharing cells, the local cell maintains a look-up table, in which each accessible channel occupies one entry consisting of the following two fields. The first field indicates the current state of an associated channel. The state in the first field may be "DISABLED", "IDLE", or "BUSY", described as follows. An accessible channel labeled "DISABLED" is *not enabled* in the local cell. This indicates that the channel is concurrently enabled in the sharing cell associated with that channel. The local cell can use only those accessible channels labeled "BUSY" or "IDLE" (i.e., these channels are the enabled channels in the local cell). In this case the labels further indicate whether channels are currently occupied by mobile users in the local cell. The second field simply records the names of the sharing cells associated with the accessible channels.

Initially, for each accessible channel, the channel controller may arbitrarily set its state in the look-up table of the local cell "IDLE" or "DISABLED"; concurrently, the state in the look-up table of the sharing cell associated with that accessible channel must be inversely set "DISABLED" or "IDLE", respectively.

Our protocol can be described in three main parts, corresponding to three different possible scenarios: *ar-*

rival of a call, sharing a request from a sharing cell, and *departure of a call.*

3.1.1. Arrival of a call

The protocol for handling the arrival of a call is shown in Figure 6. When a call arrives, the channel controller checks if there are any accessible channels labeled "IDLE" in the look-up table of the local cell. If there are, the arriving call is accepted and assigned an idle channel, and the state of that channel is then changed to "BUSY." Otherwise, the channel controller attempts to obtain an idle accessible channel from some sharing cell, as follows. The channel controller first looks up all accessible channels currently labeled "DISABLED" in the local cell and obtains a list of the sharing cells associated with those "DISABLED" accessible channels. The channel controller then chooses one of the sharing cells on this list and sends it a *sharing request.* The sharing cell, upon receiving the sharing request, then executes the procedure in Section 3.1.2. If the sharing request is granted, the channel controller accepts the arriving call by assigning the accessible channel specified in the return message from the sharing cell, and setting the state of that channel "BUSY." If the request is denied, the channel controller proceeds to send another sharing request to one of the remaining sharing cells on the list. The process is continued until the sharing request is accepted or denied by all sharing cells on the list, in which case the call is rejected (blocked). The way to choose one of the sharing cells for directing a sharing request may be totally random, as done later in this paper for simplicity, or may follow some heuristic rules, such as starting from the one associated with the largest number of accessible channels currently labeled "DISABLED" in the local cell.

3.1.2. Sharing request from a sharing cell

The protocol for handling the sharing request from a sharing cell is illustrated in Figure 7. When a sharing request is received from a sharing cell, the channel controller first checks whether there is any accessible channel U, associated with that sharing cell, currently labeled "IDLE" in the local cell. If so, the channel controller grants the sharing request by sending back the identification number of channel U in the return message, and setting channel U "DISABLED" in the local look-up table. Otherwise, the channel controller

attempts to obtain such an idle channel U by *swapping channels* as follows. The channel controller checks whether there is any accessible channel V currently labeled "IDLE" in the local cell. If so, the channel controller finds a user currently using an accessible channel U associated with the sharing cell (we can always find such a user because, from Section 3.1.1, a sharing request is directed to the local cell only if in the sharing cell there are sharable channels labeled "DISABLED", which must be either "BUSY" or "IDLE" in the local cell). That user then releases channel U and grabs channel V, so that the channel controller can grant the sharing request by returning the identification number of channel U and setting channel U as "DISABLED" in the local look-up table. If no accessible channels are in the "IDLE" state, the channel controller rejects the sharing request, for simplicity, as illustrated in Figure 7.

For example, suppose that in the linear cellular system shown in Figure 1, cell A, after receiving a call request, sends a sharing request to cell B. The channel controller in cell B first checks whether there is any idle channel U of set I in cell B (see Figure 2). If so, channel U is labeled "DISABLED" in cell B and consequently it can be assigned to that call arrival and labeled "BUSY" in cell A. Otherwise, the channel controller then checks whether there is any idle channel V in cell B, which in this case must belong to channel set II. If so, the channel controller lets a user, who is currently using a channel U of set I in cell B, grab channel V, so that channel U can be released to cell A. Otherwise, the sharing request is rejected, according to the protocol of Figure 7.

It should be pointed out, however, that even in the above case, rejecting a sharing request may not be necessary. Instead, the channel controller may further send another sharing request to the sharing cells of the local cell, the same way as in Section 3.1.1, so that the channel controller may obtain an idle accessible channel and grant the original sharing request. This process may be repeated from cell to cell (i.e., sharing requests are propagated from one cell to another) until one of the sharing requests can be granted. We will quantitatively investigate the performance improvement when applying this sharing propagation strategy in Section 5.3.

3.1.3. Departure of a call

Figure 8 depicts the protocol to handle the scenario when a call leaves the local cell. This scenario arises when a call terminates in the local cell, or when a call migrates to another cell. In this case, the channel controller simply labels the associated channel "IDLE."

Consider again the example in the last section. When channel U, which was granted from cell B to cell A by sharing, is released, it remains "IDLE" and is not immediately returned to cell B (unless there is a sharing request from cell B).

3.2. Salient Features of the Channel Sharing Protocol

The following are some of the important features of our channel sharing protocol:

1. *Channel sharing within a meta-cell is localized* between two adjacent cells and can therefore be done in a decentralized fashion. No global coordination is necessary in our protocol, thus facilitating implementation. At the same time, our channel assignment scheme ensures that there is no co-channel interference due to channel movement. The major computational effort in the local cell includes communication with the sharing cells, channel swappings, and simple table look-ups. We will investigate the complexity of our protocol later in Section 5.1 by estimating the expected number of inter-cell communication and channel swappings for each call arrival.

2. *Channel utilization is improved* because channels are assigned to meta-cells instead of to individual cells. Clearly, an idle channel can be accessed by calls in either of its component cells, thus effectively reducing the fraction of idle periods of channels. Consequently, *the blocking of handoff requests occurs relatively rarely* in our protocol because it requires all three of the following conditions to be simultaneously true:

(a) All sharable channels between the handoff originating cell and the destination cell are already occupied in the destination cell.

(b) All channels in the destination cell are occupied.

(c) In each of the adjacent cells of the destination cell, either there are no idle channels, or there are no channels sharable with the destination cell.

For example, suppose a user in the local cell desires to move into a neighboring (destination) cell. If there is a channel in the local cell (whether busy or idle) that can be shared with the destination cell, then the user can move to the neighboring cell without experiencing handoff blocking. In this case, the first condition above does not hold.

3. *Handoff processing may be easier* when using our protocol. A special case of the example scenario pointed out above is when a user moves from one cell to another, and the user is using a sharable channel between the two cells. In this case, not only can the user change cells with no risk of handoff blocking, but the processing of the handoff can also be simplified by continuing the service using the same channel during handoff. Moreover, if we model and predict the mobility of a particular user, we can further reduce the incidence of handoff blocking by reassigning (if necessary) to the user a channel that can be shared with the next destination cell. The benefit here is that we effectively have a mechanism for processing handoffs by anticipating the movement of a mobile user, and the time available to do this processing is the time a user spends in a given cell. This is in contrast to the potentially much shorter time available to conventionally process a handoff call, typically only when a user is at the boundary between two cells. This feature is especially important for cellular systems with small-sized cells, such as micro-cellular systems.

4. Refinements

In the previous section, we presented the basic assignment scheme and protocol for our channel sharing strategy. To make our scheme practically useful, we next discuss two refinements.

4.1. Combined Scheme

It is instructive to compare the effective channel capacity using the LCS scheme and the tightest fixed channel assignment scheme. In our scheme, the maximum possible channel capacity of each cell is clearly just the total number of distinct accessible channels for each cell. As we pointed out above, in an individual cell, the number of accessible channels in our scheme is generally larger than that of the fixed scheme. Note that, however, this number is an upper bound on the effective channel capacity since it assumes that the statistical sharing advantage can fully be exploited. On the other hand, if we totally ignore the statistical sharing advan-

tage, we may then obtain a lower bound for the channel capacity. To be specific, we equally distribute channels that are assigned to each meta-cell into two component cells and then count the total number of distinct channels now available for each cell. For example, the lower bound capacity in the linear case is $\frac{N}{r'}$ channels. Hence, the effective channel capacity using the LCS scheme is bounded by these two extreme scenarios and depends on the extent to which the statistical sharing advantage is actually obtained.

Next, we present a combined scheme that attempts to maximize the effective channel capacity for each cell. Specifically, we divide all the N channels into two distinct groups of size N_1 and N_2 such that

$$N = N_1 + N_2. \qquad (4.1)$$

The first group of N_1 channels is assigned to cells using the tightest fixed channel assignment scheme and thus cannot be shared between adjacent cells. The remaining group of N_2 channels, however, is assigned to meta-cells according to our channel sharing assignment scheme, and can be shared within meta-cells, the same as in the previous sections.

The combined scheme above defines a family of channel assignments that encompasses both the fixed and the basic LCS schemes. At one end of the spectrum, where $N_2 = N$ (corresponding to the basic LCS scheme), the maximum number of channels are assigned to meta-cells. In this case, every channel can be shared by two adjacent cells. Thus, the upper bound of the effective channel capacity is largest, but the lower bound is smallest at the same time. With decreasing N_2, the upper bound is decreased while the lower bound is increased, until $N_2 = 0$ (corresponding to the tightest fixed channel assignment) where there is no channel sharing. In this case, the upper and lower bounds coincide and are equal to the effective channel capacity.

Varying N_2 allows us to maximize the effective channel capacity. Specifically, the parameter N_2 enables us to trade off the potential advantage from statistical sharing with a reduction in the average number of channels for each cell. The larger the value of N_2 in the combined scheme, the more the gain we expect from statistical sharing, but at the same time the higher the price we pay by reducing the average number of channels for each cell. The reduction in this average number, relative to its maximum value when $N_2 = 0$, is given by $d = \frac{N_2}{r} - \frac{N_2}{r'} = \frac{N_2}{r(r+1)}$ in the linear case, or $d = \frac{N_2}{R} - \frac{N_2}{R'} = \frac{N_2(R'-R)}{RR'}$ in the 2-D case, while the number of sharable channels for each cell is $s = \frac{N_2}{r'}$ in the linear case, or $s = \frac{N_2}{R'}$ in the 2-D case. Further, s and d are related by $\frac{s}{d} = r$ in the linear case, or $\frac{s}{d} = \frac{R}{R'-R}$ in the 2-D case. Clearly, for the same price we pay in the combined scheme in terms of d, the number of sharable channels s increases with increasing r in the linear case or $\frac{R}{R'-R}$ in the 2-D case.

Figure 9 illustrates the partitioning of accessible channels in a cell into the two groups described above. The number of accessible channels in each of these groups is N_1/R and $2N_2/R'$, respectively (in the 2-D case). Note that the number of enabled channels in the first (N_1/R) group is fixed, whereas the number of enabled channels in the second group can vary between 0 and $2N_2/R'$.

4.2. Threshold Handoff Scheme

In our basic LCS scheme, we do not distinguish between new and handoff call arrivals. However, studies have shown that one of the most important user concerns is that service not be cut off during an on-going call. Therefore, blocking a handoff arrival is even less desirable than blocking a new arrival. Various schemes have been proposed to prioritize handoff calls (e.g., [10]). The *threshold* scheme is particularly well known. Specifically, a number of channels can be reserved solely for the use of handoffs, allowing both handoff and new calls to compete for the remaining channels.

To illustrate the main idea underlying the threshold scheme, we now describe a popular scheme called *channel reservation*. Consider the tightest fixed channel assignment. A threshold K is set in each cell ($K \leq N/r$ for the linear case and $K \leq N/R$ for the 2-D case). If the number of channels currently used in the cell is below K, both new and handoff calls are accepted. Otherwise, if the number of channels used exceeds this threshold, incoming new calls are blocked and only handoff calls are admitted.

To prioritize handoff calls in our LCS scheme, we apply a threshold idea similar to the channel reservation scheme above. Our threshold scheme is composed of two parts, as described next. Note that the threshold restrictions apply only to new call requests.

4.2.1. K_1 threshold

The first part of our threshold scheme is the same as the channel reservation scheme. Specifically, a new call arriving at a cell will be blocked if the number of current users in that cell exceeds a threshold K_1, with $K_1 \leq \frac{N_1}{r} + \frac{2N_2}{r'}$ in the linear case or $K_1 \leq \frac{N_1}{R} + \frac{2N_2}{R'}$ in the 2-D case. As in the case of the channel reservation scheme (for the tightest fixed channel assignment), here also we set the threshold K_1 to avoid overall excessive use of accessible channels by new calls. For example, in some scenarios, accessible channels may be accumulated in one cell because of channel movement. In this case, it is desirable to limit excessive access to those channels by new calls, waiting instead for potential sharing requests from sharing cells. Note that the K_1 threshold takes effect only if the number of enabled channels (as described in Section 3.1) is greater than K_1 (otherwise, we apply another threshold, K_2, described in the next section).

Figure 10 provides an illustration of the K_1 threshold scheme. In the figure, we assume that the number of enabled channels is greater than K_1. As illustrated, if the number of channels being used does not exceed K_1, then new calls are accepted; otherwise, they are blocked.

Note that to achieve a given quality of service requirement for handoff, the threshold K_1 in our scheme may generally be chosen higher than K in the channel reservation scheme because now handoff requests have access to more channel capacity due to sharing. In other words, we need to reserve fewer channels *a priori* for handoff calls. This helps increase the efficiency of our handoff scheme compared to the conventional reservation scheme, as will be demonstrated in Section 5.2.

4.2.2. K_2 threshold

If the new call is not blocked by the first part of the threshold scheme, it is accepted if there are idle channels in the cell. Otherwise, if there are no idle channels (from which we infer that the number of enabled channels is less than or equal to K_1), we then attempt to obtain an accessible channel from sharing cells, as described in Section 3.1. The second part of the threshold scheme is now applied to limit the sharing accessibility associated with individual sharing cells. Specifically, we first set the value of a second threshold K_2, where $K_2 \leq \frac{N_2}{r'}$ in the linear case, or $K_2 \leq \frac{N_2}{R'}$ in the 2-D case. Then,

in the protocol described in subsection 3.1.1, we send out sharing requests only to the adjacent cells that have fewer than K_2 sharable channels currently being used in the local cell. In this way we prevent new calls from excessively using up sharable channels associated with any particular sharing cell, and thus prioritize potential handoffs from that sharing cell.

Figure 11 illustrates the K_2 threshold scheme. Note that the number of enabled channels here is not more than K_1 (for otherwise the K_2 threshold does not take effect). In the figure, we use the term *rich neighbor* to denote a neighboring cell that has fewer than K_2 sharable channels *in the local cell*. If the neighboring cell has more than or equal to K_2 channels *in the local cell*, we use the term *poor neighbor*. In other words, we send out sharing requests for new calls only to rich neighbors.

5. Simulation Results

In this section, we provide simulation results to compare the performance of our LCS scheme with the tightest fixed channel assignment scheme. We consider the following two scenarios. In the first scenario, we do not distinguish new calls from handoff calls in the channel assignment. In this case, the quality of service (QoS) measure that we are interested in is P_b, the blocking probability of a call arrival into a cell. In the second scenario, we investigate the performance of our LCS scheme with handoff prioritization, as well as the channel reservation scheme based on the tightest fixed channel assignment. Here, we distinguish between the blocking of new and handoff calls. The QoS measures we are interested in this case are: P_{bN}, the blocking probability of new calls, and P_{bH}, the blocking probability of handoff calls. We conclude the section by showing an example of further improvements that may be obtained if sharing requests are allowed to propagate across more than one cell.

We investigate both the linear and 2-D hexagonal cases by simulation. Our simulation model for the linear cellular system consists of 30 cells, where each cell has two adjacent cells. The boundary cells on the two sides are then connected to each other to avoid the "edge" effect at the boundaries. To model the 2-D cellular system, we use a 36-cell configuration, with each cell having six adjacent cells. Again, the cells on the boundary

of one side of the configuration are connected to the cells on the boundary of the other side. For both the linear and 2-D cases, the call traffic is assumed to be symmetrically distributed over all the cells. The simulation is discrete-event driven. There are three types of events: new call request arrival, handoff request arrival, and call termination. New calls are assumed to arrive at each cell according to a Poisson process with rate λ_n. The time until a call terminates is assumed to be exponentially distributed with mean $1/\mu$. The time a user spends in a cell before making a handoff request to go to another cell is assumed to be exponentially distributed with mean $1/\lambda_H$. In our simulation model, users in a cell may direct a handoff request to each of the adjacent cells with equal probability. The blocking probabilities P_{bN} and P_{bH} are estimated as follows:

$$P_{bN} \approx \frac{\text{number of new call requests rejected}}{\text{number of new call requests generated}} \quad (5.1)$$

$$P_{bH} \approx \frac{\text{number of unsuccessful handoffs}}{\text{number of handoff requests generated}} \quad (5.2)$$

To estimate P_{bN} and P_{bH}, we count the events of new call request generations, handoff request generations, new call requests rejected, and handoff requests rejected. Since we are interested in the performance of a typical cell, the statistics obtained are averaged over all cells.

5.1. Channel Allocation without Handoff

In this study, we do not consider handoffs. Further, in our simulation, users that arrive in each cell do not migrate to other cells. This is typical of assumptions made in the literature (e.g., in [9]).

Maximum call arrival rate

We compare the maximum call arrival rate λ_n that can be admitted by our LCS scheme and the tightest fixed channel assignment scheme, respectively, for various blocking probabilities P_b. More precisely, we define the following optimization problem for the LCS scheme:

$$\underset{\lambda_n, N_2}{\text{maximize}} \; \lambda_n$$
$$\text{subject to } P_b \leq B_{max} \quad (5.3)$$

The constraint B_{max} used in our simulation varies between 3×10^{-3} and 5×10^{-2} and the corresponding maximum value of λ_n is obtained by tuning the parameters N_2 and λ_n. We define a similar optimiza-

tion problem for the tightest fixed channel allocation scheme: $\text{maximize}_{\lambda_n} \; \lambda_n$, subject to $P_b \leq B_{max}$. In Figure 12, we plot the optimal values of λ_n versus B_{max} for both schemes for the linear case with $r = 2$ and $r = 4$. In Figure 13, we plot the optimal values of λ_n versus B_{max} for both schemes for the 2-D case with $R = 3, 7, 12,$ and 19. For both figures, we use $\mu = 1$. To make our results comparable for different minimum reuse factors, we keep $N/r = 15$ for all the curves in Figure 12. Thus, $N = 30$ when $r = 2$, and $N = 60$ when $r = 4$. Similarly in Figure 13, we set $N/R = 15$ for all R.

From Figures 12 and 13, we observe that for any P_b constraint, the LCS scheme allows a higher call rate than the tightest fixed scheme. For a typical constraint of $P_b \leq 10^{-2}$, our scheme can admit approximately 20% more calls into the network than the fixed scheme with $r = 4$ in the linear case or with $R = 7$ in the 2-D case. Note that in the 2-D case, even when the minimum possible reuse factor $R = 3$, our scheme outperforms the fixed scheme more than 10%. Of course, when the reuse factor becomes larger, for example for $R = 19$, the improvement is about 30%. Also, as shown in the figures, for lower blocking probability constraints, the improvement is even greater.

An observation from Figures 12 and 13 is that the improvement of the LCS scheme becomes more significant as the value of reuse factor increases. This can be explained as follows. First note that in Figures 12 and 13, we keep N/r and N/R fixed, respectively. In the tightest fixed channel allocation scheme, as long as we keep N/r or N/R (the number of channels allocated per cell) fixed, the performance metrics remain unchanged. This is why in each figure, for the tightest fixed allocation scheme, we only have one curve for different values of r (or R), since N/r (or N/R) is kept constant. However, when we increase r (and correspondingly increase N), in the case of the sharing scheme (for the linear case), the price we need to pay for channel mobility $N/r - N/(r+1) = 1/(r(r+1))$ decreases. Hence, the improvement of our sharing scheme over the FCA scheme is also higher.

Another interesting observation in our simulation is that for any given value of R, the optimal tuning parameter N_2 takes on only a few values. For example, in Figure 13, $N_2 = 15, 50, 96$ ($\frac{N_2}{R} = 3, 5, 6$), for the curves of $R = 3, 7, 12$, respectively. That is, the optimal N_2 actually remains constant for each of the corresponding

curves. When $R = 19$, $N_2 = 192$ ($\frac{N_2}{R'} = 8$) for B_{max} less than 2.44×10^{-2}, and $N_2 = 96$ ($\frac{N_2}{R'} = 4$) for the remaining portion of the curve. Moreover, if we use $N_2 = 192$ for the entire curve, the performance degradation, in terms of λ_n for a given B_{max}, is less than 2%. In fact, we have observed that the performance metric is insensitive to moderate variations in N_2 around the optimal value. For simplicity, we will use a fixed value of N_2 for each individual curve in the next section.

We next investigate the protocol complexity for those optimum combined LCS schemes obtained for Figures 12 and 13. We first estimate the expected number of inter-cell communications used to serve a call arrival, by dividing the total number of sharing requests that have been submitted in simulation to the total number of call arrivals. Here we count all sharing request signals, including those that are not granted. We find that the expected number of sharing requests per call arrival does not exceed 0.2 in all the cases shown in Figure 12, or 0.6 for those in Figure 13. There is a difference between the linear and 2-D cases because, in the latter, each cell has more adjacent cells, and thus more sharing requests have to be sent. Note that the expected number of sharing requests per call arrival depends on both the traffic load and the combined LCS scheme (N_1, N_2). For a given N_1, N_2 setting, it increases with the traffic load.

We next estimate the expected number of intra-cell channel swappings needed to serve a call arrival, by dividing the total number of channel swappings observed in simulation to the total number of call arrivals. We find that the maximum number of channel swappings per call arrival needed is less than 0.04 for the combined LCS schemes in Figure 12, or less than 0.25 for those in Figure 13. These results suggest that the computational overhead to implement our protocol is not significant.

5.2. Channel Allocation with Handoff

In this study, we evaluate the performance of our LCS scheme for the handoff problem by taking into account handoffs in the simulation traffic model. To systematically compare our handoff scheme with the channel reservation scheme, we investigate three design problems. Note that in reality the parameters N_2, K_1, and K_2 in the LCS scheme can only be optimized according to one design criterion, and that generally the

optimal parameters for one problem may not be optimal for another. The reason that we provide comparisons for three optimization problems is to evaluate our scheme under a variety of design criteria. In the interest of saving space, we provide only simulation results for the 2-D case.

Minimum blocking probability of new calls

Here we provide plots of P_{bN} under varying load conditions for the LCS and reservation schemes. The performance measures depend on the parameters N_2, K_1, and K_2 in the LCS scheme, and the parameter K in the reservation scheme. To meaningfully compare our combined scheme with the reservation scheme, we determine the optimal values of P_{bN} for the two schemes, given a constraint on P_{bH}. Here, for simplicity, we use a fixed value of N_2 in the LCS scheme for a given reuse factor. Therefore, in the LCS scheme, to appropriately choose K_1 and K_2, we consider the following optimization problem:

$$\underset{K_1, K_2}{\text{minimize}} \; P_{bN}$$
$$\text{subject to } P_{bH} \leq H_{max} \qquad (5.4)$$

where H_{max} denotes a prespecified maximum level for P_{bH}. A similar optimization problem can be defined for the reservation scheme, where the decision variables are now replaced with the threshold parameter K. For a fair comparison of the LCS scheme with the reservation scheme, we calculate the optimal values of P_{bN} for the two schemes, given the same H_{max}.

Figure 14 shows plots of the optimal values of P_{bN} for the reservation and LCS schemes under varying λ_n. For this figure we use the following parameters: $\lambda_H = 5$, $\mu = 1$, $N/R = 15$, (for example $N = 45$ when $R = 3$), and $N_2 = 30, 90, 144, 264$, for $R = 3, 7, 12, 19$, respectively. The call handoff blocking probability P_{bH} is constrained by $H_{max} = 10^{-4}$, a typical value. The new arrival rate λ_n ranges from 6 to 11. From the figure, we can see that these traffic loads are, in fact, quite heavy for the channel reservation scheme, because in order to meet the QoS constraint of P_{bH}, the threshold K must be set sufficiently low, thus resulting in fairly high new call blocking probability ($P_{bN} > 10^{-1}$ for the whole range of λ_n in the figure). Figure 14 shows that the combined LCS scheme achieves uniformly lower values of P_{bN} than the reservation scheme. We also notice that at low traffic load, there is virtually no new call

blocking for the LCS scheme. To provide some insight into the optimization, in Table 1 we list the set of K_1 and K_2 data that were used to generate the curve for $R = 7$ in Figure 14.

Note that in Figure 14, some of the curves for the LCS scheme do not start from $\lambda_n = 6$. The reason is that when λ_n is low, P_{bN} is too small to be estimated accurately in our simulation. The same applies to Figure 15.

Maximum call arrival rate

In this experiment, we compare the maximum new call arrival rate λ_n that can be admitted by the LCS and the reservation schemes for various handoff blocking probabilities P_{bH}. More precisely, we define the following optimization problem for the LCS scheme:

$$\underset{K_1,K_2,\lambda_n}{\text{maximize}} \ \lambda_n$$
$$\text{subject to } P_{bN} \leq N_{max} \qquad (5.5)$$
$$P_{bH} = H$$

Here, the constraint H for P_{bH} is varied between 10^{-6} and 10^{-2} and the corresponding maximum value of λ_n is obtained. Again, a similar optimization problem is defined for the reservation scheme by replacing K_1, and K_2 by K. In Figure 15, we plot the optimal values of λ_n versus P_{bH} for the LCS scheme and the reservation scheme scheme with $R = 3$, 7, 12, and 19. For this figure we use the following parameters: $\lambda_H = 5$, $\mu = 1$, $N/R = 15$, $N_{max} = 10^{-2}$, and $N_2 = 30, 70, 144, 264$, for $R = 3, 7, 12, 19$, respectively. We observe that the LCS scheme allows a higher new call rate than the reservation scheme over all values of P_{bH}. For a typical value of $P_{bH} = 10^{-4}$, the LCS scheme with $R = 19$ can admit approximately 64% more calls into the network than the reservation scheme. For the same P_{bH} constraint, the performance improvement for the LCS scheme is about 50% when $R = 7$, a typical reuse factor value, and is 20% when $R = 3$, the minimum possible value. As is also shown in the figure, for lower handoff probability constraints, this difference is even larger. Improving the admissible arrival rate results in increased revenue for the network provider.

Maximum utilization

From the point of view of a network provider, a useful parameter of interest is the *normalized channel utiliza-* *tion*, γ, defined as

$$\gamma = \frac{\text{average number of users in one cell}}{\text{total number of available channels in one cell}}, \qquad (5.6)$$

where the total number of available channels in one cell is N/R. The parameter γ is directly related to the revenue of a cellular network because it incorporates both new and handoff calls.

To plot the values of γ under varying loads for the LCS scheme, we define the optimization problem

$$\underset{K_1,K_2}{\text{maximize}} \ \gamma$$
$$\text{subject to } P_{bH} \leq H_{max}. \qquad (5.7)$$

Once again, we define a similar optimization problem for the reservation scheme by replacing the decisions variables by K.

In Figure 16, we plot values of γ under varying λ_n. The parameters used for this figure are: $\lambda_H = 5$, $\mu = 1$, $N/R = 15$, $H_{max} = 10^{-4}$, and $N_2 = 30, 90, 144, 264$, for $R = 3, 7, 12, 19$, respectively. The LCS scheme achieves uniformly higher values of γ under various loads. The difference between the combined and reservation schemes is most apparent at high loads. At such loads, a low value of K is required in the reservation scheme to maintain the QoS constraint on P_{bH}, thus resulting in a low value of γ. On the other hand, due to channel sharing, the threshold to maintain the QoS constraint on P_{bH} is not as low. When $R = 19$, the channel utilization for the LCS scheme at high loads is over 64% more than the reservation scheme. The performance improvement for the LCS scheme is about 33% for $R = 7$, a typical reuse factor value, and is 22% for $R = 3$, the minimum possible value.

5.3. Sharing requests across more than one cell

So far, in all of the simulation results shown (Sections 5.1 and 5.2), when a sharing request is received from an adjacent cell, if the request cannot be granted, it is simply rejected. In other words the sharing request is allowed to *propagate only one step*. However, as we have discussed earlier in Sections 2.1 and 3.1.2, to further exploit the advantage of channel sharing, we could allow sharing requests to propagate across more than one cell. Clearly, increasing the number of propagation steps will improve performance at the cost of increased complexity (due to more sharing requests that need to be processed, etc.).

We next quantitatively investigate the performance improvement as more propagation steps are allowed for sharing. For simplicity, we consider the case without handoffs, as in Section 5.1. We define the following optimization problem for the LCS scheme, similarly to that in Section 5.1 (Equation (5.3)):

$$\underset{\lambda_n, N_2}{\text{maximize}} \ \lambda_n$$
$$\text{subject to } P_b \leq B_{max} \tag{5.8}$$
$$\text{number of propagation steps} \leq S_{max}$$

For illustration, we show the results for the linear case with $r = 4$ in Figure 17. For this figure, we use the following parameters: $B_{max} = 10^{-2}$, $\mu = 1$, $N/r = 15$. The constraint S_{max} is allowed to vary from 0 to 12 in our simulation, where $S_{max} = 0$ represents the case when no sharing is allowed, i.e., the fixed channel assignment scheme. In Figure 17, we plot the optimal values of λ_n versus S_{max}. As expected, for a given constraint of blocking probability, the maximum admissible arrival rate increases as more propagation steps are allowed. The improvement is most significant when the value of S_{max} is small, but it reaches a point of diminishing returns around $S_{max} = 6$. Hence, depending on the allowable implementation complexity and latency, one could conceive of improving the performance by increasing the maximum allowable propagation steps, although only a small increase would be justified.

6. Conclusion

We have presented a novel LCS scheme to improve system capacity and QoS in wireless cellular systems. Our basic idea is to allow channels to be shared between adjacent cells without co-channel coordination with other cells. For this purpose, we introduce the concept of meta-cells to facilitate localized channel management. Further, to maximize channel reuse efficiency, we develop a channel assignment method based on the distance measure between meta-cells. We then illustrate our channel assignment for both the linear and 2-D hexagonal cellular models. In general, the LCS scheme leads to channel access in a statistical multiplexed fashion, but at the expense of some nominal capacity. An attractive feature of the LCS scheme is that it does not require complex power control techniques, global channel coordination, or on-line optimization, which simplifies its implementation.

To make the LCS scheme practically useful, we then propose two important refinements, which provide useful design parameters to maximize system performance under various QoS constraints. Via simulation, we compare the LCS scheme with the fixed channel assignment scheme (for channel assignment considerations) and the channel reservation scheme (for handoff considerations). Simulation results show that our scheme significantly improves system capacity over a large range of traffic conditions and a variety of QoS requirements, in some cases resulting in over 60% better network utilization than the channel reservation scheme (in the 2-D hexagonal case).

References

[1] Y. Akaiwa and H. Andoh, "Channel segregation - a self organized dynamic allocation method: application to TDMA/FDMA microcellular system," *IEEE Journal On Selected Areas In Communications*, vol. 11, pp. 949–954, 1993.

[2] M.-L. Cheng and J.-I. Chuang, "Performance evaluation of distributed measurement-based dynamic channel assignment in local wireless communications," *IEEE Journal On Selected Areas In Communications*, vol. 14, pp. 698–710, May 1996.

[3] T.-P. Chu and S. Rappaport, "Generalized fixed channel assignment in microcellular communication system," *IEEE Transactions on Vehicle Technology*, vol. 43, pp. 713–721, August 1994.

[4] D. Cox and D. Reudink, "Dynamic channel assignment in high-capacity mobile communication systems," *Bell System Technical Journal*, vol. 50, pp. 1833–1857, 1971.

[5] D. Cox and D. Reudink, "Dynamic channel assignment in two dimension large-scale mobile radio systems," *Bell System Technical Journal*, vol. 51, pp. 1611–1628, 1972.

[6] D. Goodman, J. Grandhi, and A. Sudheer, "Distributed channel assignment schemes," in *Proc. IEEE Vehicle Technology Conference*, pp. 532–535, 1993.

[7] D. Hong and S. Rappaport, "Traffic model and performance analysis for cellular mobile radio telephone systems with prioritized and non-prioritized handoff procedures," *IEEE Transactions on Vehicle Technology*, vol. 35, pp. 77–92, 1986.

[8] C.-L. I and P.-H. Chao, "Local packing - distributed dynamic channel allocation at cellular base station," in *Proc. IEEE GLOBECOM*, 1993.

[9] H. Jiang and S. Rappaport, "CBWL: A new channel assignment and sharing method for cellular communication systems," *IEEE Transactions on Vehicle Technology*, vol. 43, pp. 313–322, May 1994.

[10] H. Jiang and S. Rappaport, "Handoff analysis for CBWL schemes in cellular communications," in *Proc. IEEE In-*

ternational Conference on Universal Personal Communications, ICUPC'94, pp. 496–500, 1994.

[11] H. Jiang and S. Rappaport, "Hybrid CBWL and directed retry in cellular communications," in Proc. IEEE Vehicle Technology Conference, pp. 716–720, 1996.

[12] I. Katzela and M. Naghshineh, "Channel assignment schemes for cellular mobile telecommunication systems: a comprehensive survey," IEEE Personal Communications Magazine, pp. 10–31, June 1996.

[13] S. Kuek and W. Wong, "Ordered dynamic channel assignment scheme with reassignment in highway microcells," IEEE Transactions on Vehicle Technology, vol. 41, no. 3, pp. 271–276, 1992.

[14] W. Lee, Mobile Cellular Communication Systems. Wiley, 1989.

[15] J. Li, N. Shroff, and E. Chong, "Channel carrying: a novel handoff scheme for mobile cellular networks," in Proc. IEEE INFOCOM, pp. 909–917, 1997.

[16] J. Li, N. B. Shroff, and E. K. P. Chong, "A New Localized Channel Sharing Scheme for Cellular Networks," tech. rep., Purdue University, West Lafayette, IN 47907, June 1998.

[17] S. Oh and D. Tcha, "Prioritized channel assignment in a cellular radio networks," IEEE Transactions On Communications, vol. 40, pp. 1259–1269, 1992.

[18] K. Okada and F. Kubota, "A proposal of a dynamic channel assignment strategy with information of moving directions," IEICE Transactions on Fundamentals, vol. E75-a, pp. 1667–1673, 1992.

[19] R. Ramjee, R. Nagarajan, and D. Towsley, "On optimal call admission control in cellular networks," in Proc. IEEE INFOCOM, pp. 43–50, 1996.

[20] G. Senarath and D. Everitt, "Performance of handover priority and queueing systems under different handoff request strategies for microcellular mobile communication systems," in Proc. IEEE Vehicle Technology Conference, pp. 897–901, 1995.

[21] S. Tekinay and B. Jabbari, "Handover and channel assignment in mobile cellular networks," IEEE Communications Magazine, pp. 42–46, November 1991.

[22] J. W.C. Jakes, Microwave mobile communications. New York: Wiley, 1974.

[23] C. Yoon and C. Un, "Performance of personal portable radio telephone systems with and without guard channels," IEEE Journal On Selected Areas In Communications, vol. 11, pp. 911–917, 1993.

[24] M. Zhang and T.-S. Yum, "Comparisons of channel-assignment strategies in cellular mobile telephone systems," IEEE Transactions on Vehicle Technology, vol. 38, pp. 211–215, 1989.

[25] M. Zhang and T.-S. Yum, "The non-uniform compact pattern allocation algorithm for cellular mobile systems," IEEE Transactions on Vehicle Technology, vol. 40, pp. 387–391, 1991.

Junyi Li (S'97, M'98) received the B.S. degree and M.S.E.E. degrees from Shanghai Jiao Tong University, in China. His M.S. thesis "Intelligent Predictive Control" was awarded the prize 1991 Best Science and Technology Papers of Shanghai Young Scholars Under the Age of 35. From 1991 to 1994, he was an assistant professor in the Department of Automatic Control at Shanghai Jiao Tong University. In 1998, he received a PhD degree in Electrical and Computer Engineering from Purdue University, and has been working in Digital Communications Research at Bell Labs, Lucent Technologies, Holmdel, NJ since Feb. 1998.

Ness B. Shroff (S'90, M'94) received the B.S. degree in from the University of Southern California, the M.S.E. degree from the University of Pennsylvania, and the M.Phil and Ph.D. degrees from Columbia University. He is currently an Assistant Professor in the School of Electrical and Computer Engineering at Purdue University. During his doctoral study Dr. Shroff worked at AT&T Bell Labs (1991) and Bell Communications Research (1992), on problems involving fault management in telephone networks. His current research interests are in High Speed Broadband and Wireless Communication networks. He is especially interested in studying issues related to Performance Modeling and Analysis, Routing, Network Management, Scheduling, and Control in such networks. Dr. Shroff has received research and equipment grants to conduct fundamental work in broadband and wireless networks, and source coding from the National Science Foundation, AT&T, Hewlett Packard, Intel, LG Electronics, and the Purdue Research Foundation. He received the NSF CAREER award from the National Science Foundation in 1996. Dr. Shroff has served on the technical program committees of various conferences and on NSF review panels. He is the Program Chair for the 14th Annual IEEE Computer Communications Workshop (CCW) to be held in October 1999.

Edwin K.P. Chong (S'86, M'91, SM'96) joined the School of Electrical and Computer Engineering at Purdue University in 1991, where he is currently an Associate Professor. He received the B.E.(Hons.) degree with First Class Honors from the University of Adelaide, South Australia, in 1987; and the M.A. and Ph.D. degrees in 1989 and 1991, respectively, both from Princeton University, where he held an IBM Fellowship. He received the NSF CAREER Award in 1995 and the ASEE Frederick Emmons Terman Award in 1998. He is a Senior Member of IEEE, and is chairman of the IEEE Control Systems Society Technical Committee on Control Theory and the Working Group on Discrete Event Systems. He has served on the editorial board of the IEEE Transactions on Automatic Control, and

on various conference committees. His current interests are in communication networks and optimization methods. He spent a sabbatical at Bell Laboratories, Holmdel, in the fall of 1998. He coauthored a recent book, An Introduction to Optimization, Wiley-Interscience, 1996.
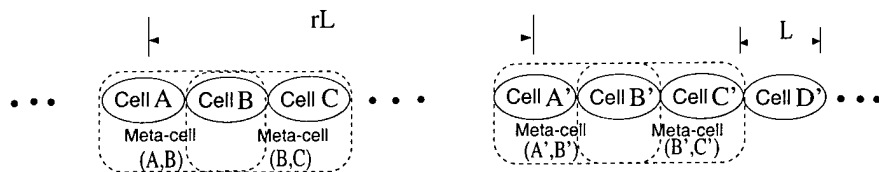
Figure 1. Cells and meta-cells in the linear cellular system.
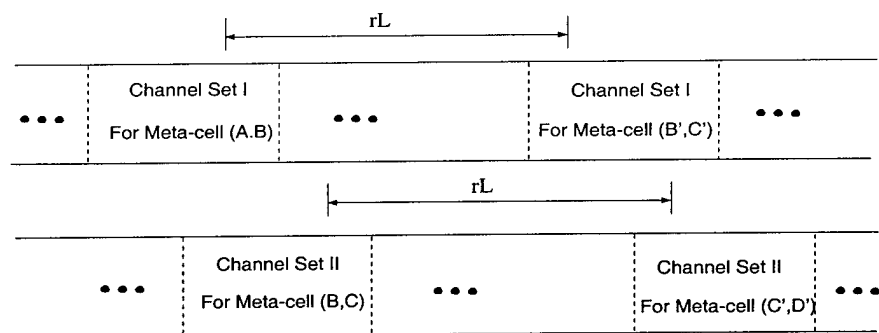
Figure 2. Channel assignment scheme that allows channel sharing in the linear cellular system.

R=12
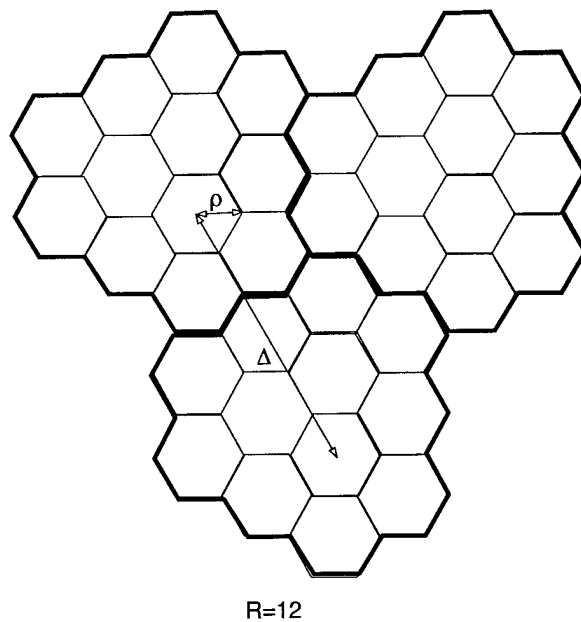
Figure 3. Hexagonal cells in a 2-D system.

λ_n	6	7	7.5	8	9	10	11
K_1	24	24	24	24	10	9	8
K_2	3	3	2	2	2	2	2

Table 1

Optimal K_1, K_2 used for the curve of $R = 7$ in Figure 14
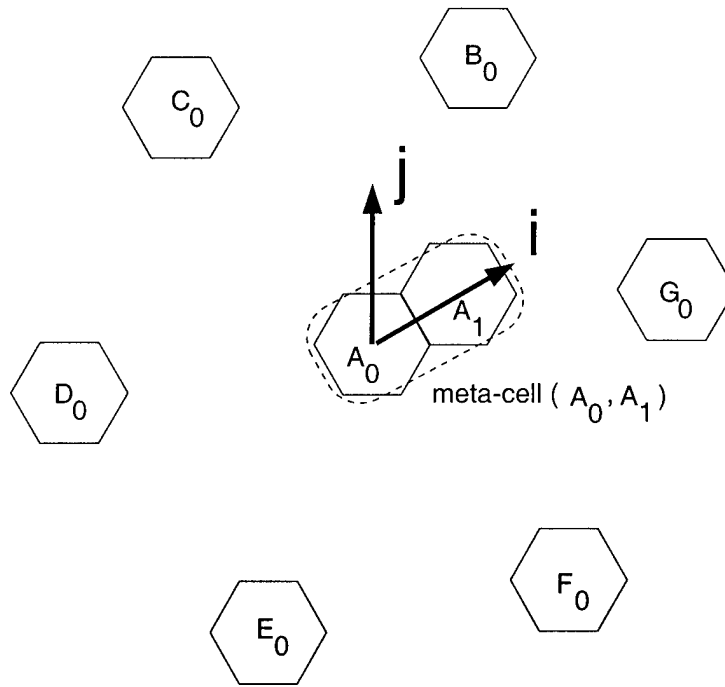
Figure 4. The set of i-j coordinates in a 2-D hexagonal system.
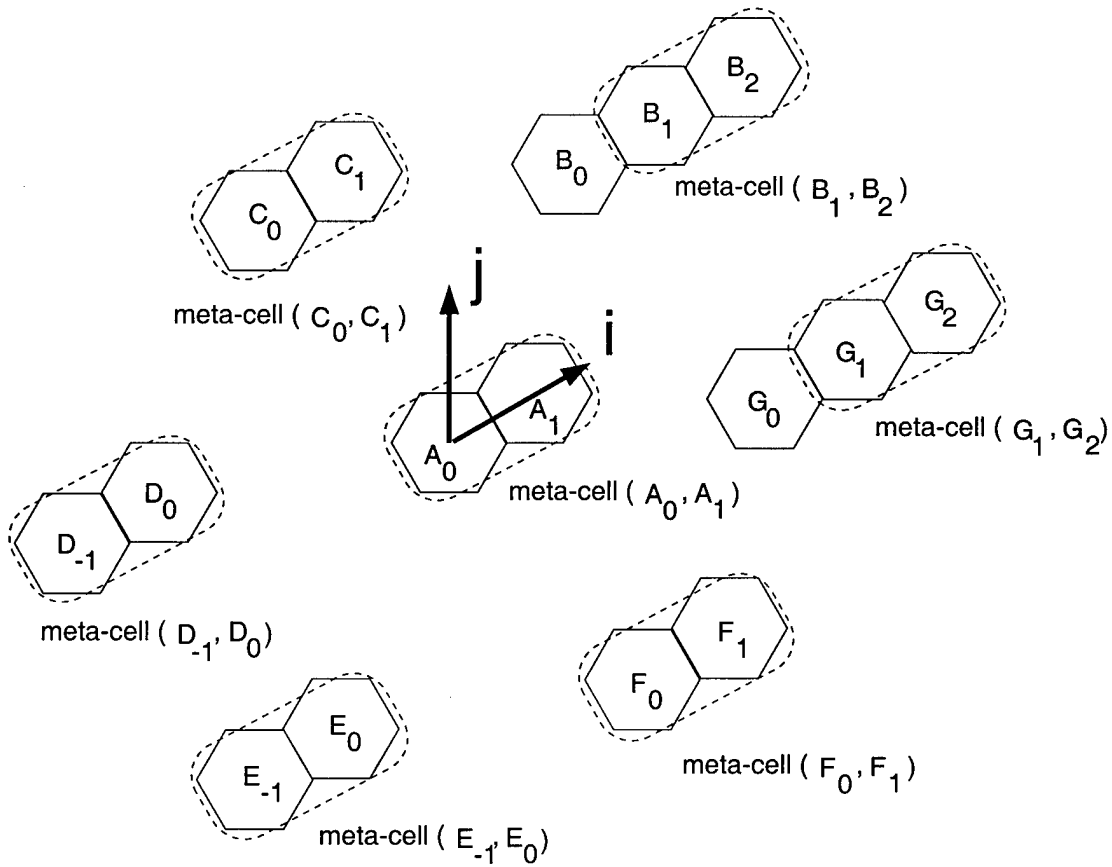
Figure 5. Configuration of co-channel meta-cells in the case of $p + 1 \geq p$.
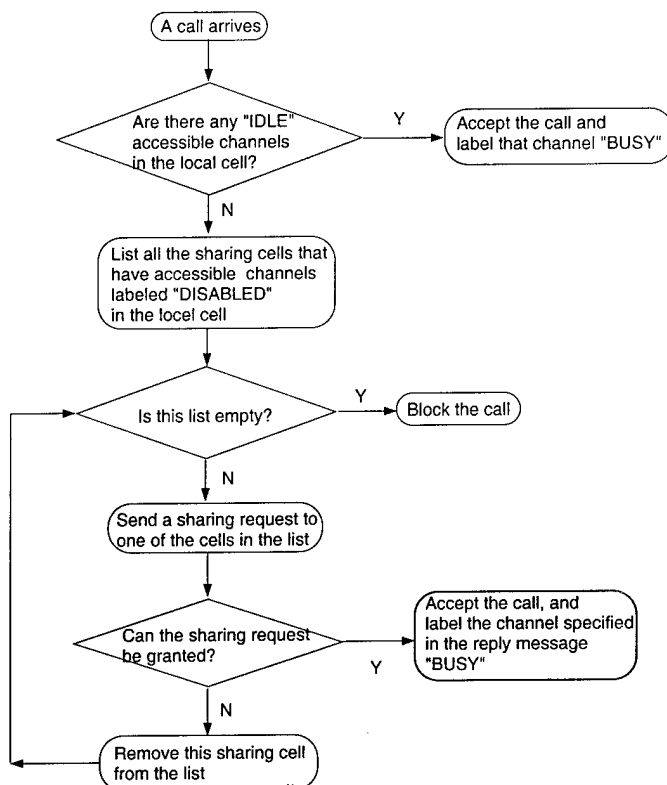
Figure 6. Protocol for handling a call arrival.
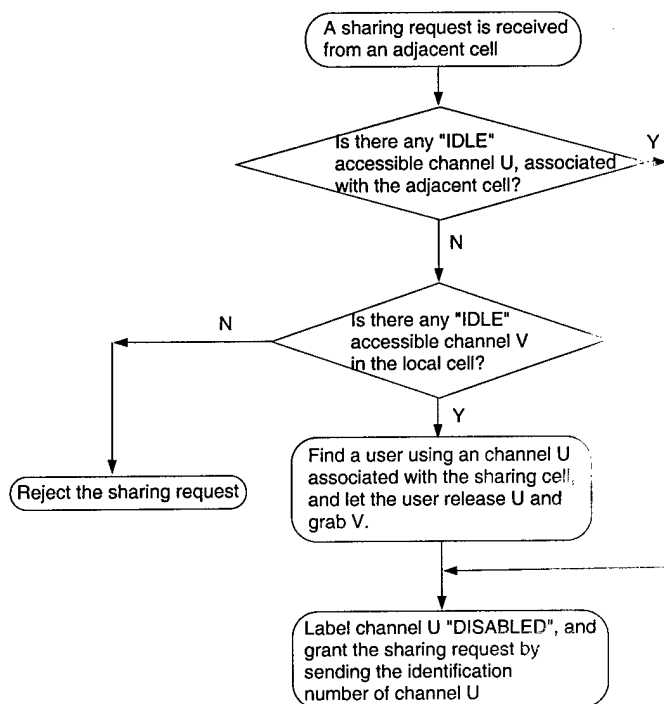
Figure 7. Protocol for handling the sharing request from a sharing cell.
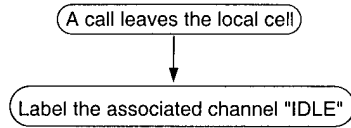
Figure 8. Protocol for handling a call departure.

Accessible Channels

Enabled Channels

Channels not sharable with any neighbors

Channels sharable with a neighbor
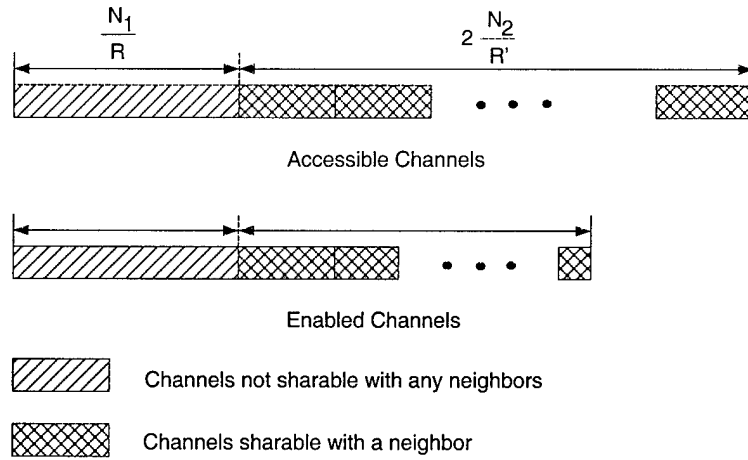
Figure 9. Partition of channels in local cell (for 2-D case).

Enabled Channels

K_1

New calls accepted   New calls blocked
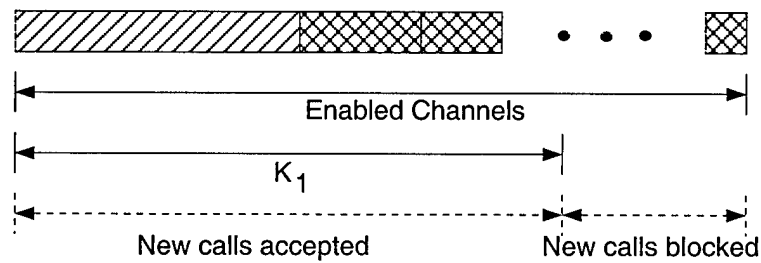
Figure 10. K_1 threshold scheme.

K_1

Enabled Channels

Poor neighbor

K_2

Rich neighbor

K_2
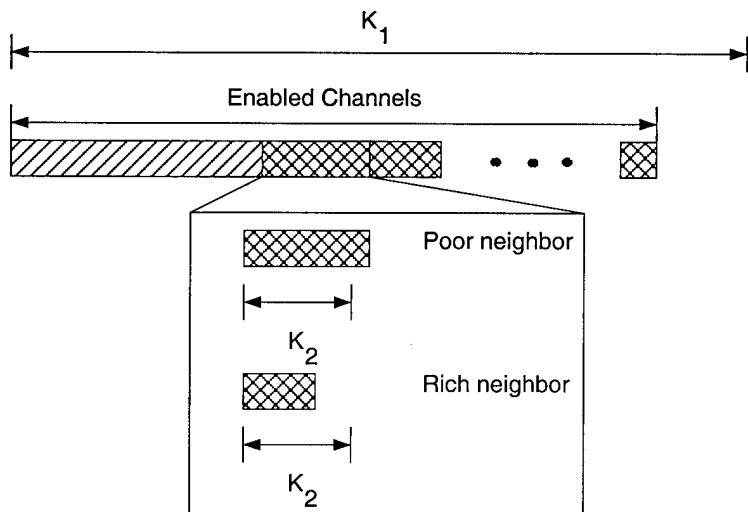
Figure 11. K_2 threshold scheme.
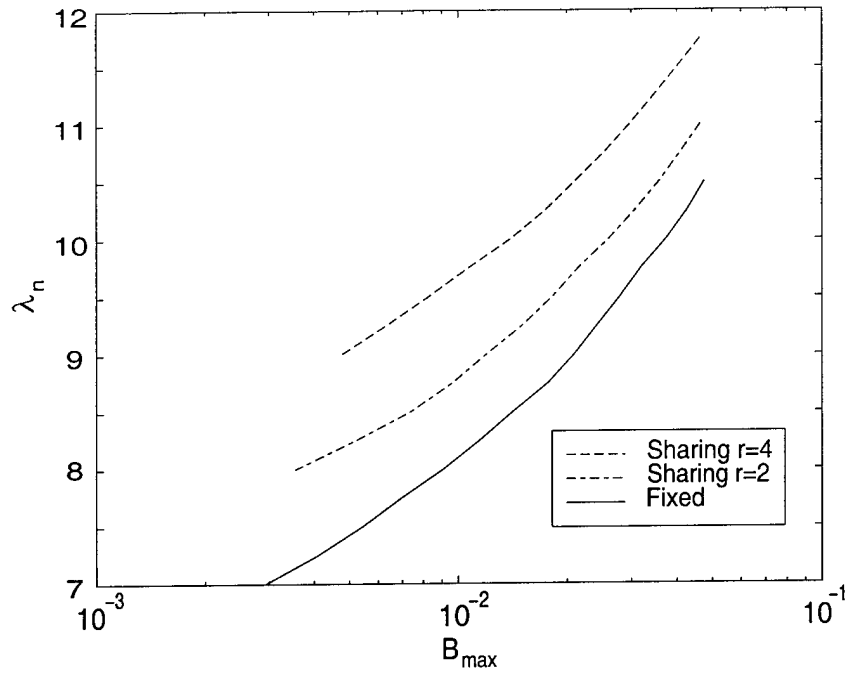
Figure 12. Plot of optimal λ_n versus B_{max} in the linear case, for the problem defined in Equation (5.3). The parameters used in this plot are: $N/r = 15$, $\mu = 1$.
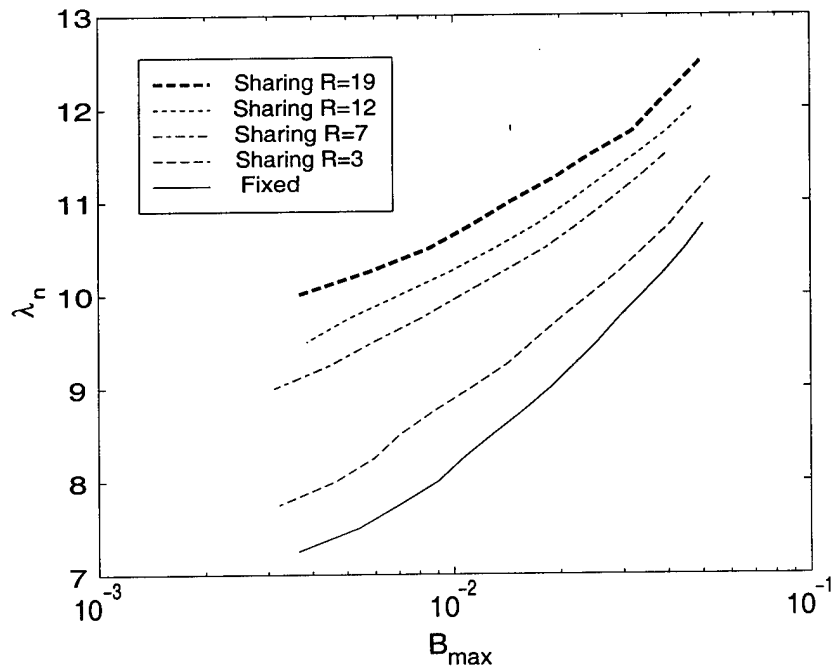
Figure 13. Plot of optimal λ_n versus B_{max} in the 2-D case, for the problem defined in Equation (5.3). The parameters used in this plot are: $N/R = 15$, $\mu = 1$.
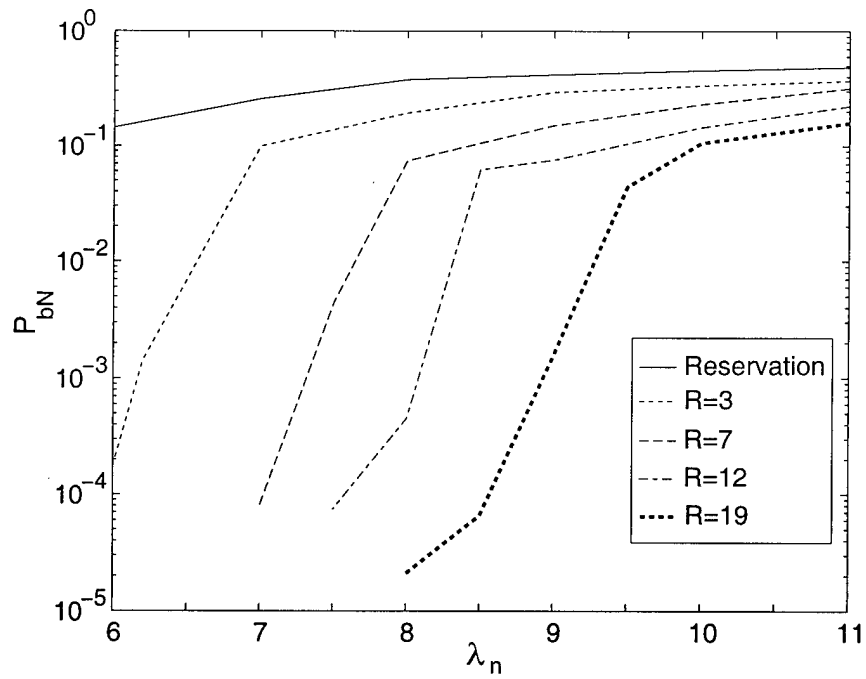
Figure 14. Plot of optimal P_{bN} versus λ_n for the problem defined in Equation (5.4). The parameters used in this plot are: $N/R = 15$, $\lambda_H = 5$, $\mu = 1$, $H_{max} = 10^{-4}$.
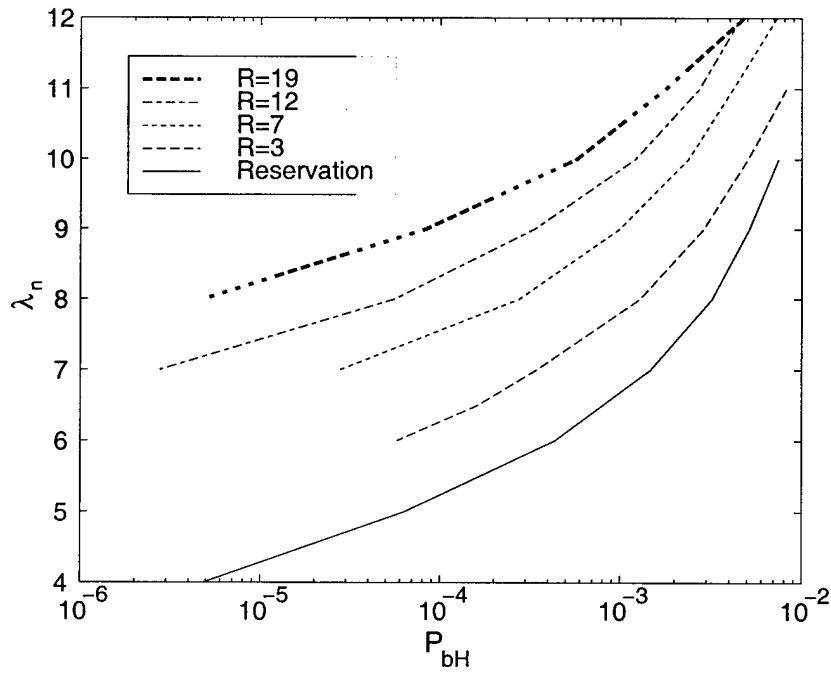
Figure 15. Plot of optimal λ_n versus P_{bH} for the problem defined in Equation (5.5). The parameters in this figure are: $N/R = 15$, $\lambda_H = 5$, $\mu = 1$, $N_{max} = 10^{-2}$.
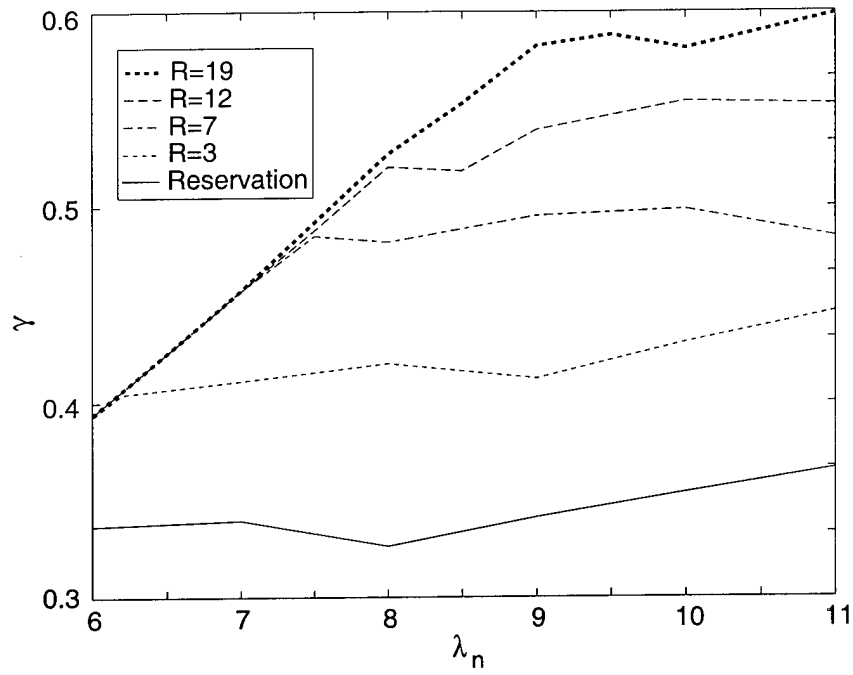
Figure 16. Plot of optimal γ versus λ_n for the problem defined in Equation (5.7). The parameters used in this figure are: $N/R = 15$, $\lambda_H = 5$, $\mu = 1$, $H_{max} = 10^{-4}$.
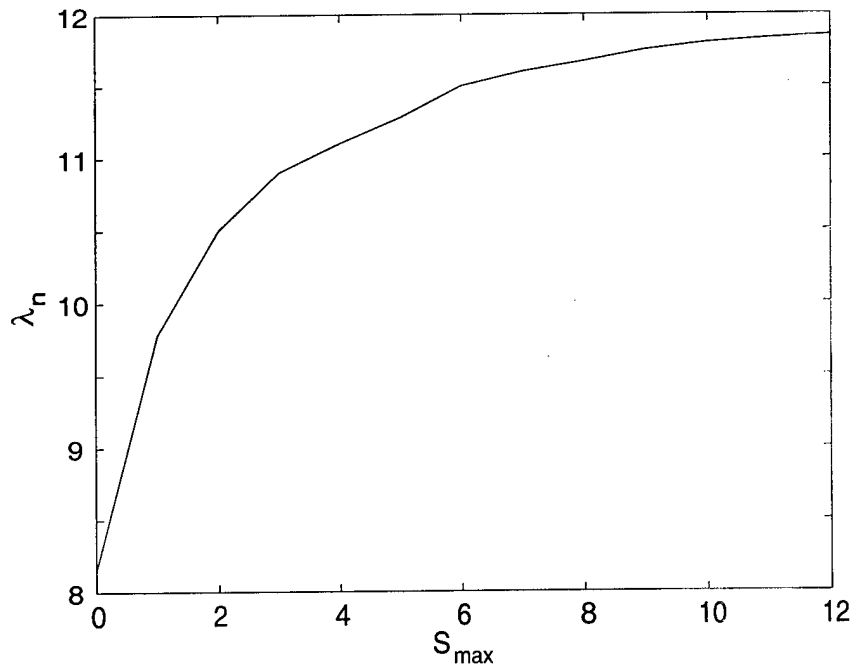
Figure 17. Plot of optimal λ_n versus S_{max} in the linear case, for the problem defined in Equation (5.8). The parameters used in this plot are: $N/r = 15$, $B_{max} = 10^{-2}$, $\mu = 1$.

An Efficient Scheme to Reduce Handoff Dropping in LEO Satellite Systems*

Suresh Kalyanasundaram, Edwin K. P. Chong and Ness B. Shroff[†]

Abstract

The problem of handoffs in cellular networks is compounded in a LEO satellite-based cellular network due to the relative motion of the satellites themselves with respect to a stationary observer on earth. But the velocity of motion of mobiles can be ignored when compared to the very high velocity of the footprints of satellites. We exploit this property of the LEO satellite systems and propose a handoff scheme based on [5] that results in a significant decrease in handoff dropping. For the same handoff dropping probability, our scheme has significantly lower new call blocking probability than the conventional reservation scheme. We present an analytical approximation that is in very good accord with simulation results.

1 Introduction

Low Earth Orbit (LEO) satellite systems can provide users low-cost and truly global wireless services regardless of user locations. Hence, there has been a lot of recent interest in developing efficient schemes for channel allocation and handoff in such systems [1, 2, 6, 12]. LEO satellite systems have certain unique features not found in other satellite and ground-based wireless communication systems. We list some of them here.

While the orbits of geo-synchronous satellites are at an altitude of about 36,000 km, LEO satellites have their orbits in the 500-2000 km altitude range. Besides reducing the propagation delay suffered by signals, the lower orbital altitude also means a lower power requirement at the hand-held terminals, thus making the terminal truly portable. LEO satellite systems can provide communication services even to those areas that do not have a terrestrial wired network in place. In areas where there is a ground-based wireless network in operation, the satellite network can either be used in conjunction with the ground-based network for handling overflow traffic, or in isolation. Since LEO satellites are smaller and lighter than geo-synchronous satellites, they are easily launched.

[†]The authors are with the School of Electrical and Computer Engineering, Purdue University, West Lafayette, IN 47907, U.S.A. E-mail:{kalyanas, echong, shroff}@ecn.purdue.edu

A large number of satellites will be required to ensure that there is always at least one satellite in view for every location on earth. For example, the IRIDIUM system envisages a 66-satellite network to provide global coverage. A typical LEO satellite system will consist of a number of low-earth orbits with a fixed number of satellites going around in each orbit. The footprint of each satellite is divided into several cells with each cell being served by a "spot-beam". Like in terrestrial cellular systems, a channel that is used in a given cell cannot be used in another cell if it is at a distance smaller than the *minimum reuse distance*.

Another unique feature relates to the fact that the LEO satellites are not in geo-synchronous orbit and hence will not appear stationary to a stationary observer on earth. Instead, the satellites move at a constant velocity relative to a stationary observer on earth. Thus, in addition to the mobile users' random motion we will have to handle the deterministic motion of the footprint of the satellite on earth. Fortunately, the velocity of the footprint on earth is so high that we can ignore the velocity of the mobile, in comparison. For example, a typical value for the velocity of the footprint is 7.39 km/s.

Some areas on earth will have overlapping coverage from different satellites. We will be able to make use of this macrodiversity advantage to reduce erroneous transmission due to channel noise. Additionally, the presence of a large number of satellites ensures survivable communications since the malfunctioning of a single satellite will not adversely affect the operation of the network.

Our objective here is to exploit the fact that the relative motion of the mobile is almost deterministic, to improve the handoff dropping performance of LEO satellite systems. This paper is organized as follows: In Section 2, we discuss the importance of handling handoffs efficiently and delineate the most important source of handoff call dropping in non-geostationary satellite systems. In Section 3, we propose our technique, based on the channel sharing scheme [5], to reduce the incidence of handoff call dropping. We will see that our technique is ideally suited to handle the handoff problem because the allocation of channels is done with the knowledge of the direction of the mobile's relative motion. In Section 4, we provide an analytical approximation for the analysis of our handoff technique. In Section 5, we compare our handoff scheme to the fixed channel assignment (FCA) scheme with channel reservation, and present numerical results. Conclusions are drawn in the final section.

2 Problem Description

We are interested in two different QoS measures: *new call blocking probability* and *handoff call dropping probability*. Handoff calls are those calls that have already been admitted in some cell and later try to move to a different cell. If the new cell to which the call is moving does not have an idle channel to allocate to this call, the call is dropped. This is known as *handoff call dropping*. When a cell is unable to allocate an idle channel to a new call, *new call blocking* occurs. Handoff call dropping has the undesirable effect of the user being cut-off in the middle of a call. Thus, it is important to reduce handoff call dropping even if it is at the expense of increased new call blocking. A very popular approach proposed in terrestrial cellular systems to reduce handoff

dropping is the reservation policy (sometimes called the guard channel policy) [7]. Other approaches include queuing of handoff attempts [3] and queuing of handoff attempts based on measured SIR values [11].

As we have already observed, ensuring successful handoffs becomes more complicated in the LEO satellite scenario due to the motion of the satellites relative to any stationary observer on earth. The velocity of motion of the footprints is of the order of kilometers/sec. So, it is common to make the simplifying assumption that the velocity of the mobile can be ignored when compared to the high velocity of the footprint ([8], [9]). With this assumption, the motion of the mobile relative to a satellite becomes totally deterministic. Our view is that we can use this knowledge about the mobiles' motion to substantially reduce handoff dropping while, at the same time, not adversely affecting the new call blocking probability.

The following are the assumptions we make in our analysis:

1. All cells are identical with length L and the relative motion of the mobile is along the length of the cells.

2. The *call holding time* (or the call duration), t_d, is exponentially distributed with mean $1/\mu$.

3. The velocity of motion of mobiles can be neglected in comparison to the velocity of motion of the footprint on earth, V. Equivalently, we assume that the mobiles are moving with a velocity of V relative to the stationary satellite footprint.

4. The distance new calls have to travel before their first handoff attempt is uniformly distributed between 0 and L.

As in [8], we call the cell of origination of a call as its "source cell" and the cell to which a call has handed off as its "transit cell". A mobile in its source cell has to travel a distance that is uniformly distributed between 0 and L before its first handoff. A mobile in a transit cell has to travel a fixed distance of L before its next handoff. Let Y denote the random variable that denotes the distance a call has to travel in its source cell before it makes a handoff. Then, the probability that a mobile in its source cell will give rise to a handoff, P_{h1}, is

$$P_{h1} = \int_0^L P\{t_d > y/V\} f_Y(y) dy$$

where

$$f_Y(y) = \begin{cases} 1/L & \text{if } 0 \le y < L \\ 0 & \text{otherwise.} \end{cases}$$

Thus,

$$P_{h1} = \frac{1 - e^{-\mu L/V}}{\mu L/V}.$$

In the following, we denote $\mu L/V$ as x. Similarly, a call in a transit cell will give rise to a handoff with a probability

$$P_{h2} = e^{-\mu L/V} = e^{-x}. \tag{1}$$

3
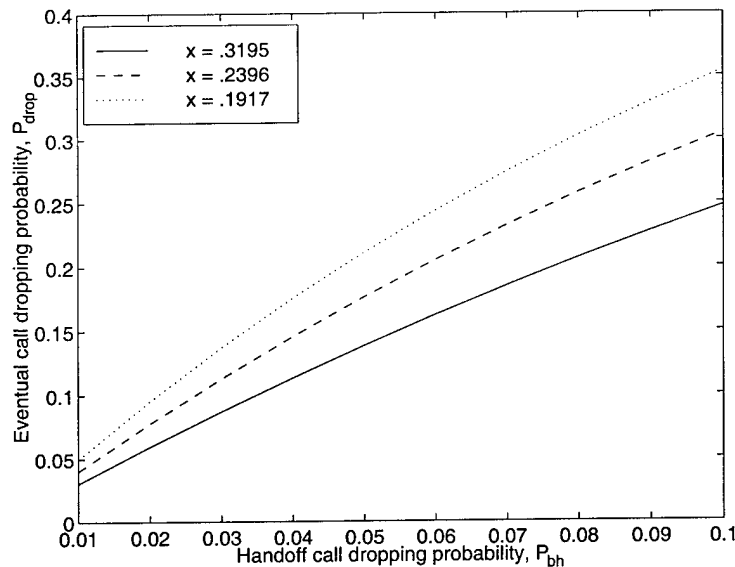
Figure 1: Comparison of P_{bh} and P_{drop} for a few typical values of x

We denote the new call blocking probability by P_{bn} and the handoff call dropping probability by P_{bh}. From the point of view of the mobile user, a quantity that is often more relevant than the handoff call dropping probability is the probability that the call gets dropped eventually due to a handoff failure. We denote this quantity as P_{drop}. Under the above assumptions, it has been shown in [8] that

$$P_{drop} = \frac{P_{h1} P_{bh}}{1 - P_{h2}(1 - P_{bh})},$$

where $P_{h1} = \frac{1 - e^{-\mu L/V}}{\mu L/V}$ is the probability that a call in its cell of origin makes a handoff attempt and $P_{h2} = e^{-\mu L/V}$ is the probability that a call in its "transit cell" makes a handoff attempt.

In Figure 1, we plot the *eventual call dropping probability* (P_{drop}) against the handoff call dropping probability (P_{bh}) for some typical values of x and for the most interesting range of P_{bh}. We find that P_{drop} is much higher than P_{bh} in this range. This is due to the high number of handoffs that a call is likely to make due to the high relative velocity of the mobile. Therefore, we see that it becomes more important to handle handoffs efficiently in LEO satellite systems. The values of x in Figure 1 are typical of the values that are obtained in a practical LEO satellite system [8]. For example, $x = .1917$ has been obtained with $1/\mu = 180$ seconds, $L = 425$ km, and $V = 7.39$ km/s.

We next delineate a primary cause for handoff dropping in LEO satellite networks. In Figure 2 we illustrate a typical case where handoff dropping occurs. We assume that each cell shown in the figure is allocated N channels and is capable of handling no more than N simultaneous calls. Since the velocities of the mobiles are deterministic and identical, the reason for handoff call dropping is the random initial location of the mobile. Figure 2(a) illustrates such a scenario. The worst situation will be when there are exactly N active mobiles in the two shaded areas in Figure 2(a). Since all the mobiles move with the same velocity, we will have as many as N dropped handoff calls, if there are no natural call terminations in the meantime.

4
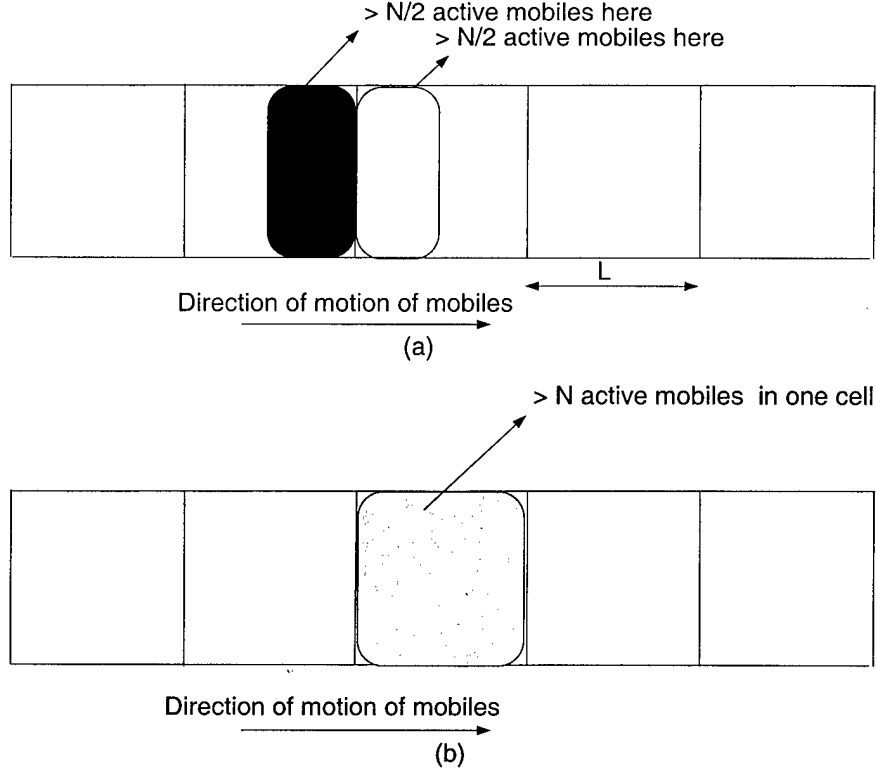
Figure 2: A typical case where handoff dropping occurs

In the next section we propose a scheme to reduce handoff dropping based on the channel sharing scheme in [5]. This scheme, as we will see, anticipates the motion of the mobiles and allocates channels accordingly.

3   Channel Sharing Handoff Scheme

We adopt the channel allocation scheme proposed in [5], called the *channel sharing scheme*. We first describe this scheme briefly. The sharing scheme allows channels to be shared between neighboring cells. For illustration, we consider a linear cellular network. To facilitate the description, we need some terminology. A *meta-cell* is a pair of neighboring cells. The two adjacent cells that form a meta-cell are called the *component cells*. For example, Figure 3 shows a family of meta-cells in a linear cellular system, each comprising two adjacent cells.

The channel sharing scheme allows channels to be shared between neighboring cells (namely, cells belonging to the same meta-cell). Consider Figure 3. For this simple linear cellular system, the distance measure $d(X, Y)$ between two cells X and Y is traditionally given as $d(X, Y) = |c_X - c_Y|$ where c_X and c_Y denote the positions of the centers of cells X and Y, respectively. Suppose that the minimum reuse distance is $\Delta = rL$, where L is the length of a single cell and r is an integer. Cells that are assigned the same set of channels are called *co-channel cells*. In the conventional scheme for fixed channel allocation, each channel is assigned to cells that are exactly a distance Δ
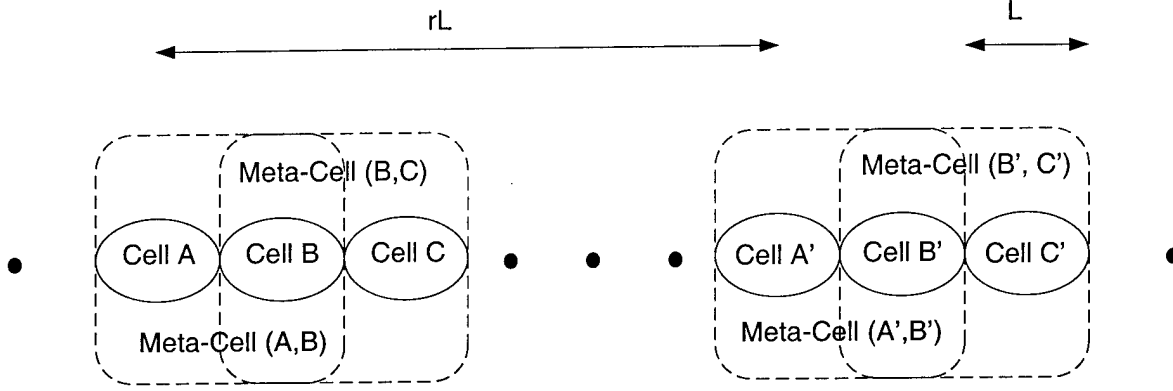
Figure 3: Linear Cellular system
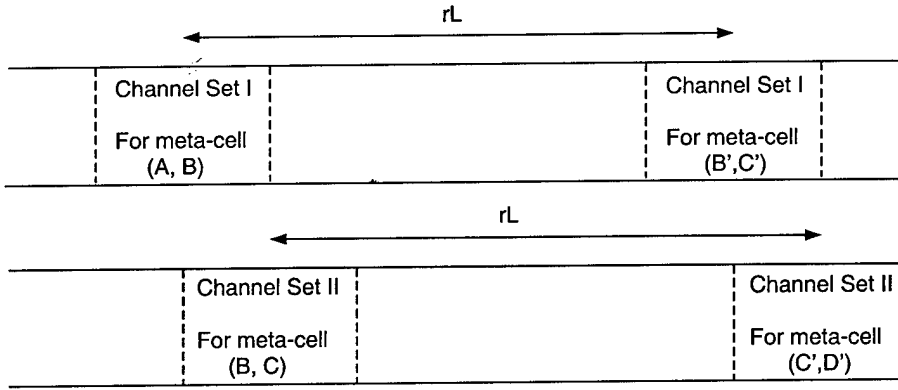
Figure 4: The same set of channels can be used in meta-cells (A, B) and (B', C') and in meta-cells (B, C) and (C', D')

apart. We refer to this scheme as the *tightest fixed channel assignment scheme*, in which co-channel cells are exactly r cells apart. For example, in Figure 3, cells A and A' are co-channel cells. Let T denote the total number of distinct channels that are available in this linear cellular system. Thus, the total number of distinct channels available for each cell is T/r (i.e., the reuse factor is r).

A meta-cell can be designated by the pair of its component cells. For example, in Figure 3, cells A and B are components of meta-cell (A, B). To assign channels to meta-cells, we next derive the distance measure $d((X, Y), (X', Y'))$ between two meta-cells (X, Y) and (X', Y'). Recall that in the sharing scheme, when a channel is assigned to a meta-cell, it can be used by a mobile user in any cell belonging to that meta-cell. Thus, we have to ensure that the distance between any component cells of two meta-cells assigned the same set of channels complies with the minimum reuse distance requirement. Consequently, we define $d((X, Y), (X', Y'))$ as the minimum of the distance measures between the component cells of meta-cells (X, Y) and (X', Y'), i.e.,

$$d((X, Y), (X', Y')) = \tag{2}$$
$$\min\{d(X, X'), d(X, Y'), d(Y, X'), d(Y, Y')\}.$$

6

For example, in Figure 3, the distance measure between meta-cells (A, B) and (A', B') is given by $(r-1)L$, which is the distance between cells B and A'.

We call meta-cells that are assigned the same set of channels *co-channel meta-cells*. To allocate a maximum number of channels to each meta-cell, co-channel meta-cells must be deployed as close as possible. Therefore, we assign the same set of channels to meta-cells that are exactly the minimum reuse distance apart, i.e., rL in this case.

It is easy to see that in the channel sharing scheme, each meta-cell is assigned $T/(r+1)$ distinct channels. In other words, the reuse factor of the channel sharing scheme is $r' = r + 1$. However, in the tightest fixed channel assignment scheme, the number of channels assigned to each meta-cell is T/r, so the cost we pay for allowing channels to be "shared" is $T/r - T/r' = T/r(r+1)$. Nevertheless, by increasing the reuse distance in this fashion we facilitate a simple way for channels to be shared between cells with little increase in complexity over fixed channel allocation techniques.

Our handoff handling scheme assumes that the channel sharing scheme is chosen as the method of channel allocation. We now describe how our handoff scheme works assuming the channel sharing scheme has been implemented. Without loss of generality, we assume that the relative motion of mobiles is such that they move towards higher numbered cells. Thus, all mobiles in cell 1 move towards cell 2, those in cell 2 move towards cell 3 and so on. Whenever there is a new call in cell i, it is allocated a channel only if there are idle channels belonging to meta-cell $(i, i+1)$. Otherwise, the new call is blocked. This procedure is shown schematically in Figure 5. By doing the allocation in this way we can allow the mobiles to "carry" their channel to cell $(i+1)$ during handoff. Handoff calls arriving at cell i are allocated a channel belonging to meta-cell $(i, i+1)$ if there is an idle one available. Otherwise, if the call was using a channel belonging to meta-cell $(i-1, i)$, it is allowed to carry the same channel over to cell i and is queued in a FIFO queue for channels belonging to meta-cell $(i, i+1)$. But, at the time of handoff, if the call was using a channel belonging to meta-cell $(i-2, i-1)$, then the call is dropped. The flowchart for processing a handoff call arrival is given in Figure 6. Each time a channel belonging to meta-cell $(i, i+1)$ becomes free (either due to a handoff or due to a call termination) the channel is allocated to the first call in the queue waiting for channels belonging to meta-cell $(i, i+1)$. If the queue is empty, the channel is idle for future new call or handoff call arrivals. Figure 7 is a schematic representation of the procedure for handling a freed channel. We see that our channel sharing handoff scheme allocates channels to mobiles knowing its direction of relative motion. Each mobile can travel one complete cell-length and look for a free channel during this time. This reduces handoff dropping significantly.

We next note that it is possible to achieve the same handoff dropping performance with the conventional FCA scheme using channel reservation. The channel reservation seeks to give preferential treatment to handoff calls by reserving channels for them. The channel reservation technique works as follows: Suppose there are N channels assigned to each cell. Then, new calls are admitted in a cell only if the total number of active calls is less than some threshold, P. Handoff calls, on the other hand, are admitted as long as there are idle channels. By tuning the parameter P the channel reservation scheme can be made to achieve the same handoff dropping performance as our handoff handling scheme. But, as we will see in Section 5, our handoff scheme offers a significantly lower
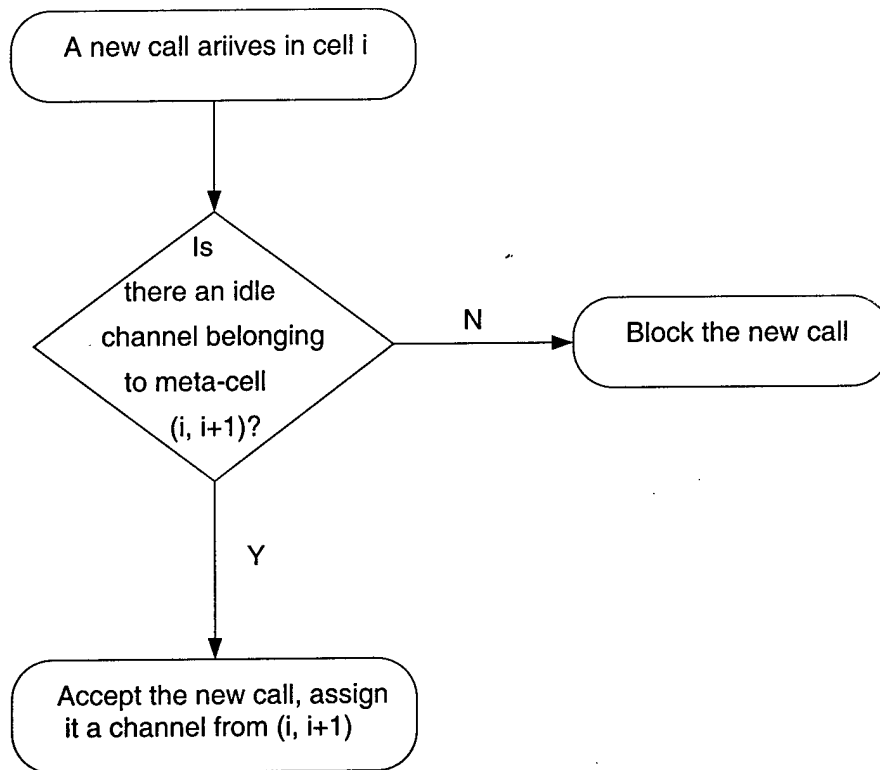
Figure 5: Flow chart for processing a new call
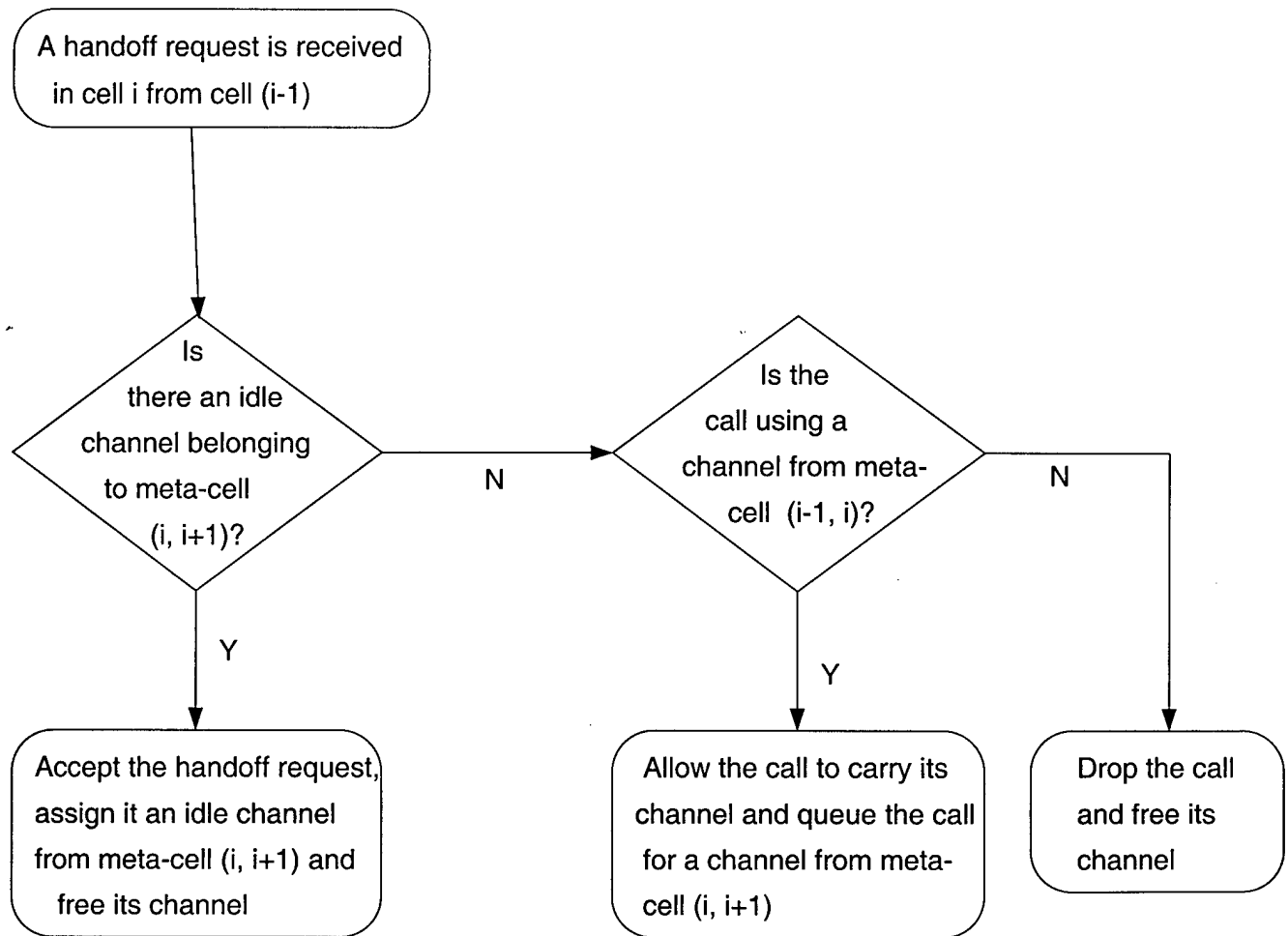
Figure 6: Flow chart for processing a handoff call
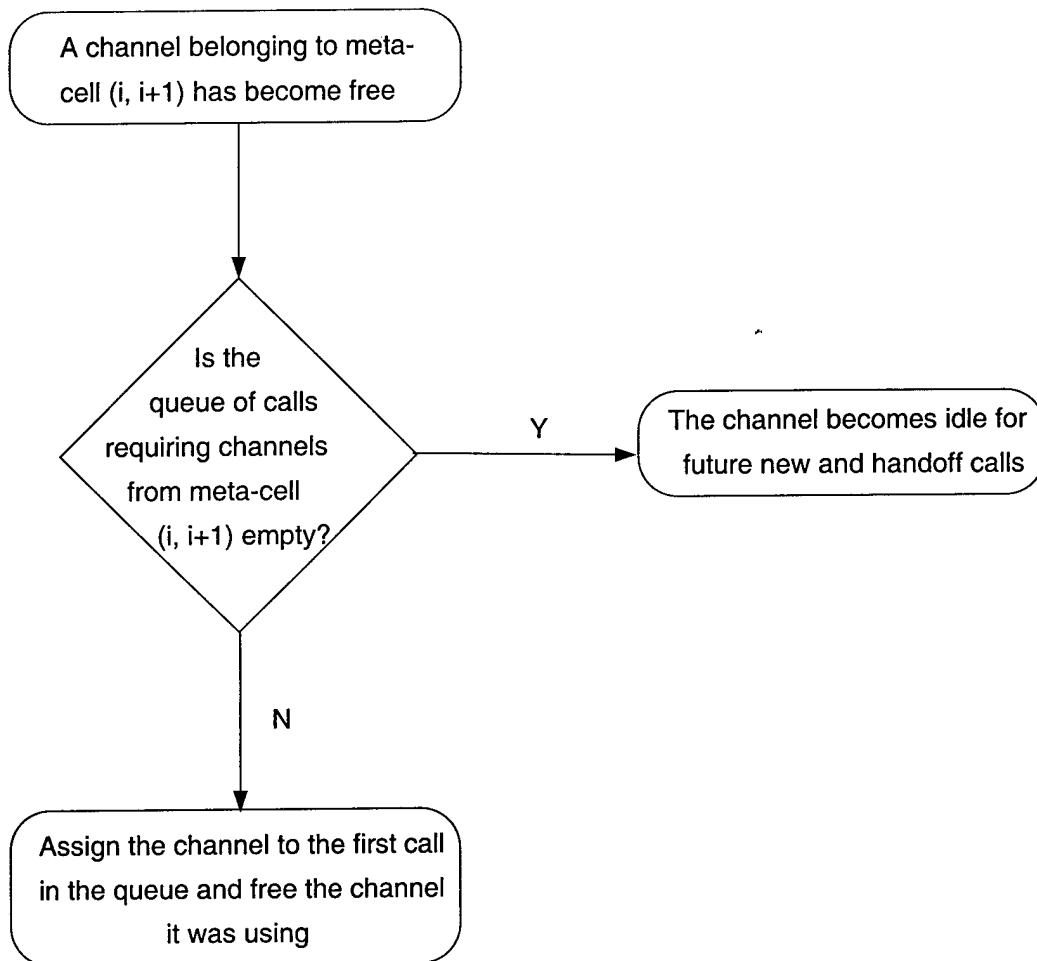
Figure 7: Flow chart for processing a freed channel
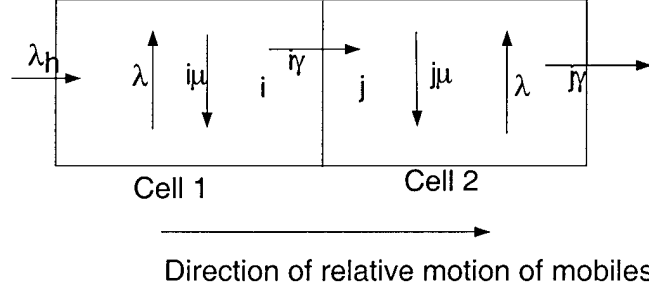
Figure 8: Reference scenario for the two-cell approximation

new call blocking probability for the same performance with the handoff dropping probability.

4 Performance Analysis

In this section, we analyze our handoff scheme using an analytical technique (*the two-cell approximation* [10]). We apply the same technique to analyze the FCA scheme with channel reservation. could use the *single-cell approximation* Another approximation, called the *single-cell approximation*, has been used in several studies for modeling traffic in LEO systems ([8], [9]). The single cell approximation assumes that the handoff call arrival into a cell is Poisson with rate λ_h and is independent of the new call arrivals [3]. This approximation is used for analytical tractability. Although the single cell approximation could be used to analyze the channel reservation scheme, it is not suited for the analysis of our channel sharing handoff scheme.

The single-cell approximation does not adequately capture the essence of our channel sharing handoff scheme. For example, the number of idle channels in a given cell, say i, not only depends on the number of active calls in that cell but also on the number of channels belonging to meta-cell $(i, i+1)$ that are in use in cell $(i+1)$. Therefore, we use the following two-cell approximation to obtain the quantities of interest for our handoff scheme.

Sidi and Starobinski [10] studied the two-cell approximation for terrestrial cellular networks. We use a similar model for our LEO satellite-based cellular network. The single-cell approximation suffers from the disadvantage that the handoff traffic into the cell is Poisson with the same rate λ_h irrespective of the state of the cell from which handoff traffic arrives. To overcome this problem, the authors of [10] suggest isolating a group of cells and approximating the handoff traffic into the group from outside the group by a Poisson process, but make no such assumption about the handoff traffic originating from within the group. Then, we choose the statistics of that cell from among the group whose statistics will closely approximate the actual P_{bn} and P_{bh}. We choose a group of two cells and carry out an approximate analysis. For the analysis to be tractable the number of cells within the group should not be too large.

The reference scenario is shown in Figure 8 where i and j refer to the number of active mobiles in cells 1 and 2 respectively. The following are the assumptions in this section:

1. Each cell has independent Poisson new call arrivals at the rate of λ.

2. The *call holding time* (or the call duration), t_d, is exponentially distributed with mean $1/\mu$.

3. The *cell residence time* (the time for which a call resides in a given cell) is exponentially distributed with mean $1/\gamma = L/V$, where L is the length of a cell and V is the relative velocity of the mobile. This approximation yields results which are in very good agreement with the simulation results (see [8] for a similar assumption).

4. Handoff arrival from outside the group into cell 1 is Poisson with rate λ_h. We compute λ_h as follows: The average rate at which new calls are carried in each cell is $\lambda(1 - P_{bn})$. The probability that a new call will attempt a first handoff is $P_{h1} = \frac{1-e^{-x}}{x}$ where $x = \mu L/V$. Thus the average rate at which calls that are making their first handoff arrive in each cell is $\lambda(1 - P_{bn})P_{h1}$. The average rate at which calls which are making their second handoff arrive in each cell is $\lambda(1 - P_{bn})P_{h1}(1 - P_{bh})P_{h2}$. Thus,

$$
\begin{aligned}
\lambda_h &= \lambda(1 - P_{bn})P_{h1} \sum_{i=0}^{\infty} (1 - P_{bh})^i P_{h2}^i \\
&= \frac{\lambda(1 - P_{bn})P_{h1}}{1 - (1 - P_{bh})P_{h2}}.
\end{aligned}
\tag{3}
$$

The above model can be described as a two-dimensional continuous-time Markov chain because new call arrivals in either cell and handoff call arrivals to cell 1 are mutually independent Poisson processes. Additionally, the duration of a call and the cell residence time are distributed exponentially and all of the above mentioned parameters are independent.

FCA with $N - P$ guard channels: We denote states of the two-dimensional Markov Chain by (i, j) where i refers to the number of active mobiles in cell 1 and j refers to the number of active mobiles in cell 2. Each cell is assigned N channels with $N - P$ channels reserved for handoff calls. Let $P(i, j), 0 \leq i, j \leq N$ be the stationary probabilities of the chain being in state (i, j). New call arrivals are admitted only so long as there are fewer than P active mobiles in the cell while handoff calls are accepted as long as there are idle channels.

The state transition diagram is shown in Figure 9. To write the balance equations, we need to define the following functions:

$$
\delta^{(i)} = \begin{cases} 0 & \text{if } i = 0 \\ 1 & \text{otherwise.} \end{cases}
\tag{4}
$$

$$
\beta^{(i)} = \begin{cases} 1 & \text{if } i < N \\ 0 & \text{if } i = N. \end{cases}
\tag{5}
$$

$$
\eta^{(i)} = \begin{cases} 1 & \text{if } i < P \\ 0 & \text{otherwise.} \end{cases}
$$

We can now write the detailed balance equations as follows:

$$
P(i, j)\{\lambda\eta^{(i)} + \lambda\eta^{(j)} + \lambda_h\beta^{(i)} + (i + j)\mu + (i + j)\gamma\} =
$$

12
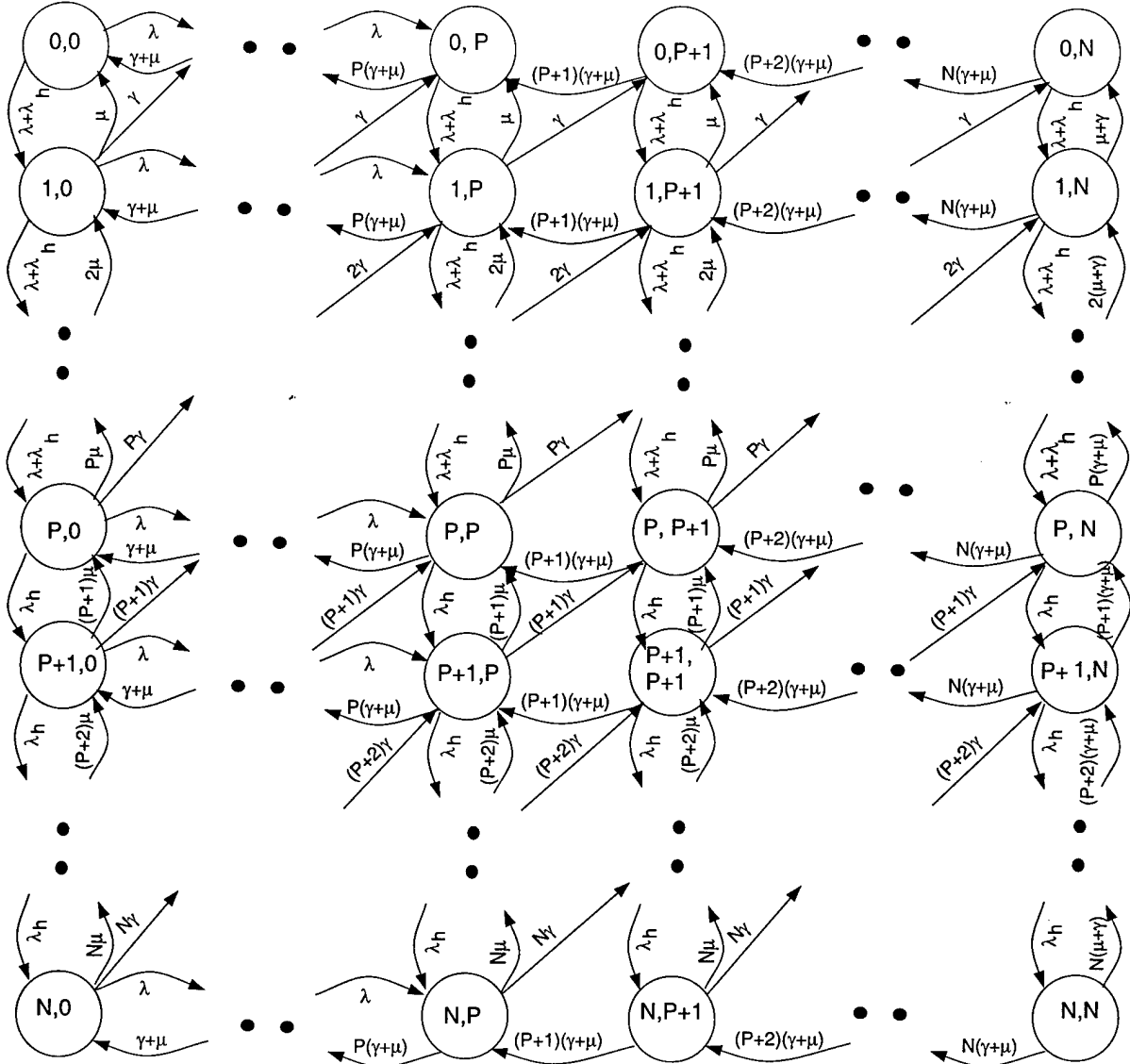
Figure 9: CTMC for two-cell approximation for fixed channel allocation with $N - P$ guard channels

13

$$P(i, j-1)\lambda\delta^{(j)}\eta^{(j-1)} + P(i, j+1)(j+1)(\gamma+\mu)\beta^{(j)} +$$
$$P(i-1, j)\{\lambda_h\delta^{(i)} + \lambda\delta^{(i)}\eta^{(i-1)}\} + \tag{6}$$
$$P(i+1, j)\{(i+1)\mu\beta^{(i)} + (i+1)\gamma\beta^{(i)}(1-\beta^{(j)})\} +$$
$$P(i+1, j-1)(i+1)\gamma\delta^{(j)}\beta^{(i)}, \text{for all } 0 \le i, j \le N.$$

On the left hand side we have the rate of leaving state (i, j) and on the right hand side is the rate with which we reach state (i, j). Additionally, the stationary probabilities have to satisfy the normalization condition in the following equation:

$$\sum_{i=0}^{N}\sum_{i=0}^{N} P(i, j) = 1. \tag{7}$$

For the FCA scheme with $N - P$ guard channels, the new call blocking probability can be derived by invoking the PASTA property as

$$P_{bn} = \sum_{j=P}^{N}\sum_{i=0}^{N} P(i, j) \tag{8}$$

and the handoff call dropping can be obtained from

$$P_{bh} = \frac{\sum_{i=0}^{N} iP(i, N)}{\sum_{i=0}^{N}\sum_{j=0}^{N} iP(i, j)}. \tag{9}$$

Eq. (8) is the new call blocking probability experienced by calls originating in cell 2. We note that this is a good approximation of the actual new call dropping probability. Eq. (9) is derived by taking the ratio of the number of unsuccessful handoffs to the total number of handoff attempts. A recursive method has to be employed to evaluate P_{bn} and P_{bh} using Eqs. (3), (6), (7), (8) and (9).

Channel sharing handoff scheme: In the channel sharing handoff scheme each meta-cell is allocated $k = \frac{Nr}{r+1}$ channels where N is the number of channels allocated to each cell in the FCA scheme. New calls are accepted in cell 1 only if there are unused channels belonging to meta-cell $(1, 2)$. The states are denoted by (i, j) where i denotes the number of active mobiles in cell 1 and j denotes the number of active mobiles in cell 2. Apart from the obvious restriction that $0 \le i, j \le 2k$, we also have the additional constraint that $0 \le i + j \le 3k$. Hence, the set of all feasible states, $S(k)$, can be defined as follows:

$$S(k) = \{(i, j) : 0 \le i, j \le 2k; 0 \le i + j \le 3k\}.$$

Let $P(i, j)$, $(i, j) \in S(k)$ be the stationary probabilities of the system being in state (i, j). The state transition diagram of the two-cell approximation for the channel sharing handoff scheme is given in Figure 10. We define the following functions to write the balance equations (the definition of $\delta^{(i)}$ is the same as given in Eq. (4)):

$$\beta^{(i)} = \begin{cases} 1 & \text{if } i < 2k \\ 0 & \text{otherwise.} \end{cases}$$

14
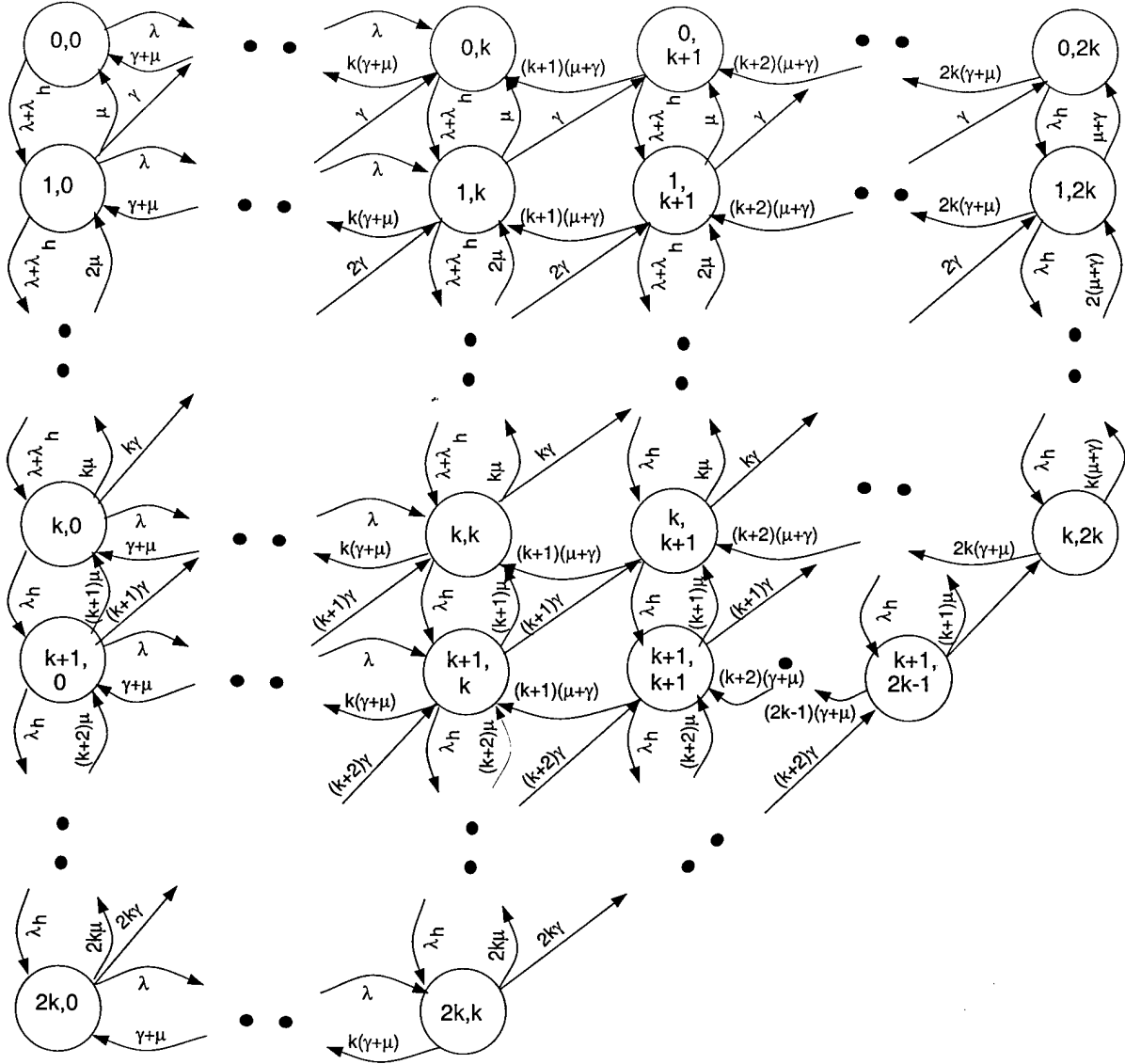
Figure 10: CTMC for two-cell approximation for channel sharing scheme

15

$$\eta^{(i)} = \begin{cases} 1 & \text{if } i < k \\ 0 & \text{otherwise.} \end{cases}$$

$$\theta^{(i,j)} = \begin{cases} 1 & \text{if } i + j < 2k \\ 0 & \text{otherwise.} \end{cases}$$

With these definitions the detailed balance equations are:

$$
\begin{aligned}
P(i,j)\lambda(\eta^{(j)} + \eta^{(i)}\theta^{(i,j)}) + \\
P(i,j)\lambda_h\beta^{(i)}\theta^{(i,j-k)} + (i+j)(\mu+\gamma) = \\
P(i,j-1)\lambda\eta^{(j-1)}\delta^{(j)} + \\
P(i+1,j-1)(i+1)\gamma\delta^{(j)}\beta^{(i)} + \\
P(i-1,j)\{\lambda_h\delta^{(i)} + \lambda\eta^{(i-1)}\delta^{(i)}\theta^{(i-1,j)}\} + \\
P(i+1,j)\{(i+1)(\mu\beta^{(i)}\theta^{(i,j-k)} + \gamma(1-\beta^{(j)})\eta^{(i)})\} \\
P(i,j+1)(j+1)(\mu+\gamma)\beta^{(j)}\theta^{(i,j-k)} \\
\text{for all } (i,j) \in S(k)
\end{aligned}
\tag{10}
$$

On the left hand side of the above equation is the rate of leaving state (i,j) and on the right hand side we have the rate of reaching state (i,j). We note that whenever cell 1 has more than k active mobiles it is unlikely that handoff calls from cell 1 to cell 2 can be dropped. This is because we have at least one channel from meta-cell $(1,2)$ in use in cell 1. And it will be this channel which will be used for a handoff from cell 1 to cell 2 due to our strategy of queuing calls which need a channel from meta-cell $(1,2)$ in a FIFO manner along with the near deterministic velocities of the mobiles. Additionally, the stationary probabilities have to satisfy the following normalization condition:

$$\sum_{(i,j) \in S(k)} P(i,j) = 1.$$

The new call and handoff call dropping probabilities are given as follows:

$$P_{bn} = \sum_{i=0}^{2k} \sum_{j \in S_i(k),\ j \geq k} P(i,j) \tag{11}$$

$$P_{bh} = \frac{\sum_{i=0}^{k} iP(i,2k)}{\sum_{(i,j) \in S(k)} iP(i,j)} \tag{12}$$

where $S_i(k) = \{j : (i,j) \in S(k)\}$.

Eq. (11) is the new call blocking probability experienced by calls originating in cell 2. We note that this is a good approximation of the actual new call dropping probability. Eq. (12) is derived by taking the ratio of the number of unsuccessful handoffs to the total number of handoff attempts arriving in cell 2. A recursive procedure has to be followed to compute P_{bh} and P_{bn}.

5   Numerical Results

In this section, we provide numerical results to compare our handoff scheme and the conventional FCA scheme with channel reservation. We use both simulation and the analytical technique presented in the last section to perform the comparison.

The following is the reference scenario for the simulation:

1. We have a linear array of 30 cells, with the end cells being connected.

2. The new call arrival, λ, is the same in all the cells.

3. Each cell is allocated 12 channels in the fixed channel allocation scheme; that is, $N = 12$.

4. The length of each cell, L, is assumed to be 425 km.

5. The relative velocity of mobiles, V, is 26,600 km/h.

6. The mean call holding time, $1/\mu$, is 3 minutes.

We observe that there is no loss of generality in assuming a linear array of cells for the LEO satellite system. This is because handoffs take place in only one direction if we ignore the overlapping region where a mobile could potentially handoff to a cell diagonally across. For the analytical results the same values of L, μ, and V are used. In all the results presented here, we use the normalized call arrival rate as a paramenter. The normalized call arrival rate is obtained by dividing the actual call arrival rate by $N\mu$.

The handoff dropping probability for our handoff scheme is too low to obtain reliable estimates using simulation. Therefore, we use the two-cell approximation to obtain estimates of the handoff dropping probabilities. In Figure 11, we plot the handoff call dropping probabilities of our handoff scheme for reuse factors 2 and 3. These values have been obtained from the two-cell approximation.

In order to do a fair comparison between the reservation scheme and our channel sharing handoff scheme, we choose the parameter P in the channel reservation scheme such that the handoff dropping probability of the channel reservation scheme closely approximates the handoff dropping probability obtained from our handoff scheme. We choose the parameter P of the channel reservation scheme as follows:

$$P_r^* = \min\{P : P_{bh}^{res}(N - P) \geq P_{bh}^{sh}(r) \text{ for } \lambda/N\mu = .5625\}$$

where $P_{bh}^{res}(N - P)$ is the handoff dropping probability of the reservation scheme with $N - P$ guard channels and $P_{bh}^{sh}(r)$ is the handoff dropping probability of the channel sharing handoff scheme for a reuse factor of r.

The choice of λ in the above equation was arbitrary. In Figure 12 we compare the new call blocking probabilities of the FCA scheme with $N - P_2^*$ guard channels and our handoff scheme (for reuse factor = 2). Similarly, in Figure 13 we compare our handoff scheme ($r = 3$) with the channel reservation scheme with $N - P_3^*$ guard channels. We see that we obtain several orders of
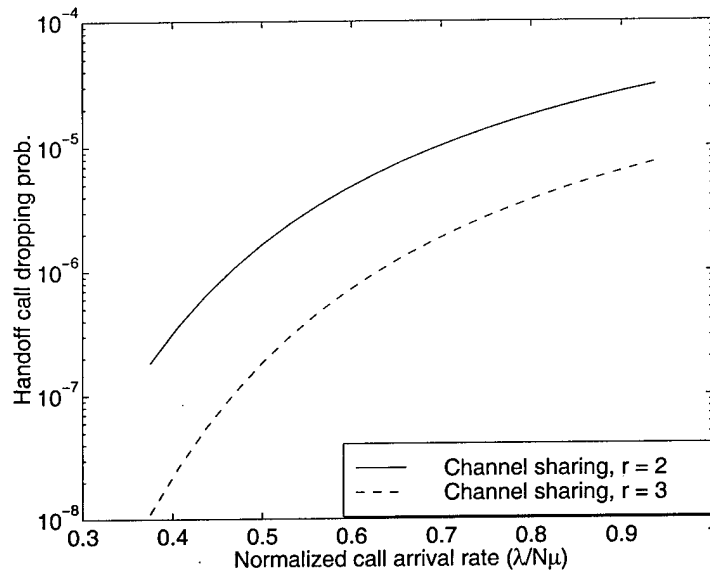
Figure 11: Comparison of two-cell approximations of handoff dropping probabilities for our channel sharing handoff scheme for reuse factors 2 and 3

magnitude improvement. Intuitively, such an improvement can be explained as follows: To obtain the same performance with the channel reservation scheme we should reserve as many channels as the number allowed to be carried in the channel sharing handoff scheme. While these channels are idle most of the time in the channel reservation scheme, in the channel sharing handoff scheme the channels can be used in adjacent cells to reduce the new call blocking probability. Figures 12 and 13 also show that the analytical results from the two-cell approximation are in very good agreement with the simulation results.

6   Conclusions

We presented a handoff handling scheme based on the channel sharing scheme in [5] for LEO satellite-based cellular networks. We obtained significant reduction in handoff dropping probability. To obtain a similar reduction in handoff dropping probability in the conventional FCA scheme would require a significant compromise in the new call blocking probability. We compared the new call blocking probabilities of our channel sharing handoff scheme to that of the reservation scheme under similar performance with handoff dropping probabilities. Our handoff scheme performs significantly better. We also developed an analytical approximation which is in very good agreement with the simulation results.

References

[1] F. Ananasso and M. Carosi. Architecture and networking issues in satellite systems for personal communications. *International Journal of satellite communications*, 12(1):33–44, January-February 1994.
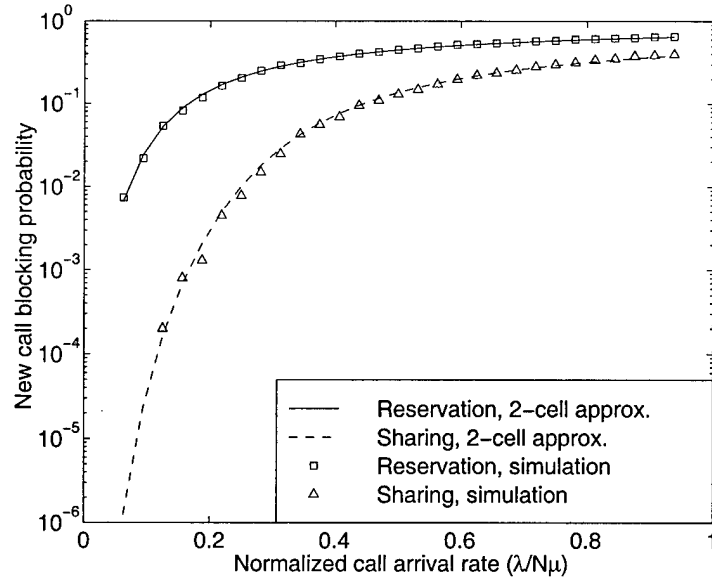
Figure 12: Comparison of simulation results and two-cell approximations for new call blocking probabilities for a reuse factor of 2.
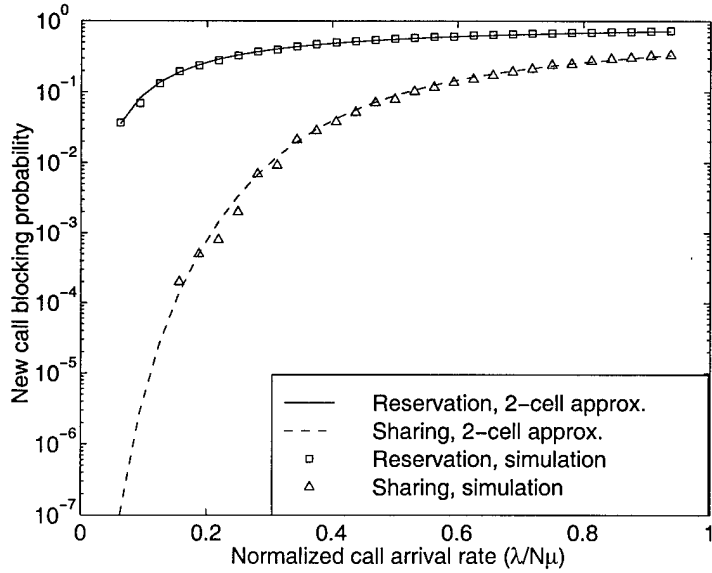
Figure 13: Comparison of simulation results and two-cell approximations for new call blocking probabilities for a reuse factor of 3.

19

[2] J. P. Havlicek, J. C. Mckeeman, and P. W. Remaklius. Networks of low-earth orbit store-and-forward satellites. *IEEE Transactions on Aerospace and Electronic Systems*, 31(2):543–553, April 1995.

[3] D. Hong and S. S. Rappaport. Traffic model and performance analysis for cellular mobile radio telephone systems with prioritized and non-prioritized handoff procedures. *IEEE Transactions on Vehicular Technology*, 35(3):77–92, 1986.

[4] J. Li, N. B. Shroff, and E. K. P. Chong. Channel carrying: a novel handoff scheme for mobile cellular networks. In *IEEE INFOCOM*, pages 909–917, 1997.

[5] J. Li, N. B. Shroff, and E. K. P. Chong. A channel sharing scheme to improve system capacity and quality of service in wireless cellular networks. In *Proceedings of the Third IEEE Symposium on Computers and Communications*, pages 700–704, 1998.

[6] G. Maral, J.-J. D. Ridder, B. G. Evans, and M. Richharia. Low earth orbit satellite systems for communications. *International Journal of satellite communications*, 9:209–225, 1991.

[7] R. Ramjee, R. Nagarajan, and D. Towsley. On optimal call admission control in cellular networks. *Wireless Networks*, 3(1):29–41, 1997.

[8] E. D. Re, R. Fantacci, and G. Giambene. Efficient dynamic channel allocation techniques with handover queuing for mobile satellite networks. *IEEE Journal on Selected Areas in Communications*, 13(2):397–405, February 1995.

[9] G. Ruiz, T. L. Dowmi, and J. G. Gardiner. Teletraffic analysis and simulation for nongeostationary mobile satellite systems. *IEEE Transactions on Vehicular Technology*, 47(1):311–320, February 1998.

[10] M. Sidi and D. Starobinski. New call blocking versus handoff blocking in cellular networks. In *IEEE INFOCOM*, volume 1, pages 35–42, 1996.

[11] S. Tekinay and B. Jabbari. A measurement based prioritization scheme for handovers in cellular and microcellular networks. *IEEE Journal on Selected Areas in Communications*, October 1992.

[12] M. Werner, A. Jahn, E. Lutz, and A. Bottcher. Analysis of system parameters for LEO/ICO-satellite communication networks. *IEEE Journal on Selected Areas in Communications*, 13(2):371–381, February 1995.

Channel Sharing Scheme for Packet-Switched Cellular Networks*

Suresh Kalyanasundaram, Junyi Li† Edwin K. P. Chong, Ness B. Shroff

School of Electrical and Computer Engineering

Purdue University

West Lafayette, IN 47907, U.S.A.

E-mail:{kalyanas, junyi, echong, shroff}@ecn.purdue.edu

Abstract

In this paper, we study an approach for sharing channels to improve network utilization in packet-switched cellular networks. Our scheme exploits unused resources in neighboring cells without the need for global coordination. We formulate a minimax approach to optimizing the allocation of channels in this sharing scheme. We develop a distributed algorithm to achieve this objective and study its convergence. We illustrate, via simulation results, that the distributed channel sharing scheme performs better than the fixed channel scheme over a wide variety of traffic conditions.

1 Introduction

The last several years has seen a tremendous growth in wireless networks all around the world. However, compared to its wired counterpart, network capacity is still very much a scarce resource in wireless systems. Hence, improving the network utilization is a very important problem in such systems. We will address this problem in the context of packet-switched networks. The reason we consider packet-switched cellular networks is that they have the advantage of statistical multiplexing and hence can deliver a higher throughput. There has been a large-scale effort to develop multiple-access schemes for packet-switched cellular networks. Studies have shown significant improvements in throughput for the packet-switched networks over those obtained for the circuit switched case. For example, Goodman et al. have shown in [1] that up to 1.64 simultaneous voice conversations can be supported in one channel.

The framework that we assume throughout this paper is that of a packet-switched cellular mobile system in which each cell contains a base station that communicates with mobile or stationary users in that cell. This communication is done over a given set of "channels." A channel can be thought of as a generic network resource such that chan-nels used in one cell cannot be used in other cells that are closer than the *minimum reuse distance*. For example, in practical TDMA/FDMA systems, two cells that are closer than the minimum reuse distance are not allowed to use the same carrier frequency. A significant body of research has been conducted on dynamically allocating channels to individual cells under this minimum reuse distance constraint (e.g., see [2] and [6], and the references therein) for circuit-switched networks. To simplify the complexities involved in dynamic channel allocation, some authors have proposed "channel borrowing" schemes to improve network utilization over fixed channel allocation ([4], [7]). However, these schemes require either channel-locking, which necessitates global coordination, or dynamic power control. To avoid these problems, in [8] and [9], the authors provide a localized "channel sharing" scheme that achieves significant throughput improvements over fixed channel allocation, without incurring significant overhead. The basic idea of the channel sharing scheme is that it attempts to alleviate call blocking by sharing channels between neighboring cells, while localizing the channel coordination.

In this paper, our objective is to extend the channel sharing scheme to packet-switched networks without the need for a central controller. We begin by defining channel sharing in the context of packet-switching. We then develop a distributed sharing scheme that optimizes a minmax objective function, in order to better utilize the network capacity. We next study the convergence of the algorithm. We then illustrate, via numerical examples, that the packet-switched sharing scheme significantly outperforms the fixed channel allocation schemes over a variety of traffic conditions.

2 The Sharing Scheme for Packet-Switched Cellular Networks

In this section, we provide an efficient but simple dynamic channel allocation scheme for packet-switched cellular networks based on the "sharing scheme" proposed in [8] and [9]. The sharing scheme attempts to alleviate call blocking by sharing channels between neighboring cells. For illustration, we consider a linear cellular network. Each cell has a base-station that communicates with mobile users in that cell using fixed-size packets. To facilitate the description, we

Figure 1: Linear Cellular system

Figure 2: The same set of channels can be used in meta-cells (A, B) and (B', C') and in meta-cells (B, C) and (C', D')
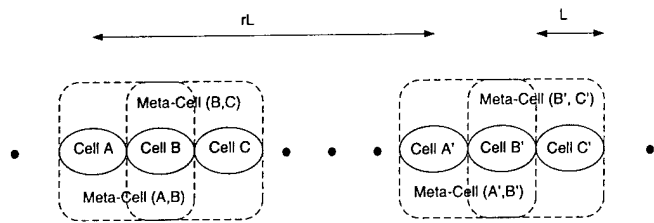
provide some terminology. For the sharing scheme, a *meta-cell* is defined to be a pair of neighboring cells. The two adjacent cells that together form a meta-cell are called the *component cells*. We allocate channels to meta-cells and allow these channels to be shared in any of the component cells of that meta-cell. Figure 1 shows a family of meta-cells in a linear cellular system, each comprising a pair of two adjacent cells. For example, in Figure 1, cells A and B are components of meta-cell (A, B). Note that the meta-cell is a logical notion that we use to help describe our distributed sharing algorithm. This notion has nothing to do with hierarchical cellular schemes in the literature.

Our channel allocation scheme for packet-switched cellular networks involves two main steps: (a) Fixed allocation of channels to meta-cells; (b) Dynamic allocation of channels to individual cells from those allocated to meta-cells.

2.1 Allocation of Channels to Meta-cells

The fixed allocation of channels to meta-cells was proposed in [8] and [9]. The number of channels allocated to a meta-cell is fixed and does not change with time. The channel sharing scheme allows channels to be shared between neighboring cells (namely, cells belonging to the same meta-cell). Consider Figure 1. For this simple linear cellular system, the distance measure $d(X, Y)$ between two cells X and Y is traditionally given as $d(X, Y) = |c_X - c_Y|$, where c_X and c_Y denote the positions of the centers of cells X and Y, respectively. The minimum reuse distance Δ is defined to be $\Delta = rL$, where L is the width of a single cell and r is an integer. Cells that are assigned the same set of channels are called co-channel cells. In the conventional scheme for fixed channel allocation, each channel is assigned to cells that are exactly a distance Δ apart. We refer to this scheme as the *tightest fixed channel assignment* scheme, in which co-channel cells are exactly r cells apart. For example, in Figure 1, cells A and A' are co-channel cells. Let T denote the total number of distinct channels that are available in this linear cellular system (over a certain period of time). Thus, the total number of distinct channels available for each cell is T/r (i.e., the reuse factor is r).

In the sharing scheme, we attempt to alleviate call blocking by sharing channels between neighboring cells, while localizing the channel coordination using the meta-cell idea. As stated above, a meta-cell can be designated by the pair of its component cells. For example, in Figure 1, cells A and B are components of meta-cell (A, B).

To assign channels to meta-cells, we next define the distance measure $d((X, Y), (X', Y'))$ between two meta-cells (X, Y) and (X', Y'). Recall that in the sharing scheme, when a channel is assigned to a meta-cell, it can be used by a mobile user in any cell belonging to that meta-cell. Thus, we have to ensure that the distance measure between any component cells of two meta-cells assigned the same set of channels complies with the minimum reuse distance requirement. Consequently, we define $d((X, Y), (X', Y'))$ as the minimum of the distance measures between the component cells of meta-cells $(X, Y), (X', Y')$, i.e.,

$$d((X, Y), (X', Y')) = \qquad (1)$$
$$\min\{d(X, X'), d(X, Y'), d(Y, X'), d(Y, Y')\}.$$

For example, in Figure 1, the distance $d((A, B), (A', B'))$ between meta-cells (A, B) and (A', B') is $(r - 1)L$, which is equal to the distance between cells B and A'.

We call meta-cells that are assigned the same set of channels *co-channel meta-cells*. To allocate a maximum number of channels to each meta-cell, co-channel meta-cells must be deployed as close as possible. Therefore, we assign the same set of channels to meta-cells that are exactly the minimum reuse distance apart, i.e., rL in this case. For example, in Figure 2, meta-cells (A, B) and (B', C') are assigned the same set of channels (i.e., they are co-channel meta-cells). Consider a particular channel in this set. Now, when the channel is used simultaneously in meta-cells (A, B) and (B', C'), the shortest possible reuse distance is between cells B and B', which is exactly the minimum reuse distance rL. Thus, the same channel can be independently used in cell A or B and cell B' or C'.

It is easy to see that in this channel assignment scheme, each meta-cell is assigned $T/(r + 1)$ distinct channels. In other words, the reuse factor of our channel assignment scheme is $r' = r + 1$. However, in the tightest fixed channel assignment scheme, the number of channels assigned to each meta-cell is T/r, so the cost we pay for allowing channels to be "shared" is $T/r - T/r' = T/r(r + 1)$. Nevertheless, by increasing the reuse distance in this fashion we facilitate a simple way for channels to be shared due to which we may be able to use as many as $2T/r'$ channels in the same cell. The increase in complexity is minimal because we do not require a central controller to allocate channels to individual calls. Moreover, unlike other channel borrowing schemes, in the
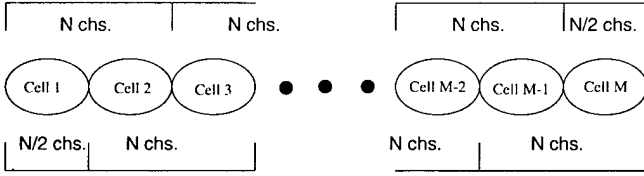
Figure 3: Number of channels allocated to different meta-cells

sharing scheme we do not need to use channel locking [10] or power control techniques [7].

2.2 Dynamic Allocation of Channels to Component Cells

We now discuss the dynamic allocation of channels to component cells from among those allocated to meta-cells. We focus on the uplink case (transmission from mobile to base-station). The allocation of channels to cells cannot take place each time a packet that has to be transmitted to the base-station arrives because the relatively short packet transmission times will require adjacent base-stations to be in constant contact to find out unused channels. This will result in an enormous overhead. Therefore, we propose the following scheme for sharing. At the end of every U time units, we allocate channels to individual cells from those allocated to meta-cells. Once the allocation is done, for the next U time units, mobiles can only use these channels for the transmission of packets to the base-station. So, this allocation has to be done in a way that will efficiently handle traffic disparities among cells.

The ability of the sharing scheme to handle the varying nature of traffic depends on the choice of U. There is clearly a trade-off in choosing U. The shorter the update duration, U, the more efficient the sharing and the more responsive the scheme to traffic variations. On the other hand, the shorter the update duration the greater the overhead and complexity of the coordination protocol between base-stations.

We assume that there are a total of M cells. We also assume that each meta-cell is allocated N channels for every U time units using the procedure described in the previous section. We assume that the two edge cells are both assigned $N/2$ channels for every U time units (as shown in Figure 3). Note that, for convenience, we have assumed that N is even.

Let us consider the time duration $[(n-1)U, nU]$. Let $\lambda_i(n)$ be the packet arrival rate in the i-th cell for the duration $[(n-1)U, nU]$. Let $x_i(n)$ be the number of channels allocated from meta-cell $(i, i+1)$ to cell i for the duration $[(n-1)U, nU]$. We note here that cell i, besides getting $x_i(n)$ channels from meta-cell $(i, i+1)$, also gets $N - x_{i-1}(n)$ channels from meta-cell $(i-1, i)$. The load ρ_i of cell i is given by:

$$\rho_1(n) = \frac{\lambda_1(n)}{N/2 + x_1(n)}$$

$$\rho_i(n) = \frac{\lambda_i(n)}{N - x_{i-1}(n) + x_i(n)} \text{ for } i = 2, 3, \ldots, (M-1) \quad (2)$$

$$\rho_M(n) = \frac{\lambda_M(n)}{N - x_{M-1}(n) + N/2}.$$

We choose the following as our objective:

$$\min_{[x_1(n), \ldots, x_{M-1}(n)]} \max_{1 \leq i \leq M} \rho_i(n) \quad (3)$$

subject to

$$0 \leq x_i(n) \leq N$$

and $x_i(n)$ integer for $i \in \{1, 2, \ldots, (M-1)\}$ and for all n.

The function $\rho(\cdot)$ is a measure of the traffic load in each cell. A higher value of ρ implies a longer waiting time and a higher packet dropping probability. Given fixed arrival rates at each cell, our objective is to find values of the allocations $x_1(n), \ldots, x_{M-1}(n)$ to minimize the worst case value of ρ over all the cells. *This strategy has the effect of allocating more channels to those cells that have higher arrival rates.*

We can take several different approaches to solving the problem. First, we can solve the above minimax problem as an integer programming problem and allocate channels based on the solution obtained. Alternatively, we can relax the requirement that $x_i(n)$ be an integer, compute the solution and then interpret the result probabilistically (as discussed in Section 5). We choose to take the latter approach because of the computational complexity involved in solving the integer programming problem. Moreover, this approach provides insights that lead to the ideas described in the distributed sharing scheme. Therefore, from now on, we will drop the integer constraints on the $x_i(n)$'s in problem (3).

We have the following theorem on the solution to our optimization problem without the integer constraints.

Theorem 1 *If the system of equations*

$$\rho_1 = \rho_2 = \cdots = \rho_M \quad (4)$$

results in a solution $\mathbf{x}^* = [x_1^*, x_2^*, \ldots, x_{M-1}^*]$ *that satisfies the constraints*

$$0 < x_i^* < N, \ i = 1, 2, \ldots, (M-1) \quad (5)$$

then, $\mathbf{x}^*$ *is the unique optimal solution to the optimization problem given in eq. (3).*

Proof: We use the following theorem from [11] to prove our result.

Theorem A *Let* $f_i(\mathbf{x}), i = 1, 2, \ldots, M$, *be continuously differentiable functions on an open set* Ω'. *Let* $\Phi(\mathbf{x}) = \max_{1 \leq i \leq M} f_i(\mathbf{x})$ *and* $R(\mathbf{x}) = \{i \in \{1, 2, \ldots, M\} : f_i(\mathbf{x}) = \Phi(\mathbf{x})\}$. *Let* Ω *be a convex closed subset of* Ω'. *Then a necessary condition for a point* $\mathbf{x}^* \in \Omega$ *to be a minimum point of* $\Phi(\mathbf{x})$ *on* Ω *is that*

$$\inf_{\mathbf{z} \in \Omega} \max_{i \in R(\mathbf{x}^*)} \left\langle \frac{\partial f_i(\mathbf{x}^*)}{\partial \mathbf{x}}, \mathbf{z} - \mathbf{x}^* \right\rangle = 0 \quad (6)$$

where $\langle \mathbf{a}, \mathbf{b} \rangle$ *denotes the inner product of* $\mathbf{a}$ *and* $\mathbf{b}$. *If* $\Phi(\mathbf{x})$ *is convex, this condition is also sufficient.*

Details of the proof can be found in [12]. □

This solution to the minimax optimization problem is intuitive. We see that any further attempt to reduce $\max\{\rho_1, \rho_2, \ldots, \rho_M\}$ from the optimal solution of $\rho_1 = \rho_2 = \cdots = \rho_M$ would have to increase the number of channels allocated to each cell. Since we have already made use of all the channels, such a reduction is impossible.

For some results in this paper we assume that the solution to eq. (4) satisfies the constraints in eq. (5). This is a reasonable assumption because a very high degree of permanent non-uniformity in traffic is required to obtain a set of λ_i's that violate this assumption. Such permanent overloaded cells can be handled by allocating more fixed channels to the meta-cell. For transient overloaded cells, our assumption is very reasonable and will almost always be satisfied. Further, in [12] we describe a method to obtain the optimal solution for the case when this assumption is relaxed.

The above solution to the minimax problem tells us that the optimal solution is obtained by making the load (ρ) in all the cells equal. This observation leads naturally to an algorithm similar to load balancing. In the following, we develop distributed strategies to dynamically allocate channels to component cells from those allocated to meta-cells based on the above minimax solution.

3 Distributed Sharing Scheme

Note that to implement the solution to our optimization problem directly, we need to know the packet arrival rates in all the M cells. This implies that there should be a central controller to allocate channels. Therefore, to do away with the requirement for a central controller, we develop a distributed algorithm to allocate channels. In our distributed scheme, the components of each meta-cell interact among themselves and decide the number of channels each cell is going to take. The number of channels each cell takes at each update time is such that the resulting load (ρ's) of the two component cells within a meta-cell will be equal. The order and manner of interaction between cells is described in Section 3.2. The cells keep interacting and re-evaluating the x_i's until the termination condition is reached. Henceforth, we will only consider the time interval $[(n-1)U, nU]$ and for simplicity we will not explicitly display the dependence of λ, x, and ρ on n.

We describe the distributed sharing scheme in the following sections.

3.1 Allocation Update Operation

Let us consider the case when cells i and $i+1$ are interacting to decide the number of channels each of them should take from among those belonging to meta-cell $(i, i+1)$. Let cell i have α channels from meta-cell $(i-1, i)$ and cell $(i+1)$ have β channels from meta-cell $(i+1, i+2)$ from the previous iteration. Then, we update x_i as follows:

$$x_i = \frac{\lambda_i(\beta + N) - \lambda_{i+1}\alpha}{\lambda_i + \lambda_{i+1}}. \tag{7}$$

The above choice of x_i would make $\rho_i = \rho_{i+1}$.

Note that the update equation (7) does not guarantee feasibility, i.e., that x_i satisfies $0 \leq x_i \leq N$. To ensure feasibility, we suggest the following modification:

$$x_i = \begin{cases} 0 & \text{if } \lambda_i(\beta + N) \leq \lambda_{i+1}\alpha \\ N & \text{if } \lambda_i\beta \geq \lambda_{i+1}(N + \alpha) \\ \frac{\lambda_i(\beta+N) - \lambda_{i+1}\alpha}{\lambda_i + \lambda_{i+1}} & \text{otherwise.} \end{cases} \tag{8}$$

Essentially, the above modification just takes the projection of the solution obtained from eq. (7) on the interval $[0, N]$.

3.2 Interaction Mechanism

In this section we describe how the sharing operation can proceed by providing three different interaction mechanisms.

3.2.1 Mechanism 1: Serial Synchronous Mechanism

At the end of each U time units, do the following:

1. Set $i := 0$, initial condition $\mathbf{x}^{(0)} = [x_1^{(0)}, x_2^{(0)}, \ldots, x_{M-1}^{(0)}]$.

2. If termination condition has not been reached (see Section 3.3), do the following:

3. Update $x_1^{(i)}, x_2^{(i)}, \ldots, x_{M-1}^{(i)}$ to $x_1^{(i+1)}, x_2^{(i+1)}, \ldots, x_{M-1}^{(i+1)}$ successively using eq. (8).

4. Set $i := i + 1$ and go to step 2.

A good choice for the initial condition $\mathbf{x}^{(0)}$ is the final allocation for the previous U time units. In words, the algorithm works as follows: We first let cells 1 and 2 interact to decide x_1, then let cells 2 and 3 decide x_2 and so on. Once x_{M-1} has been decided, we revert back to cells 1 and 2 and the variable x_1. We continue the above process until the termination condition is satisfied. The final allocation is based on the values of x_i's at the time when sharing is terminated.

3.2.2 Mechanism 2: Parallel Synchronous Mechanism

We now describe an alternative synchronous interaction mechanism. This interaction mechanism does sharing operations in parallel and hence will converge faster. The algorithm is described as follows:

At the end of each U time units, do the following:

1. Set $i := 0$, initial condition $\mathbf{x}^{(0)} = [x_1^{(0)}, x_2^{(0)}, \ldots, x_{M-1}^{(0)}]$.

2. If termination condition has not been reached (see Section 3.3), do the following:

3. Update $x_1^{(i)}, x_3^{(i)}, \ldots$ to $x_1^{(i+1)}, x_3^{(i+1)}, \ldots$ simultaneously using eq. (8). Then update $x_2^{(i)}, x_4^{(i)}, \ldots$ to $x_2^{(i+1)}, x_4^{(i+1)}, \ldots$ simultaneously using eq. (8).

4. Set $i := i + 1$ and go to step 2.

This interaction mechanism works as follows: Meta-cells (1,2), (3,4), (5,6) etc. together carry out an update operation. Then meta-cells (2,3), (4,5), (6,7) etc. together carry out an update operation using the updated values from the last operation. Then we revert back to meta-cells (1,2), (3,4), (5,6) etc. with the updated values.

3.2.3 Mechanism 3: Asynchronous Mechanism

In the asynchronous mechanism we do not require meta-cells to coordinate their update operations with other meta-cells. Instead, each meta-cell can perform update operations at arbitrary times and in an asynchronous fashion (see Section 5 for a discussion of possible rules for update initiation). Hence, we do not require a global clock to carry out this operation. Whenever an update is initiated in a meta-cell, say $(i, i+1)$, we update x_i according to eq. (8).

In Section 4 we provide convergence results for the distributed algorithm. The parallel synchronous mechanism will converge faster to the optimal solution since the sharing operations are carried out in parallel. The asynchronous mechanism simplifies implementation by eliminating the coordination and global clock required with the other two synchronous mechanisms.

3.3 Termination condition

The termination condition determines when to stop the sharing iteration. The distributed sharing scheme converges to the optimal solution and has the *descent property*, i.e., the maximum cell load (ρ_i) at the end of each iteration is at most as large as the maximum cell load at the end of the previous iteration. (We state these results in the next section). Therefore, the iterations can be terminated based on any of the following criteria: (a) Terminate after a fixed number of steps; (b) Terminate after the difference between successive iterates falls below a certain threshold, i.e., terminate once $\|\mathbf{x}^{(k+1)} - \mathbf{x}^{(k)}\|_\infty < \epsilon_a$; (c) Terminate after the relative difference between successive iterates falls below a certain threshold, i.e., terminate once $\frac{\|\mathbf{x}^{(k+1)} - \mathbf{x}^{(k)}\|_\infty}{\|\mathbf{x}^{(k)}\|_\infty} < \epsilon_r$.

4 Analysis of the Distributed Algorithm

In this section we show that the distributed algorithm has the descent property. We also show that if the optimal solution to the minimax problem results in $\rho_1(\mathbf{x}^*) = \rho_2(\mathbf{x}^*) = \cdots = \rho_M(\mathbf{x}^*)$, then the distributed algorithm converges to the optimal solution. To save space, we do not provide detailed proofs for our results. Complete details can be found in [12].

We first claim that for a fixed α and β, x_i given by eq. (8) results in the minimax solution for the two cells under consideration, namely cells i and $(i+1)$.

Lemma 1 *The value of x_i^* given by eq. (8) is the optimal solution to the following problem:*

$$\min_{x_i} \max\{\rho_i, \rho_{i+1}\} \tag{9}$$

subject to $0 \le x_i \le N$ where $\rho_i = \lambda_i/(\alpha + x_i)$ and $\rho_{i+1} = \lambda_{i+1}/(N - x_i + \beta)$.

Proof: See [12]. □

We now claim that the distributed algorithm has the descent property. This claim is easily proven using Lemma 1.

Theorem 2 *The distributed algorithm has the following descent property: If $\{\mathbf{x}^{(k)}\}$ is the sequence of iterates obtained from the distributed algorithm and if $\{\rho_i^{(k)}, i = 1, 2, \ldots, M\}$ are the corresponding function values, then*

$$\max_{1 \le i \le M} \rho_i^{(k+1)} \le \max_{1 \le i \le M} \rho_i^{(k)}. \tag{10}$$

Proof: See [12]. □

If the optimal solution $\mathbf{x}^*$ satisfies $0 < x_i^* < N$, then $\mathbf{x}^*$ is the only point that will remain unchanged under the distributed algorithm iterations. We state this result as the following proposition.

Proposition 1 *If the point $\mathbf{x}^* = [x_1^*, x_2^*, \ldots, x_{M-1}^*]$, is such that $\rho_1^* = \cdots = \rho_M^*$ and*

$$0 < x_i^* < N, \quad i = 1, 2, \ldots, (M-1), \tag{11}$$

then $\mathbf{x}^*$ is the only fixed point of the distributed algorithm iteration.

Proof: See [12]. □

The following theorem states that the distributed algorithm iterates converge to the optimal solution.

Theorem 3 *Let $\{\mathbf{x}^{(k)}\}$ be the sequence of iterates obtained from the distributed algorithm as described above and let the optimal solution $\mathbf{x}^*$ satisfy the assumption in eq. (4), then $\mathbf{x}^{(k)} \to \mathbf{x}^*$.*

Proof: See [12]. □

The distributed algorithm, as described above, has an appealing geometric interpretation. We note that when the optimal minimax solution satisfies eq. (4), it is just the solution to the following system of equations:

$$
\begin{aligned}
-(\lambda_1 + \lambda_2)x_1 + \lambda_1 x_2 &= \lambda_2 N/2 - \lambda_1 N \\
\lambda_3 x_1 - (\lambda_2 + \lambda_3)x_2 + \lambda_2 x_3 &= \lambda_3 N - \lambda_2 N \\
&\vdots \\
\lambda_M x_{M-2} - (\lambda_{M-1} + \lambda_M)x_{M-1} & \\
= \lambda_M N &- 3N\lambda_{M-1}/2.
\end{aligned}
\tag{12}
$$

The serial mechanism of our distributed algorithm works as follows: Given an initial $\mathbf{x}^{(0)}$, fixing $x_2^{(0)}$, we find an $x_1^{(1)}$ that satisfies the first of the above equations. Then, fixing $x_1^{(1)}$ and $x_3^{(0)}$, we find an $x_2^{(1)}$ that satisfies the second equation above and so on. In general, fixing $x_{i-1}^{(k+1)}$ and $x_{i+1}^{(k)}$, we find $x_i^{(k+1)}$ by solving the i-th equation above. In Figure 4, we illustrate how this scheme converges to the optimal solution for the 3-cell case.
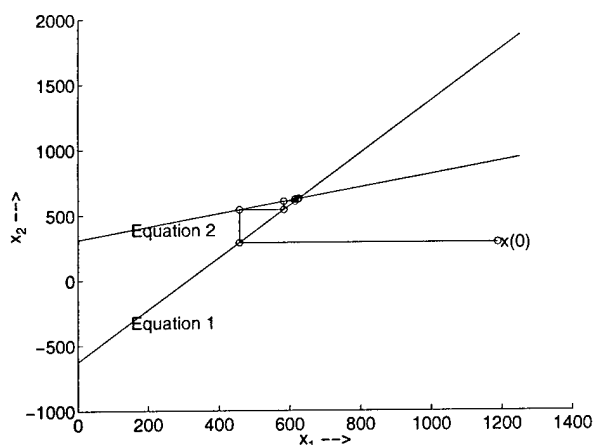
Figure 4: Convergence of the distributed algorithm

5 Discussion

In this section we discuss some issues related to our scheme.

We note that usually we will not know the exact value of the packet arrival rate $\lambda_i(n)$, beforehand. Therefore, we may need to estimate $\lambda_i(n)$. One possibility is to use the packet arrival rate over the last L time units. There is a trade-off in choosing L. If we choose L large, then our sharing algorithm will not react substantially to a change in packet arrival rate that has just begun. On the other hand, if we choose L small, then the sharing algorithm would react to even a small change in packet arrival rate that may not last very long. In the simulation, presented in the next section, we choose $L = U$.

The choice of termination condition is crucial for the distributed algorithm iterations. The longer we run the iterations the more balanced the load is over all the cells. But, each iteration increases the overhead because we require adjacent base stations to inform each other of their respective updates. In our simulation results described in the next section, we observe that for a single overloaded cell, one complete iteration is usually sufficient to give satisfactory performance.

Another factor that influences the number of iterations that need to be made is that we may have to carry out the iteration based on the estimated packet arrival rate and not the actual packet arrival rate. It might turn out that the actual packet arrival rate could be quite different from the estimated arrival rate. Thus, it may be better to carry out the iterations every once in a while based on an updated estimate rather than carry out more iterations with the same estimated packet arrival rate.

In our algorithm, we have assumed that the allocation is updated periodically. However, alternative update rules are possible. For example, an update can be initiated by an overloaded cell or by an underloaded cell. Specifically, when an overloaded cell realizes that its load (ρ) is higher than a certain maximum threshold, it can initiate an update. Similarly, when the ρ value in an underloaded cell drops

below a certain lower threshold, it can initiate an update. Alternatively, a cell can initiate an update when its ρ rises or drops by more than a certain percentage since the last update.

We have described our schemes only for a linear cellular network. These ideas can be extended to 2-D and 3-D cases. Simulation analysis for the 2-D case was carried out in a circuit switched setting in [8] and the gains were impressive. We expect similar gains in the packet-switched scenario also for the 2-D as well as 3-D cases. We are currently investigating the sharing scheme for the 2-D case in the packet-switched scenario.

We have shown the convergence of the distributed algorithm to the optimal solution only when the optimal solution satisfies eq. (4). But, as we have noted before, our distributed algorithm has the descent property irrespective of whether the optimal solution satisfies eq. (4) or not. From a practical viewpoint, we can terminate the algorithm after just a few iterations and still expect the performance gain to be substantial. For example, in the simulation results presented in the next section, we terminate the iterations after exactly one complete cycle and we still obtain fairly impressive gains over the FCA scheme.

The solution we have given assumes that x_i's are all real, while, in practice, they have to be integers. We could arbitrarily round off the x_i's or take the floor or ceiling to satisfy the integer requirements. Alternatively, we suggest the following probabilistic method of handling the integer constraints. The number of channels we allocate to cell i from meta-cell $(i, i+1)$ can be decided as follows: Allocate $\lfloor x_i \rfloor$ channels to cell i with a probability of $\lceil x_i \rceil - x_i$ and allocate $\lceil x_i \rceil$ channels with a probability of $x_i - \lfloor x_i \rfloor$. If we interpret the result this way, it can easily be seen that the expected value of the number of channels allocated to cell i is x_i.

6 Numerical Results

In this section we present simulation results. We consider a linear cellular system of 30 cells. We assume packet arrivals to be Poisson and packet sizes to be fixed at 576 bits/packet. The objective is to observe the performance of the distributed sharing scheme in the presence of traffic non-uniformities. Towards this end, we fix the packet arrival rate in all cells, except cell 15, at 500 packets/sec. We increase the packet arrival rate in cell 15 from 500 packets/sec to 2900 packets/sec and observe the results.

In the fixed channel allocation scheme, each cell is allocated a carrier that can handle 1250 packets/sec. In the simulations, we choose $U = .48$ seconds. We terminate the distributed sharing algorithm after exactly one iteration cycle and as the results show, we get fairly impressive gains over the FCA scheme. Since we need just one iteration to get satisfactory results, the overhead to implement the sharing scheme is minimal (as can be seen from Table 1). The simulations use the estimated packet arrival rates and not the exact packet arrival rates. We leave the packet arrival

	U = .16 s	U = .48 s	U = 1.6 s
reuse = 2	1.48%	.498%	.15%
reuse = 3	1.32%	.442%	.133%
reuse = 4	1.23%	.415%	.125%

Table 1: Fraction of overhead traffic for updates

rate in the congested cell as a parameter. We normalize the packet arrival rates using the packet arrival rate in the other cells, i.e., 500 packets/sec.

In Table 1, we compare the percentage overhead due to information exchange when we stop the algorithm after one iteration cycle for various update durations and reuse factors. Whenever a cell carries out an updating process, we assume that two packets will be required. For example, when x_i is being updated, one packet each would be required for cell i to first obtain information about the latest value of x_{i+1} and then to inform cell $i + 1$ about the updated value of x_i, once the updating is done. We note here that these overhead packets can be transmitted over the wired network where the resources are not as scarce.

In Figures 5(a) and 5(b), we compare the packet dropping probabilities of the sharing scheme for various reuse factors and the fixed channel allocation scheme. In Figure 5(a) we have the overall packet dropping probability and in Figure 5(b), the comparison is between packet dropping probabilities only in the most congested cell (namely, cell 15). We assume an FCFS queuing discipline for transmitting packets to the base-station and that a packet that arrives when there are 200 or more packets in the queue gets dropped. We see that the sharing scheme performs consistently better than the fixed channel scheme. As expected, we also find that the higher the reuse factor, the better the performance. For example, for an overall packet dropping probability of 0.01 while we can support a normalized packet arrival rate of only 2.8 in the fixed channel scheme we can support a normalized packet arrival rate of up to 4.8 with the sharing scheme for a reuse factor of 4. Similarly, for a typical value of packet dropping probability in the congested cell of 0.1 the improvement in the packet arrival rate that can be supported is 29% if the reuse factor is 2 and as much as 61% if the reuse factor is 4.

In Figures 6(a) and 6(b), we compare the waiting time of a packet before it gets transmitted to the base-station. In Figure 6(a) the overall average waiting time for a packet is compared. In Figure 6(b) we plot the average waiting time for a packet in the congested cell. In these figures we also plot the 99% confidence intervals. We obtain a substantial performance improvement using the sharing scheme. For example, for an overall average waiting time of 0.3 seconds, while the fixed channel scheme can support a normalized packet arrival rate of only 3.3, the sharing scheme can support a (normalized) packet arrival rate of about 4.1 if the reuse factor is 2 and about 5.3 if the reuse factor is 4. These represent improvements of about 24% and 61% respectively. Similarly, for an average waiting time of 2 seconds in the
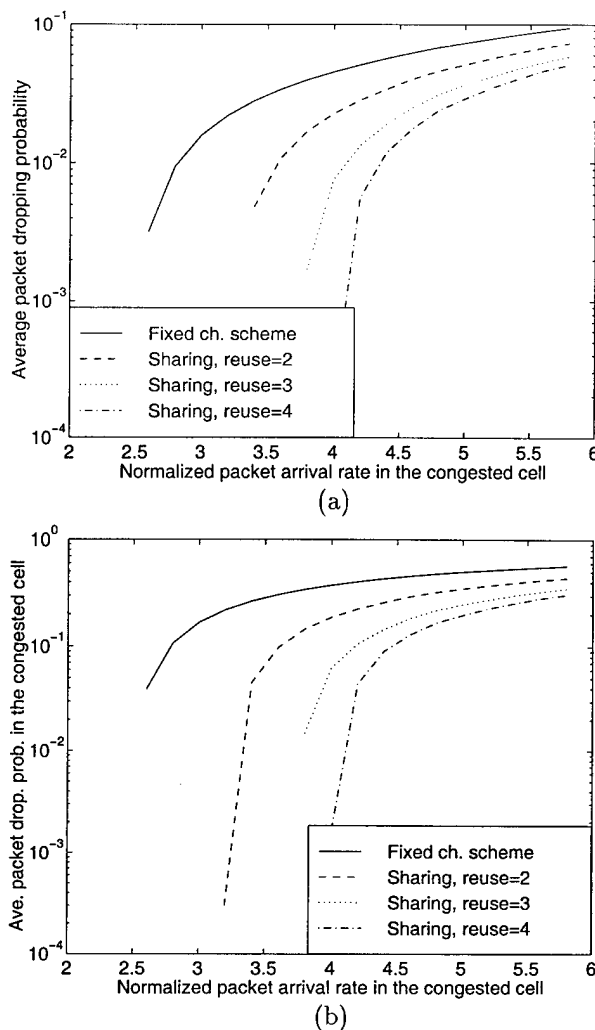
Figure 5: (a) Comparison of packet dropping probabilities for all the 30 cells (b) Comparison of packet dropping probabilities in the congested cell

congested cell, the improvement we obtain for the sharing scheme over the fixed channel scheme is about 22% if the reuse factor is 2, 43% if the reuse factor is 3, and 62% if the reuse factor is 4.

7   Conclusions

In this paper, we developed a channel sharing algorithm for packet-switched cellular networks that performs better than fixed channel allocation over a wide range of traffic conditions. We formulated our objective in terms of a minimax problem and developed distributed algorithms that achieve this objective. Our distributed sharing algorithm can easily be implemented since a central controller is not required to assign channels to cells. The asynchronous version of the distributed algorithm is even simpler to implement because, besides not requiring a central controller, it does not require cells to coordinate their sharing operations. We showed the convergence of the distributed sharing algorithm to the op-

(a)

(b)
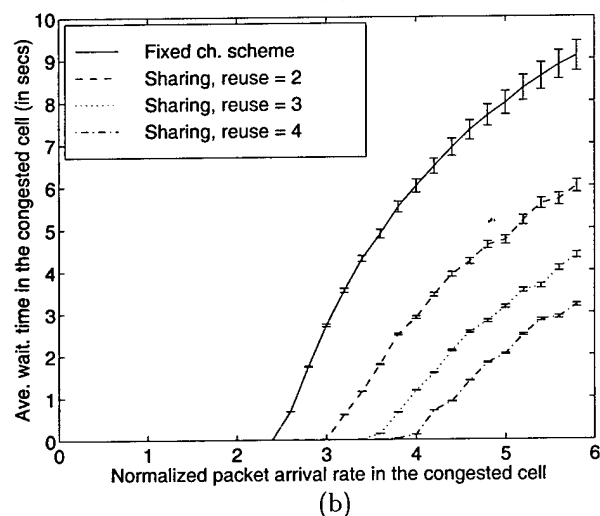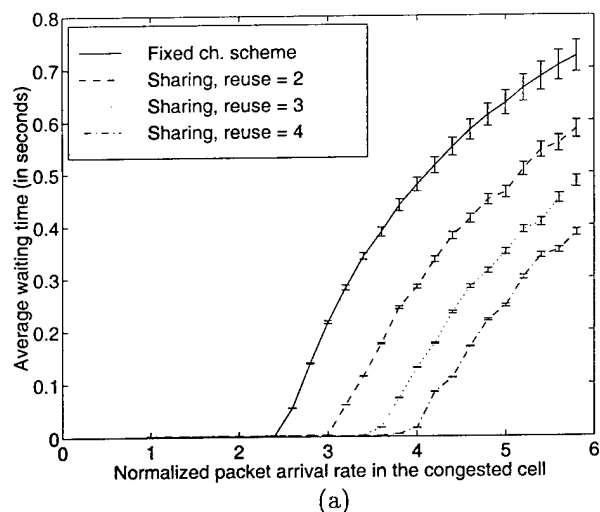
Figure 6: (a) Comparison of average waiting time in all the 30 cells with 99% confidence intervals (b) Comparison of average waiting time in the congested cell with 99% confidence intervals

timal solution for commonly occurring packet arrival patterns. Simulation results showed that our distributed channel sharing scheme performs significantly better than fixed channel allocation techniques over a variety of traffic conditions even with just a single complete iteration of the sharing algorithm.

References

[1] D. J. Goodman and S. X. Wei, "Efficiency of packet reservation multiple access," *IEEE Transactions on Vehicular Technology*, vol. 40, no. 1, pp. 170–176, February 1991.

[2] S. Tekinay and B. Jabbari, "Handover and channel assignment in mobile cellular networks," *IEEE Communications Magazine*, pp. 42–46, November 1991.

[3] C.-J. Chang, P.-C. Huang, and T.-T. Su, "A channel borrowing scheme in a cellular radio system with guard channels and finite queues," in *IEEE International Communications Conference*, pp. 1168–1172, IEEE, 1996.

[4] H. Jiang and S. Rappaport, "Prioritized channel borrowing without locking: a channel sharing strategy for cellular communications," *IEEE/ACM Transactions on Networking*, vol. 4, no. 2, pp. 163–171, 1996.

[5] H. Jiang and S. Rappaport, "A channel borrowing scheme for TDMA cellular communications systems," in *IEEE Vehicular Technology Conference*, pp. 97–101, IEEE, 1995.

[6] I. Katzela and M. Naghshineh, "Channel assignment schemes for cellular mobile telecommunication systems: a comprehensive survey," *IEEE Personal Communications Magazine*, pp. 10–31, June 1996.

[7] H. Jiang and S. Rappaport, "CBWL: a new channel assignment and sharing method for cellular communication systems," *IEEE Transactions on Vehicular Technology*, vol. 43, pp. 313–322, May 1994.

[8] J. Li, N. B. Shroff, and E. K. P. Chong, "A channel sharing scheme to improve system capacity and quality of service in wireless cellular networks," in *Proceedings of the Third IEEE Symposium on Computers and Communications*, pp. 700–704, IEEE, 1998.

[9] J. Li, N. B. Shroff, and E. K. P. Chong, "Channel carrying: a novel handoff scheme for mobile cellular networks," in *IEEE INFOCOM*, pp. 909–917, IEEE, 1997.

[10] K. L. Yeung and T.-S. P. Yum, "Cell group decoupling analysis of a channel borrowing based dynamic channel assignment strategy in microcellular radio systems," in *IEEE Global Telecommunications Conference*, pp. 281–287, IEEE, 1993.

[11] V. F. Dem'yanov and V. N. Malozemov, *Introduction to Minimax.* John Wiley and Sons, 1974.

[12] S. Kalyanasundaram, J. Li, E. K. P. Chong, and N. B. Shroff, "Channel sharing scheme for packet-switched cellular networks," Tech. Rep., Purdue University, 1998.

A Static Power Control Scheme for Wireless Cellular Networks [1]

Junyi Li   Ness B. Shroff[2]   Edwin K.P. Chong

School of Electrical and Computer Engineering
Purdue University, West Lafayette, IN 47907, U.S.A.
E-mail: {junyi, shroff, echong}@ecn.purdue.edu

Abstract—We present a novel static power control scheme to improve system capacity in wireless cellular networks. Our basic idea is to reduce intercellular interference and improve the capture probability by coordinating transmission powers of users in different cells. This coordination is determined beforehand and no real-time coordination is required. Power control is static and fixed. We formulate and solve a generic optimal scheduling problem with our coordination scheme. We find that the optimal scheduling policy is in a simple form of bang-bang control, which is illustrated for a specific case with the uniform fairness constraint. We evaluate, via numerical analysis and simulation, both throughput and delay, and compare them with other schemes. We find that the coordination scheme can achieve significant performance improvement, in terms of both maximum throughput and throughput-delay tradeoff, over a wide range of capture ratio values.

I. INTRODUCTION

In the last few years, wireless communication systems have experienced tremendous growth. Compared to its wired counterpart, the wireless spectrum is a much more scarce resource. Cellular technology is an effective means of improving spectrum utilization in the wireless environment. In a cellular system, the service area is covered by a number of contiguous small zones, called cells. The same spectral resource can be reused simultaneously in different cells, provided that their mutual interference is low enough for reliable communication in individual cells. The unit of wireless spectrum needed to serve a single user is called a *channel*. In current cellular systems, especially in the circuit-switched environment, channel reuse is separated by at least a *minimum reuse distance*, which is typically set such that the signal-to-interference ratio (SIR) on the same channel statistically exceeds some threshold. A significant body of research has been conducted on efficiently allocating channels to individual cells under this minimum reuse distance constraint, among which there are fixed and dynamic channel allocation schemes.

Next generation wireless systems are envisioned to support high-speed multimedia applications with packet-switching technology. For example, there has been a significant research effort devoted to the development of wireless ATM networks.

Experience in the wired network environment has shown that large channel capacity is needed to maintain quality of service for multimedia applications. The capacity problem becomes even more severe in the wireless environment. Thus, one of the crucial problems is to extract as much spectral capacity as possible on the wireless link, *especially by taking advantage of the mechanisms provided by packet-switching*. In packet-switched networks, the success of a transmission is measured in a packet-by-packet fashion. In particular, a packet transmission in a cell is successful if the instantaneous SIR is sufficiently high. The capability to detect a packet in the presence of interference is known as *capture*. Note that in the wireless environment, whether capture occurs or not depends on many factors, including electromagnetic signal propagation conditions (e.g., fading and shadowing) and traffic conditions (e.g., locations of interfering transmitters), and thus may fluctuate rapidly with time. Therefore, it is desirable that packet transmissions take advantage of the time periods during which capture occurs.

Based on the notion of capture, a new family of spectrum reuse methods have been recently proposed in [1], [3], which we call *capture based spectrum reuse*. The basic idea is to reuse the same channels in each cell. Thus, the capacity per cell is increased. However, since more interference is introduced due to closer channel reuse, capture failure is likely to occur. When capture fails, packets are retransmitted until capture is successful. The rationale here is that since the propagation delay between a user and its base-station is usually small (in the order of a few bits of transmission delay), recovery by retransmission is an effective mechanism of dealing with capture failure. However, we note that capture failure degrades the effective spectrum utilization, and also impacts the delay that packets may experience before being successfully delivered.

In this paper, we propose a novel power control scheme to alleviate the problem of capture failure. Power control is a technique of assigning different values of transmission power to different users. Unlike most power control schemes in the literature, in our scheme, power control is done in a coordinated fashion among users in different cells such that the intercellular interference can be effectively reduced. For simplicity of implementation, our intercellular coordination is determined *a priori*, and thus no real-time coordination is required. To fur-

[2]Please address all correspondence to this author, Tel. (317) 494-3471, FAX. (317) 494-3358.

ther simplify implementation, the power control is static and the power control levels are determined beforehand.

II. CAPTURE MODEL AND CAPTURE DIVISION PACKET ACCESS

Consider a cellular mobile system in which each cell contains a base-station that communicates with mobile users in that cell. In this paper, we consider a time-slotted framework, and assume that the size of packets in the cellular network is fixed and that exactly one packet can be transmitted in one time-slot.

Suppose that in a given time-slot of a carrier, there are two or more users transmitting packets. The transmissions may interfere with each other, and depending on the level of the interference, some of the transmissions may be unsuccessful. As discussed earlier, a successful transmission is referred to as capture. In a commonly used model, capture is said to occur (for uplink communication; for downlink communication, one can define capture similarly) for some user 0 if the signal-to-interference ratio (SIR)* exceeds some constant threshold

$$\frac{W_0}{\sum_{i \neq 0} W_i} > b. \qquad (1)$$

Here, W_0 is the received power at user 0's base-station, W_i are the received powers from other co-channel users at the same base-station, and b is called the *capture ratio*. Capture ratio is an important parameter that reflects the physical layer requirement for reliable communication. Various technologies react to interference differently. Capture ratio reflects how difficult it is for capture to occur. For example, with the same SIR, capture occurs less often for a larger value of b than a smaller value of b. Later, we will show that the value of b significantly impacts the performance of different spectrum reuse schemes.

As mentioned earlier, by taking advantage of the capture effect, the capture based spectrum reuse schemes attempt to increase spectral capacity in packet-switched wireless systems. Specifically, the distance between cells that are allowed to transmit in the same channel is shorter than the minimum reuse distance. Hence, the number of channels that can be allocated to an individual cell is significantly increased. An important example of the capture based spectrum reuse schemes is the *Capture Division Packet Access (CDPA)*, proposed in [1]. In CDPA, users in all cells can transmit in the same time-slots of each carrier, with some permission probability, and if capture does not occur, this collision is resolved by retransmitting the packet a random time later. By using a precise intracellular multiple access control mechanism, CDPA ensures that there is no contention between users within any given cell and that capture failure is only due to the interference from neighboring cells. In [1], it was shown via numerical studies that CDPA can

*the effect of thermal noise is ignored.
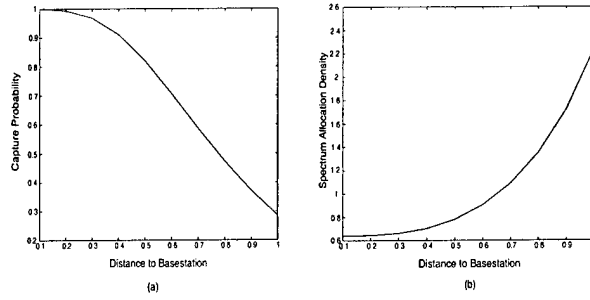
Fig. 1. Illustration of the near-far effect in CDPA (a) Users further away from the base-station may experience substantially lower capture probability. (b) More retransmission chances (hence higher capacity) have to be allocated for users that are further away from the base-station.

outperform standard TDMA, especially when the capture ratio is relatively low (e.g., $b = 6$ dB). However, the results are not satisfactory when the capture ratio is high (e.g., $b = 10$ dB).

We find that with CDPA, the probability that capture occurs (*capture probability*) depends strongly on the location of a mobile user, and that excessive retransmissions may result, especially for users that are geographically located in a way that makes capture difficult. We call this phenomenon the *near-far effect*, and illustrate it in Figure 1. In Figure 1(a), we plot a typical curve of the capture probability versus the distance of a mobile user to its base-station. It is apparent that the SIR for mobile users close to the base-station ("near" users) is high, thus leading to high capture probability. However, users far way from the base-station ("far" users), with weaker signals but stronger interference, suffer very low capture probability. Therefore, to maintain some degree of fairness among users in different locations in the cellular network, one has to allocate more retransmission opportunities to the unfavorably located users, who use a significant portion of the spectrum. For example, in Figure 1(b), we plot the density function of the spectrum allocation that keeps the same throughput for mobile users in different locations. Clearly, users far away from the base-station become the bottleneck for network efficiency. In the following sections, we present our static coordinated power control scheme to address this bottleneck problem.

III. PRIMARY/SECONDARY COORDINATION

In our scheme, we employ a simple reservation-based technique for multiple access control of users *within* a cell. In particular, a fraction of the time-slots on the uplink channel are designated as *reservation slots*. Mobile users who start/resume to send payload packets first inform the base-station by transmitting request packets on those reservation slots with some random access mechanism (e.g., ALOHA). Clearly, communication on the reservation slots could experience contention and collisions may occur. The size of the request packets is chosen to be much smaller than that of the payload packets, so that this collision probability is very small. The base-station,

Reduced Power	Full Power	Full Power	Reduced Power
(a) Transmissions on Carrier A		(b) Transmissions on Carrier B	
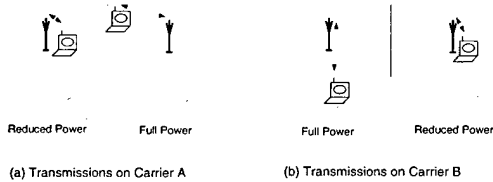
Fig. 2. Illustration of primary/secondary coordination

upon receiving a request packet, schedules the transmissions for the intended mobile user, according to some scheduling discipline, by sending commands along with downlink payload packets, on the downlink channel. In this way, uplink payload transmissions can be ensured to be contention-free. Therefore, in our coordination scheme, the transmissions on both uplink and downlink channels are completely controlled by the base-station in a given cell.

Recall from our previous discussion that the problem with CDPA is that it relies solely on random fluctuations of the SIR to combat capture failure and consequently results in excessive retransmissions for "far" users. Instead of wasting spectral resources on retransmissions, we aim to improve the probability of a successful transmission by *a priori* coordinating user transmissions over different cells. Since "far" users represent a bottleneck that requires a significant percentage of retransmissions, our basic idea is to improve the capture probability of these users by reducing the interference they experience.

Consider the following intuitive heuristic. When a "far" user is transmitting (or receiving) packets in a given cell, the idea is to reduce the power of simultaneous transmissions in the adjacent cells. On the other hand, since the power levels are reduced in the adjacent cells, only "near" users can be served in the adjacent cells, for otherwise the capture probability could become even worse. For the illustration of this heuristic, consider Figure 2, in which we show two adjacent cells in the cellular network. Here, we allow the base-station in the right cell to use one carrier (carrier A) with full power and serve a "far" user in the cell, while the left cell uses the same carrier, but with a reduced power level and serving only a "near" user. We do the reverse on another carrier (carrier B), to maintain fairness between the two cells.

In summary, in our scheme, carriers that are assigned to each cell in the cellular network are either *primary* or *secondary*. Primary carriers can be used to transmit (or receive) packets at the full allowable power W_T, while secondary carriers can only be used to transmit (or receive) packets at a reduced power level γW_T, where $0 \leq \gamma \leq 1$. We call this coordinated power control scheme the *primary/secondary coordination scheme*. Note that γ is an important tuning parameter that can be used to balance capture success in cells using primary and secondary carriers. At one end, when $\gamma = 1$, there is no difference be-

tween the primary and secondary carriers, and our scheme is indeed equivalent to CDPA. At the other end, when $\gamma = 0$, the capture probability in the secondary cells is reduced to zero. In fact, there is no communication activity at all in the secondary cells, which is similar to standard TDMA with a fixed channel reuse distance. Later we will show that, by applying an appropriate scheduling strategy, our primary/secondary coordination scheme can outperform both CDPA and TDMA.

We point out two fundamental advantages that make this scheme practically attractive:
(i) The assignment of primary/secondary carriers to any particular cell is determined beforehand, and no real-time inter-celluar coordination is required.
(ii) Power control is static, i.e., γ is a constant. In particular, here we consider two power control levels that are set *a priori* and whose values are not changed. Note that this is very different from other power control schemes in the literature, where the power is allowed to be changed dynamically and hence more sophisticated signal processing is required for their implementation.

The question to answer now is how to schedule users in different locations, under this primary/secondary coordination scheme. In our earlier heuristic discussion, illustrated via Figure 2, we suggest serving "far" users with primary carriers and "near" users with secondary carriers. To more precisely answer the above question, we next formulate an appropriate optimization problem and develop an optimal scheduling policy. Interestingly, it turns out that under certain conditions, the optimal solution agrees with our intuitive guess.

IV. OPTIMAL SCHEDULING

A. System Description

For simplicity of description, consider a linear cellular system, where the base-stations are numbered as $\{\ldots, 0, 1, 2, \ldots, \}$, and where the distance between two adjacent base-stations is normalized to be 2. Mobile users communicate with the nearest base-station. Thus, the radius of each cell is 1.

In our scheme we group all the carriers into two distinct carrier-sets A and B. All odd-numbered cells are assigned carrier-set A as the primary carrier-set, and carrier-set B as the secondary carrier-set; the even-numbered cells are assigned carrier-set B as their primary carriers, and carrier-set A as their secondary carriers. Due to symmetry, without loss of generality, we next only focus on carrier-set A, and thus call the odd-numbered cells the *primary cells* and even-numbered cells the *secondary cells*.

Let $g_P(x)$ and $g_S(x)$, with $0 \leq x \leq 1$, be the density functions of the traffic load at a distance x away from the base-station when the cell is primary and secondary, respectively. Note that these traffic load densities include both new and re-transmitted packets, and can be either downlink or uplink. The

distance parameter x is referred to as *location* x. We call the pair $\{g_P, g_S\}$ the *traffic load density pair*. Here we use g_P, g_S instead of $g_P(\cdot), g_S(\cdot)$ to simplify notation. We assume that the traffic load densities are piecewise continuous. The aggregate traffic loads in a primary and secondary cell are given by $G_P \triangleq 2 \int_0^1 g_P(x)\, dx$ and $G_S \triangleq 2 \int_0^1 g_S(x)\, dx$, respectively. We can also interpret G_P and G_S as the probabilities that a transmission occurs in a primary and secondary cell, respectively.

Let P_P and P_S denote the capture probabilities in a primary and secondary cell, respectively. The capture probabilities depend on both the location where packet transmission occurs in the cell and the interference from the adjacent cells. Thus in general, we use the notations $P_P(x, g_P, g_S)$ and $P_S(x, g_P, g_S)$ to reflect this dependence.

We define $s(x)$ to be the throughput density function, *per carrier-set*[†], at a location x, which is given by

$$s(x) = \frac{1}{2}(g_P(x)P_P(x, g_P, g_S) + g_S(x)P_S(x, g_P, g_S)) \quad (2)$$

A throughput density function is called *achieveable*, if there exist a traffic load density pair that satisfies Equation (2) for all x. We denote $\mathcal{S}$ the set of all achieveable throughput density functions.

The optimal scheduling problem is formulated as

$$\begin{aligned} \underset{s \in \mathcal{S}}{\text{maximize}} \quad & f(s) \\ \text{subject to} \quad & h(s) \geq 0 \end{aligned} \quad (3)$$

Again we use s instead of $s(\cdot)$ to simplify notation. The traffic load density pair that is associated with the optimal solution of (3) is referred to as *optimal traffic load density pair* and is denoted by $\{g_P^*, g_S^*\}$. Here, f and h are general functions satisfying the following condition:

(C1) If $h(s) \geq 0$, then for all $C > 0$, we have $f(s+C) > f(s)$ and $h(s + C) \geq 0$.

The above optimal scheduling problem is very general and captures a variety of realistic problems.

(i) $f(s) = 2 \int_0^1 s(x)\, dx$, or $f(s) = \min_x s(x)$.

(ii) $h(s) = \min_x s(x) - \max_x s(x)$. This constraint implies *uniform fairness*, i.e., the throughput is the same for different locations in the cell. The uniform fairness constraint is typically studied in the literature, for example in [1]. More generally, we can have a *non-uniform fairness constraint*: $h(s) = c - (\max_x s(x) - \min_x s(x))$, or $h(s) = c - \frac{\max_x s(x) - \min_x s(x)}{\max_x s(x)}$, where $c \geq 0$ is some constant.

B. Necessary Conditions for Optimality

Before, we proceed to solve the optimization problem (3), we impose the following condition on the capture probabilities:

[†]Note that the throughput in a cell comes from traffic on both carrier-sets A and B.

(C2) At any location in the cell, the capture probabilities depend only on the aggregate value of the traffic load pair.

Hence, we denote the capture probabilities in a primary and secondary cell as $P_P(x, G_P, G_S)$ and $P_S(x, G_P, G_S)$, respectively (instead of $P_P(x, g_P, g_S)$ and $P_S(x, g_P, g_S)$), to reflect this assumption. Note that condition (C2) exactly reflects the real situation in downlink communication. However, for uplink transmission, the received interference depends in general on the location of interferers. Thus, the capture probability in this case is determined by the traffic load distributions in the interfering cells, not just the aggregate values. Therefore this assumption represents an approximation for uplink communication. However, our simulation results will show that the mismatch can be safely ignored. It should be noted that in [1], the authors made the same assumption and they too found the impact of the approximation to be negligible.

Based on conditions (C1) and (C2), our procedure for solving the optimal scheduling problem (3) is as follows. First, for a given set of aggregate traffic loads G_P and G_S, we derive the optimal traffic load density pair $\{g_P^*, g_S^*\}$. We then obtain the overall solution by optimizing over the values of G_P and G_S (recall that $G_P, G_S \in [0, 1]$).

To proceed, we define the *family* $\{G_P, G_S\}$ to be all traffic load density pairs $\{g_P, g_S\}$ whose aggregate values are fixed and are equal to G_P and G_S, respectively. We will next derive a necessary condition for a traffic load density pair to be optimal in the family $\{G_P, G_S\}$. Note that according to the simplifying assumption, if the aggregate traffic loads are fixed, the capture probabilities are only functions of the location in a cell. Thus, when we focus on the family $\{G_P, G_S\}$, we denote the capture probabilities in the primary and secondary cells simply by P_P and P_S, respectively. It turns out that the necessary condition for solving the optimization problem can be given in the following simple form.

Theorem 1: Given values of the aggregate traffic loads G_P and G_S, suppose that $\{g_P^*, g_S^*\}$ is the optimal traffic load density pair in the family $\{G_P, G_S\}$. Then, there exists a positive constant α_0 such that

$$g_P^*(x) = 0, \text{ for all } x \text{ such that } \frac{P_P(x)}{P_S(x)} < \alpha_0, \quad (4)$$

$$g_S^*(x) = 0, \text{ for all } x \text{ such that } \frac{P_P(x)}{P_S(x)} > \alpha_0. \quad (5)$$

The proof of Theorem 1 is given in [2]. Theorem 1 states that the optimal solution to (3) is in the form of bang-bang control, in the sense that the users that are scheduled for transmission in a primary cell are selected from regions that are completely complementary to the users that are scheduled for transmission in a secondary cell. Therefore, the optimal throughput density
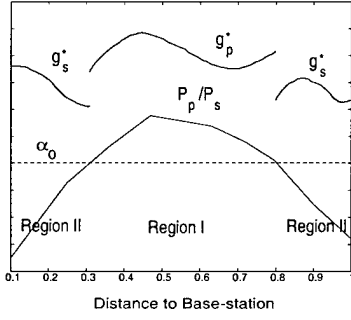
Fig. 3. Illustration of bang-bang optimal scheduling in general cases

is given by

$$s^*(x) = \begin{cases} \frac{1}{2}g_P^*(x)P_P(x), & \text{for all } x : \frac{P_P(x)}{P_S(x)} > \alpha_0 \\ \frac{1}{2}g_S^*(x)P_S(x), & \text{for all } x : \frac{P_P(x)}{P_S(x)} < \alpha_0. \end{cases} \quad (6)$$

This bang-bang type of scheduling is illustrated in Figure 3. From Figure 3, we can see that the cell is partitioned into two complementary regions, where users in Region I are scheduled for transmission only in a primary cell (i.e., $g_S^*(x) = 0$, for x in Region I), while users in Region II are scheduled for transmission only in a secondary cell (i.e., $g_P^*(x) = 0$, for x in Region II). For example, recall that so far we focus on carrier-set A and cell 1 is a primary cell. Thus, carrier A is used to serve only users in Region I of cell 1. However, when we consider carrier-set B, cell 1 becomes a secondary cell. From the same argument, we would then schedule users in Region II of cell 1 on carrier B.

We next state an important corollary when $P_P(x)/P_S(x)$ is monotonically increasing.

Corollary 1: Suppose that $P_P(x)/P_S(x)$ is a monotonically increasing function of x.[‡] Given values of the aggregate traffic loads G_P and G_S, suppose that $\{g_P^*, g_S^*\}$ is the optimal traffic load density pair in the family $\{G_P, G_S\}$. Then, there exists a number $x_0 \in (0,1)$ such that

$$g_P^*(x) = 0 \text{ for all } x \in (0, x_0) \quad (7)$$
$$g_S^*(x) = 0 \text{ for all } x \in (x_0, 1) \quad (8)$$

The proof of Corollary 1 is given in [2]. Our analysis and simulation results with standard physical layer propagation models show that $P_P(x)/P_S(x)$ is usually monotonically increasing. The corollary states that under this monotonicity condition, the optimal scheduling policy is to schedule only those users in a secondary cell that are a distance $(0, x_0)$ away from its base-station, and only those users in a primary cell that are a distance $(x_0, 1)$ away from its base-station. This corollary agrees

[‡]To obtain Equations (7) and (8) in the corollary we only require that there exists x_0 such that $P_P(x)/P_S(x) > \alpha_0$ for all $x \in (x_0, 1)$, and $P_P(x)/P_S(x) < \alpha_0$ for all $x \in (0, x_0)$, where α_0 is the parameter described in Theorem 1.

with our intuition (see Figure 2) of scheduling "far" users at higher power in a primary cell, while "near" users at a lower power in a secondary cell. What the above corollary (and Theorem 1) also tells us is that even for the optimal scheduling policy, it may not be necessary to precisely estimate the capture probability or location of each user for implementing the primary/secondary coordination scheme. Instead, a rough estimate of which region a user belongs to suffices.

C. Optimal Solution with Uniform Fairness Constraint

Theorem 1 and Corollary 1 provide necessary conditions for the optimal scheduling problem (3). However, to quantitatively calculate the optimal scheduling policy, we need to explicitly evaluate the parameter α_0 and density functions g_P^* and g_S^*. This means that the functions f and h in (3) must be explicitly defined. To illustrate the optimal scheduling solution, we next consider a specific case with the uniform fairness requirement. Consider the following optimization problem:

$$\underset{s \in S}{\text{maximize}} \quad \int_0^1 s(x)\,dx$$
$$\text{subject to} \quad \max_x s(x) - \min_x s(x) = 0 \quad (9)$$

The uniform fairness requirement indicates that the optimal through is constrained to be a constant, which we denote by s^*.

By applying the necessary condition of Theorem 1, Problem (9) is easy to solve. We integrate Equation (6) to obtain

$$s^* \int_{\Phi_P} \frac{1}{P_P(x)}\,dx = \frac{1}{2}\int_{\Phi_P} g_P^*(x)\,dx = \frac{1}{2}G_P, \quad (10)$$

$$s^* \int_{\Phi_S} \frac{1}{P_S(x)}\,dx = \frac{1}{2}\int_{\Phi_S} g_S^*(x)\,dx = \frac{1}{2}G_S, \quad (11)$$

where $\Phi_P = \{x | P_P(x)/P_S(x) > \alpha_0\}$ and $\Phi_S = \{x | P_P(x)/P_S(x) < \alpha_0\}$. Here, α_0 is the parameter described in Theorem 1 and can be determined by solving the following single-variable equation:

$$\frac{G_P}{\int_{\Phi_P} \frac{1}{P_P(x)}\,dx} = \frac{G_S}{\int_{\Phi_S} \frac{1}{P_S(x)}\,dx} \quad (12)$$

By solving either Equation (12), we can obtain the value of the parameter α_0 or x_0, and then determine the optimal throughput with Equations (10) and (11). Problem (9) has also been solved for CDPA and TDMA in [1]. In fact, as we noted previously, CDPA and TDMA can be viewed as special cases of the coordination scheme, i.e., $\gamma = 1$, $P_P(x) = P_S(x)$, and $G_P(x) = G_S(x)$ for CDPA, and $\gamma = 0$, $x_0 = 0$, and $G_S(x) = 0$ for TDMA. Therefore, their solutions can be easily derived from that for the coordination scheme. We have further investigated optimization problems with more general non-uniform fairness constraints. However, for space considerations we do not provide it here, and refer to [2].

V. PERFORMANCE EVALUATION

In this section, we evaluate the performance of our primary/secondary coordination scheme via both numerical analysis and simulation, and compare it with CDPA and TDMA schemes.

We consider a standard propagation model for performance evaluation which takes into account Rayleigh fading, lognormal shadowing, and η-th power path loss. Specifically, the power W_R (at the receiver), received from a transmitter located at a distance x away, is given by

$$W_R = \alpha^2 10^{0.1\xi} A x^{-\eta} W_T \qquad (13)$$

Here, α^2 is a Rayleigh distributed random variable with unit mean, ξ is a Gaussian random variable with zero mean and variance σ^2, $A x^{-\eta}$ accounts for the path loss and antenna gain, and W_T is the transmitted power which takes the normalized value of either 1 or γ, depending on the designation of the primary/secondary cell. As in [1], we assume for simplicity, that packet transmissions in different cells are synchronized on a common slotted time basis, so that transmissions in different cells overlap completely.

A. Analysis Model

The analytical method for determining the optimal schedule of the primary/secondary coordination scheme is as follows. First, for a given set of G_P and G_S, we compute the capture probabilities P_P and P_S. Specifically, we focus on an arbitrary cell, called "cell zero". Let the index "0" denote the intended signal in cell 0, and index "i" denote interference from cell i. Based on the propagation model (Equation (13)) and the capture model (Equation (1)), we can calculate the capture probability as follows:

$$P_P(x_0) = P\left\{ \frac{W_{R_0}}{\sum_{i:even,i\neq 0} \chi_i^P W_{R_i} + \sum_{i:odd} \chi_i^S W_{R_i} \gamma} > b \right\}$$

where $W_{R_i} = \alpha_i^2 10^{0.1\xi_i} A x_i^{-\eta}$. $P_S(x_0)$ can be calculated similarly. Here, x_0 is the distance from the intended mobile user to the base-station in cell 0, and x_i is the propagation distance associated with cell i. Binary random variables χ_i^P and χ_i^S indicate whether a transmission occurs or not in cell i when the cell is primary and secondary, respectively: $\chi_i^P = 1$ (with probability G_P), or $\chi_i^S = 1$ (with probability G_S), if a transmission occurs. For downlink communication, x_i is the distance between the intended mobile user to the base-station of cell i, which is determined by x_0. For uplink communication, x_i is the distance between the transmitter in cell i to the base-station in cell 0, which is independent of x_0. In our numerical analysis, we assume that x_i is uniformly distributed in cell i. However, this uniform assumption represents an approximation, since generally the optimal traffic load is not uniform. We

will investigate the impact of this approximation by comparing the analysis and simulation results in Section V-C.2.

We employ numerical integration methods to evaluate P_P and P_S, and then calculate the optimal traffic load pair $\{g_P^*, g_S^*\}$ in the family $\{G_P, G_S\}$, based on the necessary condition (Theorem 1). In particular, we can solve the optimal pair $\{g_P^*, g_S^*\}$ from single-variable Equations (10)–(12) for Problem (9). Finally, we obtain the overall optimal solution by enumerating the values of G_P and G_S from 0 to 1.

B. Simulation Model

We verify the numerical analysis results by comparing them with simulations. Note that in our analysis, the only performance measure that we have taken into account is the throughput. However, as noted previously, because of capture failure and packet retransmission, delay is another important performance measure of the capture based spectrum reuse method. In our simulation, we will also investigate the delay due to retransmissions.

Our simulation model is a linear cellular system consisting of 10 cells, where each cell has two adjacent cells. The boundary cells on the two sides are then connected to each other to avoid the "edge effect." In each cell there are 200 equally-spaced grids, and mobile users in the cell are located at those grids. In the simulation, packets are transmitted in the cellular system as follows. For uplink communication, during any time-slot one new packet is generated at grid i, independently from any other grid, with probability S_i. Let $S \triangleq \sum_{i=1}^{200} S_i$ be the aggregate new packet arrival rate, which is equal to the aggregate throughput if the system is stable. New packets, after arrival, are queued at the corresponding grids. We assume that by some request signaling, the base-station is immediately notified as soon as a new packet arrives at any grid. In other words, the base-station is always aware of the queue length at each grid in the cell. In any time-slot, the base-station first decides whether to transmit during that time-slot, with a permission probability β. If so, it selects a user at one grid in the cell, according to a scheduling algorithm and the cell partitioning (i.e., the bang-bang control), and then commands the user to transmit a packet in the corresponding queue. The permission probability is used to avoid congestion, as will be explained later in Section V-C.1. We use the following probabilistic scheduling algorithm for the base-station to select one of the grids in the cell. Suppose that in any time-slot, the queue lengths at all grids are q_i, $i = 1, \ldots, 200$. Then, in a primary (secondary) cell, the probability that grid i in Region I (Region II) is selected is $q_i / \sum_i q_i$, where the summation is done over all grids in Region I (Region II). The downlink case can be simulated similarly.

For both downlink and uplink communication, all transmissions in the cellular system are examined at the receivers, each of which checks Equation (1) to determine whether capture oc-

curs based on the propagation model given in Equation (13). If capture occurs, the transmitted packet is removed from the queue at the grid; otherwise, it remains in the queue, waiting for the next transmission opportunity.

C. Numerical Results

In our numerical analysis and simulation, we use the following parameters: $\eta = 4$, $\sigma = 6$ dB. The static power control parameter is $\gamma = 0.1$. When we check whether capture occurs, we take into account interference from four closest neighboring cells (i.e., two immediately adjacent, and two next-to-immediately adjacent cells). In this study, we consider three scenarios, $b = 6$, 10, and 15 dB, to represent various technologies in current and future wireless systems.

We compare our primary/secondary coordination scheme with both CDPA and TDMA. Since CDPA can be viewed as a simplified version of the coordination scheme with $G_P = G_S (\overset{\triangle}{=} G)$ and $\gamma = 1$, the methods of numerical analysis and simulation for CDPA are similar to what have been described for the coordination scheme. We also consider packet-switched TDMA which does not maintain continuous connections and allows packet retransmission. The reuse factor is set to be 2. Hence, the packet-switched TDMA system that we study here is almost the same as CDPA, except that every other cell, instead of all cells, are allowed to transmit in any time-slot.[§]

C.1 Maximum Throughput with Uniform Fairness Constraint

In this section, we investigate Problem (9) via numerical analysis. For a set of aggregate traffic loads G_P and G_S in the coordination scheme, we calculate the overall throughput S based on the discussion in Section IV-C. By varying G_P and G_S from 0 to 1, we obtain the overall optimal throughput for the coordination scheme. We can similarly investigate the optimal throughputs for CDPA and TDMA. Figure 4 plots S versus G for downlink communication in CDPA and TDMA, with $b = 6$, 10, and 15 dB. Figure 5 plots downlink S versus G_P and G_S in the coordination scheme when $b = 6$, 10, and 15 dB.

We find that when $b = 6$ dB, because capture occurs relatively easily, CDPA achieves better throughput than TDMA. However, the coordination scheme outperforms TDMA by 85% and CDPA by 35% in terms of maximum throughput. When the capture ratio is increased to 10 dB, the throughput curve of CDPA reaches a maximum for $G < 1$. This indicates that CDPA suffers congestion because of excessive intercellular interference. From Figure 4, it is clear that at $b = 10$dB,

[§]Strictly speaking, in standard TDMA, we have to adjust the reuse distance (and reuse factor) for different values of the capture ratio. Standard TDMA typically requires a reuse factor strictly larger than 2. Thus, the maximum throughput would be 1/3 at most. However, we find that in all our numerical results, the throughput of the packet-switched TDMA system that we use exceeds 0.4. Therefore, our comparison is with a fairer (and better in terms of throughput) version of TDMA.
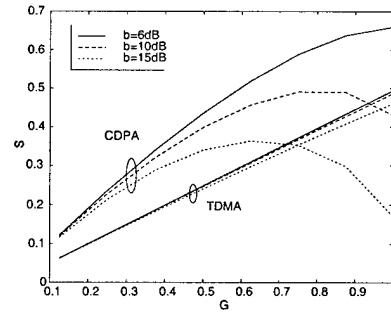
Fig. 4. Plot of downlink optimization for Problem (9) with CDPA and TDMA
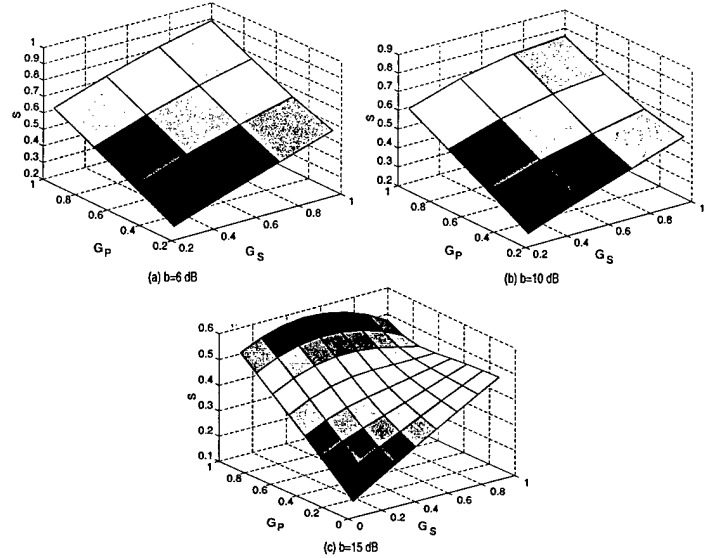
Fig. 5. Plot of downlink optimization for Problem (9) with coordination scheme: (a) $b = 6$ dB, (b) $b = 10$ dB and (c) $b = 15$ dB.

the improvement of CDPA over TDMA is marginal. However, the coordination scheme outperforms both by more than 50% in terms of maximum throughput. An interesting observation is that the throughput surface shown in Figure 5(b) reaches the maximum point at $G_P = 1$ and $G_S = 1$, which indicates that although spectrum is reused in all cells the coordinated power control scheme significantly reduces the capture probability. When the capture ratio is further increased to 15 dB, the excessive interference dramatically reduces the throughout in CDPA, which now performs even worse than TDMA. Note that in the coordination scheme, the maximum throughput is also not reached at the point where $G_P = 1$ and $G_S = 1$, indicating that many retransmissions may occur even with the static coordinated power control. From Figure 5(c), we find that the coordination scheme outperforms TDMA by 26% and CDPA by 60% in terms of maximum throughput.

Similarly, we compare the throughput performance for the uplink communication, and find that the results are similar. We summarize the maximum throughputs, for both uplink and downlink communication, of the coordination scheme, CDPA

TABLE I

A Comparison of the maximum achievable throughput using CDPA, TDMA and the coordination scheme

Capture ratio (dB)	Downlink			Uplink		
	$b = 6$	$b = 10$	$b = 15$	$b = 6$	$b = 10$	$b = 15$
Coordination	0.89	0.77	0.57	0.90	0.81	0.62
CDPA	0.66	0.49	0.36	0.80	0.65	0.41
TDMA	0.50	0.49	0.47	0.50	0.49	0.47

and TDMA for different values of the capture ratio in Table I.

C.2 Throughput-Delay Tradeoff with Uniform Fairness Constraint

In this section, we provide *simulation results* to verify the analysis presented in Section V-C.1. Recall that the results for uplink were derived based on the simplifying assumption made in Section IV-B. In simulation, we find that the coordination scheme can in fact achieve throughputs that are close to those maximum values calculated in Table I. However, the associated delays can be large. We observe similar phenomena with both CDPA and TDMA, and also in downlink communication.

To make the comparisons more meaningful, we next investigate the throughput-delay tradeoff. Specifically, for a given new packet arrival rate S (which is equal to the throughput in a stable system), we estimate the expected delay D, in terms of time-slots, that a packet experiences from the instant of arrival to the instant when the packet is successfully received. This figure includes both queueing delay and retransmissions. To maintain uniform throughput in a cell, the new packet arrival rate at any grid is thus given by $S_i = S/200$. To control congestion, we set the permission probability as the aggregate traffic load that reaches the maximum throughput in the numerical analysis of Problem (9). The cell partition parameter x_0 is determined by solving Problem (9), and is then used in the simulation of the coordination scheme. Clearly, the choice of x_0 is not optimized for minimizing the delay with a given throughput S, and therefore the performance of the coordination scheme is conservative.

We compare the expected delay versus throughput in both downlink and uplink. To save space, we summarize the simulaiton results in Table II. Detailed curves can be found in [2]. Overall the relative performance improvements of our scheme over both CDPA and TDMA, as observed from simulation, in terms of throughput-delay tradeoff are numerically close to those in terms of maximum throughput from the analysis in Section V-C.1. Specifically, For a fixed expected delay, say 10 time-slots, we compare the associated throughputs. In downlink, the coordination scheme outperforms TDMA by 80% and CDPA by 30% at $b = 6$ dB, outperforms TDMA by 55% and CDPA by 50% at $b = 10$ dB, and outperforms TDMA by 17%

TABLE II

A comparison of throughput-delay tradeoff using CDPA, TDMA and the coordination scheme.

Capture ratio (dB)	$b = 6$		$b = 10$		$b = 15$	
Delay constraint	10	10^3	10	10^3	10	10^3
Downlink						
Coordination	0.80	0.89	0.68	0.76	0.47	0.57
CDPA	0.62	0.66	0.45	0.49	0.33	0.36
TDMA	0.45	0.50	0.44	0.49	0.41	0.46
Uplink						
Coordination	0.80	0.90	0.72	0.80	0.55	0.62
CDPA	0.75	0.80	0.57	0.62	0.36	0.40
TDMA	0.45	0.50	0.44	0.49	0.41	0.46

and CDPA by 47% at $b = 15$ dB. Moreover, the performance in uplink communication is similar to that in downlink communication, and is consistent with the analysis in Section V-C.1. In particular, the maximum value observed in simulation is close to that obtained in the analysis, for all three schemes and all the choices of b. This indicates that the simplifying assumption made in Section IV-B and in [1] is reasonable.

VI. CONCLUSION

We have presented a static coordinated power control scheme in packet-switched wireless systems. Our basic idea is to reduce intercellular interference and improve the capture probability by coordinating transmission powers of users in different cells. The coordination is determined beforehand and no real-time intercellular coordination is required. The power control is static and fixed, leading to simplicity in implementation. We have formulated and solved a generic optimal scheduling problem with our coordination scheme. We find that the optimal scheduling policy is in a simple form of bang-bang control: each cell is partitioned so that users in different regions are served with different levels of transmission power. Numerical results show that the coordination scheme can achieve significant performance improvements over both CDPA and TDMA, in terms of both maximum throughput and throughput-delay tradeoff, over a wide range of the capture ratio values.

REFERENCES

[1] F. Borgonovo, M. Zorzi, L. Fratta, V. Trecordi, and G. Bianchi, "Capture-division packet access for wireless personal communications," *IEEE Journal On Selected Areas In Communications*, vol. 14, pp. 609–622, May 1996.

[2] J. Li, *Intercellular coordination schemes for improving spectrum utilization in wireless cellular networks.* Purdue University, West Lafayette, Indiana: Ph.D. dissertation, 1998.

[3] J.-P. Linnartz, "On the performance of packet-switched cellular networks for wireless data communications," *Wireless Networks*, vol. 1, pp. 129–138, 1995.

Admissibility and Network Capacity of Power-Controlled CDMA Systems in Fading Channels

Junshan Zhang   Edwin K.P. Chong*

School of Electrical and Computer Engineering
Purdue University, West Lafayette, IN 47907-1285
{junshan, echong}@ecn.purdue.edu

Abstract

Due to the fast-growing demand for network capacity in wireless networks, the characterization of network capacity has become a fundamental and pressing issue. In this paper, we study the network capacity of single-cell synchronous CDMA systems with matched filter receivers in fading channels, assuming known distributions of received powers of mobile users. We find necessary and sufficient conditions on the admissibility for both single class and multiple class systems with random signatures. For systems with deterministic signatures, we give a necessary and sufficient condition on the admissibility for single class systems, but only a sufficient condition for multiple class systems. We identify the network capacity of single class systems for both the random signature case and deterministic signature case. The network capacity can be uniquely expressed in terms of the users' QoS requirements and the distributions of the received powers.

1   Introduction

Due to the fast-growing demand for network capacity in wireless networks, it is essential to utilize efficiently the limited resources in fading channels. The characterization of network capacity is therefore one of the most fundamental and pressing issues in wireless network research. In this paper, we consider a model for the uplink of a single-cell synchronous CDMA system in fading channels.

Much of the previous research on CDMA systems has been restricted to the physical layer, focusing mainly on the performance of linear receivers in worst-case scenarios. *Near-far resistance* and *asymptotic efficiency* have been studied as two important performance measures (see [10] for a survey of the literature). At the network layer, there have been considerable efforts on power control [3, 9, 12]. The sophisticated techniques for allocating network resources at both the physical layer and network layer aim to improve network capacity. Unlike in TDMA and FDMA systems, however, there is no clean separation between resource allocation at the physical layer and network layer in CDMA systems. A natural question to address is the performance of linear receivers in power-controlled CDMA systems. In [8], Tse and Hanly characterized the network capacity for systems with several important receivers via a notion of *effective bandwidth*,

---

assuming users have random signatures. In [11], Viswanath, Anantharam, and Tse studied the joint optimization problem of designing the multiuser receiver structure, power control, and spreading sequences, and obtained simple characterizations of the resulting network capacity in various scenarios. Both [8] and [11] assumed perfect power control in characterizing network capacity. In a practical wireless communication system, however, multipath fading is ubiquitous, making perfect power control impossible. Little work has been done on network capacity of CDMA systems with multiuser receivers in fading channels. In this paper, we study the admissibility and network capacity in power-controlled CDMA systems in fading channels. All our results assume a matched filter receiver, which is the designated receiver for CDMA systems in IS-95.

The organization of the rest of this paper is as follows. In Section 2 we give some background for our model of power-controlled CDMA systems. In Section 3, we study the admissibility and network capacity for single class systems, and define the concept of *effective target SIR*. In Section 4, we extend the study to multiple class systems, and define *effective bandwidth* for power-controlled CDMA systems in fading channels. Finally, we draw some conclusions in Section 5.

2 Preliminaries

In a synchronous CDMA system, each user, say user k, is assigned a binary (± 1 valued) signature of length L, $S_k = \frac{1}{\sqrt{L}}(W_{k1}, \ldots, W_{kL})^T$, where W_{ki} is either 1 or -1 for $i = 1, \ldots, L$. The user's information symbols are spread onto its signature. We will study CDMA systems for the following two cases. The first is the deterministic signature case, by which we mean that the users' signatures are jointly designed and deterministic when they are admitted into the system (cf., [6, 11]); the second is the random signature case, by which we mean that users choose their signatures randomly and independently when they are admitted into the system, which models the situation where the information symbols are spread onto pseudo-random spreading sequences (cf., [8]).

Suppose users transmit data over a fading channel. Typically, fading channel gains are assumed to be stationary and ergodic, and all the users in one class are assumed to have independently and identically distributed channel gains (see [5]). As pointed out in [2] and [8], it is ideal to have the received powers for all the users in one class to be the same all the time. However, it is very difficult to implement perfect power control and the received powers fluctuate around the desired levels in a practical system. Assuming that the same kind of power control algorithm is applied to all users in one class, by symmetry, we model the received powers for all users in one class to be independently and identically distributed in a large network. For technical reasons, we also assume that power control is good enough to ensure that the fluctuation around the expected received power is bounded (say by d) with probability one.

We assume that the distributions of the received powers are known. This assumption is reasonable (cf., [4, Chapter 6]). From a practical viewpoint, the distributions of the received powers can usually be obtained through measurements (see [7]). We aim to study the admissibility and network capacity in the limiting regime, that is, when both M and L go to infinity. As in [8], $\beta \equiv \frac{M}{L}$ is taken to be fixed as L goes to infinity.

3 Single Class Systems

Based on [8, 9], we have the following discrete-time model for a synchronous CDMA system. Suppose there are M users in the system when the processing gain is L. For any symbol interval, the baseband received signal at the front of the receiver is

$$Y = \sum_{k=1}^{M} \sqrt{P_k^{(L)}} b_k S_k + V, \tag{1}$$

where the b_k's are the transmitted information symbols and the $P_k^{(L)}$'s are received powers for $k = 1, \ldots, M$, and V is $\mathcal{N}(0, \eta I)$ background white noise that comes from the sampling of the ambient white Gaussian noise with power spectral density η. The received powers are assumed to be i.i.d. with distribution F_L, which has a density function and mean $\mu^{(L)}$. When L goes to infinity, we assume that the sequence of functions $\{F_L\}$ converges weakly to F, which denotes the distribution of the received powers in the limiting regime. Let P_0 denote a random variable that has distribution F and mean μ. For convenience, we further assume the modulation is antipodal, that is, $b_k \in \{-1, 1\}$.

Assume the signature S_k of user k is known to the receiver for it. Then the received SIR (signal-to-interference ratio) for user k after passing the matched filter is

$$SIR_k^{(L)} = \frac{P_k^{(L)}}{\eta + \sum_{\substack{i=1 \\ i \neq k}}^{M} P_i^{(L)} (S_k^T S_i)^2} \qquad k = 1, \ldots, M. \tag{2}$$

Since the received SIR's are random variables under our assumption, we adopt a probabilistic model for the users' QoS requirements as follows:

$$P\{SIR_k^{(L)} \geq \gamma\} \geq a \qquad \forall\, k = 1, \ldots, M.$$

3.1 The Deterministic Signature Case: Admissibility and Network Capacity

In this case, the users' signatures are deterministic, and the signatures of all the M users form a signature set when the processing gain is L. When L goes to infinity, we have a sequence of signature sets. Let $\mathcal{F}$ denote the collection of sequences of signature sets satisfying the following condition:

$$\sup_{\substack{i,j \leq M \\ i \neq j}} (S_i^T S_j)^2 \log L \to 0 \qquad \text{as } L \to \infty, \tag{3}$$

where S_i and S_j are the signatures for user i and j respectively when the processing gain is L, $i, j \in \{1, \ldots, M\}$. In the proceeding parts where sequences of deterministic signature sets are chosen, we assume that all sequences are in $\mathcal{F}$.

First we define *admissibility* for a class of users as follows: when the processing gain is L, β users per degree of freedom of the processing gain are admissible in the system if and only if there exists a signature set $\{S_1, \ldots, S_M\}$ for the M users, where M equals βL, and the users' QoS requirements are satisfied when $\{S_1, \ldots, S_M\}$ are allotted to the users, that is,

$$P\{SIR_k^{(L)} \geq \gamma\} \geq a, \quad \forall k = 1, \ldots, M,$$

which is equivalent to

$$\max_{\{S_1,\ldots,S_M\}} \min_k P\{SIR_k^{(L)} \geq \gamma\} \geq a. \qquad (4)$$

Asymptotic admissibility is defined as follows: we say β users per degree of freedom of the processing gain are asymptotically admissible when the following condition holds:

$$\lim_{L\to\infty} \max_{\{S_1,\ldots,S_M\}} \min_k P\{SIR_k^{(L)} \geq \gamma\} \geq a.$$

As pointed out in [11], when $M \leq L$, we can always choose an orthogonal signature set such that there is no interference between users. Then each single user transmits data as if it were in a single-user channel. This case is not of real interest since we want to find the maximum number of users supportable by the system. For the case $M > L$, our results make use of WBE (Welch Bound Equality) signature sets. (See [6] for the definition of WBE sequence sets. Note that we use the terminology "signature set" instead of "sequence set" to avoid confusion since we will discuss sequences of such sets.)

Assuming $\lim_{L\to\infty} \max_k \sum_{j=1}^M (S_k^T S_j)^2 < \infty$, we have the following proposition on the asymptotic admissibility for the deterministic signature case.

Proposition 3.1 *Suppose all sequences of deterministic signature sets are chosen from $\mathcal{F}$. Then β users per degree of freedom of the processing gain are asymptotically admissible if and only if $\beta \leq \frac{F^{-1}(1-a)}{\gamma\mu} + 1 - \frac{\eta}{\mu}$.*

Proposition 3.1 illustrates the fact that the asymptotically admissible region is $\beta \leq \frac{F^{-1}(1-a)}{\gamma\mu} + 1 - \frac{\eta}{\mu}$. Following [8], we can call $\frac{F^{-1}(1-a)}{\gamma\mu} + 1 - \frac{\eta}{\mu}$ the *network capacity in the limiting regime* (to be distinguishable from the concept "asymptotic network capacity" which is introduced below) for the given distribution of the received powers.

In practical CDMA systems, the processing gain is finite and large. Therefore, one basic question to ask is, "How many users are admissible for some large (but finite) processing gain while the users' QoS requirements are fixed?" Basing only on Proposition 3.1, however, we cannot answer this interesting question. (The subtlety will be more clear in the proceeding discussions.) This motivates us to develop another approach that studies a sequence of network capacities indexed by the processing gain L. We proceed to elaborate on this idea in detail.

When the processing gain is L, we let C_L denote the set of all the admissible points, that is,

$$C_L = \left\{ \beta \,\middle|\, \max_{\{S_1,\ldots,S_M\}} \min_k P\{SIR_k^{(L)} \geq \gamma\} \geq a \right\}.$$

Of particular interest is the maximum number of users admissible by the system, which is defined to be the *network capacity* in terms of the number of users per degree of freedom of the processing gain. That is, the network capacity is the maximum number of users per degree of freedom of the processing gain that are admissible in the system, and depends on a. Therefore, when the processing gain is L, we can define *network capacity* as follows:

$$\beta_L(a) = \sup C_L = \sup \left\{ \beta \,\middle|\, \max_{\{S_1,\ldots,S_M\}} \min_k P\{SIR_k^{(L)} \geq \gamma\} \geq a \right\}. \qquad (5)$$

The *asymptotic network capacity* $\beta_\infty(a)$ is defined as the limit of $\beta_L(a)$ when $L \to \infty$, that is, $\beta_\infty(a) = \lim_{L\to\infty} \beta_L(a)$. Note that the network capacity in the limiting regime and

the asymptotic network capacity are different in principle (compare the two definitions). A priori, we do not know if they lead to the same expression.

We aim to identify the asymptotic network capacity. For technical reasons, we assume that the received powers in the limiting regime have a connected support, which implies that the distribution function F is strictly increasing over its support. We have the following proposition on the asymptotic network capacity for the deterministic signature case.

Proposition 3.2 *Suppose all sequences of deterministic signature sets are chosen from $\mathcal{F}$. Then the asymptotic network capacity is $\beta_\infty(a) = \frac{F^{-1}(1-a)}{\gamma\mu} + 1 - \frac{\eta}{\mu}$, which can be achieved through a sequence of WBE signature sets in $\mathcal{F}$.*

It turns out that for the deterministic signature case, the *network capacity in the limiting regime* and the *asymptotic network capacity*, which are different in principle, lead to the same result under the auxiliary assumption made on the distribution function F. In general, the network capacity in the limiting regime is an upper bound of the asymptotic network capacity. The asymptotic network capacity, however, provides a better approximation of the network capacity of a large network. In particular, by exploiting Proposition 3.2, we can conclude that for a given $\epsilon > 0$, $\beta_\infty(a) - \epsilon$ users per degree of freedom of the processing gain are admissible in the system for very large L ($L \geq L_0(\epsilon)$ for some $L_0(\epsilon)$).

Worth noting is that sequences of WBE signature sets in $\mathcal{F}$ play a very important role in both the asymptotic admissibility and asymptotic network capacity. A heuristic interpretation is that the choice of WBE signature sets is asymptotically optimal in the sense of suppressing the interference of all the users simultaneously.

3.2 The Random Signature Case: Admissibility and Network Capacity

In this case, users choose signatures randomly and independently, which models the situation where the information symbols are spread onto pseudo-random spreading sequences. When the processing gain is L, the model for random signatures is as follows: $S_k = \frac{1}{\sqrt{L}}(W_{k1}, \ldots, W_{kL})^T$, where the W_{ki}'s are i.i.d. with $P(W_{ki} = 1) = P(W_{ki} = -1) = \frac{1}{2}$ for $i = 1, \ldots, L$ and $k = 1, \ldots, M$.

Since the $P_k^{(L)}$'s are i.i.d., and the W_{ki}'s are i.i.d., the received SIR's for users are also identically distributed. Hence, $P\{SIR_k^{(L)} \geq \gamma\}$ does not depend on k, and we can study user 1 without loss of generality.

Assume that the signature for a user is known to the receiver for it. Given the distribution of the received powers, we define admissibility for a class of users with random signatures as follows: when the processing gain is L, β users per degree of freedom of the processing gain are *admissible* in the system if

$$P\{SIR_1^{(L)} \geq \gamma\} \geq a.$$

We say β users per degree of freedom of the processing gain are *asymptotically admissible* if the following condition holds:

$$\lim_{L\to\infty} P\{SIR_1^{(L)} \geq \gamma\} \geq a.$$

We have the following proposition on the asymptotic admissibility for the random signature case.

Proposition 3.3 *Suppose users choose signatures randomly and independently. Then β users per degree of freedom of the processing gain are asymptotically admissible if and only if $\beta \leq \frac{F^{-1}(1-a)}{\gamma\mu} - \frac{\eta}{\mu}$.*

We call $\frac{F^{-1}(1-a)}{\gamma\mu} - \frac{\eta}{\mu}$ the *network capacity in the limiting regime* for the given distribution of the received powers.

Similar to the deterministic signature case, when the processing gain is L, the *network capacity* is defined as the maximum number of users per degree of freedom of the processing gain that are admissible in the system, that is,

$$\beta_L(a) = \sup\left\{\beta \,\middle|\, P\{SIR_1^{(L)} \geq \gamma\} \geq a\right\}.$$

We define *asymptotic network capacity* $\beta_\infty(a)$ as the limit of $\beta_L(a)$ when $L \to \infty$, that is, $\beta_\infty(a) = \lim_{L\to\infty} \beta_L(a)$.

Again, for technical reasons, we assume the received powers in the limiting regime have a connected support and hence F is strictly increasing over its support. Then we have the following proposition on the asymptotic network capacity for the random signature case.

Proposition 3.4 *Suppose users choose their signatures randomly and independently. Then the asymptotic network capacity is $\beta_\infty(a) = \frac{F^{-1}(1-a)}{\gamma\mu} - \frac{\eta}{\mu}$.*

It turns out that for the random signature case, the *network capacity in the limiting regime* and the *asymptotic network capacity*, which are different in principle, also lead to the same expression under the auxiliary assumption made on the distribution function F. It can easily be observed that a system using optimal deterministic signatures yields precisely one more user per degree of freedom of the processing gain than one system with signatures randomly and independently chosen, which is a generalization of the result given in [11] under perfect power control.

3.3 Effective Target SIR

We proceed to look for an abstraction that can combine the information of both QoS requirements and the distributions of received powers for determining the asymptotic admissibility. In a power-controlled system, the actual received powers depend on the fading environments and the performance of the power control algorithms. Note that if β users are not asymptotically admissible for a given received power distribution, it may still be possible to make β asymptotically admissible by scaling up the received power. Referring to the definition of *scale family* in [1, p. 118], we consider the scale family $\mathcal{G} = \{F(\frac{p_0}{c}), c > 0\}$, where F is the distribution function of P_0. Define $\gamma' = \gamma c_e$, where $c_e = \frac{\mu}{F^{-1}(1-a)}$. Clearly, c_e is fixed for the scale family $\mathcal{G}$. We call γ' the *effective target SIR* for $\mathcal{G}$.

Note that in a given scale family of distributions, there exists a one-to-one correspondence between distribution and mean. Given a scale family $\mathcal{G}$ of received power distributions, a basic question to ask is if there exists a finite positive value that can be designated as μ such that β users per degree of freedom of processing gain are asymptotically admissible for the corresponding received power distribution in $\mathcal{G}$. For the deterministic signature case, it can be shown that there exists a finite positive solution for μ if and only if $\beta\frac{\gamma'}{1+\gamma'} < 1$; moreover, the minimum value for μ is $\eta\frac{\gamma'}{1+\gamma'} \,/\, 1 - \beta\frac{\gamma'}{1+\gamma'}$. For the random signature case, it is easy to obtain that there exists a finite positive solution for μ if and only if $\beta\gamma' < 1$; the minimum value for μ is $\frac{\eta\gamma'}{1-\beta\gamma'}$.

4 Multiple Class Systems

We have studied the asymptotic admissibility and identified the asymptotic network capacity for single class systems in the above section. However, future wireless systems will have to support multimedia services such as voice, data, video, and fax. Therefore, it is essential to have a level of generalization dealing with users having different QoS requirements.

Suppose there are a fixed number, say N, of classes. For $n = 1, \ldots, N$, let A_n denote the set of users in class n and M_n the cardinality of A_n. Let S_{in} denote the signature for the ith user in class n. Define $\beta_n = \frac{M_n}{L}$ and let β_n be fixed when $L \to \infty$ as in the single class case.

The received SIR for the ith user in class n is

$$SIR_{in}^{(L)} = \frac{P_{in}^{(L)}}{\eta + \sum_{\substack{j \neq n \\ l \in A_j}} P_{lj}^{(L)} (S_{in}^T S_{lj})^2 + \sum_{\substack{l \in A_n \\ l \neq i}} P_{ln}^{(L)} (S_{in}^T S_{ln})^2} , \qquad (6)$$

where $P_{in}^{(L)}$ denotes the received powers for $i \in A_n$ and $n = 1, \ldots, N$ when the processing gain is L.

Again our results are asymptotic in nature. For the sake of simplification, as in the single class case, we let P_n denote a random variable that has the same distribution F_n as the received powers of users in class n in the limiting regime, and assume that F_n has a density function and mean μ_n. For convenience, we call the collection $\{F_1, \ldots, F_N\}$ a *group of received power distributions*, and $\vec{P} = (\mu_1, \ldots, \mu_N)^T$ the *mean power vector*. Suppose it is required that the users in class n must have received SIR greater than or equal to γ_n with probability no less than $a_n \in [0, 1]$.

4.1 The Deterministic Signature Case: Admissibility, Effective Target SIR, and Effective Bandwidth

We assume that every chosen sequence of signature sets satisfies (3) and $\lim_{L \to \infty} \max_{i \in A_n} \sum_{l \in A_j} (S_{in}^T S_{lj})^2 < \infty$ for all n, $j \in \{1, \ldots, N\}$. Let $I_{in} = S_{in}^T D S_{in}$, where $D = \sum_{j=1}^N \sum_{l \in A_j} S_{lj} S_{lj}^T \mu_j$. Then we have

$$SIR_{in}^{(L)} \xrightarrow{\mathcal{D}} \frac{P_n}{\eta + I_{in} - \mu_n} \qquad \text{as } L \to \infty.$$

Similar to the argument in the single class case, it is desirable to design the signature sets such that all users' QoS requirements are satisfied. When $\sum_{n=1}^N \beta_n \leq 1$, orthogonal signature sets will work and each single user transmits data as if it were in a single-user channel. When $\sum_{n=1}^N \beta_n > 1$, however, a simple closed-form solution to the global optimization of the signature sets for this case seems unattainable. Therefore, we study a sufficient condition for the asymptotic admissibility of multiple class systems for this case.

For the sake of simplification, first we let $F_{M,n}$ denote the signature set of class n when the processing gain is L. Given the distributions of the received powers, we say a tuple $(\beta_1, \ldots, \beta_N)$ is asymptotically admissible if the following condition holds:

$$\lim_{L \to \infty} \max_{\cup_n F_{M,n}} \min_{i \in A_n} P\{SIR_{in}^{(L)} \geq \gamma\} \geq a_n \qquad \forall \, n = 1, \ldots, N.$$

We have the following proposition on the asymptotic admissibility of users of multiple classes for the deterministic signature case.

Proposition 4.1 *A tuple $(\beta_1, \ldots, \beta_N)$ is asymptotically admissible if it satisfies the following two conditions:*

$$\max_n \mu_n \leq \sum_{j=1}^{N} \beta_j \mu_j, \tag{7a}$$

$$\sum_{j=1}^{N} \beta_j \mu_j \leq \min_n \left(\frac{F_n^{-1}(1 - a_n)}{\gamma_n} + \mu_n \right) - \eta. \tag{7b}$$

As in the single class case, we introduce the scale family $\mathcal{G}_n = \{F_n(\frac{p_n}{c}), c > 0\}$ for P_n, where F_n is the distribution function of P_n, $n = 1, \ldots, N$. Define $\gamma_n' = \gamma_n c_{en}$, where $c_{en} = \frac{\mu_n}{F_n^{-1}(1-a_n)}$. As before, c_{en} is fixed for the scale family $\mathcal{G}_n$. We call γ_n' the *effective target SIR* for $\mathcal{G}_n$. For ease of reference, we call the collection $\{\mathcal{G}_1, \ldots, \mathcal{G}_N\}$ a *group of scale families*.

Observe that in a given group of scale families, there exists a one-to-one correspondence between the mean power vector and the group of received power distributions. We have the following result for a given group of scale families $\{\mathcal{G}_1, \ldots, \mathcal{G}_N\}$.

Proposition 4.2 *There exists a finite positive vector that can be assigned as the mean power vector for a tuple $(\beta_1, \ldots, \beta_N)$ to be asymptotically admissible for the corresponding group of received power distributions in $\{\mathcal{G}_1, \ldots, \mathcal{G}_N\}$ if*

$$\frac{\gamma_n'}{1 + \gamma_n'} \leq \sum_{n=1}^{N} \beta_n \frac{\gamma_n'}{1 + \gamma_n'},$$

and

$$\sum_{n=1}^{N} \beta_n \frac{\gamma_n'}{1 + \gamma_n'} < 1.$$

Observing the conditions given in Proposition 4.2, we are motivated to extend the insightful idea in [8] and define the *effective bandwidth* of class n for the deterministic signature case as $e(\gamma_n) = \frac{\gamma_n'}{1+\gamma_n'}$ degrees of freedom per user. However, we are able to give only a sufficient condition for asymptotical admissibility of a tuple $(\beta_1, \ldots, \beta_N)$ in terms of effective bandwidth. Further work is needed for this case.

4.2 The Random Signature Case: Admissibility, Effective Target SIR, and Effective Bandwidth

Similar to the approach in the single class systems with random signatures, we get

$$SIR_{in}^{(L)} \xrightarrow{\mathcal{D}} \frac{P_n}{\eta + \sum_{n=1}^{N} \beta_n \mu_n} \qquad \text{as } L \to \infty. \tag{8}$$

We can study the first user in class n without loss of generality.

Given the distributions of the received powers, we say a tuple $(\beta_1, \ldots, \beta_N)$ is asymptotically admissible if the following condition holds:

$$\lim_{L \to \infty} P\{SIR_{1n}^{(L)} \geq \gamma\} \geq a_n \qquad \forall \, n = 1, \ldots, N.$$

We have the following proposition on the asymptotic admissibility of users of multiple classes for the random signature case.

Proposition 4.3 *Suppose users choose their signatures randomly and independently. A tuple $(\beta_1, \ldots, \beta_N)$ is asymptotically admissible if and only if*

$$\sum_{n=1}^{N} \beta_n \mu_n \leq \min_n \left(\frac{F_n^{-1}(1 - a_n)}{\gamma_n} \right) - \eta. \tag{9}$$

Again we define $\gamma_n' = \gamma_n c_{en}$, where $c_{en} = \frac{\mu_n}{F_n^{-1}(1-a_n)}$ is fixed for the scale family $\mathcal{G}_n$, $n = 1, \ldots, N$. We can easily obtain the following result for a given group of scale families $\{\mathcal{G}_1, \ldots, \mathcal{G}_N\}$.

Proposition 4.4 *a). There exists a finite positive vector that can be assigned as the mean power vector for a tuple $(\beta_1, \ldots, \beta_N)$ to be asymptotically admissible for the corresponding group of received power distributions in $\{\mathcal{G}_1, \ldots, \mathcal{G}_N\}$ if and only if*

$$\sum_{n=1}^{N} \beta_n \gamma_n' < 1.$$

Similar to the deterministic signature case, we define the *effective bandwidth* of class n for the random signature case as $e(\gamma_n) = \gamma_n'$ degrees of freedom per user. Proposition 4.4 states that for a given group of scale families, a tuple $(\beta_1, \ldots, \beta_N)$ can be made asymptotically admissible through power control if and only if the sum of effective bandwidth of all classes is less than one.

5 Conclusions

We have studied single-cell synchronous CDMA systems with matched filter receivers assuming known distributions of received powers of mobile users. We studied the asymptotic admissibility for both single class systems and multiple class systems. For systems with random signatures, we gave necessary and sufficient conditions on the asymptotic admissibility in terms of effective bandwidth. For users with deterministic signatures, we gave a necessary and sufficient condition for single class systems, but only a sufficient condition for multiple class systems. Further work is needed for this case.

We have also identified the asymptotic network capacity of single class systems for both the deterministic signature case and the random signature case. The asymptotic network capacity for single class systems can be uniquely expressed in terms of the users' QoS requirements and the distributions of the received powers. We also identified the optimal sequences of signature sets for the deterministic signature case in an asymptotic setting. Furthermore, we explored the concepts of effective target SIR and effective bandwidth, which play an important role in determining the asymptotic admissibility and hence the asymptotic network capacity. Our results are useful for network-level resource allocation problems such as admission control and power control in a large network.

In this work we have focused on finding the network capacity so that we can determine how many users can be accommodated without sacrificing their QoS requirements. On the other hand, another fundamental issue is the *channel capacity*. Currently we are looking into this problem.

References

[1] G. Casella and R. L. Berger, *Statistical Inference.* Duxbury Press, 1990.

[2] K. S. Gilhousen, I. M. Jacobs, R. Padovani, A. J. Viterbi, L. A. Weaver Jr., and C. E. Wheatley III, "On the capacity of a cellular CDMA system," *IEEE Transactions on Vehicular Technology*, vol. 40, pp. 303–312, May 1991.

[3] S. V. Hanly, "Capacity and power control in spread spectrum macro-diversity radio networks," *IEEE Transactions on Communication*, vol. 4, no. 2, pp. 247–256, 1996.

[4] S. V. Hanly, *Information Capacity of Radio Networks.* PhD thesis, Cambridge University, Aug. 1993.

[5] S. V. Hanly and D. Tse, "Multi-access fading channels: Shannon and delay-limited capacities," in *Proc. 33rd Allerton conf.*, pp. 786–795, Oct. 1995.

[6] J. L. Massey and T. Mittelholzer, "Welch's bound and sequence sets for code-division multiple-access systems," in *Sequences II, Methods in Communications, Security and Computer science* (R. Capocelli, A. D. Santis, and U. Vaccaroo, eds.), Springer Verlag, 1993.

[7] Z. Rosberg and J. Zander, "Toward a framework for power control in cellular systems," *Wireless networks*, vol. 4, no. 3, pp. 215–222, Apr. 1998.

[8] D. Tse and S. V. Hanly, "Multiuser demodulation: Effective interference, effective bandwidth and capacity," preprint, Dec. 1997.

[9] S. Ulukus and R. D. Yates, "Stochastic power control for cellular radio systems," *IEEE Transactions on Communication*, vol. 46, no. 6, pp. 784–798, 1998.

[10] S. Verdú, "Multiuser detection," in *Advances in Statistical Signal Processing*, vol. 2, pp. 369–409, JAI Press Inc., 1993.

[11] P. Viswanath, V. Anantharam, and D. Tse, "Optimal sequences, power control and capacity of spread-spectrum systems with multiuser receivers," preprint, Jan. 1998.

[12] R. D. Yates, "A framework for uplink power control in cellular radio systems," *IEEE Journal on Selected Areas in Communications*, vol. 13, no. 7, pp. 1341– 1348, Sep. 1995.

CDMA Systems with Random Spreading in Fading Channels: Network Capacity and Power Control

Junshan Zhang,   Edwin K.P. Chong
School of Electrical and Computer Engineering
Purdue University, West Lafayette, IN 47907-1285
{junshan, echong}@ecn.purdue.edu

Abstract

Due to the fast-growing demand for network capacity in wireless networks, the characterization of network capacity has become one of the most fundamental and pressing issues. While there have been considerable efforts to study CDMA systems at both the physical layer and network layer, the network capacity of power-controlled CDMA systems with linear receivers, especially in fading environments, is not well-understood. In this paper, we study a single-cell synchronous CDMA system equipped with the matched filter receiver in fading channels, and identify the network capacity for single-class systems and the network capacity region for multiple-class systems assuming known distributions of received powers of mobile users. Both the network capacity and network capacity region can be uniquely expressed in terms of the users' QoS requirements and the distributions of the received powers. We also find the tightest upper bound of the network capacity over all possible distributions of received powers, and explore the concepts of effective target SIR and effective bandwidth, which play an important role in determining the admissibility and characterizing the network capacity.

1 Introduction

Wireless networks have drawn a great deal of attention in the past decade. Due to the fast-growing demand for network capacity in wireless networks, it is essential to utilize efficiently the limited resources such as scarce bandwidth and limited power in fading channels. The characterization of network capacity is therefore a fundamental and pressing issue in wireless network research. In this paper, we consider a model for the uplink of a single-cell synchronous CDMA system in fading channels. The system consists of numerous mobile subscribers communicating with one base station, which is typically interconnected to a backbone network via a wired infrastructure.

Much of the previous research on CDMA systems has been restricted to the physical layer, focusing mainly on the performance of linear receivers in worse-case scenario. *Asymptotic efficiency* and *near-far resistance* have been studied as two important performance measures (see [12] for a survey of the literature). At the network layer, there has been considerable interest on power control (see, e.g., [3, 5, 15]). Yates [15] provided a framework for understanding the issue of convergence of some deterministic power control algorithms. A generalization by Ulukus and Yates to stochastic power control algorithm can be found in [11]. Hanly [5] considered macrodiversity, derived the capacity region for the uplink of a radio network, and proposed a decentralized power adaptation algorithm.

Unlike in TDMA and FDMA systems, there is no clean separation between resource allocation at the physical layer and network layer in CDMA systems. Since the sophisticated techniques for allocating network resources at both the physical layer and network layer aim to improve network capacity, it is natural to ask how linear receivers perform in power-controlled CDMA systems. In [10], Tse and Hanly characterized the network capacity for systems with several important receivers via a notion of *effective bandwidth*, assuming users have random signatures. In [14], Viswanath, Anantharam, and Tse studied the network capacity of a synchronous power-controlled CDMA system with multiuser receivers and identified the optimal signatures and power control strategies that make the users meet their QoS requirements. However, both [10] and [14] assumed perfect power control in characterizing network capacity. In a practical wireless communication system, fading is ubiquitous, making perfect power control impossible. However, little work has been done on network capacity of power-controlled CDMA systems with linear receivers in fading channels. In this paper, we study the admissibility and network capacity in imperfect power-controlled CDMA systems in fading channels. All our results assume the matched filter receiver, which is the designated

receiver for CDMA systems in IS-95.

The organization of the rest of this paper is as follows. In Section 2, we give some preliminaries for our model of an imperfect power-controlled CDMA system. In Section 3, we study the admissibility and network capacity for single-class systems. We also address some issues on power control and define the concept of *effective target SIR*. In Section 4, we extend the study to multiple-class systems, and define *effective bandwidth* for imperfect power-controlled CDMA systems in fading channels. Section 5 contains our conclusions.

2 Preliminaries

In a synchronous CDMA system with random spreading, each user chooses its signature randomly and independently. The model for binary random signatures is as follows: $s_k = \frac{1}{\sqrt{L}}(s_{k1}, \ldots, s_{kL})^T$, where L is the processing gain, and the s_{ki}'s are i.i.d. with $P\{s_{ki} = 1\} = P\{s_{ki} = -1\} = \frac{1}{2}$, $i = 1, \ldots, L$ and $k = 1, \ldots, M$. This model is applicable to several scenarios (see, e.g., [10, 13]). First, consider the situation where users employ long pseudo-random spreading sequences with periods considerably larger than the number of chips per symbol interval (such as in IS-95 systems), which is the length of the signatures. In this case, it is sensible to adopt the model that users' signatures are randomly and independently chosen. A second scenario is the case where the signature of each user is repeated from symbol to symbol, but it is randomly and independently selected initially when the user is admitted into the system.

Suppose users transmit data over a frequency non-selective fading channel. Typically, fading channel gains are assumed to be stationary and ergodic, and all the users in one class are assumed to have independently and identically distributed channel gains [4, 7]. The above assumption is very reasonable since interleaving and de-interleaving are usually employed in practical systems. As pointed out in [3] and [10], it is ideal to have the received powers for all the users in one class to be a fixed predetermined value, a scenario called *perfect power control*. However, it is very difficult to implement perfect power control and the received powers fluctuate around the desired levels in a practical system. We model the received powers for users in one class to be independently and identically distributed. For technical reasons, we also assume that power control is good enough to ensure that the fluctuation around the expected received power is bounded (say by d) with probability one.

We assume that the distributions of the received powers are known (cf., [6, Chapter 6]). We aim to study the network capacity in the limiting regime, i.e., when both M and L go to infinity. As in [10], $\beta \equiv \frac{M}{L}$ is taken to be fixed as L goes to infinity. In fact, we only need
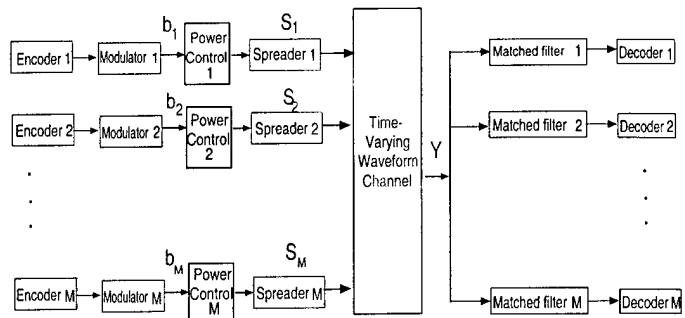
Figure 1: A simplified block diagram of the uplink of a CDMA system with the matched filter receiver

$\lim_{L \to \infty} \frac{M}{L} = \beta$; however, it is more convenient to fix the ratio in the following discussions.

3 Single-Class Systems

Figure 1 depicts a simplified block diagram of the uplink of a CDMA system with the matched filter receiver. Since our purpose is not to evaluate or optimize modulation performance, we assume for simplicity that the modulation is antipodal, that is, $b_k \in \{-1, 1\}$. This assumption is not crucial, but simplifies the analysis. Based on [10, 11], we have the following discrete-time model for a synchronous CDMA system. Suppose there are M users in the system when the processing gain is L. For any symbol interval, the baseband received signal at the front end of the receiver is

$$Y = \sum_{k=1}^{M} \sqrt{P_k^{(L)}} b_k S_k + V, \qquad (1)$$

where the b_k's are the transmitted information symbols and the $P_k^{(L)}$'s are received powers for $k = 1, \ldots, M$, and V is $\mathcal{N}(0, \eta I)$ background white noise that comes from the sampling of the ambient white Gaussian noise with power spectral density η. The received powers are assumed to be i.i.d. with distribution function $F^{(L)}$ which has a density function and mean $\mu^{(L)}$. When L goes to infinity, we assume that the sequence of functions $\{F^{(L)}\}$ converges weakly[1] to F, which denotes the distribution function of the received powers in the limiting regime. We assume that F has a density function and mean μ, and that $\lim_{L \to \infty} \mu^{(L)} = \mu$. For convenience, we let P_0 denote a random variable that has distribution function F.

Assume the signature S_k of user k is known to matched filter k. Then the received SIR (signal-to-interference ratio) for user k after passing the matched filter receiver

---

[1]See [1] for the definition of weak convergence.

is

$$SIR_k^{(L)} = \frac{P_k^{(L)}}{\eta + \sum_{\substack{i=1 \\ i \neq k}}^{M} P_i^{(L)}(S_k^T S_i)^2} \qquad (2)$$

Note that the received SIR's are random variables under our assumption. Therefore, we adopt a probabilistic model for the users' QoS requirements as follows (cf., [9]):

$$P\{SIR_k^{(L)} \geq \gamma\} \geq a, \qquad k = 1, \ldots, M,$$

where $a \in [0, 1]$. In the following sections, we will focus on the cases where $a < 1$ since our work is mainly for imperfect power-controlled systems.

3.1 Admissibility and Network Capacity

Since the $P_k^{(L)}$'s are i.i.d. and the W_{ki}'s are i.i.d., the received SIR's are also identically distributed. Hence, $P\{SIR_k^{(L)} \geq \gamma\}$ does not depend on k. We study user 1 without loss of generality.

Given the distribution of the received powers, we define admissibility for a class of users with random signatures as follows: when the processing gain is L, β users per degree of freedom of the processing gain are admissible in the system if

$$P\{SIR_1^{(L)} \geq \gamma\} \geq a. \qquad (3)$$

We say that β users per degree of freedom of the processing gain are asymptotically admissible if

$$\lim_{L \to \infty} P\{SIR_1^{(L)} \geq \gamma\} \geq a. \qquad (4)$$

Before we examine the asymptotical admissibility, we define $A_M = \frac{1}{M} \sum_{i=2}^{M} (P_i^{(L)} - \mu^{(L)})\xi_i^2$ and $B_M = \frac{1}{M} \sum_{i=2}^{M} \xi_i^2 \mu^{(L)}$, where $\xi_i = \frac{1}{\sqrt{L}} \sum_{l=1}^{L} W_{1l} W_{il}$. Then (2) boils down to

$$\begin{aligned} SIR_1^{(L)} &= \frac{P_1^{(L)}}{\eta + \sum_{i=2}^{M} P_i^{(L)}(S_1^T S_i)^2} \\ &= \frac{P_1}{\eta + \beta(B_M + A_M)}. \end{aligned} \qquad (5)$$

We have the following lemma on the limits of A_M and B_M.

Lemma 3.1 *When the processing gain L goes to infinity, A_M converges to 0 and B_M converges to μ almost surely.*

Due to space limitations, we omit the proof of Lemma 3.1 in this conference version (the proof can be found in the full version of this paper [16]). Lemma 3.1 will be used in the proofs of Proposition 3.1 and Theorem 3.1. Alternatively, Proposition 3.1 can also be

proved by applying [10, Proposition 3.3], but the proof would be more involved. Moreover, if we keep the received power profile of each user the same when $L \to \infty$, as is the case in [10], we can obtain by using Lemma 3.1 that each user's SIR converges almost surely, which is a stronger result than what can be obtained based on [10, Proposition 3.3].

Define $F^{-1}(y) = \inf\{P_0 : F(P_0) > y\}$. Since F is continuous, $F(P_0) \leq y$ if and only if $P_0 \leq F^{-1}(y)$. We have the following proposition on the asymptotical admissibility.

Proposition 3.1 *Suppose each user chooses its signature sequence randomly and independently. Then β users per degree of freedom of the processing gain are asymptotically admissible if and only if $\beta \leq \frac{F^{-1}(1-a)}{\gamma\mu} - \frac{\eta}{\mu}$.*

Proof: By Lemma 3.1, we have[2]

$$SIR_1^{(L)} \overset{\mathcal{D}}{\Longrightarrow} \frac{P_0}{\eta + \beta\mu}. \qquad (6)$$

Since P_0 is a random variable with a density function, we have

$$P\{P_0 = \gamma(\eta + \beta\mu)\} = 0.$$

Appealing to [1, Theorem 2.1], we get

$$\begin{aligned} \lim_{L \to \infty} P\{SIR_1^{(L)} \geq \gamma\} &= P\left\{\lim_{L \to \infty} SIR_1^{(L)} \geq \gamma\right\} \\ &= P\{P_0 \geq \gamma(\beta\mu + \eta)\}. \end{aligned}$$

Hence we have

$$\begin{aligned} &\lim_{L \to \infty} P\{SIR_1^{(L)} \geq \gamma\} \geq a \\ \Leftrightarrow\ & P\{P_0 \geq \gamma(\beta\mu + \eta)\} \geq a \\ \Leftrightarrow\ & F(\gamma(\beta\mu + \eta)) \leq 1 - a \\ \Leftrightarrow\ & \beta \leq \frac{F^{-1}(1-a)}{\gamma\mu} - \frac{\eta}{\mu}, \end{aligned} \qquad (7)$$

completing the proof. $\square$

Following the line of reasoning in [10], we call $\frac{F^{-1}(1-a)}{\gamma\mu} - \frac{\eta}{\mu}$ the *network capacity in the limiting regime* for the given received power distribution.

In practical CDMA systems, the processing gain is finite and large. For example, IS-95 utilizes a bandwidth of slightly less than 1.25 MHz and the processing gain equals 128. For third generation CDMA systems, it has been proposed to use a bandwidth of 5 MHz to offer high quality voice and medium rate data. It is reasonable to expect even larger processing gains for third generation CDMA systems. Therefore, one basic question to ask is, "How many users are admissible for large (but finite) processing gains while the QoS requirements are fixed?"

---

[2] The notation $\overset{\mathcal{D}}{\Longrightarrow}$ is used to denote convergence in distribution.

Based only on Proposition 3.1, however, we cannot answer this question, motivating us to develop another approach that studies a sequence of network capacities indexed by the processing gain L. We proceed to elaborate on this approach.

We define the *network capacity* when the processing gain is L as the maximum number of users (per degree of freedom of the processing gain) that are admissible in the system. That is,

$$\beta_L(a) = \sup\left\{\beta \,\middle|\, P\{SIR_1^{(L)} \geq \gamma\} \geq a\right\}.$$

We define *asymptotic network capacity* $\beta_\infty(a)$ as the limit of $\beta_L(a)$ when $L \to \infty$, that is, $\beta_\infty(a) = \lim_{L\to\infty} \beta_L(a)$.

For technical reasons, we assume that the received powers in the limiting regime have a connected support and hence F is strictly increasing over its support. Our main result is stated as follows:

Theorem 3.1 *Suppose users choose their signatures randomly and independently. Then the asymptotic network capacity is* $\beta_\infty(a) = \frac{F^{-1}(1-a)}{\gamma\mu} - \frac{\eta}{\mu}$.

The proof of Theorem 3.1 is rather technical. Again, due to space limitations, we will not present the proof of Theorem 3.1 here (the proof can be found in the full version of this paper [16]).

It turns out that the *network capacity in the limiting regime* and the *asymptotic network capacity*, which are different in principle, lead to the same result under the auxiliary assumption above. In general, the network capacity in the limiting regime is an upper bound on the asymptotic network capacity. The asymptotic network capacity, however, is a more appropriate approximation of the network capacity of a large network. In particular, by exploiting Theorem 3.1, we can conclude that for a given $\epsilon > 0$, $\beta_\infty(a) - \epsilon$ users per degree of freedom of the processing gain are admissible in the system with sufficiently large L (i.e., $L \geq L_0(\epsilon)$ for some $L_0(\epsilon)$).

Theorem 3.1 establishes the fact that the network capacity can be expressed uniquely in terms of the users' QoS requirements and the received power distribution. Figure 2 shows some plots of the network capacity as a function of the desired SIR. In this example, we assume that the received powers have a log-normal distribution, that is, we take $P_0 = \bar{T}10^{\frac{\xi}{10}}$, where $\bar{T}$ is some constant and ξ has mean zero and standard deviation $\sigma = 1.7$. Strictly speaking, we should have modeled the received power with a truncated version of the log-normal distribution by our assumption. However, the difference is insignificant and results in unnecessary increase of the computation complexity.
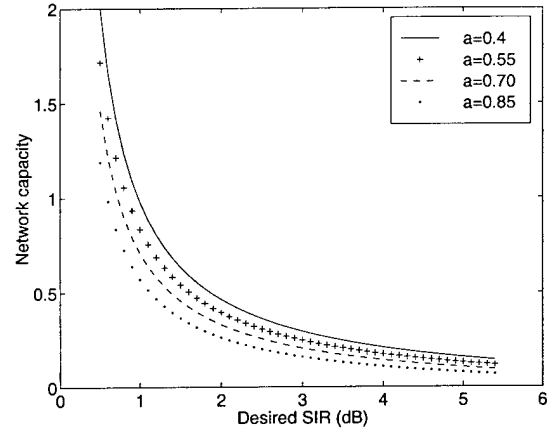
Figure 2: Network capacity vs. desired SIR

3.2 Power Control and Effective Target SIR

We have studied the admissibility and network capacity for single-class systems assuming known distribution of the received powers. On the other hand, one fundamental question to ask is, "How many users (per degree of freedom of processing gain) can be made asymptotically admissible through power control for given QoS requirements?" We study this problem in the high signal-to-noise ratio region (when the background noise power η goes to 0, as in [12]). Loosely speaking, the above problem can be regarded as the dual of the near-far resistance problem for the matched filter receiver in the following sense: on one hand, near-far resistance concerns the worse-case performance; on the other hand, optimum power-controlled capacity concerns the best-case performance.

Define

$$\tilde{\beta}_d = \sup_{F(\cdot)} \lim_{\eta\to 0} \beta_\infty(a).$$

The calculation of $\tilde{\beta}_d$ boils down to finding the supremum of the ratio of $F^{-1}(1-a)$ to μ_F over all possible distributions of received powers, where μ_F is the corresponding mean of a distribution function F. (Note that, a priori, μ_F can be any positive number.) It is straightforward to get

$$\sup_{F(\cdot)} \frac{F^{-1}(1-a)}{\mu_F} = \frac{1}{a}, \tag{8}$$

and the supremum is achieved by any distribution of the form as shown in Figure 3. Hence, $\tilde{\beta}_d = \frac{1}{a\gamma}$. Furthermore, for a given distribution function F having the form in Figure 3, it is easy to construct a sequence of continuous distribution functions that converge pointwise to F. For example, it is easy to show that $\{H_n\}$ defined below
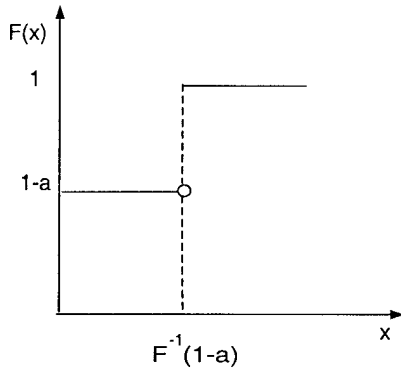
Figure 3: A distribution function that achieves the supremum of $\frac{F^{-1}(1-a)}{\mu_F}$

converges pointwise to F:

$$H_n(x) = \begin{cases} 0 & x < 0 \\ 1 - a & 0 \le x < b \\ 1 - a + na(x - b) & b \le x < b + \frac{1}{n} \\ 1 & x \ge b + \frac{1}{n}, \end{cases}$$

where $b = F^{-1}(1 - a)$. Moreover, we have

$$\lim_{n \to \infty} \frac{H_n^{-1}(1 - a)}{\mu_{H_n}} = \frac{1}{a}.$$

Therefore, there exists a distribution function for which β users (per degree of freedom) are admissible if and only if $\beta < \tilde{\beta}_d$.

Observe that the optimal power control is in the form of "bang-bang" control. To provide more insight into why the distribution function F given in Figure 3 is optimal in the sense of maximizing the capacity, we have the following heuristic and interesting interpretation. Suppose the number of users (per degree of freedom) is less than (and close to) $\tilde{\beta}_d$. Since the QoS requirement is that $P\{SIR^{(L)} \ge \gamma\} \ge a$, we implement power control such that the received SIR of each user is greater than (and close to) γ with probability a and equals 0 with probability $1 - a$. That is, very little power is wasted, which is equivalent to saying that the power control is efficient. When $a < 1$, perfect power control is no longer the best in this context by the above observations. The reason lies in the fact that we loosen the users' QoS requirements. When $a = 1$, the optimum power control strategy is perfect power control, and $\tilde{\beta}_d = \frac{1}{\gamma}$, which agrees with the expression given in [10]. (Let $\bar{P}$ denote the received power under the perfect power control scheme; we take $F^{-1}(0) = \bar{P}$.)

We proceed to look for an abstraction that combines the information of both QoS requirements and received power distributions for determining the asymptotic admissibility and characterizing the network capacity for single-class systems.

Note that if β users are not asymptotically admissible for a given received power distribution, it may still be possible to make β asymptotically admissible by scaling up the received power. Referring to the definition of *scale family* in [2, p. 118], we consider the scale family $\mathcal{G} = \{F(\frac{P_0}{c}), c > 0\}$, where F is the distribution function of P_0. Note that for any $G_1, G_2 \in \mathcal{G}$, G_1 is a scaled version of G_2, and vice versa. A very special (degenerate) example of the scale family is[3]

$$\mathcal{G} = \{F_t = I_{[t,\infty)} : t > 0\},$$

which essentially represents the totality of distribution functions under perfect power control.

Define $\gamma' = \gamma c_e$, where $c_e = \frac{\mu_H}{H^{-1}(1-a)}$, $H \in \mathcal{G}$. An important observation is that c_e is fixed for the scale family $\mathcal{G}$. That is, c_e is invariant over all the distributions in $\mathcal{G}$, and is a property of the whole scale family. Therefore, γ' is also invariant over all the distributions in $\mathcal{G}$. We call γ' the *effective target SIR* for $\mathcal{G}$. For example, we have $\gamma' = a\gamma$ for the scale family of distributions that have the form as shown in Figure 3.

Note that in a given scale family of distributions, there exists a one-to-one correspondence between distribution and mean. We have the following proposition for a given scale family $\mathcal{G}$.

Proposition 3.2 *There exists a finite positive value that can be assigned as the mean such that β users per degree of freedom of processing gain are asymptotically admissible for the corresponding received power distribution in $\mathcal{G}$ if and only if $\beta\gamma' < 1$. Moreover, the minimum value for μ_F is*

$$\tilde{\mu} = \frac{\eta\gamma'}{1 - \beta\gamma'}. \tag{9}$$

The proof of Proposition 3.2 follows directly from Proposition 3.1. Clearly, the effective target SIR plays an important role in determining the admissibility. For illustration, we show some plots of the effective target SIR as a function of the desired SIR in Figure 4. For simplicity, again we assume that the received powers have a log-normal distribution, that is, $P_0 = \bar{T}10^{\frac{\xi}{10}}$. Note that ξ is due to the channel gain estimation error. Several observations are worth noting. On one hand, the channel gain estimation has much impact on the effective target SIR, especially when a is large. The smaller the standard deviation σ of the channel gain estimation error, the smaller the slopes and hence the effective target SIR. On the other hand, it is desirable to reduce the desired SIR for fixed a as much as possible so that we can get a small effective target SIR. Sophisticated techniques of coding and modulation can be exploited to combat fading and increase the error correcting ability and hence reduce the effective target SIR.

---

[3]I_A denotes the indicator function of a set A.
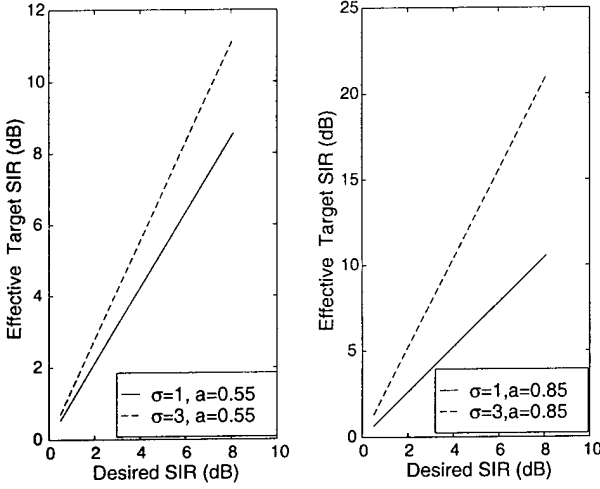
Figure 4: Effective target SIR as a function of desired SIR

Note that if β users are asymptotically admissible for some distribution of the received power, then β users are also asymptotically admissible when we scale up the received power by any constant greater than 1. For example, let H denote the distribution function corresponding to the mean given in (9). An easy observation is that β users are asymptotically admissible when we "scale up" H by any constant greater than 1 (i.e., for any distribution function $H'(p_0) = H(p_0/c)$, $c \geq 1$).

4 Multiple-Class Systems

We have studied the network capacity for single-class systems in the above section. However, future wireless systems will have to support multimedia services such as voice, data, video, and fax. Therefore, it is essential to have a level of generalization dealing with users having different QoS requirements.

Suppose there are a fixed number, say N, of classes. Let A_n denote the set of users in class n and M_n the cardinality of A_n, $n = 1, \ldots, N$. Let S_{in} denote the signature for the ith user in class n. Define $\beta_n = \frac{M_n}{L}$ and let β_n be fixed when L goes to infinity as in the single-class case.

Let $P_{in}^{(L)}$ denote the received power for $i \in A_n$ and $n = 1, \ldots, N$ when the processing gain is L. Then the received SIR for the ith user in class n is

$$SIR_{in}^{(L)} = \frac{P_{in}^{(L)}}{\eta + I_1^{(L)} + I_2^{(L)}}, \quad (10)$$

where

$$I_1^{(L)} = \sum_{\substack{l \in A_n \\ l \neq i}} P_{ln}^{(L)} (S_{in}^T S_{ln})^2,$$

$$I_2^{(L)} = \sum_{\substack{j \neq n \\ l \in A_j}} P_{lj}^{(L)} (S_{in}^T S_{lj})^2.$$

Again our results are asymptotic in nature. For the sake of notational convenience, as in the single-class case, we let P_n denote a random variable that has the same distribution F_n as the received powers of the users in class n in the limiting regime, and assume that F_n has a density function and mean μ_n. For convenience, we call the collection $\{F_1, \ldots, F_N\}$ a *group of received power distributions*, and $\vec{P} = (\mu_1, \ldots, \mu_N)^T$ the *mean power vector*. Suppose it is required that the users in class n have received SIR greater than or equal to γ_n with probability no less than $a_n \in [0, 1]$.

Similar to the approach in the single-class case, we obtain

$$SIR_{in}^{(L)} \xrightarrow{\mathcal{D}} \frac{P_n}{\eta + \sum_{n=1}^{N} \beta_n \mu_n}. \quad (11)$$

Therefore, we study the first user in class n without loss of generality.

4.1 Admissibility and Network Capacity Region

Given a group of received power distributions, we say a tuple $(\beta_1, \ldots, \beta_N)$ is asymptotically admissible if the following condition holds:

$$\lim_{L \to \infty} P\{SIR_{1n}^{(L)} \geq \gamma\} \geq a_n, \quad n = 1, \ldots, N.$$

We define the *network capacity region* to be the set of all tuples that are asymptotically admissible.

We have the following proposition on the network capacity region of multiple-class systems for the given distribution of the received powers.

Proposition 4.1 *Under the choice of random signatures, the network capacity region is given by*

$$\left\{ (\beta_1, \ldots, \beta_N) : \sum_{n=1}^{N} \beta_n \mu_n \leq \min_n \left(\frac{F_n^{-1}(1 - a_n)}{\gamma_n} \right) - \eta \right\}$$

Proof: Since P_n has a density function, we get by applying [1, Theorem 2.1],

$$\lim_{L \to \infty} P\{SIR_{1n}^{(L)} \geq \gamma\} = P\left\{ \lim_{L \to \infty} SIR_{1n}^{(L)} \geq \gamma \right\}$$

$$= P\left\{ \frac{P_n}{\eta + \sum_{n=1}^{N} \beta_n \mu_n} \geq \gamma \right\}.$$

By definition, a tuple $(\beta_1, \ldots, \beta_N)$ is asymptotically admissible if and only if for $n = 1, \ldots, N$,

$$\lim_{L \to \infty} P\{SIR_{1n}^{(L)} \geq \gamma\} \geq a_n.$$

Thus, we have for $n = 1, \ldots, N$,

$$\lim_{L \to \infty} P\{SIR_{1n}^{(L)} \geq \gamma\} \geq a_n$$

$$\Leftrightarrow \quad P\{P_n \geq \gamma(\eta + \sum_{n=1}^{N} \beta_n \mu_n)\} \geq a_n$$

$$\Leftrightarrow \quad \sum_{n=1}^{N} \beta_n \mu_n \leq \frac{F_n^{-1}(1 - a_n)}{\gamma_n} - \eta.$$

which is equivalent to

$$\sum_{n=1}^{N} \beta_n \mu_n \leq \min_n \left(\frac{F_n^{-1}(1 - a_n)}{\gamma_n} \right) - \eta. \qquad (12)$$

Then the desired result follows. $\qquad \square$

4.2 Power Control, Effective Target SIR, and Effective Bandwidth

As in the single-class case, we introduce the scale family $\mathcal{G}_n = \{F_n(\frac{P_n}{c}), c > 0\}$, where F_n is the distribution function of P_n, $n = 1, \ldots, N$. Define $\gamma_n' = \gamma_n c_{en}$, where $c_{en} = \frac{\mu_{G_n}}{G_n^{-1}(1 - a_n)}$, $G_n \in \mathcal{G}_n$. Note that c_{en} is fixed for the scale family $\mathcal{G}_n$. We call γ_n' the *effective target SIR* for $\mathcal{G}_n$. For convenience, we call the collection $\{\mathcal{G}_1, \ldots, \mathcal{G}_N\}$ a *group of scale families*. Then we have by straightforward manipulations of (12),

$$\mu_n \geq \gamma_n'[\eta + \sum_{n=1}^{N} \beta_n \mu_n] \qquad n = 1, \ldots, N. \qquad (13)$$

Let $\vec{\Gamma} = (\gamma_1', \ldots, \gamma_N')^T$, and $\vec{\beta} = (\beta_1, \ldots, \beta_N)^T$. Using the above notation, (13) boils down to

$$\vec{P} \geq \vec{\beta}^T \vec{P} \vec{\Gamma} + \eta \vec{\Gamma}. \qquad (14)$$

We want to study the feasibility of (14), that is, the condition under which there exist positive vectors $\vec{P}_d$ satisfying (14). Based on [8, 9], we draw the conclusion that a necessary and sufficient condition for the existence of a finite positive solution to (14) is the existence of a finite positive solution to the system of equations obtained by setting all inequalities in (14) to equalities. More specifically, we have the following lemma.

Lemma 4.1 *There exists a finite positive vector $\vec{P}$ satisfying (14) if and only if the following condition holds:*

$$\sum_{n=1}^{N} \beta_n \gamma_n' < 1. \qquad (15)$$

Moreover, the n-th component of the component-wise minimum mean power vector satisfying (14) is

$$\mu_n = \frac{\eta \gamma_n'}{1 - \sum_{n=1}^{N} \beta_n \gamma_n'}, \qquad n = 1, \ldots, N. \qquad (16)$$

Proof: Observe that $\vec{\Gamma} \vec{\beta}^T$ is a non-negative irreducible matrix and has rank one. Thus, the Perron-Frobenius eigenvalue of $\vec{\Gamma} \vec{\beta}^T$ is $\vec{\beta}^T \vec{\Gamma}$. Appealing to [8, Proposition 2.1], we have that a necessary and sufficient condition for the existence of a non-negative nonzero solution to (14) is

$$\sum_{n=1}^{N} \gamma_n' \beta_n < 1.$$

Define

$$\vec{P}^* = \left(I - \vec{\Gamma} \vec{\beta}^T \right)^{-1} \eta \vec{\Gamma}.$$

Then the solution $\vec{P}^*$ is Pareto optimal in the following sense: any other feasible solution to (14) will have every component not less and at least one component greater than the solution $\vec{P}^*$.

It is easy to obtain that $\vec{P}^* = \frac{\eta}{1 - \vec{\beta}^T \vec{\Gamma}} \vec{\Gamma}$. Therefore, we obtain that the n-th component of the component-wise minimum mean power vector is

$$\mu_n = \frac{\eta \gamma_n'}{1 - \sum_{n=1}^{N} \beta_n \gamma_n'}.$$

$\qquad \square$

Observe that in a given group of scale families, there exists a one-to-one correspondence between the mean power vector and the group of received power distributions. Based on Lemma 4.1, we can easily obtain the following result for a given group of scale families $\{\mathcal{G}_1, \ldots, \mathcal{G}_N\}$.

Proposition 4.2 *There exists a finite positive vector that can be assigned as the mean power vector for a tuple $(\beta_1, \ldots, \beta_N)$ to be asymptotically admissible for the corresponding group of received power distributions in $\{\mathcal{G}_1, \ldots, \mathcal{G}_N\}$ if and only if*

$$\sum_{n=1}^{N} \beta_n \gamma_n' < 1.$$

Moreover, the n-th component of the component-wise minimum mean power vector is

$$\mu_n = \frac{\eta \gamma_n'}{1 - \sum_{n=1}^{N} \beta_n \gamma_n'}, \qquad n = 1, \ldots, N.$$

The proof of Proposition 4.2 follows by combining the results of Lemma 4.1 and Proposition 4.1. Observing the conditions given in Proposition 4.2, we are motivated to extend the insightful idea in [10] and define the *effective bandwidth* of class n as $\mathcal{E}(\gamma_n) = \gamma_n'$ degrees of freedom per user. Proposition 4.2 tells us that for a given group of scale families, a tuple $(\beta_1, \ldots, \beta_N)$ can be made asymptotically admissible through power control if and only if the sum of effective bandwidth of all classes is less than one.

It is easily observed that the smaller the effective target SIR, the smaller the effective bandwidth. Under the optimum power control obtained in the single-class case, the condition given in (15) boils down to $\sum_{n=1}^{N} \beta_n a_n \gamma_n < 1$.

5 Conclusions

We study a single-cell synchronous CDMA system with the matched filter receiver in fading channels, and identify the network capacity for single-class systems and the network capacity region for multiple-class systems assuming known distributions of received powers of mobile users. Both the network capacity and network capacity region can be uniquely expressed in terms of the users' QoS requirements and the distributions of the received powers. For given scale families of distributions of received powers, we give necessary and sufficient conditions for asymptotic admissibility in terms of effective bandwidth for both single-class systems and multiple-class systems. We also find the tightest upper bound of the network capacity over all possible distributions of received powers. Our results are useful for network-level resource allocation problems such as admission control and power control in a large network. Furthermore, although we have confined ourselves to the systems with the matched filter receiver, we believe that our results can be extended to the systems equipped with the MMSE (minimum mean square error) receiver.

In this paper we have focused on characterizing the network capacity so that we can determine how many users can be accommodated without sacrificing their QoS requirements. On the other hand, another fundamental issue is the *channel capacity*. That is, how much information can be transmitted reliably through the fading channels? Currently we are looking into this problem.

References

[1] P. Billingsley, *Convergence of Probability Measures.* John Wiley & Sons, Inc., 1968.

[2] G. Casella and R. L. Berger, *Statistical Inference.* Duxbury Press, 1990.

[3] K. S. Gilhousen, I. M. Jacobs, R. Padovani, A. J. Viterbi, L. A. Weaver Jr., and C. E. Wheatley III, "On the capacity of a cellular CDMA system," *IEEE Transactions on Vehicular Technology*, vol. 40, pp. 303–312, May 1991.

[4] A. Goldsmith and P. Varaiya, "Capacity of fading channels with channel side information," *IEEE Transactions on Information Theory*, vol. 43, pp. 1986–1992, Nov. 1997.

[5] S. V. Hanly, "Capacity and power control in spread spectrum macro-diversity radio networks," *IEEE Transactions on Communications*, vol. 4, no. 2, pp. 247–256, 1996.

[6] S. V. Hanly, *Information Capacity of Radio Networks.* PhD thesis, Cambridge University, Aug. 1993.

[7] S. V. Hanly and D. Tse, "Multi-access fading channels: Shannon and delay-limited capacities," in *Proc. 33rd Allerton Conf.*, pp. 786–795, Oct. 1995.

[8] D. Mitra, "An asynchronous distributed algorithm for power control for cellular radio systems," in *Proc. 4th WINLAB Workshop on Third Generation Wireless Information Networks*, pp. 249–257, 1993.

[9] D. Mitra and J. A. Morrison, "A novel distributed power control algorithm for classes of service in cellular CDMA networks," in *Fourth Informs Telecommunication Conference*, (Boca Raton, FL), 1998.

[10] D. Tse and S. V. Hanly, "Multiuser demodulation: Effective interference, effective bandwidth and capacity," *IEEE Transactions on Information Theory*, Mar. 1999, to appear.

[11] S. Ulukus and R. D. Yates, "Stochastic power control for cellular radio systems," *IEEE Transactions on Communications*, vol. 46, no. 6, pp. 784–798, 1998.

[12] S. Verdú, "Multiuser detection," in *Advances in Statistical Signal Processing*, vol. 2, pp. 369–409, JAI Press, Inc., 1993.

[13] S. Verdú and S. Shamai (Shitz), "Spectral efficiency of CDMA with random spreading," preprint, July 1998.

[14] P. Viswanath, V. Anantharam, and D. Tse, "Optimal sequences, power control and capacity of spread-spectrum systems with multiuser linear receivers," preprint, Jan. 1998, (see http://www.eecs.berkeley.edu/~ananth).

[15] R. D. Yates, "A framework for uplink power control in cellular radio systems," *IEEE Journal on Selected Areas in Communications*, vol. 13, no. 7, pp. 1341–1348, Sept. 1995.

[16] J. Zhang and E. K. P. Chong, "CDMA systems in fading channels: Admissibility, network capacity, and power control," preprint, July 1998.

CDMA Systems in Fading Channels: Admissibility, Network Capacity, and Power Control

Junshan Zhang   Edwin K.P. Chong*

School of Electrical and Computer Engineering
Purdue University, West Lafayette, IN 47907-1285
{junshan, echong}@ecn.purdue.edu

Abstract

Due to the fast-growing demand for network capacity in wireless networks, the characterization of network capacity has become a fundamental and pressing issue. While there have been considerable efforts on CDMA systems at both the physical layer and network layer, the network capacity of imperfect power-controlled CDMA systems with linear receivers in fading environments are less well-understood. In this paper, we study a single-cell synchronous CDMA system with matched filter receivers, assuming known distributions of received powers. We find necessary and sufficient conditions on the admissibility for both single class and multiple class systems with random signatures. For systems with deterministic signatures, we give a necessary and sufficient condition on the admissibility for single class systems, but only a sufficient condition for multiple class systems. We also identify the network capacity of single class systems for both the random signature case and the deterministic signature case. The network capacity can be uniquely expressed in terms of the users' QoS requirements and the distributions of the received powers. We find the tightest upper bound on the network capacity over all possible distributions of received powers, and explore the concepts of effective target SIR and effective bandwidth, which play an important role in determining the admissibility and hence the network capacity.

Index Terms: CDMA, Matched Filter, Deterministic Signature, Random Signature, Admissibility, Network Capacity, Power Control, Fading Channel, Scale Family.

1

1 Introduction

Wireless networks have drawn a great deal of attention in the past decade. Due to the fast-growing demand for network capacity in wireless networks, it is essential to utilize efficiently the limited resources in fading channels. The characterization of network capacity is therefore a fundamental and pressing issue in wireless network research. In this work, we consider a model for the uplink of a single-cell synchronous CDMA system in fading channels. The network therein consists of numerous mobile subscribers communicating with one base station, which is typically interconnected to a backbone network via a wired infrastructure.

Much of the previous research on CDMA systems has been restricted to the physical layer [12, 13, 14, 19, 26] (see [25] for a survey of the literature). Lupas and Verdú [12] considered linear multiuser receivers that can achieve performance similar to optimal multiuser detector. Madhow and Honig [13] presented and analyzed minimum mean squared error (MMSE) interference suppression schemes. Roughly speaking, the main principle in designing these receivers is to project the signature of the desired user onto the subspace which is orthogonal to that spanned by the signatures of the interferers. In more recent work [14], Madhow and Honig further studied the performance of a finite complexity MMSE linear detector for demodulating DS-CDMA signals. These works focus mainly on the performance of linear receivers in worst-case scenarios, and *near-far resistance* and *asymptotic efficiency* have been studied as two important performance measures.

At the network level, there have been considerable efforts on power control [6, 8, 24, 31]. Yates [31] provided a framework for understanding the issue of convergence of some deterministic power control algorithms. A generalization by Ulukus and Yates to stochastic power control algorithm can be found in [24]. In [8], Hanly introduced macrodiversity, derived the capacity region for the uplink of a radio network, and proposed a decentralized power adaptation algorithm.

Unlike in TDMA and FDMA systems, there is no clean separation between resource allocation at the physical layer and network layer in CDMA systems. Since the sophisticated techniques for allocating network resources at both the physical layer and network layer aim at improving network capacity, it is natural to ask how linear receivers perform in power controlled systems. In [23], Tse and Hanly characterized network capacity for several important receivers via a notion of *effective bandwidth*, assuming users have random signatures. In [27], Viswanath, Anantharam, and Tse studied the joint optimization problem of designing the multiuser receiver structure, power control, and spreading sequences, and obtained simple characterizations of the resulting network capacity in various scenarios. However, both

2

[23] and [27] assumed perfect power control in characterizing network capacity. In a practical wireless communication system, multipath fading is ubiquitous, making perfect power control impossible. However, little work has been done on network capacity of imperfect power-controlled CDMA systems with linear receivers in fading channels.

In this paper, we study the admissibility and network capacity of imperfect power-controlled CDMA systems with matched filter receivers in fading channels. Each user in the system is assigned a signature onto which the user's information symbols are spread. Every user also has a minimum signal-to-interference (SIR) requirement. Roughly speaking, a set of users is said to be *admissible* if their simultaneous transmission does not result in violation of any of their SIR requirements; the *network capacity* is the maximum number of admissible users. Following the approach of [23, 26], we formulate the problem in an asymptotic setting in which we allow the number of users M and the degrees of freedom L (length of the signature) to grow, while keeping their ratio fixed. The results are stated in terms of this ratio of number of users per degree of freedom. A feature that distinguishes this work from [23] is that the received power for each user in our model are random. The SIR requirements in our setting are also therefore probabilistic, unlike that of [23].

We treat separately systems with single class of users and systems with multiple classes of users. In each case, we consider both deterministic and random signatures. For the random signature case, we provide necessary and sufficient conditions, in both single class and multiple class systems, for a set of users per degree of freedom to be admissible. For the deterministic signature case, we provide a necessary and sufficient condition for admissibility in single class systems, but only a sufficient condition for multiple class systems. For single class systems, we also calculate the network capacity. The analysis in the deterministic signature case involves WBE sequences and inequalities, using results of [15], as in [27] (note that the results in [27] apply only to the perfect power control case).

The organization of the rest of this paper is as follows. In Section 2 we give some preliminaries for our model of an imperfect power-controlled CDMA system in fading channels. In Section 3, we study admissibility and identify network capacity for users of a single class. We also address some issues on power control and define the concept of *effective target SIR*. In Section 4, we extend the study to users of multiple classes, and define *effective bandwidth* for imperfect power-controlled CDMA systems in fading channels. Finally, we draw some conclusions in Section 5.

2 Preliminaries

Suppose users transmit data over a fading channel. Typically, fading channel gains are assumed to be stationary and ergodic, and all the users in one class are assumed to have independently and identically distributed channel gains (see [7, 10]). The above assumption is very reasonable since interleaving and de-interleaving are usually employed in practical systems. As pointed out in [6] and [23], it is ideal to have the received powers for all the users in one class to be the same all the time. However, it is very difficult to implement perfect power control and the received powers fluctuate around the desired levels in a practical system. Assuming that all the users in one class experience independently and identically distributed channel gains and the same kind of power control algorithm is applied to all users in one class, by symmetry, we model the received powers for all users in one class to be independently and identically distributed in a large network. For technical reasons, we also assume that power control is good enough to ensure that the fluctuation around the expected received power is bounded (say by d) with probability one.

We assume that the distributions of the received powers are known. This assumption is reasonable (cf., [9, Chapter 6]). From a practical viewpoint, the distributions of the received powers can usually be obtained through measurements (see [17]). It is worth pointing out that the constraints on the power such as peak power constraint or average power constraint can easily be taken into account in the above assumptions on the received powers.

We aim to study the admissibility and network capacity in the limiting regime, that is, when both M and L go to infinity. As in [23], $\beta \triangleq \frac{M}{L}$ is taken to be fixed as L goes to infinity since it is very reasonable to keep the number of users per degree of freedom fixed while scaling up the processing gain L. In fact, we only need $\lim_{L\to\infty} \frac{M}{L} = \beta$; however, it is more convenient to fix the ratio in the following discussion.

In a synchronous CDMA system, each user, say user k, is assigned a binary (± 1 valued) signature of length L, $S_k = \frac{1}{\sqrt{L}}(W_{k1}, \dots, W_{kL})^T$, where W_{ki} is either 1 or -1 for $i = 1, \dots, L$. The user's information symbols are spread onto its signature. There are several methods to spread the information symbols onto the signature (see [16]). One method is to alter directly the information symbols by modulo-2 addition with the signature. Another way is to multiply the information symbols with the signature. For purposes of demodulation, it is convenient to adopt the second approach. We will study the admissibility and network capacity for the following two cases. The first is the deterministic signature case, by which we mean that the users' signatures are jointly designed and deterministic when they are admitted into the system (see e.g. [15, 27]); the second is the random signature case, by
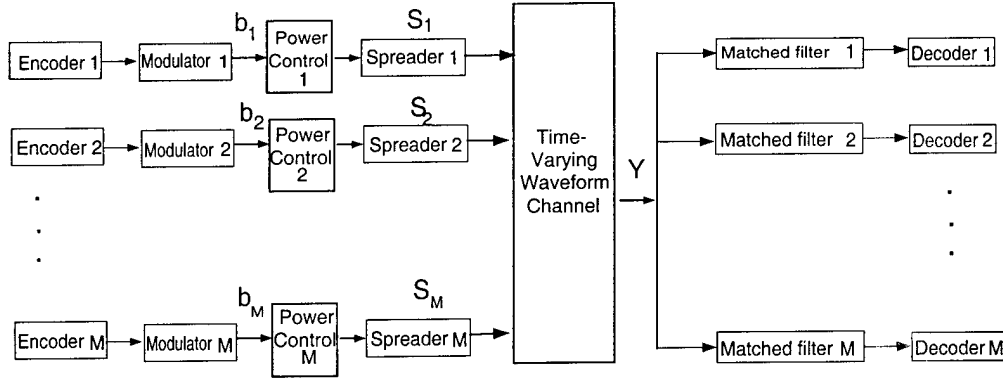
Figure 1: A simplified block diagram of the uplink of a CDMA system with matched filter receiver

which we mean that users choose their signatures randomly and independently when they are admitted into the system, which models the situation where the information symbols are spread onto pseudo-random spreading sequences (see e.g. [23, 26]).

Our main results make use of the following lemma [4, Lemma 2.4], which is a strong law for triangular arrays:

Lemma 2.1 *Let $X_{in}, i = 1, \ldots, n; \ n = 1, 2, \ldots$ be a triangular array of random variables defined on a common probability space such that for each n, $\{X_{in}, i = 1, \ldots, n\}$ are independent, and let $S_n = \sum_{i=1}^{n} X_{in}$. If $\frac{S_n}{n} \to 0$ in probability and*

$$\sum_{i=1}^{n} \frac{X_{in}^2 \log n}{n^2} \to 0 \quad a.s.,$$

then $\frac{S_n}{n} \to 0$ almost surely.

3   Single Class Systems

Figure 1 depicts a simplified block diagram of the uplink of a CDMA system with matched filter receiver. Since our purpose is not to evaluate or optimize modulation performance, for simplicity, we assume the modulation is antipodal, that is, $b_k \in \{-1, 1\}$. This assumption is not crucial, but it simplifies the analysis. Based on [23, 24], we have the following discrete-time model for the uplink of a synchronous CDMA system. Suppose there are M users in the system when the processing gain is L. For any symbol interval, the baseband received

signal at the front of the receiver is

$$Y = \sum_{k=1}^{M} \sqrt{P_k^{(L)}} b_k S_k + V, \qquad (1)$$

where the b_k's are the transmitted information symbols and the $P_k^{(L)}$'s are received powers for $k = 1, \ldots, M$, and V is $\mathcal{N}(0, \eta I)$ background noise that comes from the sampling of the ambient white Gaussian noise with power spectral density $\eta = \frac{N_0}{2}$. (We assume throughout that $\eta > 0$.) The received powers are assumed to be i.i.d. with distribution F_L, which has a density function and mean $\mu^{(L)}$. When L goes to infinity, we assume that the sequence of functions $\{F_L\}$ converges weakly to F (see [1] for the definition of weak convergence), which denotes the distribution of the received powers in the limiting regime. Let P_0 denote a random variable that has distribution F and mean μ. We assume that $\lim_{L\to\infty} \mu^{(L)} = \mu$.

Assume the signature S_k of user k is known to the receiver for it. Then the received SIR (signal-to-interference ratio) for user k after passing the matched filter is (cf., [13, 23])

$$SIR_k^{(L)} = \frac{P_k^{(L)}}{\eta + \sum_{\substack{i=1 \\ i \neq k}}^{M} P_i^{(L)} (S_k^T S_i)^2} \qquad k = 1, \ldots, M. \qquad (2)$$

Note that the received SIRs are random variables under our assumption. (See [28] for a plot of the received SIRs distributions based on the San Diego Tests.) Therefore, we adopt a probabilistic model for the users' QoS requirements as follows:

$$P\{SIR_k^{(L)} \geq \gamma\} \geq a, \qquad k = 1, \ldots, M.$$

We justify this model as follows: first, since the received SIRs depend on power control (which could be adaptive) and the status of the fading channels, it is difficult to derive a general one-to-one mapping between the average SIR and BER (bit error rate) for either coherent or noncoherent reception. Second, although much research on power control has done snapshot analysis assuming that the objective is to drive all SIR values above a given target SIR, as pointed out in [17], most often the favorite conditions for the foundation of the above approach do not hold true, making the analysis inappropriate. Furthermore, as in [20, 23], we are interested in the more general problem of extracting good estimates of the symbols of each user for soft decisions. Hence, it is sensible to adopt the above probabilistic model for the users' QoS requirements.

In the following sections, we will focus on the cases where $a < 1$ since our results are mainly for imperfect power-controlled systems.

3.1 The Deterministic Signature Case

In this case, the users' signatures are deterministic, and the signatures of all the M users form a signature set when the processing gain is L. As L goes to infinity, we have a sequence of signature sets. Let $\mathcal{F}$ denote the collection of sequences of signature sets satisfying the following condition:

$$\sup_{\substack{i,j \leq M \\ i \neq j}} (S_i^T S_j)^2 \log L \to 0 \qquad \text{as } L \to \infty, \tag{3}$$

where S_i and S_j are the signatures for user i and j respectively when the processing gain is L, $i, j \in \{1, \ldots, M\}$. Intuitively, for any sequence of signature sets not satisfying (3), there exist at least two users whose signatures are heavily correlated in a large network, which is not desirable since statistical multiplexing is an advantage of spread spectrum systems when the received powers fluctuate because of fading environments, and low cross-correlation is essential for statistical multiplexing [9].

In the following sections where sequences of deterministic signature sets are chosen, we confine ourselves to sequences in $\mathcal{F}$.

3.1.1 Asymptotic Admissibility

We define *admissibility* for a class of users as follows: when the processing gain is L, β users per degree of freedom of the processing gain are admissible in the system if and only if there exists a signature set $\{S_1, \ldots, S_M\}$ for the M users, where M equals βL, and the users' QoS requirements are satisfied when $\{S_1, \ldots, S_M\}$ are assigned to the users, that is,

$$P\{SIR_k^{(L)} \geq \gamma\} \geq a, \quad \forall k = 1, \ldots, M,$$

which is equivalent to

$$\max_{\{S_1, \ldots, S_M\}} \min_k P\{SIR_k^{(L)} \geq \gamma\} \geq a. \tag{4}$$

Asymptotic admissibility is defined as follows: we say β users per degree of freedom of the processing gain are asymptotically admissible if the following condition holds:

$$\lim_{L \to \infty} \max_{\{S_1, \ldots, S_M\}} \min_k P\{SIR_k^{(L)} \geq \gamma\} \geq a.$$

To study the issue of asymptotic admissibility, we need some intermediate results. For ease of later reference, let F_M denote the signature set $\{S_1, \ldots, S_M\}$, and define

$$A_M(F_M, k) = \sum_{\substack{i=1 \\ i \neq k}}^{M} (P_i^{(L)} - \mu^{(L)})(S_k^T S_i)^2,$$

7

$$B_M(F_M, k) = \sum_{\substack{i=1 \\ i \neq k}}^{M} (S_k^T S_i)^2 \mu^{(L)}.$$

First we study the limits of $A_M(F_M, k)$ and $B_M(F_M, k)$. As pointed out in [27], when $M \leq L$ we can always choose an orthogonal signature set so that $A_M(F_M, k) = 0$ and $B_M(F_M, k) = 0$. Then each single user transmits data as if it were in a single-user channel. This case is not of real interest since we want to find the maximum number of users supportable by the system. For the case $M > L$, our results make use of WBE (Welch Bound Equality) signature sets. Massey and Mittelholzer [15] define the binary sequences $S_1, \ldots, S_M$ of length L with unit norm satisfying the following equality as WBE sequence set:

$$\sum_{i=1}^{M} \sum_{j=1}^{M} (S_i^T S_j)^2 = \frac{M^2}{L}.$$

We use the terminology "signature set" instead of "sequence set" to avoid confusion since we will discuss sequences of such sets.

For any sequence of signature sets $\{F_M\}$, if $\lim_{L \to \infty} \max_k \sum_{j=1}^{M} (S_k^T S_j)^2$ is not finite, then $\lim_{L \to \infty} \min_k P\{SIR_k^{(L)} \geq \gamma\} = 0$, which implies at least one user cannot have its QoS requirements satisfied. Therefore, we assume $\lim_{L \to \infty} \max_k \sum_{j=1}^{M} (S_k^T S_j)^2 < \infty$ in the proceeding discussion.

Lemma 3.1 a). *For any sequence $\{F_M\}$ in $\mathcal{F}$, $\lim_{L \to \infty} A_M(F_M, k) = 0$ almost surely when $\lim_{L \to \infty} \max_k \sum_{j=1}^{M} (S_k^T S_j)^2 < \infty$;*

b). *$\lim_{L \to \infty} B_M(F_M, k) \geq (\beta - 1)\mu$ almost surely when $\beta > 1$, and equality is achieved by a sequence of WBE signature sets.*

Proof: See Appendix A. □

We define $F^{-1}(y) = \inf\{P_0 : F(P_0) > y\}$. Since F is continuous, $F(P_0) \leq y$ if and only if $P_0 \leq F^{-1}(y)$. Then we have the following result on the asymptotic admissibility for the deterministic signature case.

Theorem 3.1 *Suppose all sequences of deterministic signature sets are chosen from $\mathcal{F}$. Then β users per degree of freedom of the processing gain are asymptotically admissible if and only if $\beta \leq \frac{F^{-1}(1-a)}{\gamma \mu} + 1 - \frac{\eta}{\mu}$.*

Proof: Since $\lim_{L \to \infty} \max_k \sum_{j=1}^{M} (S_k^T S_j)^2 < \infty$, we have by Lemma 3.1,

$$\lim_{L \to \infty} (A_M(F_M, k) + B_M(F_M, k)) = \lim_{L \to \infty} B_M(F_M, k).$$

8

By assumption, the received power of every user in the limiting regime has same distribution as P_0. Hence, by Slutsky's Theorem [2, Theorem 5.3.5],

$$SIR_k^{(L)} \xRightarrow{\mathcal{D}} \frac{P_0}{\lim_{L\to\infty} B_M(F_M, k) + \eta}.$$

where the notation $\xRightarrow{\mathcal{D}}$ is used to denote convergence in distribution. Since P_0 is a random variable with a density function, it is easy to get

$$P\left\{\frac{P_0}{\eta + \lim_{L\to\infty} B_M(F_M, k)} = \gamma\right\} = 0.$$

Then, we have by [1, Theorem 2.1],

$$\lim_{L\to\infty} P\{SIR_k^{(L)} \geq \gamma\} = P\left\{\frac{P_0}{\eta + \lim_{L\to\infty} B_M(F_M, k)} \geq \gamma\right\}. \tag{5}$$

Let $F_M^* = \{S_1^*, \ldots, S_M^*\}$ and k_M^* denote a signature set and a corresponding index under which (4) achieves the max-min point, that is,

$$\max_{\{S_1,\ldots,S_M\}} \min_k P\{SIR_k^{(L)} \geq \gamma\} = P\{SIR_{k_M^*}^{(L)} \geq \gamma\},$$

where F_M^* is implicitly employed for the right side.

Observe that the sequence of the signature sets $\{F_M^*\}$ also satisfies the condition in (3), that is,

$$\lim_{L\to\infty} \sup_{j\neq k} ((S_k^*)^T S_j^*)^2 \log L = 0.$$

Clearly, $\lim_{L\to\infty} \max_k \sum_{j=1}^M ((S_k^*)^T S_j^*)^2 < \infty$. Based on (5), we apply Lemma 3.1 and get

$$\begin{aligned}
\lim_{L\to\infty} \max_{\{S_1,\ldots,S_M\}} \min_k P\{SIR_k^{(L)} \geq \gamma\} &= P\left\{\frac{P_0}{\eta + \lim_{L\to\infty} B_M(F_M^*, k_M^*)} \geq \gamma\right\} \\
&\leq P\{P_0 \geq \gamma((\beta-1)\mu + \eta)\}. \tag{6}
\end{aligned}$$

It suffices for $\{F_M^*\}$ to be optimal if it achieves the equality in (6). By Lemma 3.1, the equality in (6) holds if $\{F_M^*\}$ is a sequence of WBE signature sets in $\mathcal{F}$. Therefore, under the choice of a sequence of WBE signature sets $\{F_M\}$ in $\mathcal{F}$, we have

$$SIR_k^{(L)} \xRightarrow{\mathcal{D}} \frac{P_0}{\eta + (\beta-1)\mu} \qquad \text{as } L \to \infty.$$

Since P_0 has a density function, we obtain $P\{P_0 = \gamma[(\beta-1)\mu + \eta]\} = 0$. We get by applying [1, Theorem 2.1] again,

$$\begin{aligned}
\lim_{L\to\infty} P\{SIR_k^{(L)} \geq \gamma\} &= P\left\{\lim_{L\to\infty} SIR_k^{(L)} \geq \gamma\right\} \\
&= P\{P_0 \geq \gamma((\beta-1)\mu + \eta)\}. \tag{7}
\end{aligned}$$

9

Hence we have

$$\lim_{L\to\infty} P\{SIR_k^{(L)} \geq \gamma\} \geq a \quad \Leftrightarrow \quad P\{P_0 \geq \gamma((\beta-1)\mu+\eta)\} \geq a$$

$$\Leftrightarrow \quad \beta \leq \frac{F^{-1}(1-a)}{\gamma\mu} + 1 - \frac{\eta}{\mu}. \tag{8}$$

That is, if β users per degree of freedom of the processing gain are asymptotically admissible, then $\beta \leq \frac{F^{-1}(1-a)}{\gamma\mu} + 1 - \frac{\eta}{\mu}$. On the other hand, for any $\beta \leq \frac{F^{-1}(1-a)}{\gamma\mu} + 1 - \frac{\eta}{\mu}$, we can always choose a sequence of WBE signature sets to make it asymptotically admissible. This completes the proof. □

Theorem 3.1 illustrates the fact that the asymptotically admissible region is $\beta \leq \frac{F^{-1}(1-a)}{\gamma\mu} + 1 - \frac{\eta}{\mu}$. Following the line of reasoning in [23], we can call $\frac{F^{-1}(1-a)}{\gamma\mu} + 1 - \frac{\eta}{\mu}$ the *network capacity in the limiting regime* (to be distinguishable from the concept "asymptotic network capacity" which is introduced below) for the given distribution of the received powers.

In practical CDMA systems, the processing gain is finite and large. For example, IS-95 utilizes a bandwidth of slightly less than 1.25 MHz and the processing gain equals 128. For third generation CDMA systems, it has been proposed to use a bandwidth of 5 MHz to offer high quality voice and medium rate data. It is reasonable to expect much larger processing gains for third generation CDMA systems. Therefore, one basic question to ask is "How many users are admissible for large (but finite) processing gains while the users' QoS requirements are fixed?" Based only on Theorem 3.1, however, we cannot answer this interesting question. (The subtlety will be more clear in the next section.) This motivates us to develop another approach that studies a sequence of network capacity indexed by the processing gain L. We elaborate on this idea in detail in the following section.

3.1.2 Asymptotic Network Capacity

We let C_L denote the set of all the admissible points when the processing gain is L, that is,

$$C_L = \left\{ \beta \,\middle|\, \max_{\{S_1,\ldots,S_M\}} \min_k P\{SIR_k^{(L)} \geq \gamma\} \geq a \right\}.$$

Of particular interest is the maximum number of users admissible by the system, which is defined to be the *network capacity* in terms of the number of users per degree of freedom of the processing gain. That is, the network capacity is the maximum number of users (per degree of freedom of the processing gain) that are admissible in the system, and depends on

10

a. Therefore, when the processing gain is L, we can define *network capacity* as follows:

$$\beta_L(a) = \sup C_L = \sup \left\{ \beta \; \middle| \; \max_{\{S_1,\dots,S_M\}} \min_k P\{SIR_k^{(L)} \geq \gamma\} \geq a \right\}. \qquad (9)$$

The *asymptotic network capacity* $\beta_\infty(a)$ is defined as the limit of $\beta_L(a)$ when $L \to \infty$, that is, $\beta_\infty(a) = \lim_{L\to\infty} \beta_L(a)$. Note that the network capacity in the limiting regime and the asymptotic network capacity are different in principle (compare the two definitions). A priori, we do not know if they lead to the same expression or not. (It is worth pointing out that our approach for asymptotic network capacity is independent from Theorem 3.1 and self-contained. It could have been presented before the section on asymptotic admissibility.)

We aim to identify the asymptotic network capacity. For technical reasons, we assume the received powers in the limiting regime have a connected support, which implies that the distribution function F is strictly increasing over its support. We have the following lemma.

Lemma 3.2 *Suppose $f_n : \mathbb{R} \to [0,1]$, $n = 1, 2, \dots$, are continuous and non-increasing. Assume the sequence $\{f_n\}$ converges point-wise to f which is continuous and strictly decreasing. Define $\alpha_n(a) = \sup\{x \, | \, f_n(x) \geq a\}$. Then we have $\lim_{n\to\infty} \alpha_n(a) = f^{-1}(a)$, where f^{-1} is the inverse mapping of f.*

Proof: See Appendix A. □

Based on Lemma 3.1 and Lemma 3.2, we have the following result on the asymptotic network capacity for the deterministic signature case.

Theorem 3.2 *Suppose all sequences of deterministic signature sets are chosen from $\mathcal{F}$. Then the asymptotic network capacity is $\beta_\infty(a) = \frac{F^{-1}(1-a)}{\gamma\mu} + 1 - \frac{\eta}{\mu}$, which can be achieved through a sequence of WBE signature sets in $\mathcal{F}$.*

Proof: First we show $\beta_\infty(a)$ is upper bounded by $\frac{F^{-1}(1-a)}{\gamma\mu} + 1 - \frac{\eta}{\mu}$.

By Lemma 3.1 we have $\lim_{L\to\infty} A_M(F_M, k) = 0$ almost surely. Fix $\delta > 0$. By Egoroff's Theorem in [18], there exists a measurable set A such that $P(A) < \delta$ and $A_M(F_M, k)$ converges to 0 uniformly on $\bar{A} = \Omega \backslash A$. Therefore, fixing $\epsilon > 0$, there exists an integer L_0 such that for all $L \geq L_0$, the quantity $|A_M(F_M, k)|$ is less than or equal to ϵ for every point in $\bar{A}$.

Moreover, for any sequence $\{F_M\}$, we have by (2),

$$\{SIR_k^{(L)} \geq \gamma\} = \left\{ P_k^{(L)} \geq \gamma \left[\eta + B_M(F_M, k) + A_M(F_M, k) \right] \right\}.$$

11

Thus, for all $L \geq L_0$,

$$
\begin{aligned}
P\{SIR_k^{(L)} \geq \gamma\} &= P\{(SIR_k^{(L)} \geq \gamma) \cap A\} + P\{(SIR_k^{(L)} \geq \gamma) \cap \bar{A}\} \\
&\leq \delta + P\{(P_k^{(L)} \geq \gamma [\eta + B_M(F_M, k) + A_M(F_M, k)]) \cap \bar{A}\} \\
&\leq \delta + \overline{F_L}(\gamma(\eta + B_M(F_M, k) - \epsilon)), \quad\quad (10)
\end{aligned}
$$

where $\overline{F_L}(x) = 1 - F_L(x)$. The function $\overline{F_L}(\cdot)$ is non-increasing and continuous since $F_L(\cdot)$ is a cumulative distribution function with a density function.

Define $\alpha_L(a) = \sup\{x | \overline{F_L}(x) \geq a\}$ for any $a \in [0, 1)$. By the definition of network capacity, $P\{SIR_k^{(L)} \geq \gamma\} \geq a$ must be satisfied for all $k = 1, \ldots, M$. Thus we have

$$
\max_k B_M(F_M, k) \leq \frac{\alpha_L(a - \delta)}{\gamma} - \eta + \epsilon.
$$

Combining the above inequality with (38) in appendix A, we have

$$
\beta_L(a) \leq \frac{1}{\mu^{(L)}} \left(\frac{\alpha_L(a - \delta)}{\gamma} - \eta + \epsilon \right) + 1. \quad\quad (11)
$$

Since F_L converges point-wise to F, which is continuous and strictly increasing, $\overline{F_L}$ converges point-wise to $\overline{F}$, which is continuous and strictly decreasing. Then we have by Lemma 3.2,

$$
\lim_{L \to \infty} \alpha_L(a - \delta) = F^{-1}(1 - a + \delta).
$$

Since F is strictly increasing, and both ϵ and δ are arbitrary positive numbers, we conclude

$$
\beta_\infty(a) = \lim_{L \to \infty} \beta_L(a) \leq \frac{F^{-1}(1 - a)}{\gamma \mu} - \frac{\eta}{\mu} + 1.
$$

Next we show that the upper bound is achievable through sequences of WBE signature sets in $\mathcal{F}$.

Under the choice of WBE signature sets, we have $B_M(F_M, k) = (\beta_L - 1)\mu^{(L)}$ for all $k = 1, \ldots, M$, where $\beta_L = \frac{M}{L}$. Then we have for all $L \geq L_0$,

$$
\begin{aligned}
P\{SIR_k^{(L)} \geq \gamma\} &= P\{(SIR_k^{(L)} \geq \gamma) \cap A\} + P\{(SIR_k^{(L)} \geq \gamma) \cap \bar{A}\} \\
&\geq P\{(P_k^{(L)} \geq \gamma [\eta + B_M(F_M, k) + A_M(F_M, k)]) \cap \bar{A}\} \\
&\geq P\{(P_k^{(L)} \geq \gamma [\eta + B_M(F_M, k) + \epsilon]) \cap \bar{A}\} \\
&\geq \overline{F_L}(\gamma(\eta + (\beta_L - 1)\mu^{(L)} + \epsilon)) + P(\bar{A}) - 1 \\
&\geq \overline{F_L}(\gamma(\eta + (\beta_L - 1)\mu^{(L)} + \epsilon)) - \delta. \quad\quad (12)
\end{aligned}
$$

For $L \geq L_0$ and $\beta_L \leq \frac{1}{\mu^{(L)}}(\frac{\alpha_L(a+\delta)}{\gamma} - \eta - \epsilon) + 1$, we have

$$
\gamma[(\beta_L - 1)\mu^{(L)} + \eta + \epsilon] \leq \alpha_L(a + \delta),
$$

12

which implies

$$\overline{F_L}\{\gamma[(\beta_L - 1)\mu^{(L)} + \eta + \epsilon]\} \geq a + \delta.$$

Combining the above inequality with (12), we can get for the chosen β_L,

$$P\{SIR_k^{(L)} \geq \gamma\} \geq a.$$

Hence we have

$$\beta_L(a) \geq \frac{1}{\mu^{(L)}}\left(\frac{\alpha_L(a + \delta)}{\gamma} - \eta - \epsilon\right) + 1.$$

Again we apply Lemma 3.2 and get

$$\beta_\infty(a) = \lim_{L \to \infty} \beta_L(a) \geq \frac{F^{-1}(1 - a)}{\gamma\mu} - \frac{\eta}{\mu} + 1.$$

Hence we have *asymptotic network capacity* $\beta_\infty(a) = \frac{F^{-1}(1-a)}{\gamma\mu} + 1 - \frac{\eta}{\mu}$. This completes the proof. □

We have some final remarks on the above proof. The quantities $\beta_L(a)$ are rational numbers by definition, but $\beta_\infty(a)$ is not necessarily a rational number. In order to get across the main ideas, we neglected this constraint in the proof of the achievability of the asymptotic network capacity. However, since rationals are dense on the real line, this approach does not affect the result on the asymptotic network capacity.

It turns out that for the deterministic signature case, the *network capacity in the limiting regime* and the *asymptotic network capacity*, which are different in principle, lead to the same result under the auxiliary assumption made in this section. Certainly the result on the asymptotic network capacity is stronger than that of the network capacity in the limiting regime. Roughly speaking, by exploiting Theorem 3.2, we can conclude that for a given $\epsilon > 0$, $\beta_\infty(a) - \epsilon$ users per degree of freedom of the processing gain are admissible in the system for very large L (i.e., $L \geq L_0(\epsilon)$ for some $L_0(\epsilon)$).

Worth noting is that sequences of WBE signature sets in $\mathcal{F}$ play a very important role for both the asymptotic admissibility and asymptotic network capacity. A heuristic interpretation is that the choice of WBE signature sets is asymptotically optimal in the sense of suppressing the interference of all the users simultaneously. Another interesting observation is that the asymptotic network capacity $\beta_\infty(a)$ goes to 1 when γ increases even in the high signal-to-noise ratio region (when the background noise power η goes to 0). In this case, the optimum choice of signature set is orthogonal signaling.

WBE signature sets have great potential in spread spectrum systems (see, e.g. [15, 19]). Massey and Mittelholzer pointed out [15] that WBE signature sets enjoy an interesting

"uniformly good" property that the variance of the interuser interference experienced by a user is the same for all users under equal received power (normalized to 1) in a synchronous CDMA system. Rupf and Massey showed [19] that the sum capacity of a synchronous CDMA channel with equal average-input-energy constraints is maximized under the choice of WBE signature sets.

In [29], Welch found that a lower bound for the square of the maximum cross-correlation of the signature set $\{S_1, \cdots, S_M\}$ is $\frac{1}{M-1}(\frac{M}{L} - 1)$. It is trivial to show the condition in (3) is satisfied by sequences of signature sets that achieve this lower bound. In Appendix B we give two examples of sequences of WBE signature sets by exploiting some known results on Hamming codes and BCH codes. These sequences of WBE signature sets satisfy the condition given in (3) quite well.

3.2   The Random Signature Case

In this case users choose signatures randomly and independently, which models the situation where the information symbols are spread onto pseudo-random spreading sequences [23, 26]. When the processing gain is L, the model for random signatures is as follows: $S_k = \frac{1}{\sqrt{L}}(W_{k1}, \ldots, W_{kL})^T$, where the W_{ki}'s are i.i.d. with $P\{W_{ki} = 1\} = P\{W_{ki} = -1\} = \frac{1}{2}$ for $i = 1, \ldots, L$ and $k = 1, \ldots, M$.

Since the $P_k^{(L)}$'s are i.i.d., and the W_{ki}'s are i.i.d., the received SIRs are also identically distributed. Hence, $P\{SIR_k^{(L)} \geq \gamma\}$ does not depend on k, and we can study user 1 without loss of generality.

3.2.1   Asymptotic Admissibility

Assume that the signature for a user is known to the receiver for it. Given the distribution of the received powers, we define admissibility for a class of users with random signatures as follows: when the processing gain is L, β users per degree of freedom of the processing gain are *admissible* in the system if

$$P\{SIR_1^{(L)} \geq \gamma\} \geq a.$$

We say β users per degree of freedom of the processing gain are *asymptotically admissible* if the following condition holds:

$$\lim_{L \to \infty} P\{SIR_1^{(L)} \geq \gamma\} \geq a.$$

First we define $A_M = \frac{1}{M} \sum_{i=2}^{M} (P_i^{(L)} - \mu^{(L)})\xi_i^2$ and $B_M = \frac{1}{M} \sum_{i=2}^{M} \xi_i^2 \mu^{(L)}$, where $\xi_i =$

$\frac{1}{\sqrt{L}} \sum_{k=1}^{L} W_{1k} W_{ik}$. We can get by (2)

$$SIR_1^{(L)} = \frac{P_1^{(L)}}{\eta + \sum_{i=2}^{M} P_i^{(L)} (S_1^T S_i)^2}$$
$$= \frac{P_1}{\eta + \beta B_M + A_M}. \tag{13}$$

We have the following lemma on the limits of A_M and B_M.

Lemma 3.3 *When the processing gain L goes to infinity, A_M converges to 0 and B_M converges to μ almost surely.*

Proof: See Appendix A. $\qquad\qquad\qquad\qquad\qquad\qquad\qquad\qquad\qquad\qquad$ $\square$

Based on Lemma 3.3, we have the following result on the asymptotic admissibility for the random signature case. (Lemma 3.3 will be used in the proofs of Theorem 3.3 and Theorem 3.4. Alternatively, Theorem 3.3 can also be proved by applying [23, Proposition 3.3], but the proof would be more involved.)

Theorem 3.3 *Suppose users choose signatures randomly and independently. Then β users (per degree of freedom of the processing gain) are asymptotically admissible if and only if $\beta \leq \frac{F^{-1}(1-a)}{\gamma\mu} - \frac{\eta}{\mu}$.*

Proof: By Lemma 3.3 we have

$$SIR_1^{(L)} \overset{\mathcal{D}}{\Longrightarrow} \frac{P_0}{\eta + \beta\mu} \qquad \text{as } L \to \infty. \tag{14}$$

Since P_0 is a random variable with a density function, we have

$$P\{P_0 = \gamma(\eta + \beta\mu)\} = 0.$$

By applying [1, Theorem 2.1] again, we get

$$\lim_{L\to\infty} P\{SIR_1^{(L)} \geq \gamma\} = P\left\{\lim_{L\to\infty} SIR_1^{(L)} \geq \gamma\right\}$$
$$= P\{P_0 \geq \gamma(\beta\mu + \eta)\}.$$

Thus we have

$$\lim_{L\to\infty} P\{SIR_1^{(L)} \geq \gamma\} \geq a \quad \Leftrightarrow \quad P\{P_0 \geq \gamma(\beta\mu + \eta)\} \geq a$$
$$\Leftrightarrow \quad F(\gamma(\beta\mu + \eta)) \leq 1 - a$$
$$\Leftrightarrow \quad \beta \leq \frac{F^{-1}(1 - a)}{\gamma\mu} - \frac{\eta}{\mu}. \tag{15}$$

$\qquad\qquad\qquad\qquad\qquad\qquad\qquad\qquad\qquad\qquad\qquad\qquad\qquad\qquad\qquad\qquad\qquad$ $\square$

We call $\frac{F^{-1}(1-a)}{\gamma\mu} - \frac{\eta}{\mu}$ the *network capacity in the limiting regime* for the given distribution of the received powers.

3.2.2 Asymptotic Network Capacity

Similar to the deterministic signature case, the *network capacity* is defined as the maximum number of users (per degree of freedom of the processing gain) that are admissible in the system, and depends on a. Thus, when the processing gain is L, we can define network capacity as follows:

$$\beta_L(a) = \sup \left\{ \beta \,\Big|\, P\{SIR_1^{(L)} \geq \gamma\} \geq a \right\}.$$

We define *asymptotic network capacity* $\beta_\infty(a)$ as the limit of $\beta_L(a)$ when $L \to \infty$, that is, $\beta_\infty(a) = \lim_{L\to\infty} \beta_L(a)$.

Again, for technical reasons, we assume the received powers in the limiting regime have a connected support and hence F is strictly increasing over its support. Based on Lemma 3.3, we have the following result on the asymptotic network capacity for the random signature case.

Theorem 3.4 *Suppose users choose their signatures randomly and independently. Then the asymptotic network capacity is* $\beta_\infty(a) = \frac{F^{-1}(1-a)}{\gamma\mu} - \frac{\eta}{\mu}$.

Proof: By Lemma 3.3, $\lim_{L\to\infty} A_M = 0$ and $\lim_{L\to\infty} B_M = \mu$ with probability one. Fix $\delta > 0$. By Egoroff's Theorem in [18], there exists a measurable set A_1 such that $P(A_1) < \frac{\delta}{2}$ and $|A_M|$ converges to 0 uniformly on $\bar{A}_1 = \Omega \backslash A_1$; there exists a measurable set A_2 such that $P(A_2) < \frac{\delta}{2}$ and B_M converges to μ uniformly on $\bar{A}_2 = \Omega \backslash A_2$.

Let $A = A_1 \bigcup A_2$ and $\bar{A} = \Omega \backslash A$. Then for fixed $\epsilon > 0$, there exists an integer L_0 such that for all $L \geq L_0$, the quantity $|A_M|$ is less than or equal to ϵ for every point in $\bar{A}$; there exists an integer L_1 such that for for all $L \geq L_1$, $\mu - \frac{\epsilon}{\beta} \leq B_M \leq \mu + \frac{\epsilon}{\beta}$ for every point in $\bar{A}$.

Let $L_2 = \max(L_0, L_1)$. Then we have all $L \geq L_2$,

$$
\begin{aligned}
P\{SIR_k^{(L)} \geq \gamma\} &= P\{(SIR_k^{(L)} \geq \gamma) \cap A\} + P\{(SIR_k^{(L)} \geq \gamma) \cap \bar{A}\} \\
&\leq \delta + P\{(P_k^{(L)} \geq \gamma\,[\eta + B_M(F_M, k) + A_M(F_M, k)]) \cap \bar{A}\} \\
&\leq \delta + \overline{F_L}\{\gamma[\eta + \beta\mu^{(L)} - 2\epsilon]\},
\end{aligned}
\tag{16}
$$

and

$$
\begin{aligned}
P\{SIR_k^{(L)} \geq \gamma\} &\geq P\{(P_k^{(L)} \geq \gamma\,[\eta + B_M(F_M, k) + A_M(F_M, k)]) \cap \bar{A}\} \\
&\geq \overline{F_L}\{\gamma[\eta + \beta\mu^{(L)} + 2\epsilon]\} + P(\bar{A}) - 1 \\
&\geq \overline{F_L}\{\gamma[\eta + \beta\mu^{(L)} + 2\epsilon]\} - \delta.
\end{aligned}
\tag{17}
$$

16

Using (16), we have by definition of *network capacity*,

$$\beta_L(a) \le \frac{1}{\mu^{(L)}} \left(\frac{\alpha_L(a - \delta)}{\gamma} - \eta + 2\epsilon \right).$$

We apply Lemma 3.2 and get

$$\beta_\infty(a) = \lim_{L \to \infty} \beta_L(a) \le \frac{F^{-1}(1 - a + \delta)}{\gamma\mu} - \frac{\eta}{\mu} + \frac{2\epsilon}{\mu}.$$

Observing that both δ and ϵ are arbitrary , we have

$$\beta_\infty(a) \le \frac{F^{-1}(1 - a)}{\gamma\mu} - \frac{\eta}{\mu}.$$

Similarly by using (17) we can show for $L \ge L_2$,

$$\beta_L(a) \ge \frac{\alpha_L(a + \delta)}{\gamma\mu} - \frac{\eta}{\mu} - \frac{2\epsilon}{\mu}.$$

Hence we can draw the conclusion that

$$\beta_\infty(a) \ge \frac{F^{-1}(1 - a)}{\gamma\mu} - \frac{\eta}{\mu}.$$

Thus $\beta_\infty(a) = \frac{F^{-1}(1-a)}{\gamma\mu} - \frac{\eta}{\mu}$. $\qquad\qquad\qquad\qquad\qquad\qquad\qquad\Box$

It turns out that for the random signature case, the *network capacity in the limiting regime* and the *asymptotic network capacity*, which are different in principle, also lead to the same result under the auxiliary assumption made in this section. Moreover, we observe that the asymptotic network capacity for the random signature case $\beta_\infty(a)$ goes to 0 as γ goes to ∞ even in the high signal-to-noise ratio region (when the background noise power η goes to 0). Comparing this observation with the one that the asymptotic network capacity $\beta_\infty(a)$ goes to 1 as γ goes to ∞ in the high signal-to-noise ratio region, we conclude that matched filter receivers are not robust to the choice of signature sets.

To get a sense of the results on network capacity, we have the following example. We model that the received powers have a log-normal distribution, and take $P_0 = \bar{T}10^{\frac{\xi}{10}}$, where $\bar{T}$ is some constant and ξ has mean zero and standard deviation σ *db*. Strictly speaking, to be compatible with our assumption on the boundedness of the fluctuation of the received power, we should have modeled the received power with a truncated version of the log-normal distribution. However, the difference is insignificant and results in unnecessary increase of the computation complexity. As shown in Figure 2, a system using optimal deterministic signatures yields precisely one more user per degree of freedom of the processing gain than one with signatures randomly and independently chosen, which is a generalization of the result given in [27] for perfect power control.

17
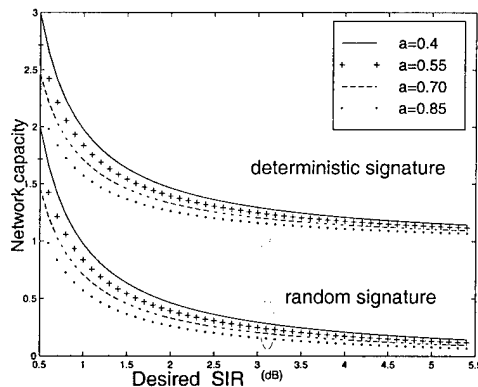
Figure 2: Network capacity as a function of desired SIR

3.3 Power Control and Effective Target SIR

We have studied the admissibility and the network capacity for single class systems assuming known distribution of the received powers. On the other hand, one fundamental question to ask is "How many users (per degree of freedom of processing gain) can be made asymptotically admissible through power control for given QoS requirements?" We study this problem in the high signal-to-noise ratio region (when the background noise power η goes to 0, as in [25]). Loosely speaking, the above problem can be regarded as the dual of the near-far resistance problem for matched filter receivers. On one hand, near-far resistance concerns the worse-case performance; on the other hand, optimum power-controlled capacity concerns the best-case performance.

First we study the deterministic signature case. Define

$$\tilde{\beta}_d = \sup_{F(x)} \lim_{\eta \to 0} \beta_\infty(a).$$

The calculation of $\tilde{\beta}_d$ boils down to finding the supremum of the ratio of $F^{-1}(1-a)$ to μ over all possible distributions of received powers. It is straightforward to get

$$\sup_{F(x)} \frac{F^{-1}(1-a)}{\mu} = \frac{1}{a},$$

and the supremum is achieved by any distribution of the form as shown in Figure 3. Hence, $\tilde{\beta}_d = \frac{1}{a\gamma} + 1$. Therefore, there exists a distribution function F for the received powers such that β users (per degree of freedom) are admissible if and only if $\beta < \tilde{\beta}_d$.

Observe that the optimal power control is in the form of "bang-bang" control. To provide more insight into why the distribution function F given in Figure 3 is optimal in the sense

18
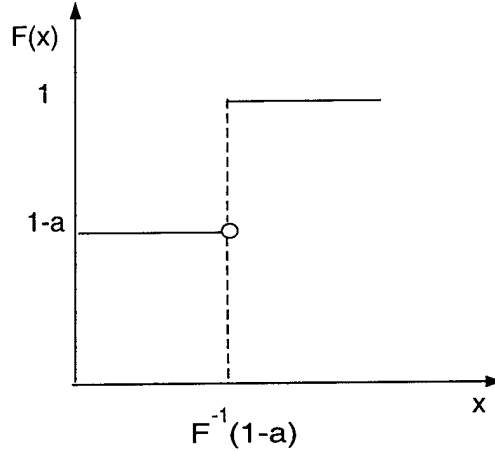
Figure 3: The distribution function that achieves the supremum of $\frac{F^{-1}(1-a)}{\mu}$

of maximizing the capacity, we have the following heuristic and interesting interpretation. Suppose the number of users (per degree of freedom) is less than (and very close to) $\tilde{\beta}_d$. Since a user's QoS requirement is that $P\{SIR^{(L)} \geq \gamma\} \geq a$, we implement power control such that the received SIR of a user is greater than (and very close to) γ with probability a and equals 0 with probability $1-a$. That is, very little power is wasted, which is equivalent to saying that the power control is efficient. When $a < 1$, perfect power control is no longer the best in this context by the above observations. The reason lies in the fact that we loosen the users' QoS requirements. When $a = 1$, the optimum power control strategy is perfect power control, and $\tilde{\beta}_d = \frac{1}{\gamma} + 1$, which agrees with the expression given in [27]. (Let P denote the received power under the perfect power control scheme; we take $F^{-1}(0) = P$.)

For the random signature case, we have

$$\tilde{\beta}_r = \sup_{F(x)} \lim_{\eta \to 0} \beta_\infty(a) = \frac{1}{a\gamma}.$$

When $a = 1$, the optimum power control strategy is perfect power control, and $\tilde{\beta}_d = \frac{1}{\gamma}$, which is as given in [23].

We proceed to look for an abstraction that can combine the information of both QoS requirements and the distributions of received powers for determining the asymptotic admissibility and characterizing network capacity for single class systems. In an imperfect power-controlled system, the actual received powers depend on the fading environments and the performance of the power control algorithms. For example, in a log-normal fading channel, it is reasonable to assume that the received powers would be log-normal distributed with smaller standard deviation if the power control is tight and with larger standard deviation

19
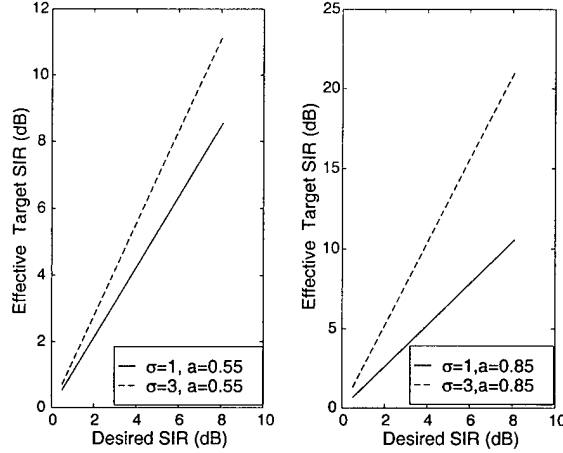
Figure 4: Effective target SIR as a function of desired SIR

if not (see [28]).

Note that if β users are not asymptotically admissible for a given received power distribution, it may still be possible to make β asymptotically admissible by scaling up the received power. Referring to the definition of *scale family* in [2, p. 118], we consider the scale family $\mathcal{G} = \{F(\frac{p_0}{c}), c > 0\}$, where F is the distribution function of P_0. Define $\gamma' = \gamma c_e$, where $c_e = \frac{\mu}{F^{-1}(1-a)}$. Clearly, c_e is fixed for the scale family $\mathcal{G}$. We call γ' the *effective target SIR* for $\mathcal{G}$. For example, we have $\gamma' = a\gamma$ for the scale family of distributions that have the form as shown in Figure 3.

Figure 4 shows some plots of effective target SIR as a function of the desired SIR. For simplicity, again we assume that the received powers have a log-normal distribution, that is, $P_0 = \bar{T}10^{\frac{\xi}{10}}$. Note that ξ is due to the channel gain estimation error (see [11]). Several observations are worth noting. First, channel gain estimation has much impact on the effective target SIR, especially when a is large. The smaller the standard deviation σ of the channel gain estimation error, the smaller the slopes and hence the effective target SIR. On the other hand, it is desirable to reduce the desired SIR for fixed a as much as possible so that we can get a small effective target SIR. Sophisticated techniques of coding and modulation can be exploited to combat fading and increase the error correcting ability and hence reduce the effective target SIR.

Note that in a given scale family of distributions, there exists a one-to-one correspondence between distribution and mean. Given a scale family $\mathcal{G}$ of received power distributions, a basic question to ask is if there exists a finite positive value that can be designated as μ such that β users per degree of freedom of processing gain are asymptotically admissible for

20

the corresponding received power distribution in $\mathcal{G}$. For the deterministic signature case, it is easy to observe from (8) that there exists a finite positive solution for μ if and only if $\beta \frac{\gamma'}{1+\gamma'} < 1$; moreover, the minimum value for μ is

$$\mu = \frac{\eta \frac{\gamma'}{1+\gamma'}}{1 - \beta \frac{\gamma'}{1+\gamma'}}. \tag{18}$$

For the random signature case, it is easy to obtain that there exists a finite positive solution for μ if and only if $\beta\gamma' < 1$; the minimum value for μ is

$$\mu = \frac{\eta\gamma'}{1 - \beta\gamma'}. \tag{19}$$

Note that if β users are asymptotically admissible for some distribution of the received power, then β users are also asymptotically admissible when we scale up the received power by any constant greater than 1. For example, let H denote the distribution function corresponding to the mean given in (18). An easy observation is that β users are asymptotically admissible when we "scale up" H by any constant greater than 1 (i.e., for any distribution function $H'(p_0) = H(p_0/c)$, $c \geq 1$).

4   Multiple Class Systems

We have studied the asymptotic admissibility and identified the asymptotic network capacity for single class systems in the above section. However, future wireless systems will have to support multimedia services such as voice, data, video, and fax. Therefore, it is essential to have a level of generalization dealing with users having different QoS requirements.

Suppose there are a fixed number, say N, of classes. Let A_n denote the set of users in class n and M_n the cardinality of A_n, $n = 1, \ldots, N$. Let S_{in} denote the signature for the ith user in class n. Define $\beta_n = \frac{M_n}{L}$ and let β_n be fixed when L goes to infinity as in the single class case. Let $\vec{\beta} = (\beta_1, \ldots, \beta_N)^T$.

The received SIR for the ith user in class n is

$$SIR_{in}^{(L)} = \frac{P_{in}^{(L)}}{\eta + \sum_{\substack{j \neq n \\ l \in A_j}} P_{lj}^{(L)} (S_{in}^T S_{lj})^2 + \sum_{\substack{l \in A_n \\ l \neq i}} P_{ln}^{(L)} (S_{in}^T S_{ln})^2}, \tag{20}$$

where $P_{in}^{(L)}$ denotes the received powers for $i \in A_n$ and $n = 1, \ldots, N$ when the processing gain is L.

Again our results are asymptotic in nature. For the sake of simplicity, as in the single class case, we let P_n denote a random variable that has the same distribution F_n as the received

powers of users in class n in the limiting regime, and assume that F_n has a density function and mean μ_n. For convenience, we call the collection $\{F_1, \ldots, F_N\}$ a *group of received power distributions*, and $\vec{P} = (\mu_1, \ldots, \mu_N)^T$ the *mean power vector*. Suppose it is required that the users in class n must have received SIR greater than or equal to γ_n with probability no less than $a_n \in [0, 1]$.

4.1 The Deterministic Signature Case

We assume that every chosen sequence of signature sets satisfies (3) and

$$\lim_{L \to \infty} \max_{i \in A_n} \sum_{l \in A_j} (S_{in}^T S_{lj})^2 < \infty \qquad \forall \, n, \, j \in \{1, \ldots, N\}.$$

Following the same line of reasoning as in the proof of Lemma 3.1, we apply Lemma 2.1 and get as $L \to \infty$,

$$
\begin{aligned}
SIR_{in}^{(L)} &= \frac{P_{in}^{(L)}}{\eta + \sum_{\substack{j \neq n \\ l \in A_j}} P_{lj}^{(L)} (S_{in}^T S_{lj})^2 + \sum_{\substack{l \in A_n \\ l \neq i}} P_{ln}^{(L)} (S_{in}^T S_{ln})^2} \\
&\overset{\mathcal{D}}{\Longrightarrow} \frac{P_n}{\eta + \sum_{j \neq n} \mu_j \sum_{l \in A_j} (S_{in}^T S_{lj})^2 + \mu_n \sum_{\substack{l \in A_n \\ l \neq i}} (S_{in}^T S_{ln})^2}.
\end{aligned}
\tag{21}
$$

Let $I_{in} = S_{in}^T D S_{in}$, where $D = \sum_{j=1}^N \sum_{l \in A_j} S_{lj} S_{lj}^T \mu_j$. Then we have

$$SIR_{in}^{(L)} \overset{\mathcal{D}}{\Longrightarrow} \frac{P_n}{\eta + I_{in} - \mu_n} \qquad \text{as } L \to \infty.$$

Similar to the argument in the single class case, it is desirable to design the signature sets such that all users' QoS requirements are satisfied. When $\sum_{n=1}^N \beta_n \leq 1$, orthogonal signature sets will work and each single user transmits data as if it were in a single-user channel. When $\sum_{n=1}^N \beta_n > 1$, however, a simple closed-form solution to the global optimization of the signature sets for this case seems unattainable. Therefore, we study a sufficient condition for the asymptotic admissibility of multiple class systems for this case.

4.1.1 Asymptotic Admissibility

For ease of reference, first we let $F_{M,n}$ denote the signature set of class n when the processing gain is L. Given a group of received power distributions, we say a tuple $(\beta_1, \ldots, \beta_N)$ is asymptotically admissible if the following condition holds:

$$\lim_{L \to \infty} \max_{\cup_n F_{M,n}} \min_{i \in A_n} P\{SIR_{in}^{(L)} \geq \gamma\} \geq a_n, \qquad n = 1, \ldots, N.$$

Assuming perfect power control, Viswanath, Anantharam, and Tse [27] developed an idea of channelizing the system with a finite processing gain and give a sufficient condition on the admissibility for users of multiple classes. Following this line, we have the following suboptimal scheme: a given processing gain L is divided into N parts and $\sum_{n=1}^{N} L_n = L$, where L_n is the degree of freedom assigned to class n. Moreover, we have $\lim_{L \to \infty} \frac{L_n}{L} = \lambda_n$ for $n = 1, \ldots, N$. Note that users in different classes do not interfere with each other under this scheme.

Observe that $I_{in} = S_{in}^{T} D S_{in}$, where D is the same for all the users. This motivates us to minimize the maximum among $\{I_{in}, i \in A_n, n = 1, \ldots, N\}$ over all the possible partitions of the processing gain and all choices of signature sets. Intuitively, we want to suppress the interference as much as possible for all the users simultaneously.

Given a partition of the processing gain, when $\lim_{L \to \infty} \frac{M_n}{L_n} \geq 1$, we have

$$\max_{i \in A_n} I_{in} \geq \frac{\beta_n}{\lambda_n} \mu_n,$$

where the equality holds if and only if the choice of the signature set for class n forms a WBE signature set. Under this choice, the I_{in}'s are the same for all the users in class n. Next we aim to find the optimum partition of the processing gain in the sense of minimizing the maximum among the I_{in}'s, that is, we have the following optimization problem:

$$\min_{\{\lambda_1, \ldots, \lambda_N\}} \max_n \frac{\beta_n}{\lambda_n} \mu_n, \tag{22a}$$

$$\text{subject to} \quad \begin{cases} \sum_{n=1}^{N} \lambda_n = 1, \\ \lambda_n > 0, \quad n = 1, \ldots, N. \end{cases} \tag{22b}$$

Let $b_n = \beta_n \mu_n$ and $\lambda = 1/\sum_{n=1}^{N} b_n$. To solve the above minimax problem, we have the following lemma by using [5, Theorem 2.1, p. 114].

Lemma 4.1 *The vector $(\lambda_1^*, \ldots, \lambda_N^*)$ is a minimax point for (22a) under the constraint given by (22b), where $\lambda_n^* = b_n \lambda$, $n = 1, \ldots, N$. Moreover, we have $\frac{\beta_n}{\lambda_n^*} \mu_n = \sum_{n=1}^{N} \beta_n \mu_n$, $n = 1, \ldots, N$.*

Proof: See Appendix A. □

In a practical spread spectrum system, it is necessary to have $L_n = \lambda_n L$ an integer for each $n \in \{1, \ldots, N\}$. In the asymptotic setting, however, the impact of the difference between L_n and $\lfloor L_n \rfloor$ on the solution to the minimax problem disappears.

Now we are ready to give the following result on the asymptotic admissibility of users of multiple classes for the deterministic signature case.

Theorem 4.1 *A tuple* $(\beta_1, \ldots, \beta_N)$ *is asymptotically admissible if it satisfies the following two conditions:*

$$\max_n \mu_n \leq \sum_{j=1}^{N} \beta_j \mu_j, \tag{23a}$$

$$\sum_{j=1}^{N} \beta_j \mu_j \leq \min_n \left(\frac{F_n^{-1}(1 - a_n)}{\gamma_n} + \mu_n \right) - \eta. \tag{23b}$$

Proof: Given a processing gain L, we partition it into N parts such that $\sum_{n=1}^{N} L_n^* = L$, where $L_n^* = \lambda_n^* L$. Observe that for $n = 1, \ldots, N$,

$$\mu_n \leq \sum_{j=1}^{N} \beta_j \mu_j \quad \Leftrightarrow \quad \frac{b_n}{\sum_{n=1}^{N} b_n} \leq \beta_n$$

$$\Leftrightarrow \quad \lim_{L \to \infty} \frac{L_n^*}{M_n} \leq 1, \tag{24}$$

Hence, under the above partitioning of the processing gain, we can choose a sequence of WBE signature sets in $\mathcal{F}$ for each class as L goes to infinity, and users in different classes do not interfere with each other. Then we have for $i \in A_n$ and $n = 1, \ldots, N$,

$$I_{in} = \frac{\beta_n}{\lambda_n^*} \mu_n = \sum_{n=1}^{N} \beta_n \mu_n,$$

and

$$SIR_{in}^{(L)} \xrightarrow{\mathcal{D}} \frac{P_n}{\eta + \sum_{j=1}^{N} \beta_j \mu_j - \mu_n} \qquad \text{as } L \to \infty.$$

By definition, a tuple $(\beta_1, \ldots, \beta_N)$ is asymptotically admissible if the following inequalities hold:

$$\lim_{L \to \infty} \max_{\cup_n F_{M,n}} \min_{i \in A_n} P\{SIR_{in}^{(L)} \geq \gamma\} \geq a_n \qquad n = 1, \ldots, N.$$

Then it suffices to show $\lim_{L \to \infty} P\{SIR_{in}^{(L)} \geq \gamma\} \geq a_n$ for $i \in A_n$ and $n = 1, \ldots, N$ under the above proposed scheme for designing signature sets. Since P_n has a density function, we have $P\{P_n = \gamma(\eta + \sum_{j=1}^{N} \beta_j \mu_j - \mu_n)\} = 0$. We apply [1, Theorem 2.1] again and get

$$\lim_{L \to \infty} P\{SIR_{in}^{(L)} \geq \gamma\} = P\left\{ \lim_{L \to \infty} SIR_{in}^{(L)} \geq \gamma \right\}$$

$$= P\left\{ P_n \geq \gamma \left(\eta + \sum_{j=1}^{N} \beta_j \mu_j - \mu_n \right) \right\}.$$

Thus, we have for $n = 1, \ldots, N$,

$$\lim_{L \to \infty} P\{SIR_{1n}^{(L)} \geq \gamma\} \geq a_n \quad \Leftrightarrow \quad P\left\{ P_n \geq \gamma \left(\eta + \sum_{j=1}^{N} \beta_j \mu_j - \mu_n \right) \right\} \geq a_n$$

$$\Leftrightarrow \quad \sum_{j=1}^{N} \beta_j \mu_j \leq \frac{F_n^{-1}(1 - a_n)}{\gamma_n} + \mu_n - \eta,$$

which is equivalent to

$$\sum_{j=1}^{N} \beta_j \mu_j \leq \min_n \left(\frac{F_n^{-1}(1 - a_n)}{\gamma_n} + \mu_n \right) - \eta.$$

This completes the proof. $\qquad\qquad\qquad\qquad\qquad\qquad\qquad\qquad\qquad\qquad\qquad\square$

4.1.2 Power Control, Effective Target SIR, and Effective Bandwidth

As in the single class case, we introduce the scale family $\mathcal{G}_n = \{F_n(\frac{p_n}{c}), c > 0\}$ for P_n, where F_n is the distribution function of P_n, $n = 1, \ldots, N$. Define $\gamma_n' = \gamma_n c_{en}$, where $c_{en} = \frac{\mu_n}{F_n^{-1}(1-a_n)}$. As before, c_{en} is fixed for the scale family $\mathcal{G}_n$. We call γ_n' the *effective target SIR* for $\mathcal{G}_n$. For ease of reference, we call the collection $\{\mathcal{G}_1, \ldots, \mathcal{G}_N\}$ a *group of scale families*.

After straightforward manipulations, (23b) can be written as

$$\mu_n \geq \gamma_n' \left[\eta + \sum_{j=1}^{N} \beta_j \mu_j - \mu_n \right] \qquad n = 1, \ldots, N.$$

Let

$$\vec{\Gamma} = (\gamma_1', \ldots, \gamma_N')^T,$$
$$\vec{B} = \left(\frac{1}{1 + \gamma_1'}, \ldots, \frac{1}{1 + \gamma_N'} \right)^T,$$
$$\vec{P}_d = ((1 + \gamma_1')\mu_1, \ldots, (1 + \gamma_N')\mu_N)^T.$$

Using this notation, (23b) further boils down to the following:

$$\vec{P}_d \geq (\vec{\beta} \odot \vec{B})^T \vec{P}_d \vec{\Gamma} + \eta \vec{\Gamma}, \qquad\qquad\qquad (25)$$

where the symbol $\odot$ denotes the operator for Hadamard product, which simply performs the element-wise multiplication of two matrices (see [21]). Note that inequality of vectors is equivalent to component-wise inequalities.

We have the following lemma regarding the feasibility of (25).

25

Lemma 4.2 *There exists a finite positive vector $\vec{P}_d$ satisfying (25) if and only if the following condition holds:*

$$\sum_{n=1}^{N} \beta_n \frac{\gamma_n'}{1 + \gamma_n'} < 1. \tag{26}$$

Moreover, the n-th component of the component-wise minimum mean power vector satisfying (25) is

$$\mu_n = \frac{\eta \frac{\gamma_n'}{1+\gamma_n'}}{1 - \sum_{n=1}^{N} \beta_n \frac{\gamma_n'}{1+\gamma_n}} \qquad n = 1, \ldots, N. \tag{27}$$

Proof: Let $\vec{e}$ denote the surplus vector for (25). Note that $\vec{e}$ is a non-negative vector. Then we have

$$\vec{P}_d = \vec{\Gamma}(\vec{\beta} \odot \vec{B})^T \vec{P}_d + \eta \vec{\Gamma} + \vec{e}. \tag{28}$$

Since $\vec{\Gamma}(\vec{\beta} \odot \vec{B})^T$ is a non-negative irreducible matrix, by [22, Theorem 2.1], a necessary and sufficient condition for the existence of a non-negative nonzero solution x to the equations

$$(I - \vec{\Gamma}(\vec{\beta} \odot \vec{B})^T)x = c$$

for any non-negative nonzero c is that the Perron-Frobenius eigenvalue of $\vec{\Gamma}(\vec{\beta} \odot \vec{B})^T$ is less than 1. Observe that $\vec{\Gamma}(\vec{\beta} \odot \vec{B})^T$ has rank one. Thus, the Perron-Frobenius eigenvalue of $\vec{\Gamma}(\vec{\beta} \odot \vec{B})^T$ is $(\vec{\beta} \odot \vec{B})^T \vec{\Gamma}$ by [22, Theorem 1.1]. Therefore, a sufficient condition for the existence of a non-negative nonzero solution to (28) is

$$(\vec{\beta} \odot \vec{B})^T \vec{\Gamma} < 1,$$

that is,

$$\sum_{n=1}^{N} \frac{\gamma_n'}{1 + \gamma_n'} \beta_n < 1.$$

Furthermore, if there exists a non-negative nonzero solution to (28) for some particular $\eta > 0$ and non-negative $\vec{e}$, then this solution must be positive and $(\vec{\beta} \odot \vec{B})^T \vec{\Gamma}$ must be less than 1 by [22, Theorem 1.6]. Hence the condition $\sum_{n=1}^{N} \beta_n \frac{\gamma_n'}{1+\gamma_n'} < 1$ is necessary for the existence of a positive power vector satisfying (25).

Moreover, we get the solution to (28) as follows:

$$\begin{aligned}
\vec{P}_d &= \left(I - \vec{\Gamma}(\vec{\beta} \odot \vec{B})^T \right)^{-1} (\eta \vec{\Gamma} + \vec{e}) \\
&= \eta \left[\vec{\Gamma} + \frac{\vec{\Gamma}(\vec{\beta} \odot \vec{B})^T \vec{\Gamma}}{1 - (\vec{\beta} \odot \vec{B})^T \vec{\Gamma}} \right] + \left(I - \vec{\Gamma}(\vec{\beta} \odot \vec{B})^T \right)^{-1} \vec{e} \\
&= \frac{\eta}{1 - (\vec{\beta} \odot \vec{B})^T \vec{\Gamma}} \vec{\Gamma} + \left(I - \vec{\Gamma}(\vec{\beta} \odot \vec{B})^T \right)^{-1} \vec{e},
\end{aligned}$$

26

where we used the following matrix inverse formula in the first step (see [3, Lemma 12.2]):

$$\left(I - \vec{\Gamma}(\vec{\beta} \odot \vec{B})^T\right)^{-1} = I + \frac{\vec{\Gamma}(\vec{\beta} \odot \vec{B})^T}{1 - (\vec{\beta} \odot \vec{B})^T\vec{\Gamma}}.$$

Under the condition $\sum_{n=1}^{N} \frac{\gamma_n'}{1+\gamma_n'}\beta_n < 1$, we have that $\left(I - \vec{\Gamma}(\vec{\beta} \odot \vec{B})^T\right)^{-1}$ is a positive matrix by [22, Corollary 1, p.31]. Hence the solution in (28) when $\vec{e}$ is set to $\vec{0}$ is the component-wise minimum $\vec{P}_d$. Recalling the relationship between $\vec{P}_d$ and the mean power vector, we find that the n-th component of the component-wise minimum mean power vector is therefore

$$\mu_n = \frac{\eta\frac{\gamma_n'}{1+\gamma_n'}}{1 - \sum_{n=1}^{N} \beta_n\frac{\gamma_n'}{1+\gamma_n}}.$$

$\square$

It is surprising that the necessary and sufficient condition in Lemma 4.2 for the existence of a finite positive solution to (25) is the same as that for the existence of a finite positive solution to the system of equations obtained by setting all inequalities in (25) to equalities. More specifically, the set of positive vectors satisfying (25) is the same as the set of positive vectors satisfying the system of equations

$$\vec{P}_d = (\vec{\beta} \odot \vec{B})^T\vec{P}_d\vec{\Gamma} + \eta\vec{\Gamma}$$

(replacing the inequality in (25) by equality). This remarkable fact is due to [22, Theorem 2.1] and a strong result called "The Subinvariance Theorem" [22, Theorem 1.6].

Observe that in a given group of scale families, there exists a one-to-one correspondence between the mean power vector and the group of received power distributions. Based on Theorem 4.1 and Lemma 4.2, we have the following result for a given group of scale families $\{\mathcal{G}_1, \ldots, \mathcal{G}_N\}$.

Proposition 4.1 *There exists a finite positive vector that can be assigned as the mean power vector for a tuple $(\beta_1, \ldots, \beta_N)$ to be asymptotically admissible for the corresponding group of received power distributions in $\{\mathcal{G}_1, \ldots, \mathcal{G}_N\}$ if*

$$\frac{\gamma_n'}{1+\gamma_n'} \leq \sum_{n=1}^{N} \beta_n\frac{\gamma_n'}{1+\gamma_n'},$$

and

$$\sum_{n=1}^{N} \beta_n\frac{\gamma_n'}{1+\gamma_n'} < 1.$$

27

Proof: We substitute (27) into (23a) and get for all $n = 1, \ldots, N$,

$$\mu_n \leq \sum_{n=1}^{N} \beta_n \mu_n$$

$$\Leftrightarrow \quad \frac{\eta \frac{\gamma_n'}{1+\gamma_n'}}{1 - \sum_{n=1}^{N} \beta_n \frac{\gamma_n'}{1+\gamma_n}} \leq \frac{\eta \sum_{n=1}^{N} \beta_n \frac{\gamma_n'}{1+\gamma_n}}{1 - \sum_{n=1}^{N} \beta_n \frac{\gamma_n'}{1+\gamma_n}}$$

$$\Leftrightarrow \quad \frac{\gamma_n'}{1 + \gamma_n'} \leq \sum_{n=1}^{N} \beta_n \frac{\gamma_n'}{1 + \gamma_n'}. \tag{29}$$

If the two conditions specified in Proposition 4.1 are satisfied, then by applying Theorem 4.1 and Lemma 4.2, the tuple $(\beta_1, \ldots, \beta_N)$ is asymptotically admissible if the power vector with n-th component given in (27) is designated as the mean power vector. □

Let $\{F_1, \ldots, F_N\}$ denote the group of received power distributions corresponding to the mean power vector given in (27). As in the single class case, it is easily observed that $(\beta_1, \ldots, \beta_N)$ is still asymptotically admissible when we "scale up" $\{F_1, \ldots, F_N\}$ uniformly by any constant greater than 1.

Observing the conditions given in Proposition 4.1, we are motivated to extend the insightful idea in [23] and define the *effective bandwidth* of class n for the deterministic signature case as $\mathcal{E}(\gamma_n) = \frac{\gamma_n'}{1+\gamma_n'}$ degrees of freedom per user. However, we are able to give only a sufficient condition for asymptotic admissibility of a tuple $(\beta_1, \ldots, \beta_N)$ in terms of effective bandwidth. Further work is needed for this case.

It is easily observed that the smaller the effective target SIR, the smaller the effective bandwidth. Under the optimum power control stated in the single class case, $\gamma_n' = a_n \gamma_n$, $n = 1, \ldots, N$. Therefore, the conditions given in Proposition 4.1 become the following:

$$\frac{a_n \gamma_n}{1 + a_n \gamma_n} \leq \sum_{n=1}^{N} \beta_n \frac{a_n \gamma_n}{1 + a_n \gamma_n},$$

and

$$\sum_{n=1}^{N} \beta_n \frac{a_n \gamma_n}{1 + a_n \gamma_n} < 1.$$

4.2 The Random Signature Case

Similar to the approach in the single class systems with random signatures, we apply Lemma 2.1 and get,

$$SIR_{in}^{(L)} \overset{\mathcal{D}}{\Longrightarrow} \frac{P_n}{\eta + \sum_{n=1}^{N} \beta_n \mu_n} \qquad \text{as } L \to \infty. \tag{30}$$

We can study the first user in class n without loss of generality.

4.2.1 Asymptotic Admissibility

Given a group of received power distributions, we say a tuple $(\beta_1, \ldots, \beta_N)$ is asymptotically admissible if the following condition holds:

$$\lim_{L \to \infty} P\{SIR_{1n}^{(L)} \geq \gamma\} \geq a_n \qquad n = 1, \ldots, N.$$

We have the following result on the asymptotic admissibility of users of multiple classes for the random signature case.

Theorem 4.2 *Suppose users choose their signatures randomly and independently. A tuple* $(\beta_1, \ldots, \beta_N)$ *is asymptotically admissible if and only if*

$$\sum_{n=1}^{N} \beta_n \mu_n \leq \min_n \left(\frac{F_n^{-1}(1 - a_n)}{\gamma_n} \right) - \eta. \tag{31}$$

Proof: Since P_n has a density function, we conclude by applying [1, Theorem 2.1] that

$$\lim_{L \to \infty} P\{SIR_{1n}^{(L)} \geq \gamma\} = P\left\{ \lim_{L \to \infty} SIR_{1n}^{(L)} \geq \gamma \right\}$$
$$= P\left\{ \frac{P_n}{\eta + \sum_{n=1}^{N} \beta_n \mu_n} \geq \gamma \right\}.$$

By definition, a tuple $(\beta_1, \ldots, \beta_N)$ is asymptotically admissible if and only if for $n = 1, \ldots, N$,

$$\lim_{L \to \infty} P\{SIR_{1n}^{(L)} \geq \gamma\} \geq a_n.$$

Thus we have for $n = 1, \ldots, N$,

$$\lim_{L \to \infty} P\{SIR_{1n}^{(L)} \geq \gamma\} \geq a_n \quad \Leftrightarrow \quad P\left\{ P_n \geq \gamma \left(\eta + \sum_{n=1}^{N} \beta_n \mu_n \right) \right\} \geq a_n$$
$$\Leftrightarrow \quad \sum_{n=1}^{N} \beta_n \mu_n \leq \frac{F_n^{-1}(1 - a_n)}{\gamma_n} - \eta,$$

which is equivalent to

$$\sum_{n=1}^{N} \beta_n \mu_n \leq \min_n \left(\frac{F_n^{-1}(1 - a_n)}{\gamma_n} \right) - \eta.$$

The proof is complete. $\qquad\qquad\qquad\qquad\qquad\qquad\qquad\qquad\qquad\quad \square$

4.2.2 Power Control, Effective Target SIR, and Effective Bandwidth

Again we define $\gamma'_n = \gamma_n c_{en}$, where $c_{en} = \frac{\mu_n}{F_n^{-1}(1-a_n)}$ is fixed for the scale family $\mathcal{G}_n$, $n = 1, \ldots, N$. Then, using similar manipulations as in the deterministic signature case, (31) can be simplified to

$$\vec{P} \geq \vec{\beta}^T \vec{P} \vec{\Gamma} + \eta \vec{\Gamma}. \tag{32}$$

We have the following lemma regarding the feasibility of (32).

Lemma 4.3 *There exists a finite positive vector $\vec{P}$ satisfying (32) if and only if the following condition holds:*

$$\sum_{n=1}^{N} \beta_n \gamma'_n < 1. \tag{33}$$

Moreover, the n-th component of the component-wise minimum mean power vector satisfying (32) is

$$\mu_n = \frac{\eta \gamma'_n}{1 - \sum_{n=1}^{N} \beta_n \gamma'_n}, \qquad n = 1, \ldots, N. \tag{34}$$

Proof: Similar to the proof of Lemma 4.2, we rearrange the terms in (32) and let $\vec{e} \geq 0$ denote the surplus vector for (32), i.e.,

$$\vec{P} = \vec{\Gamma} \vec{\beta}^T \vec{P} + \eta \vec{\Gamma} + \vec{e}. \tag{35}$$

The Perron-Frobenius eigenvalue of $\vec{\Gamma} \vec{\beta}^T$ is $\vec{\beta}^T \vec{\Gamma}$. By [22, Theorem 2.1], a sufficient condition for the existence of non-negative nonzero solution to (35) is that $\sum_{n=1}^{N} \gamma'_n \beta_n < 1$. On the other hand, the condition $\sum_{n=1}^{N} \beta_n \gamma'_n < 1$ is also necessary for the existence of a positive power vector satisfying (32) by [22, Theorem 1.6].

Furthermore, the solution to (35) is

$$\begin{aligned} \vec{P} &= \left(I - \vec{\Gamma} \vec{\beta}^T \right)^{-1} (\eta \vec{\Gamma} + \vec{e}) \\ &= \frac{\eta}{1 - \vec{\beta}^T \vec{\Gamma}} \vec{\Gamma} + (I - \vec{\Gamma} \vec{\beta}^T)^{-1} \vec{e}. \end{aligned} \tag{36}$$

Under the condition $\sum_{n=1}^{N} \gamma'_n \beta_n < 1$, we have that $(I - \vec{\Gamma} \vec{\beta}^T)^{-1}$ is a positive matrix by [22, Corollary. 2.1, p.31]. Therefore, the solution in (36) when $\vec{e}$ is set to $\vec{0}$ is the component-wise minimum mean power vector, that is, the component-wise minimum mean power vector is achieved when all the N inequalities in (32) are satisfied as equalities. The n-th component of this component-wise minimum mean power vector is

$$\mu_n = \frac{\eta \gamma'_n}{1 - \sum_{n=1}^{N} \beta_n \gamma'_n}.$$

$\square$

Based on Lemma 4.3, we can easily obtain the following result for a given group of scale families $\{\mathcal{G}_1, \ldots, \mathcal{G}_N\}$.

Proposition 4.2 *a). There exists a finite positive vector that can be assigned as the mean power vector for a tuple $(\beta_1, \ldots, \beta_N)$ to be asymptotically admissible for the corresponding group of received power distributions in $\{\mathcal{G}_1, \ldots, \mathcal{G}_N\}$ if and only if*

$$\sum_{n=1}^{N} \beta_n \gamma_n' < 1.$$

Moreover, the n-th component of the component-wise minimum mean power vector is

$$\mu_n = \frac{\eta \gamma_n'}{1 - \sum_{n=1}^{N} \beta_n \gamma_n'}, \qquad n = 1, \ldots, N.$$

b). If class n users have an average power constraint that $\mu_n \leq \bar{P}_n$, $n = 1, \ldots, N$, then there exists a finite positive vector that can be assigned as the mean power vector for a tuple $(\beta_1, \ldots, \beta_N)$ to be asymptotically admissible for the corresponding group of received power distributions in $\{\mathcal{G}_1, \ldots, \mathcal{G}_N\}$ if and only if

$$\sum_{n=1}^{N} \beta_n \gamma_n' \leq \min_n \left(1 - \frac{\eta \gamma_n'}{\bar{P}_n} \right).$$

Proof: Part (a) follows by combining the results of Lemma 4.3 and Theorem 4.2.

For part (b), we combine equation (34) with the constraint $\mu_n \leq \bar{P}_n$ to obtain

$$\frac{\eta \gamma_n'}{1 - \sum_{n=1}^{N} \beta_n \gamma_n'} \leq \bar{P}_n, \qquad n = 1, \ldots, N,$$

which is equivalent to

$$\sum_{n=1}^{N} \beta_n \gamma_n' \leq \min_n \left(1 - \frac{\eta \gamma_n'}{\bar{P}_n} \right).$$

The result then follows from Lemma 4.3 and Theorem 4.2. $\qquad\qquad\square$

Proposition 4.2 is a generalization of the result given in [23]. Similar to the deterministic signature case, we define the *effective bandwidth* of class n for the random signature case as $\mathcal{E}(\gamma_n) = \gamma_n'$ degrees of freedom per user. Proposition 4.2 tells us that for a given group of scale families, a tuple $(\beta_1, \ldots, \beta_N)$ can be made asymptotically admissible through power control (without power constraints) if and only if the sum of effective bandwidth of all classes is less than one. Under the optimum power control stated in the single class case, the condition given in (33) boils down to $\sum_{n=1}^{N} \beta_n a_n \gamma_n < 1$.

31

5 Conclusions

We have studied single-cell synchronous CDMA systems with matched filter receivers in fading channels, assuming known distributions of received powers of mobile users. We studied the asymptotic admissibility for both single class systems and multiple class systems. For systems with random signatures, we gave necessary and sufficient conditions on the asymptotic admissibility. For users with deterministic signatures, we gave a necessary and sufficient condition for single class systems, but only a sufficient condition for multiple class systems. Further work is needed for this case.

We have identified the asymptotic network capacity of single class systems for both the deterministic signature case and random signature case. The asymptotic network capacity for single class systems can be uniquely expressed in terms of the users' QoS requirements and the distributions of the received powers. We identified the optimal sequences of signature sets for the deterministic signature case in an asymptotic setting.

We also found the tightest upper bound on the asymptotic network capacity over all possible distributions of received powers, and explored the concepts of effective target SIR and effective bandwidth, which play an important role in determining the asymptotic admissibility and hence the asymptotic network capacity. Our results are useful for network-level resource allocation problems such as admission control and power control in a large network. It is easy to generalize these results to obtain asymptotic network capacity of CDMA systems that employ the techniques of sectorization and voice-activity monitoring (see [6]).

In this work we have focused on finding the network capacity so that we can determine how many users can be accommodated without sacrificing their QoS requirements. On the other hand, another fundamental issue is the *channel capacity*. That is, how much information can be transmitted reliably through fading channels in CDMA systems with linear receivers? Some work along this line is already underway (e.g., [26]). Our own preliminary study shows that there exists a tradeoff between network capacity and channel capacity. Intuitively, the more the users in the systems, the stronger the MAI (multi-access interference) that is imposed by other users, and hence the less the information that can be transmitted reliably over the channel. Currently we are looking into this problem. It will also be interesting to take into account the restriction imposed by real-time traffic, which is delay-limited.

It must also be pointed out that our results are for single-cell synchronous systems, as is the case in [23, 27]. Further work is needed to extend these results to multiple-cell asynchronous systems.

Appendices

A Proofs

A.1 Proof of Lemma 3.1

Proof: Proof for part (a): Let $\rho_{ki}^{(L)} = (S_k^T S_i)^2$. Then $A_M(F_M, k) = \sum_{\substack{i=1 \\ i \neq k}}^{M} (P_i^{(L)} - \mu^{(L)}) \rho_{ki}^{(L)}$. By Lemma 2.1, it suffices to show that $A_M(F_M, k)$ converges to 0 in probability and

$$\sum_{\substack{i=1 \\ i \neq k}}^{M} (P_i^{(L)} - \mu^{(L)})^2 (\rho_{ki}^{(L)})^2 \log L \xrightarrow{a.s.} 0.$$

(Note that $M = \beta L$ and β is fixed.)

By assumption, $|P_i^{(L)} - \mu^{(L)}|$ is bounded by d with probability one, which implies $\text{var}(P_i^{(L)})$ is bounded by d^2. Since the $P_i^{(L)}$'s are i.i.d., and $\lim_{L \to \infty} \max_k \sum_{j=1}^{M} \rho_{ki}^{(L)} < \infty$, we have

$$E(A_M(F_M, k))^2 = \sum_{\substack{i=1 \\ i \neq k}}^{M} (\rho_{ki}^{(L)})^2 \text{var}(P_i^{(L)}) \leq \sup_{\substack{i,k \leq M \\ i \neq k}} \rho_{ki}^{(L)} \sum_{\substack{i=1 \\ i \neq k}}^{M} \rho_{ki}^{(L)} d^2 \to 0,$$

where the last step follows from the fact that $\lim_{L \to \infty} \sup_{\substack{i,k \leq M \\ i \neq k}} \rho_{ki}^{(L)} = 0$. Thus $A_M(F_M, k)$ converges to 0 in probability since mean-square convergence implies convergence in probability.

Note that

$$\sum_{\substack{i=1 \\ i \neq k}}^{M} (P_i^{(L)} - \mu^{(L)})^2 (\rho_{ki}^{(L)})^2 \log L \leq (\sup_{\substack{i,k \leq M \\ i \neq k}} \rho_{ki}^{(L)} \log L) d^2 \sum_{\substack{i=1 \\ i \neq k}}^{M} \rho_{ki}^{(L)} \xrightarrow{a.s.} 0.$$

Hence $\lim_{L \to \infty} A_M(F_M, k) = 0$ almost surely.

Proof for part (b):

By Welch's bound in [15],

$$\sum_{i=1}^{M} \sum_{j=1}^{M} (S_i^T S_j)^2 \geq \frac{M^2}{L}. \tag{37}$$

This implies that

$$\sum_{i=1}^{M} \sum_{\substack{j=1 \\ j \neq i}}^{M} (S_i^T S_j)^2 \geq \frac{M^2}{L} - M,$$

and

$$\max_i \sum_{\substack{j=1 \\ j \neq i}}^{M} (S_i^T S_j)^2 \geq \beta - 1.$$

33

Thus

$$\min_{\{S_1,\ldots,S_M\}} \max_i \sum_{\substack{j=1 \\ j\neq i}}^{M} (S_i^T S_j)^2 \geq \beta - 1. \tag{38}$$

Furthermore, $\lim_{L\to\infty} \mu^{(L)} = \mu$. Hence we have

$$\lim_{L\to\infty} \min_{\{S_1,\ldots,S_M\}} \max_i B_M(F_M, k) \geq (\beta - 1)\mu. \tag{39}$$

Since the equality in (37) is achieved when $\{F_M\}$ is a WBE (Welch Bound Equality) signature set (see [15]) , the equality in (39) can be achieved by a sequence of WBE signature sets satisfying (3). □

A.2 Proof of Lemma 3.2

Proof: To show $\lim_{n\to\infty} \alpha_n(a) = f^{-1}(a)$, it suffices to show $\limsup \alpha_n(a) \leq f^{-1}(a)$ and $\liminf \alpha_n(a) \geq f^{-1}(a)$.

First suppose $\liminf \alpha_n(a) < f^{-1}(a)$. Choose s, t such that $\liminf \alpha_n(a) < s < t < f^{-1}(a)$. Then there exists $n_1 < n_2 < \ldots$ such that $\alpha_{n_j}(a) < s < t < f^{-1}(a)$ for all $j = 1, 2, \ldots$. Hence we have

$$f_{n_j}(\alpha_{n_j}(a)) \geq f_{n_j}(s) \geq f_{n_j}(t) \geq f_{n_j}(f^{-1}(a)). \tag{40}$$

By the definition of $\alpha_n(a)$, we have $f_{n_j}(\alpha_{n_j}(a)) = a$ since the f_{n_j}'s are continuous. Moreover, since $\{f_n\}$ converge to f point-wise, we have $\lim_{j\to\infty} f_{n_j}(s) = f(s)$, $\lim_{j\to\infty} f_{n_j}(t) = f(t)$, and $\lim_{j\to\infty} f_{n_j}(f^{-1}(a)) = a$. We take limit of (40) and get

$$a \geq f(s) > f(t) \geq a.$$

In the above step, we have exploited the fact that $f(s) > f(t)$ since $s < t$ and f is strictly decreasing. Thus, we get a contradiction. This implies $\liminf \alpha_n(a) \geq f^{-1}(a)$.

Following the same line, we can show $\limsup \alpha_n(a) \leq f^{-1}(a)$. Hence $\lim_{n\to\infty} \alpha_n(a) = f^{-1}(a)$, This completes the proof. □

A.3 Proof of Lemma 3.3

Proof: By assumption, the signature S_1 is known to the receiver for user 1. Thus, the ξ_i's are i.i.d. for $i = 2, \ldots, M$.

Since $E|\xi_i^2| = E\xi_i^2 = 1$ for $i = 2, \ldots, M$, we have $\frac{1}{M} \sum_{i=2}^{M} \xi_i^2 \xrightarrow{a.s.} 1$ by the Strong Law of Large Numbers. Moreover, $\lim_{L \to \infty} \mu^{(L)} = \mu$. Hence, as L goes to infinity, we have

$$B_M = \left(\frac{1}{M} \sum_{i=2}^{M} \xi_i^2 \right) \mu^{(L)} \xrightarrow{a.s.} \mu.$$

Next we show that $\lim_{L \to \infty} A_M = 0$ almost surely. To this end, by Lemma 2.1, it suffices to show A_M converges to 0 in probability and

$$\frac{\log L}{L^2} \sum_{i=2}^{M} (P_i^{(L)} - \mu^{(L)})^2 \xi_i^4 \xrightarrow{a.s.} 0.$$

Observe that

$$E\xi_i^4 = \frac{1}{L^2} \sum_{k_1} \sum_{k_2} \sum_{k_3} \sum_{k_4} E[W_{1k_1} W_{1k_2} W_{1k_3} W_{1k_4} W_{ik_1} W_{ik_2} W_{ik_3} W_{ik_4}]$$

$$\leq \frac{1}{L} + 3 < \infty.$$

Combining the above with the fact that $\mathrm{var}(P_i^{(L)}) < d^2$, we conclude that $\lim_{L \to \infty} E(A_M)^2 = 0$, and hence A_M converges to 0 in probability.

By the Strong Law of Large Numbers and the independence of $\{P_i^{(L)}\}$ and $\{\xi_i\}$, we have that

$$\frac{1}{L} \sum_{i=2}^{M} (P_i^{(L)} - \mu^{(L)})^2 \xi_i^4 \xrightarrow{a.s.} \mathrm{var}(P_0) E\xi_2^4.$$

This implies

$$\frac{\log L}{L^2} \sum_{i=2}^{M} (P_i^{(L)} - \mu^{(L)})^2 \xi_i^4 \xrightarrow{a.s.} 0.$$

Hence

$$A_M = \frac{1}{M} \sum_{i=2}^{M} (P_i^{(L)} - \mu^{(L)}) \xi_i^2 \xrightarrow{a.s.} 0.$$

This completes the proof. $\qquad \square$

A.4 Proof of Lemma 4.1

We use the following lemma, which follows directly from [5, Theorem 2.1, p.114] and [5, Property III, p. 51]:

Lemma A.1 *Let $f_n(x)$, $n \in \{1, \ldots, N\}$, be continuously differentiable convex functions on a convex closed set Ω in $\mathbb{R}^n$. Consider the problem*

$$\min_{x \in \Omega} \max_{n \in \{1, \ldots, N\}} f_n(x).$$

A point $X^* \in \Omega$ is a minimax point for the above problem (i.e., a solution to the above optimization problem) if and only if

$$\inf_{z \in \Omega} \max_{n \in R(X^*)} \left\langle \frac{\partial f_n(X^*)}{\partial x}, z - X^* \right\rangle = 0, \tag{41}$$

where $\langle \cdot, \cdot \rangle$ denotes the inner product in $\mathbb{R}^n$, and

$$R(x) = \left\{ n \in \{1, \ldots, N\} \,\middle|\, f_n(x) = \max_{n \in \{1, \ldots, N\}} f_n(x) \right\}.$$

Proof: Fix ϵ such that $0 < \epsilon < \min_{n \in \{1, \ldots, N\}} \lambda_n^*$. Define

$$\Omega = \left\{ (\lambda_1, \ldots, \lambda_N) \,\middle|\, \sum_{n=1}^{N} \lambda_n = 1, \ \lambda_n \geq \epsilon, \ n = 1, \ldots, N \right\}.$$

It is easy to verify that Ω is a closed convex set.

Let $x = (\lambda_1, \ldots, \lambda_N)$, and define $f_n(x) = \frac{b_n}{\lambda_n}$, for $n = 1, \ldots, N$. Note that $f_n(x) = \frac{b_n}{\lambda_n}$ is convex on Ω.

Observe that $X^* = (\lambda_1^*, \ldots, \lambda_N^*)$ is in Ω. Next we verify that X^* satisfies the condition specified in Lemma A.1. Let $(z - X^*) = (z_1 - \lambda_1^*, \ldots, z_N - \lambda_N^*)$. We have

$$\frac{\partial f_n(x)}{\partial x} = \left(0, \ldots, 0, \frac{-b_n}{\lambda_n^2}, 0, \ldots, 0\right),$$

which implies

$$\frac{\partial f_n(X^*)}{\partial x} = \left(0, \ldots, 0, \frac{-1}{b_n \lambda^2}, 0, \ldots, 0\right).$$

Hence

$$\left\langle \frac{\partial f_n(X^*)}{\partial x}, z - X^* \right\rangle = \frac{-1}{b_n \lambda^2}(z_n - \lambda_n^*) \qquad \text{for } n \in \{1, \ldots, N\}.$$

Note that the expression on the left hand side of (41) cannot be positive since we can always take $z = X^*$ and get a zero inner product. We will prove by contradiction that the condition in (41) is satisfied by X^*.

Suppose (41) fails to hold for X^*. Then there exists a point $Z = (z_1, \ldots, z_N) \in \Omega$ such that

$$\max_{n \in R(X^*)} \left\langle \frac{\partial f_n(X^*)}{\partial x}, Z - X^* \right\rangle < 0.$$

Since $f_n(X^*) = \sum_{n=1}^{N} \beta_n \mu_n$ for $n = 1, \ldots, N$, we have

$$\max_{n \in R(X^*)} \left\langle \frac{\partial f_n(X^*)}{\partial x}, Z - X^* \right\rangle < 0$$

$$\iff \max_{n \in \{1, \ldots, N\}} \left\langle \frac{\partial f_n(X^*)}{\partial x}, Z - X^* \right\rangle < 0, \tag{42}$$

36

that is, for any $n \in \{1, \ldots, N\}$,

$$\left\langle \frac{\partial f_n(X^*)}{\partial x}, Z - X^* \right\rangle < 0.$$

Hence, we have

$$\left\langle \frac{\partial f_n(X^*)}{\partial x}, Z - X^* \right\rangle = \frac{-1}{b_n \lambda^2}(z_n - \lambda_n^*) < 0 \quad \forall\, n \in \{1, \ldots, N\}.$$

Therefore, we get $z_n > \lambda_n^*$ for any $n \in \{1, \ldots, N\}$ since $b_n > 0$. Thus,

$$\sum_{n=1}^{N} z_n > \sum_{n=1}^{N} \lambda_n^* = 1,$$

which implies that Z is not in Ω, a contradiction. Therefore, X^* satisfies (41).

Since we can choose arbitrarily ϵ between 0 and $\min_{n \in \{1,\ldots,N\}} \lambda_n^*$, we conclude that X^* is a minimax point for (22a) over the constraint in (22b), and $\frac{\beta_n}{\lambda_n^*} \mu_n = \sum_{n=1}^{N} \beta_n \mu_n$, $n = 1, \ldots, N$.
□

B Examples of sequences of WBE signature sets satisfying (3)

In practical spread spectrum systems, the processing gain L is of the form 2^m for some integer m ($m = 7$ in IS-95). For large L, the contribution of one position in the spreading sequence to the cross-correlation of the signatures is negligible. Hence, we consider L in the form of $2^m - 1$.

As in [15], we associate a binary sequence $B = [b_1, b_2, \ldots, b_L]$ in $GF(2)^L$ with a spreading sequence $S = \frac{1}{\sqrt{L}}[s_1, s_2, \ldots, s_L]$, where the component-wise mapping is as follows:

$$b_k = \begin{cases} 0 & \text{if } s_k = 1 \\ 1 & \text{if } s_k = -1 \end{cases}.$$

Let S and S' be two arbitrary spreading sequences of length $L = 2^m - 1$, and B and B' the corresponding binary sequences in $GF(2)^L$. Then $(S^T S') = \frac{L - 2d(B,B')}{L}$, where $d(\cdot, \cdot)$ denotes the Hamming distance between the indicated vectors.

Example 1:

Let U denote a Maximum-Length Shift-Register Code of length $L = 2^m - 1$ where $m \geq 2$ and $U^\perp$ its dual code. Then U is a (L, m) linear code in which all codewords except the

all-zero codeword have identical weight 2^{m-1} ([16], p. 435). Moreover, $U^\perp$ is a Hamming code with minimum distance 3. By the corollary to Proposition 2 in [15], a binary signature set corresponding to a binary linear code is a WBE signature set if the minimum distance of its dual code is at least three. Thus, the signature set (say A) corresponding to U is a WBE set.

Let S and S' be two arbitrary and different spreading sequences chosen from A. Then $d(B, B') = 2^{m-1}$ since the code is linear, and $S^T S' = \frac{L - 2d(B, B')}{L} = \frac{-1}{L}$. As L goes to infinity, $\sup\left\{(S^T S')^2 \log L \mid S, S' \in A, S \neq S'\right\} \to 0$.

In this example, $\lim_{L \to \infty} \frac{M}{L} = 1$.

Example 2:

Let V denote a Triple-Error-Correcting Primitive Narrow-Sense Binary BCH code for $L = 2^m - 1$ and $V^\perp$ its dual code. Recall that a binary (L, K) linear code is a K-dimensional subspace of $GF(2)^L$. We conclude that $V^\perp$ is a $3m$-dimensional subspace of $GF(2)^L$. We are going to construct a linear code U which is a k-dimensional subspace of $V^\perp$ for $m < k < 3m$ by using the weight distribution of $V^\perp$ [30, p. 185].

First we consider the case $m \geq 5$, m odd (the weight distribution of $V^\perp$ for $L = 2^m - 1$, $m \geq 5$, m odd is given in Table 8-2(a) in [30, p .185]). Suppose we choose x, y, z, u, and w codewords having weights $2^{m-1} - 2^{\frac{m+1}{2}}$, $2^{m-1} - 2^{\frac{m-1}{2}}$, 2^{m-1}, $2^{m-1} + 2^{\frac{m-1}{2}}$ and $2^{m-1} - 2^{\frac{m+1}{2}}$ respectively. Moreover, it is required that $x + y + z + u + w = 2^k - 1$ so that we can construct a (L, k) block code U by using the above $2^k - 1$ nonzero codewords plus all-zero codeword. By using the MacWilliams Identity in [30, p. 90], we can get the weight enumerator of the dual code $U^\perp$. We can choose proper values for x, y, z, u, and w so that the coefficients A_1 and A_2 in the weight enumerator of $U^\perp$ are zero. This can be achieved in general since we have five variables but only three constraints. (Noting that the bounds on x, y, z, u, and w given in Table 8-2(a) in [30, p. 185] are much larger than L when m is large, we can choose x, y, z, u, and w as needed for moderate β.) Therefore, there is no codeword having weight 1 or 2 in the dual code $U^\perp$. By the corollary to Proposition 2 in [15], the signature set (say A) corresponding to $U^\perp$ is a WBE set.

Similarly by exploiting the Table 8-2(b) in [30, p. 185], we can show that the signature set corresponding to $U^\perp$ is a WBE set for the case $m \geq 5$, m even.

Again let S and S' be two arbitrary spreading sequences chosen from the above WBE set, and B and B' the corresponding binary sequences in $GF(2)^L$. From Table 8-2(a) and Table 8-2(b) in [30, p. 185], we have that $\sup\left\{|(S^T S')| \mid S, S' \in A, S \neq S'\right\} < 4L^{-\frac{1}{2}}$ and $\sup\left\{(S^T S')^2 \log L \mid S, S' \in A, S \neq S'\right\} \to 0$ as L goes to infinity.

In this example, $\beta = \lim_{L \to \infty} \frac{M}{L}$ can be chosen to be $2, 4$, etc.

References

[1] P. Billingsley, *Convergence of Probability Measures*. John Wiley & Sons, Inc., 1968.

[2] G. Casella and R. L. Berger, *Statistical Inference*. Duxbury Press, 1990.

[3] E. K. P. Chong and S. H. Żak, *An Introduction to Optimization*. John Wiley & Sons, Inc., 1996.

[4] J. Cuzick, "A strong law for weighted sums of i.i.d. random variables," *Journal of Theoretical Probability*, vol. 8, no. 3, pp. 625–641, 1995.

[5] V. Dem'yanov, *Introduction to Minimax*. John Wiley & Sons, Inc., 1974.

[6] K. S. Gilhousen, I. M. Jacobs, R. Padovani, A. J. Viterbi, L. A. Weaver Jr., and C. E. Wheatley III, "On the capacity of a cellular CDMA system," *IEEE Transactions on Vehicular Technology*, vol. 40, pp. 303–312, May 1991.

[7] A. Goldsmith and P. Varaiya, "Capacity of fading channels with channel side information," *IEEE Transactions on Information Theory*, vol. 43, pp. 1986–1992, Nov. 1997.

[8] S. V. Hanly, "Capacity and power control in spread spectrum macro-diversity radio networks," *IEEE Transactions on Communication*, vol. 4, no. 2, pp. 247–256, 1996.

[9] S. V. Hanly, *Information Capacity of Radio Networks*. PhD thesis, Cambridge University, Aug. 1993.

[10] S. V. Hanly and D. Tse, "Multi-access fading channels: Shannon and delay-limited capacities," in *Proc. 33rd Allerton conf.*, pp. 786–795, Oct. 1995.

[11] S. Kim and A. Goldsmith, "Truncated power control in code division multiple access communications," preprint, 1997.

[12] R. Lupas and S. Verdú, "Linear multiuser detectors for synchronous code-division multiple access," *IEEE Transactions on Information Theory*, vol. 35, pp. 123–136, Jan. 1989.

[13] U. Madhow and M. L. Honig, "Interference suppression for directed-sequence spread-spectrum CDMA," *IEEE Transactions on Communication*, vol. 42, pp. 3178–3188, Dec. 1994.

[14] U. Madhow and M. L. Honig, "MMSE detection of directed-sequence CDMA signals: Performance analysis for random signature sequences," *IEEE Transactions on Information Theory*, to appear.

[15] J. L. Massey and T. Mittelholzer, "Welch's bound and sequence sets for code-division multiple-access systems," in *Sequences II, Methods in Communications, Security and Computer science* (R. Capocelli, A. D. Santis, and U. Vaccaroo, eds.), Springer Verlag, 1993.

[16] J. G. Proakis, *Digital Communications*. McGraw-hill, Inc., third ed., 1995.

[17] Z. Rosberg and J. Zander, "Toward a framework for power control in cellular systems," *Wireless networks*, vol. 4, no. 3, pp. 215–222, Apr. 1998.

[18] H. L. Royden, *Real Analysis*. The Macmillan Company, New York, 1968.

[19] M. Rupf and J. L. Massey, "Optimum sequence multisets for synchronous code- division multiple-access channels," *IEEE Transactions on Information Theory*, vol. 40, pp. 1261–1266, Jul. 1994.

[20] M. Rupf, F. Tarköy, and J. L. Massey, "User-separating demodulation for code-division multiple-access systems," *IEEE Journal on Selected Areas in Communications*, vol. 12, no. 5, pp. 786– 795, Jun. 1994.

[21] J. R. Schott, *Matrix Analysis for Statistics*. John Wiley & Sons, Inc., 1997.

[22] E. Seneta, *Non-negative Matrices and Markov Chains*. Springer Verlag, second ed., 1981.

[23] D. Tse and S. V. Hanly, "Multiuser demodulation: Effective interference, effective bandwidth and capacity," preprint, Dec. 1997, (see http://www.eecs.berkeley.edu/~dtse).

[24] S. Ulukus and R. D. Yates, "Stochastic power control for cellular radio systems," *IEEE Transactions on Communication*, to appear.

[25] S. Verdú, "Multiuser detection," in *Advances in Statistical Signal Processing*, vol. 2, pp. 369–409, JAI Press Inc., 1993.

[26] S. Verdú and S. Shamai (Shitz), "Multiuser detection with random spreading and error-correction codes: Fundamental limits," in *Proc. 35th Allerton Conf.*, pp. 470–482, Oct. 1997.

[27] P. Viswanath, V. Anantharam, and D. Tse, "Optimal sequences, power control and capacity of spread-spectrum systems with multiuser receivers," preprint, Jan. 1998, (see http://www.eecs.berkeley.edu/~ananth).

[28] A. J. Viterbi and R. Padovani, "Implications of mobile cellular CDMA," *IEEE Communications Magazine*, pp. 38–41, Dec. 1992.

[29] L. R. Welch, "Lower bounds on the maximum cross-correlation of signals," *IEEE Transactions on Information Theory*, vol. 20, pp. 397–399, May 1974.

[30] S. B. Wicker, *Error Control Systems for Digital Communications and Storage*. Prentice Hall, Inc., 1995.

[31] R. D. Yates, "A framework for uplink power control in cellular radio systems," *IEEE Journal on Selected Areas in Communications*, vol. 13, no. 7, pp. 1341– 1348, Sep. 1995.

A Static Power Control Scheme for Wireless Cellular Networks *

Junyi Li   Ness B. Shroff[†]   Edwin K.P. Chong

School of Electrical and Computer Engineering
Purdue University
West Lafayette, IN 47907, U.S.A.
E-mail: {junyi, shroff, echong}@ecn.purdue.edu

October 9, 1998

Abstract

We present a novel static power control scheme to improve system capacity in wireless cellular networks. Our basic idea is to reduce intercellular interference and improve the capture probability by an *a priori* assignment of power-levels in different cells. We formulate and solve an optimal scheduling problem for our scheme. We find that the optimal scheduling policy is a simple form of bang-bang control. We illustrate our scheduling solution by considering two specific cases with uniform and nonuniform fairness constraints. We evaluate, via numerical analysis and simulation, both throughput and delay of the new scheme, and compare them with other schemes. We find that our scheme can achieve significant performance improvements, in terms of both maximum throughput and throughput-delay tradeoff, over a wide range of capture ratio values.

Submitted to IEEE/ACM Transactions on Networking

1 Introduction

In the last few years, wireless communication systems have experienced tremendous growth [19]. Compared to its wired counterpart, the wireless spectrum is a much more scarce resource. Cellular technology is an effective means of improving spectrum utilization in the wireless environment. In a cellular system, the service area is covered by a number of contiguous small zones, called cells. The same spectral resource can be reused simultaneously in different cells, provided that their mutual interference is low enough for reliable communication in individual cells [9]. The unit of wireless spectrum needed to serve a single user is called a *channel*. For example, in FDMA systems (or in a TDMA/FDMA system like GSM), a frequency carrier can be viewed as a channel. In current cellular systems, especially in the circuit-switched environment, channel reuse is separated by at least a *minimum reuse distance*, which is typically set such that the signal-to-interference ratio (SIR) on the same channel statistically exceeds some threshold. A significant body of research has been conducted on efficiently allocating channels to individual cells under this minimum reuse distance constraint [12, 21], among which there are fixed and dynamic channel allocation schemes.

Next generation wireless systems are envisioned to support high-speed multimedia applications. For example, there has been a significant research effort devoted to the development of wireless ATM networks. It is expected that packet-switching technology will prevail in future wireless multimedia systems [1, 2, 3, 4, 6, 7, 8, 10, 14, 17, 18, 19, 22]. The design and control of high-speed wireless networks is a challenging task. Experience in the wired network environment has shown that to maintain reasonable quality of service for multimedia applications, we need a very large channel capacity. The capacity problem becomes even more severe in the wireless environment. Thus, one of the crucial problems that must be solved for the next generation wireless systems is to use as much spectral capacity as possible on the wireless link, especially by taking advantage of the mechanisms provided by packet-switching.

In packet-switched networks, the success of a transmission is measured in a packet-by-packet fashion. In particular, a packet transmission in a cell is successful if the power received from the transmitter in that cell is sufficiently stronger than the power received from transmissions using the same channel in other cells. The capability to detect a packet in the presence of interference is known as *capture*. Note that in the wireless environment, whether capture occurs or not depends on many factors, including electromagnetic signal propagation conditions (e.g., fading and shadowing) and traffic conditions (e.g., locations of

interfering transmitters), and thus may fluctuate rapidly with time. Therefore, it is desirable that packet transmissions take advantage of the time periods during which capture occurs.

Based on the notion of capture, a new family of spectrum reuse methods have been recently proposed in the literature [5, 16], which we call *capture-based spectrum reuse*. The basic idea is to reuse the same channels in each cell. Thus, the capacity per cell is increased. Now, since more interference is introduced due to closer channel reuse, capture failure is likely to occur. When capture fails, packets are retransmitted until capture is successful. The rationale here is that since the propagation delay between a user and its base-station is usually small (in the order of a few bits of transmission delay), recovery by retransmission is an effective mechanism for dealing with capture failure. However, we note that capture failure degrades the effective spectrum utilization, and also impacts the delay that packets may experience before successfully being delivered.

In this paper, we propose a novel static power control (SPC) scheme to alleviate the problem of capture failure. Power control is a technique for assigning different values of transmission power to different users. Unlike most power control schemes in the literature, in our scheme, the power levels at the different cells are determined *a priori*, and thus no real-time intercellular signaling is required. To further simplify implementation, the power control is static and the power control levels are determined beforehand.

The remainder of this paper is organized as follows. In Section 2, after introducing the concept of capture, we review Capture Division Packet Access (CDPA), a capture-based spectrum reuse scheme, and discuss the problems with CDPA. We introduce our static power control (SPC) idea, namely the primary/secondary scheme, in Section 3. We formulate an optimal scheduling problem for the SPC scheme, and derive a necessary condition in Section 4. We further illustrate the optimal scheduling solutions by considering two specific optimization problems. In Section 5, we numerically evaluate the system performance via both analysis and simulation, and quantitatively compare our results with other spectrum reuse schemes.

2   Capture Model and Capture Division Packet Access

Consider a cellular mobile system in which each cell contains a base-station that communicates with mobile users in that cell. In this paper, we consider a time-slotted framework, and assume that the size of packets in the cellular network is fixed and that exactly one packet can be transmitted in one time-slot.

(a) Successful Capture　　　　　(b) Unsuccessful Capture
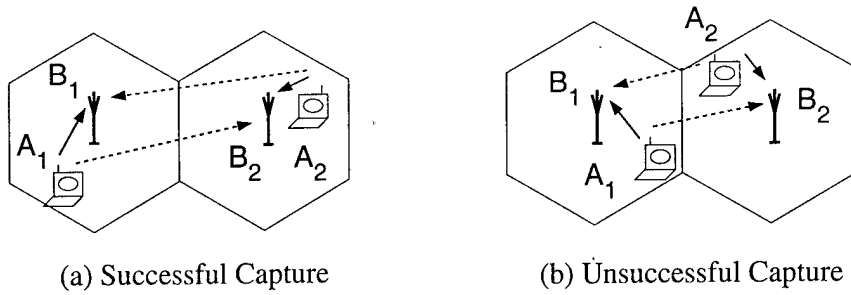
Figure 1: Capture model

Suppose that in a given time-slot of a carrier, there are two or more users transmitting packets. The transmissions may interfere with each other, and depending on the level of the interference, some of the transmissions may be unsuccessful. As discussed earlier, a successful transmission is referred to as capture. More specifically, a common capture model is that capture occurs (for uplink communication; for downlink communication, one can define capture similarly) for some user 0 if the signal-to-interference ratio (SIR) exceeds some constant threshold:

$$\frac{W_0}{\sum_{i \neq 0} W_i + \eta_0} > b. \tag{1}$$

Here, W_0 is the received power at user 0's base-station, W_i are the received powers from other co-channel users at the same base-station, η_0 represents the background noise, and b is called the *capture ratio*. For example, in Figure 1(a), the locations of users A_1 and A_2 are such that the interference between them is small compared to their signal strengths, and capture occurs, i.e., both users using the same time-slot of the same carrier successfully transmit to their respective base-stations. On the other hand, in Figure 1(b), the locations of users A_1 and A_2 are such that capture fails.

The capture ratio b is an important parameter that reflects the physical layer requirement for reliable communication. Various technologies react to interference differently [13]. For example, AMPS (Advanced Mobile Phone System) requires $b \approx 17 - 18$ dB. Other systems, including TACS (Total Access Communications System) and NMT (Nordic Mobile Telephone), are all roughly similar to AMPS in their interference characteristics. U.S. IS-54 and IS-136 TDMA reduces the requirement to 14 dB because they employ digital techniques. Due to its more robust modulation scheme, GSM (Global System for Mobile communications), however, can tolerate co-channel ratios as low as 6.5 to 9 dB. The capture ratio determines how difficult it is for capture to occur. For example, with the same SIR, capture occurs less often for a larger value of b than a smaller value of b. Later, we will find that the value of b significantly impacts the performance of different spectrum reuse schemes.

As mentioned earlier, by taking advantage of the capture effect, the capture-based spectrum reuse schemes attempt to increase spectral capacity for packet-switched wireless systems. Specifically, the distance between cells that are allowed to transmit in the same channel is shorter than the minimum reuse distance. Hence, the number of channels that can be allocated to an individual cell is significantly increased.

An important example of the capture-based spectrum reuse schemes is the *Capture Division Packet Access (CDPA)* scheme, proposed in [5]. In CDPA, users in all cells can transmit in the same time-slots of each carrier, with some permission probability, and if capture does not occur, this collision is resolved by retransmitting the packet a random time later. By using a precise *intracellular* multiple access control mechanism, CDPA ensures that there is no contention between users within any given cell and that capture failure is due only to the interference from neighboring cells. In [5], it was shown via numerical studies that CDPA can outperform standard TDMA, especially when the capture ratio is relatively low (e.g., $b = 6$ dB). However, the results are not satisfactory when the capture ratio is high (e.g., $b = 10$ dB).

With CDPA, in both uplink (mobile-to-base-station) and downlink (base-station-to-mobile) communication, the probability that capture occurs (*capture probability*) depends strongly on the location of a mobile user, and that excessive retransmissions may result, especially for users that are located geographically in a way that makes capture difficult. We call this phenomenon the *near-far effect*, and illustrate it in Figure 2. In Figure 2(a), we plot a typical curve of the capture probability versus the distance of a mobile user to its base-station. It is apparent that the SIR for mobile users close to the base-station ("near" users) is high, thus leading to high capture probabilities. However, users far way from the base-station ("far" users), with weaker signals but stronger interference, suffer very low capture probabilities. Therefore, to maintain some degree of fairness among users in different locations in the cellular network, one has to allocate more retransmission opportunities to the unfavorably located users, who use a significant portion of the spectrum. For example, in Figure 2(b), we plot the density function of the spectrum allocation that keeps the same throughput for mobile users in different locations. Clearly, users far away from the base-station become the bottleneck for network efficiency. In the following sections, we present our SPC scheme to address this bottleneck problem.
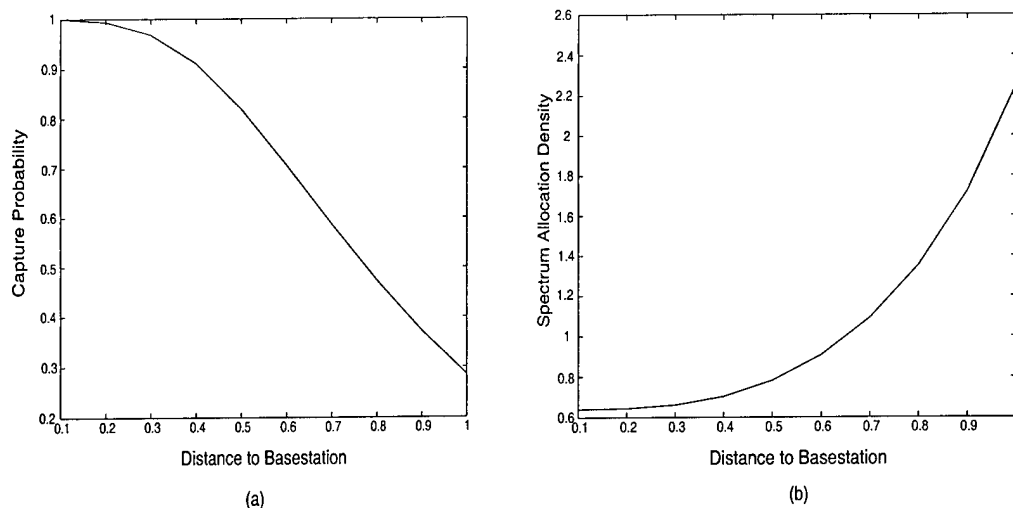
Figure 2: Illustration of the near-far effect in CDPA (a) Users further away from the base-station may experience substantially lower capture probability. (b) More retransmission chances (hence higher capacity) have to be allocated for users that are further away from the base-station.

3   Primary/Secondary Assignment

In our scheme, we employ a simple reservation-based technique, similar to the one proposed in [11], for multiple access control of users *within* a cell. In particular, a fraction of the time-slots on the uplink channel are designated as *reservation slots*. Mobile users who start/resume to send payload packets inform the base-station by transmitting request packets on those reservation slots with some random access mechanism (e.g., ALOHA). Clearly, communication on the reservation slots could experience contention, and collisions may occur. The size of the request packets is chosen to be much smaller than that of the payload packets, so that this collision probability is very small. The base-station, upon receiving a request packet, schedules the transmissions for the intended mobile user, according to some scheduling discipline, by sending commands along with downlink payload packets, on the downlink channel. In this way, uplink payload transmissions are ensured to be contention-free. Therefore, in our SPC scheme, the transmissions in a given cell on both uplink and downlink channels are completely controlled by the base-station.

Recall from our previous discussion that a problem with CDPA is that it relies solely on random fluctuations of the SIR to combat capture failure, and consequently results in excessive retransmissions, especially for "far" users. Instead of wasting spectral resources on retransmissions, we aim to improve the probability of a successful transmission by *a priori* coordinating user transmissions over different cells. Since "far" users represent a bottleneck that requires a significant percentage of retransmissions, our basic idea is to improve the

5

(a) Transmissions on Carrier A   (b) Transmissions on Carrier B
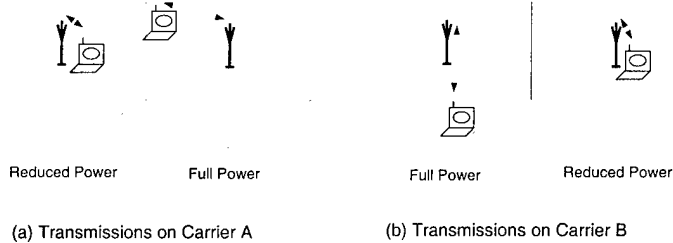
Figure 3: Illustration of primary/secondary idea

capture probability of these users by reducing the interference they experience.

Consider the following intuitive heuristic. When a "far" user is transmitting (or receiving) packets in a given cell, the idea is to reduce the power of simultaneous transmissions in the adjacent cells. On the other hand, since the power levels are reduced in the adjacent cells, only "near" users can be served in the adjacent cells, for otherwise the capture probability could become even worse. For the illustration of this heuristic, consider Figure 3, in which we show two adjacent cells in the cellular network. Here, we allow the base-station in the right cell to use one carrier (carrier A) with full power and serve a "far" user in the cell, while the left cell uses the same carrier, but with a reduced power level and serving only a "near" user. We do the reverse on another carrier (carrier B), to maintain fairness between the two cells.

In general, in our scheme, carriers that are assigned to each cell in the cellular network are either *primary* or *secondary*. Primary carriers can be used to transmit (or receive) packets at the full allowable power W_T, while secondary carriers can only be used to transmit (or receive) packets at a reduced power level γW_T, where $0 \leq \gamma \leq 1$. This primary/secondary scheme is the basis for our SPC scheme. Note that γ is an important tuning parameter that can be used to balance capture success in cells using primary and secondary carriers. At one end, when $\gamma = 1$, there is no difference between the primary and secondary carriers, and our scheme is indeed equivalent to CDPA. At the other end, when $\gamma = 0$, the capture probability in the secondary cells is reduced to zero. In fact, there is no communication activity at all in the secondary cells, which is similar to standard TDMA with a certain fixed channel reuse distance. Later we will show that, by applying an appropriate scheduling strategy, our primary/secondary SPC scheme can outperform both CDPA and TDMA.

We point out two fundamental advantages that make our SPC scheme practically attractive:

1. The assignment of primary/secondary carriers to any particular cell is determined

6
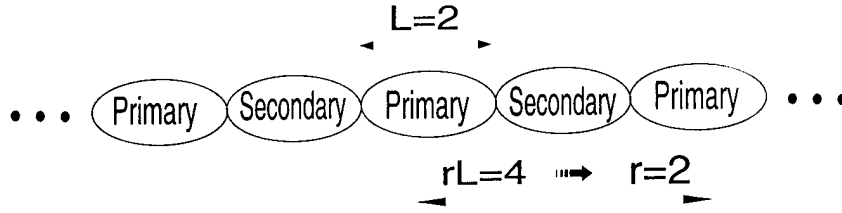
Figure 4: Linear cellular network with primary/secondary cells interleaved

beforehand, and no real-time intercelluar signaling is required.

2. Power control is static, i.e., γ is a constant. In particular, here we consider two power control levels that are set *a priori* and whose values are not changed. Note that this is very different from other power control schemes in the literature, where the power is allowed to be changed dynamically and hence more sophisticated signal processing is required for their implementation.

The question to answer now is how to schedule users in different locations, under this primary/secondary SPC scheme. In our earlier heuristic discussion, illustrated via Figure 3, we suggest serving "far" users with primary carriers and "near" users with secondary carriers. To more precisely answer the above question, we next formulate an appropriate optimization problem and develop an optimal scheduling policy. Interestingly, it turns out that under certain conditions, the optimal solution agrees with our intuitive heuristic scheme.

4 Optimal Scheduling

4.1 System Description

For simplicity of description, consider a linear cellular system, where the base-stations are numbered as $\{\ldots, 0, 1, 2, \ldots, \}$, and where the distance between two adjacent base-stations is normalized to be 2. Mobile users communicate with their nearest base-station. Thus, the radius of each cell is 1.

In our scheme, we group all the carriers into two distinct carrier-sets A and B. All odd-numbered cells are assigned carrier-set A as the primary carrier-set, and carrier-set B as the secondary carrier-set; the even-numbered cells are assigned carrier-set B as their primary carriers, and carrier-set A as their secondary carriers. Due to symmetry, without loss of generality, we next focus only on carrier-set A, and thus call the odd-numbered cells the *primary cells* and even-numbered cells the *secondary cells*.

7

Let $g_P(x)$ and $g_S(x)$, with $0 \leq x \leq 1$, be the probability density functions of the traffic load (or simply traffic load densities) at a "distance" x away from the base-station when the cell is primary and secondary, respectively. Note that these traffic load densities include both new and retransmitted packets, and can be either downlink or uplink. The distance parameter x is referred to as *location* x. Note that x may be used to represent path loss, not just physical distance from the bas-estation. We call the pair $\{g_P(\cdot), g_S(\cdot)\}$ the *traffic load density pair*. We assume that the traffic load densities are piecewise continuous. The aggregate traffic loads in a primary and secondary cell are given by $G_P \triangleq 2 \int_0^1 g_P(x)\,dx$ and $G_S \triangleq 2 \int_0^1 g_S(x)\,dx$, respectively. We can also interpret G_P and G_S as the probabilities that a transmission occurs in a primary and secondary cell, respectively.

Let P_P and P_S denote the capture probabilities in a primary and secondary cell, respectively. The capture probabilities depend on both the location where packet transmission occurs in the cell and the interference from the adjacent cells. Thus, in general, we use the notations $P_P(x, g_P(\cdot), g_S(\cdot))$ and $P_S(x, g_P(\cdot), g_S(\cdot))$ to reflect this dependence.

We define $s(x)$ to be the throughput density (or probability density function of the throughput a distance x away from the base-station), *per carrier*[1], at a location x, which is given by

$$s(x) = \frac{1}{2}(g_P(x)P_P(x, g_P(\cdot), g_S(\cdot)) + g_S(x)P_S(x, g_P(\cdot), g_S(\cdot))).$$ (2)

We now formulate the optimal scheduling problem as

$$\begin{array}{ll} \underset{g_P(\cdot), g_S(\cdot)}{\text{maximize}} & f(s(\cdot)) \\ \text{subject to} & h(s(\cdot)) \geq 0 \end{array}$$ (3)

where f and h are general functions satisfying the following condition:

(C1) If $h(s(\cdot)) \geq 0$, then for all $C > 0$, we have $f(s(\cdot) + C) > f(s(\cdot))$ and $h(s(\cdot) + C) \geq 0$.

The above optimal scheduling problem is very general and captures a variety of realistic problems. Some examples of useful functions f and h are:

- $f(s(\cdot)) = S \triangleq 2 \int_0^1 s(x)\,dx$, the overall throughput in a cell.

- $h(s(\cdot)) = \inf_x s(x)/u(x) - \sup_x s(x)/u(x)$, where $u(x) > 0$ is the user location density (representing non-uniformly distributed traffic). This constraint implies *uniform fairness*, i.e., the throughput per user is the same for different locations in the cell. The uniform fairness constraint is one that is typically studied in the literature, for example in [5].

---

[1] Note that the throughput in a cell comes from traffic on both carrier-sets A and B.

- More generally, we can have a *non-uniform fairness constraint*:

$$h(s(\cdot)) = c - \left(\sup_x s(x)/u(x) - \inf_x s(x)/u(x) \right),$$

where $c \geq 0$ is some constant. This implies that the difference between the maximum and the minimum throughputs per user is bounded by an amount c; i.e.,

$$\sup_x s(x)/u(x) - \inf_x s(x)/u(x) \leq c.$$

If we choose $c = 0$, then the above reduces to the uniform fairness constraint.

- Alternatively, we can have

$$h(s(\cdot)) = c - \frac{\sup_x s(x)/u(x) - \inf_x s(x)/u(x)}{\sup_x s(x)/u(x)},$$

which implies that the *relative* difference in throughput is constrained to be less than some constant c; i.e.,

$$\frac{\sup_x s(x)/u(x) - \inf_x s(x)/u(x)}{\sup_x s(x)/u(x)} \leq c.$$

4.2 Necessary Conditions for Optimality

Before, we proceed to solve the optimization problem (3), we impose the following condition on the capture probabilities:

(C2) At any location in the cell, the capture probabilities depend only on the aggregate values of the traffic load pair.

Hence, we denote the capture probabilities in a primary and secondary cell as $P_P(x, G_P, G_S)$ and $P_S(x, G_P, G_S)$, respectively (instead of $P_P(x, g_P(\cdot), g_S(\cdot))$ and $P_S(x, g_P(\cdot), g_S(\cdot))$), to reflect this assumption. Note that condition (C2) reflects exactly the real situation in downlink communication (since the base-stations themselves are not mobile). However, for uplink transmission, the received interference depends in general on the location of interferers. Thus, the capture probability in this case is determined by the traffic load distributions in the interfering cells, not just the aggregate values. Therefore, our assumption represents an approximation for uplink communication. However, our simulation results will show that the mismatch can be safely ignored. It should be noted that in [5], the authors made the same assumption and they too found the impact of the approximation to be negligible.

Based on conditions (C1) and (C2), our procedure for solving the optimal scheduling problem (3) is as follows. First, for a given set of aggregate traffic loads G_P and G_S, we

derive the optimal traffic load density pair $\{g_P^*(\cdot), g_S^*(\cdot)\}$. We then obtain the overall solution by optimizing over the values of G_P and G_S (recall that $G_P, G_S \in [0, 1]$).

To proceed, we define the *family* $\{G_P, G_S\}$ to be all traffic load density pairs $\{g_P(\cdot), g_S(\cdot)\}$ whose aggregate values are fixed and are equal to G_P and G_S, respectively. We will next derive a necessary condition for a traffic load density pair to be optimal in the family $\{G_P, G_S\}$. Note that according to our simplifying assumption, if the aggregate traffic loads are fixed, the capture probabilities are only functions of the location in a cell. Thus, when we focus on the family $\{G_P, G_S\}$, we denote the capture probabilities in the primary and secondary cells simply by P_P and P_S, respectively. It turns out that the necessary condition for solving the optimization problem can then be given in the following simple form.

Theorem 1 *Given values of the aggregate traffic loads G_P and G_S, suppose that $\{g_P^*(\cdot), g_S^*(\cdot)\}$ is the optimal traffic load density pair in the family $\{G_P, G_S\}$. Then, there exists a positive constant α_0 such that*

$$g_P^*(x) = 0, \text{ for all } x \text{ such that } \frac{P_P(x)}{P_S(x)} < \alpha_0, \tag{4}$$

$$g_S^*(x) = 0, \text{ for all } x \text{ such that } \frac{P_P(x)}{P_S(x)} > \alpha_0. \tag{5}$$

Proof: See appendix. ∎

Theorem 1 states that the optimal solution to (3) is in the form of bang-bang control, in the sense that the users that are scheduled for transmission in a primary cell are selected from regions that are completely complementary to the users that are scheduled for transmission in a secondary cell. Therefore, the optimal throughput density is given by

$$s^*(x) = \begin{cases} \frac{1}{2} g_P^*(x) P_P(x), & \text{for all } x \text{ such that } \frac{P_P(x)}{P_S(x)} > \alpha_0 \\ \frac{1}{2} g_S^*(x) P_S(x), & \text{for all } x \text{ such that } \frac{P_P(x)}{P_S(x)} < \alpha_0. \end{cases} \tag{6}$$

This bang-bang type of scheduling is illustrated in Figure 5. From Figure 5, we can see that the cell is partitioned into two complementary regions, where users in Region I are scheduled for transmission only in a primary cell (i.e., $g_S^*(x) = 0$, for x in Region I), while users in Region II are scheduled for transmission only in a secondary cell (i.e., $g_P^*(x) = 0$, for x in Region II). For example, recall that so far we focus on carrier-set A and cell 1 is a primary cell. Thus, carrier A is used to serve only users in Region I of cell 1. However, when we consider carrier-set B, cell 1 becomes a secondary cell. From the same argument, we would then schedule users in Region II of cell 1 on carrier B.

We next state an important corollary when $P_P(x)/P_S(x)$ is monotonically increasing.

10

Figure 5: Illustration of bang-bang optimal scheduling in general cases

Corollary 1 *Suppose that $P_P(x)/P_S(x)$ is a monotonically increasing function of x. Given values of the aggregate traffic loads G_P and G_S, suppose that $\{g_P^*(\cdot), g_S^*(\cdot)\}$ is the optimal traffic load density pair in the family $\{G_P, G_S\}$. Then, there exists a number $x_0 \in (0,1)$ such that*

$$g_P^*(x) \;=\; 0 \text{ for all } x \in (0, x_0) \tag{7}$$

$$g_S^*(x) \;=\; 0 \text{ for all } x \in (x_0, 1) \tag{8}$$

Proof: Because $P_P(x)/P_S(x)$ is a monotonically increasing function, for any α_0 given in Theorem 1, there exists a unique x_0 such that $P_P(x_0)/P_S(x_0) = \alpha_0$. The sets $\{x | P_P(x)/P_S(x) < \alpha_0\}$ and $\{x | P_P(x)/P_S(x) > \alpha_0\}$ are equivalent to intervals $(0, x_0)$ and $(x_0, 1)$, respectively. Thus, the corollary follows immediately from Theorem 1. ∎

Our analysis and simulation results with standard physical layer propagation models show that $P_P(x)/P_S(x)$ is usually monotonically increasing. However, note that to obtain Equations (7) and (8) in the corollary, we only require that there exists x_0 such that $P_P(x)/P_S(x) > \alpha_0$ for all $x \in (x_0, 1)$, and $P_P(x)/P_S(x) < \alpha_0$ for all $x \in (0, x_0)$. The result of the corollary dictates that the optimal scheduling policy is to schedule only those users in a secondary cell that are a distance $(0, x_0)$ away from its base-station, and only those users in a primary cell that are a distance $(x_0, 1)$ away from its base-station. This cell partition is illustrated in Figure 6. This corollary agrees with our intuition (see Figure 3) of scheduling "far" users at higher power in a primary cell, while "near" users at a lower power in a secondary cell. What the above corollary (and Theorem 1) also tells us is that even for the optimal scheduling policy, it may not be necessary to estimate precisely the capture

11
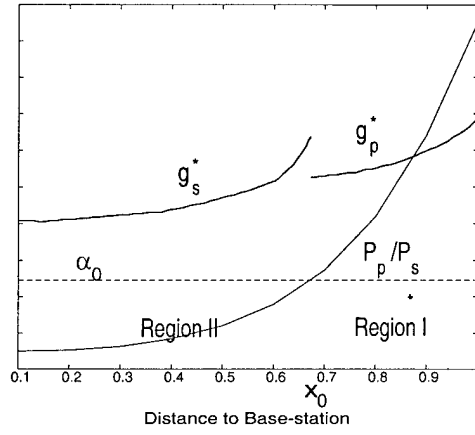
Figure 6: Illustration of bang-bang optimal scheduling when $P_P(x)/P_S(x)$ is monotonically increasing

probability or location of each user for implementing the primary/secondary SPC scheme. Instead, a rough estimate of which region a user belongs would suffice.

4.3 Specific Choices of f and h

Theorem 1 and Corollary 1 provide necessary conditions for the optimal scheduling problem (3). However, to quantitatively calculate the optimal scheduling policy, we need to evaluate explicitly the parameter α_0 and density functions $g_P^*(\cdot)$ and $g_S^*(\cdot)$. This means that the functions f and h in (3) must be explicitly defined. To illustrate the optimal scheduling solution, we will consider two specific cases in this section.

4.3.1 Problem I

Consider the following optimization problem:

$$\underset{g_P(\cdot), g_S(\cdot)}{\text{maximize}} \quad \int_0^1 s(x)\, dx$$

$$\text{subject to} \quad \sup_x \frac{s(x)}{u(x)} - \inf_x \frac{s(x)}{u(x)} = 0 \tag{9}$$

Here, $u(x)$ is the user location density. To make our discussion meaningful, we assume throughout the study that $u(\cdot)$ is piecewise continuous and $u(x) > 0$ for all $x \in [0,1]$. The constraint in Problem (9) reflects a uniform fairness constraint (in terms of throughput) among users at different locations in a cell, i.e., the optimal throughput per user is constrained to be a constant, which we denote by s_u^*.

By applying the necessary condition of Theorem 1, Problem (9) is easy to solve. We

12

integrate Equation (6) to obtain

$$s_u^* \int_{\Phi_P} \frac{u(x)}{P_P(x)} \, dx = \frac{1}{2} \int_{\Phi_P} g_P^*(x) \, dx = \frac{1}{2} G_P, \tag{10}$$

$$s_u^* \int_{\Phi_S} \frac{u(x)}{P_S(x)} \, dx = \frac{1}{2} \int_{\Phi_S} g_S^*(x) \, dx = \frac{1}{2} G_S, \tag{11}$$

where $\Phi_P = \{x | P_P(x)/P_S(x) > \alpha_0\}$ and $\Phi_S = \{x | P_P(x)/P_S(x) < \alpha_0\}$. Here, α_0 is the parameter described in Theorem 1 and can be determined by solving the following single-variable equation:

$$\frac{G_P}{\int_{\Phi_P} \frac{u(x)}{P_P(x)} \, dx} = \frac{G_S}{\int_{\Phi_S} \frac{u(x)}{P_S(x)} \, dx} \tag{12}$$

Now if $P_P(x)/P_S(x)$ is a monotonically increasing function of x, Equations (10), (11), and (12) can be simplified further as follows:

$$s_u^* \int_{x_0}^1 \frac{u(x)}{P_P(x)} \, dx = \frac{1}{4} G_P \tag{13}$$

$$s_u^* \int_0^{x_0} \frac{u(x)}{P_S(x)} \, dx = \frac{1}{4} G_S \tag{14}$$

$$\frac{G_P}{\int_{x_0}^1 \frac{u(x)}{P_P(x)} \, dx} = \frac{G_S}{\int_0^{x_0} \frac{u(x)}{P_S(x)} \, dx} \tag{15}$$

By solving either Equation (12) or (15), we can obtain the value of the parameter α_0 or x_0, and then determine the optimal throughput with Equations (10) and (11) or (13) and (14), respectively.

Problem (9) has been considered before in the literature, for example in [5]. In Section 5 we will provide extensive numerical performance comparisons with other schemes for this problem. We now present a qualitative comparison of our primary/secondary SPC scheme with CDPA, which is instructive in understanding why our scheme yields a higher throughput for Problem (9).

For simplicity, we consider the case where $P_P(x)/P_S(x)$ is monotonically increasing and assume that users are uniformly distributed in the cellular network (i.e., $u(x) = \frac{1}{2}$). For the sake of comparison with CDPA, we further restrict ourselves to the case where the aggregate traffic loads are the same for both primary and secondary cells,[2] i.e., $G_P = G_S \triangleq G$. It then follows from Equations (13)–(15) that for a given aggregate traffic load G, the optimal aggregate throughput of the primary/secondary SPC scheme is given by

$$S_{PS}^* = \frac{G}{\int_{x_0}^1 \frac{1}{P_P(x)} \, dx + \int_0^{x_0} \frac{1}{P_S(x)} \, dx}. \tag{16}$$

---

[2]We note that, however, G_P and G_S are not necessarily the same for overall optimality in our scheme.

The solution of Problem (9) for CDPA can be derived similarly [5]. In fact, recall that CDPA can be viewed as a special case of our SPC scheme when $\gamma = 1$ (i.e., no static power control). In this case, there is no difference between the primary and secondary cells, and $P_P(x) = P_S(x)$. Thus, it follows immediately from the above equation that the optimal aggregate throughput of CDPA is given by

$$S_{CDPA}^* = \frac{G}{\int_0^1 \frac{1}{P_{CDPA}(x)} dx},$$

(17)

where $P_{CDPA}(x)$ denotes the capture probability with CDPA.

We next compare the optimal throughputs of our SPC scheme and CDPA. We have,

$$
\begin{aligned}
S_{PS}^* - S_{CDPA}^* &= G\left(\frac{1}{\int_{x_0}^1 \frac{1}{P_P(x)} dx + \int_0^{x_0} \frac{1}{P_S(x)} dx} - \frac{1}{\int_0^1 \frac{1}{P_{CDPA}(x)} dx}\right) \\
&= G\frac{\int_{x_0}^1 \left(\frac{1}{P_{CDPA}(x)} - \frac{1}{P_P(x)}\right) dx - \int_0^{x_0} \left(\frac{1}{P_S(x)} - \frac{1}{P_{CDPA}(x)}\right) dx}{\left(\int_{x_0}^1 \frac{1}{P_P(x)} dx + \int_0^{x_0} \frac{1}{P_S(x)} dx\right)\left(\int_0^1 \frac{1}{P_{CDPA}(x)} dx\right)} \\
\frac{S_{PS}^* - S_{CDPA}^*}{S_{PS}^*} &= \frac{\int_{x_0}^1 \left(\frac{1}{P_{CDPA}(x)} - \frac{1}{P_P(x)}\right) dx - \int_0^{x_0} \left(\frac{1}{P_S(x)} - \frac{1}{P_{CDPA}(x)}\right) dx}{\int_0^1 \frac{1}{P_{CDPA}(x) dx}}
\end{aligned}
$$

(18)

For illustration, in Figure 7, we plot the reciprocal of the capture probabilities P_P, P_S, and P_{CDPA} versus the distance to the base-station. From Equation (18), it follows that the relative improvement in optimal throughput of the SPC scheme over CDPA (with respect to S_{PS}^*) is equal to the relative difference between the following two areas A_P and A_S (with respect to the area under the curve of $1/P_{CDPA}(x), x \in [0,1]$):

$$A_P \triangleq \int_{x_0}^1 \left(\frac{1}{P_{CDPA}(x)} - \frac{1}{P_P(x)}\right) dx$$

$$A_S \triangleq \int_0^{x_0} \left(\frac{1}{P_S(x)} - \frac{1}{P_{CDPA}(x)}\right) dx.$$

Qualitatively, since a reduced power is used in a secondary cell, the capture probability is lower with the SPC scheme than with CDPA, and the area A_S reflects the associated loss in throughput. On the other hand, the SPC scheme achieves better capture probability in a primary cell, and the gain is quantified by the area A_P. Note that in the wireless propagation environment, the capture probability drops quickly with the distance to the base-station. Hence, the gain in the interval $[x_0, 1]$ is generally larger than the loss in the interval $[0, x_0]$, and therefore the SPC scheme can achieve a higher throughput than CDPA.
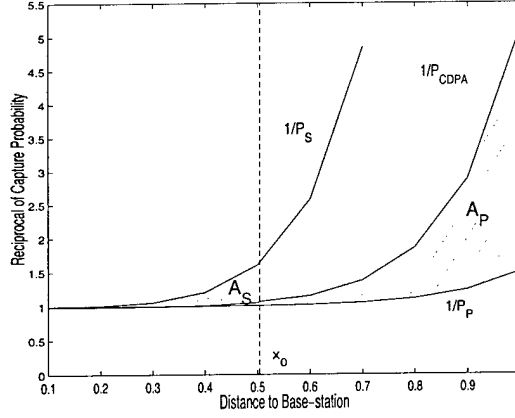
Figure 7: Qualitative comparsion of SPC scheme and CDPA

4.3.2 Problem II

In this section, we consider the following optimization problem with a more general fairness constraint:

$$
\begin{aligned}
\underset{g_P(\cdot), g_S(\cdot)}{\text{maximize}} \quad & \int_0^1 s(x)\, dx \\
\text{subject to} \quad & \sup_x \frac{s(x)}{u(x)} - \inf_x \frac{s(x)}{u(x)} \le c \left(\sup_x \frac{s(x)}{u(x)} \right)
\end{aligned}
\tag{19}
$$

when $c \in [0,1]$ is a positive number. Note that the discussion in this section is also applicable to the optimization problem when the constraint is, instead, $\sup_x \frac{s(x)}{u(x)} - \inf_x \frac{s(x)}{u(x)} \le c$. Also note that when $c = 0$, Problem (19) reduces to Problem (9). In this problem, we attempt to maximize the overall throughput, under the constraint that the relative difference between the maximum and minimum throughout per user is bounded by c.

Similar to Section 4.3.1, we next calculate the optimal traffic load in the family $\{G_P, G_S\}$. It turns out that the optimal throughput per user of Problem (19), $s_u^*(\cdot)$, can take only one of two discrete values, as stated in the following theorem.

Theorem 2 *There exist two positive numbers β_P and β_S, and two positive constants s_1 and s_2, $s_1 \ge s_2$, such that the optimal throughput per user of Problem (19) satisfies*

$$
s_u^*(x) = \begin{cases}
s_1, & \text{for all } x \ \in \Pi_{P1} \triangleq \{x \in \Phi_P | P_P(x) > \beta_P\} \\
s_2, & \text{for all } x \ \in \Pi_{P2} \triangleq \{x \in \Phi_P | P_P(x) < \beta_P\} \\
s_1, & \text{for all } x \ \in \Pi_{S1} \triangleq \{x \in \Phi_S | P_P(x) > \beta_S\} \\
s_2, & \text{for all } x \ \in \Pi_{S2} \triangleq \{x \in \Phi_S | P_P(x) < \beta_S\}
\end{cases}
\tag{20}
$$

where $\Phi_P = \{x | P_P(x)/P_S(x) > \alpha_0\}$ and $\Phi_S = \{x | P_P(x)/P_S(x) < \alpha_0\}$, and α_0 is the parameter described in Theorem 1.

15
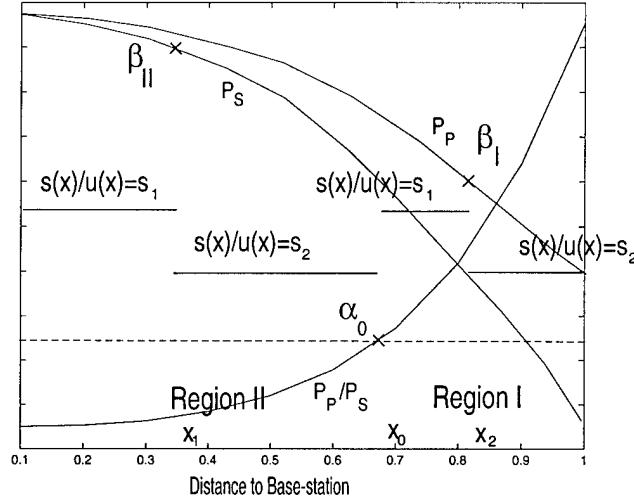
Figure 8: Illustration of two-level bang-bang optimal scheduling for Problem 19

Proof: See Appendix B.

Recall that the necessary condition (Theorem 1) partitions the cell into two complementary regions, which are served in the primary and secondary cell, respectively. Theorem 2 states that the two regions are further partitioned into four distinct subregions, in each of which the optimal throughput per user of Problem (19) remains constant. We illustrate this two-level bang-bang control in Figure 8, for the case where $P_P(x)/P_S(x)$ is monotonically increasing and $P_P(x)$ and $P_S(x)$ are themselves monotonically decreasing.

Based on Theorem 2, we can quantitatively determine the optimal scheduling scheme in the family $\{G_P, G_S\}$. Recall that $s^*(x) = \frac{1}{2}g_P^*(x)P_P(x)$, for $x \in \Phi_P$ and $s^*(x) = \frac{1}{2}g_S^*(x)P_S(x)$, for $x \in \Phi_S$. Therefore,

$$g_S^*(x) = \begin{cases} 2s_2 u(x)/P_S(x), & x \in \Pi_{S2} \\ 2s_1 u(x)/P_S(x), & x \in \Pi_{S1} \end{cases}$$

$$g_P^*(x) = \begin{cases} 2s_2 u(x)/P_P(x), & x \in \Pi_{P2} \\ 2s_1 u(x)/P_P(x), & x \in \Pi_{P1} \end{cases}$$

The key problem here is to calculate s_1, s_2, and the cell partition Π_{P1}, Π_{P2}, Π_{S1}, and Π_{S2}, which are completely determined by the parameters α_0, β_P, and β_S. Hence, we can determine the optimal schedule for Problem (19) by solving the following simple parametric optimization problem:

$$\begin{aligned} \underset{\alpha_0,\beta_P,\beta_S,s_1,s_2}{\text{maximize}} \quad & s_1\left(\int_{\Pi_{P1}} u(x)\,dx + \int_{\Pi_{S1}} u(x)\,dx\right) + s_2\left(\int_{\Pi_{P2}} u(x)\,dx + \int_{\Pi_{S2}} u(x)\,dx\right) \\ \text{subject to} \quad & s_1\int_{\Pi_{P1}} \frac{u(x)}{P_P(x)}\,dx + s_2\int_{\Pi_{P2}} \frac{u(x)}{P_P(x)}\,dx = \frac{1}{2}G_P \\ & s_1\int_{\Pi_{S1}} \frac{u(x)}{P_S(x)}\,dx + s_2\int_{\Pi_{S2}} \frac{u(x)}{P_S(x)}\,dx = \frac{1}{2}G_S \end{aligned}$$

(21)

$$s_1 - s_2 = cs_1$$

Note that unlike the functional optimization problem given by (19), the above parametric optimization problem is easy to solve. For the special case where $P_P(x)/P_S(x)$ is monotonically increasing, and $P_P(x)$ and $P_S(x)$ are monotonically decreasing, the form of the above optimization problem can further be simplified to:

$$
\begin{aligned}
\operatorname*{maximize}_{x_0, x_1, x_2, s_1, s_2} \quad & s_1 \left(\int_0^{x_1} u(x)\, dx + \int_{x_0}^{x_2} u(x)\, dx \right) + s_2 \left(\int_{x_1}^{x_0} u(x)\, dx + \int_{x_2}^{1} u(x)\, dx \right) \\
\text{subject to} \quad & s_1 \int_{x_0}^{x_2} \frac{u(x)}{P_P(x)}\, dx + s_2 \int_{x_2}^{1} \frac{u(x)}{P_P(x)}\, dx = \frac{1}{4} G_P \qquad (22) \\
& s_1 \int_0^{x_1} \frac{u(x)}{P_S(x)}\, dx + s_2 \int_{x_1}^{x_0} \frac{u(x)}{P_S(x)}\, dx = \frac{1}{4} G_S \\
& s_1 - s_2 = cs_1 \\
& 0 \le x_1 \le x_0 \le x_2 \le 1
\end{aligned}
$$

5 Performance Evaluation for the Linear Cellular System

In this section, we evaluate the performance of our primary/secondary scheme via both numerical analysis and simulation, and compare it with the CDPA and TDMA schemes.

We consider a standard propagation model for performance evaluation that takes into account Rayleigh fading, lognormal shadowing, and η-th power path loss. Specifically, the power W_R (at the receiver), received from a transmitter located at a distance x away, is given by

$$W_R = \alpha^2 10^{0.1\xi} A x^{-\eta} W_T. \qquad (23)$$

Here, α^2 is an exponentially distributed random variable with unit mean, ξ is a Gaussian random variable with zero mean and variance σ^2, $A x^{-\eta}$ accounts for the path loss and antenna gain, and W_T is the transmitted power, which takes the normalized value of either 1 or γ, depending on the primary/secondary designation of the cell. The propagation loss exponent, η, typically takes values close to 4 [23], and the shadowing parameter, σ, ranges from 5 to 12 dB [20]. As in [5], we assume for simplicity that packet transmissions in different cells are synchronized on a common time-slotted basis, so that transmissions in different cells overlap completely.

17

5.1 Analysis Model

The analytical method for determining the optimal schedule of the primary/secondary SPC scheme is as follows. First, for a given set of G_P and G_S, we compute the capture probabilities $P_P(\cdot)$ and $P_S(\cdot)$. Specifically, we focus on an arbitrary cell, called "cell 0". Let the index "0" denote the intended signal in cell 0, and index "i" denote interference from cell i. Based on the propagation model (Equation (23)) and the capture model (Equation (1)), we can calculate the capture probability as follows:

$$P_P(x_0) = P\left\{\frac{\alpha_0^2 10^{0.1\xi_0} A x_0^{-\eta}}{\sum_{i:even, i\neq 0} \chi_i^P \alpha_i^2 10^{0.1\xi_i} A x_i^{-\eta} + \sum_{i:odd} \chi_i^S \alpha_i^2 10^{0.1\xi_i} A x_i^{-\eta}\gamma} > b\right\} \quad (24)$$

$$P_S(x_0) = P\left\{\frac{\alpha_0^2 10^{0.1\xi_0} A x_0^{-\eta}\gamma}{\sum_{i:even, i\neq 0} \chi_i^S \alpha_i^2 10^{0.1\xi_i} A x_i^{-\eta}\gamma + \sum_{i:odd} \chi_i^P \alpha_i^2 10^{0.1\xi_i} A x_i^{-\eta}} > b\right\}. \quad (25)$$

Here, x_0 is the distance from the intended mobile user to the base-station in cell 0, and x_i is the propagation distance associated with cell i. The binary random variables χ_i^P and χ_i^S indicate whether or not a transmission occurs in cell i when the cell is primary and secondary, respectively: $\chi_i^P = 1$ (with probability G_P), or $\chi_i^S = 1$ (with probability G_S), if a transmission occurs. For downlink communication, x_i is the distance between the intended mobile user and the base-station of cell i, which is determined by x_0. For uplink communication, x_i is the distance between the transmitter in cell i and the base-station in cell 0, which is independent of x_0. In our numerical analysis, we assume that x_i is uniformly distributed in cell i. However, as we discussed previously in Section 4.2, this uniform assumption represents an approximation in the uplink case, since generally the optimal traffic load is not uniform. We will investigate the impact of this approximation by comparing the analysis and simulation results in Section 5.3.2.

We employ numerical integration methods to evaluate Equations (24) and (25). Since α_i^2 is an exponentially distributed random variable, Equation (24) can be simplified to (see [24]):

$$P_P(x_0) = 1 - E\left\{\prod_{i:even} \frac{1}{1 + b\chi_i^P 10^{0.1(\xi_i - \xi_0)}(x_i/x_0)^{-\eta}} \prod_{i:odd} \frac{1}{1 + b\chi_i^S 10^{0.1(\xi_i - \xi_0)}(x_i/x_0)^{-\eta}\gamma}\right\}.$$

Thus, for downlink communication,

$$P_P(x_0) = 1 - E\left\{\prod_{i:even} E\left\{\frac{1}{1 + b\chi_i^P 10^{0.1(\xi_i - \xi_0)}\left(\frac{x_i(x_0)}{x_0}\right)^{-\eta}}\bigg|\xi_0\right\}\right.$$
$$\left.\prod_{i:odd} E\left\{\frac{1}{1 + b\chi_i^S 10^{0.1(\xi_i - \xi_0)}\left(\frac{x_i(x_0)}{x_0}\right)^{-\eta}\gamma}\bigg|\xi_0\right\}\right\}$$

18

$$= 1 - E\left\{\prod_{i:even}\left(1 - G_P E\left\{\frac{b10^{0.1(\xi_i - \xi_0)}\left(\frac{x_i(x_0)}{x_0}\right)^{-\eta}}{1 + b10^{0.1(\xi_i - \xi_0)}\left(\frac{x_i(x_0)}{x_0}\right)^{-\eta}}\Bigg|\xi_0\right\}\right)\right.$$
$$\left.\prod_{i:odd}\left(1 - G_S E\left\{\frac{b10^{0.1(\xi_i - \xi_0)}\left(\frac{x_i(x_0)}{x_0}\right)^{-\eta}\gamma}{1 + b10^{0.1(\xi_i - \xi_0)}\left(\frac{x_i(x_0)}{x_0}\right)^{-\eta}\gamma}\Bigg|\xi_0\right\}\right)\right\}.$$

Here, we use the notation $x_i(x_0)$ to indicate that x_i is completely determined by x_0. For some function h of two random variables X and Y, we use the notation $E\{h(X,Y)|Y\}$ to represent the conditional expectation of $h(X,Y)$ given Y: $E\{h(X,Y)|Y\} = \int h(x,Y)dF_X(x)$, where $F_X(\cdot)$ is the distribution function of X.

For uplink communication,

$$P_P(x_0) = 1 - E\left\{\prod_{i:even}\left(1 - G_P E\left\{\frac{b10^{0.1(\xi_i - \xi_0)}\left(\frac{x_i}{x_0}\right)^{-\eta}}{1 + b10^{0.1(\xi_i - \xi_0)}\left(\frac{x_i}{x_0}\right)^{-\eta}}\Bigg|\xi_0\right\}\right)\right.$$
$$\left.\prod_{i:odd}\left(1 - G_P E\left\{\frac{b10^{0.1(\xi_i - \xi_0)}\left(\frac{x_i}{x_0}\right)^{-\eta}\gamma}{1 + b10^{0.1(\xi_i - \xi_0)}\left(\frac{x_i}{x_0}\right)^{-\eta}\gamma}\Bigg|\xi_0\right\}\right)\right\}$$

We can similarly evaluate $P_S(x_0)$ for downlink and uplink communication.

Once $P_P(\cdot)$ and $P_S(\cdot)$ are available, we calculate the optimal traffic load pair $\{g_P^*(\cdot), g_S^*(\cdot)\}$ in the family $\{G_P, G_S\}$, based on the necessary condition (Theorem 1). In particular, we can solve the optimal pair $\{g_P^*(\cdot), g_S^*(\cdot)\}$ from the single-variable Equations (10)–(12) (or Equations (13)–(15)) for Problem (9). Finally, we obtain the overall optimal solution by enumerating the values of G_P and G_S from 0 to 1.

5.2 Simulation Model

We verify the numerical analysis results by comparing them with simulations. Note that in our analysis, the only performance measure that we have taken into account is the throughput. However, as noted previously, because of capture failure and packet retransmission, delay is also an important performance measure of the capture-based spectrum reuse method. In our simulation, we also will investigate the delay due to retransmissions.

Our simulation model of the linear cellular system consists of 10 cells arranged linearly, where each cell has two adjacent cells. The boundary cells on the two sides are then connected to each other to avoid the "edge effect" at the boundaries. In each cell there are 200 equally-spaced points, and mobile users in the cell are located at those points. In the simulation, packets are transmitted in the cellular system as follows. For uplink communication, during any time-slot one new packet is generated at a point i, independently of packets generated at point $j \neq i$, with probability S_i. Let $S \triangleq \sum_{i=1}^{200} S_i$ be the aggregate new packet arrival rate, which is equal to the aggregate throughput if the system is stable. New packets, after

arrival, are queued at the corresponding points. We assume that by some request signaling, the base-station is notified immediately as soon as a new packet arrives at any point. In other words, the base-station is always aware of the queue length at each point in the cell. In any time-slot, the base-station first decides whether to transmit during that time-slot, with a permission probability β. If so, it selects a user at one point in the cell, according to a scheduling algorithm and the resulting cell partitioning (i.e., the bang-bang control shown in Figure 6), and then instructs the user to transmit a packet in the corresponding queue. The above probabilistic permission scheme is used to avoid congestion, as will be explained later in Section 5.3.1. We use the following probabilistic scheduling algorithm for the base-station to select one of the points in the cell. Suppose that in any time-slot, the queue lengths at all points are q_i, $i = 1, \ldots, 200$. Then, in a primary (secondary) cell, the probability that point i in Region I (Region II) is selected is $q_i / \sum_i q_i$, where the summation is taken over all points in Region I (Region II).

For downlink communication, the base-station of each cell maintains distinct queues for different points in the cell. In any time-slot, one new packet is added into the queue of point i, independently of each other,[3] with probability S_i, as in the uplink communication case. In any time-slot, the base-station first decides whether to transmit during that time-slot, with some given permission probability. If so, it then selects one point in the cell, according to a scheduling algorithm (e.g., the probabilistic algorithm described above) and the cell partition of the primary/secondary cell, and transmits a packet in the corresponding queue.

For both downlink and uplink communication, all transmissions in the cellular system are examined at the receivers, each of which checks Equation (1) to determine whether capture occurs based on the propagation model given in Equation (23). If capture occurs, the transmitted packet is removed from the queue at the point; otherwise, it remains in the queue, waiting for the next transmission opportunity.

5.3 Numerical Results

In our numerical analysis and simulation, we use the following parameters: $\eta = 4$, $\sigma = 6$ dB. The static power control parameter is $\gamma = 0.1$. We assume that mobile users are distributed uniformly in a cell, i.e., $u(x) = \frac{1}{2}$. When we check whether capture occurs, we take into account interference from four closest neighboring cells (i.e., two immediately adjacent, and two next-to-immediately adjacent cells). We find that the impact of interference from farther

---

[3]Here we allow multiple new packets to arrive at the same base-station during the same time-slot, to simulate the common scenario where the base-station simultaneously maintains multiple connections to the fixed network and the transmission rate in the wired link is much faster than in the wireless link.

cells is negligible. As discussed previously in Section 2, the capture ratio b is an important parameter that reflects the physical layer requirement for reliable communication, such as the requirement on bit error rate (BER) or outage probability. In this study, we consider three scenarios, $b = 6$, 10, and 15 dB, to represent various technologies in current and future wireless systems.

We compare our primary/secondary SPC scheme with both CDPA and TDMA for different values of the capture ratio. Since CDPA can be viewed as a simplified version of the SPC scheme with $G_P = G_S \triangleq G$ and $\gamma = 1$, the methods of numerical analysis and simulation for CDPA are similar to what have been described for the SPC scheme. Strictly speaking, in standard TDMA, we have to adjust the reuse distance (and reuse factor) for different values of the capture ratio. However, here we consider packet-switched TDMA, which does not maintain continuous connections and allows packet retransmission, in contrast with the circuit-switched case. We set the reuse factor to 2 (hence, the packet-switched TDMA system that we study here is almost the same as CDPA, except that every other cell, instead of all cells, are allowed to transmit in any time-slot). Note that if the standard circuit-switched TDMA is used, since no collisions are permitted, it would require a reuse factor strictly larger than 2, and hence the maximum throughput would be less than 1/3. However, we find that in all our numerical results, the throughput of the packet-switched TDMA system that we use exceeds 0.4. Therefore, our comparison is with a fairer (and better in terms of throughput) version of TDMA.

5.3.1 Maximum Throughput with the Uniform Fairness Constraint

In this section, we investigate Problem (9) via numerical analysis. Specifically, we consider the uniform fairness constraint, i.e., the throughput remains the same for users at different locations in a cell. For a set of aggregate traffic loads G_P and G_S in the SPC scheme, we calculate the overall throughput S using Equation (16). By varying G_P and G_S from 0 to 1, we obtain the overall optimal throughput for the SPC scheme. We can similarly investigate the optimal throughputs for CDPA and TDMA, using Equation (17). Note that for TDMA, the numerator of Equation (17) should be changed to $\frac{G}{2}$, instead of G, due to time-slot subdivision with reuse factor 2.

Figure 9 plots S versus G for downlink communication in CDPA and TDMA, with $b = 6$, 10, and 15 dB. Figure 10 plots downlink S versus G_P and G_S in the SPC scheme when $b = 6$, 10, and 15 dB.

We find that when $b = 6$ dB, because capture occurs relatively easily, CDPA achieves better throughput than TDMA. However, the SPC scheme outperforms TDMA by 85% and

21
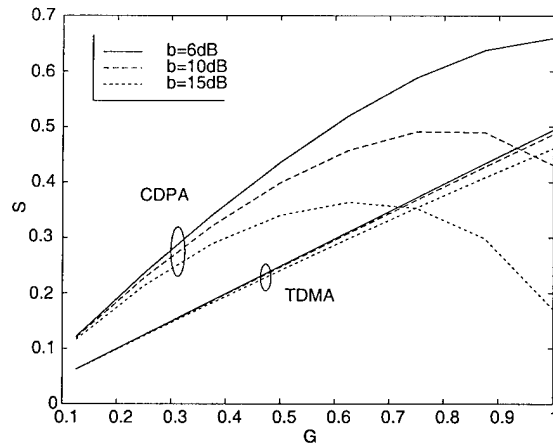
Figure 9: Plot of downlink optimization for Problem (9) with CDPA and TDMA

CDPA by 35% in terms of maximum throughput.

If we increase the capture ratio to 10 dB, the throughput curve of CDPA reaches a maximum for $G < 1$. This indicates that CDPA suffers congestion because of excessive intercellular interference. In reality, to avoid congestion and instability, we have to ensure that G does not exceed the maximum point. To limit the aggregate traffic load, in our simulation the base-station uses the probabilistic permission scheme to decide whether to transmit—if a user is scheduled for transmission, it transmits with a given fixed permission probability. From Figure 9, it is clear that at $b = 10$ dB, the improvement of CDPA over TDMA is marginal. However, the SPC scheme outperforms both by more than 50% in terms of maximum throughput. An interesting observation is that the throughput surface shown in Figure 10(b) reaches the maximum point at $G_P = 1$ and $G_S = 1$. Thus we can see that although spectrum is reused in all cells in our SPC scheme, the same as in CDPA, the interference is reduced, and the power control scheme significantly improves the capture probability.

If we further increase the capture ratio to 15 dB, the excessive interference dramatically reduces the throughout in CDPA, which performs even worse than TDMA in this case. Note that in the SPC scheme, the maximum throughput also is not reached at that point where $G_P = 1$ and $G_S = 1$, indicating that many retransmissions may occur even with the static power control scheme. From Figure 10(c), we find that the SPC scheme outperforms TDMA by 26% and CDPA by 60% in terms of maximum throughput.

Similarly, we compare the throughput performance for the uplink communication, and find that the results are similar. We summarize the maximum throughputs, for both uplink and downlink communication, of the SPC scheme, CDPA and TDMA for different values of the capture ratio in Table 1.

22
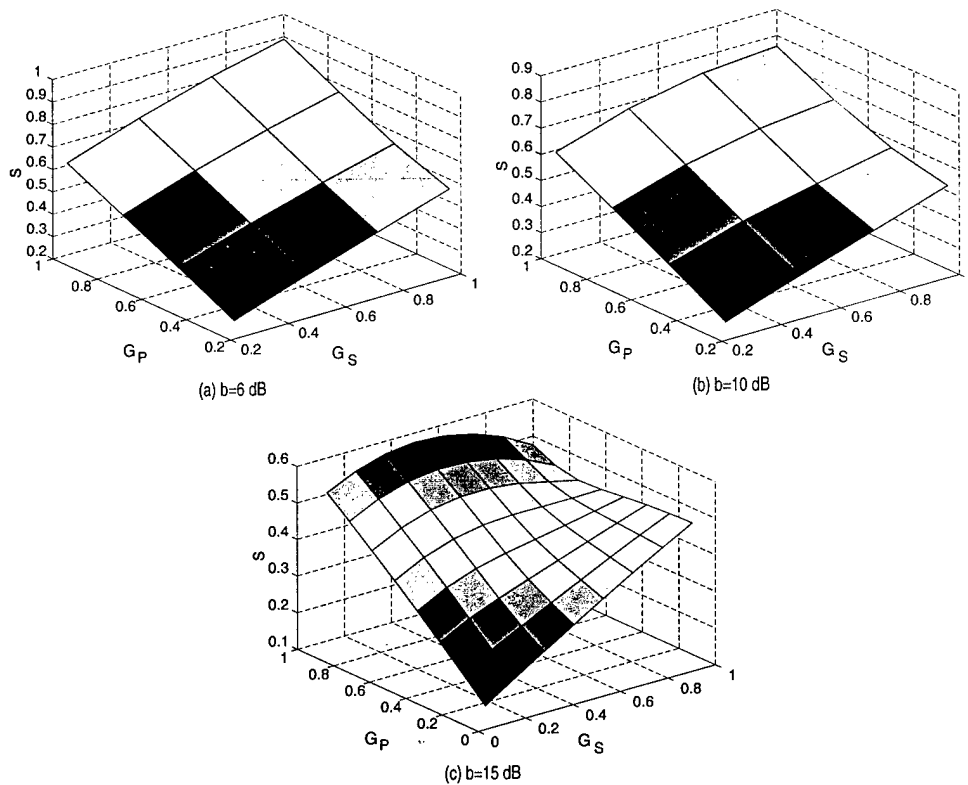
Figure 10: Plot of downlink optimization for Problem (9) with SPC scheme: (a) $b = 6$ dB, (b) $b = 10$ dB and (c) $b = 15$ dB.

5.3.2 Throughput-Delay Tradeoff with Uniform Fairness Constraint

In this section, we provide *simulation results* to verify the analysis presented in Section 5.3.1, especially for the results in uplink communication, which were derived based on the simplifying assumption made in Section 4.2.

Recall that from Table 1, in uplink communication, the SPC scheme can achieve maximum throughputs of 0.90, 0.81, and 0.62 with $b = 6$, 10, and 15 dB, respectively, for Problem (9). Through simulations, we find that the SPC scheme can in fact achieve throughputs that are close to these predicted maximum values. However, the associated delays can be large. We observe similar phenomena with both CDPA and TDMA, and also in downlink communication.

To make the comparisons more meaningful, we next investigate the throughput-delay tradeoff. Specifically, for a given new packet arrival rate S (which is equal to the throughput in a stable system), we estimate the expected delay D in terms of time-slots that a packet experiences from the instant of arrival to the instant when the packet is successfully received. This figure includes both queueing delay and retransmissions. To maintain uniform throughput in a cell, the new packet arrival rate at any point is given by $S_i = S/200$. Since we are

	Downlink			Uplink		
Capture ratio	$b = 6$ dB	$b = 10$ dB	$b = 15$ dB	$b = 6$ dB	$b = 10$ dB	$b = 15$ dB
SPC	0.88	0.73	0.51	0.90	0.81	0.62
CDPA	0.66	0.49	0.36	0.80	0.65	0.41
TDMA	0.49	0.48	0.46	0.50	0.49	0.47

Table 1: A Comparison of the maximum achievable throughput using CDPA, TDMA and the SPC scheme
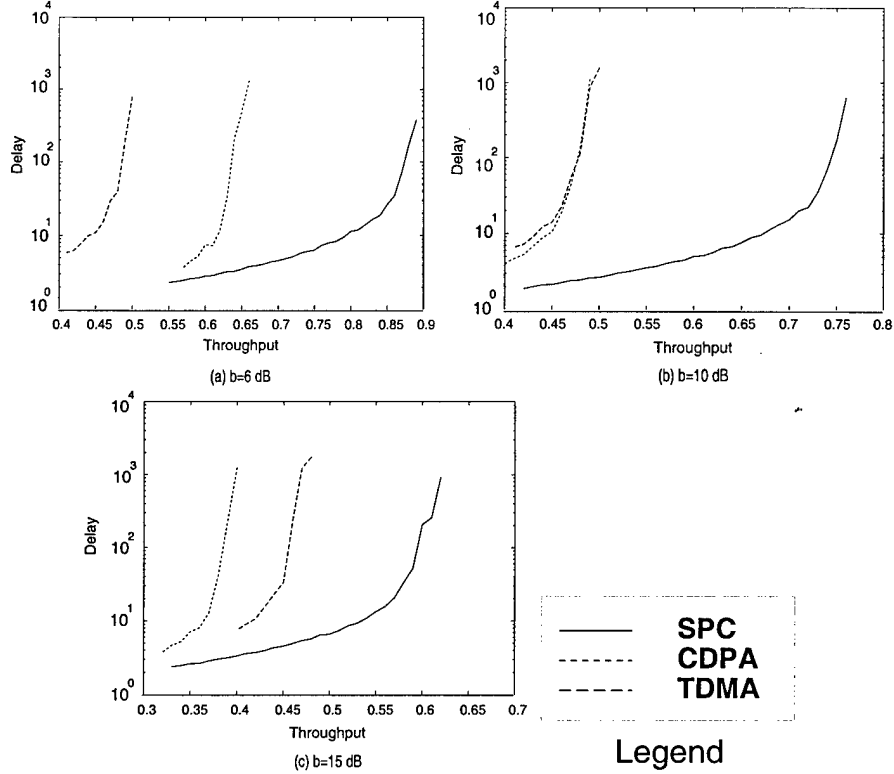
Figure 11: Downlink throughput-delay tradeoff comparison: (a) $b = 6$ dB, (b) $b = 10$ dB and (c) $b = 6$ dB (d) Legend.

interested in the performance of a typical cell, the statistics obtained are averaged over all cells.

The probabilistic permission scheduling method is used in the simulation to control congestion in CDPA and the SPC scheme, as discussed in Section 5.3.1. The value of the permission probability is set to be the aggregate traffic load(s) that achieves the maximum throughput in the numerical analysis of Problem (9). For example, with $b = 15$ dB in downlink communication, the permission probability is equal to 1 or 0.5 during the primary or secondary period, respectively, in the SPC scheme (see Figure 10(c)).

We calculate the cell partitioning parameter x_0 by solving Problem (9), and use this parameter in the simulation of the SPC scheme to obtain the individual curves in Figure 11.

Capture ratio	$b = 6$ dB		$b = 10$ dB		$b = 15$ dB	
Delay constraint (time-slots)	10	10^3	10	10^3	10	10^3
SPC	0.80	0.90	0.72	0.80	0.55	0.62
CDPA	0.75	0.80	0.57	0.62	0.36	0.40
TDMA	0.45	0.50	0.44	0.49	0.41	0.46

Table 2: A comparison of uplink throughput-delay tradeoff using CDPA, TDMA and the SPC scheme.

In Figure 11(a) we show the expected delay versus throughput for the SPC scheme, CDPA, and TDMA, in downlink communication with $b = 6$ dB. All three curves show that the delay increases with the throughput. In particular, the delay rises rapidly when the throughput approaches the maximum value, a common phenomenon in queueing theory. The maximum value of the throughput observed in the simulation given by Figures11(a)–(c) (i.e, the throughputs close to the asymptotic values of the delays in these curves) is very close to that obtained in the analysis (given by Table 1), for all three schemes. We find that the delays due to retransmission can be quite low with both the SPC scheme and CDPA, as long as we operate slightly (typically 5%) under the maximum value. For a fixed expected delay, say 10 time-slots, we compare the associated throughput of the three schemes, and find that the SPC scheme outperforms TDMA by 80% and CDPA by 30%.

In Figure 11(b), we show the expected delay versus throughput curves in downlink communication with $b = 10$ dB. It can be seen that the throughput-delay curves with CDPA and TDMA are very close. This is not surprising since the numerical analysis showed that the maximum achievable throughput with CDPA and TDMA are almost the same (see Table 1). For an expected delay of 10 time-slots, the SPC scheme outperforms TDMA by 55% and CDPA by 50%.

In Figure 11(c), we show the expected delay versus throughput in downlink communication with $b = 15$ dB. In this case, TDMA actually outperforms CDPA, which is again consistent with the observation from the analytical results in Table 1. For the expected delay of 10 time-slots, the SPC scheme outperforms TDMA by 17% and CDPA by 47%.

We also compare the expected delay versus throughput in uplink communication. To save space, we summarize the simulation results in Table 2. Detailed curves can be found in [15]. We find that the performance in uplink communication is similar to that in downlink communication, and is consistent with the analysis in Section 5.3.1. In particular, the maximum value observed in simulation is close to that obtained via analysis, for all three schemes and all the choices of b. This indicates that the simplifying assumption made in Section 4.2 and in [5] seems reasonable.
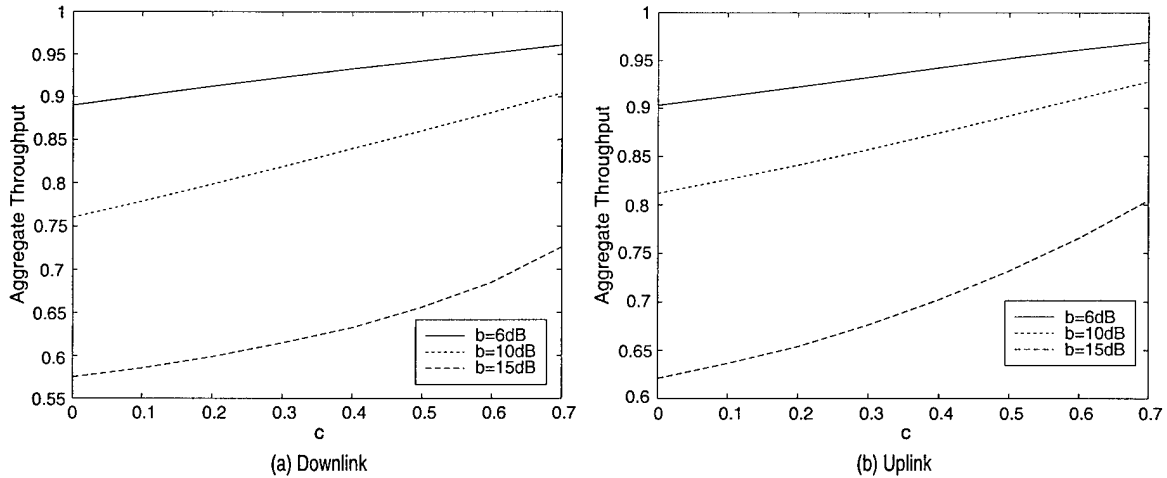
Figure 12: Aggregate throughput with nonuniform fairness constraint

5.3.3 Aggregate Throughput with Nonuniform Fairness Constraint

In all the above numerical examples, we have considered the uniform fairness constraint, which is a typical fairness constraint considered in the literature. However, in reality we may want to relax a strict fairness constraint to increase the overall throughput in the system. Here, we investigate the performance improvements with a nonuniform fairness constraint. Specifically, we consider Problem (19). We analytically determine the optimal aggregate throughput by solving the parametric optimization problem (21), when c, the relative difference between the maximum and minimum throughputs, varies from 0% to 70%. In Figure 12, we plot the optimal aggregate throughput versus c for $b = 6$, 10, and 15 dB, in downlink and uplink communication respectively. As we expect, further gains in throughput are obtained by allowing nonuniformness in the constraint, especially when b is large.

6 An Extension to the Planar (2-D) Case

So far, we have explored the primary/secondary SPC scheme for the linear cellular network. In this section, we extend the same idea to the 2-D hexagonal configuration.

Recall that in the linear case, users are scheduled for transmission in complementary locations in the primary and secondary cells. In the linear system, the location of a user is characterized by its distance to the base-station and thus can be estimated, for example, by measuring and taking the average of signal powers in previous transmissions (assuming that the user location does not change rapidly compared to the random fluctuation in the propagation conditions such as fading and shadowing). In this section, we develop a heuristic
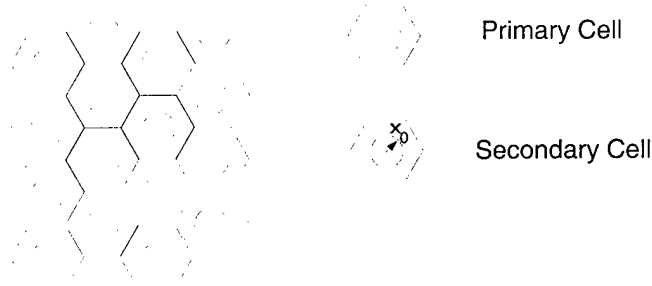
Figure 13: Primary/secondary Scheduling Scheme in 2-D Case

static power control scheme for the 2-D case based on our understanding of the optimal solution derived for the linear case.

In our 2-D scheme, primary and secondary carriers are assigned as follows. We partition all the carriers in the system into three distinct sets. Cells are also partitioned into three sets, such that every one set of cells are assigned one carrier-set as primary carriers and the remaining two sets as secondary carriers.

Our heuristic scheduling scheme is as follows. In each cell, users within a distance x_0 away from the base-station are scheduled for transmission only in a secondary cell, while users in the remaining region of the cell are scheduled for transmission only in a primary cell, as shown in Figure 13. The parameter x_0 indicates the service coverage in the secondary cell when the reduced power γW_T is employed, which is an important design parameter for balancing the traffic loads in the primary and secondary cells. We adopt the probabilistic scheduling method with permission probabilities β_P and β_S in the primary and secondary cells, respectively, to avoid excessive packet retransmission and capture failure, as described in Section 5.

We next investigate the performance of this heuristic scheduling scheme, and compare it with both TDMA and CDPA. In particular, we consider the following optimization problem for the SPC scheme:

$$\begin{array}{cl} \underset{\gamma, x_0, \beta_P, \beta_S}{\text{minimize}} & D \\ \text{subject to} & s(x, y) = \dfrac{S}{A_{cell}} \end{array} \qquad (26)$$

where D is the expected delay, and $s(x, y)$ is the throughput density at a location having coordinates (x, y) in the plane. The quantity A_{cell} represents the area of a cell, while S is the aggregate new packet arrival rate (throughput). This constraint requires that the new packet arrival density be uniform in the cell. Note that in CDPA there is no difference between the primary and secondary cells, and there is no cell partition. Thus, we have $\gamma = 1$,

27

	Downlink					
Capture ratio	$b = 6$ dB		$b = 10$ dB		$b = 15$ dB	
Delay constraint (time-slots)	40	10^3	40	10^3	40	10^3
SPC	0.413	0.437	0.294	0.303	0.152	0.158
CDPA	0.287	0.299	0.173	0.180	0.096	0.103
TDMA	0.291	0.313	0.251	0.258	0.151	0.153
	Uplink					
SPC	0.444	0.466	0.302	0.316	0.161	0.172
CDPA	0.326	0.330	0.177	0.187	0.096	0.103
TDMA	0.292	0.306	0.253	0.265	0.161	0.172

Table 3: A comparison of throughput-Delay tradeoff in the 2-D case using CDPA, TDMA and the SPC scheme.

$\beta_P = \beta_S \triangleq \beta$, and the parameter x_0 does not appear in the CDPA algorithm. Therefore, a similar optimization problem is defined for the CDPA by replacing $\gamma, x_0, \beta_P, \beta_S$ by β. For the TDMA, we simply set $\gamma = 0$, $x_0 = 0$, $\beta_P = 1$, and $\beta_S = 0$, and there is no need to optimize any parameter.

We conduct the performance evaluation via simulation. The simulation is similar to that in the linear case described in Section 5. In our simulation, we use the following parameters for the wireless propagation model: $\eta = 4$, $\sigma = 6$ dB.

The throughput-delay tradeoff curves in the 2-D case are similar to these in Figure 11. To save space, we summarize those simulation results in Table 3, where we provide the throughput of CDPA, TDMA, and the SPC scheme, when the resultant delay is 40 or 1000 time-slots, and $b = 6$, 10, and 15 dB, respectively. We next make some observations for the downlink case. Similar observations can be made for the uplink case.

We observe that the performances of CDPA and TDMA are quite close with $b = 6$. For a given expected delay requirement, say 40 time-slots, the SPC scheme has a 40% throughput gain over both CDPA and TDMA. It is interesting to recall that we had a similar observation in the linear case, but with $b = 10$ dB there.

In the case of $b = 10$ dB, it can be seen that CDPA indeed performs the worst among the three schemes. This agrees with the results in [5] where it was shown that TDMA, with reuse factor 3, can outperform CDPA when $b = 10$ dB. For the expected delay of 40 time-slots, the SPC scheme has 17% throughput gain over TDMA.

When the capture ratio is increased to $b = 15$ dB. We find that CDPA performs much worse than the SPC and TDMA schemes. It is interesting to note that the throughput gain of the SPC scheme over TDMA is relatively small. This is because with such a stringent capture ratio requirement of $b = 15$ dB, we have to choose a very low power parameter γ

28

which in turn results in a very small coverage x_0 of the secondary cell. Hence, there are very few users that can take the advantage of transmissions in the secondary cells in this case.

7 Conclusion

We have presented a static power control scheme in packet-switched wireless systems. Our basic idea is to reduce intercellular interference and improve the capture probability by setting the transmission powers of users of different cells in an optimal fashion. The assignment of powers is determined beforehand and no real-time intercellular coordination is required. The power control is static and fixed, leading to simplicity in implementation.

We have formulated and solved an optimal scheduling problem for our SPC scheme. We find that the optimal scheduling policy is in a simple form of bang-bang control: each cell is partitioned so that users in different regions are served with different levels of transmission power. We illustrate our scheduling solution by considering two specific cases with uniform and nonuniform fairness constraints.

We have evaluated, via numerical analysis and simulation, two important performance measures of the SPC scheme, throughput and delay, and compared them with both CDPA and TDMA. We find that the SPC scheme can achieve significant performance improvements, in terms of both maximum throughput and throughput-delay tradeoff, over a wide range of the capture ratio values.

APPENDIX

A Proof of Theorem 1

To prove Theorem 1, we need the following two lemmas.

Lemma 1 *Let $\{g_P(\cdot), g_S(\cdot)\}$ be a traffic load density pair in the family $\{G_P, G_S\}$, and $s(\cdot)$ the associated throughput density function. Suppose that $s'(\cdot)$ is another throughput density that satisfies the constraint $h(s'(\cdot)) \geq 0$ and there exists a subset $\Phi \subset [0,1]$ such that $s(x) > s'(x)$ for all $x \in \Phi$, and $s(x) = s'(x)$ for all $x \in [0,1] \setminus \Phi$. Then there exists another traffic load pair, $\{\hat{g}_P(\cdot), \hat{g}_S(\cdot)\}$, also in the family $\{G_P, G_S\}$, such that the resultant throughput $\hat{s}(\cdot)$ satisfies $h(\hat{s}(\cdot)) \geq 0$ and $f(\hat{s}(\cdot)) > f(s'(\cdot))$.*

Proof: We prove this lemma by construction. Let $\hat{g}_P(\cdot)$ and $\hat{g}_S(\cdot)$ be constructed as follows:

$$\hat{g}_P(x) = g_P(x)\frac{s'(x)}{s(x)} + \frac{1}{P_P(x)}\frac{\int_\Phi g_P(x)(1 - \frac{s'(x)}{s(x)})\, dx}{\int_0^1 \frac{1}{P_P(x)}\, dx}, \qquad (27)$$

29

$$\hat{g}_S(x) \;=\; g_S(x)\frac{s'(x)}{s(x)} + \frac{1}{P_S(x)}\frac{\int_\Phi g_S(x)\left(1 - \frac{s'(x)}{s(x)}\right)dx}{\int_0^1 \frac{1}{P_S(x)}\,dx}. \tag{28}$$

To show that the above traffic load pair suffices for our purpose, we need to: (1) show that it belongs to the family $\{G_P, G_S\}$; and (2) check the resultant throughput. To this end, note that

$$
\begin{aligned}
\int_0^1 \hat{g}_P(x)\,dx &= \int_0^1 g_P(x)\frac{s'(x)}{s(x)}\,dx + \int_0^1 \frac{1}{P_P(x)}\,dx\,\frac{\int_\Phi g_P(x)\left(1 - \frac{s'(x)}{s(x)}\right)dx}{\int_0^1 \frac{1}{P_P(x)}\,dx} \\
&= \int_0^1 g_P(x)\frac{s'(x)}{s(x)}\,dx + \int_\Phi g_P(x)\left(1 - \frac{s'(x)}{s(x)}\right)dx \\
&= \int_0^1 g_P(x)\frac{s'(x)}{s(x)}\,dx + \int_0^1 g_P(x)\left(1 - \frac{s'(x)}{s(x)}\right)dx \\
&= \int_0^1 g_P(x)\,dx \\
&= \frac{G_P}{2}.
\end{aligned}
$$

Similarly it can be shown that $\int_0^1 \hat{g}_S(x)\,dx = \frac{G_S}{2}$. Thus, $\{\hat{g}_P(\cdot), \hat{g}_S(\cdot)\}$ belongs to the family $\{G_P, G_S\}$. We next calculate the resultant throughput $\hat{s}(x)$:

$$
\begin{aligned}
\hat{s}(x) &= \frac{1}{2}\left(g_P(x)\frac{s'(x)}{s(x)}P_P(x) + \frac{\int_\Phi g_P(x)\left(1 - \frac{s'(x)}{s(x)}\right)dx}{\int_0^1 \frac{1}{P_P(x)}\,dx} + g_S(x)\frac{s'(x)}{s(x)}P_S(x) \right. \\
&\qquad \left. + \frac{\int_\Phi g_S(x)\left(1 - \frac{s'(x)}{s(x)}\right)dx}{\int_0^1 \frac{1}{P_S(x)}\,dx} \right) \\
&= s'(x) + \frac{1}{2}\left(\frac{\int_\Phi g_P(x)\left(1 - \frac{s'(x)}{s(x)}\right)dx}{\int_0^1 \frac{1}{P_P(x)}\,dx} + \frac{\int_\Phi g_S(x)\left(1 - \frac{s'(x)}{s(x)}\right)dx}{\int_0^1 \frac{1}{P_S(x)}\,dx} \right). \tag{29}
\end{aligned}
$$

Note that the last two terms in Equation (29) are positive constants, since $1 - \frac{s'(x)}{s(x)} > 0$ for $x \in \Phi$. From condition (C1), it follows that $h(\hat{s}(\cdot)) \geq 0$ and $f(\hat{s}(\cdot)) > f(s'(\cdot))$. ∎

Lemma 2 *Let Φ_1, Φ_2 be two subsets of $[0,1]$ satisfying*

$$\sup_{x\in\Phi_1} \frac{P_P(x)}{P_S(x)} < \inf_{x\in\Phi_2} \frac{P_P(x)}{P_S(x)}, \tag{30}$$

Suppose that $\{g_P(\cdot), g_S(\cdot)\}$ is a traffic load pair in the family $\{G_P, G_S\}$ such that $\inf_{x\in\Phi_1} g_P(x) > 0$, and $\inf_{x\in\Phi_2} g_S(x) > 0$. Then there exists another traffic load pair $\{g'_P(\cdot), g'_S(\cdot)\}$ in the family $\{G_P, G_S\}$, such that the resultant throughput satisfies $s'(x) > s(x)$ for all $x \in \Phi_2$ and $s'(x) = s(x)$ elsewhere.

Proof: We prove this lemma by construction. First, for $x \in [0,1] \setminus (\Phi_1 \cup \Phi_2)$, we simply set $g'_P(x) = g_P(x)$ and $g'_S(x) = g_S(x)$. For $x \in \Phi_1$, we "perturb" $g_P(x)$ and $g_S(x)$ as follows:

$$g'_P(x) = g_P(x) - \theta g_P(x),$$
$$g'_S(x) = g_S(x) + \Delta g_S(x),$$

with $0 < \theta \leq 1$ is a constant, and $\Delta g_S(x) > 0$. To maintain $s'(x) = s(x)$ for $x \in \Phi_1$, we set $\Delta g_S(x) = \frac{P_P(x)}{P_S(x)} \theta g_P(x)$. We will determine θ later.

Meanwhile, to keep the new traffic load within the family $\{G_P, G_S\}$, we can set $g'_P(x), g'_S(x)$ for $x \in \Phi_2$ as follows:

$$g'_P(x) = g_P(x) + \Delta_P$$
$$g'_S(x) = g_S(x) - \Delta_S$$

where Δ_P and Δ_S are two constants given by

$$\Delta_P = \theta \frac{\int_{\Phi_1} g_P(z) dz}{\int_{\Phi_2} dz}$$
$$\Delta_S = \theta \frac{\int_{\Phi_1} g_S(z) dz}{\int_{\Phi_2} dz}.$$

Since $\inf_{x \in \Phi_1} g_P(x) > 0$ and $\inf_{x \in \Phi_2} g_S(x) > 0$, we can always find sufficiently small θ such that $g'_P(x) \geq 0$ for $x \in \Phi_1$, and $g'_S(x) \geq 0$ for $x \in \Phi_2$. Thus, this new traffic load pair is valid.

Now, we need to show that for any $x \in \Phi_2$, the resultant throughput $s'(x)$ satisfies $s'(x) > s(x)$. Note that for $x \in \Phi_2$, we have

$$
\begin{aligned}
\frac{\Delta_P P_P(x)}{\Delta_S P_S(x)} &= \frac{\int_{\Phi_1} g_P(z) dz}{\int_{\Phi_1} P_P(z)/P_S(z) g_P(z) dz} \frac{P_P(x)}{P_S(x)} \\
&\geq \frac{\int_{\Phi_1} g_P(z) dz}{\sup_{z \in \Phi_1} (P_P(z)/P_S(z)) \int_{\Phi_1} g_P(z) dz} \frac{P_P(x)}{P_S(x)} \\
&> 1,
\end{aligned}
$$

where the last inequality follows immediately from Equation (30). Thus, for any $x \in \Phi_2$, we have $s'(x) > s(x)$. ∎

Lemma 2 provides an insight on the result of Theorem 1. Note that in the primary/secondary SPC scheme, the transmission power in a secondary cell is lower than that in a primary cell. Thus, in general, capture is more likely to occur in a primary cell. However,

the quantitative difference between $P_P(x)$ and $P_S(x)$ may vary for different locations x, and the optimal schedule can be achieved by intelligently distributing traffic load in the primary and secondary cells. From the proof of Lemma 2, we know that $P_P(x)/P_S(x)$, the ratio of the capture probabilities, plays a key role in determining the optimal schedule. Consider two scheduling policies that have the same value of the aggregate traffic load and only differ in two distinct intervals A and B. If the ratio of capture probabilities are always higher in interval A than in interval B, then scheduling more traffic in interval A in a primary cell and more traffic in interval B in a secondary cell yields higher throughput. Repetitively applying this observation eventually leads to the bang-bang control form of the optimal schedule.

We are now ready to prove Theorem 1.

Proof of Theorem 1: Let

$$\alpha_1 \triangleq \sup\{\alpha | g_P^*(x) = 0 \text{ for all } x \text{ such that } \frac{P_P(x)}{P_S(x)} < \alpha\}$$

$$\alpha_2 \triangleq \inf\{\alpha | g_S^*(x) = 0 \text{ for all } x \text{ such that } \frac{P_P(x)}{P_S(x)} > \alpha\}.$$

If $\alpha_1 \geq \alpha_2$, then the theorem is already proven by arbitrarily choosing $\alpha_0 \in [\alpha_2, \alpha_1]$.

Let the resultant throughput density of the optimal traffic load pair $\{g_P^*(\cdot), g_S^*(\cdot)\}$ be $s^*(\cdot)$. We next show, by contradiction, that α_1 can never be less than α_2. Assume that $\alpha_1 < \alpha_2$. By definition, we can choose two sufficiently small positive numbers ϵ_1 and ϵ_2 satisfying $\alpha_1 + \epsilon_1 < \alpha_2 - \epsilon_2$, and there exist $R_1, R_2 \in [0,1]$ such that $g_P^*(R_1) > 0$, $\frac{P_P(R_1)}{P_S(R_1)} < \alpha_1 + \epsilon_1$, and $g_S^*(R_2) > 0$, $\frac{P_P(R_2)}{P_S(R_2)} > \alpha_2 - \epsilon_2$.

Since $g_P^*(\cdot)$, $g_S^*(\cdot)$, and $\frac{P_P(\cdot)}{P_S(\cdot)}$ are piecewise continuous on $[0,1]$, we can find two intervals Φ_1 and Φ_2, covering R_1 and R_2 respectively, such that $\inf_{x_1 \in \Phi_1} g_P^*(x_1) > 0$, $\inf_{x_2 \in \Phi_2} g_S^*(x_2) > 0$, and $\sup_{x_1 \in \Phi_1} \frac{P_P(x_1)}{P_S(x_1)} < \inf_{x_2 \in \Phi_2} \frac{P_P(x_2)}{P_S(x_2)}$. Then by Lemma 2, there exists another traffic load pair $\{g_P'(\cdot), g_S'(\cdot)\}$, also in the family $\{G_P, G_S\}$, that results in a throughput which is equal to $s^*(x)$ everywhere, except on Φ_2 where the new throughput is higher than $s^*(x)$. Further, by Lemma 1, we can find another traffic load pair $\{\hat{g}_P'(\cdot), \hat{g}_S'(\cdot)\}$, also in the family $\{G_P, G_S\}$, that results in a throughput function $\hat{s}'(\cdot)$ which satisfies the constraint and has a higher value of the objective function. This contradicts the premise that $s^*(\cdot)$ is the optimal throughput. ∎

B   Proof of Theorem 2

Let $\{g_P^*(\cdot), g_S^*(\cdot)\}$ denote the optimal traffic load pair of Problem (19). Define $s_1 \triangleq \sup_x s_u^*(x)$, $s_2 \triangleq \inf_x s_u^*(x)$, and $\Pi \triangleq \{x | s_2 < s_u^*(x) < s_1\}$. We will first show, by contradiction, that Π is in fact an empty set.

Let $x_0 \in \Pi$. Since $s_u^*(\cdot)$ is piecewise continuous, there exists an interval Γ_1 covering x_0 such that for all $x \in \Gamma_1$, $s_2 < s_u^*(x) < s_1$. Now because the set $\{x | P_P(x)/P_S(x) = \alpha_0\}$ has zero length, we can always find $x_1 \in \Gamma_1$ such that $P_P(x_1)/P_S(x_1) \neq \alpha_0$. Without loss of generality, suppose that $P_P(x_1)/P_S(x_1) > \alpha_0$. Because of the continuity of $P_P(\cdot)/P_S(\cdot)$, there exists a number $\epsilon > 0$ such that for all $x \in [x_1 - \epsilon, x_1 + \epsilon]$, $P_P(x)/P_S(x) > \alpha_0$. Also note that from Equation (6), $s_u^*(x) = \frac{1}{2} g_P^*(x) P_P(x)/u(x)$ for all $x \in [x_1 - \epsilon, x_1 + \epsilon]$.

Consider now the interval $\Gamma_2 \triangleq \Gamma_1 \cap [x_1 - \epsilon, x_1 + \epsilon]$. Clearly, Γ_2 has non-zero length. For a given number $\beta \in [0,1]$, let $\Gamma_\beta \triangleq \{x \in \Gamma_2 | P_P(x) > \beta\}$. Since $P_P(x)$ is continuous, there exists a positive number β_0 such that $\int_{\Gamma_{\beta_0}} dx = \frac{1}{2} \int_{\Gamma_2} dx$.

We next "perturb" the optimal traffic load $g_P^*(x)$ for $x \in \Gamma_2$ as follows:

$$g_P'(x) = \begin{cases} g_P^*(x) + \Delta, & x \in \Gamma_{\beta_0} \\ g_P^*(x) - \Delta, & x \in \Gamma_2 \setminus \Gamma_{\beta_0} \end{cases}$$

where Δ is a sufficiently small positive number such that: (1) $\Delta \leq g_P^*(x)$ for all $x \in \Gamma_2 \setminus \Gamma_{\beta_0}$; (2) $P_P(x)\Delta/u(x) \leq s_1 - s_u^*(x)$ for all $x \in \Gamma_{\beta_0}$; and (3) $P_P(x)\Delta/u(x) \leq s_u^*(x) - s_2$ for all $x \in \Gamma_2 \setminus \Gamma_{\beta_0}$.

From the choice of β_0 we know that $\int_{\Gamma_2} g_P'(x)\, dx = \int_{\Gamma_2} g_P^*(x)\, dx$. Therefore, the new traffic load pair still belongs to the family $\{G_P, G_S\}$. Let $s_u'(\cdot)$ denote the resultant throughput per user of the new traffic load pair $\{g_P'(\cdot), g_S'(\cdot)\}$. The choice of Δ ensures that $s_u'(\cdot)$ satisfies the constraint of Problem (19), since $s_2 \leq s_u'(x) \leq s_1$.

We next compare the aggregate throughput:

$$\begin{aligned} \int_{\Gamma_2} s_u'(x)u(x)\, dx &= \int_{\Gamma_{\beta_0}} s_u'(x)u(x)\, dx + \int_{\Gamma_2 \setminus \Gamma_{\beta_0}} s_u'(x)u(x)\, dx \\ &= \int_{\Gamma_2} s_u^*(x)u(x)\, dx + \frac{1}{2}\Delta \Big(\int_{\Gamma_{\beta_0}} P_P(x)\, dx - \int_{\Gamma_2 \setminus \Gamma_{\beta_0}} P_P(x)\, dx \Big) \\ &> \int_{\Gamma_2} s_u^*(x)u(x)\, dx + \frac{1}{2}\Delta \Big(\int_{\Gamma_{\beta_0}} dx - \int_{\Gamma_2 \setminus \Gamma_{\beta_0}} dx \Big) \beta_0 \\ &= \int_{\Gamma_2} s_u^*(x)u(x)\, dx \end{aligned}$$

The above inequality holds due to the fact that for all $x_1 \in \Gamma_{\beta_0}, x_2 \in \Gamma_2 \setminus \Gamma_{\beta_0}, we have P_P(x_1) > \beta_0 \geq P_P(x_2)$. Therefore, we find that the aggregate value of s_u' is even greater than that of s_u^*. This contradicts the premise that s_u^* is the optimal throughput per user. Hence, Π must be empty. In other words, $s_u^*(x)$ can only take one of two values, s_1 or s_2.

To proceed, we next consider the optimal throughput for $x \in \Phi_P$. Let $\beta_{P1} = \inf\{P_P(x) | s_u^*(x) = s_1, x \in \Phi_P\}$ and $\beta_{P2} = \sup\{P_P(x) | s_u^*(x) = s_2, x \in \Phi_P\}$. We first assume that $\beta_{P2} > \beta_{P1}$. Then, by definition, there exist positive numbers ϵ_1, ϵ_2 and $R_1, R_2 \in \Phi_P$ such that $P_P(R_2) = \beta_{P2} - \epsilon_2 > \beta_{P1} + \epsilon_1 = P_P(R_1)$ and $s_u^*(R_1) = s_1, s_u^*(R_2) = s_2$. Since $s_u^*(\cdot)$ is

piecewise continuous and $P_P(\cdot)$ is continuous, there exist two intervals Ω_1 and $\Omega_2 \subset \Phi_P$, covering R_1 and R_2, respectively, such that: (1) $\int_{\Omega_1} dx = \int_{\Omega_2} dx$; and (2) for all $x_1 \in \Omega_1, x_2 \in \Omega_2$, $P_P(x_2) > P_P(x_1)$, $s_u^*(x_1) = s_1$, and $s_u^*(x_2) = s_2$.

We next "perturb" the optimal traffic load as follows,

$$g_P'(x) = \begin{cases} g_P^*(x) + \Delta, & x \in \Omega_2 \\ g_P^*(x) - \Delta, & x \in \Omega_1 \end{cases}$$

By choosing a sufficiently small positive Δ, similar to the previous analysis of perturbing $g_P^*(x)$ for $x \in \Gamma_2$, it can be shown that the aggregate throughput of the new traffic load $g_P'(\cdot)$ is greater than that of $g_P^*(\cdot)$, which is supposed to be the optimal. By contradiction, we conclude that $\beta_{P2} \leq \beta_{P1}$. Now by choosing any $\beta_P \in [\beta_{P2}, \beta_{P1}]$, Equation (20) follows immediately.

Clearly, the same analysis can be applied when $x \in \Phi_S$. ∎

References

[1] A. Acampora, "Wireless ATM: a perspective on issues and prospects," *IEEE Personal Communications Magazine*, pp. 8–17, August 1996.

[2] P. Agrawal, E. Hyden, P. Krzyzanowski, P. Mishra, M. Srivastava, and J. Trotter, "SWAN: a mobile multimedia wireless network," *IEEE Personal Communications Magazine*, pp. 18–33, April 1996.

[3] A. Alwan, R. Bagrodia, N. Bambos, M. Gerla, L. Kleinrock, J. Short, and J. Villasenor, "Adaptive mobile multimedia networks," *IEEE Personal Communications Magazine*, pp. 34–51, April 1996.

[4] E. Ayanoglu, K. Eng, and M. Karol, "Wireless ATM: limits, challenges, and proposals," *IEEE Personal Communications Magazine*, pp. 18–34, August 1996.

[5] F. Borgonovo, M. Zorzi, L. Fratta, V. Trecordi, and G. Bianchi, "Capture-division packet access for wireless personal communications," *IEEE Journal On Selected Areas In Communications*, vol. 14, pp. 609–622, May 1996.

[6] A. DeSimone and S. Nanda, "Wireless data: systems, standards, services," *Wireless Networks*, vol. 1, pp. 241–253, 1995.

[7] K. Eng, M. Karol, M. Veeraraghavan, E. Ayanoglu, C. Woodworth, P. Pancha, and R. Valenzuela, "BAHAMA: a broadband ad-hoc wireless ATM local-area network," in *Proc. IEEE International Communications Conference*, pp. 1216–1223, 1995.

[8] K. Eng, M. Karol, M. Veeraraghavan, E. Ayanoglu, C. Woodworth, P. Pancha, and R. Valenzuela, "A wireless broadband ad-hoc ATM local-area network," *Wireless Networks*, vol. 1, pp. 161–174, 1995.

[9] D. Everitt, "Traffic engineering of the radio interference for cellular mobile networks," *Proceedings of IEEE*, vol. 82, no. 9, pp. 1371–1382, 1994.

[10] R. Gejji, "Mobile multimedia scenario using ATM and microcellular technologies," *IEEE Transactions on Vehicle Technology*, vol. 43, no. 3, pp. 699–703, 1994.

[11] M. Karol, Z. Liu, and K. Eng, "Distributed-queueing request update multiple access (DQRUMA) for wireless packet (ATM) networks," in *Proc. IEEE International Communications Conference*, pp. 1224–1231, 1995.

[12] I. Katzela and M. Naghshineh, "Channel assignment schemes for cellular mobile telecommunication systems: a comprehensive survey," *IEEE Personal Communications Magazine*, pp. 10–31, June 1996.

[13] R. Kuruppillai, M. Dontamsetti, and F. Cosentino, *Wireless PCS*. New York: McGraw-Hill, 1997.

[14] R. LaMaire, A. Krishna, P. Bhagwat, and J. Panian, "Wireless LANs and mobile networking: standards and future directions," *IEEE Personal Communications Magazine*, pp. 86–94, August 1996.

[15] J. Li, *Intercellular coordination schemes for improving spectrum utilization in wireless cellular networks*. Purdue University, West Lafayette, Indiana: Ph.D. dissertation, 1998.

[16] J.-P. Linnartz, "On the performance of packet-switched cellular networks for wireless data communications," *Wireless Networks*, vol. 1, pp. 129–138, 1995.

[17] D. Raychaudhuri, "Wireless ATM networks: architecture, system design and prototyping," *IEEE Personal Communications Magazine*, pp. 42–49, August 1996.

[18] D. Raychaudhuri and N. Wilson, "ATM-based transport architecture for multiservices wireless personal communication networks," *IEEE Journal On Selected Areas In Communications*, vol. 12, no. 8, pp. 1401–1414, 1994.

[19] M. Schwartz, "Network management and control issues in multimedia wireless networks," *IEEE Personal Communications Magazine*, pp. 8–16, June 1995.

[20] G. Stüber, *Principles of mobile communication*. Boston: Kluwer Academic Publishers, 1996.

[21] S. Tekinay and B. Jabbari, "Handover and channel assignment in mobile cellular networks," *IEEE Communications Magazine*, pp. 42–46, November 1991.

[22] B. Walke, D. Petras, and D. Plassmann, "Wireless ATM: air interface and network protocols of the mobile broadband system," *IEEE Personal Communications Magazine*, pp. 50–56, August 1996.

[23] J. W.C. Jakes, *Microwave mobile communications*. New York: Wiley, 1974.

[24] M. Zorzi, "On the analytical computation of the interference statistics with applications to the performance evaluation of mobile radio systems," *IEEE Transactions On Communications*, vol. 45, pp. 103–109, January 1997.

Analysis of a Distributed Power Control Algorithm[*]

Jeffrey D. Herdtner and Edwin K. P. Chong

School of Electrical and Computer Engineering
Purdue University
West Lafayette, IN 47907-1285
{herdtner, echong}@ecn.purdue.edu

1 Introduction

We consider a wireless communication system consisting of mobile users communicating to base stations over a common radio channel. Since users are transmitting simultaneously over a shared channel, each user is creating interference for the others. Power control is needed to limit unnecessary interference while providing acceptable connections for all users.

We analyze a low complexity uplink power control algorithm. At each iteration, each user needs only a single bit of information from its assigned base station indicating whether its SIR is above or below its desired level. If it is above, the user decreases its power level by a fixed amount (in dB); otherwise, the power level is increased by a fixed amount. This type of algorithm has been shown to be effective in simulation studies of various types of systems [1, 3, 4]. Because of the fixed step sizes, the algorithm does not actually converge to the optimal power assignment, but we prove its stability and some performance guarantees in terms of analytically derived bounds on the convergence error. We show that the convergence error can be made as small as desirable, at the cost of reducing the convergence rate. We do not consider mobility, but rather assume that the network parameters are held constant while the algorithm runs.

2 The Power Control Problem

Consider a wireless system with M base stations and N users communicating over a common radio channel. The assignment of users to base stations is assumed to be fixed. The SIR of user i (at its assigned base station) is

$$SIR_i(\boldsymbol{p}) \triangleq \frac{h_{ii}p_i}{\sum_{j \neq i} h_{ji}p_j + \sigma_i},$$

where p_i is the transmit power level of user i, h_{ij} is the gain from user i to the assigned base station of user j, σ_i is the receiver noise at the assigned base station of user i, and $\boldsymbol{p} = [p_1, \ldots, p_N]^T$. User i's connection is considered acceptable under power assignment $\boldsymbol{p}$ if $SIR_i(\boldsymbol{p}) \geq \gamma_i$, where γ_i is the SIR requirement for user i. The power control problem is that of finding the smallest power vector for which all users have acceptable connections.

Letting H be the $N \times N$ matrix with entries $H_{ii} = 0$ and $H_{ij} = \gamma_i h_{ji}/h_{ii}$ for $j \neq i$, and letting δ be the N-vector with entries $\delta_i = \gamma_i \sigma_i/h_{ii}$, the power control problem can be written as follows:

$$\text{minimize} \quad p$$
$$\text{subject to} \quad p \geq Hp + \delta, \, p > 0,$$

where the inequalities are componentwise and the minimization is with respect to the partial order associated with $\leq$. (Previous work using this formulation includes [2, 5].) It has been shown that a unique optimal (minimum power) solution to the power control problem exists if and only if $\rho(H) < 1$, where $\rho(H)$ is the spectral radius of H.

3 Algorithm Description

We now describe the algorithm that we will analyze. At each iteration, each user increases its power level by a factor $\beta > 1$ if its SIR is below the desired level; otherwise, the power level is decreased by a factor $\alpha, 0 < \alpha < 1$. To define the algorithm, we first define the function $T : R^N \to R^N$ as follows:

$$T_i(p) = \begin{cases} \beta p_i & \text{if } SIR_i(p) < \gamma_i \\ \alpha p_i & \text{if } SIR_i(p) \geq \gamma_i \end{cases}$$

We then let $T(p) = [T_1(p), \ldots, T_N(p)]^T$. Given an initial power vector $p^{(0)} > 0$, the algorithm generates the sequence of power vectors $\left\{p^{(n)}\right\}_{n=0}^{\infty}$ according to the iteration

$$p^{(n+1)} = T\left(p^{(n)}\right) \quad n \geq 0. \tag{1}$$

This algorithm has very desirable characteristics. No global information is needed for users to update their power levels, and each user needs only a single bit of information per iteration from its assigned base station, indicating whether or not its SIR constraint is satisfied. It is assumed that the SIR is accurately measured and that the corresponding information bit is transmitted without error to the user, but simulations in [1, 4] indicate that this type of algorithm is robust in less ideal conditions

4 Stability and Convergence Analysis

An algorithm is considered to be stable if, for any initial condition $p^{(0)}$, there is a finite power vector $\overline{p}$ such that $0 \leq p^{(n)} \leq \overline{p}$ for all $n \geq 0$. In this work, we prove that the power control algorithm defined by (1) is stable for any initial power vector $p^{(0)} \geq 0$ provided $\rho(H) < 1/\beta$. The proof proceeds by constructing a set that contains $p^{(0)}$ and is invariant under T.

While algorithm stability is important, it gives little information about how close the algorithm comes to the optimal power assignment. In this work, we prove that the power control algorithm provides users with acceptable connections provided α and β are chosen appropriately. More specifically, we show that each user's SIR is within a fraction α/β of its desired level after a finite number of iterations and never drops below thereafter.

It is desirable for the power control algorithm not only to provide acceptable connections for all users, but also to prevent excess power usage. As mentioned in Section 2, it is known that if $\rho(H) < 1$, then there is a componentwise mimimum power assignment

that provides all users with acceptable connections. In this work, we establish upper and lower bounds on the users' power levels that are attained or approached as the algorithm progresses. The error is shown to be controllable by the choice of α and β, but there is a tradeoff in that reducing the error results in slower convergence.

References

[1] S. Ariyavisitakul, "Signal and interference statistics of a CDMA system with feedback power control - Part II," *IEEE Transactions on Communications*, vol. 42, pp. 597–605, 1994.

[2] S. V. Hanly, "An algorithm for combined cell-site selection and power control to maximize cellular spread spectrum capacity," *IEEE Journal on Selected Areas in Communications*, vol. 13, no. 7, pp. 1332–1340, Sept. 1995.

[3] F. Ling, B. Love, and M. M. Wang, "Behavior and performance of power controlled IS-95 reverse-link under soft handoff," in *Proc. IEEE Vehicular Technology Conference*, vol. 2, pp. 924–928, Sept. 1997.

[4] A. J. Viterbi, A. M. Viterbi, and E. Zehavi, "Performance of power-controlled wideband terrestrial digital communication," *IEEE Transactions on Communications*, vol. 41, no. 4, pp. 559–569, Apr. 1993.

[5] R. D. Yates and C.-Y. Huang, "Integrated power control and base station assignment," *IEEE Transactions on Vehicular Technology*, vol. 44, no. 3, pp. 638–644, Aug. 1995.

Decision Feedback Sequence Estimation for Unwhitened ISI Channels

Abdulrauf Hafeez[1] and Wayne E. Stark
Dept. of Elect. Engineering and Computer Science
1301 Beal Ave. , University of Michigan, Ann Arbor, MI 48109-2122.
E-mail: rauf@eecs.umich.edu, stark@eecs.umich.edu.

Abstract– In this paper, a form of decision-feedback sequence estimation (DFSE) is proposed for unwhitened inter-symbol interference (ISI) channels. DFSE which is a reduced-complexity alternative to maximum likelihood sequence estimation, performs very well on whitened (minimum-phase) ISI channels. However, it may not be feasible to compute the whitening filter for many time-varying channels like the multiuser asynchronous direct-sequence CDMA channel. On such channels, it is desirable to use the Ungerboeck formulation which operates directly on discrete-time unwhitened statistic obtained from conventional matched filtering. Unfortunately, decision-feedback sequence estimation for unwhitened channels is interference limited because the decision statistic depends on both past and future inputs. Specifically, the decision rule that chooses the path with the best accumulated metric leading to a reduced state, fails to account for interference from the future inputs not included in the reduced state. We propose a modified decision rule to be integrated into the Ungerboeck form of sequence estimation which is not sensitive to channel phase. It can be implemented as a single stage or a multistage scheme depending on the amount of dispersion present in the channel. Simulation results indicate that the algorithm used on unwhitened channels with low to moderate dispersion, provides similar performance/complexity tradeoffs as the DFSE used on the corresponding whitened minimum-phase channels. The algorithm is especially attractive for multiuser asynchronous DS-CDMA channels with long spreading codes.

1 Introduction

There are two main approaches to maximum likelihood sequence estimation (MLSE) for known inter-symbol interference (ISI) channels with additive noise. Forney's approach [1] consists of using the Viterbi algorithm on the sampled output of whitened matched filters while Ungerboeck's formulation [2] operates directly on conventional matched filter output samples without the need of noise whitening. Due to the exponential complexity of these methods, several low-complexity sub-optimal schemes have been developed. A promising reduced-complexity alternative to MLSE using Forney's approach is decision feedback sequence estimation (DFSE) [3], [4]. The scheme provides an excellent tradeoff between performance and complexity.

ISI may be the result of spectral shaping at the transmitter and/or distortion in the physical channel. Moreover, multiuser interference can also be viewed as a form of time-varying ISI. A receive filter matched to a non-Nyquist transmit pulse-shaping filter or to the overall channel impulse response, gives rise to bi-directional ISI and correlated noise. The noise has to be whitened in order to use DFSE. In case of rapidly (or periodically) time-varying ISI channels, it may not be feasible to track the whitening filter (the computation involves polynomial factorization and inversion). An example is the multiuser asynchronous direct-sequence CDMA channel where the spreading of users' transmit pulses with long non-orthogonal spreading codes gives rise to rapidly time-varying ISI over the composite data sequence. Clearly, Ungerboeck's form is better suited for such channels as noise whitening is expensive [5]. However, a reduced-state Ungerboeck variant (which we call UDFSE[2]) similar to the DFSE does not work as well. The problem arises from the nature of the unwhitened statistic which depends on both past and future input symbols. Consequently the decision rule borrowed from DFSE, which decides in favor of the path with the best accumulated (Euclidean distance) metric, leading to a reduced state, ignores interference from the future inputs not included in the reduced state. As a result, the decisions obtained in UDFSE are interference-limited even in the absence of feedback errors. The M-algorithm [7], used on unwhitened statistic, suffers from the same problem as paths are selected based on accumulated metrics which do not reflect all relevant interference components.

In the case of UDFSE, where the reduced state is pre-determined, the interfering anti-causal components are known. Thus the decision rule can be modified to nullify the effect of these components recursively. This can be accomplished in two ways: by using conventional hard decisions on the relevant anti-causal interference components or by using decisions obtained at the output of the preceding stage in a multistage scheme. In either case, the preliminary decisions do not enter the branch metrics directly. The number of stages to use depends on the amount of dispersion present in the channel. Since conventional hard decisions are used to cancel interference partially, the modified scheme may not be suitable for highly dispersive channels.

Simulation is undertaken to compare the performance of various algorithms on single-user ISI channels and multiuser asynchronous CDMA channels. It is found that the modified UDFSE scheme obtains sizable gains over UDFSE on channels with low to moderate amount of dispersion. On such channels, it provides similar performance/complexity tradeoff as DFSE used on the corresponding whitened minimum-phase channels. The proposed scheme performs very well on DS-CDMA channels as the correlations among user's spreading codes are small. It is noted that a single-stage algorithm suffices when the dispersion is low while a second stage is needed in medium dispersion. On highly dispersive channels, the performance is not that good and may be worse than UDFSE.

The paper is organized as follows. We present the system model in section 2. The two approaches to MLSE are reviewed in section 3. In section 4, we describe various methods of decision-feedback sequence estimation in detail and develop the modified UDFSE algorithm. Simulation results are presented in section 5 where the performance of the various schemes is compared for single user ISI channels and multiuser DS-CDMA channels.

---

[2]The scheme is referred to as Delayed Decision Feedback Sequence Estimation with *a standard matched filter* in [6]

2   System model

Consider the transmission of linearly-modulated digital data over a (time-varying) time-dispersive additive white Gaussian noise channel. Assume that the receiver has perfect knowledge of the carrier phase, symbol timing and the impulse response of the channel (assumed constant for symbol period T). After coherent down-conversion, the receiver employs a filter $h_n(t)$ matched to the cascade of the transmit pulse-shaping filter and the channel impulse response and samples the output at symbol spaced intervals. The sequence of sampled matched filter outputs is a sufficient statistic for estimating the transmitted data sequence. Thus an equivalent discrete-time channel model is obtained.

The matched filter output at time n is given by

$$y_n = \sum_{i=-L}^{L} s_{n,i} b_{n-i} + z_n \tag{1}$$

where $\{b_n\}$ is the transmitted data sequence assumed to be i.i.d. $b_n \in A_M$ (an M-ary alphabet). $s_{n,i}$ are channel correlations sampled at time n, given by

$$s_{n,i} = \left\{ \begin{array}{ll} h_n(t) * h_n(-t)|_{t=iT} & |i| \leq L \\ 0 & |i| > L \end{array} \right. \tag{2}$$

where $L < \infty$. $\{z_n\}$ is a complex Gaussian noise process with mean 0 and covariance $\mathrm{E}[z_n^* z_{n-i}] = N_0 s_{n,i}$. We will refer to the above model as the unwhitened model.

Let $s_n(D) = \sum_i s_{n,i} D^i$, then an equivalent discrete-time white Gaussian noise model is obtained by noting

$$s_n(D) = f_n^*(D^{-1}) f_n(D)$$

where $f_n(D) = \sum_{i=0}^{L} f_{n,i} D^i$ has all its roots inside the unit circle (minimum-phase channel). Thus the statistic obtained when $\{y_n\}$ is filtered by the anti-causal whitening filter $1/f_n^*(D^{-1})$, is given by

$$y_n' = \sum_{i=0}^{L} f_{n,i} b_{n-i} + z_n' \tag{3}$$

$\{z_n'\}$ is a proper[3] complex white Gaussian noise process with mean 0 and variance N_0.

3   Maximum likelihood sequence estimation

The maximum likelihood sequence estimator (MLSE) determines as the most likely sequence transmitted, the sequence b^N that maximizes the metric [2]

$$\mathrm{U}\left(y^N, b^N\right) = \sum_{n=1}^{N} 2\mathrm{Re}\{b_n^* y_n\} - \sum_{i=1}^{N} \sum_{k=1}^{N} b_i^* s_{i,k} b_k. \tag{4}$$

where $x^n = x_1, x_2, \ldots, x_n$. Under the condition:

$$s_{n,i} = s_{n-i,-i}^* \quad \text{or equivalently} \quad s_{n,-i} = s_{n+i,i}^*, \tag{5}$$

it can be shown that the above metric can be computed recursively as

$$\mathrm{U}(y^n, b^n) = \mathrm{U}(y^{n-1}, b^{n-1}) + \mathrm{V}(y_n, b_n, \sigma_{n-1}) \tag{6}$$

---

[3] $\mathrm{E}[\mathrm{Re}\{z_n'\} \mathrm{Im}\{z_n'\}] = 0$

where $V(.)$ is known as the branch metric, given by

$$V(y_n, b_n, \sigma_{n-1}) = \text{Re}\left\{ b_n^* \left(2y_n - s_{n,0}b_n - 2\sum_{i=1}^{L} s_{n,i}b_{n-i} \right) \right\} \quad (7)$$

and $\sigma_n = b_n, b_{n-1}, \ldots, b_{n-L+1}$ is the state at time n.

The above is a more generalized form of the Ungerboeck formulation (where $s_{n,i} = s_i$ i.e. the channel is fixed) independently derived in [8] in detail. The condition in (5) holds for time-varying channels like the asynchronous DS-CDMA channel. The application of this algorithm to the multiuser sequence estimation problem was noted by Verdu [9].

The maximum likelihood sequence can also be determined equivalently by applying the Viterbi algorithm on the whitened statistic $\{y_n'\}$ as shown by Forney [1]. The metric in this case can be written as

$$U'\left(y'^N, b^N\right) = \sum_{n=1}^{N} \left[2\text{Re}\left(y_n' \sum_{i=0}^{L} f_{n,i}^* b_{n-i}^* \right) - \left\| \sum_{i=0}^{L} f_{n,i}b_{n-i} \right\|^2 \right] \quad (8)$$

which can be computed recursively as

$$U'\left(y'^n, b^n\right) = U'(y'^{n-1}, b^{n-1}) + V'(y_n', b_n, \sigma_{n-1}) \quad (9)$$

where

$$V'(y_n', b_n, \sigma_{n-1}) = 2\text{Re}\left(y_n' \sum_{i=0}^{L} f_{n,i}^* b_{n-i}^* \right) - \left\| \sum_{i=0}^{L} f_{n,i}b_{n-i} \right\|^2. \quad (10)$$

The two algorithms have the same order of computational complexity and storage requirement proportional to M^L.

4 Decision feedback sequence estimation

A reduced-complexity sub-optimal alternative to MLSE using the Viterbi algorithm is decision feedback sequence estimation DFSE [3], [4]. A parameter called memory order J is chosen arbitrarily smaller than the channel memory L and the trellis is collapsed into M^J states corresponding to the J most recent hypothesized symbols only. Since the reduced state falls short in providing all the information needed to compute branch metrics for the next iteration, the algorithm uses the path with the best accumulated metric, leading to each state, to extract the rest of the information required. In other words, the algorithm makes tentative conditional decisions on the input symbols more than J samples in the past (given the J most recent hypothesized input symbols) to cancel their effect on the current output sample. Note that this algorithm operates on whitened statistic $\{y_n'\}$ which depends on past and present inputs only.

4.1 UDFSE

In this section, we consider decision-feedback sequence estimation in the Ungerboeck form, referred to here as UDFSE (derived in [6]).

Let $\beta_n = b_n, b_{n-1}, \ldots, b_{n-J+1}$ represent the reduced state at time n and $m(\beta_n)$ be the associated path metrics, defined as

$$m(\beta_n) \triangleq \max_{b^{n-J}} U(y^n, b^n) \quad (11)$$

then the algorithm can be summarized as:

$$m(\beta_n) = \max_{b_{n-J}}[m(\beta_{n-1}) + W(y_n, b_n, \beta_{n-1})] \tag{12}$$

$$W(y_n, b_n, \beta_{n-1}) = \mathrm{Re}\left\{ b_n^* \left(2y_n - s_{n,0}b_n - 2\sum_{i=1}^{J} s_{n,i}b_{n-i} - 2\sum_{i=J+1}^{L} s_{n,i}\hat{b}_{n-i}(\beta_{n-1}) \right) \right\} \tag{13}$$

$\{\hat{b}(\beta_n)\}$ are tentative conditional decisions on inputs more than J samples in the past, obtained from the path with the best accumulated metric, leading to reduced state β_n.

$$\hat{b}_{n-J}(\beta_n) = \arg\max_{b_{n-J}}[m(\beta_{n-1}) + W(y_n, b_n, \beta_{n-1})] \tag{14}$$

A drawback of UDFSE: Although both full-state formulations in section 3 yield the maximum likelihood sequence estimate, the corresponding reduced-state derivations perform quite dissimilarly. In fact, UDFSE does not perform nearly as well as DFSE on most channels. The problem arises from the nature of unwhitened statistic. Recall that unlike whitened statistic, unwhitened statistic $\{y_n\}$ depends on both past and future input symbols. Now note from (14) that when deciding (conditionally) b_{n-J} in the n-th step, the UDFSE algorithm has ignored interference from inputs $b_{n+1}, b_{n+2}, \ldots, b_{n-J+L}$ which directly affect output sample y_{n-J} corresponding to b_{n-J}. This means that the decision rule of (14), used to decide b_{n-J}, based on the knowledge of only J inputs in the future is inherently near-sighted unless it has some sort of side information available about another $L - J$ inputs in the future. Thus unlike the whitened channel counterpart, UDFSE suffers from a major drawback: the conditional decisions are interference-limited from future inputs even in the absence of feedback errors. The M-algorithm which operates on unwhitened statistic is also plagued by the same problem.

4.2   Modified UDFSE

When the reduced-state is pre-determined as in the case of UDFSE, the problem can be alleviated by modifying the decision rule to include a bias for cancelling the effect of the residual interference. Note that the full-state algorithm does not decide b_{n-J} until the $(n-J+L)$th step when the interference from the relevant future inputs has been averaged out. On the other hand, the reduced-state scheme accounts for the contribution of only J inputs in the future. The bias needed to cancel the residual anti-causal interference completely in the reduced-state scheme can be found by comparing UDFSE term by term against the full-state algorithm.

The modified algorithm (MUDFSE) can be outlined as follows: Path metrics are calculated as in UDFSE using equation(12). Conditional decisions are made (and the corresponding survivor paths are chosen) using the modified decision rule:

$$\hat{b}_{n-J}(\beta_n) = \arg\max_{b_{n-J}}[m(\beta_{n-1}) + W(y_n, b_n, \beta_{n-1}) + \mathrm{bias}(b_{n-J})] \tag{15}$$

where

$$\mathrm{bias}(b_n) = -2\mathrm{Re}\left\{ b_n^* \sum_{i=1}^{L-J} s_{n,-J-i}\tilde{b}_{n+J+i} \right\}, \quad \tilde{b}_n = \mathrm{sign}(y_n). \tag{16}$$

Note that tentative hard decisions $\{\tilde{b}_n\}$ (which may not be very reliable) affect branch metrics (12) only through conditional decisions $\{\hat{b}(\beta_n)\}$. Also note that the bias term does not add significantly to the computational load and storage requirement of the algorithm which is on the order of $(G - J)M^J$ (same as DFSE), where G is the decision lag. The algorithm is delayed by $L - J$ samples as y_{n+L-J} is needed in the nth step.

4.3 Multistage MUDFSE

MUDFSE can be run in a multistage configuration where decisions obtained at the output of the first stage are fed back to compute the bias in the second stage and so on. i.e.

$$(\tilde{b}_n)_1 = \text{sign}(y_n) \quad \text{and} \quad (\tilde{b}_n)_i = (\bar{b}_n)_{i-1}, \quad i > 1$$

where $\{(\bar{b}_n)_i\}$ are decisions obtained from the ith stage at lag G_i ($G_i >> L$). Note that decisions $\{(\bar{b}_n)_1\}$ are likely to be much more reliable than $\{(\tilde{b}_n)_1\}$. The complexity and delay of a Q-stage scheme is given by $\sum_{i=1}^{Q}(G_i - J_i)M^{J_i}$ and $\sum_{i=1}^{Q} G_i + L - J_1$ respectively.

Since the reliability of symbol-by-symbol decisions $\{\text{sign}(y_n)\}$ depends heavily on the amount of dispersion present in the channel, the use of these decisions in MUDFSE is warranted for channels with low-to-medium dispersion only. On highly dispersive channels, it may be better to ignore the anti-causal interference rather than try to cancel it with unreliable decisions. On such channels, UDFSE may be the preferable scheme (or the first stage followed by MUDFSE as the second stage, in a two-stage setup).

5 Performance results

Performance is evaluated via simulation. We consider binary signaling over two static time-dispersive additive white Gaussian noise channels. Channel 1 is given by $f = (0.8614394, 0.2584344, -0.1000742, -0.2740468, 0.130008, 0.1000742, -0.0375511, 0.1122497, -0.1137419, -0.22837)$ and channel 2 is given by $f = (0.7071067, -0.153016, 0.4679421, -0.306526, 0.2846515, -0.1041423, 0.2437057, 0.0679643, -0.0705263, 0.052918)$. Both channels are minimum phase and are arbitrarily chosen. The receiver has perfect knowledge of the symbol timing and the impulse response of the channel.

Figures 1 and 2 show the bit-error rate performance of various schemes on channels 1 and 2 respectively. Each simulation was run for a count of 1000 errors. The various schemes are indexed with the memory order and the decision lag (J, G). Except DFSE, all algorithms operate on symbol-spaced samples obtained at the output of conventional matched filters. Ideal noise whitening is assumed for DFSE. Channel 1 has low-to-moderate amount of dispersion. All schemes shown in Fig 1, except MLSE, have the same order of overall complexity and storage requirement. Fig 1 shows that $(5, 45)$ Modified UDFSE gains $0.5 - 1.5$ dB over $(5, 45)$ UDFSE. Another $0.5 - 2.25$ dB is gained by the two-stage scheme $[(4, 45), (4, 45)]$ 2MUDFSE over single-stage $(5, 45)$ MUDFSE. No significant amount of further gain is achieved by the three-stage scheme with the same overall complexity. Its performance, however, is almost identical to that of $(5, 45)$ DFSE on this channel. Note that, here we have neglected the effects of non-ideal noise-whitening on the performance of DFSE, resulting from fixed delay constraint. The additional delay required can be compared to the delay of a multi-stage scheme. Moreover, the performance of DFSE depends heavily on channel phase with the best performance achieved on minimum-phase channels. On the contrary, the performance of receiver structures that operate on unwhitened statistic is independent of channel phase.

Channel 2 is more dispersive than channel 1 (the main signal element f_0 contains only 50% of the total energy). Fig 2 shows that the modified single-stage scheme $(5, 45)$ MUDFSE is actually a bit worse than $(5, 45)$ UDFSE for most of the SNR range. This is because the conventional hard decisions used in the modified scheme to compute the bias term, are somewhat unreliable due to heavy dispersion. However, the two-stage scheme $[(4, 45), (4, 45)]$ 2MUDFSE, with the same overall complexity as the single-stage

algorithms, manages to gain about half a dB owing to the much improved reliability of decisions available to the second stage. Its performance is still far from that achieved by (5, 45) DFSE especially at low noise. The two-stage scheme with higher memory order, however, compares more favorably with (5, 45) DFSE.

Next, we simulate a BPSK modulated asynchronous DS-CDMA system with eight users whose signature waveforms are derived from Gold sequences of length 31. The relative delays of users are fixed for the simulation and are in an increasing order. The channel spectrum $S(D) = S_1^T D^{-1} + S_0 + S_1 D$ is given by

$$
\frac{1}{31}
\begin{bmatrix}
31 & 8-D & 7 & 6+D & -3+2D & -6+5D & -3+2D & -2+D \\
8-D^{-1} & 31 & -D & 9-2D & -6-3D & -7-2D & -D & 9-2D \\
7 & -D^{-1} & 31 & -D & -1 & -D & -1 & -2+D \\
6+D^{-1} & 9-2D^{-1} & -D^{-1} & 31 & -D & -1 & -D & -1 \\
-3+2D^{-1} & -6-3D^{-1} & -1 & -D^{-1} & 31 & -D & -1 & -D \\
-6+5D^{-1} & -7-2D^{-1} & -D^{-1} & -1 & -D^{-1} & 31 & -D & -1 \\
-3+2D^{-1} & -D^{-1} & -1 & -D^{-1} & -1 & -D^{-1} & 31 & -D \\
-2+D^{-1} & 9-2D^{-1} & -2+D^{-1} & -1 & -D^{-1} & -1 & -D^{-1} & 31
\end{bmatrix}
$$

The equivalent periodically time-varying ISI channel can be obtained from the relation

$$
s_{\kappa(n),i} = \begin{cases}
S_1(\kappa(n), \kappa(n) - i + K) & \kappa(n) - i < 1 \\
S_0(\kappa(n), \kappa(n) - i) & 1 \le \kappa(n) - i \le K \\
S_1(\kappa(n) - i - K, \kappa(n)) & \kappa(n) - i > K
\end{cases}
\tag{17}
$$

for $|i| \le K - 1$, where K is the number of users and $\kappa(n)$ is the user index given by $\kappa(n) = n \bmod K$.

Figure 3 shows the bit-error rate of user 1 for various schemes when all users have identical signal-to-noise ratio. Each simulation was run for a count of 500 errors. It is evident that even with ideal power control, the performance of the conventional single-user detector is in no comparison with optimum MLSE. With four states, (2, 28) UDFSE and (4) M-algorithm that operate directly on the matched filter output, do not improve much over the conventional detector. Linear-decorrelator that nulls out all interference, loses about $0.7 - 1.0$ dB compared to MLSE. (2, 28) DFSE and (4) M-algorithm that operate on the equivalent whitened minimum-phase channel, closely approach MLSE performance. The proposed single-stage and two-stage modified UDFSE algorithms give by far the best performance on this channel (next to MLSE). This behavior is attributable to low channel cross-correlations typical of well-designed spreading codes (compare to the channel in figure 1). The second stage of 2MUDFSE does not provide any significant gain over the decisions obtained in the first stage. (2, 28) MUDFSE (with four states) is only 0.3 dB worse than MLSE (128 states) and gains $1.0 - 3.0$ dB over UDFSE.

Figure 4 shows the bit-error rate of user 1 against the signal-to-noise ratio of the rest of the users. SNR of user 1 is held constant at 10.0 dB. It can be seen that the conventional detector, UDFSE and the unwhitened M-algorithm are limited by multiuser interference. Linear-decorrelator is ideally near-far resistant which means that its performance is the same as that of MLSE under worst case interference. In other conditions, DFSE and the whitened M-algorithm perform better. The proposed modified UDFSE schemes outperform the other methods and converge to MLSE in high multiuser interference.

Note that MUDFSE is especially suitable for long spreading codes used in today's cellular systems. Channel factorization and inversion operations are difficult to perform on the time-varying channels that result from long spreading codes and arrival and departure of users. However, partial cross-correlations of long codes can be easily generated locally at the receiver (especially at the uplink).

6 Conclusions and future work

We described a form of decision-feedback to be integrated into the Ungerboeck formulation for sequence estimation on ISI channels. The resulting reduced-complexity algorithm provides similar performance/complexity tradeoffs as the decision feedback sequence estimator on low to moderately dispersive channels. It, however, is insensitive to channel phase and does not require noise-whitening which makes it attractive for time-varying channels like the asynchronous DS-CDMA channel.

The proposed scheme requires knowledge of received signal amplitudes. Thus, it is imperative that an adaptive form of the algorithm be developed to use on fading channels. In [10], UDFSE was considered for equalization in the global system for mobile communications (GSM) receiver. It was found that UDFSE with four states provides adequate performance with some degradation for rural area, typical urban and hilly terrain channels with six rays but exhibits inferior performance for a uniform ray power profile. It would be interesting to consider the proposed algorithm for these channels.

References

[1] G. D. Forney, "Maximum-Likelihood Sequence Estimation of Digital Sequences in the Presence of Intersymbol Interference", *IEEE Trans. Information Theory*, Vol. IT-18, No. 3, pp. 363-378, May 1972.

[2] G. Ungerboeck, "Adaptive Maximum-Likelihood Receiver for Carrier-Modulated Data-Transmission Systems", *IEEE Trans. Comm. Technology*, Vol. COM-22, No. 5, pp. 624-636, May 1974.

[3] A. Duel-Hallen and C. Heegard, "Delayed Decision-Feedback Sequence Estimation", *IEEE Trans. Comm.*, Vol. 37, No. 5, pp. 428-436, May 1989.

[4] V. M. Eyuboglu and S. U. Qureshi, "Reduced-state Sequence Estimation with Set Partitioning and Decision Feedback", *IEEE Trans. Comm.*, pp. 13-20, Jan. 1988.

[5] L. Wei and L. K. Rasmussen, "A Near Ideal Noise Whitening Filter for an Asynchronous Time-Varying CDMA System", *IEEE Trans. Comm.*, Vol. 44, No. 10, pp. 1355-1361, Oct. 1996.

[6] A. Duel and C. Heegard, "Delayed Decision Feedback Sequence Estimation for QAM and Trellis Coded Systems", *20th Conf. Info. Sc. and Sys.*, pp. 367-372, Mar. 1986.

[7] J. B. Anderson and S. Mohan, "Sequential Coding Algorithms: A Survey Cost Analysis", *IEEE Trans. Comm.*, Vol. COM-32, pp. 169-176, Feb. 1984.

[8] G. E. Bottomley and S. Chennakeshu, "Adaptive MLSE Equalization Forms for Wireless Communications", *Fifth Virginia Tech. Symp. Wireless Personal Comm.*, pp. 20-1-20-12, May 1995.

[9] S. Verdu, "Minimum Probability of Error for Asynchronous Gaussian Multiple-Access Channels", *IEEE Trans. Info. Th.*, Vol. IT-32, No. 1, pp. 85-96, Jan. 1986.

[10] K. Wesolowski, R. Krenz and K. Das, "Efficient Receiver Structure for GSM Mobile Radio", *Int. J. Wireless Information Networks*, Vol. 3, No. 2, 1996.
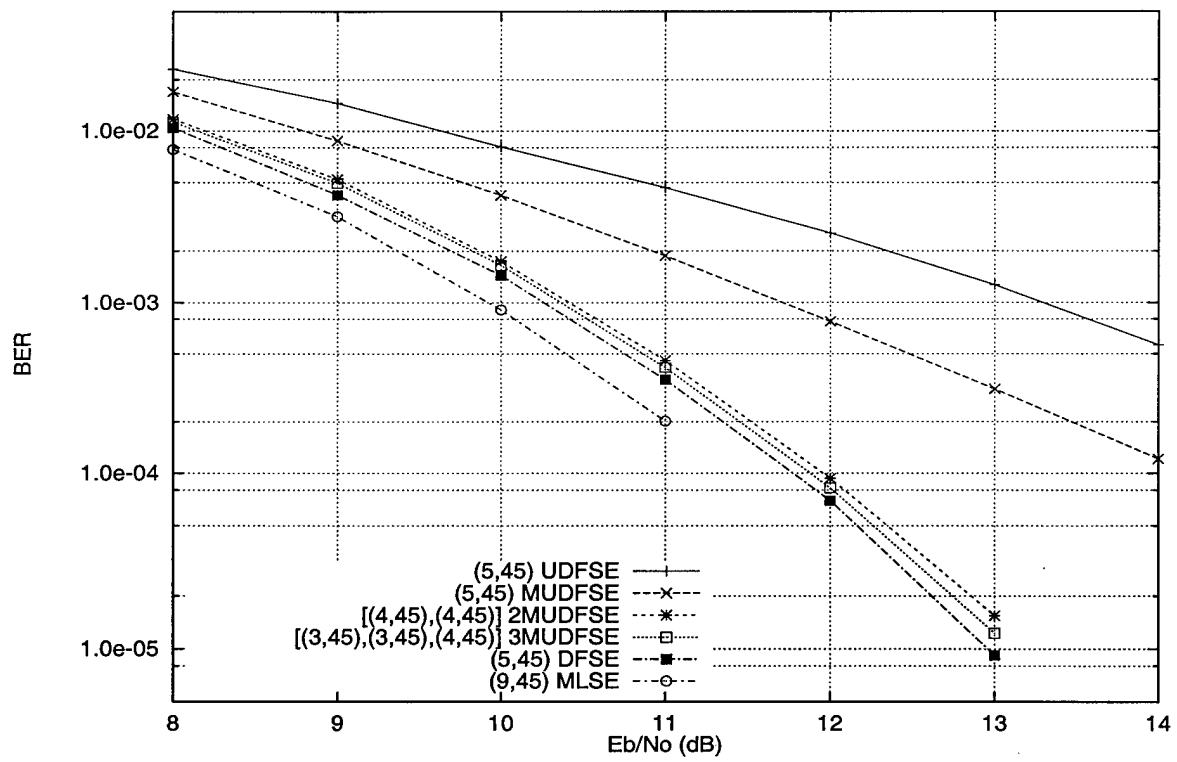
Figure 1: BER performance of various detection schemes on channel 1.
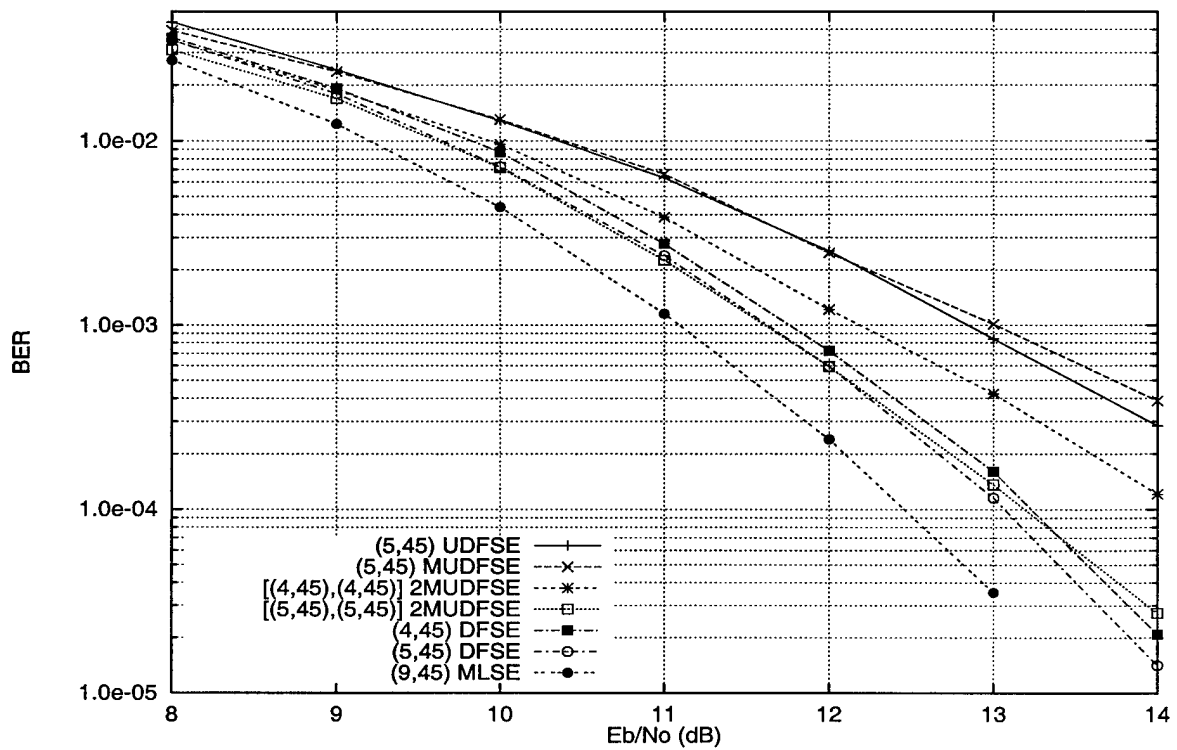

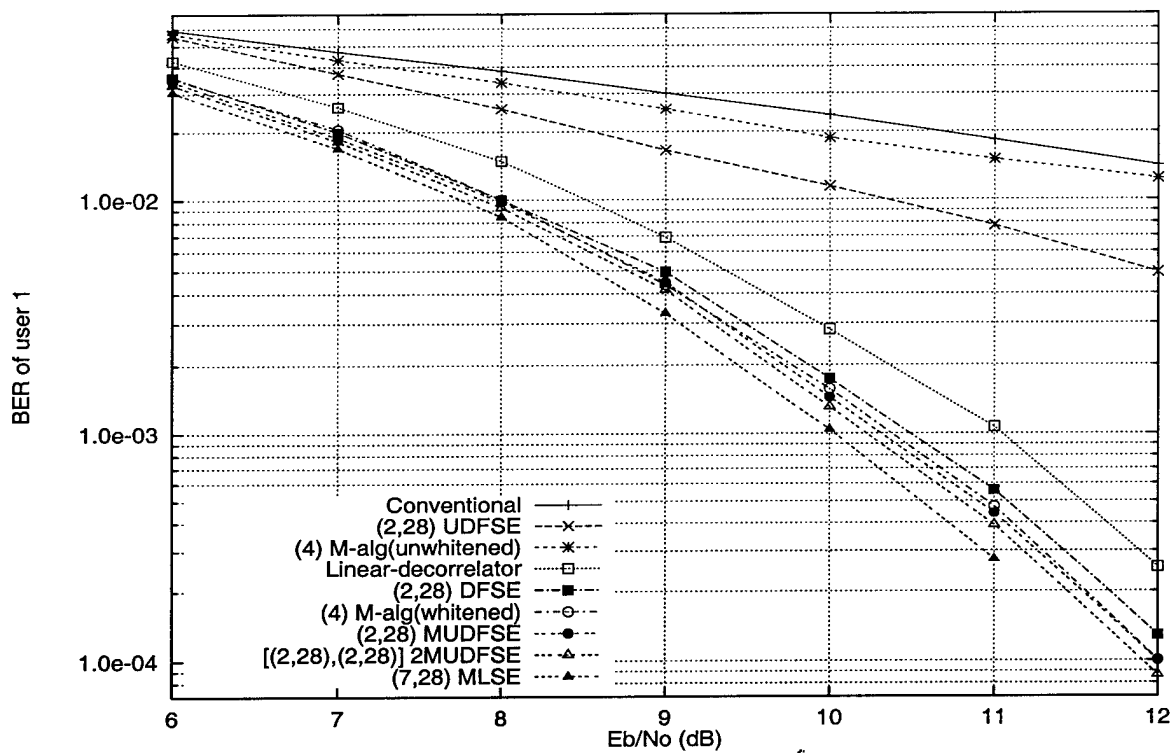Figure 2: BER performance of various detection schemes on channel 2.

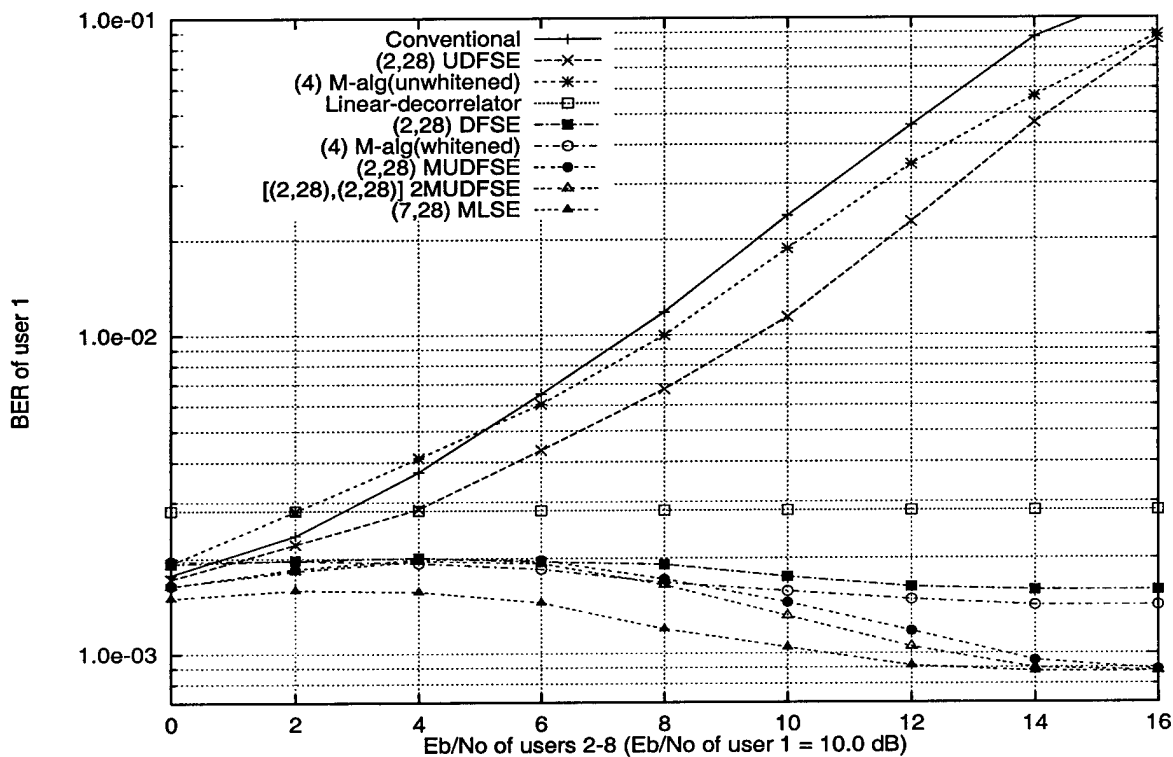Figure 3: BER performance of various detection schemes on an 8-user asynchronous DS-CDMA channel.

Figure 4: Near-far performance of various detection schemes on an 8-user asynchronous DS-CDMA channel.

A Family of Soft-Output Multiuser Demodulators for Coded Asynchronous CDMA Channels

Abdulrauf Hafeez[1] and Wayne E. Stark
Dept. of Elect. Engineering and Computer Science
University of Michigan, Ann Arbor, MI 48109-2122.

Abstract: In this paper, we consider soft-output multiuser demodulation for asynchronous CDMA channels with coding and interleaving. First, we derive an optimum soft-output multiuser estimation (OSOME) algorithm for linearly-modulated Gaussian CDMA channels. The forward-recursive algorithm generates *a posteriori* probabilities (APP) for modulator-input symbols given the received signal, which can be fed directly to single-user soft-decision decoders. Second, we outline a reduced-state soft-output multiuser estimation (RSOME) scheme, with complexity exponential in a parameter called memory order chosen arbitrarily (smaller than channel memory). These algorithms can be employed with conventional matched filtering and do not require noise whitening. Finally we present simulation results of a four-user coded asynchronous CDMA system. The results indicate that the OSOME algorithm achieves a $0.4 - 0.6$ dB gain over soft-output Viterbi algorithm (SOVA) [3] in a power controlled environment and the reduced-state schemes provide a desirable performance-complexity tradeoff.

Multiuser CDMA systems suffer from multiple-access interference (MAI), noise and other channel impairments. Two techniques are generally used to combat MAI. The first is multiuser demodulation for which there has been considerable research. The second technique is the combination of coding and interleaving. In order to make the most of error control coding, the demodulator must provide soft-inputs to the decoders in the form of likelihoods, symbol APP's, erasures, etc.. Unfortunately most multiuser detection algorithms ignore the possibility of generating this reliability information and concentrate instead on minimizing the demodulated error rate. In this paper, we attempt to derive multiuser algorithms that estimate code symbol APP's and can be effectively combined with error control coding and interleaving.

Recently considerable amount of work has been done in symbol-by-symbol detection techniques for channels with ISI (e.g. [1]). The optimum soft-output algorithm (OSA) of [1] can be applied to the multiuser case, but this requires noise whitening. Despite the strides made in the whitening technique, noise whitening requires sizable complexity and

is not very suitable for long spreading sequences and time varying channels. Hayes et. al. derived an optimal symbol-by-symbol detection (OSSD) algorithm for ISI channels with correlated noise (after matched filtering) [2]. They and other authors, however, over-estimated the complexity of this algorithm. We derive an optimum soft-output multiuser estimation (OSOME) algorithm based on their scheme. The complexity of OSOME(L) is on the order of $M^{K-1}[(M-1)(L-K+1)+1]$, where L is the decision lag, K is the number of users and M is the size of symbol alphabet. Thus the complexity of this algorithm is at par with the OSA but it does not require noise whitening. The OSOME algorithm is an optimum demodulator for a coded and linearly-modulated multiuser CDMA system with ideal interleaving, in the sense that without exploiting any information about coding in the demodulation process, it supplies each decoder with as much information as possible about the sequence of modulator-input symbols for the corresponding user while suppressing the irrelevant information about other user's sequences. This is called user-separating demodulation in [4].

The number of states in the OSOME algorithm is exponential in the number of users K minus one. The state can be truncated arbitrarily by employing conditional decision feedback in the recursion of OSOME, resulting in a family of reduced-state soft-output multiuser estimators (RSOME(J,L)), where J is a parameter called memory order and L is the decision lag. The complexity of these algorithms is exponential in J ($J \leq K - 1$) and linear in L ($L \geq K - 1$). The reduced state consists of the J most recent symbols. The idea is to make tentative conditional decisions on the next recent $K - J - 1$ symbols conditioned on the state. These conditional decisions are fed back in the next iteration to compute the branch metrics. This method of trellis truncation works very well in causal interference (that arises in a whitened Gaussian CDMA channel) [5]. However, due to the non-causal nature of multiuser interference resulting from conventional matched filtering, the conditional decisions are rendered interference limited. Thus, the performance of the reduced-state scheme becomes highly interference limited if these conditional decisions are used in computing branch metrics. We overcome this difficulty by modifying the additive metric decomposition used for the recursion such that the

---

relevant non-causal interference components are accounted for in the decision statistic of the symbols on which conditional decisions are made. The non-causal interference components are obtained by making hard decisions on the corresponding symbols (given only the respective matched filter outputs) and introducing appropriate delay in the recursion. Although this in turn adds noise to the composite metric, the reliability of conditional decisions (that play the vital role of trellis truncation) is considerably improved, resulting in an overall improvement from the modification.

Simulation with a four-user, convolutionally coded, BPSK-modulated asynchronous CDMA system on an AWGN channel indicates that the reduced-state schemes perform quite well in most interference conditions. In fact, the reduced-state schemes considered outperformed full-state SOVA in low to medium MAI. The error rate for the reduced-state schemes however, does not approach single-user performance with increasing MAI as fast as the full state schemes, as can be expected. The optimum soft-output multiuser estimator gains $0.4 - 0.6$ dB over SOVA in power control.

Figure 1: BER comparison of various algorithms.

References

[1] Y. Li, B. Vucetic, Y. Sato, "Optimum Soft-Output Detection for Channels with Intersymbol Interference", *IEEE Trans. Information Theory*, Vol. 41, No. 3, May 1995.

[2] J. F. Hayes, T. M. Cover and J. B. Riera, "Optimal Sequence Detection and Optimal Symbol-by-Symbol Detection: Similar Algorithms", *IEEE Trans. Comm.*, Vol. COM-30, No. 1, Jan. 1982.

[3] J. Hagenauer and P. Hoeher, "A Viterbi Algorithm with Soft-Decision Outputs and its Applications", *Proc. Globecom*, Vol. 3, pp. 47.1.1-47.1.7, Nov. 1989.

[4] M. Rupf, F. Tarkoy, J. L. Massey, "User-Separating Demodulation for Code-Division Multiple-Access Systems", *IEEE J. Selected Areas Comm.*, Vol. 12, No. 5, June 1994.

[5] Abdulrauf Hafeez and Wayne E. Stark, "Soft-Output Multiuser Estimation for Asynchronous CDMA Channels", *IEEE Vehicular Technology conference*, May 1997.
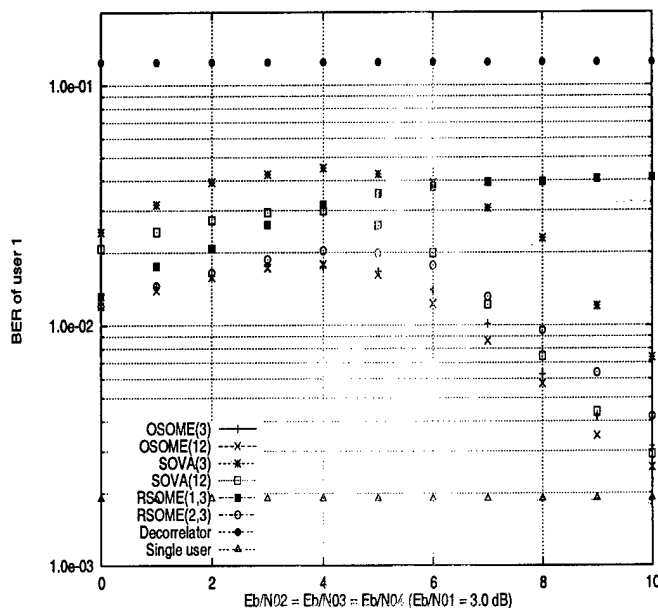
Figure 2: BER performance in near-far situation.

Decision Feedback Sequence Estimation

Abdulrauf Hafeez[1] and Wayne E. Stark
Electrical Engineering and Computer Science Department
1301 Beal Ave., Ann Arbor, MI 48109-2122.
Email: rauf@eecs.umich.edu, stark@eecs.umich.edu.

Abstract — A family of high-performance decision feedback sequence estimation receivers is described for various receive filtering approaches.

I. Summary

Maximum likelihood sequence estimation (MLSE) using the Viterbi algorithm is well-known as an optimum detection technique for signals corrupted with white Gaussian noise and inter-symbol interference (ISI). Two classic approaches to MLSE are due to Forney [1] and Ungerboeck [2]. Fig.1 shows the general structure of an MLSE receiver. A sequence of discrete-time sufficient statistic is extracted from the baseband received signal $y(t)$ by passing it through a front-end filter, followed by a sampler and optionally through a discrete-time noise-whitening filter. The front-end filter is usually matched to the transmit filter. In certain cases, the sampled output of the front-end filter depends on the past as well as future information symbols and is affected by correlated noise. This occurs in the case of fractional rate sampling, partial response signaling and multiuser DS-CDMA channels. The sampled output of a front-end filter matched to the overall channel response (transmit filter + medium) also has the above characteristic. Approaches similar to Forney utilize a noise-whitening filter as a result of which the statistic z_n depends on the past and present symbols only. Approaches similar to Ungerboeck, on the other hand, use a modified metric in the Viterbi algorithm so that the whitening filter is not needed. All of these approaches are equivalent in terms of performance, not considering joint channel/data estimation.

The complexity of MLSE is exponential in channel memory and can thus be prohibitive. Decision feedback sequence estimation [3] (DFSE) is a reduced complexity alternative to MLSE, which employs a reduced state Viterbi algorithm (RSVA) with state-conditional decision feedback. It is known that DFSE does not perform very well if the statistic is not whitened. On the other hand, the well-known form of DFSE that operates on whitened statistics performs very well (for minimum-phase channels). However, in time-varying conditions, it is difficult to compute the whitening filter. The filter would have to be recomputed every symbol period for a multiuser DS-CDMA channel employing long spreading codes. Moreover, in systems that perform bidirectional equalization like the GSM system, whitening has to be performed in both directions to get a minimum-phase response. Thus, it may be desirable to use DFSE without noise-whitening.
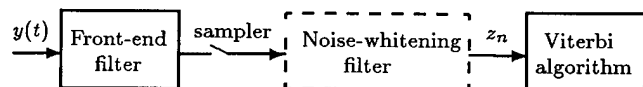
We have found that the cause for the poor performance of DFSE for unwhitened statistics is the existence of uncanceled anti-causal interference components. These components arise in the RSVA if the input statistic depends on future information symbols and affect the choice of survivor paths in the RSVA. Fortunately, the uncanceled interference components can be identified for a given model for the input statistic $\{z_n\}$ (which depends on the front-end filter and the sampler) by analyzing the pair-wise error event probability of the RSVA assuming no decision-error propagation. We propose a novel DFSE structure where the survivor paths are chosen based on the accumulated metric plus a bias term obtained from the analysis. The bias term uses tentative decisions to pre-cancel the effect of the anti-causal interference components on the choice of survivor paths. The tentative decisions are obtained from conventional symbol-by-symbol detection or from the preceding stage in a multistage scheme. The bias term does not add significantly to the complexity of DFSE.

In [4], a modified unwhitened decision feedback sequence estimation (MUDFSE) algorithm was derived for the case of the front-end filter matched to the overall channel response and symbol-rate sampling (i.e. the Ungerboeck formulation). The algorithm provides sizable gains over unwhitened DFSE for channels with low to moderate ISI and/or MAI. Simulation of an 8 user, BPSK-modulated, asynchronous DS-CDMA system with length 31 Gold spreading codes indicates that the modified algorithm with 4 states approaches the performance of MLSE with 128 states over an AWGN channel. Moreover, the modified algorithm obtains a gain of $4\frac{1}{2}$ dB over unwhitened DFSE at an error rate of 0.1% in power control.

We have derived an MLSE receiver which does not need noise-whitening like the Ungerboeck receiver but has a front-end filter matched to the transmit filter. The new receiver uses a branch metric in the Viterbi algorithm that does not depend on future medium response coefficients (unlike the Ungerboeck receiver) which is desirable when the coefficients have to be adapted. A DFSE structure corresponding to this new MLSE formulation has also been developed by examining the pair-wise error event probability of the RSVA with the new metric.

References

[1] G. D. Forney, "Maximum-Likelihood Sequence Estimation of Digital Sequences in the Presence of Intersymbol Interference," *IEEE Trans. IT*, Vol. IT-18, No. 3, pp. 363-378, May 1972.

[2] G. Ungerboeck, "Adaptive Maximum-Likelihood Receiver for Carrier-Modulated Data-Transmission Systems," *IEEE Trans. Comm.*, Vol. COM-22, No. 5, pp. 624-636, May 1974.

[3] A. Duel and C. Heegard, "Delayed Decision Feedback Sequence Estimation for QAM and Trellis Coded Systems," *20th Conf. Info. Sc. and Sys.*, pp. 367-372, Mar. 1986.

[4] A. Hafeez and W. E. Stark, "Decision Feedback Sequence Estimation for Unwhitened ISI Channels with Applications to Multiuser Detection," submitted to *IEEE JSAC*, April 1998.

Fig. 1: Receiver.

Decision Feedback Sequence Estimation for Unwhitened ISI and Multiuser CDMA Channels

Abdulrauf Hafeez[1] and Wayne E. Stark

Electrical Engineering and Computer Science Department

1301 Beal Ave., University of Michigan, Ann Arbor, MI 48109-2122.

E-mail: rauf@eecs.umich.edu, stark@eecs.umich.edu.

Abstract– Decision feedback sequence estimation (DFSE), which is a reduced-complexity alternative to maximum likelihood sequence estimation, performs very well for whitened (minimum-phase) inter-symbol interference (ISI) channels. However, it may not be feasible to compute the whitening filter for many time-varying channels like the multiuser asynchronous direct-sequence CDMA channel. Moreover, the performance of DFSE is not very good for many non-minimum-phase whitened ISI channels and for channels for which it is desirable to perform bidirectional equalization as in the GSM system. In these scenarios, it is beneficial to use the Ungerboeck formulation for sequence estimation which operates directly on the discrete-time unwhitened statistic obtained from conventional matched filtering. In this paper, we show that conventional decision-feedback sequence estimation in the Ungerboeck form is interference limited. An error probability analysis leads us to a modified unwhitened decision feedback sequence estimator (MUDFSE). Simulation results indicate that the modified algorithm used on unwhitened ISI channels with low to moderate dispersion, provides similar performance/complexity tradeoffs as the DFSE used on the corresponding whitened *minimum-phase* channels. The algorithm is especially attractive for multiuser detection for asynchronous DS-CDMA channels with long spreading codes, where it obtains sizable gains over the (unwhitened) M-algorithm.

1 Introduction

There are two main approaches to maximum likelihood sequence estimation (MLSE) for inter-symbol interference (ISI) channels with additive noise. Forney's approach [1] consists of using the Viterbi algorithm on the sampled output of whitened matched filters while Ungerboeck's formulation [2] operates directly on conventional matched filter output samples without the need for noise whitening. Due to the exponential complexity of these methods, several low-complexity sub-optimal schemes have been developed. A promising reduced-complexity alternative to MLSE using Forney's approach is decision feedback sequence esti-

mation (DFSE) [3], [4]. The scheme provides an excellent tradeoff between performance and complexity.

The performance of DFSE is sensitive to channel phase. While the best performance is obtained for minimum-phase channels, the performance may not be adequate for non-minimum phase channels. In the GSM system, training sequences are inserted in the middle of the burst to aid channel estimation. Equalization over the data field is then performed bi-directionally starting out from the training sequence [5]. If the channel response is minimum-phase in one direction, it is maximum-phase in the other. DFSE performs poorly in maximum-phase conditions.

Decision feedback sequence estimation can be employed for multiuser detection. In direct-sequence CDMA systems, the spreading of users' transmit pulses with long non-orthogonal spreading codes, and the arrival and departure of users gives rise to a rapidly time-varying multiuser interference channel. Conventional matched filter outputs are affected by non-causal interference and correlated noise. Thus, noise whitening has to be employed in order to use DFSE. However, noise whitening in a time-varying environment [6] is computationally expensive.

Ungerboeck's formulation for sequence estimation is better suited in conditions such as mentioned above. A reduced-state Ungerboeck variant to DFSE, which we call unwhitened decision feedback sequence estimation (UDFSE)[2], was derived in [7][2] and [5]. It operates on discrete-time unwhitened statistics obtained from conventional matched filtering and is thus insensitive to channel phase. However, the scheme does not perform as well as DFSE on most channels. The problem arises from the nature of unwhitened statistics which depend on both past and future input symbols. Thus, a decision rule similar to DFSE, which decides in favor of the path with the best accumulated (Euclidean distance) metric, leading to a reduced state, fails to account for interference from the future inputs not included in the reduced state. As a result, the decisions obtained in UDFSE are interference-limited even in the absence of feedback errors. The M-algorithm [8], used on unwhitened statistics, suffers from a similar problem: paths selected based on accumulated metrics do not reflect the effect of anti-causal interference com-

---

[2]The scheme is referred to as Delayed Decision Feedback Sequence Estimation with *a standard matched filter* in [7]

ponents. Thus, its performance is rather poor as noted by Wei *et. al* for CDMA systems [9].

In the case of UDFSE, where the reduced state is pre-determined, the decision rule can be modified to take into account the effect of the relevant anti-causal components. The decision rule in the modified UDFSE algorithm selects survivor paths based on the accumulated Ungerboeck metric plus a bias term that pre-cancels the effect of the interfering anti-causal inputs on the choice of survivor paths using tentative decisions. The bias term follows from an error probability analysis of the UDFSE algorithm. It can be obtained by using conventional hard decisions on the anti-causal inputs or by using decisions obtained at the output of the preceding stage in a multistage scheme.

The paper is organized as follows. We present the system model in section 2. The two approaches to MLSE are reviewed in section 3. In section 4, we describe various methods of decision-feedback sequence estimation in detail. We show that UDFSE is interference limited which leads us to the modified UDFSE algorithm. In section 5, we analyze the error performance of the proposed detector. Simulation results are presented in section 6 where the performance of the various schemes is compared for single user ISI and multiuser DS-CDMA channels.

2   System model

Consider the transmission of linearly-modulated digital data over a (time-varying) time-dispersive additive white Gaussian noise channel. Assume that the receiver has perfect knowledge of the carrier phase, the symbol timing and the impulse response of the channel. After coherent down-conversion, the receiver employs a filter $h_n(t)$ matched to the cascade of the transmit pulse-shaping filter and the channel impulse response and samples the output at symbol spaced intervals. The sequence of sampled matched filter outputs is a sufficient statistic for estimating the transmitted sequence in the absence of excess bandwidth. Thus, an equivalent discrete-time channel model is obtained.

The matched filter output at time n is given by

$$y_n = \sum_{i=-L}^{L} s_{n,i} b_{n-i} + z_n \tag{1}$$

where $\{b_n\}$ is the transmitted data sequence assumed to be i.i.d. ($b_n \in A_M$, an M-ary alphabet), $\{z_n\}$ is a complex Gaussian noise process with mean 0 and covariance $E[z_n^* z_{n-i}] = N_0 s_{n,i}$, and $\{s_{n,i}\}$ is the sampled channel autocorrelation function at time n, given by

$$s_{n,i} = \begin{cases} h_n^*(-t) * h_n(t)|_{t=iT} & |i| \le L \\ 0 & |i| > L \end{cases} \tag{2}$$

where L is the (finite) channel memory in symbol intervals. We will refer to the above model as the unwhitened model.

Let $s_n(D) = \sum_i s_{n,i} D^i$, then an equivalent discrete-time white Gaussian noise model is obtained by noting that

$$s_n(D) = f_n^*(D^{-1}) f_n(D)$$

where $f_n(D) = \sum_{i=0}^{L} f_{n,i} D^i$ has all its roots inside the unit circle (minimum-phase channel). The statistic obtained from filtering $\{y_n\}$ using the anti-causal whitening filter $1/f_n^*(D^{-1})$, is given by

$$y_n' = \sum_{i=0}^{L} f_{n,i} b_{n-i} + z_n' \tag{3}$$

where $\{z_n'\}$ is a proper[3] complex white Gaussian noise process with mean 0 and variance N_0.

3   Maximum likelihood sequence estimation

The maximum likelihood sequence estimator (MLSE) determines as the most likely sequence transmitted, the sequence b^N that maximizes the metric [2]

$$U\left(y^N, b^N\right) = \sum_{n=1}^{N} 2\mathrm{Re}\{b_n^* y_n\} - \sum_{i=1}^{N}\sum_{k=1}^{N} b_i^* s_{i,k} b_k \tag{4}$$

where $x^n = x_1, x_2, \ldots, x_n$. Under the condition:

$$s_{n,i} = s_{-i,-i}^* \text{ or equivalently } s_{n,-i} = s_{n+i,i}^*, \tag{5}$$

the above metric can be computed recursively as

$$U(y^n, b^n) = U(y^{n-1}, b^{n-1}) + V(y_n, b_n, \sigma_n) \tag{6}$$

where $V(\cdot)$ is known as the branch metric and is given by

$$V(y_n, b_n, \sigma_n) = \mathrm{Re}\left\{ b_n^* \left(2y_n - s_{n,0}b_n - 2\sum_{i=1}^{L} s_{n,i} b_{n-i} \right) \right\} \tag{7}$$

and $\sigma_n = b_{n-1}, b_{n-2}, \ldots, b_{n-L}$ is the state at time n.

The above is a more generalized form of the Ungerboeck formulation (where $s_{n,i} = s_i$ i.e. the channel is fixed), independently derived in [10] in detail. Condition (5) holds for time-varying channels like the asynchronous DS-CDMA channel. The application of this algorithm to optimum multiuser detection for DS-CDMA was noted in [11].

The maximum likelihood sequence can be determined equivalently by applying the Viterbi algorithm on the whitened statistic $\{y_n'\}$ as shown in [1], using the metric

$$U'\left(y'^N, b^N\right) = \sum_{n=1}^{N} \left[2\mathrm{Re}\left(y_n' \sum_{i=0}^{L} f_{n,i}^* b_{n-i}^* \right) - \left\| \sum_{i=0}^{L} f_{n,i} b_{n-i} \right\|^2 \right] \tag{8}$$

which can be computed recursively as

$$U'\left(y'^n, b^n\right) = U'(y'^{n-1}, b^{n-1}) + V'(y_n', b_n, \sigma_n) \tag{9}$$

where

$$V'(y_n', b_n, \sigma_n) = 2\mathrm{Re}\left(y_n' \sum_{i=0}^{L} f_{n,i}^* b_{n-i}^* \right) - \left\| \sum_{i=0}^{L} f_{n,i} b_{n-i} \right\|^2 . \tag{10}$$

The two algorithms require the same order of computational complexity and storage proportional to M^L.

---

[3] $E[\mathrm{Re}\{z_n'\}\mathrm{Im}\{z_n'\}] = 0$

4 Decision feedback sequence estimation

A reduced-complexity sub-optimal alternative to MLSE using the Viterbi algorithm is decision feedback sequence estimation DFSE [3], [4]. A parameter called memory order J is chosen arbitrarily smaller than channel memory L and the trellis is collapsed into M^J states corresponding to the J most recent hypothesized symbols only. Since the reduced state falls short in providing all the information needed to compute branch metrics, the algorithm uses the path with the best accumulated metric leading to each state to extract the rest of the information. Note that this algorithm operates on whitened statistics $\{y'_n\}$ which depend on past and present inputs only.

4.1 UDFSE

In this section, we outline decision-feedback sequence estimation in the Ungerboeck form (UDFSE, derived in [7]).

Let $\beta_n = b_{n-1}, b_{n-2}, \ldots, b_{n-J}$ represent the reduced state at time n and $m(\beta_n)$ be the associated path metric, defined as

$$m(\beta_n) \triangleq \max_{b^{n-J-1}} U(y^n, b^n). \tag{11}$$

Then the algorithm can be summarized as:

$$m(\beta_{n+1}) = \max_{b_{n-J}}[m(\beta_n) + W(y_n, b_n, \beta_n)] \tag{12}$$

where $W(y_n, b_n, \beta_n)$ is the branch metric, given by

$$
\begin{aligned}
W(y_n, b_n, \beta_n) =\ & \mathrm{Re}\left\{ b_n^* \left(2y_n - s_{n,0} b_n - 2\sum_{i=1}^{J} s_{n,i} b_{n-i} \right.\right. \\
& \left.\left. - 2\sum_{i=J+1}^{L} s_{n,i} \hat{b}_{n-i}(\beta_n) \right) \right\},
\end{aligned} \tag{13}
$$

where $\{\hat{b}(\beta_n)\}$ are tentative conditional decisions on inputs more than J samples in the past, obtained from the path with the best accumulated metric, leading to state β_n, as

$$\hat{b}_{n-J}(\beta_{n+1}) = \arg\max_{b_{n-J}}[m(\beta_n) + W(y_n, b_n, \beta_n)]. \tag{14}$$

4.1.1 A Drawback of UDFSE

Although both full-state formulations in section 3 yield the maximum likelihood sequence estimate, the reduced-state derivation UDFSE does not perform nearly as well as its whitened channel counterpart (DFSE) on most channels. The problem arises from the nature of unwhitened statistic $\{y_n\}$ which depends on both past and future input symbols. Note that the UDFSE algorithm, when deciding b_{n-J} (conditionally) in the n-th step (14), ignores interference from inputs $b_{n+1}, b_{n+2}, \ldots, b_{n-J+L}$ which directly affect output sample y_{n-J} (corresponding to b_{n-J}). Thus, the

decision rule of (14) which is based on the knowledge of only J inputs in the future is inherently near-sighted. Unlike DFSE, the decisions obtained in UDFSE are therefore interference-limited even in the absence of feedback errors. This observation is quantified by the following analysis.

Let $\{\dot{b}_n\}$ be the sequence transmitted, which is eliminated in the UDFSE algorithm in favor of another sequence $\{\bar{b}_n\}$. Let $\{\dot{\beta}_n\}$ be the sequence of states in the path of $\{\dot{b}_n\}$ and $\{\bar{\beta}_n\}$ be the sequence of states in the path of $\{\bar{b}_n\}$. An error event occurs between times n_1 and n_2 if:

$$\bar{\beta}_n = \dot{\beta}_n \text{ for } n = n_1, n_2 \text{ and } \bar{\beta}_n \neq \dot{\beta}_n \text{ for } n_1 < n < n_2. \tag{15}$$

We will show that the probability of this error event (i.e. the pairwise error probability) depends on the value of inputs $\dot{b}_{n_2}, \dot{b}_{n_2+1}, \ldots, \dot{b}_{n_2-1+L-J}$ in the absence of error propagation (from any previous error events).

Proof: Let $e_n = \bar{b}_n - \dot{b}_n$ be the error sequence. Assume:

$$e_n = 0 \text{ for } n_1 - L \leq n \leq n_1 - J - 1, \tag{16}$$

i.e. there are no errors $L - J$ steps prior to the error event. The error event occurs if the accumulated metric on the incorrect path is greater than that on the correct path at the point where the two paths merge i.e.

$$\sum_{n=n_1}^{n_2-1} W(y_n, \bar{b}_n, \bar{\beta}_n) > \sum_{n=n_1}^{n_2-1} W(y_n, \dot{b}_n, \dot{\beta}_n). \tag{17}$$

Substituting branch metrics from (13) and noting that $\{\hat{b}_{n-i}(\bar{\beta}_n)\}$ and $\{\hat{b}_{n-i}(\dot{\beta}_n)\}$ are decisions taken from paths corresponding to the sequence of states $\{\bar{\beta}_n\}$ and $\{\dot{\beta}_n\}$ respectively, (17) is equivalent to

$$
\begin{aligned}
& \sum_{n=n_1}^{n_2-1} \mathrm{Re}\left\{ \bar{b}_n^* \left(2y_n - s_{n,0}\bar{b}_n - 2\sum_{i=1}^{L} s_{n,i}\bar{b}_{n-i} \right) \right\} > \\
& \sum_{n=n_1}^{n_2-1} \mathrm{Re}\left\{ \dot{b}_n^* \left(2y_n - s_{n,0}\dot{b}_n - 2\sum_{i=1}^{L} s_{n,i}\dot{b}_{n-i} \right) \right\} \tag{18}
\end{aligned}
$$

Using (1), (16) and noting that $e_n = 0$ for $n_2 - J \leq n \leq n_2 - 1$ as $\bar{\beta}_{n_2} = \dot{\beta}_{n_2}$, it can be shown that the above inequality holds if

$$
\begin{aligned}
& \sum_{n=n_1}^{n_2-1-J} \mathrm{Re}\{2e_n^* z_n\} > \sum_{n=n_1}^{n_2-1-J} \mathrm{Re}\left\{ e_n^* \left(s_{n,0}e_n + 2\sum_{i=1}^{L} s_{n,i}e_{n-i} \right) \right\} \\
& \quad - \sum_{n=n_2-L}^{n_2-1-J} \mathrm{Re}\left\{ e_n^* \left(2\sum_{i=n_2-n}^{L} s_{n,-i}\dot{b}_{n+i} \right) \right\} \tag{19}
\end{aligned}
$$

The left hand side of (19) is a Gaussian random variable with mean 0 and variance that depends on the error sequence. While the first term on the right hand side of (19) depends on the error sequence only, the second term in addition, depends on inputs $\dot{b}_{n_2}, \dot{b}_{n_2+1}, \ldots, \dot{b}_{n_2-1+L-J}$. $\square$

The above analysis suggests that if the term which depends on the $L-J$ future inputs is absorbed in the decision

rule of UDFSE, the pairwise error probability of the modified detector will depend on the error sequence only. This, of course, requires knowledge of some future inputs. In practice, tentative hard decisions can be used instead as described in the following section.

4.2 Modified UDFSE

The modified algorithm (MUDFSE) can be outlined as follows: path metrics are computed as in UDFSE using (12). Conditional decisions are made (and the corresponding survivor paths are chosen) using the modified rule:

$$\hat{b}_{n-J}(\beta_{n+1}) = \arg\max_{b_{n-J}}[m(\beta_n) + W(y_n, b_n, \beta_n) - \text{bias}(\beta_n)]$$

(20)

where

$$\text{bias}(\beta_n) = \sum_{j=n-L+1}^{n-J} \text{Re}\left\{2b_j^* \sum_{i=n-j+1}^{L} s_{j,-i}\tilde{b}_{j+i}\right\}, \quad (21)$$

$$\tilde{b}_n = \text{sign}(y_n). \quad (22)$$

The algorithm is delayed by $L - J$ samples as y_{n+L-J} is needed in the nth step. Note that (21) depends on b_{n-J} (the bit falling out of the state) and $b_{n-J-1}, \ldots, b_{n-L+1}$ for which conditional decisions, taken from the path leading to state β_n, are used. The bias can be simplified to include only the leading term which depends on b_{n-J} as follows:

$$\text{bias}(\beta_n) \approx \text{bias}(b_{n-J}) = \text{Re}\left\{2b_{n-J}^* \sum_{i=J+1}^{L} s_{n-J,-i}\tilde{b}_{n-J+i}\right\}.$$

(23)

The approximate bias is independent of the state. It does not add significantly to the computational load and storage requirement of the algorithm which is on the order of $(G - J)M^J$ (same as DFSE), where G is the decision lag.

4.3 Multistage MUDFSE

The MUDFSE algorithm can be run in a multistage configuration where decisions obtained at the output of the first stage are fed back to compute the bias in the second stage and so on, i.e.

$$(\tilde{b}_n)_1 = \text{sign}(y_n) \text{ and } (\tilde{b}_n)_i = (\bar{b}_n)_{i-1}, \quad i > 1$$

where $\{(\bar{b}_n)_i\}$ are decisions obtained from the ith stage at lag G_i ($G_i \gg L$). Note that decisions $\{(\bar{b}_n)_1\}$ are likely to be much more reliable than $\{(\tilde{b}_n)_1\}$. The complexity and delay of a Q-stage scheme is given by $\sum_{i=1}^{Q}(G_i - J_i)M^{J_i}$ and $\sum_{i=1}^{Q} G_i + L - J_1$ respectively.

5 Error performance

Assuming stationarity (i.e. $s_{n,i} = s_i$) and the absence of decision errors prior to the start of an error event, the beginning of the error event can be arbitrary aligned with time $n = 1$. In the following sections, we find the probability that an error event occurs in modified UDFSE.

5.1 Genie-aided MUDFSE

Assume that perfect information is provided by a genie on the future inputs needed to compute the bias in (21) (i.e. $\tilde{b}_n = \dot{b}_n$ (21)). Then, it follows from (19)-(21) that an error event ε of length n_ε symbols occurs if

$$\sum_{n=1}^{n_\varepsilon} \text{Re}\{2e_n^* z_n\} > \delta^2(\varepsilon) \quad (24)$$

where $\delta^2(\varepsilon)$ is called the distance of ε and is given by

$$\delta^2(\varepsilon) = \sum_{n=1}^{n_\varepsilon} \sum_{k=1}^{n_\varepsilon} e_n^* s_{n-k} e_k. \quad (25)$$

The left-hand side of (24) is a Gaussian random variable with mean zero and variance $4\delta^2(\varepsilon)N_0$. Thus, the probability that the error event occurs is given by

$$\Pr(\varepsilon) = Q\left(\frac{\delta(\varepsilon)}{2\sqrt{N_0}}\right). \quad (26)$$

Note that this expression for the pairwise error event probability of genie-aided MUDFSE is identical to the expression derived in [2] for MLSE. However, there is an important distinction in the definition of error events for MUDFSE and MLSE. A valid error sequence for J-order MUDFSE ($1 \le J \le L$) can have no more than $J - 1$ consecutive zeros according to the definition in (15), whereas $J = L$ for MLSE. When $J = 0$, all error sequences have length $n_\varepsilon = 1$ symbol. This implies that $\delta^2(\varepsilon) = |e|^2 s_0 \ \forall \varepsilon$. In other words, a 0-order genie-aided MUDFSE approaches the performance of the ISI-free channel. Notice that the analysis does not consider decision error propagation.

5.2 MUDFSE

The error event probability for MUDFSE in the absence of ideal bias depends, in addition to the distance of the error event, on the residual interference arising from decision errors on the $L - J$ inputs ($\dot{b}_{n_\varepsilon+J+1}, \ldots, \dot{b}_{n_\varepsilon+L}$) following the error event. Using (19)-(21), we get

$$\Pr(\varepsilon) = Q\left(\frac{\delta^2(\varepsilon) + \gamma(\varepsilon)}{2\delta(\varepsilon)\sqrt{N_0}}\right) \quad (27)$$

where $\gamma(\varepsilon)$ is the residual interference, given by

$$\gamma(\varepsilon) = \sum_{n=\max(n_\varepsilon+J+1-L,1)}^{n_\varepsilon} \text{Re}\left\{e_n^*\left(2\sum_{i=n_\varepsilon+J+1-n}^{L} s_{-i}\lambda_{n+i}\right)\right\}$$

(28)

and $\lambda_n = \tilde{b}_n - \dot{b}_n$ is the decision error.

Note that when $J = 0$, MUDFSE reduces to the zero-forcing decision-feedback detector for unwhitened channels (without the feed-forward filter). Unlike DFSE, where error event distances diminish in general when memory order J is decreased as compared to channel memory L, the distances for MUDFSE remain the same as in the case
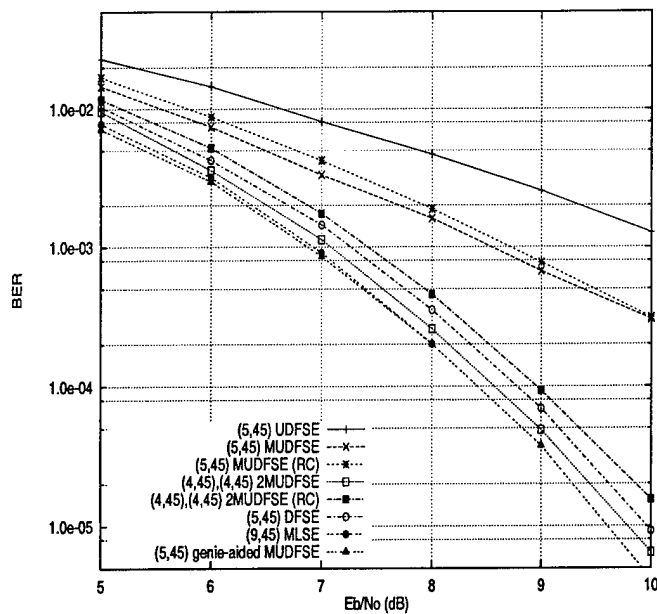
Figure 1: BER performance of various detection schemes over an ISI channel.

Figure 2: BER performance of various detection schemes on an 8-user asynchronous DS-CDMA channel.

$J = L$ (MLSE). The variance of the residual interference $\gamma(\varepsilon)$, however, increases from zero as the memory order J is made smaller than L in MUDFSE. This sharp contrast between the behavior of MUDFSE and DFSE is consistent with the fact that the operation of matched filtering collects all the energy of the pulse transmitted at time n into the corresponding output sample y_n [2], while the operation of noise whitening results in the scattering of some of this energy into subsequent output samples.

6   Performance results

Performance is evaluated via simulation. First, we consider binary signaling over a static time-dispersive additive white Gaussian noise channel, given by $f = (0.8614394, 0.2584344, -0.1000742, -0.2740468,$ $0.130008, 0.1000742, -0.0375511, 0.1122497, -0.1137419,$ $- 0.22837)$. The channel is minimum phase and is arbitrarily chosen. The receiver has perfect knowledge of the symbol timing and the impulse response of the channel.

Figure 1 shows the bit-error rate performance of various schemes on the ISI channel. Each simulation was run for a count of 1000 errors. The various schemes are indexed with the memory order and the decision lag (J, G). Except DFSE, all algorithms operate on symbol-spaced samples obtained at the output of conventional matched filters. Ideal noise whitening is assumed for DFSE. All schemes shown in Fig. 1, except MLSE, require similar overall complexity and storage. Fig. 1 shows that the $(5, 45)$ Modified UDFSE algorithm gains $1.0 - 1.7$ dB over $(5, 45)$ UDFSE. The two-stage scheme $[(4, 45), (4, 45)]$ 2MUDFSE closely approaches MLSE performance and obtains $0.6 - 2.2$ dB
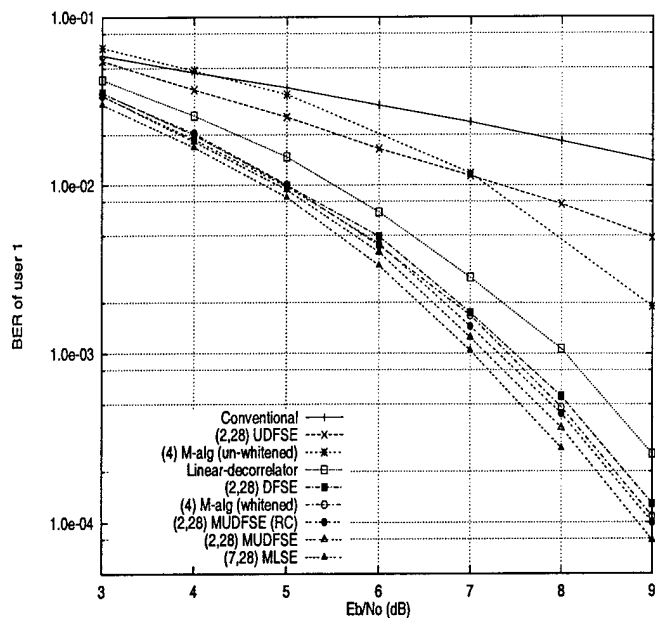
gain over the single-stage scheme $(5, 45)$ MUDFSE. With bias approximation (23), the corresponding MUDFSE (reduced computation) schemes, lose less than 0.5 dB. The error rate of $(5, 45)$ genie-aided MUDFSE is slightly better than MLSE as discussed in section 5.1.

The performance of $(5, 45)$ DFSE is also close to MLSE for the ISI channel as shown in Fig. 1. Here we have neglected the effects of non-ideal noise-whitening (due to fixed delay constraint) on the performance of DFSE. The delay incurred from anti-causal filtering can be compared to the delay of a multi-stage MUDFSE scheme. As the channel used for Fig. 1 is minimum-phase, the performance achieved by DFSE is the best possible. The performance of MUDFSE, however, is independent of channel phase.

Next, we simulate a BPSK modulated asynchronous DS-CDMA system with eight users whose signature waveforms are derived from Gold sequences of length 31. The relative delays of users are fixed for the simulation and are in an increasing order. Figure 2 shows the bit-error rate of user 1 for various schemes when all users have identical signal-to-noise ratio. Each simulation was run for a count of 500 errors. It is evident that even with ideal power control, the performance of the conventional single-user detector is significantly worse than optimum MLSE. With four states, $(2, 28)$ UDFSE and (4) M-algorithm that operate directly on the matched filter output, do not improve much over the conventional detector. Linear-decorrelator that nulls out all interference, loses about $0.7 - 1.0$ dB compared to MLSE. $(2, 28)$ DFSE and (4) M-algorithm that operate on the equivalent whitened minimum-phase channel, obtain near MLSE performance. The proposed single-stage modified UDFSE algorithms by far give the best performance on this channel (next to MLSE). This
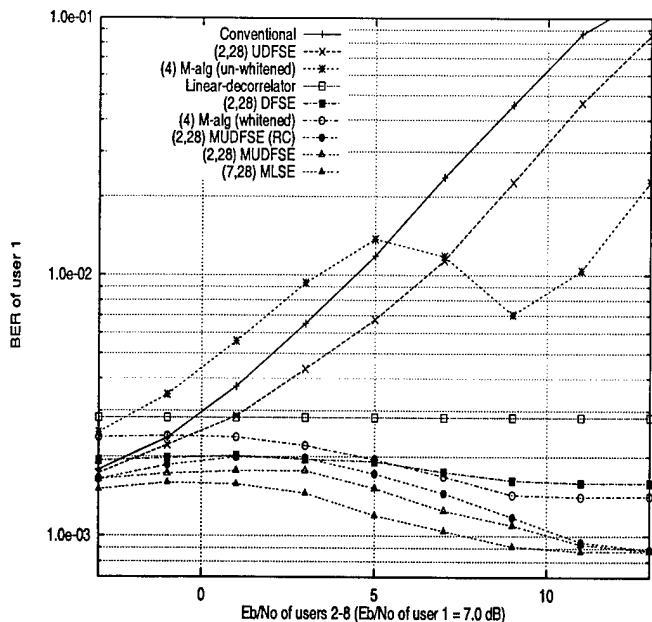
Figure 3: Near-far performance of various detection schemes on an 8-user asynchronous DS-CDMA channel.

behavior is attributable to low channel cross-correlations typical of well-designed spreading codes (compare to the channel in Figure 1). $(2,28)$ MUDFSE (with four states only) closely approaches the performance of MLSE (128 states) and gains $1.2 - 3.2$ dB over UDFSE.

Figure 3 shows the bit-error rate of user 1 versus the signal-to-noise ratio of the rest of the users. SNR of user 1 is held constant at 7.0 dB. It can be seen that the conventional detector, UDFSE and the unwhitened M-algorithm are limited by multiuser interference. The error-rate of linear-decorrelator is the same as that of MLSE under worst case interference. In other conditions, DFSE and the whitened M-algorithm perform better. The proposed modified UDFSE schemes outperform the other methods and converge to MLSE in high multiuser interference.

7 Conclusions

In this paper, we show that conventional decision feedback sequence estimation with the Ungerboeck formulation as proposed in [7] (for unwhitened ISI channels) is interference-limited. We derive a modified unwhitened decision feedback sequence estimation algorithm which alleviates this problem. On channels with low-to-moderate dispersion, the algorithm provides excellent performance/complexity tradeoffs. The algorithm is insensitive to channel phase and does not require noise-whitening. These attributes make it especially attractive for bi-directional equalization in the GSM system and multiuser detection in asynchronous DS-CDMA systems.

References

[1] G. D. Forney, "Maximum-Likelihood Sequence Estimation of Digital Sequences in the Presence of Intersymbol Interference", *IEEE Trans. Information Theory*, Vol. IT-18, No. 3, pp. 363-378, May 1972.

[2] G. Ungerboeck, "Adaptive Maximum-Likelihood Receiver for Carrier-Modulated Data-Transmission Systems", *IEEE Trans. Comm. Technology*, Vol. COM-22, No. 5, pp. 624-636, May 1974.

[3] A. Duel-Hallen and C. Heegard, "Delayed Decision-Feedback Sequence Estimation", *IEEE Trans. Comm.*, Vol. 37, No. 5, pp. 428-436, May 1989.

[4] V. M. Eyuboglu and S. U. Qureshi, "Reduced-state Sequence Estimation with Set Partitioning and Decision Feedback", *IEEE Trans. Comm.*, pp. 13-20, Jan. 1988.

[5] K. Wesolowski, R. Krenz and K. Das, "Efficient Receiver Structure for GSM Mobile Radio", *Int. J. Wireless Information Networks*, Vol. 3, No. 2, 1996.

[6] L. Wei and L. K. Rasmussen, "A Near Ideal Noise Whitening Filter for an Asynchronous Time-Varying CDMA System", *IEEE Trans. Comm.*, Vol. 44, No. 10, pp. 1355-1361, Oct. 1996.

[7] A. Duel and C. Heegard, "Delayed Decision Feedback Sequence Estimation for QAM and Trellis Coded Systems", *20th Conf. Info. Sc. and Sys.*, pp. 367-372, Mar. 1986.

[8] J. B. Anderson and S. Mohan, "Sequential Coding Algorithms: A Survey Cost Analysis", *IEEE Trans. Comm.*, Vol. COM-32, pp. 169-176, Feb. 1984.

[9] L. Wei, L. K. Rasmussen and R. Wyrwas, "Near Optimum Tree-Search Detection Schemes for Bit-Synchronous Multiuser CDMA Systems over Gaussian and Two-Path Rayleigh-Fading Channels", *IEEE Trans. Comm.*, Vol. 45, No. 6, pp. 691-700, June 1997.

[10] G. E. Bottomley and S. Chennakeshu, "Adaptive MLSE Equalization Forms for Wireless Communications", *Fifth Virginia Tech. Symp. Wireless Personal Comm.*, pp. 20-1-20-12, May 1995.

[11] S. Verdu, "Minimum Probability of Error for Asynchronous Gaussian Multiple-Access Channels", *IEEE Trans. Info. Th.*, Vol. IT-32, No. 1, pp. 85-96, Jan. 1986.

Decision Feedback Sequence Estimation for Unwhitened ISI Channels with Applications to Multiuser Detection

Abdulrauf Hafeez[1] and Wayne E. Stark

Electrical Engineering and Computer Science Department

1301 Beal Ave., University of Michigan, Ann Arbor, MI 48109-2122.

E-mail: rauf@eecs.umich.edu, stark@eecs.umich.edu.

Abstract– Decision feedback sequence estimation (DFSE), which is a reduced-complexity alternative to maximum likelihood sequence estimation, can be used effectively for equalization of inter-symbol interference as well as for multiuser detection. The algorithm performs very well for whitened (minimum-phase) channels. For non-minimum-phase channels, however, the algorithm is not very effective. Moreover, DFSE requires a noise-whitening filter, which may not be feasible to compute for time-varying channels like a multiuser DS-CDMA channel. Noise-whitening is also cumbersome for applications that involve bi-directional equalization such as the GSM system. In such conditions, it is desirable to use the Ungerboeck formulation for sequence estimation which operates directly on the discrete-time unwhitened statistic obtained from conventional matched filtering. Unfortunately, decision feedback sequence estimation based on matched filter statistics is severely limited by untreated interference components. In this paper, we identify the anti-causal interference components using an error probability analysis. This leads us to a modified unwhitened decision feedback sequence estimator (MUDFSE) where the components are canceled using tentative decisions. We obtain approximate error probability bounds for the proposed algorithm. Performance results indicate that the modified algorithm used on unwhitened channels with relatively small channel correlations, provides similar

1

performance/complexity tradeoffs as the DFSE used on the corresponding whitened *minimum-phase* channels. The algorithm is especially attractive for multiuser detection for asynchronous direct sequence CDMA channels with long spreading codes, where it can achieve near-MLSE performance with exponentially lower complexity.

Index Terms– Equalizers, decision feedback equalizers, intersymbol interference, multiuser detection, multiuser channels, sequence estimation, Viterbi detection, CDMA.

1 Introduction

There are two main approaches to maximum likelihood sequence estimation (MLSE) for inter-symbol interference (ISI) channels with additive noise. Forney's approach [1] consists of using the Viterbi algorithm on the sampled output of whitened matched filters while Ungerboeck's formulation [2] operates directly on conventional matched filter output samples without the need for noise whitening. Due to the exponential complexity of these methods, several low-complexity sub-optimal schemes have been developed. A promising reduced-complexity alternative to MLSE using Forney's approach is decision feedback sequence estimation (DFSE) [3], [4]. This scheme provides an excellent tradeoff between performance and complexity by reducing the memory order of the Viterbi algorithm and employing conditional decision feedback to cancel the tail of the ISI.

A drawback of DFSE is that its performance is sensitive to channel phase. While the best performance is obtained for minimum-phase channels, the performance may not be adequate for non-minimum phase channels. In the GSM system, training sequences are inserted in the middle of the burst to aid channel estimation. Equalization over the data field is then performed bi-directionally starting out from the training sequence [5]. If the channel response is minimum-phase in one direction, it is maximum-phase in the other[2]. DFSE performs poorly in maximum-phase conditions and is thus unsuitable for equalization in this case.

Besides channels with inter-symbol interference, decision feedback sequence estimation can be employed for multiuser detection. In direct-sequence CDMA systems, the use of long spreading codes, and the arrival and departure of users gives rise to a time-varying multiuser interference channel. The sequence of statistics obtained at the output of a bank of matched filters is affected by non-causal multiple-access

---

[2]Minimum-phase response can be obtained for both directions by means of appropriate all-pass filters.

interference and correlated noise [6]. In order to use DFSE, the statistic has to be filtered to make the noise white and the interference causal. Noise whitening filters have been proposed for a time-varying environment [7]. However, the operation is computationally expensive.

Ungerboeck's formulation for sequence estimation is better suited in conditions such as those mentioned above. A reduced-state Ungerboeck-type variant to DFSE, which we call unwhitened decision feedback sequence estimation (UDFSE), was derived in [8][3] and [5]. It operates on discrete-time unwhitened statistics obtained from conventional matched filtering. UDFSE is thus insensitive to channel phase and does not require a noise-whitening filter. However, the scheme does not perform as well as DFSE on most channels. This is because unlike whitened statistics, which depend on the past input symbols only, unwhitened statistics depend on both the past and future input symbols. The decision rule of DFSE selects the survivor path with the best accumulated (Euclidean distance) metric leading to a reduced state. The same decision rule when used with an Ungerboeck metric (as in UDFSE), fails to account for interference from the future inputs not represented in the reduced state (but would have been represented in the full-blown state). As a result, the decisions obtained in UDFSE are affected by untreated interference even in the absence of feedback errors. The M-algorithm [9], used on unwhitened statistics, suffers from a similar problem: survivor paths are chosen on the basis of an accumulated metric which does not reflect the effect of some anti-causal interference components. Thus, the performance of the unwhitened M-algorithm is rather poor as noted by Wei *et. al* for CDMA systems [10].

In the case of UDFSE, the decision rule can be modified to take into account the effect of the interfering anti-causal components. The decision rule in the modified UDFSE algorithm selects survivor paths based on the accumulated Ungerboeck metric plus a *bias* term that pre-cancels the effect of the interfering anti-causal inputs on the choice of survivor paths using tentative decisions. The *bias* term is determined by examining the pairwise error probability of the UDFSE algorithm. It can be computed by using conventional decisions based on matched filter outputs or by using decisions obtained at the output of the preceding stage in a multistage scheme. A reduced computation form of the modified detector was proposed in [11].

The rest of the paper is organized as follows. We present the system model in Section 2. The two classic approaches to MLSE are reviewed in Section 3. In

---

[3]The scheme is referred to as Delayed Decision Feedback Sequence Estimation with *a standard matched filter* in [8].

3

Section 4, we describe various methods for decision-feedback sequence estimation in detail. We show that UDFSE performance is limited by untreated ISI which leads us to the modified UDFSE algorithm. In Section 5, we obtain approximate bounds on the symbol error probability of UDFSE and the modified algorithm. In Section 6, we illustrate how the bounds can be evaluated using error-state diagrams. Performance results are presented in Section 7 where the BER performance of the various schemes is compared for single user ISI and multiuser DS-CDMA channels using analysis and simulation.

2 System model

Consider the transmission of linearly-modulated digital data over a (time-varying) time-dispersive additive white Gaussian noise channel. Assume that the receiver has perfect knowledge of the carrier phase, the symbol timing and the impulse response of the channel. After coherent down-conversion, the receiver employs a filter matched to the cascade of the transmit pulse-shaping filter and the channel impulse response (assumed to be fixed for the duration of the transmit filter) and samples the output at symbol spaced intervals. The sequence of sampled matched filter outputs is known to be a sufficient statistic for estimating the transmitted sequence. Thus, an equivalent discrete-time channel model is obtained. The matched filter output at time n is given by

$$y_n = \sum_{i=-L}^{L} s_{n,i} b_{n-i} + z_n \qquad (1)$$

where $\{b_n\}_{n=1}^{N}$ is the transmitted data sequence assumed to be independent and identically distributed ($b_n \in A_M$, an M-ary alphabet), $\{z_n\}$ is a complex Gaussian noise process with mean 0 and covariance $\mathrm{E}[z_n z_{n-i}^*] = N_0 s_{n,i}$, and $s_{n,i}$ is the sampled channel autocorrelation function, given by

$$s_{n,i} = \begin{cases} \int h^*(t - nT; t) h(t - nT + iT; t) dt & |i| \le L \\ 0 & |i| > L \end{cases} \qquad (2)$$

where $h(\tau; t)$ is the overall channel impulse response with (finite) span L in symbol intervals, where τ represents delay and t represents time variation. We will refer to the above model as the unwhitened model.

Let $s_n(D) = \sum_i s_{n,i} D^i$, then an equivalent discrete-time white Gaussian noise model is obtained by noting that

$$s_n(D) = f_n^*(D^{-1}) f_n(D)$$

4

where $f_n(D) = \sum_{i=0}^{L} f_{n,i} D^i$ has all its roots inside the unit circle (minimum-phase channel). The statistic obtained by filtering $\{y_n\}$ with the anti-causal noise-whitening filter $1/f_n^*(D^{-1})$ (assuming that it exists), is given by

$$y_n' = \sum_{i=0}^{L} f_{n,i} b_{n-i} + z_n' \tag{3}$$

where $\{z_n'\}$ is a proper[4] complex white Gaussian noise process with mean 0 and variance N_0.

3 Maximum likelihood sequence estimation

A maximum likelihood sequence estimator (MLSE) based on the unwhitened model, determines as the most likely sequence transmitted, the sequence $\{b\}_{n=1}^{N}$ that maximizes the metric [2, 12]

$$U\left(\underline{y}_N, \underline{b}_N\right) = \sum_{n=1}^{N} 2\mathrm{Re}\{b_n^* y_n\} - \sum_{i=1}^{N} \sum_{k=1}^{N} b_i^* s_{i,k} b_k \tag{4}$$

where $\underline{x}_n = x_1, x_2, \ldots, x_n$. Due to the symmetry in the sampled channel correlations: $s_{n,i} = s_{n-i,-i}^*$, the above metric can be computed recursively as

$$U(\underline{y}_n, \underline{b}_n) = U(\underline{y}_{n-1}, \underline{b}_{n-1}) + V(y_n, b_n, \sigma_n) \tag{5}$$

where $V(\cdot)$ is known as the branch metric and is given by

$$V(y_n, b_n, \sigma_n) = \mathrm{Re}\left\{ b_n^* \left(2y_n - s_{n,0} b_n - 2\sum_{i=1}^{L} s_{n,i} b_{n-i} \right) \right\} \tag{6}$$

and $\sigma_n = b_{n-1}, b_{n-2}, \ldots, b_{n-L}$ represents the state at time n.

The above is a generalized form of the Ungerboeck formulation (where $s_{n,i} = s_i$ i.e. the channel is fixed), independently obtained in [12]. An optimum multiuser detector proposed by Verdu [6] for asynchronous DS-CDMA systems can be obtained from this formulation.

The maximum likelihood sequence can be determined equivalently by applying the Viterbi algorithm to the whitened statistic $\{y_n'\}$ as shown in [1], using the metric

$$U'\left(\underline{y}_N', \underline{b}_N\right) = \sum_{n=1}^{N} \left[2\mathrm{Re}\left(y_n' \sum_{i=0}^{L} f_{n,i}^* b_{n-i}^* \right) - \left| \sum_{i=0}^{L} f_{n,i} b_{n-i} \right|^2 \right] \tag{7}$$

---

[4] $E[\mathrm{Re}\{z_n'\}\mathrm{Im}\{z_n'\}] = 0$.

which can be computed recursively as

$$U'\left(\underline{y}'_n, \underline{b}_n\right) = U'(\underline{y}'_{n-1}, b^{n-1}) + V'(y'_n, b_n, \sigma_n) \tag{8}$$

where

$$V'(y'_n, b_n, \sigma_n) = 2\mathrm{Re}\left(y'_n \sum_{i=0}^{L} f^*_{n,i} b^*_{n-i}\right) - \left|\sum_{i=0}^{L} f_{n,i} b_{n-i}\right|^2. \tag{9}$$

The two algorithms require the same order of computational complexity and storage proportional to M^L.

4 Decision feedback sequence estimation

A reduced-complexity sub-optimal alternative to MLSE using the Viterbi algorithm is decision feedback sequence estimation DFSE [3], [4]. A parameter called memory order J is chosen arbitrarily smaller than channel memory L and the trellis is collapsed into M^J states corresponding to the J most recent hypothesized symbols. Since the reduced state falls short in providing all the information needed to compute branch metrics, the algorithm uses the path with the best accumulated metric leading to each state to extract the rest of the information. Note that this algorithm operates on whitened statistics $\{y'_n\}$ which depend on past and present inputs only (cf. (3)).

4.1 UDFSE

The unwhitened decision-feedback sequence estimation (UDFSE) algorithm [8] follows the Ungerboeck formulation for sequence estimation. The algorithm is given by the recursion

$$m(\beta_{n+1}) = \max_{b_{n-J}}[m(\beta_n) + W(y_n, b_n, \beta_n)] \tag{10}$$

where $\beta_n = b_{n-1}, b_{n-2}, \ldots, b_{n-J}$ represents the reduced state at time n, $m(\beta_n)$ is the accumulated metric of the path associated with the state β_n and $W(y_n, b_n, \beta_n)$ is the branch metric, given by

$$\begin{aligned}
W(y_n, b_n, \beta_n) &= \mathrm{Re}\Bigg\{ b^*_n \Bigg(2y_n - s_{n,0}b_n - 2\sum_{i=1}^{J} s_{n,i} b_{n-i} \\
&\qquad\qquad -2 \sum_{i=J+1}^{L} s_{n,i} \hat{b}_{n-i}(\beta_n) \Bigg) \Bigg\}.
\end{aligned} \tag{11}$$

In (11), $\{\hat{b}_{n-i}(\beta_n)\}$ are tentative conditional decisions on inputs more than J samples in the past, obtained from the path with the best accumulated metric, leading to the

state β_n, as

$$\hat{b}_{n-J}(\beta_{n+1}) = \arg\max_{b_{n-J}}[\mathrm{m}(\beta_n) + \mathrm{W}(y_n, b_n, \beta_n)]. \tag{12}$$

Although both full-state formulations in Section 3 yield the maximum likelihood sequence estimate, it has been noted that the reduced-state derivation UDFSE does not perform nearly as well as its whitened channel counterpart (DFSE) on most channels [10, 11]. The problem arises from the nature of unwhitened statistics $\{y_n\}$ which depend on both the past and future input symbols. Note that the UDFSE algorithm, when deciding b_{n-J} (conditionally) in the n-th step (12), ignores interference from inputs $b_{n+1}, b_{n+2}, \ldots, b_{n-J+L}$ which directly affect output sample y_{n-J} (corresponding to b_{n-J}). Thus, the decision rule of (12) which is based on the knowledge of only J inputs in the future is inherently near-sighted. Unlike DFSE, the decisions obtained in UDFSE are affected by untreated interference components even in the absence of feedback errors. This observation is quantified by the following analysis.

Let $\{\dot{b}_n\}$ be the transmitted sequence of symbols and $\{\dot{\beta}_n\}$ be the sequence of states in the path of $\{\dot{b}_n\}$ in the reduced trellis. Let $\{\bar{b}_n\}$ be a hypothetical sequence of symbols and $\{\bar{\beta}_n\}$ be the corresponding sequence of states in the reduced trellis that diverges from the correct sequence of states at time n_1 and re-merges with it at a later time n_2, i.e.

$$\bar{\beta}_n = \dot{\beta}_n \ \text{ for } \ n = n_1, n_2 \ \text{ and } \ \bar{\beta}_n \neq \dot{\beta}_n \ \text{ for } \ n_1 < n < n_2. \tag{13}$$

An error event occurs at time n_2 if the algorithm picks $\{\bar{b}_n\}$ as the correct sequence over $\{\dot{b}_n\}$.

Proposition 4.1 *The occurrence of the error event depends on the value of inputs* $\dot{b}_{n_2}, \dot{b}_{n_2+1}, \ldots, \dot{b}_{n_2-1+L-J}$ *in the absence of error propagation (from any previous error events).*

Proof: The error event occurs if the accumulated metric on the incorrect path is greater than that on the correct path at the point where the two paths merge i.e.

$$\sum_{n=n_1}^{n_2-1} \mathrm{W}(y_n, \bar{b}_n, \bar{\beta}_n) > \sum_{n=n_1}^{n_2-1} \mathrm{W}(y_n, \dot{b}_n, \dot{\beta}_n). \tag{14}$$

Assume:

$$\bar{b}_n = \dot{b}_n \ \text{ for } \ n_1 - L \leq n \leq n_1 - J - 1, \tag{15}$$

i.e. there are no errors $L - J$ steps prior to the error event. Substituting branch metrics from (11) and noting that $\{\hat{b}_{n-i}(\bar{\beta}_n)\}$ and $\{\hat{b}_{n-i}(\dot{\beta}_n)\}$ are decisions taken from

7

the paths corresponding to the sequences of states $\{\bar{\beta}_n\}$ and $\{\dot{\beta}_n\}$ respectively, (14) can be written as

$$2\mathrm{Re}\{\bar{\underline{b}}^H \underline{y}\} - \bar{\underline{b}}^H S \bar{\underline{b}} > 2\mathrm{Re}\{\dot{\underline{b}}^H \underline{y}\} - \dot{\underline{b}}^H S \dot{\underline{b}} \qquad (16)$$

where $\underline{x} = [x_{n_1}, x_{n_1+1}, \ldots, x_{n_2-1}]^T$ and S is a banded Hermitian matrix given by

$$S = \begin{bmatrix} s_{n_1,0} & \cdots & s_{n_1,-L} & 0 & 0 & \cdots & 0 \\ s_{n_1+1,1} & s_{n_1+1,0} & \cdots & s_{n_1+1,-L} & 0 & \cdots & 0 \\ \vdots & \ddots & & \ddots & & & \vdots \\ s_{n_1+L,L} & \cdots & s_{n_1+L,0} & \cdots & s_{n_1+L,-L} & \ddots & 0 \\ 0 & \ddots & & & & & \vdots \\ \vdots & & \ddots & & \ddots & & 0 \\ 0 & \ddots & s_{n_2-1-L,L} & \cdots & s_{n_2-1-L,0} & \cdots & s_{n_2-1-L,-L} \\ \vdots & & \ddots & & \ddots & & \vdots \\ 0 & \cdots & 0 & s_{n_2-2,L} & \cdots & s_{n_2-2,0} & s_{n_2-2,-1} \\ 0 & \cdots & 0 & 0 & s_{n_2-1,L} & \cdots & s_{n_2-1,0} \end{bmatrix} \qquad (17)$$

Let $\underline{e} = \frac{1}{2}(\bar{\underline{b}} - \dot{\underline{b}})$ be the error sequence. Using (1) and (15) and noting that $e_n = 0$ for $n_2 - J \le n \le n_2 - 1$ as $\bar{\beta}_{n_2} = \dot{\beta}_{n_2}$, it can be shown that the above inequality holds if

$$2\mathrm{Re}\{\underline{e}^H \underline{z}\} > \underline{e}^H S \underline{e} - \underline{e}'^H S' \dot{\underline{b}}' \qquad (18)$$

where $\underline{z} = [z_{n_1}, z_{n_1+1}, \ldots, z_{n_2-1}]^T$, $\dot{\underline{b}}' = [\dot{b}_{n_2}, \dot{b}_{n_2+1}, \ldots, \dot{b}_{n_2-1+L-J}]^T$, $\underline{e}' = [e_{n_2-L}, e_{n_2-L+1}, \ldots, e_{n_2-1-J}]^T$ and S' is a lower triangular matrix given by

$$S' = \begin{bmatrix} s_{n_2-L,-L} & 0 & \cdots & 0 \\ s_{n_2-L+1,-L+1} & s_{n_2-L+1,-L} & 0 & 0 \\ \vdots & & & \vdots \\ \vdots & & \ddots & 0 \\ s_{n_2-1-J,-J-1} & \cdots & s_{n_2-1-J,-L+1} & s_{n_2-1-J,-L} \end{bmatrix} \qquad (19)$$

Conditioned on the error sequence $\underline{e}$, the left hand side of (18) is a Gaussian random variable with mean 0 and variance that depends on the error sequence. While the first term on the right hand side of (18) depends on the error sequence only, the second term in addition, depends on the inputs $\dot{b}_{n_2}, \dot{b}_{n_2+1}, \ldots, \dot{b}_{n_2-1+L-J}$. $\square$

The above analysis suggests that if the term which depends on the $L - J$ future inputs is absorbed in the decision rule of UDFSE, the occurrence of the error event in

the modified detector will depend on the error sequence only. This, of course, requires knowledge of some future inputs. In practice, tentative decisions can be used instead as described in the following section.

4.2   Modified UDFSE

The modified algorithm (MUDFSE) can be outlined as follows: path metrics are computed as in UDFSE using (10). Conditional decisions are made (and the corresponding survivor paths are chosen) using the modified rule:

$$\hat{b}_{n-J}(\beta_{n+1}) = \arg \max_{b_{n-J}}[\mathrm{m}(\beta_n) + \mathrm{W}(y_n, b_n, \beta_n) - \mathrm{bias}(\beta_n)] \tag{20}$$

where

$$\mathrm{bias}(\beta_n) = \sum_{j=n-L+1}^{n-J} \mathrm{Re}\left\{ 2b_j^* \sum_{i=n-j+1}^{L} s_{j,-i}' \tilde{b}_{j+i} \right\}, \tag{21}$$

$$\tilde{b}_n = \mathrm{sign}(y_n). \tag{22}$$

The algorithm is delayed $L-J$ samples as y_{n+L-J} is needed in the nth step. Note that the bias in (21) depends on b_{n-J} (the bit falling out of the state) and $b_{n-J-1}, \ldots, b_{n-L+1}$ for which conditional decisions, taken from the path history of state β_n, are used. Note that the bias is used only for survivor path selection and does not constitute the accumulated path metric. The bias can be simplified to include only the leading term which depends on b_{n-J}, as follows:

$$\mathrm{bias}(\beta_n) \approx \mathrm{bias}(b_{n-J}) = \mathrm{Re}\left\{ 2b_{n-J}^* \sum_{i=J+1}^{L} s_{n-J,-i} \tilde{b}_{n-J+i} \right\}. \tag{23}$$

The approximate bias is independent of the state. It does not contribute significantly to the computational load and storage requirement of the algorithm which is on the order of $(G-J)M^J$ (same as DFSE), where G is the decision lag. This reduced computation form of MUDFSE was first proposed in [11].

4.3   Multistage MUDFSE

The MUDFSE algorithm can be run in a multistage configuration where decisions obtained at the output of the first stage are fed back to compute the bias in the second stage and so on, i.e.

$$(\tilde{b}_n)_1 = \mathrm{sign}(y_n) \quad \text{and} \quad (\bar{b}_n)_i = (\bar{b}_n)_{i-1}, \quad i > 1$$

9

where $\{(\bar{b}_n)_i\}$ are decisions obtained from the ith stage at lag G_i ($G_i \gg L$). Note that the decisions $\{(\bar{b}_n)_1\}$ are likely to be much more reliable than $\{(\tilde{b}_n)_1\}$. The complexity and delay of a Q-stage scheme is given by $\sum_{i=1}^{Q}(G_i - J_i)M^{J_i}$ and $\sum_{i=1}^{Q} G_i + L - J_1$ respectively.

5 Error performance

Assuming stationarity (i.e. $s_{n,i} = s_i$) and the absence of decision errors prior to the start of an error event, the beginning of the error event can be aligned with time $n = 1$ without loss of generality. In the following sections, we find the pairwise error probability and an upper-bound on the symbol error probability for UDFSE and modified UDFSE.

5.1 Genie-aided MUDFSE

An error event ε of length n_ε symbols occurs in modified UDFSE if

$$\sum_{n=1}^{n_\varepsilon+J} W(y_n, \bar{b}_n, \bar{\beta}_n) - \text{bias}(\bar{\beta}_{n_\varepsilon+J}) > \sum_{n=1}^{n_\varepsilon+J} W(y_n, \dot{b}_n, \dot{\beta}_n) - \text{bias}(\dot{\beta}_{n_\varepsilon+J}). \tag{24}$$

Assume that perfect information is provided by a genie on the future inputs needed to compute the bias in MUDFSE. Then, using (21) with $\tilde{b}_n$ replaced by $\dot{b}_n$ in the above inequality, it follows that the error event occurs in the genie-aided MUDFSE if

$$\sum_{n=1}^{n_\varepsilon} \text{Re}\{e_n^* z_n\} > \delta^2(\mathbf{e}) \tag{25}$$

where $\delta(\mathbf{e})$ is called the distance[5] of the error sequence $\mathbf{e} = \{e_1, e_2, \dots, e_{n_\varepsilon}\}$ and is given by

$$\delta^2(\mathbf{e}) = \sum_{n=1}^{n_\varepsilon} \sum_{k=1}^{n_\varepsilon} e_n^* s_{n-k} e_k. \tag{26}$$

The left-hand side of (25) is a Gaussian random variable with mean zero and variance $\delta^2(\mathbf{e})N_0$. Thus, the probability that the error event ε occurs is given by

$$\Pr(\varepsilon) = Q\left(\frac{\delta(\mathbf{e})}{\sqrt{N_0}}\right). \tag{27}$$

Note that this expression for the pairwise event error probability of genie-aided MUDFSE (GA-MUDFSE) is identical to the expression derived in [2] for MLSE. However, there is an important distinction in the definition of error events for MUDFSE

---

[5]Notice that this definition of distance is different from the one given in [2].

and MLSE. A valid error sequence for a J-th order MUDFSE ($1 \leq J \leq L$) can have no more than $J - 1$ consecutive zeros according to the definition in (13), whereas $J = L$ for MLSE. When $J = 0$, all error sequences have length $n_\varepsilon = 1$ symbol. In this case, $\delta^2(\mathbf{e}) = |e|^2 s_0$. In other words, a 0-th order genie-aided MUDFSE approaches the performance of the ISI-free channel. Notice that the analysis does not consider decision error propagation.

5.2 MUDFSE

In the absence of ideal bias, the occurrence of the error event in MUDFSE depends, in addition to the distance of the error sequence, on the residual interference arising from tentative decision errors on the $L - J$ inputs $(\dot{b}_{n_\varepsilon+J+1}, \ldots, \dot{b}_{n_\varepsilon+L})$ following the error event. Note that the tentative decision errors following an error event in the main detector are correlated with the main decision errors due to memory in the channel. In order to simplify analysis, we assume that tentative and main decisions errors occur independently and the tentative decision error process is stationary. Thus, we get the pairwise error probability for MUDFSE using (24), (18 and (21) as

$$\Pr(\varepsilon) \approx \sum_{\mathbf{t}} Q\left(\frac{\delta(\mathbf{e}) + \gamma(\mathbf{e}, \mathbf{t})}{\sqrt{N_0}}\right) P_{\mathbf{t}} \tag{28}$$

where $P_{\mathbf{t}}$ is the probability that the sequence of tentative decision errors $\mathbf{t} = \{t_{n_\varepsilon+J+1}, \ldots, t_{n_\varepsilon+L}\}$ (where $t_n = \frac{1}{2}(\tilde{b}_n - \dot{b}_n)$) follows the error event ε and $\gamma(\mathbf{e}, \mathbf{t})$ is the residual interference, given by

$$\gamma(\mathbf{e}, \mathbf{t}) = \sum_{n=\max(n_\varepsilon+J+1-L,1)}^{n_\varepsilon} \text{Re}\left\{e_n^*\left(2\sum_{k=n_\varepsilon+J+1}^{n+L} s_{n-k}t_k\right)\right\} \Big/ \delta(\mathbf{e}). \tag{29}$$

The residual interference $\gamma(\mathbf{e}, \mathbf{t})$ can be viewed as the projection of the tentative decision error vector $\mathbf{t}$ onto the main decision error vector $\mathbf{e}$ as determined by the channel correlation spectrum $\mathbf{s}$.

Note that unlike DFSE, where error distances diminish in general when memory order J is decreased as compared to channel memory L, the distances for MUDFSE remain the same as in the case $J = L$ (MLSE). The variance of the residual interference $\gamma(\mathbf{e}, \mathbf{t})$, however, increases from zero as the memory order J is made smaller than L in MUDFSE. This sharp contrast between the behavior of MUDFSE and DFSE is consistent with the fact that the operation of matched filtering collects all the energy w_n of the pulse transmitted at time n into the corresponding output sample y_n

$(s_{n,0} = w_n)$ [2], while the operation of noise whitening results in the scattering of some of this energy into L subsequent output samples $(\sum_{i=0}^{L} |f_{n,i}|^2 = w_n)$.

When $J = 0$, $n_\varepsilon = 1$, $\delta^2(\mathbf{e}) = |e_1|^2 s_0$ and $\gamma(\mathbf{e}, \mathbf{t})$ is given by

$$\gamma(\mathbf{e}, \mathbf{t}) = \text{Re}\left\{ e_1^* \left(2 \sum_{k=2}^{L+1} s_{1-k} t_k \right) \right\} \Big/ |e_1| \sqrt{s_0} \tag{30}$$

i.e. MUDFSE reduces to a zero-forcing decision-feedback detector for unwhitened channels (where feed-forward filtering is replaced by tentative decision feedback).

5.3   UDFSE

Using (18), the pairwise error probability in the case of UDFSE can be written as

$$\text{Pr}(\varepsilon) = \sum_{\mathbf{b}} Q\left(\frac{\delta(\mathbf{e}) + \mu(\mathbf{e}, \mathbf{b})}{\sqrt{N_0}} \right) P_{\mathbf{b}} \tag{31}$$

where $P_{\mathbf{b}}$ is the probability that the sequence of inputs $\mathbf{b} = \{b_{n_\varepsilon+J+1}, \ldots, b_{n_\varepsilon+L}\}$ follows the error event ε ($P_{\mathbf{b}} = M^{J-L}$ for i.i.d. equiprobable inputs) and $\mu(\mathbf{e}, \mathbf{b})$ is the untreated interference, given by

$$\mu(\mathbf{e}, \mathbf{b}) = \sum_{n=\max(n_\varepsilon+J+1-L,1)}^{n_\varepsilon} \text{Re}\left\{ e_n^* \left(-\sum_{k=n_\varepsilon+J+1}^{n+L} s_{n-k} b_k \right) \right\} \Big/ \delta(\mathbf{e}). \tag{32}$$

Note that (31) provides an exact expression for the pairwise error probability of UDFSE unlike (28) for MUDFSE.

5.4   Symbol error probability

Assuming that all input sequences are equally likely, the symbol error probability for UDFSE, genie-aided MUDFSE and MUDFSE can be union-bounded as [3]

$$P_s \leq \sum_{\varepsilon} \text{w}(\mathbf{e}) \left(\prod_{n=1}^{n_\varepsilon} \frac{M - |e_n|}{M} \right) \text{Pr}(\varepsilon) \tag{33}$$

where $\text{w}(\mathbf{e})$ is the number of symbol errors entailed by the error sequence $\mathbf{e}$ and $\prod_{n=1}^{n_\varepsilon}(M - |e_n|)/M$ is the number of input sequences that can have $\mathbf{e}$ as the error sequence, where the symbol alphabet is given as $A_M = \{\pm1, \pm3, \ldots, \pm(M-1)\}$ for M even. In the case of BPSK modulation, (33) simplifies to

$$P_s \leq \sum_{\varepsilon} \frac{\text{w}(\mathbf{e})}{2^{\text{w}(\mathbf{e})}} \text{Pr}(\varepsilon). \tag{34}$$

$$a_0 = \tfrac{1}{2}D^{s_0}$$
$$a_1 = \tfrac{1}{2}D^{(s_0+2s_1)}$$
$$a_2 = \tfrac{1}{2}D^{(s_0-2s_1)}$$
$$a_3 = \tfrac{1}{2}D^{(s_0+2s_1+2s_2)}$$
$$a_4 = \tfrac{1}{2}D^{(s_0-2s_1-2s_2)}$$
$$a_5 = \tfrac{1}{2}D^{(s_0-2s_1+2s_2)}$$
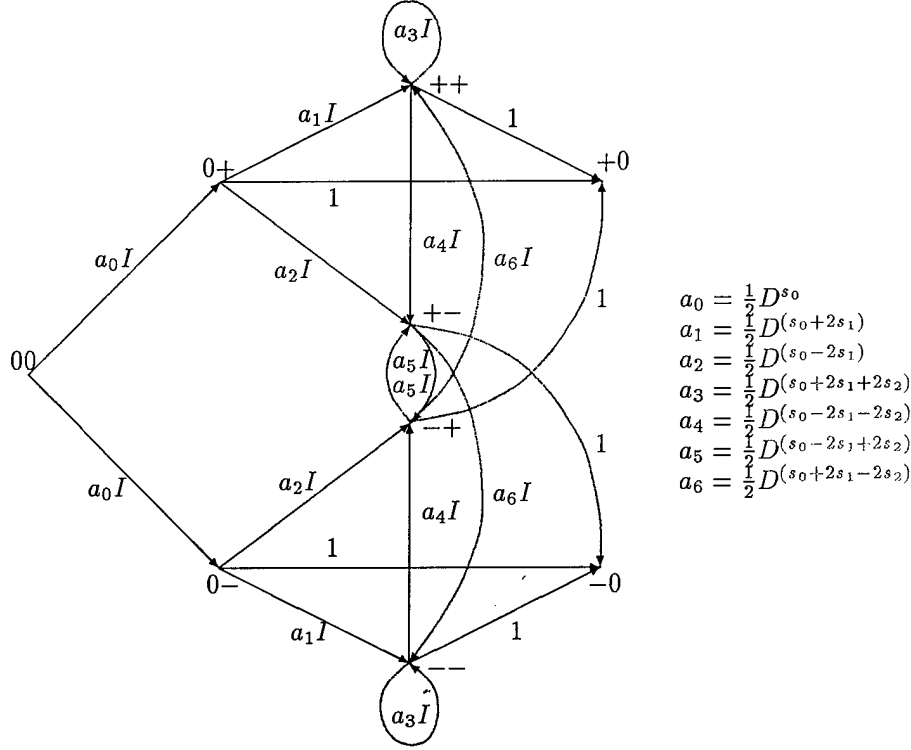$$a_6 = \tfrac{1}{2}D^{(s_0+2s_1-2s_2)}$$

Figure 1: Error state diagram for $L = 2, J = 1$.

Note that the above bounds on the probability of symbol error are obtained assuming no decision error propagation (a separation of more than $L - J$ symbols between error events). However, the effect of error propagation is usually small at medium to high signal-to-noise ratio.

6   Bound evaluation

To evaluate the symbol error probability for MUDFSE, we make use of the error-state diagram as in [13]. The error-state diagram used for determining the generating function of channel codes for maximum-likelihood sequence estimation [13, pp. 283] has to be modified in the case of MUDFSE so that the error sequences satisfy (13). The modified diagram is shown in Fig. 1 for the case of binary signaling over an AWGN channel with memory $L = 2$ and memory order $J = 1$ chosen for MUDFSE. It has dimensionality 3^L. The nodes are labeled with the error states which are ternary L-tuples with components that take values in $\{0, +1, -1\}$. The transitions are labeled with the branch generating function $\mathrm{Re}\left\{e_n^* \left(s_0 e_n + 2\sum_{i=1}^{L} s_i e_{n-i}\right)\right\}$ as the exponent of dummy variable D, and the number of symbol errors entailed by the

transition as the exponent of variable I. A factor of $1/2$ is used to account for the weighing factor in (34) if the transition involves an error. The transitions which lead back to the $0+$ and $0-$ states (except from the 00 state) have been eliminated because error sequences which contain a zero in the middle are not allowed in the case $J = 1$, according to the definition in (13).

Instead of enumerating all allowable error paths through the channel code trellis, we are interested in enumerating the paths that terminate with a $+1$ and -1 separately because the residual interference given by (29) depends on the tail of the error path $\mathbf{e}' = \{e_{\max(n_\epsilon + J + 1 - L, 1)}, \ldots, e_{n_\epsilon}\}$. Thus, in general, we seek $2 \times 3^{L-J-1}$ generating functions ($J < L$) corresponding to the paths which terminate with a given tail (such that $e_{n_\epsilon} \neq 0$).

Let $T_j(D, I)$ be the generating function for the error paths which terminate in the tail $\mathbf{e}'_j$ ($j = 1, \ldots, 2 \times 3^{L-J-1}$), found by solving the state equations simultaneously. Each generating function can be series expanded as follows

$$\frac{\partial}{\partial I} T_j(D, I) \bigg|_{I=1} = \sum_k B_{j,k} D^{\delta_{j,k}^2} \tag{35}$$

where $B_{j,k}$ is the number of error paths (weighted by the number of symbol errors on the path per the number of the corresponding input sequences) with Euclidean distance $\delta_{j,k}$ that terminate in the tail $\mathbf{e}'_j$. Then, the symbol error probability for MUDFSE can be computed as

$$P_s \leq \sum_{j=1}^{2 \times 3^{L-J-1}} \sum_k \sum_t B_{j,k} D^{\delta_{j,k} + \gamma(\mathbf{e}'_j, \delta_{j,k}, \mathbf{t})} P_t \bigg|_{D^x = Q(x/\sqrt{N_0})} \tag{36}$$

where we use the fact that the residual interference $\gamma(\mathbf{e}, \mathbf{t})$ depends on the error sequence $\mathbf{e}$ only through the tail of the error sequence $\mathbf{e}'$ and the distance of the error sequence $\delta(\mathbf{e})$.

Note from Fig. 1 that the error state pairs that are negative of each other are indistinguishable on the basis of branch values. Thus, they can be combined as in [13]. It follows that the number of paths that terminate in the tail $\mathbf{e}'$ is the same as the number of paths that terminate in the tail $-\mathbf{e}'$. Moreover, since $\gamma(\mathbf{e}'_j, \delta_{j,k}, \mathbf{t}) = \gamma(-\mathbf{e}'_j, \delta_{j,k}, -\mathbf{t})$, (36) simplifies to

$$P_s \leq 2 \sum_{j=1}^{3^{L-J-1}} \sum_k \sum_t B_{j,k} D^{\delta_{j,k} + \gamma(\mathbf{e}'_j, \delta_{j,k}, \mathbf{t})} P_t \bigg|_{D^x = Q(x/\sqrt{N_0})}. \tag{37}$$

In general, the reduced error-state diagram for binary signaling comprises $(3^L - 1)/2$ non-zero nodes with 3^{L-J-1} terminating nodes.
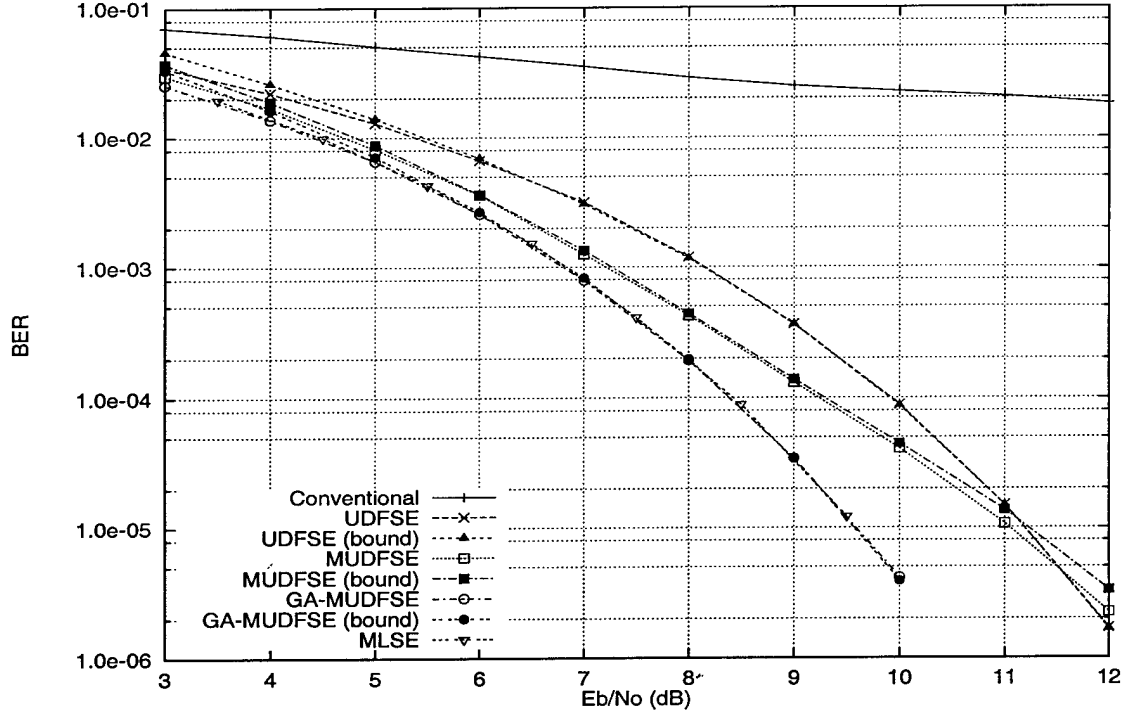
Figure 2: BER performance of various detection schemes on channel 1.

In order to compute (37), we assume that the sequence of tentative decision errors t is an i.i.d. sequence which is independent of the sequence of main decision errors e and has distribution

$$
t_n = \begin{cases} 0 & 1-p \\ +1 & \frac{1}{2}p \\ -1 & \frac{1}{2}p \end{cases} \tag{38}
$$

where p is the probability of tentative decision error which, in the case of a single-stage MUDFSE algorithm, is the symbol error probability of a conventional matched-filter detector.

As the noise is correlated, tentative decision errors are correlated with each other as well as with main decision errors. Our assumptions are thus, optimistic because errors in the tentative detector will tend to occur in bursts, inducing errors in the main detector. Nevertheless, independence can be assumed in case noise correlations are small.

15

7 Performance results

In this section, we compare the performance of the various detection algorithms discussed in this paper via simulation and analysis using several example channels. First, we consider binary signaling over static time-dispersive AWGN channels. The receiver is assumed to have perfect knowledge of the symbol timing and the impulse response of the channel. We run each simulation for a count of 1000 errors.

Channel 1 is given by $s' = (0.2, -0.25, 1.0, -0.25, 0.2)$, where s' represents the normalized channel correlations. The ISI channel has memory $L = 2$. Fig. 2 shows the BER performance of the various detection schemes on this channel. The memory order J is chosen to be 1 for UDFSE and modified UDFSE. The bounds in Fig. 2 are computed using (34) by averaging over all error sequences e with squared distance $\delta^2(e) \leq 10.0$. For MUDFSE, the probability of tentative decision error (p in (38)) is found from simulation. The bounds are tight especially for moderate to high signal-to-noise ratio (SNR) as can be expected of union bounds (the curves are virtually indistinguishable from those for simulation in the case of UDFSE and GA-MUDFSE at high SNR). Note that the bounds are approximate as they do not account for decision error propagation. However, the effect of error propagation is usually small in schemes that employ conditional decision feedback at medium to high SNR, as noted in [3]. The semi-analytic bound for MUDFSE shown in Fig. 2 seems to diverge somewhat from the simulation curve although it can be expected to cross over the simulation curve at high SNR due to dependence between the tentative and main decisions.

For channel 1, modified UDFSE provides some gain over UDFSE in the low to medium SNR range. But at high SNR, its performance is worse than UDFSE. The performance differential depends on how effectively the anti-causal interference components affecting UDFSE (Section 4.1) are canceled in the modified algorithm by means of tentative decisions based on matched filter outputs. Genie-aided MUDFSE that cancels the anti-causal interference ideally, performs slightly better than MLSE as shown in Fig. 2. This is due to the reasons discussed in Section 5.1.

Fig. 3 shows the BER performance (simulated) of various detection schemes over an ISI channel (2) with memory $L = 9$. Channel 2 is given by $f = (0.861, 0.258, -0.100, -0.274, 0.130, 0.100, -0.038, 0.112, -0.114, -0.228)$. The channel is minimum-phase and is arbitrarily chosen. The various schemes are indexed with the memory order and the decision lag (J, G). Except DFSE, all algorithms operate on symbol-spaced samples obtained from conventional matched filtering. Ideal noise whitening
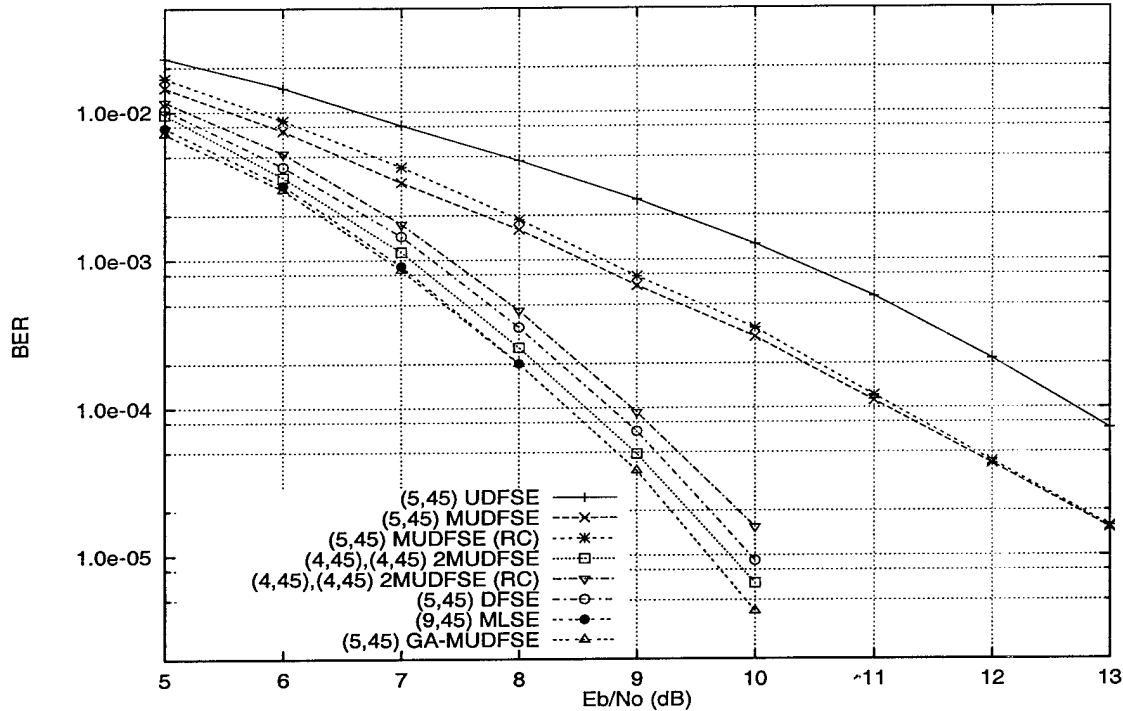
16

Figure 3: BER performance of various detection schemes on channel 2.

is assumed for DFSE. All schemes shown in Fig. 3, except MLSE, require similar overall complexity and storage. Fig. 3 shows that $(5,45)$ Modified UDFSE gains $1.0 - 1.5$ dB over $(5,45)$ UDFSE in the SNR range shown. The two-stage scheme $[(4,45),(4,45)]$ 2MUDFSE closely approaches MLSE performance and obtains a gain of 4 dB over UDFSE at an error rate of 10^{-4}. The single-stage and two-stage MUDFSE (reduced computation) schemes lose less than 0.5 dB due to bias approximation (23).

The performance of $(5,45)$ DFSE is also close to MLSE for channel 2 as shown in Fig. 3. We have neglected the effects of non-ideal noise-whitening (due to fixed delay constraint) on the performance of DFSE. The delay incurred from anti-causal (noise-whitening) filtering needed in DFSE can be compared to the delay of a multi-stage MUDFSE scheme. As channel 2 is minimum-phase, the performance achieved by DFSE is the best possible for any channel phase. The performance of UDFSE and MUDFSE, however, is independent of channel phase.

Fig. 4 shows the BER performance (simulated) over another ISI channel (3) with memory $L = 9$. Channel 3 is given by $f = (0.707, -0.153, 0.468, -0.306, 0.285, -0.104, 0.244, 0.068, -0.070, 0.053)$. Channel 3 is more dispersive than channel 2. Note that the $(5,45)$ MUDFSE schemes do a little worse than $(5,45)$ UDFSE. This is partly because conventional hard decisions are unreliable (BER $\approx \frac{1}{5}$). The two-
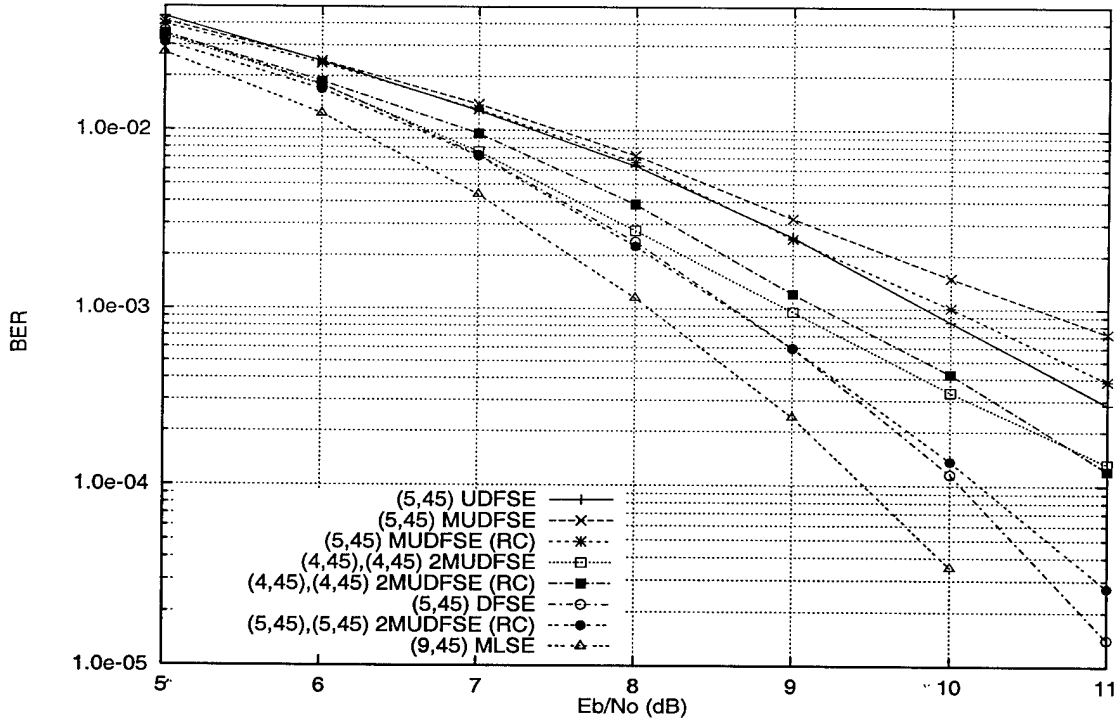
17

Figure 4: BER performance of various detection schemes on channel 3.

stage MUDFSE schemes, therefore, obtain better performance. Due to the heavy correlation between tentative and main decisions, however, the two-stage schemes are unable to provide as much improvement over UDFSE as obtained for channel 2.

Next, we simulate a BPSK modulated asynchronous DS-CDMA system with eight users whose signature waveforms are derived from Gold sequences of length 31. The relative delays of users are fixed for the simulation and are in an increasing order. The multiuser channel is static and has the same spectrum as given in [11][6]. Fig. 5 shows the BER of user 1 for various detection schemes when all users have identical SNR. Each simulation was run for a count of 500 errors. It is evident that even with ideal power control, the performance of the conventional single-user detector is significantly worse than optimum MLSE. $(2, 28)$ UDFSE provides some improvement over the conventional detector. The four-state (unwhitened) M-algorithm that operates directly on the matched filter output is about 2 dB worse than the M-algorithm that operates on the equivalent whitened minimum-phase channel. The linear-decorrelator, that nulls out all interference, loses about $0.5 - 1.0$ dB compared to MLSE due to noise enhancement. $(2, 28)$ DFSE also obtains near MLSE performance. However, DFSE,

---

[6]The simulation results reported in [11] are off by 3 dB (worse) due to a mistake in normalization of symbol energies.
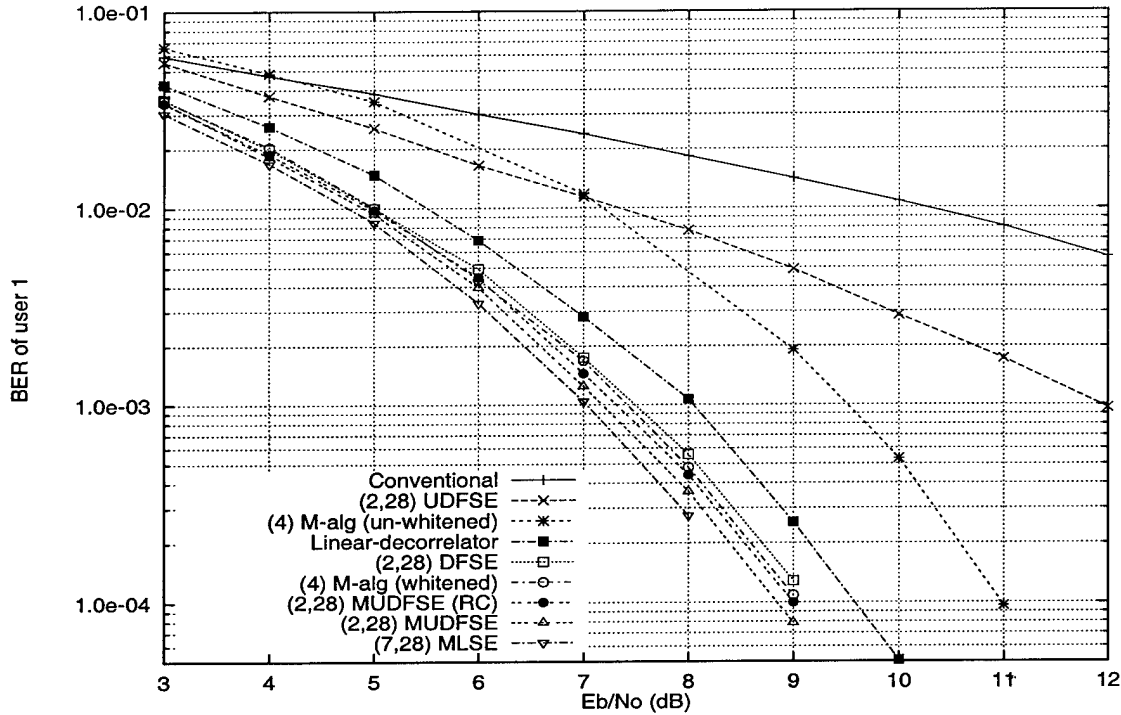
18

Figure 5: BER performance of various detection schemes over an 8-user asynchronous DS-CDMA channel.

the linear-decorrelator and the (whitened) M-algorithm require multiuser channel inversion and/or factorization which has complexity quadratic in the number of users. Moreover, the M-algorithm requires sorting of survivor paths at each iteration which is not needed for DFSE or UDFSE as they are trellis based.

The single-stage modified UDFSE algorithms which require a bank of matched filters only, obtain the best performance on this channel (next to MLSE). $(2, 28)$ MUDFSE (with four states only) closely approaches the performance of MLSE which requires 128 states in the Viterbi algorithm. With bias approximation, $(2, 28)$ MUDFSE (RC) obtains a gain of 4.5 dB over UDFSE at an error-rate of 0.1%.

Fig. 6 shows the BER of user 1 versus the SNR of the rest of the users. The SNR of user 1 is held constant at 7.0 dB. It can be seen that the conventional detector, UDFSE and the unwhitened M-algorithm do not perform well in a near-far situation. The linear-decorrelator, DFSE and the whitened M-algorithm perform well. However, the modified UDFSE schemes outperform the other methods and converge to MLSE in high SNR of interfering users on this channel.

The improvement afforded by the modified UDFSE algorithm over UDFSE depends on several factors. Among these factors is the amount of ISI, the reliability of
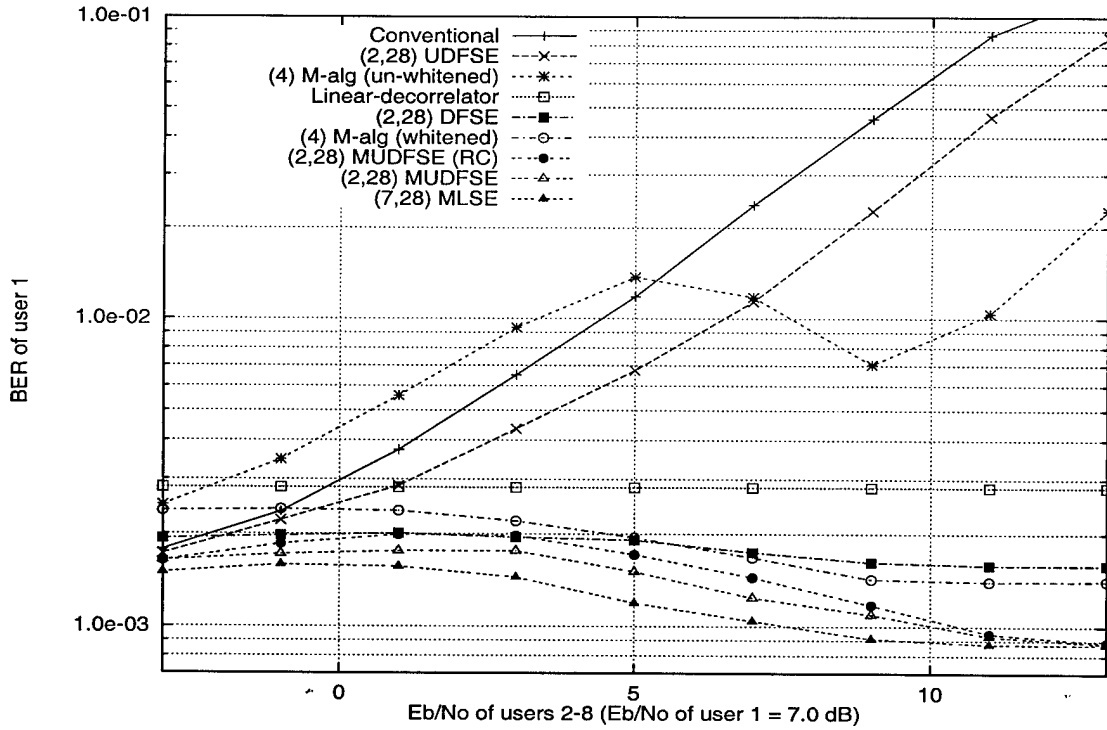
19

Figure 6: Near-far performance of various detection schemes over an 8-user asynchronous DS-CDMA channel.

tentative decisions and the choice of the memory order. On channels with small sampled correlations, the conventional matched filter detector makes relatively reliable decisions. The reliability of tentative decisions can be improved further by means of an auxiliary stage. If the memory order is not too small, the error performance of the modified detector (28) is dominated by error event distances in the main stage rather than the residual interference. Close to MLSE performance is achieved in this case. Unlike DFSE, error event distances in MUDFSE do not diminish with the memory order as discussed in Section 5.1. Thus, MUDFSE generally outperforms DFSE (with similar complexity) on channels with small correlations since the residual interference is reliably removed. An example is the multiuser DS-CDMA channel where well-designed spreading codes or long spreading codes, in a not so highly loaded system, provide low channel cross-correlations.

The modified UDFSE algorithm may perform worse than UDFSE (as well as DFSE) for channels with large sampled correlations (highly dispersive ISI channels or heavily loaded multiuser channels). This is not mainly due to the unreliability of tentative decisions. An auxiliary stage can render relatively reliable tentative decisions. However, due to the strong dependence between error events in the auxiliary

20

and the main stage, the main stage can not significantly improve upon the decisions obtained in the auxiliary stage.

8   Conclusions

In this paper, we show that decision feedback sequence estimation based on conventional matched filter outputs (a reduced-state version of the Ungerboeck MLSE formulation) is affected by untreated interference components. We derive a modified unwhitened decision feedback sequence estimation algorithm which uses tentative decisions to cancel the anti-causal interference components. The algorithm, which operates on matched filter outputs, provides excellent performance/complexity tradeoffs on channels with relatively small sampled correlations. The algorithm is insensitive to channel phase and does not require noise-whitening. These attributes make it attractive for bi-directional equalization in the GSM system and multiuser detection in asynchronous DS-CDMA systems.

The algorithm can be improved by using soft tentative decisions instead of hard decisions. An adaptive form of the algorithm should be considered for time-varying media. The algorithm can be modified to provide soft outputs for coded systems. An approximate error probability analysis is conducted in this paper which provides some insight into the proposed algorithm. An in-depth analysis is needed, however, to better identify the class of channels for which gains are afforded by the modified algorithm and to quantify the gains for a given channel with given complexity.

References

[1] G. D. Forney, "Maximum-Likelihood Sequence Estimation of Digital Sequences in the Presence of Intersymbol Interference," *IEEE Trans. Info. Theory*, vol. IT-18, no. 3, pp. 363-378, May 1972.

[2] G. Ungerboeck, "Adaptive Maximum-Likelihood Receiver for Carrier-Modulated Data-Transmission Systems," *IEEE Trans. Comm. Technology*, vol. COM-22, no. 5, pp. 624-636, May 1974.

[3] A. Duel-Hallen and C. Heegard, "Delayed Decision-Feedback Sequence Estimation," *IEEE Trans. Communication*, vol. 37, no. 5, pp. 428-436, May 1989.

[4] V. M. Eyuboglu and S. U. Qureshi, "Reduced-State Sequence Estimation with Set Partitioning and Decision Feedback," *IEEE Trans. Communication*, pp. 13-20, Jan. 1988.

[5] K. Wesolowski, R. Krenz and K. Das, "Efficient Receiver Structure for GSM Mobile Radio," *Int. J. Wireless Information Networks*, vol. 3, no. 2, pp. 117-122, April 1996.

[6] S. Verdu, "Minimum Probability of Error for Asynchronous Gaussian Multiple-Access Channels," *IEEE Trans. Info. Theory*, vol. IT-32, no. 1, pp. 85-96, Jan. 1986.

[7] L. Wei and L. K. Rasmussen, "A Near Ideal Noise Whitening Filter for an Asynchronous Time-Varying CDMA System," *IEEE Trans. Communication*, vol. 44, no. 10, pp. 1355-1361, Oct. 1996.

[8] A. Duel and C. Heegard, "Delayed Decision Feedback Sequence Estimation for QAM and Trellis Coded Systems," *20th Conf. Info. Sc. and Sys.*, pp. 367-372, Mar. 1986.

[9] J. B. Anderson and S. Mohan, "Sequential Coding Algorithms: A Survey Cost Analysis," *IEEE Trans. Communication*, vol. COM-32, pp. 169-176, Feb. 1984.

[10] L. Wei, L. K. Rasmussen and R. Wyrwas, "Near Optimum Tree-Search Detection Schemes for Bit-Synchronous Multiuser CDMA Systems over Gaussian and Two-Path Rayleigh-Fading Channels," *IEEE Trans. Communication*, vol. 45, no. 6, pp. 691-700, June 1997.

[11] Abdulrauf Hafeez and W. E. Stark, "Decision Feedback Sequence Estimation for Unwhitened ISI Channels," *Proc. 35th Annual Allerton Conf. on Communication, Control and Computing*, pp. 493-502, Sept. 1997.

[12] G. E. Bottomley and S. Chennakeshu, "Unification of MLSE receivers and extension to time-varying channels," *IEEE Trans. Communication*, vol. 46, pp. 464-472, April 1998.

[13] A. J. Viterbi and J. K. Omura, "Principles of Digital Communication and Coding," McGraw-Hill, 1979.

List of Figures

Abdulrauf Hafeez was born on January 4, 1969 in Karachi, Pakistan. He received the B.S. degree in Electrical Engineering from NED University of Engineering and Technology, Karachi in 1991. He joined Alcatel (Pakistan) Ltd. as a site engineer where he worked on the deployment of a fiber-optic transmission network for a year. He received the M.S. degree in Electrical Engineering from the University of Michigan, Ann Arbor in 1994. He is currently pursuing the Ph.D. degree at the University of Michigan. His research interests include equalization, multiuser detection and coding for land-line and mobile communication systems and spread spectrum techniques. He has several conference publications in these areas. In 1997, he was at Ericsson Inc., Raleigh, North Carolina where he was engaged in research on baseband techniques for narrow-band mobile communication systems. He has a patent pending in the area of co-channel interference cancellation for cellular and PCS systems applied for by Ericsson Inc. Mr. Hafeez is a member of the IEEE Communication society.

Wayne Stark received the B.S. (with highest honors), M.S., and Ph.D. degrees in electrical engineering from the University of Illinois, Urbana in 1978, 1979, and 1982 respectively. Since September 1982 he has been a faculty member in the Department of Electrical Engineering and Computer Science at the University of Michigan, Ann Arbor where he is currently Professor. From 1984-1989 he was Editor for Communication Theory of the IEEE Transactions on Communication in the area of Spread-Spectrum Communications. He was involved in the planning and organization of the 1986 International Symposium on Information Theory which was held in Ann Arbor, Michigan. He was selected by the National Science Foundation as a 1985 Presidential Young Investigator. He is principal investigator of a Army Research Office Multidisciplinary University Research Initiative (MURI) project on Low Energy Mobile Communications. His research interests are in the areas of coding and communication theory, especially for spread-spectrum and wireless communication networks. Dr. Stark is a member of Eta Kappa Nu, Phi Kappa Phi and Tau Beta Pi and a Fellow of the IEEE.

A New Fractional MLSE Receiver for Time-varying Channels

Abdulrauf Hafeez[1] and Wayne E. Stark

Electrical Engineering and Computer Science Department

1301 Beal Ave., University of Michigan, Ann Arbor, MI 48109-2122.

E-mail: rauf@eecs.umich.edu, stark@eecs.umich.edu.

Abstract– In this paper, we derive a new maximum-likelihood sequence estimation (MLSE) receiver that operates on fractionally-spaced samples obtained at the output of an analog filter matched to the transmit pulse-shaping filter. A fractional MLSE receiver was proposed by Hamied *et al.* that requires a fixed noise-whitening filter to whiten noise samples at the output of the transmit matched filter. Due to the presence of nulls in the Nyquist bandwidth of practical pulse-shaping filters like the square-root raised cosine filter, the noise-whitening filter has a long slowly-damped delay response and any practical length truncation results in significant distortion. The new receiver does not need noise-whitening. The branch metric of the Viterbi algorithm in the receiver accounts for the correlation in the noise samples. The receiver is insensitive to sampler timing phase. An adaptive form of the receiver requires only one step prediction of medium response coefficients. These features make the receiver attractive for fast time-varying channels.

Index Terms– Adaptive equalizers, equalizers, fading channels, intersymbol interference, maximum likelihood estimation, sequence estimation, time-varying channels, Viterbi detection.

---

1 Introduction

Maximum-likelihood sequence estimation (MLSE) is an optimum detection technique for signals corrupted with intersymbol interference (ISI) and additive white Gaussian noise (AWGN). Forney [2] and Ungerboeck [9] derived MLSE receivers for known time-invariant channels. The latter formulation was extended for the case of known time-varying channels by Bottomley *et al.* [1]. Adaptive channel estimation using (tentative) decision feedback is assumed in the case of unknown time-varying channels.

In wireless communication systems, the channel is generally considered as comprising a time-invariant transmit (pulse-shaping) filter followed by a time-varying transmission medium. Forney and Ungerboeck's receivers employ an analog front-end filter which is matched to the overall channel response. If the transmission medium is time-varying or unknown at the receiver, the front-end filter has to be adaptive. This is not desirable for implementation purposes. Ungerboeck also described an adaptive receiver in [9] which uses a discrete-time transversal filter at the front end to synthesize matched filter characteristics. The receiver, however, does not take advantage of the fact that the transmit filter is generally known at the receiver and this information can be exploited to improve channel estimation in the presence of excess signal bandwidth.

Many wireless radio systems have transmitted signals with bandwidth more than the data rate. Narrowband TDMA systems based on the IS-54/IS-136 and PDC standards employ 35% and 50% excess bandwidth respectively. In the presence of excess signal bandwidth, fractional sampling is effective due to its insensitivity to sampler timing phase [7]. Some authors [5, 6] have considered using an analog front-end filter which is matched to the transmit filter response (transmit matched filter) followed by a fractional sampler. They, however, assume that the noise affecting the sampled statistic is white. The branch metric of the Viterbi algorithm ignores the correlation in the noise samples. As a result the performance improvement is marginal.

Hamied *et al.* [3] derived an MLSE receiver for systems that employ at most 100% excess bandwidth. Their receiver employs a transmit matched filter followed by a fractional sampler and a fixed noise-whitening filter. The statistic thus obtained is white. However, we note that practical pulse-shaping filters like the square-root raised cosine filter have nulls in the Nyquist spectrum, due to which the noise-whitening filter has a long slowly-damped delay response. Any practical length truncation of the filter leads to severe distortion.

2

Following the development in [1], we derive an Ungerboeck-type receiver which does not need noise-whitening. The branch metric of the Viterbi algorithm accounts for the correlation in the noise samples affecting the fractionally sampled statistic obtained at the output of a transmit matched filter. An adaptive algorithm exploits the knowledge of the pulse-shaping filter and adapts just the fractionally-spaced medium response coefficients. However, the branch metric for the receiver depends on future medium response coefficients up to the span of the medium response. The prediction of these future coefficients using an adaptive algorithm would result in excess estimation error and thus degrade performance. We derive an alternative formulation for the branch metric which depends on causal medium response coefficients only. Thus, only one step prediction is needed to adapt the medium response coefficients. The receiver is suitable for systems with excess signal bandwidth and rapidly time-varying channels.

The paper is organized as follows. In Section 2, we describe the system model and in Section 3, we define an MLSE receiver. In Section 4, we re-visit the Ungerboeck-Bottomley formulation for time-varying channels. We describe the channel model for a system with excess signal bandwidth in Section 5. A fractional Ungerboeck-type receiver is then derived in Section 6. Section 7 deals with the receiver of Hamied *et al.* [3]. A new fractional MLSE receiver that does not need noise-whitening and minimizes channel prediction is described in Section 8.

2   System model

Consider the transmission of linearly-modulated digital data over a linear, time-dispersive medium. The system model consists of a transmitter, a linear time-varying transmission medium and a receiver. The baseband transmitted signal is modeled as

$$x(t) = \sum_{n=0}^{N-1} a_n q(t - nT) \tag{1}$$

where $q(t)$ is the impulse response of the transmit filter and $\{a_n\}_{n=0}^{N-1}$ is a finite sequence of complex symbols (taken from a finite alphabet $\mathcal{A}$). The radio signal transmitted propagates through the medium to reach the receiver where it is converted to a complex-valued, baseband signal $y(t)$, given by

$$
\begin{aligned}
y(t) &= g(\tau; t) * x(t) + w(t) \\
&= \int g(t - \lambda; t) x(\lambda) d\lambda + w(t)
\end{aligned}
\tag{2}
$$

3

where $g(\tau; t)$ is the output of the transmission medium at time t when an impulse is applied at time $t - \tau$ and $w(t)$ is a complex white Gaussian noise process with power spectral density N_0. Substituting (1) in (2), we get

$$y(t) = \sum_{n=0}^{N-1} a_n h(t - nT; t) + w(t) \qquad (3)$$

where $h(\tau; t)$ models the overall response of the transmit filter and the transmission medium and is given by

$$h(\tau; t) = \int g(\tau - \lambda; t) x(\lambda) d\lambda. \qquad (4)$$

The received signal $y(t)$ is collected over a finite time interval, denoted I which is much larger than $[0, (N-1)T]$. The response $h(\tau; t)$ is assumed to be square integrable over the interval I, i.e.

$$\int_{-\infty}^{\infty} |h(\tau; t)|^2 d\tau < \infty \quad \text{for} \quad t \in I. \qquad (5)$$

3 Maximum likelihood sequence estimation

A maximum likelihood sequence estimation (MLSE) receiver finds the hypothetical sequence of symbols $\{\alpha_n\}$ ($\alpha_n \in \mathcal{A}$) that maximizes the likelihood of the received signal $y(t)$ given that $\{\alpha_n\}$ was transmitted. Assuming equiprobable symbols, an MLSE receiver maximizes the log-likelihood function derived from the *a posteriori* distribution of the received signal. Ignoring constant scaling factors and additive terms, the log-likelihood function reduces to

$$J_H = - \int_{t \in I} |y(t) - y_H(t)|^2 \, dt = - \int_{t \in I} \left| y(t) - \sum_{n=0}^{N-1} \alpha_n h(t - nT; t) \right|^2 dt, \qquad (6)$$

where H is the hypothesis corresponding to the sequence $\{\alpha_n\}$. It is assumed that $y(t)$ is band-limited in the receiver front end, using a bandwidth larger than the signal bandwidth, so that the integral in (6) is well defined.

4 The Ungerboeck-Bottomley formulation

In this section, we re-derive an MLSE receiver following the development of Bottomley *et al.* [1]. The receiver is an extension of Ungerboeck's MLSE formulation [9] to time-varying channels. Expressions developed here will be used in later sections, where we derive fractional MLSE receivers.

4

The log-likelihood function J_H can be expanded as

$$J_H = A + B_H + C_H, \tag{7}$$

where

$$A = -\int_{t \in I} |y(t)|^2 dt, \tag{8}$$

$$B_H = \int_{t \in I} 2\mathrm{Re}\left\{ \sum_{n=0}^{N-1} \alpha_n^* h^*(t - nT; t) y(t) \right\} dt, \tag{9}$$

$$C_H = -\int_{t \in I} \sum_{n=0}^{N-1} \sum_{k=0}^{N-1} \alpha_n^* \alpha_k h^*(t - nT; t) h(t - kT; t) dt. \tag{10}$$

Since term A is independent of the sequence hypothesis, an MLSE receiver chooses the sequence hypothesis that maximizes the metric

$$\Lambda_H = B_H + C_H. \tag{11}$$

Terms B_H and C_H can be written as

$$B_H = \sum_{n=0}^{N-1} 2\mathrm{Re}\left\{ \alpha_n^* z(n) \right\}, \tag{12}$$

$$C_H = -\sum_{n=0}^{N-1} \sum_{k=0}^{N-1} \alpha_n^* \alpha_k s(n - k; n), \tag{13}$$

where $\{z(n)\}_{n=0}^{N-1}$ is the sequence of symbol-spaced samples obtained at the output of a receive filter matched to the channel impulse response $h(\tau; t)$, as

$$z(n) = h^*(-\tau; t - \tau) * y(t)|_{t=nT} = \int_{t \in I} h^*(t - nT; t) y(t) dt \tag{14}$$

and the s parameter is the sampled channel autocorrelation function, given by

$$s(l; n) = \int_{t + nT \in I} h^*(t; t + nT) h(t + lT; t + nT) dt \tag{15}$$

where $n \in \{0, 1, \ldots, N-1\}$ and $l \in \{0, \pm 1, \ldots, \pm(N-1)\}$. Noting that $s^*(k - n; k) = s(n - k; n)$ and using the following identity for multi-dimensional summation

$$\sum_{n=i}^{f} \sum_{k=i}^{f} x(n, k) = \sum_{n=i}^{f} \left[x(n, n) + \sum_{k=i}^{n-1} (x(n, k) + x(k, n)) \right], \tag{16}$$

term C_H can be expanded as

$$C_H = -\sum_{n=0}^{N-1} \left[\alpha_n^* \alpha_n s(0; n) - \sum_{k=0}^{n-1} 2\mathrm{Re}\{\alpha_n^* \alpha_k s(n - k; n)\} \right]. \tag{17}$$

5

Substituting (12) and (17) in (11) and letting L be the smallest integer such that $s(l; n) = 0$ for $|l| > L$, we get the metric as

$$\Lambda_H = \sum_{n=0}^{N-1} \Gamma_n(\alpha_n, \sigma_n) \tag{18}$$

where σ_n represents the subsequence hypothesis $\sigma_n : \alpha_{n-1}, \alpha_{n-2}, \ldots, \alpha_{n-L}$ and $\Gamma_n(\alpha_n, \sigma_n)$ is the branch metric, given by

$$\Gamma_n(\alpha_n, \sigma_n) = \text{Re}\left\{ \alpha_n^* \left[2z(n) - s(0; n)\alpha_n - 2\sum_{l=1}^{L} s(l; n)\alpha_{n-l} \right] \right\}. \tag{19}$$

The receiver can be implemented as shown in Fig. 1. The front-end filter in the receiver is matched to the overall channel response $h(\tau; t)$. The Viterbi algorithm in Fig. 1 finds the sequence $\{\alpha_n\}$ that maximizes the metric of (18). The number of states in the Viterbi algorithm is $|\mathcal{A}|^L$, where $|\mathcal{A}|$ is the size of the input alphabet and L is the overall channel memory in symbols (assumed finite).
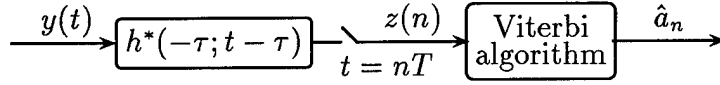
Figure 1: Ungerboeck-Bottomley receiver

5 Channel model

If the baseband transmitted signal $x(t)$ has bandwidth $W \leq M/2T$, where M is an integer, then an arbitrary medium response $g(\tau; t)$ can be modeled as a fractionally-spaced tapped delay line [10, pp. 488]

$$g(\tau; t) = \sum_j c(jT/M; t)\delta(\tau - jT/M) \tag{20}$$

where

$$c(jT/M; t) = c(j; t) = \int g(\tau; t)\text{sinc}\left(\frac{\tau - jT/M}{T/M}\right) d\tau. \tag{21}$$

Assuming that the medium response can be well-approximated by $L_c + 1$ fractionally-spaced taps (i.e. $c(j; t) = 0$ for $j > L_c$), the overall channel impulse response can be written as

$$h(\tau; t) = g(\tau; t) * q(\tau) = \sum_{j=0}^{L_c} c(j; t)q(\tau - jT/M). \tag{22}$$

6

Typically, $\frac{1}{2} < WT < 1$ for full-response signaling and $WT < \frac{1}{2}$ for partial-response signaling (continuous phase modulation) used in narrowband mobile communication systems. Symbol-spaced channel models have been used to develop MLSE receivers [8, 4]. Symbol-spaced MLSE receivers yield close to optimum performance if the excess signal bandwidth (WT in excess of $\frac{1}{2}$) is small. However, the performance of these receivers is highly sensitive to the timing phase [3] in the presence of excess bandwidth. This is due to the inability of a symbol-spaced transversal filter to invert a null in the sampled signal spectrum without excessive noise enhancement [7]. Fractionally-spaced MLSE receivers, on the other hand, are insensitive to the timing phase as aliasing does not occur in the sampled signal spectrum in the case of a fractionally-spaced transversal filter.

6 A fractional Ungerboeck-type receiver

Adaptation of channel parameters is usually needed for an MLSE receiver on time-varying channels. Ungerboeck's adaptive receiver [9] consists of a fractionally-spaced transversal filter followed by a symbol-rate sampler and a Viterbi algorithm. The coefficients of the front-end filter and the sampled channel autocorrelation function 's' are adapted using a stochastic steepest descent algorithm. The s parameters are needed to compute the branch metric (19) in the Viterbi algorithm. Note that the s parameters depend on the transmit filter response and the medium response. Since the transmit filter response is known at the receiver, channel estimation can be improved by adapting the medium response coefficients directly instead of adapting the s parameters. The formulation of Section 4 can be modified for this purpose as shown in [1] for the case of symbol-spaced channel models.

Substituting (22) in (14) and (15), and assuming that the the medium response coefficients $c(j; t)$ are fixed (time-invariant) over the span of the transmit filter response[2] $q(t)$, we get

$$z(n) \approx \sum_{j=0}^{L_c} c^* \left(j; n + \frac{j}{M}\right) Y \left(n + \frac{j}{M}\right), \qquad (23)$$

$$s(l; n) \approx \sum_{j=0}^{L_c} \sum_{k=0}^{L_c} c^* \left(j; n + \frac{j}{M}\right) c \left(k; n - l + \frac{k}{M}\right) r_q(lM + j - k), \qquad (24)$$

where the discrete-time medium response coefficients are defined as $c(j; i) = c(jT; iT)$ for values of i in multiples of T/M, and $\{Y(\cdot)\}$ is the sequence of fractionally-spaced

---

[2]The assumption makes sense when the time variation in the channel coefficients $c(j; t)$ is slow relative to the span of the transmit filter.

samples obtained at the output of a receive filter matched to the transmit filter response $q(t)$, as

$$Y\left(n + \frac{j}{M}\right) = \int_{t \in I} q^*\left(t - \left(n + \frac{j}{M}\right)T\right) y(t) dt \qquad (25)$$

and $r_q(i)$ is the fractionally-sampled autocorrelation function of the transmit filter, given by

$$r_q(i) = \int_{t \in I} q^*(t) q\left(t + \frac{iT}{M}\right) dt. \qquad (26)$$
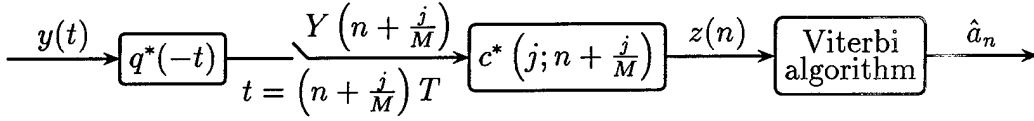
Figure 2: A fractional Ungerboeck-type receiver.

The receiver is shown in Fig. 2. It has a front-end filter matched to the transmit filter response $q(t)$, followed by a fractional-rate sampler. The fractionally-sampled statistic is filtered by an adaptive discrete-time filter and fed to a Viterbi algorithm. The Viterbi algorithm uses the branch metric of (19) with the s parameters given by (24). Note that the receiver in Fig. 2 has a fixed analog front-end filter unlike the receiver of Fig. 1, where the front-end filter is adaptive.

Note from (23) and (24), that the branch metric at time nT given by (19), depends on medium response coefficients for times up to $(n + L_c/M)T$. Thus, medium response coefficients have to be predicted (for $L_c + 1$ future steps) in the adaptive receiver of Fig. 2. The accuracy of prediction decreases in general with the number of steps over which prediction is required. This makes the adaptive receiver of Fig. 2 unsuitable for channels with rapid time variation.

7 A fractional Forney-type receiver

An alternative receiver is obtained by noting that the statistic given by (25) can also be expressed as

$$Y\left(n + \frac{j}{M}\right) = \sum_{i=0}^{L_c} c\left(i; n + \frac{j}{M}\right) \sum_{l=-L_q}^{L_q} r_q(l) a_{n + \frac{i-i-l}{M}} + v\left(n + \frac{j}{M}\right) \qquad (27)$$

8

where $\{v(\cdot)\}$ is a complex Gaussian noise sequence with autocorrelation

$$\mathrm{E}\left[v\left(n + \frac{j}{M}\right)v^*\left(m + \frac{i}{M}\right)\right] = N_0 r_q((n-m)M + j - i), \qquad (28)$$

$$a_{k/M} = \begin{cases} a_i & \text{if } k = iM, \ i \text{ is an integer} \\ 0 & \text{otherwise} \end{cases} \qquad (29)$$

and L_q is the smallest integer such that $r_q(i) = 0$ for $|i| > L_q$. Thus, it is assumed that the transmit filter has a finite impulse response. In practice, transmit pulse-shaping filters like the square-root raised cosine (SRRC) filter are truncated to a span of several symbols. Let the D-transform of the transmit filter autocorrelation function $r_q(n)$ (the sampled autocorrelation spectrum) be defined as

$$R_q(D) = \sum_{n=-L_q}^{L_q} r_q(n)D^n \qquad (30)$$

where D stands for fractional symbol duration.

Hamied *et al.* [3] obtain an adaptive MLSE receiver by assuming that the statistic $\{Y(\cdot)\}$ obtained at the output of the front-end filter in Fig. 2 can be whitened by using a fixed noise-whitening filter. The noise-whitening filter is determined by factoring the sampled autocorrelation spectrum $R_q(D)$ as

$$R_q(D) = F_q^*(D^{-1})F_q(D). \qquad (31)$$

In case the transmit filter spectrum has no roots on the unit circle, the factor $F_q(D) = \sum_{n=0}^{L_q} f_q(n)D^n$ is chosen such that all its roots are outside the unit circle. The anti-causal noise-whitening filter is then given by $(F_q^*(D^{-1}))^{-1}$ which is stable in the sense that its coefficients are square summable.

For many practical pulse-shaping filters like the SRRC filter, the sampled auto-correlation spectrum has zeros on the unit circle. This is illustrated in Fig. 3 which shows the amplitude of the sampled autocorrelation spectrum for SRRC pulses (truncated to a span of 500 symbols) with various roll-off factors. The spectrum exhibits nulls in the Nyquist bandwidth $1/T$ (corresponding to $M = 2$). This is true for all SRRC pulses with roll off factor $\beta \in [0,1]$. The noise-whitening filter does not exist for these pulses as the nulls in the Nyquist band can not be inverted. Fig. 4 shows the sampled autocorrelation spectra for the same SRRC pulses but with a truncation of 10 symbols. Note that the nulls are less severe in this case. Strictly speaking, the noise-whitening filter exists for all practical finite-length transmit pulse-shaping filters. However, due to the presence of zeros near the unit circle, the noise-whitening

9
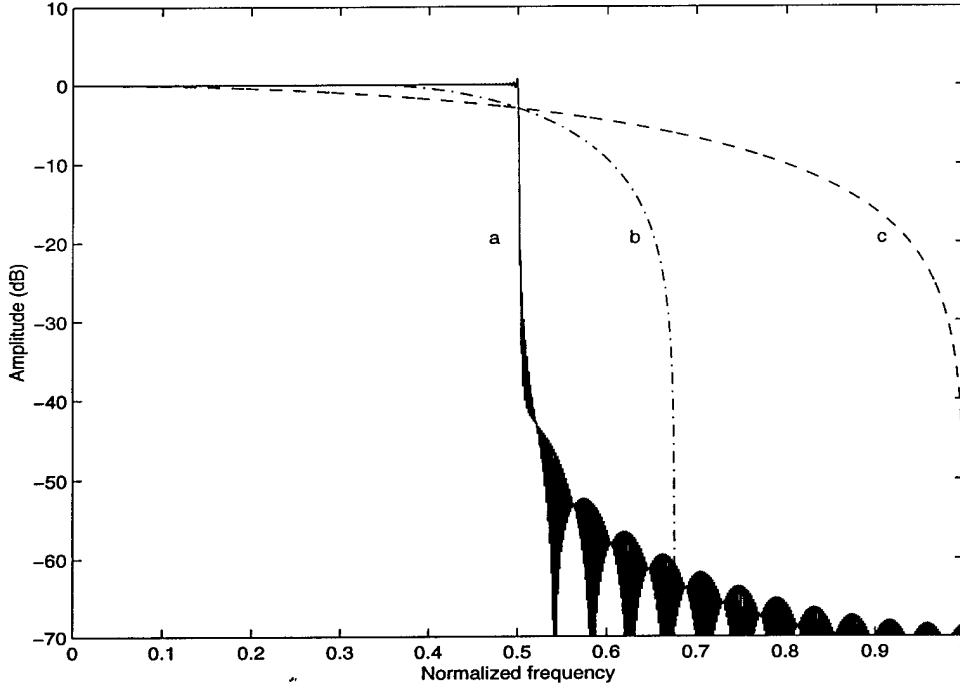
Figure 3: Sampled autocorrelation spectra for SRRC pulses truncated to 500 symbols
(a) $\beta = 0$, (b) $\beta = 0.35$, (c) $\beta = 1$.

filter has a long slowly-damped impulse response and any practical length truncation
results in severe distortion. Fig. 5 shows the effect of truncation of the noise-whitening
filter. The squared error resulting from truncation is given by

$$\|\hat{F}_q(D) - F_q(D)\|^2 \tag{32}$$

where $\hat{F}_q(D)$ is the whitened channel spectrum obtained from using a truncated noise-
whitening filter $W(D^{-1})$ as $\hat{F}_q(D) = W(D^{-1})R_q(D)$. Fig. 5 shows the squared error
for the SRRC pulse of Fig. 4 (truncated to 10 symbols) with $\beta = 0.35$ and $M =$
2. Note that the squared error exhibits damped oscillations and is significant even
with 500 taps of the noise-whitening filter (spanning 250 symbols). The error would
increase with the length of the SRRC pulse because the nulls would be deeper as
demonstrated in Fig. 3.

8 A new fractional MLSE receiver

In this section, we derive an alternative fractional MLSE receiver that does not require
noise-whitening unlike the receiver of Hamied *et al.* [3]. Moreover, it does not require
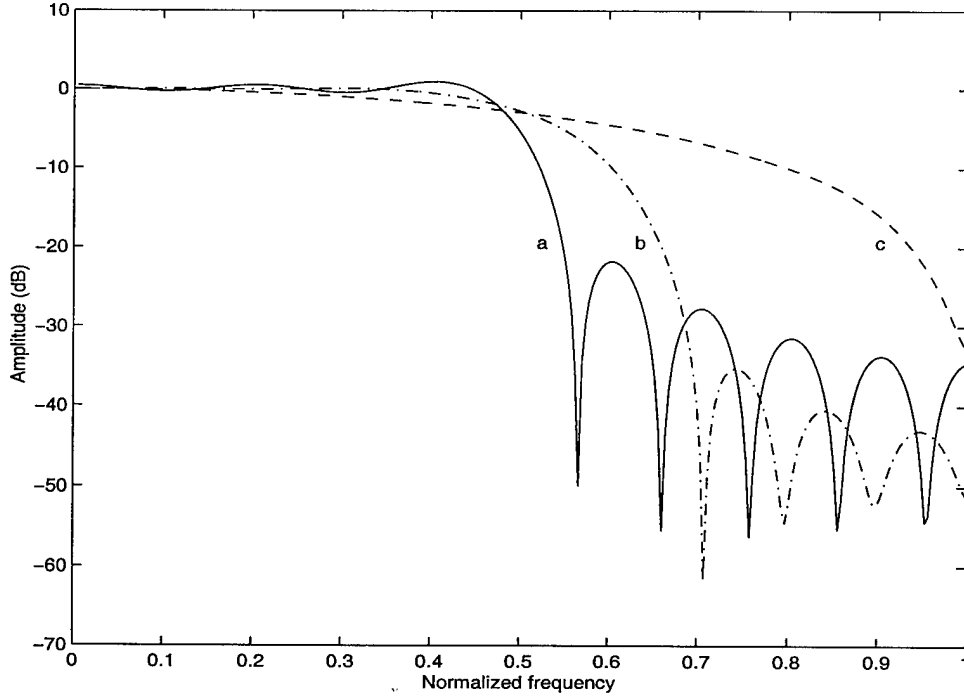
Figure 4: Sampled autocorrelation spectra for SRRC pulses truncated to 10 symbols
(a) $\beta = 0$, (b) $\beta = 0.35$, (c) $\beta = 1$.

extra prediction of medium response coefficients unlike the Ungerboeck-type receiver
of Fig. 2.

Substituting (23) in (12) and making a change of variables gives

$$B_H = \sum_{n=0}^{N-1}\sum_{m=0}^{M-1} 2\mathrm{Re}\left\{ \sum_{j=0}^{L_c} \alpha^*_{n+\frac{m-j}{M}} c^*\left(j; n+\frac{m}{M}\right) Y\left(n+\frac{m}{M}\right)\right\}. \tag{33}$$

Substituting (24) in (13) and making a change of variables gives

$$C_H = -\sum_{n=0}^{(N-1)M}\sum_{j=0}^{L_c}\sum_{k=0}^{(N-1)M}\sum_{l=0}^{L_c} \alpha^*_{\frac{n-j}{M}}\alpha_{\frac{k-l}{M}} c^*\left(j; \frac{n}{M}\right) c\left(l; \frac{k}{M}\right) r_q(n-k). \tag{34}$$

Using (16), term C_H can be written as

$$C_H = -\sum_{n=0}^{N-1}\sum_{m=0}^{M-1}\sum_{j=0}^{L_c}\mathrm{Re}\left\{ c^*\left(j; n+\frac{m}{M}\right) \alpha^*_{n+\frac{m-j}{M}}\left[r_q(0)\sum_{l=0}^{L_c} c\left(l; n+\frac{m}{M}\right)\alpha_{n+\frac{m-l}{M}}\right.\right.$$
$$\left.\left. + 2\sum_{i=1}^{L_q} r_q(i)\sum_{l=0}^{L_c} c\left(l; n+\frac{m-i}{M}\right)\alpha_{n+\frac{m-i-l}{M}}\right]\right\}. \tag{35}$$

Thus, the metric Λ_H in (11) can be written as

$$\Lambda_H = \sum_{n=0}^{N-1}\Gamma'_n(\alpha_n, \sigma_n) \tag{36}$$

11
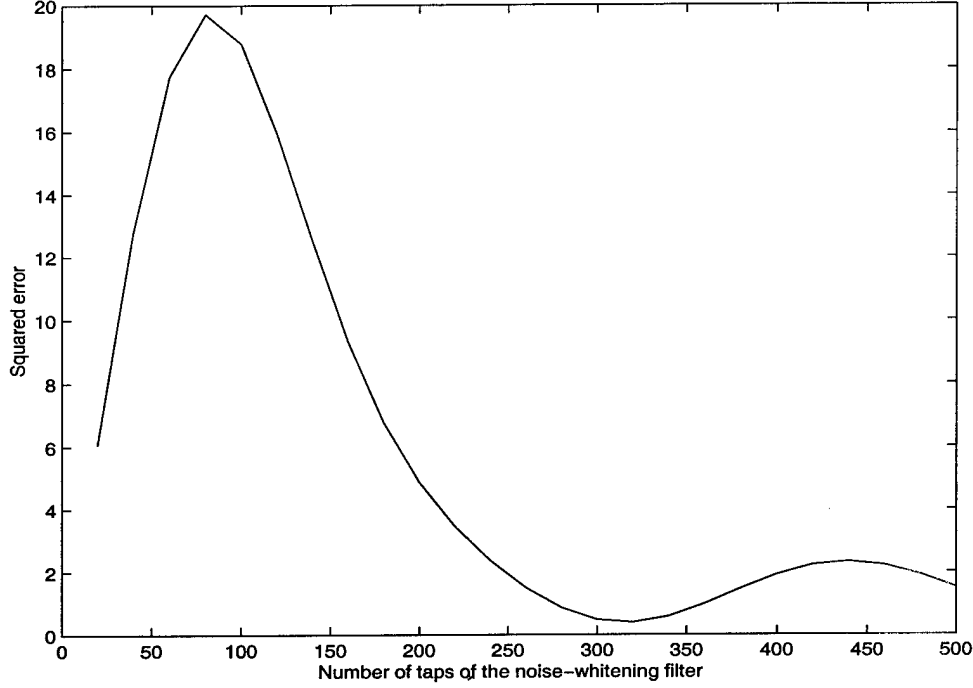
Figure 5: Squared error due to truncation of the noise-whitening filter for SRRC pulse truncated to 10 symbols with $\beta = 0.35$.

where $\Gamma'_n(\alpha_n, \sigma_n)$ is the branch metric, given by

$$
\Gamma'_n(\alpha_n, \sigma_n) =
$$
$$
\sum_{m=0}^{M-1} \sum_{j=0}^{L_c} \mathrm{Re} \left\{ c^* \left(j; n + \frac{m}{M} \right) \alpha^*_{n+\frac{m-j}{M}} \left[2Y \left(n + \frac{m}{M} \right) \right.\right.
$$
$$
\left.\left. - r_q(0) \sum_{l=0}^{L_c} c \left(l; n + \frac{m}{M} \right) \alpha_{n+\frac{m-l}{M}} - 2 \sum_{i=1}^{L_q} r_q(i) \sum_{l=0}^{L_c} c \left(l; n + \frac{m-i}{M} \right) \alpha_{n+\frac{m-i-l}{M}} \right] \right\} \quad (37)
$$

Again using (16) for the term involving $r_q(0)$ in (37), the branch metric can alternatively be written as

$$
\Gamma'_n(\alpha_n, \sigma_n) =
$$
$$
\sum_{m=0}^{M-1} \sum_{j=0}^{L_c} \mathrm{Re} \left\{ c^* \left(j; n + \frac{m}{M} \right) \alpha^*_{n+\frac{m-j}{M}} \left[2Y \left(n + \frac{m}{M} \right) - r_q(0) \left(c \left(j; n + \frac{m}{M} \right) \alpha_{n+\frac{m-j}{M}} \right.\right.\right.
$$
$$
\left.\left.\left. + 2 \sum_{l=1}^{L_c-j} c \left(j+l; n + \frac{m}{M} \right) \alpha_{n+\frac{m-j-l}{M}} \right) - 2 \sum_{i=1}^{L_q} r_q(i) \sum_{l=0}^{L_c} c \left(l; n + \frac{m-i}{M} \right) \alpha_{n+\frac{m-i-l}{M}} \right] \right\} \quad (38)
$$

The receiver is shown in Fig. 6. It employs a fixed front-end filter matched to the transmit filter response. The output of the front-end filter is sampled at the

12

fractional-rate and fed to a Viterbi algorithm. The number of states in the Viterbi algorithm is $|\mathcal{A}|^L$, where $L = \left\lceil \frac{L_c + L_q}{M} \right\rceil$ is the overall channel memory in symbols. The Viterbi algorithm processes M samples of the input statistic every symbol time T. The branch metric given by (37) or (38) has M terms corresponding to each sample. Note that an M step prediction of medium response coefficients is needed to compute the branch metric at each recursion. An alternative approach is to process one sample of the input statistic every T/M seconds by computing one component (of the M components) of the branch metric at each recursion followed by an update of the medium response coefficients. An advantage of this method is that the medium response coefficients can be estimated more accurately as only one step prediction is performed at the fractional rate.
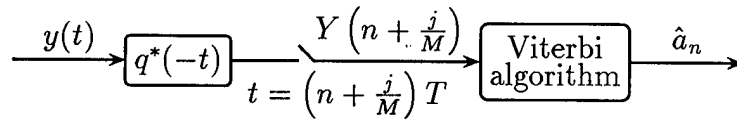
Figure 6: A new fractional MLSE receiver

For a symbol-spaced channel model ($M = 1$), the branch metric given by (38) simplifies to

$$
\Gamma'_n(\alpha_n, \sigma_n) = \\
\sum_{j=0}^{L_c} \mathrm{Re} \left\{ c^*(j; n) \, \alpha^*_{n-j} \left[2Y(n) - r_q(0) \left(c(j; n) \, \alpha_{n-j} + 2 \sum_{l=1}^{L_c - j} c(j+l; n) \, \alpha_{n-j-l} \right) \right. \right. \\
\left. \left. - 2 \sum_{i=1}^{L_q} r_q(i) \sum_{l=0}^{L_c} c(l; n-i) \, \alpha_{n-i-l} \right] \right\}.
\tag{39}
$$

which reduces to the "Partial Ungerboeck" formulation of Bottomley [1] for the case of Nyquist pulse-shaping (i.e. $r_q(n) = \delta(n)$).

9   Conclusions

In this paper, we derived a new fractional MLSE receiver for time-varying channels. The receiver consists of a fixed analog front-end filter matched to the transmit pulse-shaping filter, a fractional sampler and a Viterbi algorithm. The branch metric of the Viterbi algorithm accounts for the correlation in the noise samples which is known

13

at the receiver. The branch metric depends on causal fractionally-spaced medium response coefficients which can be adapted using only one step prediction. The rceiver is suitable for communication systems with excess signal bandwidth and rapidly time-varying channels.

References

[1] G. E. Bottomley and S. Chennakeshu, "Unification of MLSE receivers and extension to time-varying channels," *IEEE Transactions on Communications*, vol. 46, no. 4, pp. 464–472, April 1998.

[2] G. D. Forney, "Maximum-likelihood sequence estimation of digital sequences in the presence of intersymbol interference," *IEEE Transactions on Information Theory*, vol. IT-18, no. 3, pp. 363–378, May 1972.

[3] K. Hamied and G. L. Stuber, "A fractionally spaced MLSE receiver," *IEEE International Conference on Communication*, pp. 7–11, 1995.

[4] H. Kubo, K. Murakami, and T. Fujino, "An adaptive maximum-likelihood sequence estimator for fast time-varying intersymbol interference channels," *IEEE Transactions on Communications*, vol. 42, pp. 1872–1880, Feb./Mrach/April 1994.

[5] Q. Liu and Y. Wan, "A unified MLSE detection technique for TDMA digital cellular radio," *IEEE Vehicular Technology Conference*, pp. 265–268, 1993.

[6] K. Okanoue, A. Ushirokawa, H. Tomita, and Y. Furuya, "New MLSE receiver free from sample timing and input level controls," *IEEE Vehicular Technology Conference*, pp. 408–411, 1993.

[7] S. U. H. Qureshi, "Adaptive equalization," *Proceedings of the IEEE*, vol. 73, no. 9, pp. 1349–1387, September 1985.

[8] N. Seshadri, "Joint data and channel estimation using blind trellis search algorithms," *IEEE Transactions on Communications*, vol. 42, pp. 1000–1011, Feb./Mrach/April 1994.

[9] G. Ungerboeck, "Adaptive maximum-likelihood receiver for carrier-modulated data-transmission systems," *IEEE Transactions on Communication Technology*, vol. COM-22, no. 5, pp. 624–636, May 1974.

[10] H. L. VanTrees, *Detection, Estimation and Modulation Theory Part III: Radar-Sonar Signal Processing and Gaussian Signals in Noise*, New York: John Wiley & Sons, 1968.

Reduced Trellis and Tree Search Algorithms: The Effect of The Receive Filter and The Branch Metric

Abdulrauf Hafeez[1] and Wayne E. Stark

Electrical Engineering and Computer Science Department

1301 Beal Ave., University of Michigan, Ann Arbor, MI 48109-2122.

E-mail: rauf@eecs.umich.edu, stark@eecs.umich.edu.

Abstract– In this paper, we examine the role of the receive filter and the branch metric in decision feedback sequence estimation (DFSE) and M-algorithm receivers. We consider a generalized receiver which consists of a front-end filter (matched to the overall channel response or the transmit filter response) followed by a general transversal processing filter and a reduced trellis or tree search algorithm. A first event error analysis of the generalized receiver indicates that a proper combination of the processing filter and the branch metric is necessary to avoid bias (untreated interference components) in the receiver. Bias occurs in a DFSE or M-algorithm receiver due to a mismatch between the processing filter and the branch metric. We show that the processing filter must either be the appropriate noise-whitening filter or the zero-forcing filter in order to achieve unbiasedness. We obtain the branch metric for the reduced trellis and tree search algorithms for each case of matched filtering. The well-known DFSE and M-algorithm receivers where the search algorithm operates on whitened statistics belong to the class of unbiased receivers, while the receivers where the search algorithm operates on standard matched filter statistics belong to the class of biased receivers. We characterize the error performance of various DFSE and truncated memory MLSE receivers in terms of a parameter called the *error distance* which includes the effect of noise enhancement. We show that the whitening filter DFSE receiver is optimum among unbiased DFSE and truncated memory MLSE receivers (with pre-filtering) in the sense that it maximizes the error distance. We

---

obtain upper bounds on the symbol error probability of the various DFSE receivers and outline a generating function approach to evaluate the bounds. Simulation and analytical results are presented for the case of a symbol-sampled channel model and a fractionally-sampled channel model.

Index Terms– Equalizers, decision feedback equalizers, intersymbol interference, M-algorithm, sequence estimation, Viterbi detection, multiuser detection.

1 Introduction

Maximum-likelihood sequence estimation (MLSE) [11, 22, 4, 23] is an optimum detection technique for channels with memory and additive noise. As the complexity of the various MLSE algorithms is exponential in the channel memory, several low-complexity suboptimal methods have been proposed. One method is to ignore the tail of the delay response or to select a subset of states in the Viterbi algorithm for reduced state detection [24, 12]. The residual interference that arises as a result limits the performance of these methods even at modest ISI levels [18]. Another approach is to pre-cancel the tail of the delay response using a linear or a decision feedback equalizer (DFE). The DFE approach [16, 27] suffers from severe error propagation on channels where the tail contains a significant fraction of the total energy in the channel while the linear pre-filtering approach [10, 19] enhances noise.

Decision feedback sequence estimation (DFSE) [6, 5, 8, 9, 28, 21, 13, 14, 15] and the M-algorithm [1, 26, 29] are two well-known reduced-complexity alternatives to MLSE. These algorithms find applications in equalization of inter-symbol interference (ISI) [6, 5, 8, 28, 21, 13, 14, 15], detection of partial response signals, trellis-coded modulation [6, 8, 9] and multiuser detection [26, 29, 13, 14, 15]. DFSE is a trellis-based method where the complexity is controlled by reducing the memory of the trellis in the Viterbi algorithm. On the other hand, the M-algorithm is a tree-based method where the complexity is reduced by pruning the tree (representing sequence hypotheses) to maintain a given number of branches at each step. Both schemes feed back conditional decisions taken from survivor paths to cancel the tail of the delay response. This manner of decision feedback has been shown to alleviate the problem of error propagation that arises in the conventional DFE approach.

DFSE and M-algorithm receivers were originally proposed to operate on discrete-time statistics containing white noise for which case they have been thoroughly investigated [6, 8, 21, 1, 26]. However, receivers that operate on matched filter statistics have also been proposed for various applications [5, 28, 13, 26, 29]. The main advantage of

these receivers is that they do not require noise-whitening. Computing the whitening filter can be cumbersome for some applications like bidirectional equalization in the GSM system and multiuser detection of direct-sequence CDMA (DS-CDMA) signals [28, 13, 14]. An investigation of the DFSE and M-algorithm receivers with matched filter statistics is given in [15] and [26] respectively. It has been noted that the receive filter has a significant influence on the bit-error performance of these receivers.

In this paper, we extend the techniques of DFSE and M-algorithm to operate on the output of a general transversal processing filter which follows a front-end matched filter. We provide two different formulations of the branch metric — one for the case of standard matched filtering (front-end filter matched to the overall channel response) and the other for the case of transmit matched filtering (front-end filter matched to the transmit filter response). The latter formulation is in terms of causal medium response coefficients. It is desirable if adaptive channel estimation is needed for fractionally spaced medium response coefficients in case of excess signal bandwidth. We conduct a first event error analysis of the various receivers which indicates that the error performance of some of the receivers is affected by "untreated or raw" interference components (bias). Bias occurs in a DFSE or M-algorithm receiver due to a mismatch between the processing filter and the branch metric. This leads to the classification of the various receivers as biased and unbiased, where the notion of "unbiasedness" is devised to mean that an error event is independent of the transmitted sequence given the error sequence.

We find that there exist only two processing filters for each case of matched filtering described above that result in unbiased receivers, namely the filter that whitens (or partially decorrelates) the effect of the matched filter and the filter that zero-forces (or completely decorrelates) the effect of the matched filter. The whitening filter DFSE (WF-DFSE) and whitening filter M-algorithm (WF-MA) receivers with a standard matched filter are the well-known receivers described in [6, 8, 21, 1, 26]. The zero-forcing DFSE (ZF-DFSE) receiver with a standard matched filter was derived in [20]. The class of biased receivers includes matched filter DFSE (MF-DFSE) and matched filter M-algorithm (MF-MA) receivers where the matched filter statistic is fed directly into the reduced trellis or tree search algorithm without further processing. The MF-DFSE(S)[2] receiver was proposed in [5, 28]. The MF-MA(S) receiver was proposed in [29] for multiuser detection.

We find the probability $\Pr(\varepsilon)$ of the occurrence of a given first error event ε for the various DFSE receivers. The probability $\Pr(\varepsilon)$ in the case of unbiased DFSE receivers

---

[2]Where 'S' stands for standard matched filtering.

3

is completely characterized by the error distance $\delta(\varepsilon)$ of the receiver. We use a broader definition of the error distance (than given in [11]) that includes the effect of noise enhancement. In the case of BPSK modulation, the probability $\Pr(\varepsilon)$ for an unbiased DFSE receiver is equal to the error probability of a memoryless system with signal amplitude equal to $\frac{1}{2}\delta(\varepsilon)$. We show that the error distance is maximized by the MF-DFSE(S) receiver. However, the error performance of the MF-DFSE(S) receiver is dominated by untreated interference components (bias) for most channels of interest and is therefore not very good. Among unbiased DFSE receivers, the error distance is maximized by the WF-DFSE receivers for each case of matched filtering. We also show that the error distance of truncated memory MLSE receivers that employ pre-filtering to reduce memory [10, 19], is lower than the error distance of WF-DFSE. Thus, WF-DFSE receivers have the best error performance among these unbiased trellis-based receivers, not considering the effects of error propagation. However, bias-compensated MF-DFSE receivers, where the bias is canceled using tentative decisions (proposed in [14, 15]), can outperform the WF-DFSE receivers of commensurate complexity for channels where reliable tentative decisions can be obtained.

We obtain upper bounds on the symbol error probability of the various DFSE receivers. We show that these bounds can be evaluated using a generating function method similar to MLSE, clearing the misconception that a generating function method is not applicable to the case of DFSE due to the use of decision feedback [21].

The paper is organized as follows. The system model is given in Section 2. MLSE receivers that consist of a front-end matched filter followed by a general transversal processing filter are described in Section 3. The corresponding DFSE and M-algorithm receivers are described in Sections 4 and 5 respectively. In Section 6, we conduct a first event error analysis of the various receivers. Sections 7 and 8 deal with unbiased and biased receivers respectively. Section 9 deals with a truncated memory MLSE receiver that employs pre-filtering. In Section 10, we derive bounds on the symbol error probability and in Section 11, we compare the error distances of the various receivers. In Section 12, we show how the bounds can be evaluated using error state diagrams. In Section 13, we compare the error-rate performance of the various receivers for a symbol-sampled system and a fractionally sampled system via simulation and analysis using some example channels.

2 System model

Consider the transmission of linearly-modulated digital data over a linear, time-dispersive medium. The system model consists of a transmitter, a linear time-invariant transmission medium and a receiver. The baseband transmitted signal is modeled as

$$s_t(t) = \sum_{n=0}^{N-1} a_n d(t - nT) \tag{1}$$

where $\{a_n\}_{n=0}^{N-1}$ is a finite sequence of complex symbols (taken from a finite alphabet $\mathcal{A}$) and $d(t)$ is the impulse response of the transmit filter. The signal transmitted propagates through the medium to reach the receiver where it is converted to a complex-valued, baseband signal $y(t)$, given by

$$
\begin{aligned}
y(t) &= g(t) * s_t(t) + w(t) \\
&= \int g(t - \lambda) s_t(\lambda) d\lambda + w(t)
\end{aligned}
\tag{2}
$$

where $w(t)$ is a complex white Gaussian noise process with power spectral density N_0 and $g(t)$ is the impulse response of the transmission medium (assumed stationary). The medium response is modeled as a tapped delay line with L_c complex-valued symbol-spaced tap coefficients $c(i)$, i.e.

$$g(t) = \sum_{i=0}^{L_c} c(i) \delta(t - iT). \tag{3}$$

Substituting (1) in (2), we get the received signal as

$$y(t) = \sum_{n=0}^{N-1} a_n h(t - nT) + w(t) \tag{4}$$

where $h(t)$ models the overall response of the transmit filter and the transmission medium and is given by

$$h(t) = \sum_{i=0}^{L_c} c(i) d(t - iT). \tag{5}$$

The response $h(t)$ is assumed to be square integrable.

3 Maximum Likelihood Sequence Estimation

Maximum likelihood sequence estimation (MLSE) is an optimal detection algorithm that minimizes the probability of sequence error for *a priori* equiprobable sequences. In this section, we describe an MLSE receiver with a general transversal processing

5

filter. The processing filter has no influence on MLSE performance as we will see in the next section. However, the expressions developed in this section will be useful when we consider the effect of the processing filter on reduced trellis and tree search algorithms.

It is well-known [11, 22, 4] that the sequence of symbol-spaced samples $\{z(n)\}_{n=0}^{N-1}$ obtained at the output of a receive filter matched to the overall channel impulse response $h(t)$ forms a set of sufficient statistics for detecting the transmitted sequence $\{a_n\}_{n=0}^{N-1}$ given the received signal $y(t)$. The matched-filter statistic $z(n)$ is given by

$$z(n) = h^*(-t) * y(t)|_{t=nT} = \int h^*(t-nT)y(t)dt. \tag{6}$$

In vector notation, the sequence of matched-filter statistics is given by

$$\underline{z} = S\underline{a} + \underline{u} \tag{7}$$

where $\underline{a} = [a_0, a_1, \ldots, a_{N-1}]^T$, $\underline{z} = [z(0), z(1), \ldots, z(N-1)]^T$, $\underline{u} = [u(0), u(1), \ldots, u(N-1)]^T$, and S is an $N \times N$ Hermitian Toeplitz[3] matrix known as the channel spectrum. The (i,j)-th element of S is given by

$$s(i,j) = s(i-j) = \int h^*(t)h(t+(i-j)T)dt. \tag{8}$$

The elements $s(i)$ are samples of the autocorrelation function of the overall channel response which is assumed to have finite span. The smallest integer L such that $s(i) = 0$ for $|i| > L$ is known as the channel memory. We assume that the channel memory L is much smaller than the length N of the transmitted sequence. The matrix S is thus banded. The vector $\underline{u}$ is a discrete Gaussian noise vector with elements

$$u(n) = \int_{t \in I} h^*(t-nT)w(t)dt \tag{9}$$

and autocorrelation $\mathrm{E}[\underline{u}^H\underline{u}] = N_0 S$.

Consider a transversal processing filter P which processes the output of the matched filter. The output of the processing filter which is an $N \times N$ matrix, is given by

$$\underline{x} = P\underline{z} = P(S\underline{a} + \underline{u}) \tag{10}$$

From (7), it follows that $\underline{x} = [x(0), x(1), \ldots, x(N-1)]^T$ is a Gaussian random vector with mean $PS\underline{a}$ and autocovariance $N_0 PSP^H$, given the information sequence $\underline{a}$. Assume that the inverse processing filter P^{-1} exists. Then, it is possible to recover the original sequence $\underline{z}$ from the filtered sequence $\underline{x}$. Thus, the sequence $\underline{x}$ forms a
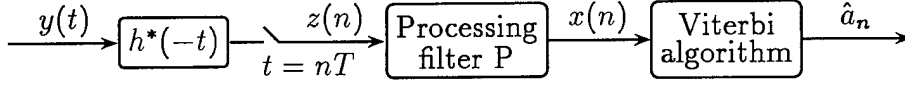
Figure 1: A generalized MLSE receiver

set of sufficient statistics for detecting the transmitted sequence $\underline{a}$ given the received signal $y(t)$.

Consider the receiver shown in Fig. 1. The receiver finds the hypothetical sequence of symbols $\{\alpha_n\}$ $(\alpha_n \in \mathcal{A})$ that maximizes the likelihood of the received signal $y(t)$ given that $\{\alpha_n\}$ was transmitted. Assuming equiprobable symbols, the receiver maximizes the log-likelihood function derived from the *a posteriori* distribution of the received signal. Ignoring constant scaling factors and additive terms, the log-likelihood function reduces to

$$J_H = -(\underline{x} - PS\underline{\alpha})^H (PSP^H)^{-1} (\underline{x} - PS\underline{\alpha}) \tag{11}$$

where the superscript H stands for Hermitian transpose and the subscript H corresponds to the hypothesized sequence $\underline{\alpha}$. Neglecting terms common to all hypotheses, the metric to be maximized by the Viterbi algorithm can be written as

$$\Lambda_H = 2\mathrm{Re}\{\underline{\alpha}^H P^{-1} \underline{x}\} - \underline{\alpha}^H S \underline{\alpha} \tag{12}$$

Assume that the matrix S is positive definite. Then, it can be decomposed into its unique Cholesky factors as

$$S = \tilde{F}^H \tilde{F} \tag{13}$$

where $\tilde{F}$ is an $N \times N$ invertible lower-triangular matrix. For $N \gg L$, the matrix $\tilde{F}$ is near Toeplitz[4]. Also note that

$$S = F_+^H F_+ \tag{14}$$

where F_+ is an $N + L \times N$ matrix with elements

$$f(i,j) = \begin{cases} f(i-j) & 0 \le i - j \le L \\ 0 & \text{otherwise} \end{cases} \tag{15}$$

---

[3]i.e. the elements of S satisfy $s(i,j) = s(i-j)$.

[4]The matrix has constant elements along each diagonal except the elements in some bottom rows.

7

obtained from the inverse z-transform of the minimum-phase Cholesky factor $F(z)$ of the z-transform of $\{s(i)\}$. Then, the metric in (12) can be written as

$$\Lambda_H = 2\text{Re}\{\underline{\alpha}^H P^{-1} \underline{x}\} - \|F_+ \underline{\alpha}\|^2. \tag{16}$$

The metric can be approximated as

$$\Lambda_H \approx 2\text{Re}\{\underline{\alpha}^H P^{-1} \underline{x}\} - \|F \underline{\alpha}\|^2 \tag{17}$$

where F is an $N \times N$ lower-triangular Toeplitz matrix with elements given by (15). The approximation in (17) is a result of premature trellis termination in the Viterbi algorithm at the tail of the transmitted sequence. We adopt the approximate expression for the total metric (17) rather than (16) for simplicity of notation and analysis. In order to be consistent then, we let $S = F^H F$ throughout the rest of the paper, without loss of generality.

The two expressions for the total metric (12) and (17) lead to two different additive decompositions (branch metrics). In order to obtain a general expression for the branch metric, we write the channel spectrum as

$$S = RQ \tag{18}$$

where R is an $N \times N$ upper-triangular Toeplitz matrix with elements

$$r(i,j) = \begin{cases} r(i-j) & -l_r \le i - j \le 0 \\ 0 & \text{otherwise} \end{cases} \tag{19}$$

where l_r is either 0 or L and Q is an $N \times N$ Toeplitz matrix with elements

$$q(i,j) = \begin{cases} q(i-j) & -L + l_r \le i - j \le L \\ 0 & \text{otherwise} \end{cases} \tag{20}$$

In (12), $R = I$ and $Q = S$ while in (17), $R = Q^H = F^H$.

Assume that the inverse processing filter consists of $l_p + l_f + 1$ coefficients ($l_p + 1$ causal and l_f anti-causal). The elements of the $N \times N$ banded Toeplitz matrix P^{-1} are given by

$$p'(i,j) = \begin{cases} p'(i-j) & -l_f \le i - j \le l_p \\ 0 & \text{otherwise} \end{cases} \tag{21}$$

This structure for the inverse processing filter encompasses many filters of interest, including the zero-forcing filter and the noise-whitening filter.

Using (19), (20) and (21), the total metric in (12) can then be written as

$$\Lambda_H = 2\mathrm{Re}\{\underline{\alpha}^H[(P^{-1})^L \underline{x}]\} + 2\mathrm{Re}\{[\underline{\alpha}^H(P^{-1})^{UD}]\underline{x}\} - [\underline{\alpha}^H R][(Q)^L \underline{\alpha}] - [\underline{\alpha}^H R(Q)^{UD}]\underline{\alpha}$$

$$(22)$$

where the superscripts L, U and D denote the lower-triangular, the upper-triangular and the diagonal part of a matrix respectively. The above form for the total metric leads to the additive decomposition

$$\Lambda_H = \sum_{n=0}^{N-1} \Gamma(\alpha_n, \sigma_n) \tag{23}$$

where $\Gamma(\alpha_n, \sigma_n)$ is the branch metric corresponding to the state $\sigma_n : \alpha_{n-1}, \ldots, \alpha_{n-L_v}$ ($L_v = \max(L, l_f)$) in the trellis of the Viterbi algorithm, given by

$$\Gamma(\alpha_n, \sigma_n) = 2\mathrm{Re}\left\{ \alpha_n^* \sum_{l=1}^{l_p} p'(l)x(n-l) + x(n)\sum_{l=0}^{l_f} p'(-l)\alpha_{n-l}^* \right\}$$

$$- \left(\sum_{l=0}^{l_r} r(-l)\alpha_{n-l}^* \right) \left(\sum_{l=1}^{L} q(l)\alpha_{n-l} \right) - \alpha_n \sum_{l=0}^{l_r} r(-l) \sum_{k=0}^{L-l_r} q(-k)\alpha_{n-l-k}^* \tag{24}$$

where $\alpha_n = 0$ for $N - 1 < n < 0$. The Viterbi algorithm recursively computes the accumulated metric defined as

$$\mathcal{M}(\sigma_n) \triangleq \max_{\alpha_1, \alpha_2, \ldots, \alpha_{n-L_v-1}} \sum_{i=0}^{n-1} \Gamma(\alpha_i, \sigma_i) \tag{25}$$

for all subsequence hypotheses (or states) σ_n. The recursion follows from (24) and (25) as

$$\mathcal{M}(\sigma_{n+1}) = \max_{\alpha_{n-L_v}} \left[\mathcal{M}(\sigma_n) + \Gamma(\alpha_n, \sigma_n) \right]. \tag{26}$$

The number of states in the Viterbi algorithm is $|\mathcal{A}|^{L_v}$ (note that the memory of the Viterbi algorithm L_v may be greater than the channel memory L). The output of the Viterbi algorithm is the estimated sequence $\{\hat{a}_n\}$.
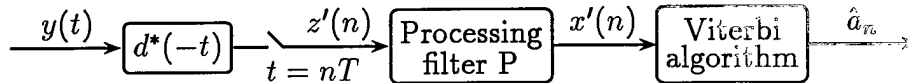

Figure 2: An alternative MLSE receiver

An alternative MLSE receiver is shown in Fig. 2. It differs from the receiver of Fig. 1 in that it has a front-end filter which is matched to just the transmit

filter response $d(t)$ instead of the overall channel response $h(t)$. The transmit filter matched-filter statistic $z'(n)$ is given by

$$
\begin{aligned}
z'(n) &= d^*(-t) * y(t)|_{t=nT} = \int d^*(t-nT)y(t)dt \\
&= \sum_{l=-L_d}^{L_d} \sum_{i=0}^{L_c} c(i)\phi(n,n-l)a_{n-l-i} + u'(n).
\end{aligned} \tag{27}
$$

which can be written in vector notation as

$$
\underline{z}' = \Phi C \underline{a} + \underline{u}' \tag{28}
$$

where $\underline{z}' = [z'(0), z'(1), \ldots, z'(N-1)]^T$, $\underline{u}' = [u'(0), u'(1), \ldots, u'(N-1)]^T$. The matrix C is a lower-triangular Toeplitz matrix with elements

$$
c(i,j) = \begin{cases} c(i-j) & 0 \le i-j \le L_c \\ 0 & \text{otherwise} \end{cases} \tag{29}
$$

and the matrix Φ is a Hermitian Toeplitz matrix with elements which are samples of the transmit filter autocorrelation function

$$
\phi(i,j) = \phi(i-j) = \int d^*(t)d(t+(i-j)T)dt. \tag{30}
$$

Let $\phi(i) = 0$ for $|i| > L_d$. The overall channel memory is then $L = L_c + L_d$. The vector $\underline{u}'$ is a Gaussian random vector with mean zero and autocorrelation $\mathrm{E}[\underline{u}'^H \underline{u}'] = N_0 \Phi$. Note that the statistic $\underline{z}$ can be obtained from the statistic $\underline{z}'$ as $\underline{z} = C^H \underline{z}'$. The sequence $\underline{z}'$, thus, forms a set of sufficient statistics for detecting the transmitted sequence given $y(t)$. The statistic $\underline{x}'$ input to the Viterbi algorithm is given by

$$
\underline{x}' = P\underline{z}' = P(\Phi C \underline{a} + \underline{u}'). \tag{31}
$$

The log-likelihood function in this case is given by

$$
J'_H = -(\underline{x}' - P\Phi C \underline{\alpha})^H (P\Phi P^H)^{-1}(\underline{x}' - P\Phi C \underline{\alpha}) \tag{32}
$$

which yields the likelihood metric to be maximized by the Viterbi algorithm in Fig. 2, as

$$
\Lambda'_H = 2\mathrm{Re}\{\underline{\alpha}^H C^H P^{-1} \underline{x}'\} - \underline{\alpha}^H C^H \Phi C \underline{\alpha}. \tag{33}
$$

Again two different additive decompositions of the above metric are possible corresponding to the two decompositions of the matrix Φ, i.e.

$$
\Phi = R'Q' \tag{34}
$$

10

where the elements of R' are given by

$$r'(i,j) = \begin{cases} r'(i-j) & -l_{r'} \leq i-j \leq 0 \\ 0 & \text{otherwise} \end{cases} \tag{35}$$

where $l_{r'}$ is either 0 or L_d and the elements of Q' are given by

$$q'(i,j) = \begin{cases} q'(i-j) & -L_d + l_{r'} \leq i-j \leq L_d \\ 0 & \text{otherwise} \end{cases} \tag{36}$$

In one case $R' = I$, $Q' = \Phi$ and in the other case $R' = Q'^H = F'^H$. The matrix F' is a lower-triangular Toeplitz matrix with elements $f'(i)$ given by the inverse z-transform of the minimum-phase Cholesky factor $F'(z)$ of the z-transform of $\{\phi(i)\}$. Then, (33) can be written as

$$\Lambda'_H = \sum_{n=0}^{N-1} \Gamma'(\alpha_n, \sigma_n) = 2\text{Re}\{\underline{\alpha}^H C^H P^{-1} \underline{x}'\} - \underline{\alpha}^H C^H R' Q' C \underline{\alpha}. \tag{37}$$

where the branch metric $\Gamma'(\alpha_n, \sigma_n)$ is given by

$$\begin{aligned}
\Gamma'(\alpha_n, \sigma_n) &= 2\text{Re}\left\{ \left(\sum_{l=0}^{L_c} c^*(l)\alpha^*_{n-l} \right) \left(\sum_{l=1}^{l_p} p'(l)x'(n-l) \right) + x'(n) \sum_{l=0}^{L_c} c^*(l) \sum_{k=0}^{l_f} p'(-k)\alpha^*_{n-l-k} \right\} \\
&\quad - \left(\sum_{l=0}^{L_c} c^*(l) \sum_{k=0}^{l_{r'}} r'(-k)\alpha^*_{n-l-k} \right) \left(\sum_{l=0}^{L_c} c(l) \sum_{k=1}^{L_d} q'(k)\alpha_{n-l-k} \right) \\
&\quad - \left(\sum_{l=0}^{L_c} c^*(l) \sum_{k=0}^{l_{r'}} r'(-k) \sum_{m=0}^{L_d-l_{r'}} q'(-m)\alpha^*_{n-l-k-m} \right) \left(\sum_{l=0}^{L_c} c(l)\alpha_{n-l} \right).
\end{aligned} \tag{38}$$

The memory of the Viterbi algorithm in this case is $L'_v = \max(L, L_c + l_f)$. Note that the receiver of Fig. 2 can be easily extended for the case of a fractionally-spaced medium response model. In this case, the output of the transmit matched filter in Fig. 2 is sampled at a multiple of the symbol rate (say ν/T). The memory of the Viterbi algorithm is $\lceil L'_v/\nu \rceil$ and the branch metric is modified by replacing α_n in (38) by π_n, given by

$$\pi_n = \begin{cases} \alpha_{n/\nu} & n/\nu \text{ integer} \\ 0 & \text{otherwise} \end{cases}. \tag{39}$$

4 Decision Feedback Sequence Estimation

Decision feedback sequence estimation (DFSE) is a reduced complexity alternative to maximum likelihood sequence estimation which provides an adjustable performance/complexity tradeoff. Proposed by Duel-Hallen et al. [5, 6][5] and Eyuboglu

---

[5]The algorithm is referred to as Delayed Decision Feedback Sequence Estimation in [5, 6]

11

et al. [8], the scheme employs a reduced trellis search algorithm to search through a subset of sequence hypotheses searched by the full-blown Viterbi algorithm. The complexity is controlled by a parameter called memory order J, which is chosen arbitrarily smaller than the memory of the Viterbi algorithm. The trellis in the reduced trellis search algorithm then comprises $|\mathcal{A}|^J$ states corresponding to the J most recent symbol hypotheses. Survivor paths or sequences are chosen in the reduced trellis search algorithm on the basis of the same cost function as in MLSE (i.e. the accumulated likelihood metric). A transition in the reduced trellis specifies the $J + 1$ most recent hypothesized symbols. The remaining $L - J$ symbols needed to compute the branch metric are obtained from decisions taken from the survivor history (past decisions) of the path.

Figure 3: A generalized DFSE receiver

The DFSE algorithms proposed by Duel-Hallen *et al.* operate on matched-filter and whitened statistics obtained from conventional matched filtering and whitened matched filtering respectively. Here we generalize the DFSE algorithm to operate with a general transversal processing filter. The receiver is shown in Fig. 3. The reduced trellis search algorithm has memory order J chosen such that $0 \leq J \leq L_v$. It employs the recursion:

$$\mathcal{M}(\beta_{n+1}) = \max_{\alpha_{n-J}} \left[\mathcal{M}(\beta_n) + \Gamma(\alpha_n, \beta_n) \right] \tag{40}$$

where $\beta_n : \alpha_{n-1}, \alpha_{n-2}, \ldots, \alpha_{n-J}$ represents states in the reduced trellis at time n, $\mathcal{M}(\beta_n)$ is the accumulated metric of the survivor path associated with state β_n and $\Gamma(\alpha_n, \beta_n)$ is the corresponding branch metric given by

$$
\begin{aligned}
\Gamma(\alpha_n, \beta_n) &= 2\mathrm{Re}\left\{ \alpha_n^* \sum_{l=1}^{l_p} p'(l) x(n-l) + x(n) \sum_{l=0}^{l_f} p'(-l)\eta_{n-l}^* \right\} \\
&- \left(\sum_{l=0}^{l_r} r(-l)\eta_{n-l}^* \right) \left(\sum_{l=1}^{L} q(l)\eta_{n-l} \right) - \alpha_n \sum_{l=0}^{l_r} r(-l) \sum_{k=0}^{L-l_r} q(-k)\eta_{n-l-k}^* \tag{41}
\end{aligned}
$$

12

where at time n

$$\eta_{n-i} = \begin{cases} \alpha_{n-i} & 0 \leq i \leq J \\ \hat{\alpha}_{n-i}(\beta_n) & J+1 \leq i \leq L_v \end{cases} \tag{42}$$

In (42), $\{\hat{\alpha}_i(\beta_n)\}$ are tentative conditional decisions on symbols more than J samples in the past obtained from the history of the survivor path associated with state β_n, as

$$\hat{\alpha}_{n-J}(\beta_n) = \arg\max_{\alpha_{n-J}} [\mathcal{M}(\beta_n) + \Gamma(\alpha_n, \beta_n)]. \tag{43}$$

The reduced trellis branch metric $\Gamma(\alpha_n, \beta_n)$ of (41) corresponds to the full trellis branch metric $\Gamma(\alpha_n, \sigma_n)$ given by (24). Note that the (whitened matched filter) DFSE algorithm of [6] is obtained by substituting $P^{-1} = R = Q^H = F^H$ and the DFSE algorithm with the standard matched filter, proposed in [5], is obtained by substituting $P^{-1} = R = I$, $Q = S$. In the first case, the whitened channel F with coefficients $\{f(n)\}$ is minimum-phase.
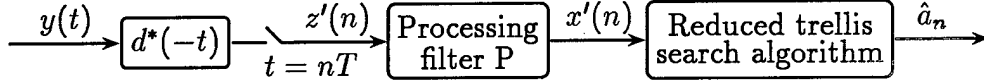
Figure 4: An alternative DFSE receiver

An alternative DFSE receiver shown in Fig. 4 corresponds to the MLSE receiver of Fig. 2, in that the front-end filter is matched to the transmit filter response. It follows the recursion:

$$\mathcal{M}'(\beta_{n+1}) = \max_{\alpha_{n-J}} [\mathcal{M}'(\beta_n) + \Gamma'(\alpha_n, \beta_n)] \tag{44}$$

where the memory order is chosen in the range $0 \leq J \leq L'_v$ and the reduced trellis branch metric $\Gamma'(\alpha_n, \beta_n)$ is obtained by replacing α_{n-i} in (38) by

$$\eta'_{n-i} = \begin{cases} \alpha_{n-i} & 0 \leq i \leq J \\ \hat{\alpha}'_{n-i}(\beta_n) & J+1 \leq i \leq L'_v \end{cases} \tag{45}$$

where $\{\hat{\alpha}'_i(\beta_n)\}$ are tentative conditional decisions obtained as

$$\hat{\alpha}'_{n-J}(\beta_n) = \arg\max_{\alpha_{n-J}} [\mathcal{M}'(\beta_n) + \Gamma'(\alpha_n, \beta_n)]. \tag{46}$$

13

The branch metric is given by

$$\Gamma'(\alpha_n, \sigma_n) = 2\mathrm{Re}\left\{\left(\sum_{l=0}^{L_c} c^*(l)\eta_{n-i}'^*\right)\left(\sum_{l=1}^{l_p} p'(l)x'(n-l)\right) + x'(n)\sum_{l=0}^{L_c} c^*(l)\sum_{k=0}^{l_f} p'(-k)\eta_{n-l-k}'^*\right\}$$

$$- \left(\sum_{l=0}^{L_c} c^*(l)\sum_{k=0}^{l_{r'}} r'(-k)\eta_{n-l-k}'^*\right)\left(\sum_{l=0}^{L_c} c(l)\sum_{k=1}^{L_d} q'(k)\eta_{n-l-k}'\right)$$

$$- \left(\sum_{l=0}^{L_c} c^*(l)\sum_{k=0}^{l_{r'}} r'(-k)\sum_{m=0}^{L_d-l_{r'}} q'(-m)\eta_{n-l-k-m}'^*\right)\left(\sum_{l=0}^{L_c} c(l)\eta_{n-l}'\right). \qquad (47)$$

With $P = R' = Q' = I$, we get the case of Nyquist pulse-shaping[6] at the transmitter and transmit-filter matched-filtering at the receiver with no further processing. This results in the DFSE receiver of [6] where the statistic is white and the channel C with coefficients $\{c(n)\}$ may have any phase (minimum, mixed, or maximum phase). With $P^{-1} = R' = Q'^H = F'^H$, the whitened channel $F'C$ with coefficients $\{f'(n) * c(n)\}$ has mixed phase in general.

5   M-Algorithm

The M-algorithm (MA) [1] is well-known as another reduced complexity alternative to MLSE. The scheme was originally proposed to operate on white (or whitened) statistics. However, it has also been used with the standard matched filter (see for example [29, 26]). The M-algorithm is essentially a reduced tree search algorithm. At each step, M survivor paths (hypothesized sequences) are extended to $M\mathcal{A}$ paths, of which the M paths with the best accumulated likelihood metric are retained and the rest are discarded.
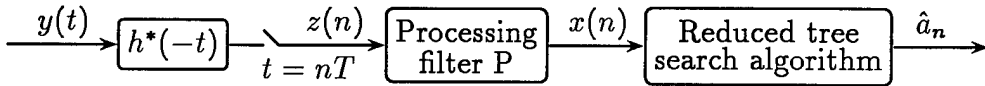

Figure 5: A generalized M-algorithm receiver

In this section, we extend the M-algorithm to operate with a general transversal processing filter. The receiver is shown in Fig. 5. Let $\underline{\alpha}_n(j) = (\alpha_0, \alpha_1, \ldots, \alpha_{n-1})$ be

---

[6]Using transmit pulses that satisfy the Nyquist criterion for ISI free transmission.

one of the M survivor paths $(j = 1, \ldots, M)$ at time n. At time $n + 1$, the reduced tree search algorithm extends each survivor into $\mathcal{A}$ paths $\underline{\alpha}_{n+1} = (\underline{\alpha}_n(j), \alpha_n)$ and computes their accumulated likelihood metric using

$$\mathcal{M}(\underline{\alpha}_{n+1}) = \mathcal{M}(\underline{\alpha}_n(j)) + \Gamma(\alpha_n, \sigma_n(j)) \tag{48}$$

where the branch metric $\Gamma(\alpha_n, \sigma_n(j))$ which depends on the last L_v hypothetical symbols $\sigma_n(j)$ in the survivor path $\underline{\alpha}_n(j)$, is given by (24). The M paths with the highest accumulated metric are then selected.

An alternative M-algorithm receiver has a front-end filter matched to the transmit filter response and uses the branch metric of the MLSE receiver of Fig. 2, given by (38).

6 First Event Error Analysis

In this section, we examine the first event error (FEE) probability of the generalized DFSE receiver of Section 4 (Fig. 3) and the generalized M-algorithm receiver of Section 5 (Fig. 5). We say that a *first event error* is made in the reduced trellis or tree search algorithm (at time j) if the correct path is abandoned for the first time in favor of a competitor path or paths that diverge from the correct path at time j. Note that our definition of a first event error is different from the definition given in [17], in that we consider the start time of an error event as the time of its occurrence as opposed to the end time as in [17]. We assume that the channel is stationary. Thus, a first event error is independent of the time and time 0 can be chosen without loss of generality.

6.1 Trellis Search Algorithms

Consider the generalized DFSE receiver of Fig. 3. Let $\{a_n\}$ be the sequence of symbols transmitted and $\{b_n\}$ ($b_n : a_{n-1}, a_{n-2}, \ldots, a_{n-J}$) be the sequence of states in the path of $\{a_n\}$ in the reduced trellis of the DFSE receiver (with memory order J). Let $\{\bar{a}_n\}$ be a hypothetical sequence of symbols and $\{\bar{b}_n\}$ be the corresponding sequence of states in the reduced trellis that diverges from the correct sequence of states at time unit 0 and re-merges with it at a later time (say k), i.e.

$$\bar{b}_n = b_n \text{ for } n = 0, k \text{ and } \bar{b}_n \neq b_n \text{ for } 0 < n < k. \tag{49}$$

A first event error occurs at time 0 if the reduced trellis search algorithm picks $\{\bar{a}_n\}$ as the survivor sequence over $\{a_n\}$. It follows from (40) that the event occurs if the

metric accumulated on the incorrect path is greater than the metric accumulated on the correct path i.e.

$$\sum_{n=0}^{k-1} \Gamma(\bar{a}_n, \bar{b}_n) > \sum_{n=0}^{k-1} \Gamma(a_n, b_n) \tag{50}$$

where $\{\Gamma(a_n, b_n)\}$ and $\{\Gamma(\bar{a}_n, \bar{b}_n)\}$ are branch metrics corresponding to the paths $\{a_n\}$ and $\{\bar{a}_n\}$ respectively, computed using (41). Note that the conditional decisions $\{\hat{a}_{n-l}(b_n)\}$ and $\{\hat{a}_{n-l}(\bar{b}_n)\}$ which are fed back to compute the branch metrics, are taken from the paths corresponding to the sequences of states $\{b_n\}$ and $\{\bar{b}_n\}$ respectively. Thus, $\hat{a}_{n-l}(b_n) = a_{n-l}$ and $\hat{a}_{n-l}(\bar{b}_n) = \bar{a}_{n-l}$ and (50) can be written in matrix notation as

$$2\mathrm{Re}\{\bar{\underline{a}}_k^H (P^{-1})_k \underline{x}_k\} - \bar{\underline{a}}_k^H R_k Q_k \bar{\underline{a}}_k > 2\mathrm{Re}\{\underline{a}_k^H (P^{-1})_k \underline{x}_k\} - \underline{a}_k^H R_k Q_k \underline{a}_k \tag{51}$$

where $\underline{a}_k = [a_0, a_1, \ldots, a_{k-1}]^T$, $\bar{\underline{a}}_k = [\bar{a}_0, \bar{a}_1, \ldots, \bar{a}_{k-1}]^T$ and $\underline{x}_k = [x(0), x(1), \ldots, x(k-1)]^T$. The matrices $(P^{-1})_k$, R_k and Q_k are principal submatrices[7] of dimension k of the matrices P^{-1}, R and Q respectively given by (18), (19), (20) and (21). Defining $\underline{e}_k = \bar{\underline{a}}_k - \underline{a}_k$ as the error sequence and noting that $R_k Q_k = Q_k^H R_k^H$, (51) can also be expressed as

$$2\mathrm{Re}\{\underline{e}_k^H (P^{-1})_k \underline{x}_k\} > \underline{e}_k^H R_k Q_k \underline{e}_k + 2\mathrm{Re}\{\underline{e}_k^H R_k Q_k \underline{a}_k\} \tag{52}$$

From (10), it follows that

$$\underline{x}_k = P_{k \times N}(S\underline{a} + \underline{u}) \tag{53}$$

where $P_{k \times N}$ is the $k \times N$ matrix comprising the top k rows of the matrix P. Using (53), (52) can be written as

$$2\mathrm{Re}\{\underline{e}_k^H (P^{-1})_k P_{k \times N} \underline{u}\} > \underline{e}_k^H R_k Q_k \underline{e}_k + 2\mathrm{Re}\{\underline{e}_k^H R_k Q_k \underline{a}_k\} - 2\mathrm{Re}\{\underline{e}_k^H (P^{-1})_k P_{k \times N} S\underline{a}\} \tag{54}$$

which is the condition for the error event ε : $\underline{a}_k$ is eliminated in favor of $\underline{a}_k + \underline{e}_k$ (with $\underline{a}_k$ and $\underline{e}_k$ given i.e. non-random). The error event ε is associated with the error sequence $\underline{e}_k$. The length of the error event is $k - J$ symbols, not counting the last J components of $\underline{e}_k$ which must be zero as $\bar{b}_k = b_k$ according to (49).

6.1.1 MLSE

In the case of maximum likelihood sequence estimation, the memory order is $J = L_v$ (Viterbi algorithm). Thus, we have $e_{k-i} = 0$ for $i = 1, 2, \ldots, L_v$. Using the fact that

---

[7]The principal submatrix of dimension k of a square matrix A (with dimension $\geq k$) is obtained by erasing all but the first k rows and columns of A.

$R_k Q_k$ is a square banded matrix with $L \leq L_v$ elements in the right band[8], we get

$$\underline{e}_k^H R_k Q_k \underline{e}_k = \underline{e}_{k-L_v}^H S_{k-L_v} \underline{e}_{k-L_v} \tag{55}$$

$$\underline{e}_k^H R_k Q_k \underline{a}_k = \underline{e}_{k-L_v}^H S_{k-L_v \times k} \underline{a}_k \tag{56}$$

where $\underline{e}_{k-L_v} = [e_0, e_1, \ldots, e_{k-L_v-1}]^T$ and $S_{k-L_v \times k}$ is a $(k - L_v) \times k$ matrix comprising the top $k - L_v$ rows of S_k. Since $(P^{-1})_k$ is a banded matrix with $l_f \leq L_v$ elements in the right band), the top $k - L_v$ rows of $(P^{-1})_k P_{k \times N}$ are given by $[I_{k-L_v} | O_{k-L_v \times N+L_v-k}]$ and we have

$$\underline{e}_k^H (P^{-1})_k P_{k \times N} S \underline{a} = \underline{e}_{k-L_v}^H S_{k-L_v \times k} \underline{a}_k \tag{57}$$

Combining (55), (56) and (57) with (54), we see that the error event ε occurs in an MLSE receiver if

$$2\mathrm{Re}\{\underline{e}_{k-L_v}^H \underline{u}_{k-L_v}\} > \underline{e}_{k-L_v}^H S_{k-L_v} \underline{e}_{k-L_v}. \tag{58}$$

Given the error sequence $\underline{e}_k$, the left hand side of (58) is a Gaussian random variable with mean 0 and variance $4N_0 \underline{e}_{k-L_v}^H S_{k-L_v} \underline{e}_{k-L_v}$. Thus, the probability of the error event ε is given by

$$\mathrm{Pr}(\varepsilon) = \mathrm{Q}\left(\frac{1}{2} \sqrt{\frac{\underline{e}_{k-L_v}^H S_{k-L_v} \underline{e}_{k-L_v}}{N_0}} \right) \tag{59}$$

It follows from (49) and (59) that the first event error probability can be overbounded using a union bound, as

$$P_{FEE} \leq \sum_{\underline{e} \in E} p_{\underline{e}} \mathrm{Q}\left(\frac{\delta(\underline{e})}{2\sqrt{N_0}} \right) \tag{60}$$

where E is the set of all error sequences $\underline{e} = e_0, e_1, \ldots, e_{l-1}$ (such that $l > 0$, $e_{l-1} \neq 0$) with less than J consecutive zeros in the midst of the sequence, $p_{\underline{e}}$ is the *a priori* probability of the error sequence $\underline{e}$ and $\delta(\underline{e})$ is known as the distance of the error sequence $\underline{e}$ and is given by

$$\delta(\underline{e}) = \sqrt{\underline{e}^H S_l \underline{e}} = \sqrt{\sum_{i=0}^{l-1} \sum_{j=0}^{l-1} e_i^* s(i-j) e_j} \tag{61}$$

Notice that the first event error probability given by (60) is independent of the processing filter P and the form of the branch metric used. It is the same as obtained by Forney [11] and Ungerboeck [22] for MLSE receivers with specific processing filter and branch metric combinations. Our result validates the fact that the Viterbi algorithm does in fact yield maximum likelihood sequence estimates regardless of the

---

[8]The elements on the right hand side of (but not including) the diagonal.

form of the processing filter as long as the inverse processing filter P^{-1} exists and the trellis is expanded by $l_f - L$ symbols if the number of anticausal taps l_f of P^{-1} is greater than the channel memory L.

6.1.2 DFSE

For a memory order $J < L$, the first term on the right hand side of (54) depends on the error sequence $\underline{e}_k$ only while the other two terms depend, in addition, on the transmitted sequence $\underline{a}$. These terms do not cancel for a general transversal processing filter P and thus represent "raw or untreated" interference. The error performance of a DFSE receiver thus depends on the processing filter unlike the case of an MLSE receiver. Moreover, the error performance also depends on the branch metric formulation employed by the reduced trellis-search algorithm. This can be seen by noting that the two branch metric formulations: $R_k = Q_k^H = F_k^H$ and $R_k = I_k$, $Q_k = S_k$ result in different error distance and interference terms as $F_k^H F_k \neq S_k$. Note that the asymptotic equivalence of the matrices S and $F^H F$ (for N large) assumed in Section 3 does not apply here, as error events are generally short, i.e. $k \ll N$.

In view of the above discussion, it is desirable to have a processing filter + branch metric combination which eliminates the problem of untreated interference and maximizes the error distance. We devise the notion of "unbiasedness" to describe such DFSE receivers whose error performance is not affected by untreated interference (or bias).

Definition 6.1 *A DFSE receiver is termed "unbiased" if the error event ε is conditionally independent of the transmitted sequence $\underline{a}$ given the error sequence $\underline{e}_k$, for any memory order $0 \leq J < L_v$.*

It can be expected that an unbiased DFSE receiver would have good error performance for any memory order. On the other hand, a biased DFSE receiver would be affected by untreated interference components and could thus exhibit an error floor. In order to obtain an unbiased DFSE receiver, one must find a processing filter that causes the cancelation of the interference terms in (54) for any memory order. It follows that such a processing filter P must satisfy the condition:

$$(P^{-1})_k P_{k \times N} S = R_k Q_k [I_k | O_{k \times N - k}] \quad \forall\, 1 \leq k < N \tag{62}$$

or equivalently (noting that $R_k Q_k = Q_k^H R_k^H$ for the cases in hand):

$$(P^{-1})_k P_{k \times N} = Q_k^H (Q^{-H})_{k \times N} \quad \forall\, 1 \leq k < N \tag{63}$$

18

where the matrix $(Q^{-H})_{k \times N}$ comprises the top k rows of the matrix Q^{-H}.

It follows from (54) and (62) that the probability of the error event ε for an unbiased DFSE receiver is given by

$$\Pr(\varepsilon) = Q \left(\frac{\underline{e}_k^H R_k Q_k \underline{e}_k}{2\sqrt{N_0 \underline{e}_k^H R_k Q_k (S^{-1})_k R_k Q_k \underline{e}_k}} \right) \tag{64}$$

The first event error probability for an unbiased DFSE receiver can then be over-bounded as

$$P_{FEE} \leq \sum_{\underline{e} \in E'} p_{\underline{e}} Q \left(\frac{\delta(\underline{e})}{2\sqrt{N_0}} \right) \tag{65}$$

where E' is the set of all error sequences in the set E with J zeros appended and $\delta(\underline{e})$ is the distance of the error sequence $\underline{e}$ defined, in general, as

$$\delta(\underline{e}) \triangleq \frac{\underline{e}^H R_k Q_k \underline{e}}{\sqrt{\underline{e}^H R_k Q_k (S^{-1})_k R_k Q_k \underline{e}}} \tag{66}$$

where the subscript k denotes the length of the composite error sequence $\underline{e}$. Note that the above definition of the error distance includes the effect of noise enhancement (the term in the denominator of (66)).

A first event error analysis of the alternative DFSE receiver of Fig. 4 is similar to the analysis presented above and is given in Appendix A.

6.2   Tree Search Algorithms

Consider the generalized M-algorithm receiver of Fig. 5. Let $\{a_n\}$ be the sequence of symbols transmitted. Let $\underline{a}_k(i)$ ($i \in \{0, 1, \dots, M\mathcal{A} - 1\}$) be the $M\mathcal{A}$ paths extended at a time unit $k > \log_{\mathcal{A}} M$, including the correct path $\underline{a}_k(0) = \underline{a}_k$. A first event error occurs at time 0 in the M-algorithm receiver if the tree search algorithm eliminates the path $\underline{a}_k$. It follows from (48) that the error event occurs if the metric accumulated on the correct path is less than the metric accumulated on at least M of the other extended paths, i.e.

$$\mathcal{M}(\underline{a}_k) < \mathcal{M}(\underline{a}_k(i)) \tag{67}$$

for at least M values of $i \in \mathcal{I} = \{1, 2, \dots, M\mathcal{A} - 1\}\}$. Let $\{\sigma_n(i)\}_{n=0}^{k-1}$ be the sequence of states[9] in the path of $\underline{a}_k(i)$. Then, using (48), (67) can be written as

$$\sum_{n=0}^{k-1} \Gamma(a_n(i), \sigma_n(i)) > \sum_{n=0}^{k-1} \Gamma(a_n, \sigma_n(0)) \tag{68}$$

---

[9] The notion of state in a tree search algorithm is as defined in Section 5.

Defining $\underline{e}_k(i) = \underline{a}_k(i) - \underline{a}_k$ as an error sequence and following the development of (54), we get equivalently

$$2\text{Re}\{\underline{e}_k(i)^H(P^{-1})_k P_{k \times N}\underline{u}\} \;>\; \underline{e}_k(i)^H R_k Q_k \underline{e}_k(i) + 2\text{Re}\{\underline{e}_k(i)^H R_k Q_k \underline{a}_k\}$$
$$-2\text{Re}\{\underline{e}_k(i)^H(P^{-1})_k P_{k \times N} S\underline{a}\} \tag{69}$$

for at least M values of $i \in \mathcal{I}$. This is the condition for the error event ε' : $\underline{a}_k$ is eliminated in favor of M of the extended paths $\underline{a}_k + \underline{e}_k(i)$ (with $\underline{a}_k$ and $\underline{e}_k(i)$ given, $i \in \mathcal{I}$).

Notice that like the case of the DFSE receiver, the error performance of the generalized M-algorithm receiver depends on the processing filter and is, in general, affected by untreated interference components. Thus, the concept of "unbiasedness" also applies to M-algorithm receivers. Specifically, we define a class of unbiased M-algorithm receivers as follows

Definition 6.2 *An M-algorithm receiver is termed "unbiased" if the error event ε' is conditionally independent of the transmitted sequence $\underline{a}$ given the error sequences $\underline{e}_k(i)$ ($i \in \mathcal{I}$).*

Clearly the processing filter P of an unbiased M-algorithm receiver must satisfy (63) as in the case of unbiased DFSE receivers. The probability of the error event ε' for an unbiased M-algorithm receiver is, thus, given by

$$\text{Pr}(\varepsilon') = \text{Pr}\left(X(\underline{e}_k(i)) > \underline{e}_k(i)^H R_k Q_k \underline{e}_k(i), \quad \text{for } M \text{ values of } i \in \mathcal{I}\right) \tag{70}$$

where $X(\underline{e}_k(i))$ are jointly Gaussian random variables with mean zero and covariance $\text{E}[X(\underline{e}_k(i))X^*(\underline{e}_k(j))] = 4N_0\underline{e}_k(i)^H R_k Q_k (S^{-1})_k R_k Q_k \underline{e}_k(j)$.

7 Unbiased receivers

In Appendix B, we show that the processing filters that satisfy the unbiasedness conditions of (63) and (133) (corresponding to the case where the front-end filter is matched to the overall channel response and where it is matched to the transmit filter response respectively) are unique (within a scaling factor) and are given by

$$P = Q^{-H} \tag{71}$$

and

$$P = Q'^{-H} \tag{72}$$

20

respectively. In the first case, the processing filter P that results in an unbiased receiver when used with a reduced trellis or tree search algorithm with branch metric formulation $R = Q^H = F^H$, is the noise-whitening filter F^{-H}, while for the formulation $R = I$ and $Q = S$, it is the zero-forcing filter S^{-1}. In the second case, the processing filter in the case of branch metric formulation $R' = Q'^H = F'^H$, is the appropriate noise-whitening filter F'^{-H}, while for the formulation $R' = I$ and $Q' = \Phi$, it is the appropriate zero-forcing filter Φ^{-1}. Note that the processing filters in both cases correspond to the autocorrelation spectrum of the front-end filter in the receiver. The processed statistics given by

$$\underline{x} = R^H \underline{a} + Q^{-H} \underline{u} \tag{73}$$

in the first case, and

$$\underline{x}' = R'^H C \underline{a} + Q'^{-H} \underline{u}' \tag{74}$$

in the second case, depend on the past transmitted symbols only and not on any future transmitted symbols. Thus, the statistics fed to a reduced trellis or tree search algorithm must have causal dependence only, for unbiased operation. Note that it is also necessary to match a given processing filter with the proper branch metric of the reduced trellis or tree search algorithm in order to achieve unbiasedness.

We considered two additive decompositions of the likelihood metric in each case of the front-end filter, which led to two different unbiased receivers. The two branch metric formulations correspond to the two decompositions of the front-end filter autocorrelation matrix (S or Φ)- one actually being no decomposition and the other being the unique Cholesky decomposition. Note that there is no other decomposition of a positive definite and banded matrix of the form RQ (or equivalently $R^H Q^H$), where the matrix R is upper-triangular and both matrices R and Q are banded. The matrix R is constrained to be upper-triangular to get a causal form for the additive metric. Both R and Q are constrained to be banded in order for the branch metric to have finite complexity. Thus, our treatment of unbiased receivers is complete in this sense.

In the case of an infinite length transmitted sequence, the processing filters described above have infinite impulse responses. In practice, these filters can be implemented by truncating the impulse response at a sufficient length. However, this leads to some bias (untreated interference) in the receiver. Thus, there is no truly unbiased DFSE or M-algorithm receiver for an infinite length transmitted sequence. An exception to this is the case of Nyquist pulse-shaping at the transmitter and

21

transmit-filter matched-filtering at the receiver. No processing filter is required in this case for unbiased operation.

7.1 Receivers with a whitening filter

One type of unbiased DFSE and M-algorithm receivers have a noise-whitening filter. Henceforth, they will be referred to as whitening filter DFSE (WF-DFSE) and whitening filter M-algorithm (WF-MA) receivers. In case the front-end filter is matched to the overall channel response with autocorrelation spectrum S (standard matched filtering), the noise-whitening filter is given by F^{-H}. The branch metric for the WF-DFSE(S) and WF-MA(S) receivers[10] is obtained by replacing $P^{-1} = R = Q^H = F^H$ in (41) and (24) respectively. An upper bound on the first event error probability of the WF-DFSE(S) receiver is given by (65), with the error distance obtained by substituting $R_k = Q_k^H = F_k^H$ in (66) and noting that

$$(S^{-1})_k = (F^{-1}F^{-H})_k = (F^{-1})_k(F^{-H})_k = (F_k)^{-1}(F_k)^{-H} \tag{75}$$

where the second and third equalities follow from the identity:

If X and Y are $N \times N$ matrices and Y is upper-triangular (or X is lower-triangular), then

$$(XY)_k = X_k Y_k \tag{76}$$

where $(XY)_k$ is the principal submatrix of dimension $k < N$ of the matrix XY.

The error distance is then given by

$$\delta(\underline{e}) = \|F_k \underline{e}\| \tag{77}$$

In case the front-end filter is matched to the transmit filter response with autocorrelation spectrum Φ (transmit matched filtering), the noise-whitening filter is given by F'^{-H}. The branch metric is obtained by replacing $P^{-1} = R' = Q'^H = F'^H$ in (47) and (38) respectively for the WF-DFSE(T)[11] and WF-MA(T) receivers. The error distance for the WF-DFSE(T) receiver follows from (135) as

$$\delta(\underline{e}) = \|F_k' C_k \underline{e}\|. \tag{78}$$

Note that the two expressions for the error probability of the WF-DFSE receivers differ from each other due to the different phase characteristic of the whitened channel

---

[10]Where 'S' stands for standard matched filtering.

[11]Where 'T' stands for transmit matched filtering.

in each case. In the first case, the whitened channel $\{f(n)\}$ has minimum-phase while in the second case, the whitened channel $\{f'(n) * c(n)\}$ has mixed phase, in general. We will see later that the error distance and hence the error probability is superior in the case of the minimum-phase channel. Note that the first event error probability expressions derived here are equivalent to the expression obtained in [6].

7.2 Receivers with a zero-forcing filter

The other type of unbiased DFSE and M-algorithm receivers consist of a zero-forcing filter. Henceforth, they will be referred to as zero-forcing filter DFSE (ZF-DFSE) and zero-forcing filter M-algorithm (ZF-MA) receivers. In the case of standard matched filtering, the zero-forcing filter is given by S^{-1}. The branch metric for the ZF-DFSE(S) and ZF-MA(S) receivers is obtained by replacing $P^{-1} = Q = S$, $R = I$ in (41) and (24) respectively. Substituting these values in (66) gives the error distance for the ZF-DFSE(S) receiver as

$$\delta(\underline{e}) = \frac{\underline{e}^H S_k \underline{e}}{\sqrt{\underline{e}^H S_k (S^{-1})_k S_k \underline{e}}}. \tag{79}$$

In the case of transmit matched filtering, the zero-forcing filter is given by Φ^{-1}. The branch metric is obtained by replacing $P^{-1} = Q' = \Phi$, $R' = I$ in (47) and (38) respectively for the ZF-DFSE(T) and ZF-MA(T) receivers. The error distance for the ZF-DFSE(T) receiver follows from (135) as

$$\delta(\underline{e}) = \frac{\underline{e}^H C_k^H \Phi_k C_k \underline{e}}{\sqrt{\underline{e}^H C_k^H \Phi_k (\Phi^{-1})_k \Phi_k C_k \underline{e}}}. \tag{80}$$

Note that the zero-forcing filter Φ^{-1} in the latter case does not null out inter-symbol interference entirely. It decorrelates only the part due to the autocorrelation of the front-end filter response while the part which is due to the dispersion caused by the medium response $\{c(n)\}$ is left untouched.

8 Biased receivers

Several biased receivers are possible. One example is a DFSE receiver considered in [20]. It comprises a front-end filter matched to the overall channel response followed by the noise-whitening filter $P = F^{-H}$. The reduced trellis search algorithm uses the branch metric formulation $R = I$, $Q = S$. To see that the receiver is biased, note that $F_k^H F_k \neq S_k$ ($k \ll N$). It follows from (54) that the error event ε depends on the transmitted sequence $\underline{a}$ through $(S_k - F_k^H F_k)\underline{a}_k$.

23

Note that a transversal processing filter adds complexity to a receiver. The computation of a noise-whitening or zero-forcing filter requires channel inversion and factorization operations. Moreover, the filter has to track the variation in the channel if the channel is time-varying. One solution to this problem is to omit the processing filter and pass the output of the matched filter directly to the trellis or tree search algorithm, resulting in a class of receivers which we refer to as matched filter receivers. Matched filter receivers, however, are biased. In other words, their error performance is limited by untreated interference components. Some useful matched filter receivers are described in the following sections.

8.1 Matched filter receivers

An important type of matched filter DFSE (MF-DFSE) and matched filter M-algorithm (MF-MA) receivers have a front-end filter matched to the overall channel response followed by a reduced trellis or tree search algorithm with branch metric obtained by replacing $P^{-1} = R = I$, $Q = S$ in (41) and (24) respectively. The MF-DFSE receiver of this type was proposed in [5, 28]. The MF-MA receiver of this type was considered in [26, 29]. An upper bound on the first event error probability of the MF-DFSE(S) receiver was derived in [15, 14]. It follows from (54) as

$$P_{FEE} \leq \sum_{\underline{e} \in E'} p_{\underline{e}} \mathrm{E}_{\underline{a}} \left[\mathrm{Q} \left(\frac{\delta(\underline{e}) - \gamma(\underline{e}, \underline{a})}{2\sqrt{N_0}} \right) \right] \tag{81}$$

where $\delta(\underline{e})$ is the error distance given by

$$\delta(\underline{e}) = \sqrt{\underline{e}^H S_k \underline{e}} \tag{82}$$

and $\gamma(\underline{e}, \underline{a})$ is the untreated interference given by

$$\gamma(\underline{e}, \underline{a}) = 2\mathrm{Re}\{\underline{\xi}^H \dot{S}_{L-J}^H \dot{\underline{a}}_k\}/\delta(\underline{e}) \tag{83}$$

where $\dot{\underline{a}}_k = [a_k, \ldots, a_{k+L-J-1}]^T$, $\underline{\xi}$ is the tail of the error sequence $\underline{e}$ given by[12]

$$\underline{\xi} = [e_{k-L}, \ldots, e_{k-J-1}]^T \tag{84}$$

and $\dot{S}$ is an $L \times L$ matrix given by

$$\dot{S} = \begin{bmatrix} s(L) & \cdots & s(2) & s(1) \\ 0 & \ddots & & \vdots \\ \vdots & \ddots & s(L) & s(L-1) \\ 0 & \cdots & 0 & s(L) \end{bmatrix}. \tag{85}$$

---

[12]In (84), k ($> J$) denotes the length of the sequence $\underline{e}$ and $e_i = 0$ for $i < 0$.

24

McLane investigated truncated-state Viterbi detectors (TSVD) with standard matched filters in [18]. The difference between the TSVD algorithm of [18] and the MF-DFSE algorithm is that the MF-DFSE algorithm uses conditional tentative decisions to cancel the tail of the channel response while the TSVD algorithm simply ignores it. The error bounds obtained by McLane indicate the presence of untreated interference. However, the untreated interference in his bounds arises due to ignoring the tail of the channel response in the TSVD algorithm. Such interference term does not appear in the bounds for DFSE as it is canceled by means of tentative conditional decisions in the DFSE algorithm. The untreated interference component that appears in the DFSE bound of (81) is, however, absent in McLane's bounds. The cause of this latter untreated interference component can be intuitively explained as follows. The matched filter statistics at the input of a reduced trellis search algorithm depend on L past and L future transmitted symbols (cf. (7)). The reduced trellis search algorithm (with memory order J) selects survivor paths extending up to time n on the basis of the metric accumulated up to time $n + J$. This premature elimination of candidate paths does not account for the interference arising from the $L - J$ future transmitted symbols. Clearly, this type of untreated interference affects both the DFSE and TSVD algorithms. Hence, the bounds in [18] should be corrected to include this interference component.

A second type of matched filter receivers is obtained in the case the front-end filter is matched to the transmit filer response. The reduced trellis and tree search algorithms of MF-DFSE(T) and MF-MA(T) receivers employ the branch metric given by (47) and (38) respectively with $P^{-1} = R' = I$, $Q' = \Phi$. Substituting these values in (131), we see that an upper bound on the first event error probability of the MF-DFSE(T) receiver is given by (81), where the error distance $\delta(\underline{e})$ is given by

$$\delta(\underline{e}) = \underline{e}^H C_k^H \Phi_k C_k \underline{e} \tag{86}$$

and the untreated interference $\gamma(\underline{e}, \underline{a})$ is given by

$$\gamma(\underline{e}, \underline{a}) = 2\mathrm{Re}\{\underline{\xi}^H (\ddot{C}_{L_d \times L - J})^H \ddot{\Phi} \ddot{C} \ddot{\underline{a}}_k\}/\delta(\underline{e}) \tag{87}$$

where $\ddot{\underline{a}}_k = [a_{k-L_c}, \ldots, a_k, \ldots, a_{k+L_d-1}]^T$ and $\ddot{C}$ and $\ddot{\Phi}$ are $L_d \times L$ and $L_d \times L_d$ matrices respectively, given by

$$\ddot{C} = \begin{bmatrix} c(L_c) & \cdots & c(1) & c(0) & 0 & \cdots & 0 \\ 0 & \ddots & & & \ddots & \ddots & \vdots \\ \vdots & \ddots & \ddots & & & \ddots & 0 \\ 0 & \cdots & 0 & c(L_c) & \cdots & c(1) & c(0) \end{bmatrix}, \tag{88}$$

25

$$\ddot{\Phi} = \begin{bmatrix} \phi(-L_d) & \cdots & \phi(-2) & \phi(-1) \\ 0 & \ddots & & \vdots \\ \vdots & \ddots & \phi(-L_d) & \phi(-L_d+1) \\ 0 & \cdots & 0 & \phi(-L_d) \end{bmatrix}. \tag{89}$$

The matrix $\ddot{C}_{L_d \times L-J}$ comprises the first $L - J$ columns of the matrix $\ddot{C}$.

Note from (81) that the untreated interference increases or decreases the error distance of the MF-DFSE receivers with equal probability in the case of i.i.d. transmitted symbols. Due to convexity of the $Q(\cdot)$ function, the error performance is, however, dominated by the destructive effect of the untreated interference and is, thus, rather poor. Without giving an expression for the error probability of the MF-MA receivers, it can be noted that the MF-MA receivers also suffer from untreated interference.

8.2 Bias-compensated matched-filter receivers

An intuitive solution to the problem of untreated interference (bias) in matched filter receivers is to cancel the bias by means of tentative decisions. With reliable tentative decisions, the error performance can be expected to improve significantly. A bias-compensated MF-DFSE(S) (BC-MF-DFSE(S)) receiver was proposed in [15][13] where the front-end filter is matched to the overall channel response and conventional matched filter decisions are used to cancel bias. The algorithm computes path metrics as in MF-DFSE(S) using (40). However, conditional decisions are made (and the corresponding survivor paths are selected) using the modified rule:

$$\hat{\alpha}_{n-J}(\beta_n) = \arg \max_{\alpha_{n-J}} \left[\mathcal{M}(\beta_n) + \Gamma(\alpha_n, \beta_n) - \mathrm{bias}(\beta_n) \right], \tag{90}$$

where $\mathcal{M}(\beta_n)$ and $\Gamma(\alpha_n, \beta_n)$ are the accumulated metric and the branch metric of MF-DFSE(S) respectively and the bias term is given by

$$\mathrm{bias}(\beta_n) = \underline{\mu}_n^H \dot{S}_{L-J}^H \underline{\tilde{a}}_n \tag{91}$$

where $\underline{\mu}_n = [\eta_{n-L+1}, \ldots, \eta_{n-J-1}, \eta_{n-J}]^T$ are the $L - J$ most recent symbols in the survivor path associated with state β_n, $\underline{\tilde{a}}_n = [\tilde{a}_{n+1}, \ldots, \tilde{a}_{n+L-J}]^T$ are tentative decisions on future symbols obtained by using conventional symbol-by-symbol detection as $\tilde{a}_n = \mathrm{sign}(z_n)$ and $\dot{S}_{L-J}$ is the principal submatrix of dimension $L - J$ of the matrix $\dot{S}$. The bias term follows from the expression for the untreated interference given

---

[13]The algorithm is referred to as modified unwhitened DFSE (MUDFSE) in [15].

by (83). A reduced computation form of the algorithm (BC-MF-DFSE$\sim$) uses the approximate bias:

$$\text{bias}(\beta_n) \approx \alpha_{n-J}^* [s(-J-1), \ldots, s(-L)] \tilde{\underline{a}}_n \tag{92}$$

A simplified error performance analysis of the BC-MF-DFSE(S) algorithm can be found in [15].

Note that a bias-compensated MF-MA can also be derived on the same principle as described above for BC-MF-DFSE i.e. using tentative decisions to cancel untreated interference components. The untreated interference in the case of MF-MA (with the standard matched filter) follows from (69) as $2\text{Re}\{\underline{\xi}(i)^H \dot{S}^H \underline{\ddot{a}}_k\}/\delta(\underline{e}(i))$, where $\underline{\xi}(i) = [e_{k-L}(i), \ldots, e_{k-1}(i)]^T$ is the tail of the error sequence $\underline{e}(i)$ corresponding to the ith contender path and $\underline{\ddot{a}}_k = [a_k, \ldots, a_{k+L-1}]^T$. The interference can be canceled by choosing survivor paths in the M-algorithm on the basis of the accumulated metric minus a bias term, computed using tentative decisions. Note that the bias term in this case depends on the last L symbols in the survivor path rather than the last $L - J$, as in the case of BC-MF-DFSE. This is because unlike DFSE, the M-algorithm is a tree search algorithm where contender paths are not constrained to merge. Since contender paths in DFSE always agree on the J most recent symbols, the bias term does not depend on them. However, this is not the case with the M-algorithm. Consequently, bias compensation requires more computation in the case of MF-MA.

A bias-compensated MF-DFSE receiver can also be obtained for the case of transmit matched filtering (BC-MF-DFSE(T)). In this case, the algorithm computes path metrics as in MF-DFSE(T) using (44). Conditional decisions are made using the modified rule:

$$\hat{\alpha}'_{n-J}(\beta_n) = \arg\max_{\alpha_{n-J}}[\mathcal{M}'(\beta_n) + \Gamma'(\alpha_n, \beta_n) - \text{bias}'(\beta_n)]. \tag{93}$$

where $\mathcal{M}'(\beta_n)$ and $\Gamma'(\alpha_n, \beta_n)$ are the accumulated metric and the branch metric of MF-DFSE(T) respectively and the bias term is given by

$$\text{bias}'(\beta_n) = \underline{\mu}_n'^H (\ddot{C}_{L_d \times L-J})^H \ddot{\Phi} \ddot{C} \tilde{\underline{a}}_n' \tag{94}$$

where $\underline{\mu}_n' = [\eta'_{n-L+1}, \ldots, \eta'_{n-J-1}, \eta'_{n-J}]^T$ are the $L - J$ most recent symbols in the survivor path associated with state β_n and $\tilde{\underline{a}}_n' = [\eta'_{n-L_c+1}, \ldots, \eta'_n, \tilde{a}'_{n+1}, \ldots, \tilde{a}'_{n+L_d}]^T$, where $\{\tilde{a}'_n\}$ are tentative decisions obtained as $\tilde{a}'_n = \text{sign}(z'_n)$. The bias term follows from (87).

9 Truncated memory MLSE receivers

Linear pre-filtering was proposed in [10, 19] as a means to truncate the memory of the Viterbi algorithm in an MLSE receiver. In [10], the overall response of the channel/pre-filter combination is forced to a truncated and causal desired impulse response (DIR) of acceptably short span (say J symbols). Pre-filtering colors the noise in the output statistic. However, the Viterbi algorithm is used on the pre-filtered statistic as if the noise were white. An important difference between this approach and our generalized DFSE approach is that the receive filter in the case of DFSE is not specifically designed for a memory order. This allows one to vary the memory order of the trellis search algorithm without changing the receive filter. In the following, we look at the error performance of the pre-filtering method.

Let $\underline{x}$ be the statistic obtained after matched filtering/noise-whitening, i.e.

$$\underline{x} = F\underline{a} + \underline{w} \tag{95}$$

where $\underline{w}$ is a white Gaussian noise sequence with covariance $E[\underline{w}\underline{w}^H] = N_0 I$. Let G be an $N \times N$ lower-triangular banded Toeplitz matrix (with band width $J < L$) representing the DIR and H be the corresponding pre-filter matrix, given by $HF = G$. The pre-filtered statistic is given by

$$\underline{x}^p = G\underline{a} + \underline{w}^p \tag{96}$$

where $\underline{w}^p = H\underline{w}$ is the filtered noise.

Consider a path $\{\bar{a}_n\}$ in a truncated memory MLSE (TM-MLSE) receiver that diverges from the correct path $\{a_n\}$ at time 0 and remerges with it at a later time k. A first event error occurs at time 0 if $\{\bar{a}_n\}$ is picked as a survivor path. The error event occurs if the metric accumulated on the incorrect path is greater than the metric on the correct path, i.e.

$$-\|\underline{x}_k^p - G_k\bar{\underline{a}}_k\|^2 > -\|\underline{x}_k^p - G_k\underline{a}_k\|^2. \tag{97}$$

Using (96), we get

$$2\text{Re}\{\underline{e}_k^H G_k^H \underline{w}_k^p\} > \|G_k\underline{e}_k\|^2. \tag{98}$$

where $\underline{e}_k = \bar{\underline{a}}_k - \underline{a}_k$ is the error sequence. Note that H is a lower-triangular matrix. Therefore, $E[\underline{w}_k^p\underline{w}_k^{pH}] = N_0 H_k H_k^H$ and the probability of the error event ε: the sequence $\underline{a}_k$ is eliminated in favor of the sequence $\underline{a}_k + \underline{e}_k$, is given by

$$\Pr(\varepsilon) = Q\left(\frac{\delta(\underline{e})}{2\sqrt{N_0}}\right). \tag{99}$$

28

where $\delta(\underline{e})$ is the error distance given by

$$\delta(\underline{e}) = \frac{\|G_k\underline{e}\|^2}{\sqrt{\underline{e}^H G_k^H H_k H_k^H G_k\underline{e}}}.$$ (100)

10 Symbol error probability

Consider a path in the reduced trellis of a DFSE receiver that diverges from the correct path at time n_1 and remerges with it at a later time n_2. Due to feedback incorporated in the reduced trellis search algorithm, the event that the correct path is eliminated in favor of the incorrect path (an error event) depends on previous error events. The effect of the error propagation is, however, small in DFSE receivers as compared to simple decision feedback equalizers (DFE). This is because the decisions fed back in DFSE are conditioned on the state of the reduced trellis unlike the decisions in DFE. Moreover, the effect of error propagation is small at medium to high signal-to-noise ratio (SNR). This was shown to be the case for WF-DFSE receivers in [6, 7]. Assuming no error propagation (i.e. a separation of more than $L - J$ correct decisions between error events), the probability that an error event occurs in a DFSE receiver can be upperbounded by the first event error probability [17]. The symbol error probability for unbiased DFSE receivers can then be upperbounded as [11, 6]

$$P_s \leq \sum_{\underline{e} \in E'} \mathrm{w}(\underline{e}) p_{\underline{e}} Q\left(\frac{\delta(\underline{e})}{2\sqrt{N_0}}\right)$$ (101)

where $\mathrm{w}(\underline{e})$ is the number of symbol errors entailed by the error sequence $\underline{e}$, $\delta(\underline{e})$ is the distance of the error sequence and $p_{\underline{e}}$ is the probability that a transmitted sequence can have $\underline{e}$ as an error sequence. For i.i.d. transmitted sequences and input alphabet $\mathcal{A} = \{\pm 1, \pm 3, \ldots, \pm(|\mathcal{A}| - 1)\}$ (for $|\mathcal{A}|$ even), we have

$$p_{\underline{e}} = \prod_{n=0}^{k-1-J} \frac{|\mathcal{A}| - \frac{1}{2}|e_n|}{|\mathcal{A}|}$$ (102)

which reduces to

$$p_{\underline{e}} = 2^{-\mathrm{w}(\underline{e})}$$ (103)

in the case of BPSK modulation. The error distance $\delta(\underline{e})$ is given by (77) and (78) for WF-DFSE receivers with the standard and transmit matched filters respectively. The error distance for ZF-DFSE receivers given by (79) and (80), depends on the location and length of the error event. This is because the correlation in the noise samples given by S^{-1} varies over the length of the data sequence. However, note that

29

the noise correlation is constant in the middle of a long sequence (i.e. S^{-1} is nearly Toeplitz except at the edges for $N \gg L$). In Appendix C, we obtain expressions for the error distance that assume the noise correlation to be constant. The error distance in the case of standard and transmit matched filtering is given by (150) and (151) respectively. The symbol error probability bound of (101) also holds for the truncated memory MLSE receiver of Section 9 with the error distance given by (100). In this case, it is a strict upper bound as there is no decision feedback and thus no error propagation.

For moderate SNRs, the upper bound given by (101) is dominated by the term

$$Q\left(\frac{\delta_{min}}{2\sqrt{N_0}}\right) \sum_{\underline{e} \in E'_{min}} \text{w}(\underline{e}) p_{\underline{e}} \qquad (104)$$

where E'_{min} is the set of error sequences in E' that achieve the minimum distance (known as minimum distance sequences)

$$\delta_{min} = \min_{\underline{e} \in E'} \delta(\underline{e}). \qquad (105)$$

The symbol error probability for MF-DFSE receivers can similarly be upper-bounded as

$$P_s \leq \sum_{\underline{e} \in E'} \text{w}(\underline{e}) p_{\underline{e}} \text{E}_{\underline{a}} \left[Q\left(\frac{\delta(\underline{e}) - \gamma(\underline{e}, \underline{a})}{2\sqrt{N_0}}\right) \right] \qquad (106)$$

where the error distance $\delta(\underline{e})$ and the untreated interference $\gamma(\underline{e}, \underline{a})$ are given by (82) and (83) for the case of standard matched filtering and (86) and (87) for the case of transmit matched filtering respectively. Due to the presence of untreated interference, the upper bound in (106) is not dominated by the minimum distance error sequences only, unlike the bound for unbiased DFSE receivers. Higher distance error sequences should also be considered with worst case interference.

11   Error distance

The various DFSE receivers derived in the previous sections can be compared on the basis of their error distance. Error distances characterize an upper bound on the symbol error probability. In the case of an unbiased DFSE receiver, the minimum error distance squared per noise spectral density can be considered as its effective SNR [6]. For a given channel and memory order, the distance of a given error sequence depends on the type of the DFSE receiver. Specifically, it depends on the receive

filter and the branch metric. In this section, we compare the error distance for various receivers.

Let $\underline{e} = [e_0, e_1, \ldots, e_{k-1-J}, 0, \ldots, 0]^T$ be an error sequence of length k belonging to the set E'_J (the set E' of allowable error sequences for a DFSE receiver with memory order $J < L$). Let $\underline{e}_+ = [\underline{e}^T, 0, \ldots, 0]^T$ (length $l = k + L - J$). Then, $\underline{e}_+ \in E'_L$, the set of allowable error sequences for an MLSE receiver. The distance of this sequence in the case of an MLSE receiver is given by

$$\delta(\underline{e}_+) = \underline{e}_+^H S_l \underline{e}_+ = \underline{e}^H S_k \underline{e} \tag{107}$$

which is equal to the distance of the corresponding error sequence in the case of a MF-DFSE receiver with the standard matched filter. Let E''_J be the set of all error sequences in E'_J appended by $L - J$ zeros ($L > J$). Note that $E''_J \subset E'_L$, i.e. the upper bounds given by (101) and (106) for DFSE receivers are determined using only a subset of the error sequences considered for an MLSE receiver[14]. Thus, if the untreated interference in the case of MF-DFSE(S) could be removed ideally with the aid of a genie, the upper bound for the receiver would be lower than MLSE. In fact, the error rate performance of the genie-aided receiver is generally better than MLSE in moderate SNRs where error propagation is negligible. For the other DFSE receivers, we will show that the error distance is smaller, in general, compared to the MF-DFSE(S) receiver (or an MLSE receiver).

11.1 WF-DFSE

Note that

$$\underline{e}_+^H S_l \underline{e}_+ = \underline{e}_N^H S \underline{e}_N = \|F \underline{e}_N\|^2 = \|F_l \underline{e}_+\|^2 = \|F_k \underline{e}\|^2 + \|\dot{\Psi} \underline{\xi}\|^2 \tag{108}$$

where $\underline{e}_N = [\underline{e}_+^T 0, \ldots, 0]^T$ (length N) and $\dot{\Psi}$ is an $L - J \times L - J$ matrix given by

$$\dot{\Psi} = \begin{bmatrix} f(L) & \cdots & \cdots & f(J+1) \\ 0 & \ddots & & \vdots \\ \vdots & \ddots & f(L) & f(L-1) \\ 0 & \cdots & 0 & f(L) \end{bmatrix}. \tag{109}$$

The matrix $\dot{\Psi}$ is illustrated in Fig. 6. The distance of a given error sequence is thus

---

[14]The error sequences excluded have more than $J - 1$ consecutive zeros in the midst and hence cause a reduced trellis encoder with memory J to flush.
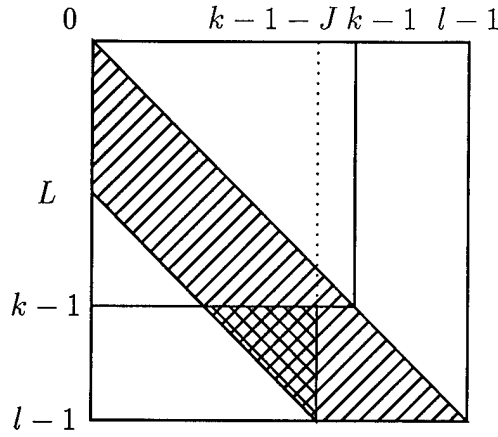
Figure 6: Illustration of $\dot{\Psi}$ within F_l.

smaller for WF-DFSE(S) as compared to MF-DFSE(S).

Let

$$v(i, j) = \begin{cases} v(i - j) & 0 \leq i - j \leq L \\ 0 & \text{otherwise} \end{cases} \tag{110}$$

be the coefficients of the lower-triangular Toepltiz matrix $V = F'C$. Then, similar to (108), we can write

$$\underline{e}_+^H S_l \underline{e}_+ = \|F_l' C_l \underline{e}_+\|^2 = \|F_k' C_k \underline{e}\|^2 + \|\ddot{\Psi} \underline{\xi}\|^2 \tag{111}$$

where $\ddot{\Psi}$ is an $L - J \times L - J$ matrix given by

$$\ddot{\Psi} = \begin{bmatrix} v(L) & \cdots & \cdots & v(J+1) \\ 0 & \ddots & & \vdots \\ \vdots & \ddots & v(L) & v(L-1) \\ 0 & \cdots & 0 & v(L) \end{bmatrix}. \tag{112}$$

Note that the matrix F of the whitened channel coefficients $\{f(n)\}$ (in the case of standard matched filtering), is invertible since $F(z)$, the z-transform of $\{f(n)\}$, is minimum-phase (has all roots inside the unit circle). Similarly, $F'(z)$, the z-transform of $\{f'(n)\}$, is minimum-phase. However, the z-transform $C(z)$ of the medium response coefficients $\{c(n)\}$ may be non-minimum phase. Therefore, $V(z) = F'(z)C(z)$, the z-transform of the coefficients of the whitened channel $\{v(n)\}$ (in the case of transmit matched filtering), is mixed-phase in general. The whitened channels in the two cases have the same magnitude response, as

$$F^*(z^{-1})F(z) = V^*(z^{-1})V(z) = S(z) \tag{113}$$

32

where $S(z)$ is the z-transform of the sampled channel autocorrelation function $\{s(n)\}$. Note that channels with identical magnitude response but different phase responses have different energy distribution among tap coefficients. The minimum-phase channel has most of its energy contained in the leading tap coefficients, while the maximum-phase channel (with all roots outside the unit circle) has most of its energy contained in the lagging tap coefficients. Note from (108) and (111) that the loss in squared distance for WF-DFSE compared to MLSE is given by $\|\dot{\Psi}\underline{\xi}\|^2$ and $\|\ddot{\Psi}\underline{\xi}\|^2$ in the case of standard and transmit matched filtering respectively. The coefficients of the matrix $\dot{\Psi}$ (belonging to the minimum-phase channel F) have smaller energy, in general, than the coefficients of the matrix $\ddot{\Psi}$. Thus, the loss in distance is smaller in the first case.

11.2 ZF-DFSE

In appendix C, we show that the error distance in the case of ZF-DFSE(S) is given by

$$\frac{\underline{e}^H S_k \underline{e}}{\sqrt{\underline{e}^H S_k (S^{-1})_k S_k \underline{e}}} = \frac{\underline{e}^H S_k \underline{e}}{\sqrt{\underline{e}^H S_k \underline{e} + \underline{\xi}^H \dot{S}_{L-J}^H (S_{22}^I)_L \dot{S}_{L-J} \underline{\xi}}} \tag{114}$$

where $(S_{22}^I)_L$ is a submatrix of the matrix S^{-1} and is thus positive definite. Note that the second term in the denominator of the RHS of (114) is greater than zero as the matrix $\dot{S}$ is full rank (since $s(-L) \neq 0$). Thus, the error distance for ZF-DFSE(S) is less than MF-DFSE(S). Similarly, it can be shown that the error distance in the case of ZF-DFSE(T) is smaller than MF-DFSE(T).

11.3 Optimum unbiased DFSE receivers

In this section, we show that WF-DFSE receivers are optimum in the sense that they minimize the first event error probability of unbiased DFSE receivers. Equivalently, we show that WF-DFSE receivers maximize the distance of a given error sequence in the class of DFSE receivers that satisfy the unbiasedness condition, i.e.

$$\frac{\underline{e}^H R_k Q_k \underline{e}}{\sqrt{\underline{e}^H R_k Q_k (S^{-1})_k R_k Q_k \underline{e}}} \leq \|F_k \underline{e}\| \tag{115}$$

with equality only if $Q_k = F_k$, where $(R, Q) = (I, S)$ or (F^H, F) and

$$\frac{\underline{e}^H C_k^H R_k' Q_k' C_k \underline{e}}{\sqrt{\underline{e}^H C_k^H R_k' Q_k' (\Phi^{-1})_k R_k' Q_k' C_k \underline{e}}} \leq \|F_k' C_k \underline{e}\| \tag{116}$$

with equality only if $Q_k' = F_k'$, where $(R', Q') = (I, \Phi)$ or (F'^H, F').

33

To prove Proposition (115), we note that

$$
\begin{aligned}
\underline{e}^H R_k Q_k \underline{e} &= \underline{e}^H (F_k)^H (F_k)^{-H} R_k Q_k \underline{e} \\
&\leq \|F_k \underline{e}\| \|(F_k)^{-H} R_k Q_k \underline{e}\| \\
&= \|F_k \underline{e}\| \sqrt{\underline{e}^H Q_k^H R_k^H (S^{-1})_k R_k Q_k \underline{e}}
\end{aligned}
\tag{117}
$$

where the inequality in (117) is the Schwartz inequality which becomes an equality only if $R_k = Q_k^H = F_k^H$. The last equality in (117) follows from (75). Proposition (116) can be shown similarly.

Comparing the error distance of the WF-DFSE receiver with the truncated memory MLSE receiver of Section 9 (with the same memory order), we note that

$$
\begin{aligned}
\underline{e}^H G_k^H G_k \underline{e} &= \underline{e}^H G_k^H H_k F_k \underline{e} \\
&\leq \|H_k^H G_k \underline{e}\| \|F_k \underline{e}\|
\end{aligned}
\tag{118}
$$

where $G_k = (HF)_k = H_k F_k$ follows from (76) as H is a lower-triangular matrix and we again use the Schwartz inequality. Thus, we get

$$
\frac{\|G_k \underline{e}\|^2}{\sqrt{\underline{e}^H G_k^H H_k H_k^H G_k \underline{e}}} \leq \|F_k \underline{e}\|.
\tag{119}
$$

In conclusion, we see that the distance of a given error sequence for a DFSE receiver depends on the type of filtering and the branch metric. The distance for the MF-DFSE(S) receiver is the same as in the case of an MLSE receiver. For the unbiased DFSE receivers – WF-DFSE and ZF-DFSE, the distance is smaller. This is due to the fact that the standard matched filter collects all the energy of the pulse transmitted at a given time in the corresponding output sample (in other words, it maximizes the output SNR, given by $|s(0)|^2/N_0$). The noise-whitening filter spreads out the signal energy into $L + 1$ output samples in the process of whitening noise ($\sum_{i=0}^{L} |f(i)|^2 = |s(0)|^2$). The linear zero-forcing filter decorrelates all interfering signal components but enhances (and correlates) noise in the process. The reduced trellis-search algorithms that follow these filters recover part of the signal energy (or SNR) that is spread out but are unable to recover all of it. Thus, WF-DFSE and ZF-DFSE suffer from a loss of the effective SNR, while MF-DFSE(S) does not. Of course, the drawback with MF-DFSE is that the reduced trellis search algorithm is unable to resolve some anticausal interfering signal components. This problem is alleviated in BC-MF-DFSE where the untreated components are canceled using tentative decisions. If reliable tentative decisions can be obtained, the BC-MF-DFSE receiver presents an advantage over the unbiased DFSE receivers in terms of SNR.

34

The noise-whitening filter removes only the anti-causal signal components which is necessary for unbiasedness. The causal signal components forming the tail of the channel response are equalized using decision feedback which does not enhance noise. The zero-forcing filter on the other hand performs complete signal decorrelation. This leads to noise enhancement and a further loss of the error distance. Similarly, the use of pre-filtering to remove some of the causal signal components in a truncated memory MLSE receiver enhances noise. Thus, WF-DFSE has greater error distance than ZF-DFSE and truncated memory MLSE receivers with pre-filtering. Practically, error propagation slightly degrades DFSE performance at moderate SNRs. Error propagation, however, does not occur in a truncated memory MLSE receiver with pre-filtering as there is no decision feedback.

12 Bound evaluation

In this section, we describe a generating function method to evaluate the symbol error probability bounds given in Section 10. In [15], a generating function method was proposed to evaluate the error probability bound for the MF-DFSE(S) receiver and an approximate bound for the BC-MF-DFSE(S) receiver. Here, we describe a generating function method for unbiased DFSE receivers.

Note that a generating function method has never been considered for WF-DFSE receivers. In [8] and [6], the minimum distance was used to approximate the symbol error probability. However, the approximation may not be very good depending on the system, even at high SNRs [21]. In [21], a stack algorithm was proposed to obtain a chosen number of the largest terms in the Union upper bound of (101). It was stated in [21] that a generating function method can not be applied to the case of DFSE because unlike MLSE, branch distances in DFSE can not be uniquely determined from pairs of error states due to decision feedback incorporated in the branch metric calculation. We note that the problem with the approach in [21] is that the branch distance depends on $L + 1$ error symbols (where L is the channel memory) while the states in the error state diagram of [21] represent $J + 1$ error symbols (where $J < L$ is the memory order of DFSE). In the following, we show how an error state diagram used to obtain error distances in MLSE, can be modified in the case of DFSE.

An error state diagram (ESD) in the case of DFSE enumerates the distance $\delta(\underline{e})$, the number of symbol errors $w(\underline{e})$ and the *a priori* probability $p(\underline{e})$ of all error sequences $\underline{e}$ in the set of allowable sequences E'. Each path through the ESD corresponds to an error sequence in E'. For WF-DFSE, ZF-DFSE and MF-DFSE, the

35

branch distance (defined later for each case) depends on $L+1$ error symbols identified uniquely by a pair of error states, where an error state is defined as the value of L consecutive error symbols: $\{e_{j-L}, e_{j-L+1}, \ldots, e_{j-1}\}$. Since, an error symbol can take on any of $|\mathcal{A}|(|\mathcal{A}|-1)+1$ values (including zero), the diagram has $[|\mathcal{A}|(|\mathcal{A}|-1)+1]^L$ error states or nodes, as in MLSE [25]. The nodes are connected to each other through branches. Since an error sequence in the set E' can have no more than $J-1$ consecutive zeros in the middle of the sequence, the nodes and branches that correspond to J or more consecutive zeros in the middle of the error path are expurgated. The modified error state diagram is shown in Fig. 7 for the case of binary symbol alphabet, channel memory $L=3$ and memory order $J=1$. The error states or nodes are ternary L-tuples that take values in $\{0, +2, -2\}$. The pairs of error states that are negative of each other have been combined, as in [25]. This is because the branch distances for such error states are identical, as we will see later. Note that with $L=3$, there should be $(3^3-1)/2 = 13$ non-zero error state pairs in the ESD. However, the nodes $\pm 0\pm$ and $\pm 0\mp$ do not appear in the ESD of Fig. 7. Moreover, the nodes 0 ± 0, $\pm\pm 0$, $\pm\mp 0$ and ± 00 have only one outgoing branch each. This is because the nodes and branches that correspond to a zero in the middle of the error path, have been eliminated because with $J=1$, an allowable error sequences can not have any zeros in the middle of the sequence. The branches are labeled with the branch distance parameter λ and the number of symbol errors entailed by the transition as the exponent of dummy variable I. A factor of $1/2$ is used to account for the *a-priori* probability of error if the transition involves an error.

In the case of WF-DFSE, the error distance (squared) $\delta^2(\underline{e})$ is given by

$$\delta^2(\underline{e}) = \sum_{j=0}^{k-1+L-J} b_j \tag{120}$$

where k is the length of the error sequence $\underline{e} = \{e_0, e_1, \ldots, e_{k-1}\} \in E'_J$ and b_j is the branch distance given by[15]

$$b_j = \begin{cases} \left(\sum_{i=0}^{L} f(i) e_{j-i}\right)^2 & j = 0, 1, \ldots, k-1 \\ 0 & \text{otherwise} \end{cases} \tag{121}$$

Note that the segment of an error path $\underline{e}$ between the node $\{e_{k-L}, \ldots, e_{k-1-J}, 0, \ldots, 0\}$ $(e_{k-1-J} \neq 0)$ and the all-zeros node corresponds to the tail of the error sequence $\underline{\xi}$. Note from (121) that the branches within this segment of an error path (which we

---

[15] In the case of transmit matched filtering, $f(i)$ should be replaced by $v(i)$.

36

Figure 7: Error state diagram for DFSE ($L = 3, J = 1$).

refer to as tail branches) have distance zero. This is in accordance with (108) and (111), where the loss in squared distance (compared to MLSE) given by $\|\dot{\Psi}\underline{\xi}\|^2$ and $\|\ddot{\Psi}\underline{\xi}\|^2$ respectively, occurs on the tail branches.

Table 1 lists the branch distance parameters λ_i for Fig. 7 in the case of WF-DFSE (also see footnote 15). The branch distance appears as the exponent of a dummy variable D. Let $T(D, I)$ be the generating function for the error paths in the case of WF-DFSE, found by solving the state equations in the ESD of Fig. 7 simultaneously. The generating function can be series expanded as

$$\left.\frac{\partial}{\partial I}T(D, I)\right|_{I=1} = \sum_l N_l D^{\delta^2(l)} \tag{122}$$

where N_l is the number of error path pairs (negative of each other) with distance $\delta(l)$, per the number of symbol errors and the number of the corresponding input sequences. Then, the symbol error probability bound of (101) for WF-DFSE can be computed as[16]

$$P_s \leq \left.\sum_l 2N_l D^{\delta^2(l)}\right|_{D^x = Q\left(\sqrt{x/2N_0}\right)}. \tag{123}$$

---

[16]Note that for real symbol alphabet, the noise is real with power spectral density $N_0/2$.

Table 1: Branch distance parameters for WF-DFSE ($L = 3, J = 1$)

$\lambda_0 = D^{4f(0)^2}$	$\lambda_1 = D^{4[f(0)+f(1)]^2}$
$\lambda_2 = D^{4[f(0)-f(1)]^2}$	$\lambda_3 = D^{4f(1)^2}$
$\lambda_4 = D^{4[f(0)+f(1)+f(2)]^2}$	$\lambda_5 = D^{4[f(1)+f(2)]^2}$
$\lambda_6 = D^{4[f(0)-f(1)-f(2)]^2}$	$\lambda_7 = D^{4[f(0)+f(1)-f(2)]^2}$
$\lambda_8 = D^{4[f(1)-f(2)]^2}$	$\lambda_9 = D^{4[f(0)-f(1)+f(2)]^2}$
$\lambda_{10} = D^{4[f(0)+f(1)+f(2)+f(3)]^2}$	$\lambda_{11} = D^{4[f(0)-f(1)-f(2)-f(3)]^2}$
$\lambda_{12} = D^{4[f(0)-f(1)-f(2)+f(3)]^2}$	$\lambda_{13} = D^{4[f(0)+f(1)-f(2)-f(3)]^2}$
$\lambda_{14} = D^{4[f(0)+f(1)-f(2)+f(3)]^2}$	$\lambda_{15} = D^{4[f(0)-f(1)+f(2)-f(3)]^2}$
$\lambda_{16} = D^{4[f(0)+f(1)+f(2)-f(3)]^2}$	$\lambda_{17} = D^{4[f(0)-f(1)+f(2)+f(3)]^2}$
$\lambda_{18} = D^{4[f(1)+f(2)+f(3)]^2}$	$\lambda_{19} = D^{4[f(1)+f(2)-f(3)]^2}$
$\lambda_{20} = D^{4[f(1)-f(2)-f(3)]^2}$	$\lambda_{21} = D^{4[f(1)-f(2)+f(3)]^2}$
$\lambda_{22} = \lambda_{23} = \lambda_{24} = \lambda_{25} = 1$	

In the case of ZF-DFSE(S), the squared error distance is given by $\delta^2(\underline{e}) = b_n^2/b_d$, where

$$b_n = \sum_{j=0}^{k-1+L-J} b_{n,j} \tag{124}$$

is the numerator distance and

$$b_d = \sum_{j=0}^{k-1+L-J} b_{d,j} \tag{125}$$

is the denominator distance, and $b_{n,j}$ and $b_{d,j}$ are the corresponding branch distances which follow from (150) as

$$b_{n,j} = \text{Re}\left\{ e_j^* \left(s(0)e_j + 2\sum_{i=1}^{L} s(i)e_{j-i} \right) \right\} \tag{126}$$

$$b_{d,j} = \begin{cases} b_{n,j} & j = 0, 1, \ldots, k-1 \\ \underline{\xi}^H \dot{S}_{L-J}^H S_{L-J}' \dot{S}_{L-J} \underline{\xi} & j = k \\ 0 & \text{otherwise} \end{cases} \tag{127}$$

Note that the numerator and denominator branch distances differ only at the tail branches according to (150).

38

Table 2: Branch distance parameters for ZF-DFSE(S) ($L = 3, J = 1$)

$\lambda_i = D_1^{4\lambda_{1,i}} D_2^{4\lambda_{2,i}}$	
$\lambda_{1,0} = s(0)$	$\lambda_{1,1} = s(0) + 2s(1)$
$\lambda_{1,2} = s(0) - 2s(1)$	$\lambda_{1,4} = s(0) + 2s(1) + 2s(2)$
$\lambda_{1,6} = s(0) - 2s(1) - 2s(2)$	$\lambda_{1,7} = s(0) + 2s(1) - 2s(2)$
$\lambda_{1,9} = s(0) - 2s(1) + 2s(2)$	$\lambda_{1,10} = s(0) + 2s(1) + 2s(2) + 2s(3)$
$\lambda_{1,11} = s(0) - 2s(1) - 2s(2) - 2s(3)$	$\lambda_{1,12} = s(0) - 2s(1) - 2s(2) + 2s(3)$
$\lambda_{1,13} = s(0) + 2s(1) - 2s(2) - 2s(3)$	$\lambda_{1,14} = s(0) + 2s(1) - 2s(2) + 2s(3)$
$\lambda_{1,15} = s(0) - 2s(1) + 2s(2) - 2s(3)$	$\lambda_{1,16} = s(0) + 2s(1) + 2s(2) - 2s(3)$
$\lambda_{1,17} = s(0) - 2s(1) + 2s(2) + 2s(3)$	$\lambda_{1,3} = \lambda_{1,5} = \lambda_{1,8} = \lambda_{1,18-25} = 0$
$\lambda_{2,i} = \lambda_{1,i}$ for $i = 0, 1, \ldots, 21, 25$	
$\lambda_{2,22} = \big(s(2) + s(3)\big)[s'(0)(s(2) + s(3)) + 2s'(1)s(3)] + s'(0)s(3)^2$	
$\lambda_{2,23} = s(2)[s'(0)s(2) + 2s'(1)s(3)] + s'(0)s(3)^2$	
$\lambda_{2,24} = \big(s(2) - s(3)\big)[s'(0)(s(2) - s(3)) + 2s'(1)s(3)] + s'(0)s(3)^2$	

Table 2 lists the branch distance parameters λ_i for Fig. 7 in the case of ZF-DFSE(S). Dummy variables D_1 and D_2 are used to enumerate the numerator distance and the denominator distance respectively. Let $T(D_1, D_2, I)$ be the generating function for the error paths in this case, which can be series expanded as

$$\frac{\partial}{\partial I} T(D_1, D_2, I) \Big|_{I=1} = \sum_l M_l D_1^{b_n(l)} D_2^{b_d(l)}. \tag{128}$$

where M_l is the number of error path pairs with numerator distance $b_n(l)$ and denominator distance $b_d(l)$, per the number of symbol errors and the number of the corresponding input sequences. Then, the symbol error probability bound of (101) for ZF-DFSE(S) can be computed as

$$P_s \leq \sum_l 2M_l D_1^{b_n(l)} D_2^{b_d(l)} \Big|_{D_1^x D_2^y = Q\left(\sqrt{x^2/2N_0 y}\right)}. \tag{129}$$

A similar approach can be applied to evaluate the symbol error probability bound for ZF-DFSE(T). A generating function method for MF-DFSE(S) was described in [15].

13 Performance results

In this section, we compare the performance of the various receivers described in this paper via simulation and analysis. We consider BPSK modulation and single-user static time-dispersive AWGN channels. We consider the cases of a symbol-spaced channel model (symbol-rate sampling) and a half symbol-spaced channel model (fractional sampling). The receiver is assumed to have perfect estimates of the symbol timing and the impulse response of the channel. Each simulation was run for a count of 600 errors.

The first example is taken from [21]. The overall channel response is given by symbol-spaced tap coefficients[17] $f = (0.6335, 0.5456, 0.4479, 0.3167)$. The channel has memory $L = 3$ and is minimum-phase. Nyquist pulse-shaping is assumed. Fig. 8 shows the bit-error rate (BER) performance of various receivers for the channel in Example 1 with standard matched filtering. The memory order for the DFSE receivers is set to $J = 1$. With memory order one, the minimum distance in the DFSE receivers is achieved by the error sequences $\pm(2, -2, 0)$. For the MF-DFSE, WF-DFSE and ZF-DFSE receivers, the minimum distance as given by (82), (77) and (150) respectively,

---
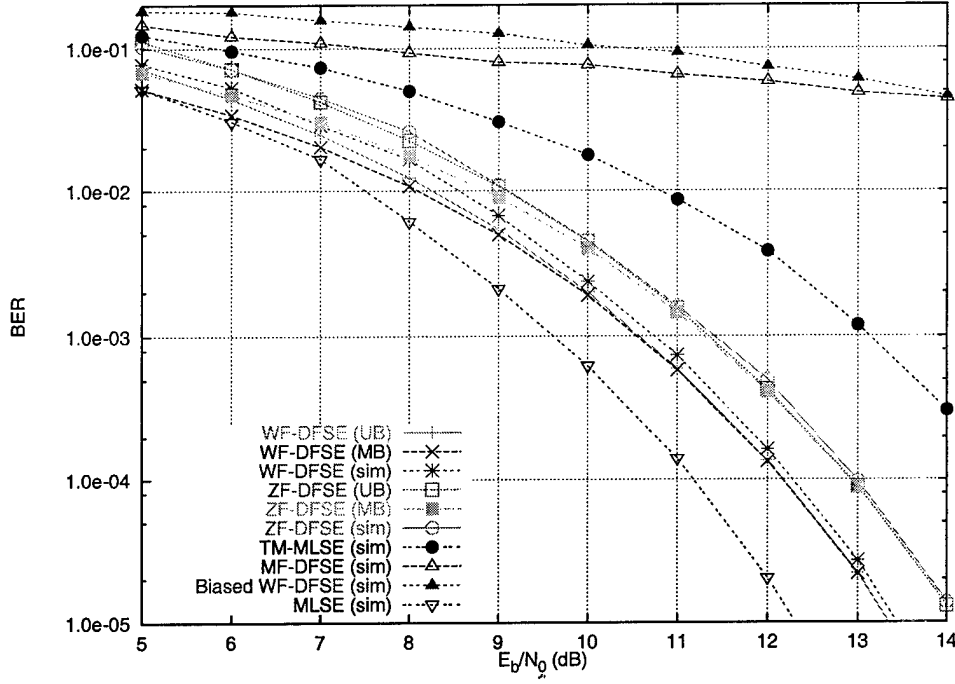
[17]Normalized so that $\sum_{i=0}^{L} |f(i)|^2 = 1$.

Figure 8: BER performance of various receivers in Example 1.

equals 0.7322, 0.6470 and 0.5936 respectively[18]. Fig. 8 shows the upper bound (UB) on the symbol error probability given by (101) and the minimum distance bound (MB) given by (104) for WF-DFSE and ZF-DFSE. Note that the bounds were obtained assuming absence of error propagation. The simulated BER is marginally higher than the upper bound for both receivers. In the simulations, final decisions were obtained at a lag of 30 symbols. The minimum distance bound converges to the upper bound at high signal-to-noise ratio (SNR) as minimum distance sequences dominate the performance.

Also shown in Fig. 8 is the simulated performance of an optimum two-tap TM-MLSE receiver with desired impulse response $(0.7071, 0.7071)$ taken from [10]. Note that the WF-DFSE receiver performs better than the ZF-DFSE and TM-MLSE receivers at all SNRs as discussed in Section 11.3. Although the zero-forcing filter in the case of ZF-DFSE, performs more signal decorrelation (which results in noise enhancement) than the prefilter of TM-MLSE, ZF-DFSE performs better than TM-MLSE in this example. This is because, unlike the case of TM-MLSE, the trellis search algorithm in the case of ZF-DFSE takes into account the correlation in the noise samples and is thus able to recover some of the lost signal energy.

---

[18]After dividing by two.

41
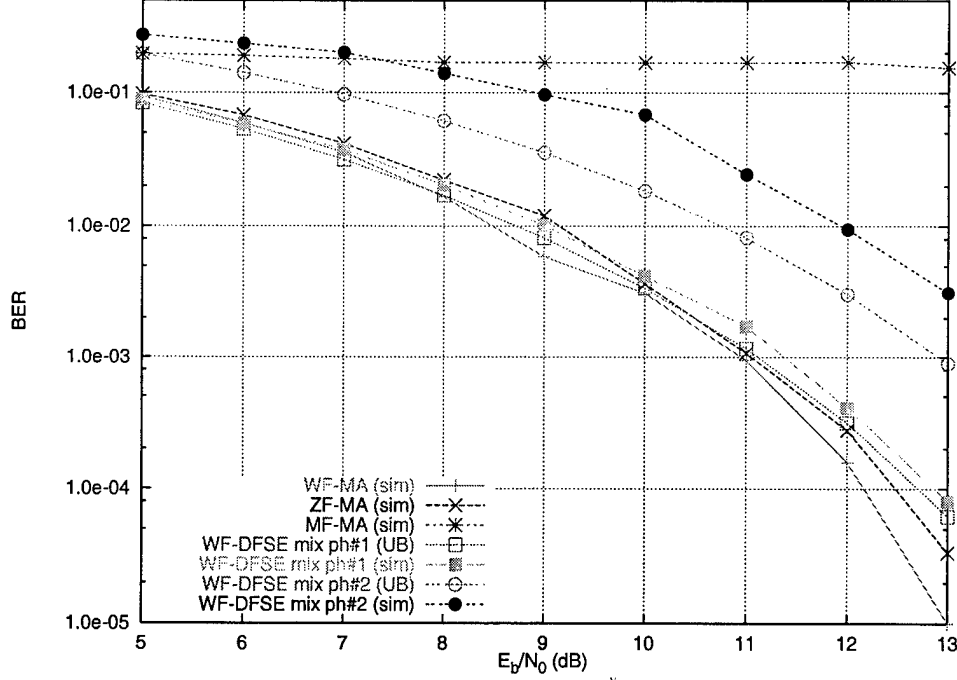
Figure 9: BER performance of various receivers in Example 1.

The MF-DFSE receiver achieves the maximum error distance equal to that of the MLSE receiver. However, it performs quite poorly due to the presence of untreated interference components. Also shown in Fig. 8 is a biased WF-DFSE receiver with the configuration $P^{-1} = F^H, Q = S, R = I$, considered in [20]. Again the effect of untreated interference is evident. The untreated interference arises due to a mismatch between the processing filter and the branch metric as discussed in Section 8.

Fig. 9 shows the simulated BER performance of the WF-MA, ZF-MA and MF-MA receivers for the channel in Example 1. The number of paths in the M-algorithm receivers is set to $M = 2$. The WF-MA receiver obtains the best performance. The MF-MA receiver exhibits a (high) error floor like the MF-DFSE and the biased WF-DFSE receivers, all of which belong to the class of biased receivers. Fig. 9 also shows the BER performance of WF-DFSE(T) receivers on mixed-phase channels with symbol-spaced medium responses $c = (0.4930, 0.6745, 0.3693, 0.4070)$ (#1) and $c = (0.4070, 0.3693, 0.6745, 0.4930)$ (#2). The channels have the same magnitude response as the channel in Example 1, which is minimum-phase. Note that the performance deteriorates as the channel phase increases. The deterioration in performance is due to two factors: the increase in the distance loss with the channel phase as discussed in Section 11 and the increase in error propagation. The latter effect is not captured

42

in the upper bound, so the bound diverges as error propagation becomes significant.

For our second example, the medium response is given by half-symbol spaced tap coefficients $c = (0.6335, 0.5456, 0.4479, 0.3167)$ (same as the minimum-phase channel of Example 1 but with fractional spacing). The medium response memory is $L_c = 3$. We consider two different transmit filters specified by the sampled autocorrelation function $\phi = (0.045, 0.0, 0.4053, 1.0, 0.4053, 0.0, 0.045)$ (T1) and $\phi = (0.33, 0.33, 0.33, 1.0, 0.33, 0.33, 0.33)$ (T2). The first one is a Nyquist-1 pulse (truncated to seven half-symbol samples) taken from [2, (5.5)] while the second one is arbitrarily chosen. The transmit filter memory is $L_d = 3$. The overall channel memory is thus $L = (L_c + L_d)/2 = 3$. The memory order is chosen as $J = 1$ for the DFSE receivers.

Fig. 10 shows the BER performance of various receivers for the two transmit filters (T1 and T2) with transmit matched filtering. In the case of T1, the WF-DFSE receiver achieves close to MLSE performance while the performance of MF-DFSE is less than a dB worse. ZF-DFSE is not shown for the case of T1 as its BER is very close to WF-DFSE at all SNRs. Note that the zero-forcing filter in ZF-DFSE(T) decorrelates only the transmit filter response, unlike ZF-DFSE(S) where the zero-forcing filter decorrelates the overall channel response. For the case of T2, we show upper bounds for WF-DFSE and ZF-DFSE which are marginally lower than the simulated results due to error propagation. Note that WF-DFSE performs better than ZF-DFSE at all SNRs as in Example 1. MF-DFSE in the case of T2 is much worse than MLSE as the sampled correlations in the case of T2 are more severe than T1.

14 Conclusions

We have presented a unified analysis of DFSE and M-algorithm receivers for channels with finite memory that examines the role of the receive filter and the branch metric. The analysis indicates that the error performance of certain receivers (called biased receivers) is affected by untreated interference components (bias) which arise due to a mismatch between the receive filter and the branch metric. We have shown that an unbiased receiver consists of a front-end filter (matched to the overall channel response or the transmit filter response) followed by the appropriate noise-whitening or zero-forcing filter and a reduced trellis or tree search algorithm. We have shown that the DFSE receivers with the noise-whitening filter (and the proper branch metric) are optimum among unbiased DFSE and truncated memory MLSE receivers (with pre-
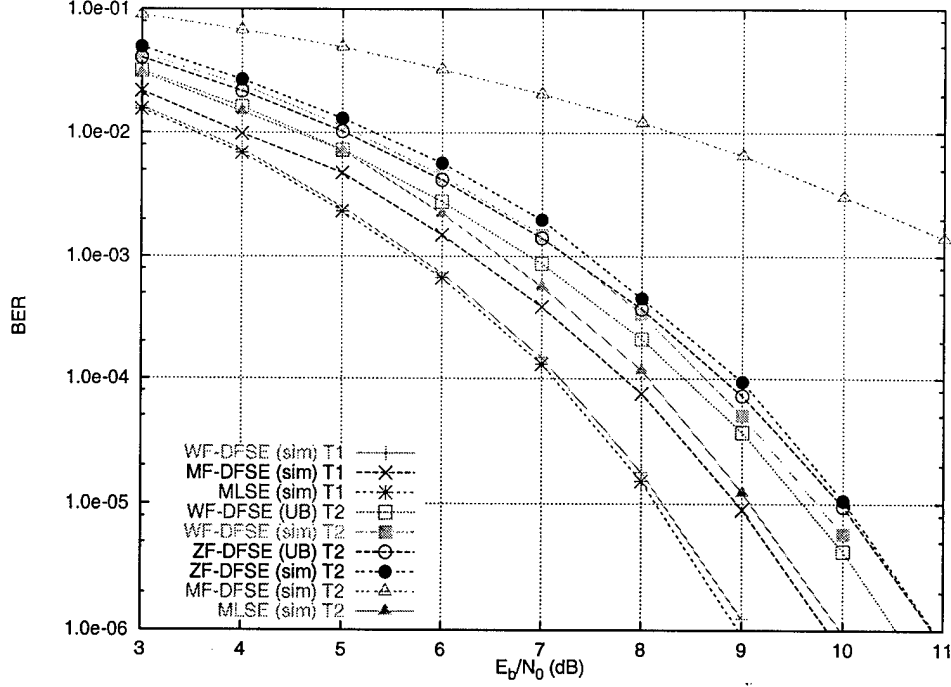
Figure 10: BER performance of various receivers in Example 2.

filtering) in the sense that they maximize the error distance. We have obtained novel receiver structures which employ transmit matched filtering and are thus suitable for adaptive channel estimation in the presence of excess signal bandwidth. We have obtained upper bounds on the symbol error probability of the various DFSE receivers and described a generating function approach to evaluate the bounds. Simulation and analytical results were presented for the various receivers using a symbol-spaced channel model and a fractionally-spaced channel model. The bounds were found to be tight in each case.

A Analysis of the alternative DFSE receiver

Consider the DFSE receiver of Fig. 4. Following the treatment given in Section 6.1, we see that a first event error occurs at time 0 in the reduced trellis search algorithm of Fig. 4 if

$$2\mathrm{Re}\{\bar{\underline{a}}_k^H C_k^H (P^{-1})_k \underline{x}_k'\} - \bar{\underline{a}}_k^H C_k^H R_k' Q_k' C_k \bar{\underline{a}}_k > 2\mathrm{Re}\{\underline{a}_k^H C_k^H (P^{-1})_k \underline{x}_k'\} - \underline{a}_k^H C_k^H R_k' Q_k' C_k \underline{a}_k$$

$$(130)$$

where $\underline{x}'_k = [x'(0), x'(1), \ldots, x'(k-1)]^T$ and the matrices C_k, R'_k and Q'_k are principal submatrices of dimension k of the matrices C, R' and Q' respectively. Using (31), (130) can equivalently be written as

$$2\mathrm{Re}\{\underline{e}^H_k C^H_k (P^{-1})_k P_{k \times N} \underline{u}'\} > \underline{e}^H_k C^H_k R'_k Q'_k C_k \underline{e}_k + 2\mathrm{Re}\{\underline{e}^H_k C^H_k R'_k Q'_k C_k \underline{a}_k\}$$
$$- 2\mathrm{Re}\{\underline{e}^H_k C^H_k (P^{-1})_k P_{k \times N} \Phi C \underline{a}\} \tag{131}$$

which is the condition for the error event ε defined in Section 6.1. The unbiasedness condition for this receiver can then be written as

$$C^H_k (P^{-1})_k P_{k \times N} \Phi C = C^H_k R'_k Q'_k C_k [I_k | O_{k \times N-k}] \quad \forall\, 1 \le k < N \tag{132}$$

or equivalently using the fact that $R'_k Q'_k = Q'^H_k R'^H_k$:

$$(P^{-1})_k P_{k \times N} = Q'^H_k (Q'^{-H})_{k \times N} \quad \forall\, 1 \le k < N \tag{133}$$

where the matrix $(Q'^{-H})_{k \times N}$ comprises the top k rows of the matrix Q'^{-H}. It follows from (131) and (132) that the probability of the error event ε for an unbiased DFSE receiver with the front-end filter matched to the transmit filter response, is given by

$$\Pr(\varepsilon) = Q\left(\frac{\underline{e}^H_k C^H_k R'_k Q'_k C_k \underline{e}_k}{2\sqrt{N_0 \underline{e}^H_k C^H_k R'_k Q'_k (\Phi^{-1})_k R'_k Q'_k C_k \underline{e}_k}}\right). \tag{134}$$

An upper bound on the first event error probability is given by (65) with the error distance $\delta(\underline{e})$ in this case defined as

$$\delta(\underline{e}) \triangleq \frac{\underline{e}^H_k C^H_k R'_k Q'_k C_k \underline{e}_k}{\sqrt{\underline{e}^H_k C^H_k R'_k Q'_k (\Phi^{-1})_k R'_k Q'_k C_k \underline{e}_k}}. \tag{135}$$

B Filters that satisfy unbiasedness

Let Y be an $N \times N$ Toeplitz matrix with elements

$$y(i,j) = \begin{cases} 1 & i = j \\ y(i-j) & 0 < |i-j| \le L_y \\ 0 & \text{otherwise} \end{cases} \tag{136}$$

Let P^{-1} be the $N \times N$ Toeplitz matrix defined in (21) with the diagonal element $p'(0)$ set to 1. Assume that the inverses of the submatrices Y_k and $(P^{-1})_k$ exist for all $k \le N$.

45

Proposition B.1 *Let* $\max(L_y, l_f, l_p) + 1 < N < \infty$. *If*

$$(P^{-1})_k P_{k \times N} = Y_k (Y^{-1})_{k \times N} \quad \forall\, k = 1, 2, \ldots, N - 1 \qquad (137)$$

then

$$P = Y^{-1}. \qquad (138)$$

In order to prove the above proposition, we make use of the following lemma [3]:

Lemma B.1 *Let* T *be an* $m \times m$ *invertible Toeplitz matrix subdivided into* $k \times k$, $k \times (m - k)$, $(m - k) \times k$ *and* $(m - k) \times (m - k)$ *submatrices* T_{11}, T_{12}, T_{21} *and* T_{22} *as shown below. Then* $S = T^{-1}$ *is partitioned similarly into* S_{11}, S_{12}, S_{21} *and* S_{22}:

$$T = \begin{bmatrix} T_{11} & T_{12} \\ T_{21} & T_{22} \end{bmatrix}, \quad S = \begin{bmatrix} S_{11} & S_{12} \\ S_{21} & S_{22} \end{bmatrix},$$

where, assuming T_{11} *is invertible,*

$$
\begin{aligned}
S_{11} &= T_{11}^{-1} + T_{11}^{-1} T_{12} (T_{22} - T_{21} T_{11}^{-1} T_{12})^{-1} T_{21} T_{11}^{-1}, \\
S_{12} &= -T_{11}^{-1} T_{12} (T_{22} - T_{21} T_{11}^{-1} T_{12})^{-1}, \\
S_{21} &= -(T_{22} - T_{21} T_{11}^{-1} T_{12})^{-1} T_{21} T_{11}^{-1}, \\
S_{22} &= (T_{22} - T_{21} T_{11}^{-1} T_{12})^{-1}.
\end{aligned}
$$

Let the matrices P^{-1} and Y be subdivided into $k \times k$, $k \times (N - k)$, $(N - k) \times k$ and $(N - k) \times (N - k)$ submatrices P'_{11}, P'_{12}, P'_{21} and P'_{22} and Y_{11}, Y_{12}, Y_{21} and Y_{22} respectively as shown below

$$P^{-1} = \begin{bmatrix} P'_{11} & P'_{12} \\ P'_{21} & P'_{22} \end{bmatrix}, \quad Y = \begin{bmatrix} Y_{11} & Y_{12} \\ Y_{21} & Y_{22} \end{bmatrix}, \qquad (139)$$

for $k = 1, 2, \ldots, N - 1$. Then, using Lemma B.1, (137) can be broken into two equations concerning the first k and the last $N - k$ columns of the $k \times N$ matrices on either side of (137), given by

$$
\begin{aligned}
P'_{11}[P'^{-1}_{11} + P'^{-1}_{11} P'_{12}(P'_{22} - P'_{21} P'^{-1}_{11} P'_{12})^{-1} P'_{21} P'^{-1}_{11}] = \\
Y_{11}[Y_{11}^{-1} + Y_{11}^{-1} Y_{12}(Y_{22} - Y_{21} Y_{11}^{-1} Y_{12})^{-1} Y_{21} Y_{11}^{-1}] \qquad (140)
\end{aligned}
$$

and

$$P'_{11}[-P'^{-1}_{11} P'_{12}(P'_{22} - P'_{21} P'^{-1}_{11} P'_{12})^{-1}] = Y_{11}[-Y_{11}^{-1} Y_{12}(Y_{22} - Y_{21} Y_{11}^{-1} Y_{12})^{-1}] \qquad (141)$$

46

respectively for $k = 1, 2, \ldots, N - 1$. Substituting (141) into (140) and simplifying, we get

$$P'_{21}P'^{-1}_{11} = Y_{21}Y^{-1}_{11}. \tag{142}$$

Let $k = 1$, then $P'_{11} = Y_{11} = 1$ and (142) implies that the first column of the matrix P^{-1} is equal to the first column of the matrix Y. Since P^{-1} and Y are Toepltiz matrices, all elements in the lower triangle of P^{-1} are equal to the corresponding elements of Y, i.e. $P'_{21} = Y_{21}$ for all $k = 1, 2, \ldots, N - 1$. Thus, (142) implies that

$$P'_{11} = Y_{11} \tag{143}$$

for all $k = 1, 2, \ldots, N - 1$. Since $N > \max(L_y, l_f, l_p) + 1$, (143) involves all non-zero elements of the matrices P^{-1} and Y. Thus,

$$P = Y^{-1}. \tag{144}$$

Note that the diagonal elements of the matrices P^{-1} and Y were set to 1 to factor out a scaling factor. In general, we have

$$P = cY^{-1} \tag{145}$$

where c is a constant scaling factor.

C   Error distance for ZF-DFSE

Let the matrices S and S^{-1} be subdivided into $k \times k$, $k \times (N - k)$, $(N - k) \times k$ and $(N - k) \times (N - k)$ submatrices S_{11}, S_{12}, S_{21} and S_{22} and S^I_{11}, S^I_{12}, S^I_{21} and S^I_{22} respectively as shown below

$$S = \begin{bmatrix} S_{11} & S_{12} \\ S_{21} & S_{22} \end{bmatrix}, \quad S^{-1} = \begin{bmatrix} S^I_{11} & S^I_{12} \\ S^I_{21} & S^I_{22} \end{bmatrix}. \tag{146}$$

Then, using Lemma B.1, we get

$$\begin{aligned} S_k(S^{-1})_k S_k &= S_k + S_{12}(S_{22} - S_{21}S^{-1}_{11}S_{12})^{-1}S_{21} \\ &= S_k + S_{12}S^I_{22}S_{21}. \end{aligned} \tag{147}$$

For $k \geq L$, we have

$$S_k(S^{-1})_k S_k = S_k + \begin{bmatrix} 0_{k-L} & 0 \\ 0 & \dot{S}^H(S^I_{22})_L \dot{S} \end{bmatrix}. \tag{148}$$

47

Note that for $N \gg L$, S^{-1} is near Toeplitz in the middle of the matrix. Thus, we can replace the matrix $(S_{22}^I)_L$ in (148) by the principal submatrix S_L' of an $N \times N$ Toeplitz matrix S' with elements $s'(i,j) = s'(i-j)$, given by the inverse z-transform of $1/S(z)$. Thus, for an error sequence $\underline{e} \in E'$ with tail $\underline{\xi}$ as defined in (84), we have

$$\underline{e}^H S_k (S^{-1})_k S_k \underline{e} \approx \underline{e}^H S_k \underline{e} + \underline{\xi}^H \dot{S}_{L-J}^H S_{L-J}' \dot{S}_{L-J} \underline{\xi}. \tag{149}$$

The error distance for ZF-DFSE(S) given by (79) can then be approximated as

$$\delta(\underline{e}) \approx \frac{\underline{e}^H S_k \underline{e}}{\sqrt{\underline{e}^H S_k \underline{e} + \underline{\xi}^H \dot{S}_{L-J}^H S_{L-J}' \dot{S}_{L-J} \underline{\xi}}}. \tag{150}$$

The above expression is approximate for error events occurring near the edges of the data burst where the noise correlation is not the same as in the middle, while it is exact for short error events occurring toward the middle of the burst.

Similarly, it can be shown that the error distance for ZF-DFSE(T) given by (80) can be approximated as

$$\delta(\underline{e}) \approx \frac{\underline{e}^H C_k^H \Phi_k C_k \underline{e}}{\sqrt{\underline{e}^H C_k^H \Phi_k C_k \underline{e} + \underline{\xi}^H (\ddot{C}_{L_d \times L - J})^H \ddot{\Phi}^H (\Phi')_{L_d} \ddot{\Phi} \ddot{C}_{L_d \times L - J} \underline{\xi}}} \tag{151}$$

where Φ' is an $N \times N$ Toeplitz matrix with elements $\phi'(i,j) = \phi'(i-j)$ obtained from the inverse z-transform of $1/\Phi(z)$ (where $\Phi(z)$ is the z-transform of $\{\phi(i)\}$).

References

[1] J. B. Anderson and S. Mohan, "Sequential coding algorithms: A survey cost analysis," *IEEE Transactions on Communications*, vol. 32, pp. 169–176, February 1984.

[2] J. W. M. Bergmans, *Digital Baseband Transmission and Recording*, Boston: Kluwer Academic Publishers, 1996.

[3] A. Bjorck, *Large Scale Matrix Problems*, New York: Elsevier North Holland, 1981.

[4] G. E. Bottomley and S. Chennakeshu, "Unification of MLSE receivers and extension to time-varying channels," *IEEE Transactions on Communications*, vol. 46, no. 4, pp. 464–472, April 1998.

[5] A. Duel and C. Heegard, "Delayed decision feedback sequence estimation for QAM and trellis coded systems," *Conference on Information Siences and Systems*, vol. 20, pp. 367–372, March 1986.

[6] A. Duel and C. Heegard, "Delayed decision-feedback sequence estimation," *IEEE Transactions on Communications*, vol. 37, no. 5, pp. 428–436, May 1989.

[7] A. Duel-Hallen, *Detection algorithms for Intersymbol Interfence Channels*, PhD thesis, Cornell University, August 1987.

[8] V. M. Eyuboglu and S. U. H. Qureshi, "Reduced-state sequence estimation with set partitioning and decision feedback," *IEEE Transactions on Communications*, pp. 13–20, January 1988.

[9] V. M. Eyuboglu and S. U. H. Qureshi, "Reduced-state sequence estimation for coded modulation on intersymbol interference channels," *IEEE Journal on Selected Areas in Communications*, vol. 7, no. 6, pp. 989–995, August 1989.

[10] D. D. Falconer and F. R. Magee Jr., "Adaptive channel memory truncation for maximum likelihood sequence estimation," *Bell Systems technical Journal*, vol. 52, pp. 1541–1562, November 1973.

[11] G. D. Forney, "Maximum-likelihood sequence estimation of digital sequences in the presence of intersymbol interference," *IEEE Transactions on Information Theory*, vol. IT-18, no. 3, pp. 363–378, May 1972.

[12] G. J. Foschini, "A reduced state variant of maximum likelihood sequence detection attaining optimum performance for high signal-to-noise ratios," *IEEE Transactions on Information Theory*, vol. 23, pp. 605–609, September 1977.

[13] A. Hafeez and W. E. Stark, "Decision feedback sequence estimation for unwhitened ISI channels," *Annual Allerton Conference on Communication, Control and Computing*, vol. 35, pp. 493–502, September 1997.

[14] A. Hafeez and W. E. Stark, "Decision feedback sequence estimation for unwhitened ISI and multiuser CDMA channels," *IEEE Vehicular Technology Conference*, pp. 424–429, May 1998.

[15] A. Hafeez and W. E. Stark, "Decision feedback sequence estimation for unwhitened ISI channels with applications to multiuser detection," *IEEE Journal*

on Selected Areas in Communications, vol. 16, no. 9, pp. 1785–1795, December 1998.

[16] W. U. Lee and F. S. Hill Jr., "A maximum likelihood sequence estimator with decision feedback equalization," *IEEE Transactions on Communications*, vol. COM-25, pp. 971–980, September 1977.

[17] S. Lin and D. J. Costello Jr., *Error Control Coding: Fundamentals and Applications*, New Jersey: Prentice-Hall, 1983.

[18] P. J. McLane, "A residual interference error bound for truncated-state Viterbi detectors," *IEEE Transactions on Information Theory*, vol. IT-26, pp. 549–553, September 1980.

[19] S. Qureshi and E. Newhall, "An adaptive receiver for data transmission over time-dispersive channels," *IEEE Transactions on Information Theory*, vol. IT-19, pp. 448–457, July 1973.

[20] C. Schlegel, "The receiver filter influence on reduced-state trellis decoding on channels with ISI," *IEEE Transactions on Vehicular Technology*, 1995. Under revision.

[21] W. Sheen and G. L. Stuber, "Error probability for reduced-state sequence estimation," *IEEE Journal on Selected Areas in Communications*, vol. 10, no. 3, pp. 571–578, April 1992.

[22] G. Ungerboeck, "Adaptive maximum-likelihood receiver for carrier-modulated data-transmission systems," *IEEE Transactions on Communication Technology*, vol. COM-22, no. 5, pp. 624–636, May 1974.

[23] S. Verdu, "Minimum probability of error for asynchronous gaussian multiple-access channels," *IEEE Transactions on Information Theory*, vol. IT-32, no. 1, pp. 85–96, January 1986.

[24] F. L. Vermeulen and M. E. Hellman, "Reduced state Viterbi decoders for channels with intersymbol interference," *IEEE International Conference on Communication*, pp. 37B-1–37B-4, 1974.

[25] A. Viterbi and J. K. Omura, *Principles of Digital Communication and Coding*, McGraw-Hill, 1979.

[26] L. Wei, L. K. Rasmussen, and R. Wyrwas, "Near optimum tree-search detection schemes for bit-synchronous multiuser CDMA systems over gaussian and two-path rayleigh-fading channels," *IEEE Transactions on Communications*, vol. 45, no. 6, pp. 691–700, June 1997.

[27] K. Wesolowski, "An efficient DFE & ML suboptimum receiver for data transmission over dispersive channels using two-dimensional signal constellations," *IEEE International Symposium on Information Theory*, pp. 23–28, June 1985.

[28] K. Wesolowski, R. Krenz, and K. Das, "Efficient receiver structure for GSM mobile radio," *International Journal on Wireless Information Networks*, vol. 3, no. 2, pp. 117–122, 1996.

[29] Z. Xie, C. Rushforth, R. Short, and T. K. Moon, "Joint signal detecetion and parameter estimation in multiuser communications," *IEEE Transactions on Communications*, vol. 41, pp. 1208–1215, August 1993.

Trellis-Based Multiuser Detection for DS-CDMA Systems with Frequency-Selective Fading

Do-Sik Yoo, Abdulrauf Hafeez and Wayne E. Stark

Electrical Engineering and Computer Science Department

1301 Beal Ave., University of Michigan, Ann Arbor, MI 48109-2122.

E-mail: dyoo@eecs.umich.edu, rauf@eecs.umich.edu, stark@eecs.umich.edu.

Summary

Wideband CDMA (WCDMA) has been chosen by ETSI as the basic radio-access technology for UMTS to allow high-rate data services [1]. Due to the use of wide bandwidth signals, system design must consider frequency-selective multipath fading along with multiple-access interference (MAI). A base station has knowledge of the spreading codes of all users in its cell and fading levels and user timings can be estimated effectively and tracked at the receiver. In this paper, we consider a trellis-based multiuser detector that fully exploits these parameters to provide an excellent performance/complexity tradeoff.

Decision feedback sequence estimation (DFSE) [2] is a reduced complexity alternative to maximum likelihood sequence estimation, where the complexity is controlled by reducing the memory of the trellis in the Viterbi algorithm. For purposes of multiuser detection of DS-CDMA signals, it is desirable to use the DFSE algorithm of [3] that operates on unwhitened matched filter statistics (UDFSE), as it does not require noise-whitening. Hafeez and Stark showed in [4] that the UDFSE algorithm suffers from untreated anti-causal interference components (bias). A modified unwhitened decision feedback sequence estimation (MUDFSE) algorithm was proposed which compensates for the bias using tentative decisions. A simplified version of this algorithm uses an approximate bias term which is independent of the state in the trellis and does not add significant complexity. In this paper, we consider a receiver with a Rake front-end for each user followed by the simplified MUDFSE algorithm that operates on the statistics of all users (assumed to be asynchronous). The Rake optimally combines the multipath fading components for each user while the MUDFSE algorithm resolves the multiuser interference components. The MUDFSE algorithm is provided with partial channel correlations which are computed on line by means of Rake correlators.

We consider an 8 user, BPSK modulated asynchronous DS-CDMA system with length
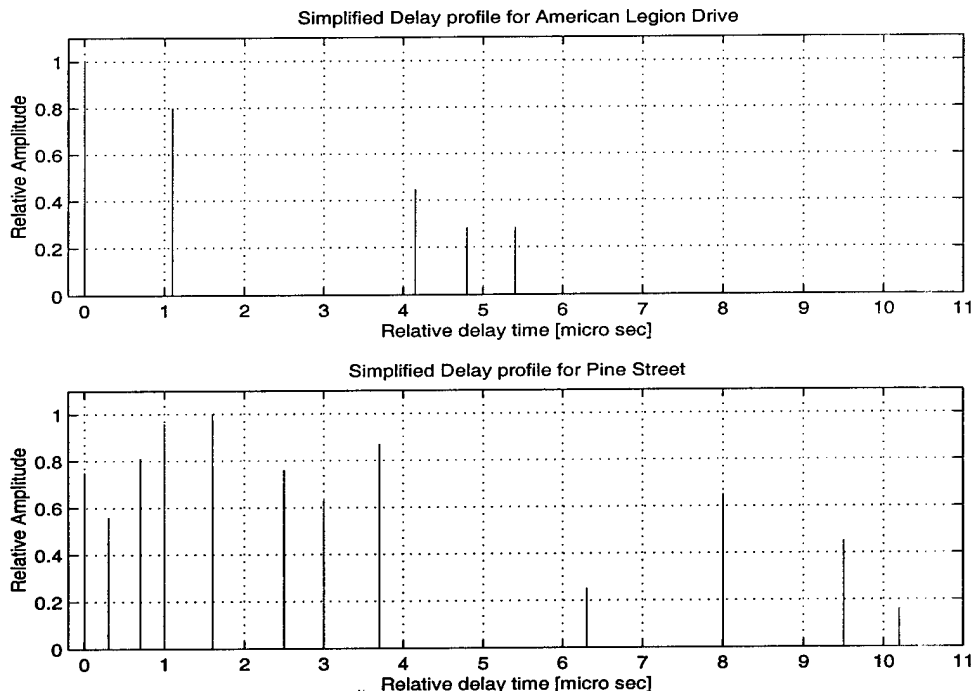
Figure 1: Sampled delay profiles for ALD and PS.

31 Gold spreading codes, chip rate 4.096 Mcps, data rate 132 kbps, carrier frequency 910 MHz and vehicle speed of 67.5 mph. We consider two different channel environments for each user based on the measurements of Cox et. al for a suburban [5] and an urban area [6]. The delay profiles are shown in Fig. 1. Relative user delays are fixed for the simulation and are assumed known at the receiver. Fading levels are also assumed to be known at the receiver.

Fig. 2 shows the average user bit-error rate (BER) for various receivers on American Legion Drive. The parameters in the figure specify the memory order of the trellis search algorithm and the decision lag. The multiuser channel has memory 7, not considering inter-symbol interference and MAI components caused by the multipaths of non-overlapping symbols. Fig. 3 shows the bit-error rate (BER) performance on Pine Street. It can be noted that with memory order 2, the MUDFSE algorithm provides close to MLSE performance in the case of ALD and obtains a huge gain over UDFSE (with the same memory order) for moderate signal-to-noise ratios (SNR). The gain over UDFSE is less in the case of PS which is more dispersive than ALD.

We will compare MUDFSE against other non-linear multiuser detection methods like parallel interference cancellation and successive interference cancellation. A soft-input version of MUDFSE which uses soft tentative decisions to cancel bias will also be considered. Moreover, we will provide numerical results with adaptive channel estimation.
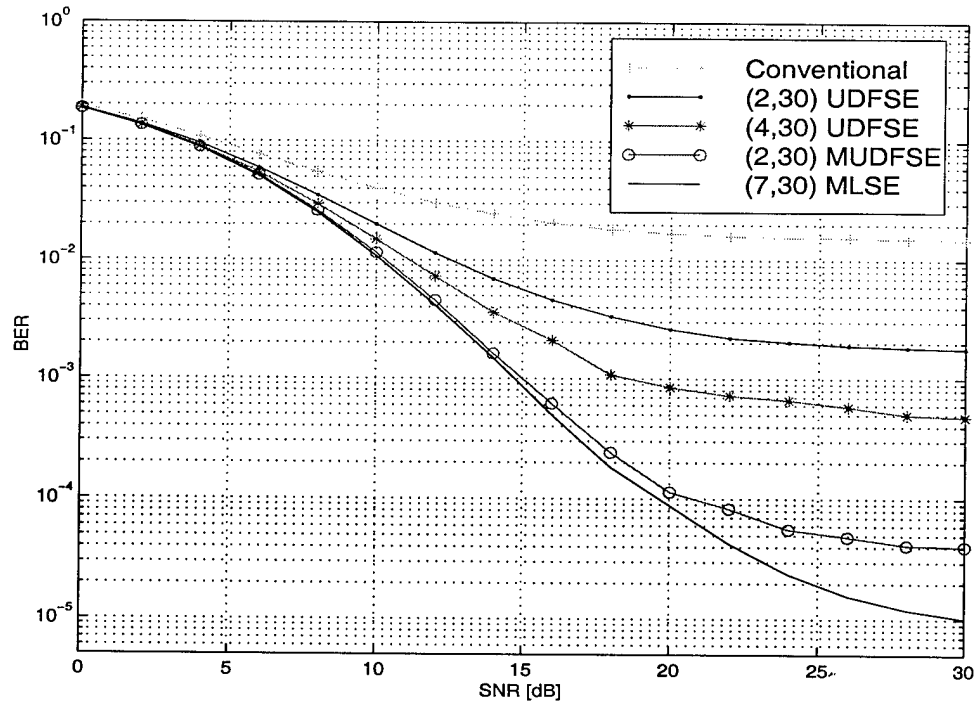
Figure 2: BER performance for various receivers on ALD.
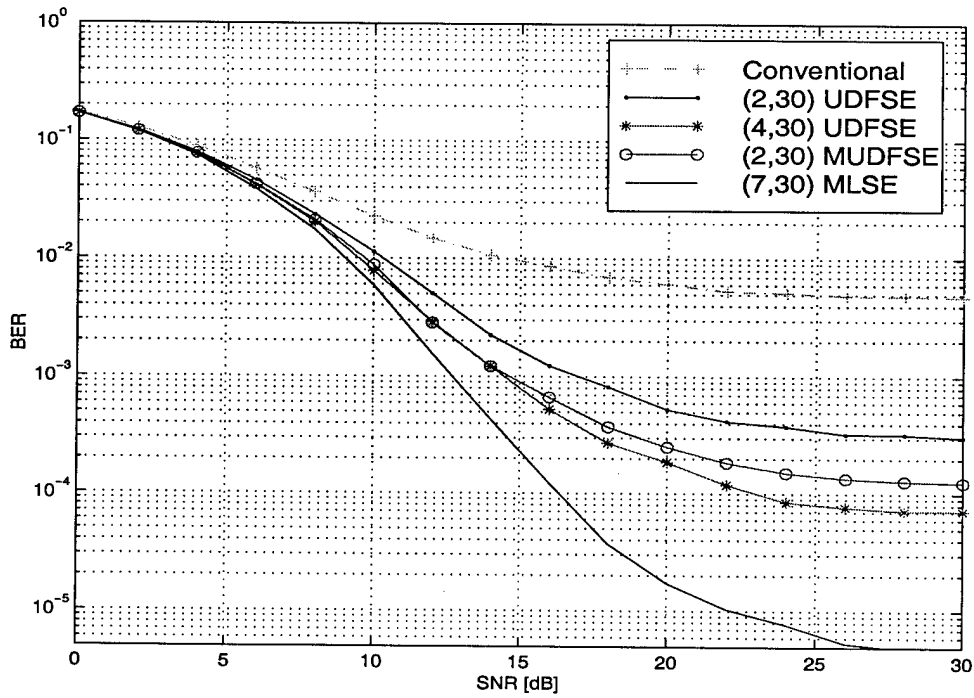
Figure 3: BER performance for various receivers on PS.

References

[1] E. Dahlman, P. Beming, J. Knutsson, F. Ovesjo, M. Persson and C. Roobol, "WCDMA – The Radio Interface for Future Mobile Multimedia Communications," *IEEE Trans. Vehicular Technology*, pp. 1105-1118, vol. 47, no. 4, Nov. 1998.

[2] A. Duel-Hallen and C. Heegard, "Delayed Decision-Feedback Sequence Estimation," *IEEE Trans. Communication*, vol. 37, no. 5, pp. 428-436, May 1989.

[3] A. Duel and C. Heegard, "Delayed Decision Feedback Sequence Estimation for QAM and Trellis Coded Systems," *20th Conf. Info. Sc. and Sys.*, pp. 367-372, Mar. 1986.

[4] Abdulrauf Hafeez and W. E. Stark, "Decision Feedback Sequence Estimation for Unwhitened ISI Channels with Applications to Multiuser Detection," *IEEE Journal Selected Areas Communications*, pp. 1785-1795, vol. 16, no. 9, Dec. 1998.

[5] D. C. Cox, "Delay-Doppler characteristics of Multipath Propagation at 910MHz in a suburban Mobile Radio Environment," *IEEE Trans. Antennas and Propagation*, pp. 625–635, vol. 20, Sept. 1972.

[6] D. C. Cox, "910MHz Urban Mobile Radio Propagation: Multipath characteristics in New York City," *IEEE Trans. Communications*, pp. 1188-1194, vol. 21, Nov. 1973.

CO-CHANNEL INTERFERENCE CANCELLATION FOR D-AMPS HANDSETS

Abdulrauf Hafeez*, Karl J. Molnar**, Gregory E. Bottomley**

* EECS Dept., U. of Michigan, Ann Arbor, MI 48109-2122
** Ericsson Inc., Research Triangle Park, NC 27709

Abstract – Co-channel interference is a major impairment for IS-136 handsets. Joint estimation of co-channel signals can be used to minimize this effect, but traditional approaches require transmissions from different base-stations to be synchronized. In this paper, we consider a semi-blind approach for cancelling asynchronous interference using generalized per-survivor processing for channel acquisition and tracking. Signal delays and medium responses are jointly estimated for symbol-asynchronous co-channel signals assuming knowledge of the signal structure. Simulation results are presented that show C/I gains of 15 dB in the presence of one interferer.

I INTRODUCTION

Digital AMPS (D-AMPS) based on the IS-136 standard is a popular technology for wireless cellular and PCS services in the Americas and elsewhere. System design must consider multipath fading and time dispersion, as well as co-channel interference (CCI). At the base station, these impairments can be mitigated using diversity or phased array antennas. However, at the handset, it is preferable to use only one antenna and receive chain due to size, weight and cost constraints. Joint adaptive demodulation of co-channel signals provides an attractive alternative for obtaining vital gains near cell boundaries where typically one or two co-channel interferers are dominant. It enables tighter frequency reuse in the network, improves coverage or allows a combination of both. This paper focuses on a semi-blind approach for joint demodulation suitable for slot and symbol asynchronous interference.

Coherent joint demodulation of co-channel user signals has previously been considered by several authors. Analytical bounds on performance have been derived for joint maximum likelihood (ML) detection of symbol-synchronous users in fading channels [1]. Joint maximum likelihood sequence estimation (MLSE) of co-channel signals in known, time-invariant ISI channels is investigated in [2] and [3]. Since fading channels are unknown *a priori*, it is critical to estimate the channels accurately for successful signal separation. Transmission of synchronized training sequences for multiple co-channel signals greatly facilitates the channel acquisition process, and is used in [4]. In current D-AMPS systems, base-stations are not synchronized, precluding joint training. However, it is possible to exploit the training sequences of individual signals, and is considered in [5] for stationary channels. For the D-AMPS burst interval length, the fading channel estimates must be adapted over the slot, even at fairly low vehicle speeds. Adaptive estimation of co-channel signals aided by joint training is considered in [6], and blind adaptive joint MLSE and MAP algorithms without training are investigated in [7].

In this paper, we investigate joint adaptive estimation of asynchronous co-channel signals. A novel, semi-blind approach to signal acquisition is given, in which initial channel estimates are obtained using only the training sequence of the desired signal. This approach addresses the fact that user signals are both slot and symbol asynchronous. To handle additional ISI from the interferer misalignment, the MLSE state space is increased, and pulse-shape side information is used to aid channel estimation. Acquisition and demodulation are based on a generalization of per-survivor processing (PSP) [8], which has been used for single-user acquisition [9]. Generalized PSP is the concept of per-path parallel feedback extended to an arbitrary tree search algorithm. Specifically, we apply multiple survivor PSP [10] for semi-blind joint acquisition of co-channel signals over the training sequence of the desired signal and for jointly demodulating all signals.

The overall response for each co-channel signal consists of a transmit pulse-shaping filter, a medium response and a receive filter matched to the transmit pulse. The transmit and receive filter responses are known *a priori* and are used to constrain the overall channel impulse responses in the case of asynchronous co-channel signals. However, this method requires the knowledge of signal delays. During acquisition, we jointly estimate the delays and medium responses of co-channel signals using pulse-shape side information, with the joint MLSE metric formulated in terms of the pulse-shape autocorrelation and the medium response.

The paper is organized as follows. Section II describes the system model and the joint detection problem is formulated in section III. Section IV describes

adaptive channel estimation and semi-blind acquisition. Performance results are presented and discussed in section V and section VI concludes the paper.

II SYSTEM MODEL

Figure 1 shows the model of a co-channel communication system with K users in baseband equivalent form. The kth transmitter transmits an independent sequence of N complex symbols $\{a_{k,n}\}_{n=1}^{N}$ (taken from an M-ary alphabet) after passing it through a linear time-invariant pulse-shaping transmit filter with impulse response $f(t - \tau_k)$[1], where τ_k is the kth signal's delay. Transmit signal k passes through a time-varying transmission medium with delay response $g_k(\tau; t)$, where τ and t are the delay and the time indices, respectively. The co-channel signals are summed and added with $w(t)$, which is assumed to be a zero-mean AWGN process with a one-sided noise power spectral density N_0.
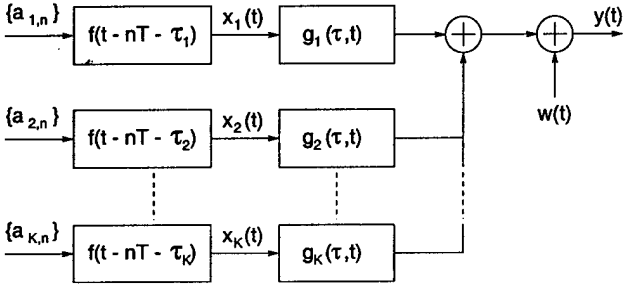
Figure 1: A co-channel communication system model.

III JOINT DETECTION

Joint detection of multiuser sequences, assuming *a priori* equiprobable transmitted sequences can be performed using a maximum likelihood sequence detector (MLSD). For $\underline{a}_n = \{a_{k,i} : k = 1, \ldots, K; i = 1, \ldots, n\}$, the optimum joint MLSD receiver finds the sequence $\underline{\hat{a}}_N$ that maximizes the likelihood of receiving $y(t)$ given that the sequence $\underline{a}_N$ was transmitted. This detector is derived in the appendix for signals with excess bandwidth under the assumption of a time-varying, frequency selective channel response. However, this approach requires sampling the filtered receive signal non-uniformly at the delays of the fractionally-spaced medium response. Alternatively, in this section, we derive a sub-optimum joint MLSD receiver for detecting $\underline{a}_N$ based on symbol-spaced sampling of the receive signal, leading to a simplified receiver.

Let $r(t)$ be the received signal filtered by a time-invariant filter matched to the transmit pulse-shaping filter i.e. $r(t) = f^*(-t) * y(t)$. Let the first co-channel signal be the desired signal with signal delay $\tau_1 = 0$,

[1] $f(t)$ is normalized to have unit energy

then the medium response for each user can be modeled as a tapped delay line with symbol-spaced taps

$$g_k(\tau, t) = \sum_{l} c_{k,l}(t)\delta(\tau - lT), \qquad (1)$$

where T is the symbol period. The filtered signal $r(t)$ sampled at times nT is denoted as $r_n = r(nT)$, with

$$r_n = \sum_{k=1}^{K} \sum_{l=0}^{L_k} c_{k,l,n} \sum_{j \in J} a_{k,n-l-j}\rho_{k,j} + w_n. \qquad (2)$$

L_k is the memory length of the kth co-channel medium in symbol periods, and $c_{k,l,n} = c_{k,l}(nT)$ are the taps of the medium response filter which are approximated as constant over the duration of the pulse-shaping filter response. The sampled autocorrelation function of the pulse-shaping filter, $\rho_{k,j}$, is given by $\rho_{k,j} = f^*(-t) * f(t - \tau_k)|_{t=jT}$ and is assumed to be Nyquist. Interval J is chosen such that the sampled autocorrelation function for the kth signal $\rho_{k,j}$ has negligible energy for $j \notin J$.

Equation (2) can be written in matrix form as

$$r_n = \underline{c}_n^H \Phi \underline{a}_n + w_n, \qquad (3)$$

where $\underline{a}_n$ and $\underline{c}_n$ are *stacked* vectors of the transmitted symbols and medium response samples, respectively. The matrix Φ is a block diagonal matrix with the kth block Φ_k containing the sampled pulse-shape autocorrelation values $\rho_{k,j}$ corresponding to user k. As an example, consider two flat-faded co-channel signals using Nyquist pulse-shaping with the received signal sampled ideally for the desired signal. The sampled pulse autocorrelation function for the second signal modeled as three taps ($j \in \{-1, 0, 1\}$) to account for its delay. In this case, $\underline{a}_n = (a_{1,n}, a_{2,n+1}, a_{2,n}, a_{2,n-1})^T$, $\underline{c}_n = (c_{1,0,n}, c_{2,0,n})^H$, and Φ is given by

$$\Phi = \begin{bmatrix} 1 & 0 & 0 & 0 \\ 0 & \rho_{2,-1} & \rho_{2,0} & \rho_{2,1} \end{bmatrix}. \qquad (4)$$

A joint MLSD based on the model of (3) determines the most likely transmitted sequence $\underline{\hat{a}}_N$ that minimizes the metric

$$J(\underline{\hat{a}}_N) = \sum_{n=1}^{N} \left\| r_n - \underline{c}_n^H \Phi \underline{\hat{a}}_n \right\|^2. \qquad (5)$$

It follows ([11], [12], [2]) that the ML sequence can be determined recursively by using the Viterbi algorithm with branch metrics based on (5).

IV ADAPTIVE CHANNEL ESTIMATION

Channel estimation plays a key role in successful cancellation of co-channel interference through coherent

demodulation. Independent fading of co-channel signals makes it possible to distinguish between signal states at the output with high probability only if the fading channels are known or can be estimated accurately at the receiver. For the D-AMPS system, although the desired channel can be estimated individually over its sync word, the estimate is not accurate at low carrier-to-interference (C/I) ratios. Joint data/channel estimation is thus employed for semi-blind channel acquisition over the training sequence of the desired signal.

Per-survivor processing allows effective channel estimation aided by zero-delay survivor sequences. Assuming knowledge of signal delays, we estimate the medium responses using branch metrics computed as

$$e(\sigma_n|\sigma_{n-1}) = r_n - \hat{\underline{c}}_n^H(\sigma_{n-1})\Phi\hat{\underline{a}}_n, \qquad (6)$$

where $\hat{\underline{c}}_n(\sigma_{n-1})$ are medium response estimates obtained using the survivor sequence associated with the state σ_{n-1}. Using Least Mean Square (LMS) channel identification, the channel update is calculated as

$$\hat{\underline{c}}_{n+1}(\sigma_n) = \hat{\underline{c}}_n(\sigma_{n-1}) + \beta\Phi\hat{\underline{a}}_n e^*(\sigma_n|\sigma_{n-1}), \qquad (7)$$

where β is selected as a compromise between tracking capability and excess mean square error.

Blind single channel acquisition can be enhanced over conventional PSP by resorting to an extended data sequence search. The primary cause of mis-acquisitions in the single channel case is the existence of *indistinguishable*, i.e. *equivalent* sequences, including sequences such as the inverted and shifted versions of the transmitted data sequence. In order to improve acquisition, the number of sequences eliminated is minimized during the early stages in a generalized PSP algorithm [9].

Blind acquisition of multiple co-channels is more difficult, since mis-acquisitions may be caused by transmitted co-channel sequences that happen to be highly correlated over a large enough window of overlapping symbol positions. As an example, consider the case of two co-channel signals: both flat-faded and stationary. Assume that the transmitted sequences are symbol-aligned. A PSP-based joint MLSE algorithm requires only one state. Let $a_{1,n} = a_{2,n}$ for $n = 1, \ldots, N_s$, then equivalent accumulated metrics $J(\underline{a}_{N_s})$ along the correct path are given by

$$\sum_{n=1}^{N_s} \left\| r_n - \sum_{k=1}^2 \hat{c}_{k,0,n} a_{k,n} \right\|^2 = \sum_{n=1}^{N_s} \left\| r_n - a_{1,n} \sum_{k=1}^2 \hat{c}_{k,0,n} \right\|^2. \qquad (8)$$

With the co-channels initialized to zero, the single channel estimator along the correct path (if not eliminated) is equally likely to converge (if it does) to any of the co-channel states belonging to the infinite set

$\{(\hat{c}_{1,0,N_s}, \hat{c}_{2,0,N_s}) : \hat{c}_{1,0,N_s} + \hat{c}_{2,0,N_s} = c_{1,0,N_s} + c_{2,0,N_s}\}$. This problem can be alleviated by using a generalized PSP algorithm during acquisition. We consider *multiple survivor* PSP, since it allows survivors with identical recent path histories (but different channel histories) to continue if they possess good accumulated metrics. This reduces the chance of mis-acquisition of the correct channel.

For asynchronous co-channel interference, two approaches for channel estimation are considered. In the first approach, independent taps are estimated for the composite response of the interferer. The composite response is the medium response convolved with the transmit and receive filter pulse shape autocorrelation function. In the second approach, the channel estimator estimates only the medium response for each co-channel signal using (7). The sequence estimator uses the knowledge of the sampled pulse autocorrelation matrix Φ to compute branch metrics that depend on the overall response using (6). The latter approach requires estimation of ray delays, which are estimated by employing hypothesis testing of the delay value during acquisition. We restrict this approach to the case where a single interferer path (flat fading) is assumed, and choose the hypothesized delay for this path with the best metric from the Viterbi algorithm.

The path metric and the medium response estimates must be initialized prior to acquisition. We assume that the length of multi-path spread in symbol intervals (L_k) is known for all co-channel signals. The desired medium response is initialized to its least squares estimate which is found using the known sync word. The interferer channel is initialized based on the residual signal after estimation and removal of the desired signal. The interferer channel's amplitude is estimated by subtracting the reconstructed desired signal from the received signal and averaging over the training sequence. The phase of the estimate is obtained from the phase of one of the samples of the residual signal.

If the transmission medium is non-stationary, channel estimates obtained over the training sequence are not valid for the entire slot. D-AMPS at 1990 MHz has a slot-normalized fading rate of 1.23 at a speed of 100 km/h. Thus, fully adaptive channel tracking is required at high speeds, but it also helps overcome poor initial channel estimates at low speeds. Here, the least mean square (LMS) algorithm is considered for tracking as it has been shown to have similar tracking capabilities as the more complex recursive least squares (RLS) algorithm [13]. In the case that composite channel estimates are computed, LMS is used in the conventional manner to update the desired signal and interferer taps jointly. When knowledge of the pulse shape is used, the channel estimates are adap-

tively updated via the LMS algorithm using the hypothesized symbols convolved with the pulse shape [14], and is called Pulse-shape Assisted Channel Estimation (PACE).

V PERFORMANCE RESULTS

Performance is evaluated via simulation for the downlink of the D-AMPS system. A 40 ms frame is divided into six slots, giving each user a 30 kHz channel for two slots per frame. The user transmits at 24.3 k-Baud using $\pi/4$-DQPSK modulation with 1990 MHz carrier and square-root raised cosine pulse-shaping (35% rolloff). The slot comprises 162 differential symbols out of which the first fourteen are used for training. The receiver mixes down the signal coherently, filters it with a matched square-root raised cosine filter and samples at eight times the symbol rate. Synchronization (sync) is performed for the desired user, decimating the signal to the symbol rate based upon the symbol timing estimate. The received signal comprises a desired signal and one interfering signal. Results are presented separately for acquisition and demodulation.

Figure 2 shows results for acquisition of channel estimates using the known training sequence of the desired signal. For this case, two taps are used for the desired signal and one for the interferer. Each signal, however, is flat faded with 0 Hz fading (fixed over the slot, but independent from slot to slot). The interferer is symbol synchronous, but slot asynchronous, to the desired signal and ideal sampling based on the desired signal is assumed at the receiver. Each simulation was run for 500 slots with $\beta = 0.28$. The plots show the number of slots with a root mean square error of E_{rms} versus E_{rms}, where RMS error is the error between the first ray of the desired channel and its estimate after the training period. The top and bottom plots show results when PSP-MLSE and 32 survivor paths are used, respectively, when C/I is fixed at 0 dB and E_s/N_0 equals 23 dB. For the case that PSP-MLSE is used, an E_{rms} value greater than 0.1 is observed in roughly 20% of the slots, leading to misacquisition of the channel. This is because sometimes the random data of the interferer happens to be highly correlated with the desired signal's sync word over several symbol periods. Using 32 survivor paths, only a handful of slots experience $E_{rms} > 0.1$, both reducing the average and maximum E_{rms} values, as shown in the figure.

Next, we compare the bit error-rate (BER) performance of various PACE approaches when the desired and the interfering signals are symbol asynchronous. Both signals again have 0 Hz fading which is independent from slot to slot. The desired signal's timing is either known or estimated by correlating the data
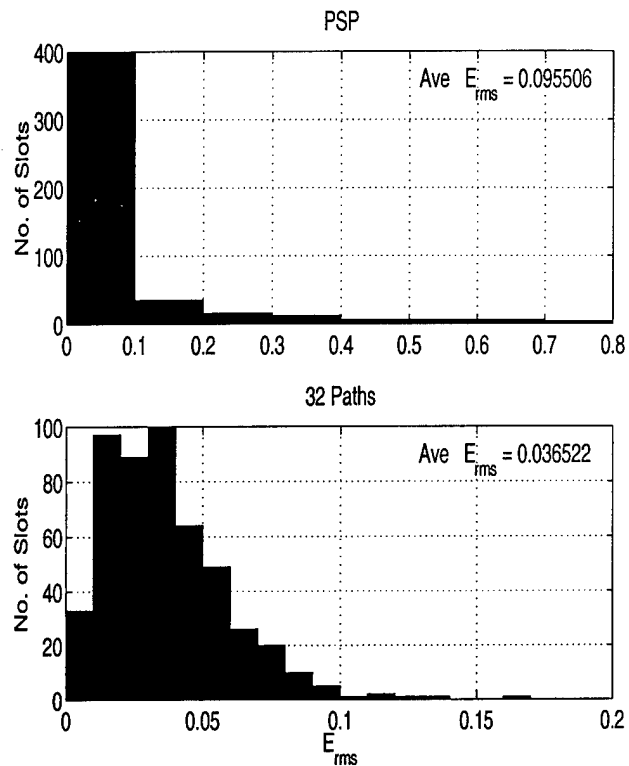

Figure 2: Histogram of the slots with a given rms error after semi-blind acquisition.

with the known training sequence of the desired signal. The overall response for the desired co-channel signal is modeled as one tap while, for the interferer, it is modeled as three taps. When using PACE mode, only one medium tap is estimated. Acquisition is achieved with 64 survivor paths, while tracking mode uses one survivor path (PSP-MLSE). Signal misalignment is estimated during acquisition mode for each slot by hypothesizing delays 0 to half symbol in increments of 1/8th symbol, choosing the delay that yields the best accumulated metric over the training field of the desired signal. LMS step sizes are set to 0.2 and 0.1 for training and tracking modes, respectively.

Figure 3 shows the performance in an interference limited environment ($E_s/N_0 = 33$ dB) when the two signals are quarter symbol misaligned. The bottom curve shows performance using joint demodulation with PACE mode under known medium conditions. The next curve uses PACE mode with estimated sync and medium response, but known interferer misalignment. The following curve is the same as the last, but estimates the interferer misalignment. The second curve from the top uses joint demodulation, but estimates the composite channel, and the top curve shows performance without joint demodulation. Note that the joint demodulation performance with known sync and channel is not very good at low C/I. This
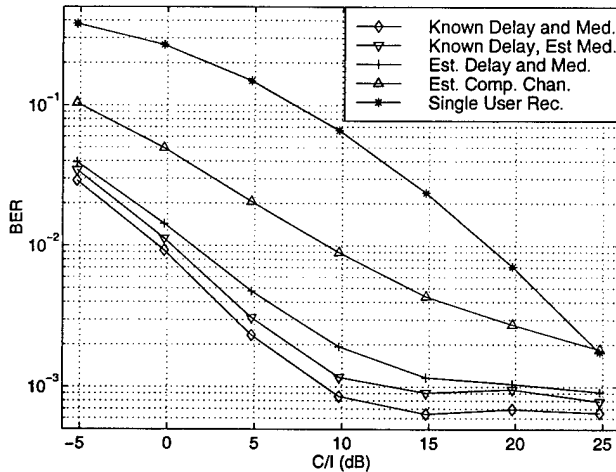
Figure 3: Performance with $T/4$ symbol misalignment.

is mainly because the three taps for the interferer do not account for all the ringing arising from the sampling offset. With known misalignment, the receiver that uses this information and estimates the medium responses only, performs better than the receiver that estimates the overall responses. Even when the delay is estimated, the first receiver outperforms the second and provides about 15 dB gain over the conventional single user receiver at 1% BER.

Figure 4 shows the bit error-rate performance when $E_s/N_0 = 33$ dB and the desired signal and interferer are flat faded and symbol aligned, but the Doppler frequency is 46 Hz (25 km/h at 1990 MHz). One tap is assumed for each signal's channel, and LMS step sizes are set at 0.7 and 0.6 for training and tracking modes, respectively. At 1% bit error rate, a 5 dB C/I gain is achieved compared to without interference cancellation. The cause of the degradation in performance when the channels are time varying is partly due to the reasons discussed previously. When the data sequences of the interfering signals happen to be highly correlated over several consecutive symbols, the per-survivor channel trackers can be thrown off the correct channel state even on the correct survivor path. Multiple survivor tracking can help reduce the probability of this event. Figure 4 shows that a further 4 dB C/I gain is achieved at an error rate of 1% when 4 path channel tracking is used over the data field. We note, however, the large step sizes used in the LMS approach indicate that it has difficulty estimating the channel and alternate adaptive trackers should be considered.

VI CONCLUSIONS

In this paper, we propose joint maximum likelihood sequence estimation together with per-survivor-processing and multiple survivor search to jointly de-
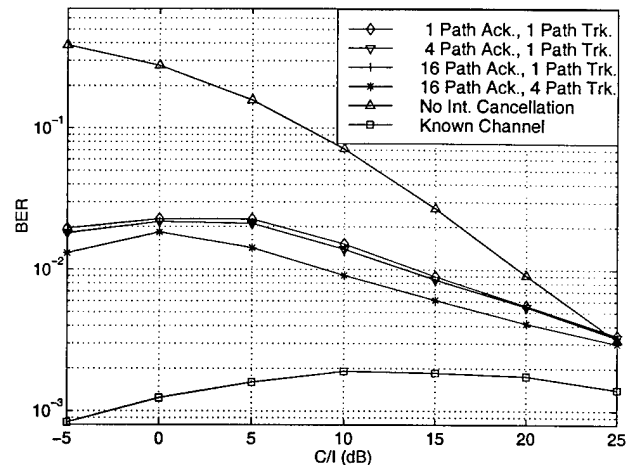
Figure 4: Tracker performance at 25 km/h.

modulate a single dominant co-channel interferer to improve the performance for the desired signal. LMS-based channel estimation is used in a D-AMPS terminal with single antenna and symbol-spaced sampling. In the case of symbol-asynchronous signals, we estimate signal delays and exploit the knowledge of pulse shaping filters for the symbol sampled receive signal. Simulation results indicate that gains of 5-15 dB C/I can be achieved over the conventional single-user receiver. Further work includes improving performance at high speeds using more sophisticated tracking.

REFERENCES

[1] S.J. Grant and J.K. Cavers, "Performance enhancement through joint detection of cochannel signals using diversity arrays", *IEEE Trans. Comm.*, vol. 46, pp. 1038–1049, Aug. 1998.

[2] W. van Etten, "Maximum likelihood receiver for multiple channel transmission systems", *IEEE Trans. Comm.*, vol. 24, pp. 276–283, Feb. 1976.

[3] K. Giridhar, S. Chari, J.J. Shynk, and R.P. Gooch, "Joint demodulation of cochannel signals using MLSE and MAPSD algorithms", in *Proc. IEEE ICASSP*, pp. IV–160–IV–163, Apr. 1993.

[4] P.A. Ranta, A. Hottinen, and Z. Honkasalo, "Co-channel interference cancelling receiver for TDMA mobile systems", in *Proc. IEEE ICC*, pp. 17–21, Feb. 1995.

[5] S.W. Wales, "Technique for cochannel interference suppression in TDMA mobile radio systems", *IEE Proc. Comm.*, vol. 142, Apr. 1995.

[6] H. Yoshino, K. Fukawa, and H. Suzuki, "Interference canceling equalizer (ICE) for mobile radio communication", *IEEE Trans. in Veh. Tech.*, vol. 46, pp. 849–861, Nov. 1997.

[7] K. Giridhar, J.J. Shynk, A. Mathur, S. Chari, and R.P. Gooch, "Nonlinear techniques for the joint

estimation of cochannel signals", *IEEE Trans. Comm.*, vol. 45, pp. 473–483, Apr. 1997.

[8] R. Raheli, A. Polydoros, and C. Tzou, "Per-survivor processing: A general approach to MLSE in uncertain environments", *IEEE Trans. Comm.*, vol. 43, pp. 354–364, Feb./Mar./Apr. 1995.

[9] K.M. Chugg, "Blind acquisition characteristics of PSP-based sequence detectors", *IEEE Journal on Sel. Areas of Comm.*, vol. 16, pp. 1518–1529, Oct. 1998.

[10] K.M. Chugg and A. Polydoros, "On the existence and uniqueness of joint channel and data estimates", in *Proc. IEEE Int. Sym. Inf. Th.*, p. 402, 1995.

[11] G.D. Forney, "Maximum likelihood sequence estimation of digital sequences in the presence of intersymbol interference", *IEEE Trans. Inf. Theory*, vol. IT-18, pp. 363–378, May 1972.

[12] G.E. Bottomley and S. Chennakeshu, "Unification of MLSE receivers and extension to time-varying channels", *IEEE Trans. Comm.*, vol. 46, pp. 464–472, Apr. 1998.

[13] E. Eleftheriou and D.D. Falconer, "Tracking properties and steady-state performance of RLS adaptive filter algorithms", *IEEE Trans. Acoustics, Speech and Sig. Proc.*, vol. ASSP-34, pp. 1097–1109, Oct. 1986.

[14] K.J. Molnar, G.E. Bottomley, and R. Ramesh, "A novel fractionally-spaced MLSE receiver and channel tracking with side information", in *Proc. IEEE VTC*, May 1998.

[15] G. Ungerboeck, "Adaptive maximum-likelihood receiver for carrier-modulated data transmission systems", *IEEE Trans. Comm.*, vol. COM-22, pp. 624–636, May 1974.

APPENDIX

Here we derive a receiver that finds the sequence $\underline{\hat{a}}_N$ which maximizes the likelihood of the received signal $y(t)$, given that $\underline{\hat{a}}_N$ was transmitted. This is equivalent to maximizing the log-likelihood function derived from the *a posteriori* distribution of the received signal, assuming equally probable transmitted symbols. Ignoring constant scaling factors and additive terms [15], the log-likelihood function reduces to

$$\Lambda_H = -\int_{t \in I} \left| y(t) - \sum_{k=1}^{K} \sum_{n=1}^{N} \hat{a}_{k,n} h_k(t - nT; t) \right|^2 dt, \tag{9}$$

where I is the finite time interval over which $y(t)$ is collected [15] and H is the hypothesis corresponding to the sequence $\underline{\hat{a}}_N$. The composite channel for user k is denoted as $h_k(\tau, t)$, and is equal to

$$h_k(\tau, t) = \sum_{l} c_{k,l}(t) f(\tau - \tau_k - lT/Q), \tag{10}$$

where Q is an integer chosen s.t. the signal bandwidth is less than $Q/2T$. Following the development in [12], the log-likelihood function Λ_H can be expanded as

$$\Lambda_H = A + B_H + C_H, \tag{11}$$

where

$$A = -\int_{t \in I} |y(t)|^2 dt, \tag{12}$$

$$B_H = \int_{t \in I} 2\mathrm{Re}\left\{ \sum_{k=1}^{K} \sum_{n=1}^{N} \hat{a}_{k,n}^* h_k^*(t - nT; t) y(t) \right\} dt, \tag{13}$$

and

$$C_H = -\int_{t \in I} \sum_{k=1}^{K} \sum_{n=1}^{N} \tag{14}$$

$$\sum_{l=1}^{K} \sum_{m=1}^{N} \hat{a}_{k,n}^* \hat{a}_{l,m} h_k^*(t - nT; t) h_l(t - mT; t) dt.$$

Term A can be omitted and

$$B_H = \sum_{n=1}^{N} 2\mathrm{Re}\left\{ \sum_{k=1}^{K} \hat{a}_{k,n}^* z_{k,n} \right\}, \tag{15}$$

where

$$z_{k,n} = \sum_{l} c_{k,l}^*(nT + lT/Q + \tau_k) r(nT + lT/Q + \tau_k), \tag{16}$$

$r(t) = f^*(-t) * y(t)$, and the medium response $c_{k,l}(t)$ is approximated as constant for the duration of the pulse shaping filter $f(t)$.

Term C_H can be written as

$$C_H = -\sum_{k=1}^{K} \sum_{n=1}^{N} \sum_{l=1}^{K} \sum_{m=1}^{N} \hat{a}_{k,n}^* \hat{a}_{l,m} s_{k,l;n,m}, \tag{17}$$

where

$$s_{k,l;n,m} = \tag{18}$$

$$\int_{t+mT \in I} h_k^*(t - (n-m)T; t + mT) h_l(t; t + mT) dt.$$

The RHS in (17) can be expanded using the fact that $s_{k,l;n,m} = s_{l,k;m,n}^*$. Combining the terms B_H and C_H, the log-likelihood metric can be expressed as

$$\Lambda_H = \sum_{n=1}^{N} \sum_{k=1}^{K} \mathrm{Re}\{\hat{a}_{k,n}^* \tag{19}$$

$$(2z_{k,n} - \hat{a}_{k,n} s_{k,k;n,n} - 2 \sum_{l<k} \sum_{m<n} \hat{a}_{l,m} s_{k,l;n,m})\}.$$

The sequence that maximizes this metric can be determined by using the Viterbi algorithm.

ABSTRACT

Trellis and Tree Search Algorithms for Equalization and Multiuser Detection

by

Abdulrauf Hafeez

Chair: Wayne E. Stark

This thesis deals with the detection of digital signals in the presence of inter-symbol interference (ISI) and/or multiple-access interference. We develop a new fractional maximum likelihood sequence estimation (MLSE) receiver which is suitable for wireless communication systems with excess signal bandwidth and fast time-varying channels. We investigate the effect of the receive filter and the branch metric on decision feedback sequence estimation (DFSE) and M-algorithm receivers, which are reduced-complexity alternatives to MLSE. The analysis leads to the classification of these receivers on the basis of the presence of untreated interference components, referred to as bias, which dominate the error-rate performance of the receiver. Bias arises in a DFSE or M-algorithm receiver due to a mismatch between the receive filter and the branch metric. We show that an unbiased receiver comprises a front-end filter matched to the overall channel or the transmit filter response followed by the appropriate noise-whitening or zero-forcing filter and a reduced trellis or tree search algorithm. Receivers with just a matched filter followed by a reduced trellis or tree search algorithm belong to the class of biased receivers.

We compare various trellis-based receivers on the basis of the distance of a given error sequence, which characterizes the probability of the associated error event. We show that whitening filter DFSE receivers maximize the error distance among unbiased DFSE receivers and truncated-memory MLSE receivers with pre-filtering. For matched filter DFSE

receivers, we describe bias compensation methods employing hard as well as soft tentative decisions, which significantly enhance performance in most cases without adding much complexity. Union bounds on the error probability of the various receivers are derived and evaluated using a modified generating function approach.

We derive an optimum forward-recursive soft-output algorithm which operates on the standard matched filter statistics and has complexity that grows exponentially with the channel memory only. We also derive a reduced-state soft-output algorithm which provides good symbol reliability estimates with reduced complexity. The performance of the various algorithms is compared for equalization of ISI and multiuser detection for direct-sequence code-division multiple-access systems via simulation and analytical examples.

To my dear parents, aunts, uncles and siblings.

ACKNOWLEDGEMENTS

TABLE OF CONTENTS

LIST OF TABLES

LIST OF FIGURES

LIST OF APPENDICES

CHAPTER 1

Introduction

Bandwidth efficient data transmission over wireline and wireless channels is made possible by the use of equalization techniques to compensate for the inter-symbol interference (ISI) introduced by the channel. In wireline channels like telephone lines, time dispersion results from non-ideal amplitude and phase characteristics of the medium and causes adjacent transmitted pulses to interfere with each other. In radio and undersea channels, the signal traverses several paths with differing amplitude and delay responses to reach the receiver. This phenomenon, known as multipath propagation, causes ISI. The problem of ISI also occurs in magnetic and optical recording channels due to non-ideal characteristics of the inductive read head. The medium is not always responsible for causing ISI. Bandwidth efficient design of signals, known as partial-response signaling, generally introduces controlled ISI to enable high-rate transmission.

Many wireline and wireless communication systems suffer from the impairment of multiple-access interference (MAI) in varying degrees. In code-division multiple-access (CDMA) systems, users share a common physical channel to transmit/receive non-orthogonal signals which interfere with each other. In hybrid time-division multiple-access/frequency-division multiple-access (TDMA/FDMA) systems, users reusing the frequency of the desired user in nearby cells cause co-channel interference. In twisted-pair local subscriber lines, crosstalk between users occurs due to the coupling of signals in adjacent wires. The problem of MAI can be alleviated by means of a multiuser detection technique. Such techniques have gained popularity especially in the case of direct-sequence CDMA (DS-CDMA) systems and are being considered for the next generation wireless systems as a key to improve capacity. Co-channel interference cancellation techniques are also being considered for the TDMA/FDMA

1

system based on the digital advanced mobile phone system (D-AMPS) standard.

The mitigation of ISI has been a prolific area of research for several decades [34]. Several techniques have been developed for equalization of ISI for pulse-amplitude modulated (PAM) systems which have been adopted for related problems, including MAI suppression. Maximum likelihood sequence estimation (MLSE) [6,13,22,40,43] is an optimal detection technique for channels with memory and additive noise. It minimizes the probability of sequence error for *a-priori* equiprobable sequences. The technique was first proposed by Forney [13] for optimum equalization of linear finite ISI channels with additive white Gaussian noise (AWGN). Later, other authors discovered applications of the MLSE algorithm to related problems. Verdú [43] derived an optimum multiuser detector for DS-CDMA systems by noting that the MAI in a DS-CDMA system can be viewed as cyclo-stationary ISI in a single-user system. The detector finds the joint maximum likelihood sequence of symbols for all users.

Maximum *a-posteriori* symbol-by-symbol detection (MAPSSD) is an optimal detection technique for channels with memory and additive noise which minimizes the probability of symbol error [1,3,23,28,42]. Conventional implementation of a MAPSSD receiver, compared to an MLSE receiver, has the added benefit of obtaining symbol *a-posteriori* probabilities (APP) which are useful for concatenated systems. Central to an MLSE (MAPSSD) receiver is a non-linear processor called the Viterbi algorithm (optimum soft-output algorithm). For a channel with delay response with finite length L (measured in symbol periods) and input alphabet size $\mathcal{A}$, the Viterbi algorithm employs a trellis with $\mathcal{A}^L$ states or nodes. The size of the trellis and the computational complexity of the algorithm become prohibitive if the channel has a long delay response. The algorithm can not be implemented for channels with infinite delay response. The same is true for an optimum soft-output algorithm (OSA). Thus, several low-complexity linear and non-linear techniques have been considered for equalization [34] as well as for multiuser detection [44]. Some of the most powerful complexity reduction techniques are non-linear techniques which are derived from an MLSE or MAPSSD receiver. These include decision feedback sequence estimation (DFSE) [7,8,10,11,17,19,20,39,50], truncated memory MLSE (TM-MLSE) [12,26,35,49], the M-algorithm [2,48,51] and Bayesian conditional decision feedback estimation (BCDFE) [18,25]. This thesis deals with analysis and derivation of MLSE and MAPSSD receivers and some of their most prominent reduced-complexity derivatives. New techniques are de-

2

veloped for applications in equalization and multiuser detection. Existing techniques are compared to each other and to the new techniques via analysis and simulation. Most work in this thesis is focussed on MLSE and related receiver structures. For this purpose, Chapter 2 sets up the system models for a single-user ISI system and a multiuser DS-CDMA system and describes optimum equalization and multiuser detection methods based on the MLSE technique. The notation developed there is followed throughout the thesis.

In wireless communication systems, the channel is generally considered as comprising a time-invariant transmit pulse-shaping filter and a time-varying and dispersive transmission medium. Forney's MLSE receiver comprises a front-end filter matched to the overall channel impulse response (the standard matched filter), followed by a symbol-rate sampler and a discrete-time noise-whitening filter to whiten the filtered noise affecting the statistics. The Viterbi algorithm operates on the whitened statistics to search for the most likely sequence transmitted using the Euclidean distance metric. Ungerboeck [40] derived an alternative MLSE formulation where the Viterbi algorithm operates directly on the statistics obtained after standard matched filtering, using a modified metric. In a time-varying environment, both receivers require an adaptive front-end filter which is not desirable for implementation purposes. Moreover, if the signal bandwidth is greater than the data rate, sampling at the symbol rate results in high sensitivity to the sampler timing phase [34]. Many narrowband communication systems utilize excess signal bandwidth. To handle these problems, Hamied et al. [22] proposed a receiver with a non-adaptive front-end filter matched to the transmit filter response (transmit matched filter), followed by a fractional-rate sampler and a fixed noise-whitening filter. However, due to the presence of nulls in the Nyquist band of practical pulse-shaping filters like the square-root raised cosine filter, the noise-whitening filter has a long slowly-damped delay response and any practical length truncation results in significant distortion. In Chapter 3, we derive a new fractional MLSE receiver that does not need a noise-whitening filter. The receiver is insensitive to the sampler timing phase. It exploits the knowledge of the pulse-shaping filter at the receiver and requires only one-step prediction for the medium response coefficients. These features make the receiver attractive for systems with excess signal bandwidth and fast time-varying media.

DFSE and TM-MLSE are trellis-based techniques where the complexity is controlled by reducing the memory of the trellis in the Viterbi algorithm. On the other hand, the M-algorithm is a tree-based technique where the complexity is reduced by pruning the tree

3

(representing sequence hypotheses) to maintain a given number of branches at each step. In TM-MLSE [12,35], the tail of the delay response of the channel is canceled by means of linear pre-filtering. In DFSE [7,8] and the M-algorithm [2], the tail of the delay response is canceled by feeding back past decisions taken from survivor paths in the trellis or tree. This manner of conditional decision feedback has been shown to alleviate the problem of error propagation that limits the conventional decision feedback equalizers. DFSE and M-algorithm receivers have been proposed to operate with whitened as well as standard matched filter statistics. It has been noted that the receive filter has a profound influence on the performance of these receivers [37,48,50]. However, this effect has not been quantified and understood.

In Chapter 4, we examine the effect of the receive filter and the branch metric on a generalized receiver comprising a front-end filter followed by a general transversal processing filter and a reduced trellis or tree search algorithm with conditional decision feedback. We consider two different formulations for the branch metric — in one case the front-end filter is the standard matched filter while in the other case, it is the transmit matched filter. The latter formulation is desirable for fractional equalization in the presence of excess signal bandwidth. A first error event analysis of the generalized receiver indicates that a proper combination of the processing filter and the branch metric is necessary to avoid *bias* (untreated interference components). The presence of bias severely limits the error-rate performance of a DFSE or M-algorithm receiver for most channels of interest. The various receivers are thus classified as biased and unbiased. Bias occurs in a DFSE or M-algorithm receiver due to a mismatch between the processing filter and the branch metric. We show that the processing filter must either be the appropriate noise-whitening filter (WF) or the zero-forcing filter (ZF) in order to achieve unbiasedness. Thus, the well-known DFSE and M-algorithm receivers with the whitening filter (WF-DFSE and WF-MA, respectively) belong to the class of unbiased receivers, while the receivers with just the matched filter (MF-DFSE and MF-MA) belong to the class of biased receivers.

The error-rate performance of the various DFSE and TM-MLSE receivers can be characterized by a parameter called the *error distance*. The error distance, in our case, does not merely mean the distance between two hypothesized signal sequences as in Forney [13], but it also includes the effect of noise enhancement. The distance of a given error sequence for a DFSE receiver depends on the type of filtering and the branch metric. The distance is max-

imized by the MF-DFSE receiver with the standard matched filter, while it is smaller for WF-DFSE and ZF-DFSE. This is due to the fact that the standard matched filter maximizes the output signal-to-noise ratio (SNR) by collecting all the energy of the pulse transmitted at a given time in the corresponding output sample. The noise-whitening filter spreads out the signal energy into several output samples in the process of whitening noise. The linear zero-forcing filter decorrelates all interfering signal components but enhances (and correlates) noise in the process. The reduced trellis-search algorithms which follow these filters recover part of the SNR that is spread out but are unable to recover all of it. Unfortunately, the drawback of MF-DFSE is that the reduced trellis search algorithm, in this case, is unable to resolve some anti-causal interfering signal components which generally dominate the error performance. Since the noise-whitening filter removes only the anti-causal signal components, which is necessary for unbiasedness, it maximizes the error distance among unbiased DFSE receivers. ZF-DFSE and TM-MLSE perform additional signal decorrelation and have lower error distance and thus inferior error-rate performance than WF-DFSE. The analysis ignores the effect of error propagation on DFSE receivers which, however, is small for most channels of interest. We obtain upper bounds on the symbol error probability of the various trellis based receivers assuming no error propagation and describe a generating function method to evaluate the union bounds.

Despite the unbiasedness and excellent error distance properties of WF-DFSE, its applicability is limited by the requirement of the noise-whitening filter. In applications where the noise at the output of the front-end filter is white, the algorithm can be employed without noise-whitening. However, the error performance in this case is highly sensitive to channel phase. While the best performance is obtained if the channel has minimum-phase, the performance may be rather poor if the channel has maximum or mixed phase. An all-pass filter is needed to get the minimum-phase channel. Computation of the additional processing filter requires channel inversion and/or factorization operations. This may not be desirable for applications involving time-varying channels and channels with deep spectral nulls. MF-DFSE is suitable for such applications. However, its performance is severely limited by the presence of bias as described earlier.

An intuitive solution to the problem of anti-causal interference components in MF-DFSE is to cancel them by means of tentative decision feedback. This results in bias-compensated MF-DFSE (BC-MF-DFSE) receivers which are described and analyzed in

Chapter 5. With reliable tentative decisions, the bias can be compensated effectively. As a result, the performance is no longer dominated by untreated interference components but rather by the excellent error distance. Tentative decisions can be obtained by using a decision device which delivers hard or soft decisions based on just the current input sample or by using a multistage configuration. Linear and non-linear minimum mean square error estimates of the symbols are considered as soft decisions. We obtain approximate upper bounds on the error probability for the various BC-MF-DFSE receiver configurations and describe a generating function technique to evaluate the bounds. Using several simulation and analytical examples, we find that a MF-DFSE receiver with soft bias compensation (SBC-MF-DFSE) provides a significant gain over MF-DFSE for most channels of interest without much added complexity. The receiver is particularly suitable for multiuser detection in DS-CDMA systems and performs quite well in near-far conditions.

Chapter 6 deals with soft-output algorithms. The optimum soft-output algorithm (OSA) of Li *et al.* [28] has complexity which grows exponentially with the channel memory and linearly with the decision lag. The algorithm operates on discrete-time statistics containing white noise. The algorithm of Hayes *et al.* [23] operates on the standard matched filter statistics but has complexity which is exponential in the decision lag. The optimum soft-output multiuser estimation algorithm of Verdú [42] requires a backward-forward recursion, due to which it has high latency. We derive an optimum soft-output algorithm with a forward-only-recursion which operates on the standard matched filter statistics. The algorithm has complexity similar to the OSA of Li *et al.*. We derive a reduced-complexity sub-optimal version of this algorithm which requires add-compare-select operations mostly. We also derive a reduced-state alternative to the OSA algorithm. The algorithm is obtained by modifying the algorithm of Lee *et al.* [25] which fails to generate reliable soft information. The complexity of the various algorithms is tabulated. The error-rate performance of the various algorithms is compared via simulation of a DS-CDMA system with convolutional coding and interleaving.

The thesis is organized as follows. In Chapter 2, we describe the system models for a single-user system with ISI and a multiuser DS-CDMA system. We describe optimum equalization and joint equalization/multiuser detection techniques for time-varying transmission media. In Chapter 3, we develop a new fractional MLSE receiver for systems with excess signal bandwidth and discuss its merits compared to other receivers. Chapter 4 deals

6

with analysis, classification and comparison of reduced trellis and tree search algorithms. In Chapter 5, we describe bias-compensation for matched-filter type receivers and compare the performance of the various receivers via simulation and approximate bounds which are obtained in this chapter. In Chapter 6, we derive novel soft-output algorithms and compare their performance via simulation. Conclusions are drawn and future work is discussed in Chapter 7.

CHAPTER 2

Optimum equalization and multiuser detection

2.1 Introduction

Maximum-likelihood sequence estimation (MLSE) is an optimum detection technique for signals corrupted with intersymbol interference (ISI) and additive white Gaussian noise (AWGN). The technique minimizes the probability of sequence error for *a priori* equiprobable sequences. Forney [13] provided the first MLSE formulation by noting the application of the Viterbi algorithm to equalization over a known time-dispersive, linear and time-invariant channel. Forney's formulation employs a filter matched to the overall channel impulse response (the standard matched filter) followed by a discrete-time noise-whitening filter[1] to produce discrete-time sufficient statistics which are processed by the Viterbi algorithm. Ungerboeck [40] later derived an alternative MLSE formulation which consists of just the standard matched filter and the Viterbi algorithm with a modified metric. The latter formulation was extended for the case of known time-varying channels by Bottomley *et al.* [6]. Verdú [43] derived an optimum multiuser detector for direct-sequence code-division multiple-access (DS-CDMA) channels with AWGN. The detector finds the joint maximum likelihood sequence of symbols for all users transmitted asynchronously over a common channel. Verdu's multiuser receiver is really an extension of Ungerboeck's MLSE formulation to joint detection of multiuser signals.

In this chapter, we describe optimum receivers for single-user equalization and joint equalization/multiuser detection for DS-CDMA systems in a known time-varying environment. This chapter sets up the system models and notation which is followed throughout

---

[1]The cascade of the two filters is referred to as the whitened matched filter.

the thesis. The chapter is organized as follows. In Section 2.2, we present the model for a single-user system with ISI. In Section 2.3, we describe the functionality of an MLSE receiver. In Section 2.4, we re-derive the Ungerboeck-Bottomley formulation for time-varying channels. In Section 2.5, we describe the model for a multi-user DS-CDMA system. In Section 2.6, we obtain an optimum receiver for joint equalization/multiuser detection as an extension of the Ungerboeck-Bottomley formulation.

2.2 System model

Consider the transmission of linearly-modulated digital data over a linear, time-dispersive medium. The system model consists of a transmitter, a linear time-varying transmission medium and a receiver. The baseband transmitted signal is modeled as

$$s_t(t) = \sum_{n=0}^{N-1} a_n d(t - nT) \tag{2.1}$$

where $d(t)$ is the impulse response of the transmit filter and $\{a_n\}_{n=0}^{N-1}$ is a finite sequence of complex symbols (taken from a finite alphabet $\mathcal{A}$). The radio signal transmitted propagates through the medium to reach the receiver where it is converted to a complex-valued, baseband signal $y(t)$, given by

$$\begin{aligned} y(t) &= g(\tau; t) * s_t(t) + w(t) \\ &= \int g(t - \lambda; t) s_t(\lambda) d\lambda + w(t) \end{aligned} \tag{2.2}$$

where $g(\tau; t)$ is the output of the transmission medium at time t when an impulse is applied at time $t - \tau$ and $w(t)$ is a complex white Gaussian noise process with power spectral density N_0. Substituting (2.1) in (2.2), we get

$$y(t) = \sum_{n=0}^{N-1} a_n h(t - nT; t) + w(t) \tag{2.3}$$

where $h(\tau; t)$ models the overall response of the transmit filter and the transmission medium and is given by

$$h(\tau; t) = \int g(\tau - \lambda; t) d(\lambda) d\lambda. \tag{2.4}$$

The received signal $y(t)$ is collected over a finite time interval, denoted I, which is much larger than $[0, (N - 1)T]$. The response $h(\tau; t)$ is assumed to be square integrable over the

interval I, i.e.

$$\int_{-\infty}^{\infty} |h(\tau;t)|^2 d\tau < \infty \quad \text{for } t \in I. \tag{2.5}$$

2.3 Maximum likelihood sequence estimation

A maximum likelihood sequence estimation (MLSE) receiver finds the hypothetical sequence of symbols $\{\alpha_n\}$ ($\alpha_n \in \mathcal{A}$) that maximizes the likelihood of the received signal $y(t)$ given that $\{\alpha_n\}$ was transmitted. Assuming equiprobable symbols, an MLSE receiver maximizes the log-likelihood function derived from the *a posteriori* distribution of the received signal. Ignoring constant scaling factors and additive terms, the log-likelihood function reduces to

$$J_H = -\int_{t \in I} |y(t) - y_H(t)|^2 \, dt = -\int_{t \in I} \left| y(t) - \sum_{n=0}^{N-1} \alpha_n h(t - nT; t) \right|^2 dt, \tag{2.6}$$

where H is the hypothesis corresponding to the sequence $\{\alpha_n\}$. It is assumed that $y(t)$ is band-limited in the receiver front end, using a bandwidth larger than the signal bandwidth, so that the integral in (2.6) is well defined.

2.4 The Ungerboeck-Bottomley formulation

In this section, we re-derive an MLSE formulation following the development of Bottomley *et al.* [6]. The receiver is an extension of Ungerboeck's MLSE formulation [40] to time-varying channels.

The log-likelihood function J_H can be expanded as

$$J_H = A + B_H + C_H, \tag{2.7}$$

where

$$A = -\int_{t \in I} |y(t)|^2 dt, \tag{2.8}$$

$$B_H = \int_{t \in I} 2\mathrm{Re} \left\{ \sum_{n=0}^{N-1} \alpha_n^* h^*(t - nT; t) y(t) \right\} dt, \tag{2.9}$$

$$C_H = -\int_{t \in I} \sum_{n=0}^{N-1} \sum_{k=0}^{N-1} \alpha_n^* \alpha_k h^*(t - nT; t) h(t - kT; t) dt. \tag{2.10}$$

10

Since term A is independent of the sequence hypothesis, an MLSE receiver chooses the sequence hypothesis that maximizes the metric

$$\Lambda_H = B_H + C_H. \tag{2.11}$$

Terms B_H and C_H can be written as

$$B_H = \sum_{n=0}^{N-1} 2\text{Re}\left\{\alpha_n^* z(n)\right\}, \tag{2.12}$$

$$C_H = -\sum_{n=0}^{N-1}\sum_{k=0}^{N-1} \alpha_n^* \alpha_k s(n-k; n), \tag{2.13}$$

where $\{z(n)\}_{n=0}^{N-1}$ is the sequence of symbol-spaced samples obtained at the output of a receive filter matched to the channel impulse response $h(\tau; t)$, as

$$z(n) = h^*(-\tau; t-\tau) * y(t)|_{t=nT} = \int_{t \in I} h^*(t - nT; t) y(t) dt \tag{2.14}$$

and the s parameter is the sampled channel autocorrelation function, given by

$$s(l; n) = \int_{t \in I} h^*(t - nT; t) h(t - (n-l)T; t) dt \tag{2.15}$$

where $n \in \{0, 1, \ldots, N-1\}$ and $l \in \{0, \pm 1, \ldots, \pm(N-1)\}$. Noting that $s^*(k-n; k) = s(n-k; n)$ and using the following identity for multi-dimensional summation

$$\sum_{n=i}^{f}\sum_{k=i}^{f} x(n,k) = \sum_{n=i}^{f}\left[x(n,n) + \sum_{k=i}^{n-1}\left(x(n,k) + x(k,n)\right)\right], \tag{2.16}$$

the term C_H can be expanded as

$$C_H = -\sum_{n=0}^{N-1}\left[\alpha_n^* \alpha_n s(0; n) - \sum_{k=0}^{n-1} 2\text{Re}\{\alpha_n^* \alpha_k s(n-k; n)\}\right]. \tag{2.17}$$

Substituting (2.12) and (2.17) into (2.11) and letting L be the smallest integer such that $s(l; n) = 0$ for $|l| > L$, we get the metric as

$$\Lambda_H = \sum_{n=0}^{N-1} \Gamma_n(\alpha_n, \sigma_n) \tag{2.18}$$

where σ_n represents the subsequence hypothesis $\sigma_n : \alpha_{n-1}, \alpha_{n-2}, \ldots, \alpha_{n-L}$ and $\Gamma_n(\alpha_n, \sigma_n)$ is the branch metric, given by

$$\Gamma_n(\alpha_n, \sigma_n) = \text{Re}\left\{\alpha_n^*\left[2z(n) - s(0; n)\alpha_n - 2\sum_{l=1}^{L} s(l; n)\alpha_{n-l}\right]\right\}. \tag{2.19}$$

11

The receiver can be implemented as shown in Fig. 2.1. The front-end filter in the receiver is matched to the overall channel response $h(\tau;t)$. The Viterbi algorithm in Fig. 2.1 finds the sequence $\{a_n\}$ that maximizes the metric of (2.18). It does so by computing recursively the accumulated metric defined as

$$\mathcal{M}_n(\sigma_n) \triangleq \max_{\alpha_1,\alpha_2,\ldots,\alpha_{n-L-1}} \sum_{i=0}^{n-1} \Gamma_n(\alpha_i,\sigma_i) \tag{2.20}$$

for all subsequence hypotheses (or states) σ_n. The recursion follows from (2.19) and (2.20) as

$$\mathcal{M}_n(\sigma_{n+1}) = \max_{\alpha_{n-L}} \left[\mathcal{M}_n(\sigma_n) + \Gamma_n(\alpha_n,\sigma_n) \right]. \tag{2.21}$$

The number of states in the Viterbi algorithm is $|\mathcal{A}|^L$, where $|\mathcal{A}|$ is the size of the input alphabet and L is the overall channel memory in symbols (assumed finite). The output of the Viterbi algorithm is the estimated sequence $\{\hat{a}_n\}$.
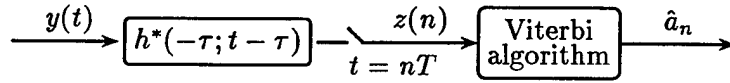
Figure 2.1: Ungerboeck-Bottomley receiver

2.5 Multiuser DS-CDMA system model

Consider a linear, time-dispersive channel shared by K users who transmit independent unsynchronized data streams by linearly modulating assigned signal waveforms. The system model consists of K transmitters, K independent time-varying and dispersive transmission media and one receiver. The baseband signal transmitted by user k is modeled as

$$s_{t,k}(t) = \sum_{m=0}^{N'-1} a_k(m) d_k(t - mT) \tag{2.22}$$

where $\{a_k(m)\}_{m=0}^{N'-1}$ is a finite sequence of complex symbols taken from a finite alphabet $\mathcal{A}$ (common to all users $k = 1,\ldots,K$). The filter $d_k(t)$ models the transmit filter for user k which, in general, includes a pulse-shaping filter common to all users and a signature waveform (spreading code) uniquely assigned to each user which may be pseudo-randomly

12

time-varying over the duration of several symbols (long code). The radio signal transmitted by each user propagates through a dispersive transmission medium to reach the receiver. The receiver sees the sum of the K signals in AWGN. The received signal is converted to a complex-valued, baseband signal $y(t)$, given by

$$y(t) = \sum_{k=1}^{K} g_k(\tau; t) * s_{t,k}(t - \tau_k) + w(t) \tag{2.23}$$

where $g_k(\tau; t)$ is the output of the transmission medium for user k at time t when an impulse is applied at time $t - \tau$, τ_k is the relative delay for user k and $w(t)$ is a complex white Gaussian noise process with power spectral density N_0. Substituting (2.22) into (2.23), we get

$$y(t) = \sum_{m=0}^{N'-1} \sum_{k=1}^{K} a_k(m) h_k(t - mT; t) + w(t) \tag{2.24}$$

where $h_k(\tau; t)$ models the overall response of the transmit filter and the transmission medium for user k and is given by

$$h_k(\tau; t) = \int g_k(\tau - \lambda; t) d_k(\lambda - \tau_k) d\lambda. \tag{2.25}$$

The above model accurately represents the uplink (mobile station to base station) of a DS-CDMA cell. The model can be simplified for the downlink (base station to mobile station) by considering synchronized user transmission over a single transmission medium.

From the viewpoint of joint multiuser detection/equalization, the multiuser system model of (2.24) can be represented equivalently in a single-user form as

$$y(t) = \sum_{n=0}^{N-1} a_{\kappa(n)}(\eta(n)) h_{\kappa(n)}(t - \eta(n)T; t) + w(t) \tag{2.26}$$

where $\kappa(n)$ and $\eta(n)$ represent the user index and the time index respectively and are given by

$$\kappa(n) = (n \bmod K) + 1 \tag{2.27}$$

$$\eta(n) = \left\lfloor \frac{n}{K} \right\rfloor \tag{2.28}$$

and $N = N'K$ is the length of the combined data stream of all users $\{a_{\kappa(n)}(\eta(n))\}_{n=0}^{N-1}$ which is ordered in increasing user and time indices assuming $\tau_k < \tau_{k+1}$ $\forall k$, without loss of generality . Henceforth, we will use the notation $\{a_n\}_{n=0}^{N-1}$ for the combined data sequence of all users for brevity.

13

Note that the above model has the same form as the single-user model of Section 2.2. This allows us to provide a unified treatment for problems of single-user equalization and multiuser detection. Throughout this thesis, we will consider receivers for single-user equalization which also find applications in multiuser detection. A special mention will be made where different considerations apply.

2.6 Joint equalization/multiuser detection

Noting the similarity between the multiuser system model of (2.26) and the single-user model of (2.3), it can be seen that a receiver that performs joint equalization and multiuser detection for DS-CDMA systems has the form of the Ungerboeck-Bottomley receiver of Section 2.4. The receiver is shown in Fig. 2.2. It consists of a bank of filters each of which is matched to the overall channel impulse response of a user. The sequence of joint statistics obtained at the output of the bank of filters is given by

$$z(n) = h_{\kappa(n)}^*(-\tau; t - \tau) * y(t)\Big|_{t=\eta(n)T} = \int_{t \in I} h_{\kappa(n)}^*(t - \eta(n)T; t)y(t)dt. \qquad (2.29)$$

The receiver processes the joint sequence of matched filter statistics using the Viterbi algorithm which hypothesizes the symbols of all users jointly using the recursion of (2.21), where the branch metric is given by (2.19). The sampled channel autocorrelation function in this case is given by

$$s(l; n) = \int_{t \in I} h_{\kappa(n)}^*(t - \eta(n)T; t)h_{\kappa(n-l)}(t - \eta(n - l)T; t)dt. \qquad (2.30)$$

The receiver is a generalization of Verdu's optimum multiuser detector [43] to linearly dispersive and time-varying transmission media. Note that the number of states in the Viterbi algorithm is $|\mathcal{A}|^L$, where the memory L is defined as the smallest integer such that $s(l; n)$ (given by (2.30)) equals zero for $|l| > L$. For non-dispersive media, $L = K - 1$, while for dispersive (frequency-selective) media, $L > K - 1$.

For the case of non-dispersive and time-invariant AWGN channels, a baseband asynchronous DS-CDMA system, with symbol-length (short) spreading codes and rectangular transmit pulses, is generally specified in terms of a code partial-correlation matrix polynomial known as the channel spectrum $S(D)$, given by

$$S(D) = S_1^T D^{-1} + S_0 + S_1 D \qquad (2.31)$$

14
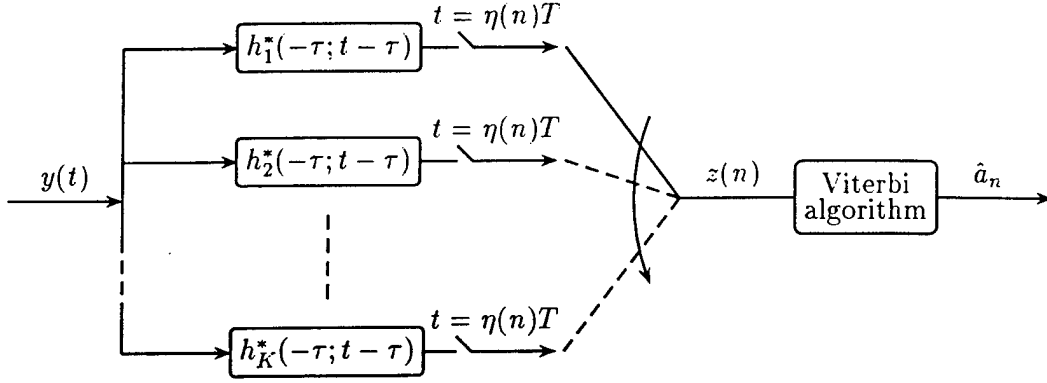
Figure 2.2: Multiuser receiver

where S_0 is a $K \times K$ Hermitian matrix and S_1 is a $K \times K$ upper-triangular matrix, assuming that the users are ordered in increasing delay. The element $S_0(i,j)$ of the matrix S_0 is the partial correlation of the code of user i with the code of user j for the current symbol period, i.e.

$$S_0(i,j) = \int d_i^*(t - \tau_i)d_j(t - \tau_j)dt. \tag{2.32}$$

The element $S_1(i,j)$ of the matrix S_1 is the partial correlation of the code of user i with the code of user j for the past symbol period, given by

$$S_1(i,j) = \int d_i^*(t - \tau_i)d_j(t - \tau_j + T)dt. \tag{2.33}$$

In this case, the normalized sampled channel correlations $\bar{s}(l;n) = s(l;n)/s(0;n)$ are given by

$$\bar{s}(l;n) = \begin{cases} S_1(\kappa(n), \kappa(n) - l + K) & \kappa(n) - l < 1 \\ S_0(\kappa(n), \kappa(n) - l) & 1 \leq \kappa(n) - l \leq K \\ S_1(\kappa(n) - l - K, \kappa(n)) & \kappa(n) - l > K \end{cases} \cdot \tag{2.34}$$

The memory of the multiuser channel is $K - 1$ and there is no ISI.

15

CHAPTER 3

Fractionally-spaced MLSE receivers

3.1 Introduction

In wireless communication systems, the channel is generally considered as comprising a time-invariant transmit (pulse-shaping) filter followed by a time-varying transmission medium. Forney and Ungerboeck's maximum-likelihood sequence estimation (MLSE) receivers [13,40] employ an analog front-end filter which is matched to the overall channel impulse response. If the transmission medium is time-varying or unknown at the receiver, the front-end filter has to be adaptive. This is not desirable for implementation purposes. Ungerboeck also described an adaptive receiver in [40] which uses a discrete-time transversal filter at the front end to synthesize matched filter characteristics. The receiver, however, does not take advantage of the fact that the transmit filter is generally known at the receiver and this information can be exploited to improve channel estimation.

Many wireless radio systems transmit signals with a bandwidth more than the data rate. Narrowband TDMA systems based on the IS-54/IS-136 and PDC standards employ 35% and 50% excess bandwidth, respectively. In the presence of excess signal bandwidth, fractional sampling is effective due to its insensitivity to the sampler timing phase [34]. Some authors [30,33] have considered using an analog front-end filter which is matched to the transmit filter response (transmit matched filter) followed by a fractional sampler. They, however, assume that the noise affecting the sampled statistics is white. The branch metric of the Viterbi algorithm ignores the correlation in the noise samples. As a result the performance improvement is marginal.

Hamied *et al.* [22] derived an MLSE receiver for systems that employ at most 100%

16

excess bandwidth. Their receiver employs a transmit matched filter followed by a fractional sampler and a fixed noise-whitening filter. The sequence of statistics thus obtained has white noise. However, we note that practical pulse-shaping filters like the square-root raised cosine filter have nulls in the Nyquist spectrum, due to which the noise-whitening filter has a long slowly-damped delay response. Any practical length truncation of the filter leads to severe distortion.

Following the development in [6], we derive an Ungerboeck-type receiver which does not need noise-whitening. The branch metric of the Viterbi algorithm accounts for the correlation in the noise samples affecting the fractionally sampled statistic obtained at the output of a transmit matched filter. An adaptive algorithm exploits the knowledge of the pulse-shaping filter and adapts just the fractionally-spaced medium response coefficients. However, the branch metric for the receiver depends on future medium response coefficients up to the span of the medium response. The prediction (adaptation) of these future coefficients using decision feedback would result in excess estimation error and thus degrade performance. We derive an alternative formulation for the branch metric which depends on causal medium response coefficients only. Thus, only one step prediction is needed to adapt the medium response coefficients. The receiver is suitable for systems with excess signal bandwidth and rapidly time-varying channels.

The chapter is organized as follows. In Section 3.2, we describe the channel model for a single-user system with excess signal bandwidth. A fractional Ungerboeck-type receiver is then derived in Section 3.3. In Section 3.4, we discuss the receiver of Hamied *et al.*. A new fractional MLSE receiver that does not need noise-whitening and minimizes channel prediction is described in Section 3.5.

3.2 Channel model

Consider the single-user system model of Section 2.2. If the baseband transmitted signal $s_t(t)$ has bandwidth $W \leq \nu/2T$, where ν is an integer, then an arbitrary medium response $g(\tau; t)$ can be modeled as a fractionally-spaced tapped delay line [41, pp. 488]

$$g(\tau; t) = \sum_j c(jT/\nu; t)\delta(\tau - jT/\nu) \tag{3.1}$$

where

$$c(jT/\nu; t) = c(j; t) = \int g(\tau; t) \mathrm{sinc} \left(\frac{\tau - jT/\nu}{T/\nu} \right) d\tau. \qquad (3.2)$$

Assuming that the medium response can be well-approximated by $L_c + 1$ fractionally-spaced taps (i.e. $c(j; t) = 0$ for $j > L_c$), the overall channel impulse response can be written as

$$h(\tau; t) = g(\tau; t) * d(\tau) = \sum_{j=0}^{L_c} c(j; t) d(\tau - jT/\nu). \qquad (3.3)$$

Typically, $\frac{1}{2} < WT < 1$ for full-response signaling and $WT < \frac{1}{2}$ for partial-response signaling (continuous phase modulation) used in narrowband mobile communication systems. Symbol-spaced channel models have been used to develop MLSE receivers [24, 38]. Symbol-spaced MLSE receivers yield close to optimum performance if the excess signal bandwidth (WT in excess of $\frac{1}{2}$) is small. However, the performance of these receivers is highly sensitive to the timing phase [22] in the presence of excess bandwidth. This is due to the inability of a symbol-spaced transversal filter to invert a null in the sampled signal spectrum without excessive noise enhancement [34]. Fractionally-spaced MLSE receivers, on the other hand, are insensitive to the timing phase as aliasing does not occur in the sampled signal spectrum in the case of a fractionally-spaced transversal filter.

3.3 A fractional Ungerboeck-type receiver

Adaptation of channel parameters is usually needed for an MLSE receiver on time-varying channels. Ungerboeck's adaptive receiver [40] consists of a fractionally-spaced transversal filter followed by a symbol-rate sampler and a Viterbi algorithm. The coefficients of the front-end filter and the sampled channel autocorrelation function 's' are adapted using a stochastic steepest descent algorithm. The s parameters are needed to compute the branch metric (2.19) in the Viterbi algorithm. Note that the s parameters depend on the transmit filter response and the medium response. Since the transmit filter response is known at the receiver, channel estimation can be improved by adapting the medium response coefficients directly instead of adapting the s parameters. The formulation of Section 2.4 can be modified for this purpose as shown in [6] for the case of symbol-spaced channel models.

Substituting (3.3) in (2.14) and (2.15), and assuming that the medium response coeffi-

cients $c(j:t)$ are fixed (time-invariant) over the span of the transmit filter response[1] $d(t)$, we get

$$z(n) \approx \sum_{j=0}^{L_c} c^* \left(j; n + \frac{j}{\nu} \right) Y \left(n + \frac{j}{\nu} \right),$$ (3.4)

$$s(l; n) \approx \sum_{j=0}^{L_c} \sum_{k=0}^{L_c} c^* \left(j; n + \frac{j}{\nu} \right) c \left(k; n - l + \frac{k}{\nu} \right) \phi(l\nu + j - k),$$ (3.5)

where the discrete-time medium response coefficients are defined as $c(j; i) = c(jT; iT)$ for values of i in multiples of T/ν and $\{Y(\cdot)\}$ is the sequence of fractionally-spaced samples obtained at the output of a receive filter matched to the transmit filter response $d(t)$, as

$$Y \left(n + \frac{j}{\nu} \right) = \int_{t \in I} d^* \left(t - \left(n + \frac{j}{\nu} \right) T \right) y(t) dt$$ (3.6)

and $\phi(i)$ is the fractionally-sampled autocorrelation function of the transmit filter, given by

$$\phi(i) = \int_{t \in I} d^*(t) d \left(t + \frac{iT}{\nu} \right) dt.$$ (3.7)
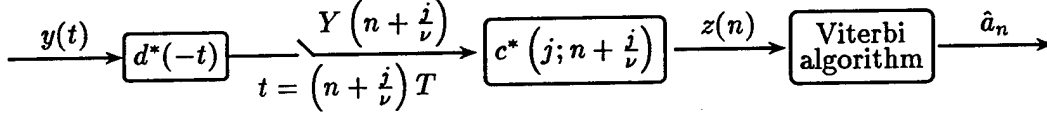
Figure 3.1: A fractional Ungerboeck-type receiver.

The receiver is shown in Fig. 3.1. It has a front-end filter matched to the transmit filter response $d(t)$, followed by a fractional-rate sampler. The fractionally-sampled statistic is filtered by an adaptive discrete-time filter and fed to a Viterbi algorithm. The Viterbi algorithm uses the branch metric of (2.19) with the s parameters given by (3.5). Note that the receiver in Fig. 3.1 has a fixed analog front-end filter unlike the receiver of Fig. 2.1, where the front-end filter is adaptive.

Note from (3.4) and (3.5), that the branch metric at time nT given by (2.19), depends on medium response coefficients for times up to $(n + L_c/\nu)T$. Thus, medium response coefficients have to be predicted (for $L_c + 1$ future steps) in the adaptive receiver of Fig. 3.1. The accuracy of prediction decreases in general with the number of steps over which prediction

---

[1]The assumption makes sense when the time variation in the channel coefficients $c(j; t)$ is slow relative to the span of the transmit filter.

is required. This makes the adaptive receiver of Fig. 3.1 unsuitable for channels with rapid time variation.

3.4 Hamied's fractional MLSE receiver

An alternative receiver is obtained by noting that the statistic given by (3.6) can also be expressed as

$$Y\left(n + \frac{j}{\nu}\right) = \sum_{i=0}^{L_c} c\left(i; n + \frac{j}{\nu}\right) \sum_{l=-L_d}^{L_d} \phi(l)a_{n+\frac{l-i-l}{\nu}} + v\left(n + \frac{j}{\nu}\right) \qquad (3.8)$$

where $\{v(\cdot)\}$ is a complex Gaussian noise sequence with autocorrelation

$$E\left[v\left(n + \frac{j}{\nu}\right)v^*\left(m + \frac{i}{\nu}\right)\right] = N_0\phi((n-m)\nu + j - i), \qquad (3.9)$$

$$a_{k/\nu} = \begin{cases} a_i & \text{if } k = i\nu, \ i \text{ is an integer} \\ 0 & \text{otherwise} \end{cases} \qquad (3.10)$$

and L_d is the smallest integer such that $\phi(i) = 0$ for $|i| > L_d$. Thus, it is assumed that the transmit filter has a finite impulse response. In practice, transmit pulse-shaping filters like the square-root raised cosine (SRRC) filter are truncated to a span of several symbols. Let the D-transform of the transmit filter autocorrelation function $\phi(n)$ (the sampled autocorrelation spectrum) be defined as

$$\Phi(D) = \sum_{n=-L_d}^{L_d} \phi(n)D^n \qquad (3.11)$$

where D stands for fractional symbol duration.

Hamied *et al.* [22] obtain an adaptive MLSE receiver by assuming that the statistic $\{Y(\cdot)\}$ obtained at the output of the front-end filter in Fig. 3.1 can be whitened by using a fixed noise-whitening filter. The noise-whitening filter is determined by factoring the sampled autocorrelation spectrum $\Phi(D)$ as

$$\Phi(D) = F'^*(D^{-1})F'(D). \qquad (3.12)$$

In case the transmit filter spectrum has no roots on the unit circle, the factor $F'(D) = \sum_{n=0}^{L_d} f'(n)D^n$ is chosen such that all its roots are outside the unit circle. The anti-causal noise-whitening filter is then given by $F'^*(D^{-1}))^{-1}$ which is stable in the sense that its coefficients are square summable.
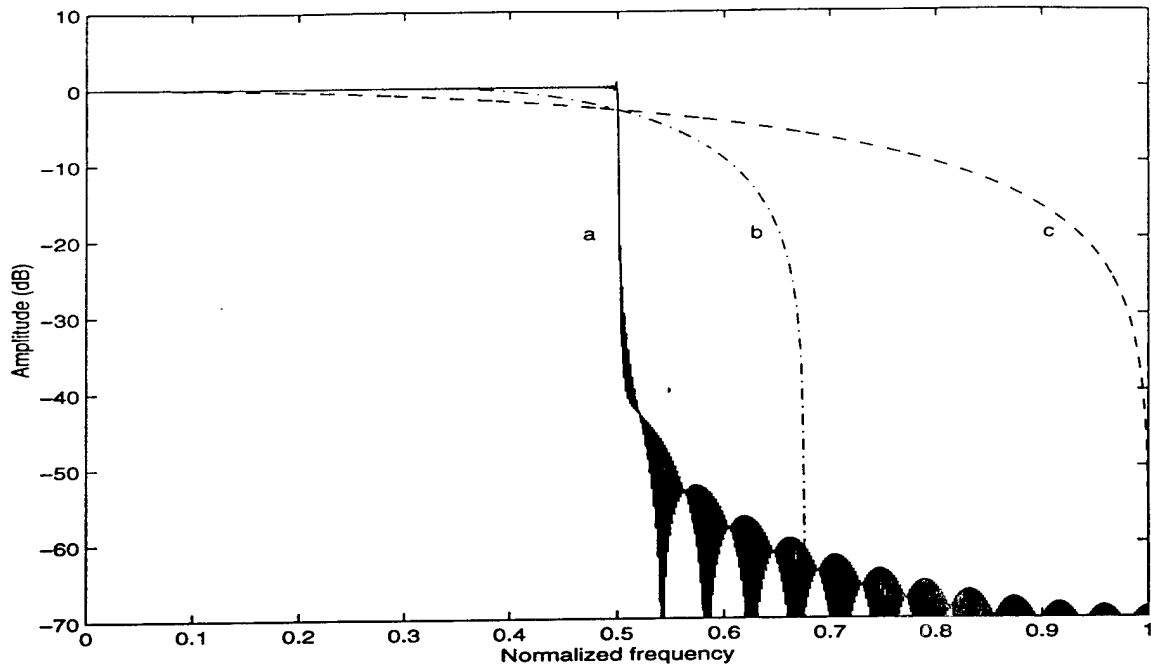
Figure 3.2: Sampled autocorrelation spectra for SRRC pulses truncated to 500 symbols (a) $\beta = 0$, (b) $\beta = 0.35$, (c) $\beta = 1$.
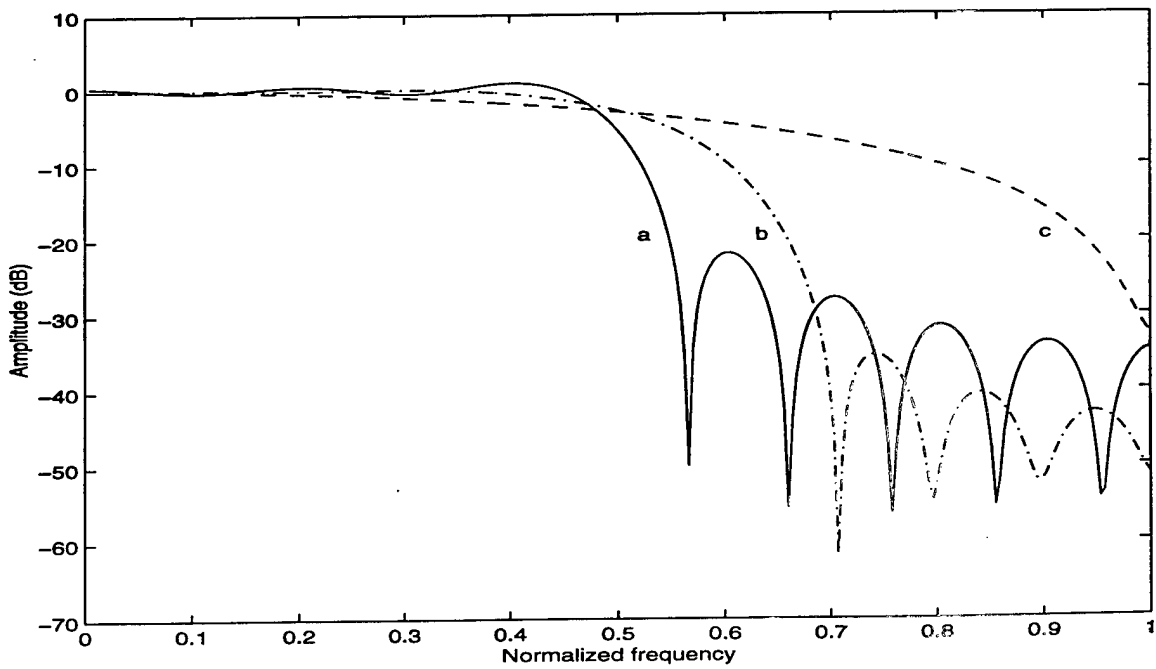
Figure 3.3: Sampled autocorrelation spectra for SRRC pulses truncated to 10 symbols (a) $\beta = 0$, (b) $\beta = 0.35$, (c) $\beta = 1$.

For many practical pulse-shaping filters like the SRRC filter, the sampled autocorrelation spectrum has zeros on the unit circle. This is illustrated in Fig. 3.2 which shows the amplitude of the sampled autocorrelation spectrum for SRRC pulses (truncated to a span of 500 symbols) with various roll-off factors. The spectrum exhibits nulls in the Nyquist bandwidth $1/T$ (corresponding to $\nu = 2$). This is true for all SRRC pulses with roll off factor $\beta \in [0, 1]$. The noise-whitening filter does not exist for these pulses as the nulls in the Nyquist band can not be inverted. Fig. 3.3 shows the sampled autocorrelation spectra for the same SRRC pulses but with a truncation of 10 symbols. Note that the nulls are less severe in this case. Strictly speaking, the noise-whitening filter exists for all practical finite-length transmit pulse-shaping filters. However, due to the presence of zeros near the unit circle, the noise-whitening filter has a long slowly-damped impulse response and any practical length truncation results in severe distortion. Fig. 3.4 shows the effect of truncation of the noise-whitening filter. The squared error resulting from truncation is given by

$$\|\hat{F}'(D) - F'(D)\|^2 \tag{3.13}$$

where $\hat{F}'(D)$ is the whitened channel spectrum obtained from using a truncated noise-whitening filter $\mathcal{W}(D^{-1})$ as $\hat{F}'(D) = \mathcal{W}(D^{-1})\Phi(D)$. Fig. 3.4 shows the squared error for the SRRC pulse of Fig. 3.3 (truncated to 10 symbols) with $\beta = 0.35$ and $\nu = 2$. Note that the squared error exhibits damped oscillations and is significant even with 500 taps of the noise-whitening filter (spanning 250 symbols). The error would increase with the length of the SRRC pulse because the nulls would be deeper as demonstrated in Fig. 3.2.

3.5 A new fractional MLSE receiver

In this section, we derive an alternative fractional MLSE receiver that does not require noise-whitening unlike the receiver of Hamied *et al.* [22]. Moreover, it does not require extra prediction for the medium response coefficients, unlike the Ungerboeck-type receiver of Fig. 3.1.

Substituting (3.4) into (2.12) and making a change of variables gives

$$B_H = \sum_{n=0}^{N-1} \sum_{m=0}^{\nu-1} 2\text{Re} \left\{ \sum_{j=0}^{L_c} \alpha^*_{n+\frac{m-j}{\nu}} c^* \left(j; n + \frac{m}{\nu} \right) Y \left(n + \frac{m}{\nu} \right) \right\}. \tag{3.14}$$
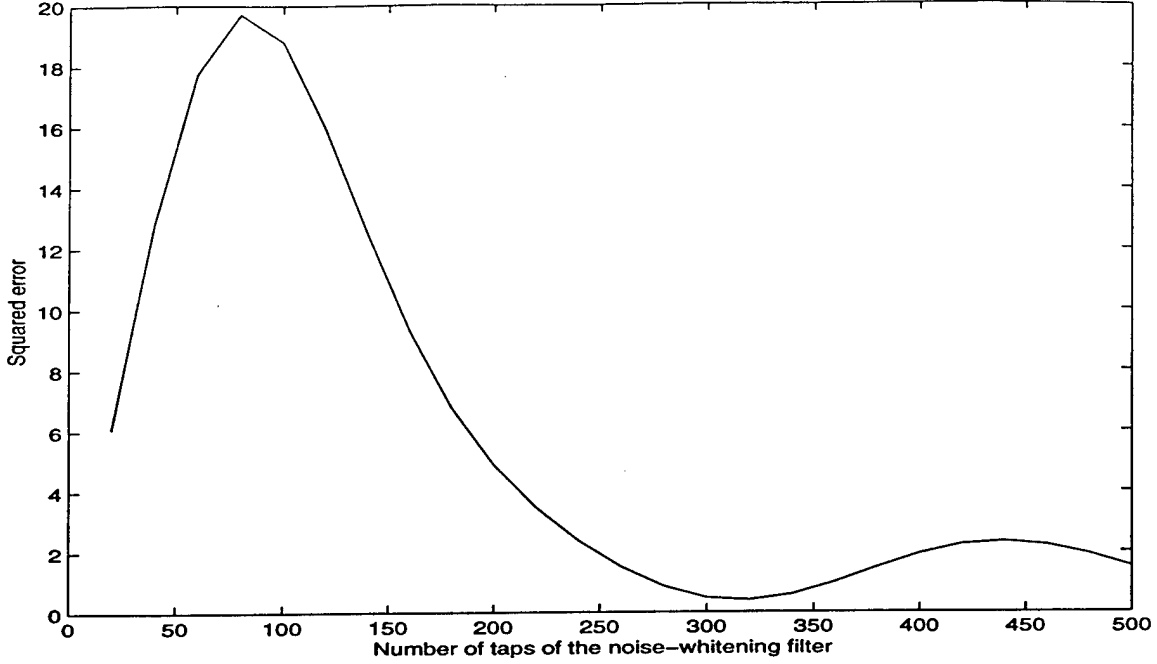
Figure 3.4: Squared error due to truncation of the noise-whitening filter for SRRC pulse truncated to 10 symbols with $\beta = 0.35$.

Substituting (3.5) into (2.13) and making a change of variables gives

$$C_H = - \sum_{n=0}^{(N-1)\nu} \sum_{j=0}^{L_c} \sum_{k=0}^{(N-1)\nu} \sum_{l=0}^{L_c} \alpha^*_{\frac{n-j}{\nu}} \alpha_{\frac{k-l}{\nu}} c^* \left(j; \frac{n}{\nu} \right) c \left(l; \frac{k}{\nu} \right) \phi(n - k). \qquad (3.15)$$

Using (2.16), C_H can be written as

$$C_H = - \sum_{n=0}^{N-1} \sum_{m=0}^{\nu-1} \sum_{j=0}^{L_c} \mathrm{Re} \left\{ c^* \left(j; n + \frac{m}{\nu} \right) \alpha^*_{n+\frac{m-j}{\nu}} \left[\phi(0) \sum_{l=0}^{L_c} c \left(l; n + \frac{m}{\nu} \right) \alpha_{n+\frac{m-l}{\nu}} \right. \right.$$

$$\left. \left. + \ 2 \sum_{i=1}^{L_d} \phi(i) \sum_{l=0}^{L_c} c \left(l; n + \frac{m - i}{\nu} \right) \alpha_{n+\frac{m-i-l}{\nu}} \right] \right\}. \qquad (3.16)$$

Thus, the metric Λ_H in (2.11) can be written as

$$\Lambda_H = \sum_{n=0}^{N-1} \Gamma'_n(\alpha_n, \sigma_n) \qquad (3.17)$$

where $\Gamma'_n(\alpha_n, \sigma_n)$ is the branch metric, given by

$$\Gamma'_n(\alpha_n, \sigma_n) =$$
$$\sum_{m=0}^{\nu-1} \sum_{j=0}^{L_c} \mathrm{Re} \left\{ c^* \left(j; n + \frac{m}{\nu} \right) \alpha^*_{n+\frac{m-j}{\nu}} \left[2Y \left(n + \frac{m}{\nu} \right) \right. \right.$$

$$
- \phi(0) \sum_{l=0}^{L_c} c\left(l; n + \frac{m}{\nu}\right) \alpha_{n + \frac{m-l}{\nu}} - 2 \sum_{i=1}^{L_d} \phi(i) \sum_{l=0}^{L_c} c\left(l; n + \frac{m-i}{\nu}\right) \alpha_{n + \frac{m-i-l}{\nu}} \Bigg] \Bigg\} \quad (3.18)
$$

Again using (2.16) for the term involving $\phi(0)$ in (3.18), the branch metric can alternatively be written as

$$
\Gamma'_n(\alpha_n, \sigma_n) =
$$

$$
\sum_{m=0}^{\nu-1} \sum_{j=0}^{L_c} \mathrm{Re} \left\{ c^* \left(j; n + \frac{m}{\nu}\right) \alpha^*_{n + \frac{m-j}{\nu}} \left[2Y\left(n + \frac{m}{\nu}\right) - \phi(0) \left(c\left(j; n + \frac{m}{\nu}\right) \alpha_{n + \frac{m-j}{\nu}} \right. \right. \right.
$$

$$
\left. \left. + 2 \sum_{l=1}^{L_c - j} c\left(j + l; n + \frac{m}{\nu}\right) \alpha_{n + \frac{m-j-l}{\nu}} \right) - 2 \sum_{i=1}^{L_d} \phi(i) \sum_{l=0}^{L_c} c\left(l; n + \frac{m-i}{\nu}\right) \alpha_{n + \frac{m-i-l}{\nu}} \right] \right\} \quad (3.19)
$$

The receiver is shown in Fig. 3.5. It employs a fixed front-end filter matched to the transmit filter response. The output of the front-end filter is sampled at the fractional-rate and fed to a Viterbi algorithm. The number of states in the Viterbi algorithm is $|\mathcal{A}|^L$, where $L = \left\lceil \frac{L_c + L_d}{\nu} \right\rceil$ is the overall channel memory in symbols. The Viterbi algorithm processes ν samples of the input statistic every symbol time T. The branch metric given by (3.18) or (3.19) has ν terms corresponding to each sample. Note that an ν step prediction of medium response coefficients is needed to compute the branch metric at each recursion. An alternative approach is to process one sample of the input statistic every T/ν seconds by computing one component (of the ν components) of the branch metric at each recursion followed by an update of the medium response coefficients. An advantage of this method is that the medium response coefficients can be estimated more accurately as only one step prediction is performed at the fractional rate.
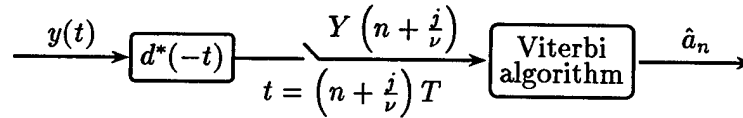
Figure 3.5: A new fractional MLSE receiver

For a symbol-spaced channel model ($\nu = 1$), the branch metric given by (3.19) simplifies to

$$
\Gamma'_n(\alpha_n, \sigma_n) =
$$

$$\sum_{j=0}^{L_c} \mathrm{Re} \left\{ c^*(j;n) a_{n-j}^* \left[2Y(n) - o(0) \left(c(j;n) a_{n-j} + 2 \sum_{l=1}^{L_c-j} c(j+l;n) a_{n-j-l} \right) \right. \right.$$

$$\left. \left. - 2 \sum_{i=1}^{L_d} \phi(i) \sum_{l=0}^{L_c} c(l;n-i) a_{n-i-l} \right] \right\} \tag{3.20}$$

which reduces to the "Partial Ungerboeck" formulation of Bottomley [6] for the case of Nyquist pulse-shaping (i.e. $\phi(n) = \delta(n)$).

3.6 Conclusions

In this chapter, we derived a new MLSE receiver for linearly-dispersive time-varying channels with additive white Gaussian noise. The receiver consists of a fixed analog front-end filter matched to the transmit pulse-shaping filter, a fractional sampler and a Viterbi algorithm. The branch metric of the Viterbi algorithm accounts for the correlation in the noise samples (due to fractional sampling) which is known at the receiver. The branch metric depends on causal fractionally-spaced medium response coefficients which can be adapted using only one step prediction. The receiver is suitable for communication systems with excess signal bandwidth and rapidly time-varying channels.

CHAPTER 4

Reduced Trellis and Tree Search Algorithms

4.1 Introduction

Maximum-likelihood sequence estimation (MLSE) [6,13,40,43] is an optimum detection technique for channels with memory and additive noise. As the complexity of the various MLSE algorithms is exponential in the channel memory, several low-complexity suboptimal methods have been proposed. One method is to ignore the tail of the delay response or to select a subset of states in the Viterbi algorithm for reduced state detection [14,45]. The residual interference that remains limits the performance of these methods even at modest intersymbol interference (ISI) levels [32]. Another approach is to pre-cancel the tail of the delay response using a linear or a decision feedback equalizer (DFE). The DFE approach [26,49] suffers from severe error propagation on channels where the tail contains a significant fraction of the total energy in the channel while the linear pre-filtering approach [12,35] enhances noise.

Decision feedback sequence estimation (DFSE) [7,8,10,11,17,19,20,39,50] and the M-algorithm [2,48,51] are two well-known reduced-complexity alternatives to MLSE. These algorithms find applications in equalization of ISI [7,8,10,17,19,20,39,50], detection of partial response signals, trellis-coded modulation [8,10,11] and multiuser detection [17,19, 20,48,51]. DFSE is a trellis-based method where the complexity is controlled by reducing the memory of the trellis in the Viterbi algorithm. On the other hand, the M-algorithm is a tree-based method where the complexity is reduced by pruning the tree (representing sequence hypotheses) to maintain a given number of branches at each step. Both schemes feed back conditional decisions taken from survivor paths to cancel the tail of the delay

response. This manner of decision feedback has been shown to alleviate the problem of error propagation that arises in the conventional DFE approach.

DFSE and M-algorithm receivers were originally proposed and thoroughly investigated for discrete-time statistics containing white noise for which case they have been thoroughly investigated [2,8,10,39,48]. However, receivers that operate on matched filter statistics have also been proposed for various applications [7,17,48,50,51]. The main advantage of these receivers is that they do not require noise-whitening. Computing the noise-whitening filter involves channel inversion and/or factorization operations which may not be feasible for time-varying, cyclo-stationary or bidirectional channels, or for channels with deep spectral nulls. Applications that particularly involve such channels include multiuser detection for direct-sequence code-division multiple-access (DS-CDMA) systems [19], bidirectional equalization for the global system for mobile communications (GSM) system [50] and fractional equalization for narrowband systems with excess signal bandwidth. An investigation of the DFSE and M-algorithm receivers with matched filter statistics is given in [20] and [48] respectively. It has been noted that the receive filter has a significant influence on the bit-error performance of these receivers.

In this chapter, we consider DFSE and M-algorithm receivers operating on the output of a general transversal processing filter which follows a front-end matched filter. We provide two different formulations of the branch metric — one for the case of standard matched filtering (front-end filter matched to the overall channel response) and the other for the case of transmit matched filtering (front-end filter matched to the transmit filter response). The latter formulation is desirable for fractional equalization in the presence of excess signal bandwidth. We conduct a first event error analysis of the various receivers which indicates that error events in certain receivers depend on the transmitted sequence. The error-rate performance of such receivers is affected, and generally dominated, by untreated interference components which we call *bias*. Bias occurs in a DFSE or M-algorithm receiver due to a mismatch between the processing filter and the branch metric. This leads to the classification of the various receivers as biased and unbiased, where the notion of "unbiasedness" means that error events are independent of the transmitted sequence given the error sequence.

We find that there exist only two processing filters for each type of matched filtering (i.e. standard and transmit) that result in unbiased receivers, namely the filter that whitens

(or partially decorrelates) the effect of the matched filter and the filter that zero-forces (or completely decorrelates) the effect of the matched filter. The whitening filter DFSE (WF-DFSE) and whitening filter M-algorithm (WF-MA) receivers with a standard matched filter are the well-known receivers described in [2, 8, 10, 39, 48]. The zero-forcing DFSE (ZF-DFSE) receiver with a standard matched filter was derived in [37]. The class of biased receivers includes matched filter DFSE (MF-DFSE) and matched filter M-algorithm (MF-MA) receivers where the matched filter statistic is fed directly into the reduced trellis or tree search algorithm without further processing. The MF-DFSE(S)[1] receiver was proposed in [7,50]. The MF-MA(S) receiver was proposed in [51] for multiuser detection.

We find the probability $\Pr(\varepsilon)$ of the occurrence of a given first event error ε for the various DFSE receivers. The probability $\Pr(\varepsilon)$ in the case of unbiased DFSE receivers is completely characterized by the error distance $\delta(\varepsilon)$ of the receiver. We use a broader definition for the error distance (than given in [13]) that includes the effect of noise enhancement. In the case of BPSK modulation, the probability $\Pr(\varepsilon)$ for an unbiased DFSE receiver is equal to the error probability of a memoryless system with signal amplitude equal to $\frac{1}{2}\delta(\varepsilon)$. We show that the error distance is maximized by the MF-DFSE(S) receiver. However, the error performance of the MF-DFSE(S) receiver is dominated by untreated interference components (bias) for most channels of interest and is therefore not very good. Among unbiased DFSE receivers, the error distance is maximized by the WF-DFSE receivers for each type of matched filtering. We also show that the error distance of truncated memory MLSE receivers that employ pre-filtering to reduce memory [12,35], is lower than the error distance of WF-DFSE. Thus, WF-DFSE receivers have the best error performance among these unbiased trellis-based receivers, not considering the effects of error propagation.

We obtain approximate upper bounds on the symbol error probability of the various DFSE receivers assuming absence of error propagation. We show that these bounds can be evaluated using a generating function method similar to MLSE, clearing the misconception that a generating function method is not applicable to DFSE receivers due to the use of decision feedback [39].

The chapter is organized as follows. The system model is given in Section 4.2. MLSE receivers that consist of a front-end matched filter followed by a general transversal processing filter are described in Section 4.3. The corresponding DFSE and M-algorithm receivers

---

[1]Where 'S' stands for standard matched filtering.

are described in Sections 4.4 and 4.5, respectively. In Section 4.6. we conduct a first event error analysis of the various receivers. Sections 4.7 and 4.8 deal with unbiased and biased receivers, respectively. In Section 4.9, we discuss truncated memory MLSE receivers that employs pre-filtering to reduce memory. In Section 4.10, we derive bounds on the symbol error probability of the various trellis-based receivers and in Section 4.11, we compare the error distance of the various receivers. In Section 4.12, we show how the bounds can be evaluated using an error state diagram. We compare the error-rate performance of the various receivers in Section 4.13 for a symbol-sampled system and a fractionally sampled system via simulation and analysis for some example channels.

4.2 System model

In this chapter, we assume the same system model as in Section 2.2 except with a time-invariant transmission medium. Thus, the baseband received signal is given by

$$y(t) = \sum_{n=0}^{N-1} a_n h(t - nT) + w(t) \tag{4.1}$$

where $h(t)$ represents the overall response of a transmit filter $d(t)$ and a time-invariant transmission medium, which is modeled as a tapped delay line with L_c complex-valued symbol-spaced tap coefficients $c(i)$,

$$h(t) = \sum_{i=0}^{L_c} c(i)d(t - iT). \tag{4.2}$$

4.3 A generalized MLSE receiver

Maximum likelihood sequence estimation (MLSE) is an optimal detection algorithm that minimizes the probability of sequence error for *a priori* equiprobable sequences. In this section, we describe an MLSE receiver with a general transversal processing filter. The processing filter has no influence on MLSE performance as we will see in the next section. However, the expressions developed in this section will be useful when we consider the effect of the processing filter on reduced trellis and tree search algorithms.

It is well-known [6,13,40] that the sequence of symbol-spaced samples $\{z(n)\}_{n=0}^{N-1}$ obtained at the output of a receive filter matched to the overall channel impulse response $h(t)$ forms a set of sufficient statistics for detecting the transmitted sequence $\{a_n\}_{n=0}^{N-1}$ given the

received signal $y(t)$. The matched-filter statistic $z(n)$ is given by

$$z(n) = h^*(-t) * y(t)|_{t=nT} = \int h^*(t - nT)y(t)dt \qquad (4.3)$$

$$= \sum_i s(i)a_{n-i} + u_n. \qquad (4.4)$$

In vector notation, the sequence of matched-filter statistics can be written as

$$\underline{z} = S\underline{a} + \underline{u} \qquad (4.5)$$

where $\underline{a} = [a_0, a_1, \ldots, a_{N-1}]^T$, $\underline{z} = [z(0), z(1), \ldots, z(N-1)]^T$, $\underline{u} = [u(0), u(1), \ldots, u(N-1)]^T$, and S is an $N \times N$ Hermitian Toeplitz[2] matrix known as the channel spectrum. The (i, j)-th element of S is given by

$$s(i, j) = s(i - j) = \int h^*(t)h(t + (i - j)T)dt. \qquad (4.6)$$

The elements $s(i)$ are samples of the autocorrelation function of the overall channel response which is assumed to have finite span. The smallest integer L such that $s(i) = 0$ for $|i| > L$ is known as the channel memory. We assume that the channel memory L is much smaller than the length N of the transmitted sequence. The matrix S is thus banded. The vector $\underline{u}$ is a discrete Gaussian noise vector with elements

$$u(n) = \int_{t \in I} h^*(t - nT)w(t)dt \qquad (4.7)$$

and autocorrelation $\mathrm{E}[\underline{u}^H \underline{u}] = N_0 S$.

Consider a transversal processing filter P which processes the output of the matched filter. The output of the processing filter, which is an $N \times N$ matrix, is given by

$$\underline{x} = P\underline{z} = P(S\underline{a} + \underline{u}). \qquad (4.8)$$

From (4.5), it follows that $\underline{x} = [x(0), x(1), \ldots, x(N-1)]^T$ is a Gaussian random vector with mean $PS\underline{a}$ and autocovariance $N_0 PSP^H$, given the information sequence $\underline{a}$. Assume that the inverse processing filter P^{-1} exists. Then, it is possible to recover the original sequence $\underline{z}$ from the filtered sequence $\underline{x}$. Thus, the sequence $\underline{x}$ forms a set of sufficient statistics for detecting the transmitted sequence $\underline{a}$ given the received signal $y(t)$.

Consider the receiver shown in Fig. 4.1. The receiver finds the hypothetical sequence of symbols $\{\alpha_n\}$ ($\alpha_n \in \mathcal{A}$) that maximizes the likelihood of the received signal $y(t)$ given

---

[2]i.e. the elements of S satisfy $s(i, j) = s(i - j)$.
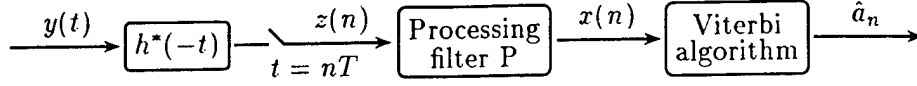
Figure 4.1: A generalized MLSE receiver

that $\{\alpha_n\}$ was transmitted. Assuming equiprobable symbols, the receiver maximizes the log-likelihood function derived from the *a posteriori* distribution of the received signal. Ignoring constant scaling factors and additive terms, the log-likelihood function reduces to

$$J_H = -(\underline{x} - PS\underline{\alpha})^H (PSP^H)^{-1}(\underline{x} - PS\underline{\alpha}) \tag{4.9}$$

where the superscript H stands for Hermitian transpose and the subscript H corresponds to the hypothesized sequence $\underline{\alpha}$. Neglecting terms common to all hypotheses, the metric to be maximized by the Viterbi algorithm can be written as

$$\Lambda_H = 2\mathrm{Re}\{\underline{\alpha}^H P^{-1}\underline{x}\} - \underline{\alpha}^H S\underline{\alpha}. \tag{4.10}$$

Assume that the matrix S is positive definite. Then, it can be decomposed into its unique Cholesky factors as

$$S = \tilde{F}^H \tilde{F} \tag{4.11}$$

where $\tilde{F}$ is an $N \times N$ invertible lower-triangular matrix. For $N \gg L$, the matrix $\tilde{F}$ is near Toeplitz[3]. Also note that

$$S = F_+^H F_+ \tag{4.12}$$

where F_+ is an $(N + L) \times N$ matrix with elements

$$f(i, j) = \begin{cases} f(i - j) & 0 \le i - j \le L \\ 0 & \text{otherwise} \end{cases} \tag{4.13}$$

obtained from the inverse z-transform of the minimum-phase Cholesky factor $F(z)$ of the z-transform of $\{s(i)\}$. Then, the metric in (4.10) can be written as

$$\Lambda_H = 2\mathrm{Re}\{\underline{\alpha}^H P^{-1}\underline{x}\} - \|F_+\underline{\alpha}\|^2. \tag{4.14}$$

---

[3]The matrix has constant elements along each diagonal except the elements in some bottom rows.

The metric can be approximated as

$$\Lambda_H \approx 2\mathrm{Re}\{\underline{a}^H P^{-1}\underline{x}\} - \|F\underline{a}\|^2 \qquad (4.15)$$

where F is an $N \times N$ lower-triangular Toeplitz matrix with elements given by (4.13). The approximation in (4.15) is a result of premature trellis termination in the Viterbi algorithm at the tail of the transmitted sequence. We adopt the approximate expression for the total metric (4.15) rather than (4.14) for simplicity of notation and analysis. In order to be consistent then, we let $S = F^H F$ throughout the rest of the chapter, without loss of generality.

The two expressions for the total metric (4.10) and (4.15) lead to two different additive decompositions (branch metrics). In order to obtain a general expression for the branch metric, we write the channel spectrum as

$$S = RQ \qquad (4.16)$$

where R is an $N \times N$ upper-triangular Toeplitz matrix with elements

$$r(i,j) = \begin{cases} r(i-j) & -l_r \le i-j \le 0 \\ 0 & \text{otherwise} \end{cases} \qquad (4.17)$$

where l_r is either 0 or L and Q is an $N \times N$ Toeplitz matrix with elements

$$q(i,j) = \begin{cases} q(i-j) & -L+l_r \le i-j \le L \\ 0 & \text{otherwise} \end{cases} \qquad (4.18)$$

In (4.10), $R = I$ and $Q = S$ while in (4.15), $R = Q^H = F^H$.

Assume that the inverse processing filter consists of $l_p + l_f + 1$ coefficients ($l_p + 1$ causal and l_f anti-causal). The elements of the $N \times N$ banded Toeplitz matrix P^{-1} are given by

$$p'(i,j) = \begin{cases} p'(i-j) & -l_f \le i-j \le l_p \\ 0 & \text{otherwise} \end{cases} \qquad (4.19)$$

This structure for the inverse processing filter encompasses many filters of interest, including the zero-forcing filter and the noise-whitening filter.

Using (4.17), (4.18) and (4.19), the total metric in (4.10) can then be written as

$$\Lambda_H = 2\mathrm{Re}\{\underline{a}^H[(P^{-1})^L\underline{x}]\} + 2\mathrm{Re}\{[\underline{a}^H(P^{-1})^{UD}]\underline{x}\} - [\underline{a}^H R][(Q)^L\underline{a}] - [\underline{a}^H R(Q)^{UD}]\underline{a} \quad (4.20)$$

where the superscripts L, U and D denote the lower-triangular, the upper-triangular and the diagonal part of a matrix, respectively. The above form for the total metric leads to the additive decomposition

$$\Lambda_H = \sum_{n=0}^{N-1} \Gamma(\alpha_n, \sigma_n) \tag{4.21}$$

where $\Gamma(\alpha_n, \sigma_n)$ is the branch metric corresponding to the state $\sigma_n : \alpha_{n-1}, \ldots, \alpha_{n-L_v}$ ($L_v = \max(L, l_f)$) in the trellis of the Viterbi algorithm, given by

$$
\begin{aligned}
\Gamma(\alpha_n, \sigma_n) = {} & 2\mathrm{Re}\left\{ \alpha_n^* \sum_{l=1}^{l_p} p'(l) x(n-l) + x(n) \sum_{l=0}^{l_f} p'(-l) \alpha_{n-l}^* \right\} \\
& - \left(\sum_{l=0}^{l_r} r(-l)\alpha_{n-l}^* \right) \left(\sum_{l=1}^{L} q(l)\alpha_{n-l} \right) - \alpha_n \sum_{l=0}^{l_r} r(-l) \sum_{k=0}^{L-l_r} q(-k)\alpha_{n-l-k}^* \tag{4.22}
\end{aligned}
$$

where $\alpha_n = 0$ for $N-1 < n < 0$ and $x(n) = 0$ for $n < 0$. The Viterbi algorithm recursively computes the accumulated metric given by

$$\mathcal{M}(\sigma_{n+1}) = \max_{\alpha_{n-L_v}} \left[\mathcal{M}(\sigma_n) + \Gamma(\alpha_n, \sigma_n) \right]. \tag{4.23}$$

for all subsequence hypotheses (or states) σ_n. The number of states in the Viterbi algorithm is $|\mathcal{A}|^{L_v}$ (note that the memory of the Viterbi algorithm L_v may be greater than the channel memory L). The output of the Viterbi algorithm is the estimated sequence $\{\hat{a}_n\}$.
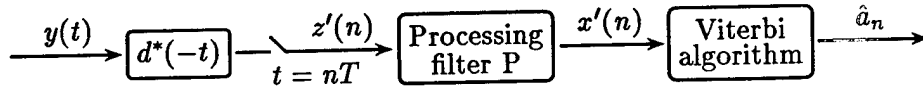
Figure 4.2: An alternative MLSE receiver

An alternative MLSE receiver is shown in Fig. 4.2. It differs from the receiver of Fig. 4.1 in that it has a front-end filter which is matched to just the transmit filter response $d(t)$ instead of the overall channel response $h(t)$. The transmit filter matched-filter statistic $z'(n)$ is given by

$$
\begin{aligned}
z'(n) &= d^*(-t) * y(t)|_{t=nT} = \int d^*(t - nT) y(t)\, dt \\
&= \sum_{l=-L_d}^{L_d} \sum_{i=0}^{L_c} c(i)\phi(n, n-l)a_{n-l-i} + u'(n) \tag{4.24}
\end{aligned}
$$

which can be written in vector notation as

$$\underline{z}' = \Phi C \underline{a} + \underline{u}' \tag{4.25}$$

where $\underline{z}' = [z'(0), z'(1), \ldots, z'(N-1)]^T$, $\underline{u}' = [u'(0), u'(1), \ldots, u'(N-1)]^T$. The matrix C is a lower-triangular Toeplitz matrix with elements

$$c(i,j) = \begin{cases} c(i-j) & 0 \le i-j \le L_c \\ 0 & \text{otherwise} \end{cases} \tag{4.26}$$

and the matrix Φ is a Hermitian Toeplitz matrix with elements which are samples of the transmit filter autocorrelation function

$$\phi(i,j) = \phi(i-j) = \int d^*(t)d(t+(i-j)T)dt. \tag{4.27}$$

Let $\phi(i) = 0$ for $|i| > L_d$. The overall channel memory is then $L = L_c + L_d$. The vector $\underline{u}'$ is a Gaussian random vector with mean zero and autocorrelation $E[\underline{u}'^H \underline{u}'] \doteq N_0 \Phi$. Note that the statistic $\underline{z}$ can be obtained from the statistic $\underline{z}'$ as $\underline{z} = C^H \underline{z}'$. The sequence $\underline{z}'$, thus, forms a set of sufficient statistics for detecting the transmitted sequence given $y(t)$. The statistic $\underline{x}'$ input to the Viterbi algorithm is given by

$$\underline{x}' = P\underline{z}' = P(\Phi C \underline{a} + \underline{u}'). \tag{4.28}$$

The log-likelihood function in this case is given by

$$J'_H = -(\underline{x}' - P\Phi C \underline{\alpha})^H (P\Phi P^H)^{-1} (\underline{x}' - P\Phi C \underline{\alpha}) \tag{4.29}$$

which yields the likelihood metric to be maximized by the Viterbi algorithm in Fig. 4.2, as

$$\Lambda'_H = 2\text{Re}\{\underline{\alpha}^H C^H P^{-1} \underline{x}'\} - \underline{\alpha}^H C^H \Phi C \underline{\alpha}. \tag{4.30}$$

Again two different additive decompositions of the above metric are possible corresponding to the two decompositions of the matrix Φ, i.e.

$$\Phi = R'Q' \tag{4.31}$$

where the elements of R' are given by

$$r'(i,j) = \begin{cases} r'(i-j) & -l_{r'} \le i-j \le 0 \\ 0 & \text{otherwise} \end{cases} \tag{4.32}$$

34

where $l_{r'}$ is either 0 or L_d and the elements of Q' are given by

$$q'(i,j) = \begin{cases} q'(i-j) & -L_d + l_{r'} \le i - j \le L_d \\ 0 & \text{otherwise} \end{cases} . \qquad (4.33)$$

In one case $R' = I$, $Q' = \Phi$ and in the other case $R' = Q'^H = F'^H$. The matrix F' is a lower-triangular Toeplitz matrix with elements $f'(i)$ given by the inverse z-transform of the minimum-phase Cholesky factor $F'(z)$ of the z-transform of $\{\phi(i)\}$. Then, (4.30) can be written as

$$\Lambda'_H = \sum_{n=0}^{N-1} \Gamma'(\alpha_n, \sigma_n) = 2\text{Re}\{\underline{\alpha}^H C^H P^{-1} \underline{x}'\} - \underline{\alpha}^H C^H R' Q' C \underline{\alpha} \qquad (4.34)$$

where the branch metric $\Gamma'(\alpha_n, \sigma_n)$ is given by

$$
\begin{aligned}
\Gamma'(\alpha_n, \sigma_n) =\ & 2\text{Re}\left\{ \left(\sum_{l=0}^{L_c} c^*(l)\alpha^*_{n-l} \right) \left(\sum_{l=1}^{l_p} p'(l)x'(n-l) \right) + x'(n) \sum_{l=0}^{L_c} c^*(l) \sum_{k=0}^{l_f} p'(-k)\alpha^*_{n-l-k} \right\} \\
& - \left(\sum_{l=0}^{L_c} c^*(l) \sum_{k=0}^{l_{r'}} r'(-k)\alpha^*_{n-l-k} \right) \left(\sum_{l=0}^{L_c} c(l) \sum_{k=1}^{L_d} q'(k)\alpha_{n-l-k} \right) \\
& - \left(\sum_{l=0}^{L_c} c^*(l) \sum_{k=0}^{l_{r'}} r'(-k) \sum_{m=0}^{L_d - l_{r'}} q'(-m)\alpha^*_{n-l-k-m} \right) \left(\sum_{l=0}^{L_c} c(l)\alpha_{n-l} \right) . \qquad (4.35)
\end{aligned}
$$

The memory of the Viterbi algorithm in this case is $L'_v = \max(L, L_c + l_f)$. Note that the receiver of Fig. 4.2 can be easily extended for the case of a fractionally-spaced medium response model. In this case, the output of the transmit matched filter in Fig. 4.2 is sampled at a multiple of the symbol rate (say ν/T). The memory of the Viterbi algorithm is $\lceil L'_v/\nu \rceil$ and the branch metric is modified by replacing α_n in (4.35) by π_n, given by

$$\pi_n = \begin{cases} \alpha_{n/\nu} & n/\nu \text{ integer} \\ 0 & \text{otherwise} \end{cases} . \qquad (4.36)$$

4.4 Decision Feedback Sequence Estimation

Decision feedback sequence estimation (DFSE) is a reduced complexity alternative to maximum likelihood sequence estimation which provides an adjustable performance/complexity tradeoff. Proposed by Duel-Hallen et al. [7,8][4] and Eyuboglu et al. [10], the scheme employs a reduced trellis search algorithm to search through a subset of sequence hypotheses searched by the full-blown Viterbi algorithm. The complexity is controlled by a parameter

---

[4]The algorithm is referred to as Delayed Decision Feedback Sequence Estimation in [7, 8]

called the memory order J, which is chosen arbitrarily smaller than the memory of the Viterbi algorithm. The trellis in the reduced trellis search algorithm then comprises $|\mathcal{A}|^J$ states corresponding to the J most recent symbol hypotheses. Survivor paths or sequences are chosen in the reduced trellis search algorithm on the basis of the same cost function as in MLSE (i.e. the accumulated likelihood metric). A transition in the reduced trellis specifies the $J+1$ most recent hypothesized symbols. The remaining $L-J$ symbols needed to compute the branch metric are obtained from decisions taken from the survivor history (past decisions) of the path.
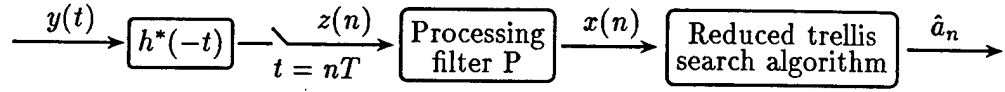
Figure 4.3: A generalized DFSE receiver

The DFSE algorithms proposed by Duel-Hallen *et al.* operate on matched-filter and whitened statistics obtained from conventional matched filtering and whitened matched filtering respectively. Here we generalize the DFSE algorithm to operate with a general transversal processing filter. The receiver is shown in Fig. 4.3. The reduced trellis search algorithm has memory order J chosen such that $0 \leq J \leq L_v$. It employs the recursion:

$$\mathcal{M}(\beta_{n+1}) = \max_{\alpha_{n-J}} [\mathcal{M}(\beta_n) + \Gamma(\alpha_n, \beta_n)] \tag{4.37}$$

where $\beta_n : \alpha_{n-1}, \alpha_{n-2}, \ldots, \alpha_{n-J}$ represents states in the reduced trellis at time n, $\mathcal{M}(\beta_n)$ is the accumulated metric of the survivor path associated with state β_n and $\Gamma(\alpha_n, \beta_n)$ is the corresponding branch metric given by

$$\Gamma(\alpha_n, \beta_n) = 2\text{Re}\left\{ \alpha_n^* \sum_{l=1}^{l_p} p'(l)x(n-l) + x(n) \sum_{l=0}^{l_f} p'(-l)\eta_{n-l}^* \right\}$$
$$- \left(\sum_{l=0}^{l_r} r(-l)\eta_{n-l}^* \right) \left(\sum_{l=1}^{L} q(l)\eta_{n-l} \right) - \alpha_n \sum_{l=0}^{l_r} r(-l) \sum_{k=0}^{L-l_r} q(-k)\eta_{n-l-k}^* \tag{4.38}$$

where at time n

$$\eta_{n-i} = \begin{cases} \alpha_{n-i} & 0 \leq i \leq J \\ \hat{\alpha}_{n-i}(\beta_n) & J+1 \leq i \leq L_v \end{cases} . \tag{4.39}$$

36

In (4.39), $\{\hat{\alpha}_i(\beta_n)\}$ are tentative conditional decisions on symbols more than J samples in the past obtained from the history of the survivor path associated with state β_n, as

$$\hat{\alpha}_{n-J}(\beta_n) = \arg\max_{\alpha_{n-J}} [\mathcal{M}(\beta_n) + \Gamma(\alpha_n, \beta_n)]. \qquad (4.40)$$

The reduced trellis branch metric $\Gamma(\alpha_n, \beta_n)$ of (4.38) corresponds to the full trellis branch metric $\Gamma(\alpha_n, \sigma_n)$ given by (4.22). Note that the (whitened matched filter) DFSE algorithm of [8] is obtained by substituting $P^{-1} = R = Q^H = F^H$ and the DFSE algorithm with the standard matched filter, proposed in [7], is obtained by substituting $P^{-1} = R = I, Q = S$. In the first case, the whitened channel F with coefficients $\{f(n)\}$ is minimum-phase.
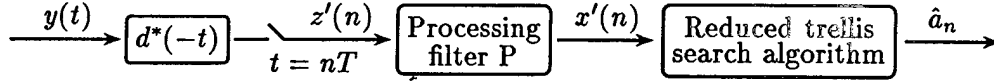
Figure 4.4: An alternative DFSE receiver

An alternative DFSE receiver shown in Fig. 4.4 corresponds to the MLSE receiver of Fig. 4.2, in that the front-end filter is matched to the transmit filter response. It follows the recursion:

$$\mathcal{M}'(\beta_{n+1}) = \max_{\alpha_{n-J}} [\mathcal{M}'(\beta_n) + \Gamma'(\alpha_n, \beta_n)] \qquad (4.41)$$

where the memory order is chosen in the range $0 \le J \le L'_v$ and the reduced trellis branch metric $\Gamma'(\alpha_n, \beta_n)$ is obtained by replacing α_{n-i} in (4.35) by

$$\eta'_{n-i} = \begin{cases} \alpha_{n-i} & 0 \le i \le J \\ \hat{\alpha}'_{n-i}(\beta_n) & J+1 \le i \le L'_v \end{cases} \qquad (4.42)$$

where $\{\hat{\alpha}'_i(\beta_n)\}$ are tentative conditional decisions obtained as

$$\hat{\alpha}'_{n-J}(\beta_n) = \arg\max_{\alpha_{n-J}}[\mathcal{M}'(\beta_n) + \Gamma'(\alpha_n, \beta_n)]. \qquad (4.43)$$

The branch metric is given by

$$\Gamma'(\alpha_n, \sigma_n) = 2\mathrm{Re}\left\{ \left(\sum_{l=0}^{L_c} c^*(l)\eta'^*_{n-i} \right) \left(\sum_{l=1}^{l_p} p'(l)x'(n-l) \right) + x'(n) \sum_{l=0}^{L_c} c^*(l) \sum_{k=0}^{l_f} p'(-k)\eta'^*_{n-l-k} \right\}$$

$$- \left(\sum_{l=0}^{L_c} c^*(l) \sum_{k=0}^{l_{r'}} r'(-k) \eta'^*_{n-l-k} \right) \left(\sum_{l=0}^{L_c} c(l) \sum_{k=1}^{L_d} q'(k) \eta'_{n-l-k} \right)$$

$$- \left(\sum_{l=0}^{L_c} c^*(l) \sum_{k=0}^{l_{r'}} r'(-k) \sum_{m=0}^{L_d - l_{r'}} q'(-m) \eta'^*_{n-l-k-m} \right) \left(\sum_{l=0}^{L_c} c(l) \eta'_{n-l} \right). \qquad (4.44)$$

With $P = R' = Q' = I$, we get the case of Nyquist pulse-shaping[5] at the transmitter and transmit-filter matched-filtering at the receiver. This results in the DFSE receiver of [8] where the statistic is white without any linear processing and the channel C with coefficients $\{c(n)\}$ may have any phase (minimum, mixed, or maximum phase). With $P^{-1} = R' = Q'^H = F'^H$, the whitened channel $F'C$ with coefficients $\{f'(n)*c(n)\}$ has mixed phase in general. With $P^{-1} = R' = I$, $Q' = \Phi$, we get the DFSE receiver corresponding to the new fractional MLSE formulation of Section 3.5.

4.5 M-Algorithm

The M-algorithm (MA) [2] is well-known as another reduced complexity alternative to MLSE. The scheme was originally proposed to operate on white (or whitened) statistics. However, it has also been used with the standard matched filter (see for example [48,51]). The M-algorithm is essentially a reduced tree search algorithm. At each step, M survivor paths (hypothesized sequences) are extended to MA paths, of which the M paths with the best accumulated likelihood metric are retained and the rest are discarded.

$$y(t) \rightarrow \boxed{h^*(-t)} \xrightarrow[t = nT]{z(n)} \boxed{\begin{array}{c}\text{Processing}\\\text{filter P}\end{array}} \xrightarrow{x(n)} \boxed{\begin{array}{c}\text{Reduced tree}\\\text{search algorithm}\end{array}} \xrightarrow{\hat{a}_n}$$
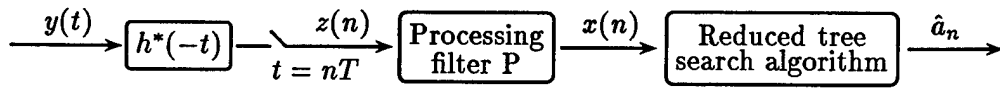
Figure 4.5: A generalized M-algorithm receiver

In this section, we extend the M-algorithm to operate with a general transversal processing filter. The receiver is shown in Fig. 4.5. Let $\underline{\alpha}_n(j) = (\alpha_0, \alpha_1, \ldots, \alpha_{n-1})$ be one of the M survivor paths $(j = 1, \ldots, M)$ at time n. At time $n + 1$, the reduced tree search algorithm extends each survivor into A paths $\underline{\alpha}_{n+1} = (\underline{\alpha}_n(j), \alpha_n)$ and computes their accumulated

---

[5]Using transmit pulses that satisfy the Nyquist criterion for ISI free transmission.

38

likelihood metric using

$$\mathcal{M}(\underline{a}_{n+1}) = \mathcal{M}(\underline{a}_n(j)) + \Gamma(a_n, \sigma_n(j)) \tag{4.45}$$

where the branch metric $\Gamma(a_n, \sigma_n(j))$ which depends on the last L_v hypothetical symbols $\sigma_n(j)$ in the survivor path $\underline{a}_n(j)$, is given by (4.22). The M paths with the highest accumulated metric are then selected.

An alternative M-algorithm receiver has a front-end filter matched to the transmit filter response and uses the branch metric of the MLSE receiver of Fig. 4.2, given by (4.35).

4.6 First Event Error Analysis

In this section, we examine the first event error (FEE) probability of the generalized DFSE receiver of Section 4.4 (Fig. 4.3) and the generalized M-algorithm receiver of Section 4.5 (Fig. 4.5). We say that a *first event error* is made in the reduced trellis or tree search algorithm (at time j) if the correct path is abandoned for the first time in favor of a competitor path or paths that diverge from the correct path at time j. Note that our definition of a first event error is different from the definition given in [29], in that we consider the start time of an error event as the time of its occurrence as opposed to the end time as in [29]. We assume that the channel is stationary. Thus, a first event error is independent of the start time and time 0 can be chosen as the start time without loss of generality.

4.6.1 Trellis Search Algorithms

Consider the generalized DFSE receiver of Fig. 4.3. Let $\{a_n\}$ be the sequence of symbols transmitted and $\{b_n\}$ $(b_n : a_{n-1}, a_{n-2}, \ldots, a_{n-J})$ be the sequence of states in the path of $\{a_n\}$ in the reduced trellis of the DFSE receiver (with memory order J). Let $\{\bar{a}_n\}$ be a hypothetical sequence of symbols and $\{\bar{b}_n\}$ be the corresponding sequence of states in the reduced trellis that diverges from the correct sequence of states at time unit 0 and re-merges with it at a later time (say k), i.e.

$$\bar{b}_n = b_n \text{ for } n = 0, k \text{ and } \bar{b}_n \neq b_n \text{ for } 0 < n < k. \tag{4.46}$$

A first event error occurs at time 0 if the reduced trellis search algorithm picks $\{\bar{a}_n\}$ as the survivor sequence over $\{a_n\}$. It follows from (4.37) that the event occurs if the metric

accumulated on the incorrect path is greater than the metric accumulated on the correct path i.e.

$$\sum_{n=0}^{k-1} \Gamma(\bar{a}_n . \bar{b}_n) > \sum_{n=0}^{k-1} \Gamma(a_n . b_n) \qquad (4.47)$$

where $\{\Gamma(a_n, b_n)\}$ and $\{\Gamma(\bar{a}_n, \bar{b}_n)\}$ are branch metrics corresponding to the paths $\{a_n\}$ and $\{\bar{a}_n\}$ respectively, computed using (4.38). Note that the conditional decisions $\{\hat{a}_{n-l}(b_n)\}$ and $\{\hat{a}_{n-l}(\bar{b}_n)\}$ which are fed back to compute the branch metrics, are taken from the paths corresponding to the sequences of states $\{b_n\}$ and $\{\bar{b}_n\}$ respectively. Thus, $\hat{a}_{n-l}(b_n) = a_{n-l}$ and $\hat{a}_{n-l}(\bar{b}_n) = \bar{a}_{n-l}$ and (4.47) can be written in matrix notation as

$$2\text{Re}\{\underline{\bar{a}}_k^H (P^{-1})_k \underline{x}_k\} - \underline{\bar{a}}_k^H R_k Q_k \underline{\bar{a}}_k > 2\text{Re}\{\underline{a}_k^H (P^{-1})_k \underline{x}_k\} - \underline{a}_k^H R_k Q_k \underline{a}_k \qquad (4.48)$$

where $\underline{a}_k = [a_0, a_1, \ldots, a_{k-1}]^T$, $\underline{\bar{a}}_k = [\bar{a}_0, \bar{a}_1, \ldots, \bar{a}_{k-1}]^T$ and $\underline{x}_k = [x(0), x(1), \ldots, x(k-1)]^T$. The matrices $(P^{-1})_k$, R_k and Q_k are principal submatrices[6] of dimension k of the matrices P^{-1}, R and Q respectively given by (4.16), (4.17), (4.18) and (4.19). Defining $\underline{e}_k = \underline{\bar{a}}_k - \underline{a}_k$ as the error sequence and noting that $R_k Q_k = Q_k^H R_k^H$, (4.48) can also be expressed as

$$2\text{Re}\{\underline{e}_k^H (P^{-1})_k \underline{x}_k\} > \underline{e}_k^H R_k Q_k \underline{e}_k + 2\text{Re}\{\underline{e}_k^H R_k Q_k \underline{a}_k\}. \qquad (4.49)$$

From (4.8), it follows that

$$\underline{x}_k = P_{k \times N}(S\underline{a} + \underline{u}) \qquad (4.50)$$

where $P_{k \times N}$ is the $k \times N$ matrix comprising the top k rows of the matrix P. Using (4.50), (4.49) can be written as

$$2\text{Re}\{\underline{e}_k^H (P^{-1})_k P_{k \times N} \underline{u}\} > \underline{e}_k^H R_k Q_k \underline{e}_k + 2\text{Re}\{\underline{e}_k^H R_k Q_k \underline{a}_k\} - 2\text{Re}\{\underline{e}_k^H (P^{-1})_k P_{k \times N} S\underline{a}\} \qquad (4.51)$$

which is the condition for the error event ε : $\underline{a}_k$ is eliminated in favor of $\underline{a}_k + \underline{e}_k$ (with $\underline{a}_k$ and $\underline{e}_k$ given, i.e. non-random). The error event ε is associated with the error sequence $\underline{e}_k$. The length of the error event is $k - J$ symbols, not counting the last J components of $\underline{e}_k$ which must be zero as $\bar{b}_k = b_k$ according to (4.46).

MLSE

In the case of maximum likelihood sequence estimation, the memory order is $J = L_v$ (Viterbi algorithm). Thus, we have $e_{k-i} = 0$ for $i = 1, 2, \ldots, L_v$. Using the fact that $R_k Q_k$

---

[6]The principal submatrix of dimension k of a square matrix A (with dimension $\geq k$) is obtained by erasing all but the first k rows and columns of A.

is a square banded matrix with $L \leq L_v$ elements in the right band[7], we get

$$\underline{e}_k^H R_k Q_k \underline{e}_k = \underline{e}_{k-L_v}^H S_{k-L_v} \underline{e}_{k-L_v} \tag{4.52}$$

$$\underline{e}_k^H R_k Q_k \underline{a}_k = \underline{e}_{k-L_v}^H S_{k-L_v \times k} \underline{a}_k \tag{4.53}$$

where $\underline{e}_{k-L_v} = [e_0, e_1, \ldots, e_{k-L_v-1}]^T$ and $S_{k-L_v \times k}$ is a $(k - L_v) \times k$ matrix comprising the top $k - L_v$ rows of S_k. Since $(P^{-1})_k$ is a banded matrix with $l_f \leq L_v$ elements in the right band), the top $k - L_v$ rows of $(P^{-1})_k P_{k \times N}$ are given by $[I_{k-L_v} | O_{k-L_v \times N+L_v-k}]$ and we have

$$\underline{e}_k^H (P^{-1})_k P_{k \times N} S \underline{a} = \underline{e}_{k-L_v}^H S_{k-L_v \times k} \underline{a}_k \tag{4.54}$$

Combining (4.52), (4.53) and (4.54) with (4.51), we see that the error event ε occurs in an MLSE receiver if

$$2\mathrm{Re}\{\underline{e}_{k-L_v}^H \underline{u}_{k-L_v}\} > \underline{e}_{k-L_v}^H S_{k-L_v} \underline{e}_{k-L_v}. \tag{4.55}$$

Given the error sequence $\underline{e}_k$, the left hand side of (4.55) is a Gaussian random variable with mean 0 and variance $4N_0 \underline{e}_{k-L_v}^H S_{k-L_v} \underline{e}_{k-L_v}$. Thus, the probability of the error event ε is given by

$$\mathrm{Pr}(\varepsilon) = \mathrm{Q}\left(\frac{1}{2}\sqrt{\frac{\underline{e}_{k-L_v}^H S_{k-L_v} \underline{e}_{k-L_v}}{N_0}}\right) \tag{4.56}$$

It follows from (4.46) and (4.56) that the first event error probability can be over-bounded using a union bound, as

$$P_{FEE} \leq \sum_{\underline{e} \in E} p_{\underline{e}} \mathrm{Q}\left(\frac{\delta(\underline{e})}{2\sqrt{N_0}}\right) \tag{4.57}$$

where E is the set of all error sequences $\underline{e} = e_0, e_1, \ldots, e_{l-1}$ (such that $l > 0$, $e_{l-1} \neq 0$) with less than J consecutive zeros in the midst of the sequence, $p_{\underline{e}}$ is the *a priori* probability of the error sequence $\underline{e}$ and $\delta(\underline{e})$ is known as the distance of the error sequence $\underline{e}$ and is given by

$$\delta(\underline{e}) = \sqrt{\underline{e}^H S_l \underline{e}} = \sqrt{\sum_{i=0}^{l-1} \sum_{j=0}^{l-1} e_i^* s(i-j) e_j}. \tag{4.58}$$

Notice that the first event error probability given by (4.57) is independent of the processing filter P and the form of the branch metric used. It is the same as obtained by Forney [13] and Ungerboeck [40] for MLSE receivers with specific processing filter and branch metric combinations. Our result validates the fact that the Viterbi algorithm does in fact yield

---

[7]The elements on the right hand side of (but not including) the diagonal.

maximum likelihood sequence estimates regardless of the form of the processing filter as long as the inverse processing filter P^{-1} exists and the trellis is expanded by $l_f - L$ symbols if the number of anti-causal taps l_f of P^{-1} is greater than the channel memory L.

DFSE

For a memory order $J < L$, the first term on the right hand side of (4.51) depends on the error sequence $\underline{e}_k$ only, while the other two terms depend, in addition, on the transmitted sequence $\underline{a}$. These terms do not cancel for a general transversal processing filter P and thus represent "raw or untreated" interference. The error performance of a DFSE receiver thus depends on the processing filter unlike the case of an MLSE receiver. Moreover, the error performance also depends on the branch metric formulation employed by the reduced trellis-search algorithm. This can be seen by noting that the two branch metric formulations: $R_k = Q_k^H = F_k^H$ and $R_k = I_k$, $Q_k = S_k$ result in different error distance and interference terms as $F_k^H F_k \neq S_k$. Note that the asymptotic equivalence of the matrices S and $F^H F$ (for N large) assumed in Section 4.3 does not apply here, as error events are generally short, i.e. $k \ll N$.

In view of the above discussion, it is desirable to have a processing filter plus branch metric combination which eliminates the problem of untreated interference and maximizes the error distance. We devise the notion of "unbiasedness" to describe such DFSE receivers whose error performance is not affected by untreated interference (or bias). Let E' be the set of all error sequences in the set E with J zeros appendid at the tail.

Definition 4.6.1 *A DFSE receiver is termed "unbiased" if each error event ε (corresponding to an error sequence in E') is conditionally independent of the transmitted sequence $\underline{a}$ given the error sequence $\underline{e}_k$, for any memory order $0 \leq J < L_v$.*

It can be expected that an unbiased DFSE receiver would have good error performance for any memory order. On the other hand, a biased DFSE receiver would be affected by untreated interference components and could thus exhibit an error floor. In order to obtain an unbiased DFSE receiver, one must find a processing filter that causes the cancelation of the interference terms in (4.51) for any memory order. It follows that such a processing filter P must satisfy the condition:

$$(P^{-1})_k P_{k \times N} S = R_k Q_k [I_k | O_{k \times N-k}] \quad \forall \, 1 \leq k < N \tag{4.59}$$

or equivalently (noting that $R_k Q_k = Q_k^H R_k^H$ for the cases in hand):

$$(P^{-1})_k P_{k \times N} = Q_k^H (Q^{-H})_{k \times N} \quad \forall \; 1 \le k < N \qquad (4.60)$$

where the matrix $(Q^{-H})_{k \times N}$ comprises the top k rows of the matrix Q^{-H}.

It follows from (4.51) and (4.59) that the probability of the error event ε for an unbiased DFSE receiver is given by

$$\Pr(\varepsilon) = Q \left(\frac{\underline{e}_k^H R_k Q_k \underline{e}_k}{2\sqrt{N_0 \underline{e}_k^H R_k Q_k (S^{-1})_k R_k Q_k \underline{e}_k}} \right) . \qquad (4.61)$$

The first event error probability for an unbiased DFSE receiver can then be overbounded as

$$P_{FEE} \le \sum_{\underline{e} \in E'} p_{\underline{e}} Q \left(\frac{\delta(\underline{e})}{2\sqrt{N_0}} \right) \qquad (4.62)$$

where $\delta(\underline{e})$ is the distance of the error sequence $\underline{e}$ defined, in general, as

$$\delta(\underline{e}) \triangleq \frac{\underline{e}^H R_k Q_k \underline{e}}{\sqrt{\underline{e}^H R_k Q_k (S^{-1})_k R_k Q_k \underline{e}}} \qquad (4.63)$$

where the subscript k denotes the length of the composite error sequence $\underline{e}$. Note that the above definition of the error distance includes the effect of noise enhancement (the term in the denominator of (4.63)).

A first event error analysis of the alternative DFSE receiver of Fig. 4.4 is similar to the analysis presented above and is given in Appendix A.

4.6.2 Tree Search Algorithms

Consider the generalized M-algorithm receiver of Fig. 4.5. Let $\{a_n\}$ be the sequence of symbols transmitted. Let $\underline{a}_k(i)$ ($i \in \{0, 1, \ldots, M\mathcal{A} - 1\}$) be the $M\mathcal{A}$ paths extended at a time unit $k > \log_{\mathcal{A}} M$, including the correct path $\underline{a}_k(0) = \underline{a}_k$. A first event error occurs at time 0 in the M-algorithm receiver if the tree search algorithm eliminates the path $\underline{a}_k$. It follows from (4.45) that the error event occurs if the metric accumulated on the correct path is less than the metric accumulated on at least M of the other extended paths, i.e.

$$\mathcal{M}(\underline{a}_k) < \mathcal{M}(\underline{a}_k(i)) \qquad (4.64)$$

for at least M values of $i \in \mathcal{I} = \{1, 2, \ldots, MA - 1\}\}$. Let $\{\sigma_n(i)\}_{n=0}^{k-1}$ be the sequence of states[8] in the path of $\underline{a}_k(i)$. Then, using (4.45), (4.64) can be written as

$$\sum_{n=0}^{k-1} \Gamma(a_n(i), \sigma_n(i)) > \sum_{n=0}^{k-1} \Gamma(a_n, \sigma_n(0)). \tag{4.65}$$

Defining $\underline{e}_k(i) = \underline{a}_k(i) - \underline{a}_k$ as an error sequence and following the development of (4.51), we get equivalently

$$2\mathrm{Re}\{\underline{e}_k(i)^H (P^{-1})_k P_{k \times N} \underline{u}\} > \underline{e}_k(i)^H R_k Q_k \underline{e}_k(i) + 2\mathrm{Re}\{\underline{e}_k(i)^H R_k Q_k \underline{a}_k\}$$
$$- 2\mathrm{Re}\{\underline{e}_k(i)^H (P^{-1})_k P_{k \times N} S \underline{a}\} \tag{4.66}$$

for at least M values of $i \in \mathcal{I}$. This is the condition for the error event ε' : $\underline{a}_k$ is eliminated in favor of M of the extended paths $\underline{a}_k + \underline{e}_k(i)$ (with $\underline{a}_k$ and $\underline{e}_k(i)$ given, $i \in \mathcal{I}$).

Notice that like the case of the DFSE receiver, the error performance of the generalized M-algorithm receiver depends on the processing filter and is, in general, affected by untreated interference components. Thus, the concept of "unbiasedness" also applies to M-algorithm receivers. Specifically, we define a class of unbiased M-algorithm receivers as follows

Definition 4.6.2 *An M-algorithm receiver is termed "unbiased" if each error event ε' (for each depth k) is conditionally independent of the transmitted sequence $\underline{a}$ given the error sequences $\underline{e}_k(i)$ ($i \in \mathcal{I}$).*

Clearly the processing filter P of an unbiased M-algorithm receiver must satisfy (4.60) as in the case of unbiased DFSE receivers. The probability of the error event ε' for an unbiased M-algorithm receiver is, thus, given by

$$\mathrm{Pr}(\varepsilon') = \mathrm{Pr}\left(X(\underline{e}_k(i)) > \underline{e}_k(i)^H R_k Q_k \underline{e}_k(i), \quad \text{for } M \text{ values of } i \in \mathcal{I}\right) \tag{4.67}$$

where $X(\underline{e}_k(i))$ are jointly Gaussian random variables with mean zero and covariance $E[X(\underline{e}_k(i)) X^*(\underline{e}_k(j))] = 4N_0 \underline{e}_k(i)^H R_k Q_k (S^{-1})_k R_k Q_k \underline{e}_k(j)$.

4.7 Unbiased receivers

In Appendix B, we show that the processing filters that satisfy the unbiasedness conditions of (4.60) and (A.4) (corresponding to the case where the front-end filter is matched

---

[8]The notion of state in a tree search algorithm is as defined in Section 4.5.

to the overall channel response and where it is matched to the transmit filter response respectively) are unique (within a scaling factor) and are given by

$$P = Q^{-H} \qquad (4.68)$$

and

$$P = Q'^{-H} \qquad (4.69)$$

respectively. In the first case, the processing filter P that results in an unbiased receiver when used with a reduced trellis or tree search algorithm with branch metric formulation $R = Q^H = F^H$, is the noise-whitening filter F^{-H}, while for the formulation $R = I$ and $Q = S$, it is the zero-forcing filter S^{-1}. In the second case, the processing filter in the case of branch metric formulation $R' = Q'^H = F'^H$, is the appropriate noise-whitening filter F'^{-H}, while for the formulation $R' = I$ and $Q' = \Phi$, it is the appropriate zero-forcing filter Φ^{-1}. Note that the processing filters in both cases correspond to the autocorrelation spectrum of the front-end filter in the receiver. The processed statistics given by

$$\underline{x} = R^H \underline{a} + Q^{-H} \underline{u} \qquad (4.70)$$

in the first case, and

$$\underline{x}' = R'^H C \underline{a} + Q'^{-H} \underline{u}' \qquad (4.71)$$

in the second case, depend on the past transmitted symbols only and not on any future transmitted symbols. Thus, the statistics fed to a reduced trellis or tree search algorithm must have causal dependence only, for unbiased operation. Note that it is also necessary to match a given processing filter with the proper branch metric of the reduced trellis or tree search algorithm in order to achieve unbiasedness.

We considered two additive decompositions of the likelihood metric in each case of the front-end filter, which led to two different unbiased receivers. The two branch metric formulations correspond to the two decompositions of the front-end filter autocorrelation matrix (S or Φ)- one actually being no decomposition and the other being the unique Cholesky decomposition. Note that there is no other decomposition of a positive definite and banded matrix of the form RQ (or equivalently $R^H Q^H$), where the matrix R is upper-triangular and both matrices R and Q are banded. The matrix R is constrained to be upper-triangular to get a causal form for the additive metric. Both R and Q are constrained

45

to be banded in order for the branch metric to have finite complexity. Thus, our treatment of unbiased receivers is complete in this sense.

In the case of an infinite length transmitted sequence, the processing filters described above have infinite impulse responses. In practice, these filters can be implemented by truncating the impulse response at a sufficient length. However, this leads to some bias (untreated interference) in the receiver. Thus, there is no truly unbiased DFSE or M-algorithm receiver for an infinite length transmitted sequence. An exception to this is the case of Nyquist pulse-shaping at the transmitter and transmit-filter matched-filtering at the receiver. No processing filter is required in this case for unbiased operation.

4.7.1 Receivers with a noise-whitening filter

One type of unbiased DFSE and M-algorithm receivers have a noise-whitening filter. Henceforth, they will be referred to as whitening filter DFSE (WF-DFSE) and whitening filter M-algorithm (WF-MA) receivers. For the case where the front-end filter is matched to the overall channel response with autocorrelation spectrum S (standard matched filtering), the noise-whitening filter is given by F^{-H}. The branch metric for the WF-DFSE(S) and WF-MA(S) receivers[9] is obtained by replacing $P^{-1} = R = Q^H = F^H$ in (4.38) and (4.22) respectively. An upper bound on the first event error probability of the WF-DFSE(S) receiver is given by (4.62), with the error distance obtained by substituting $R_k = Q_k^H = F_k^H$ in (4.63) and noting that

$$(S^{-1})_k = (F^{-1}F^{-H})_k = (F^{-1})_k(F^{-H})_k = (F_k)^{-1}(F_k)^{-H} \tag{4.72}$$

where the second and third equalities follow from the following identity.

If X and Y are $N \times N$ matrices and Y is upper-triangular (or X is lower-triangular), then

$$(XY)_k = X_k Y_k \tag{4.73}$$

where $(XY)_k$ is the principal submatrix of dimension $k < N$ of the matrix XY.

The error distance is then given by

$$\delta(\underline{e}) = \|F_k \underline{e}\| \tag{4.74}$$

For the case where the front-end filter is matched to the transmit filter response with autocorrelation spectrum Φ (transmit matched filtering), the noise-whitening filter is given

---

[9]Where 'S' stands for standard matched filtering.

by F'^{-H}. The branch metric is obtained by replacing $P^{-1} = R' = Q'^H = F'^H$ in (4.44) and (4.35) respectively for the WF-DFSE(T)[10] and WF-MA(T) receivers. The error distance for the WF-DFSE(T) receiver follows from (A.6) as

$$\delta(\underline{e}) = \|F_k' C_k \underline{e}\|. \tag{4.75}$$

Note that the two expressions for the error distance of WF-DFSE receivers (4.74) and (4.75) differ from each other due to the different phase characteristic of the whitened channel in each case. In the first case, the whitened channel $\{f(n)\}$ has minimum-phase while in the second case, the whitened channel $\{f'(n) * c(n)\}$ has mixed phase, in general. We will see later that the error distance and hence the error probability is superior in the case of the minimum-phase channel. Note that the first event error probability expressions derived here are equivalent to the expression obtained in [8].

4.7.2 Receivers with a zero-forcing filter

The other type of unbiased DFSE and M-algorithm receivers consist of a zero-forcing filter. Henceforth, they will be referred to as zero-forcing filter DFSE (ZF-DFSE) and zero-forcing filter M-algorithm (ZF-MA) receivers. For the case of standard matched filtering, the zero-forcing filter is given by S^{-1}. The branch metric for the ZF-DFSE(S) and ZF-MA(S) receivers is obtained by replacing $P^{-1} = Q = S$, $R = I$ in (4.38) and (4.22) respectively. Substituting these values in (4.63) gives the error distance for the ZF-DFSE(S) receiver as

$$\delta(\underline{e}) = \frac{\underline{e}^H S_k \underline{e}}{\sqrt{\underline{e}^H S_k (S^{-1})_k S_k \underline{e}}}. \tag{4.76}$$

For the case of transmit matched filtering, the zero-forcing filter is given by Φ^{-1}. The branch metric is obtained by replacing $P^{-1} = Q' = \Phi$, $R' = I$ in (4.44) and (4.35), respectively for the ZF-DFSE(T) and ZF-MA(T) receivers. The error distance for the ZF-DFSE(T) receiver follows from (A.6) as

$$\delta(\underline{e}) = \frac{\underline{e}^H C_k^H \Phi_k C_k \underline{e}}{\sqrt{\underline{e}^H C_k^H \Phi_k (\Phi^{-1})_k \Phi_k C_k \underline{e}}}. \tag{4.77}$$

Note that the zero-forcing filter Φ^{-1} in the latter case does not null out inter-symbol interference entirely. It decorrelates only the part due to the autocorrelation of the front-end filter response while the part which is due to the dispersion caused by the medium response $\{c(n)\}$ is left untouched.

---

[10]Where 'T' stands for transmit matched filtering.

47

4.8 Biased receivers

Several biased receivers are possible. One example is a DFSE receiver considered in [37]. It comprises a front-end filter matched to the overall channel response followed by the noise-whitening filter $P = F^{-H}$. The reduced trellis search algorithm uses the branch metric formulation $R = I$, $Q = S$. To see that the receiver is biased, note that $F_k^H F_k \neq S_k$ ($k \ll N$). It follows from (4.51) that the error event ε depends on the transmitted sequence $\underline{a}$ through $(S_k - F_k^H F_k)\underline{a}_k$.

Note that a transversal processing filter adds complexity to a receiver. The computation of a noise-whitening or zero-forcing filter requires channel inversion and factorization operations. Moreover, the filter has to track the variation in the channel if the channel is time-varying. One solution to this problem is to omit the processing filter and pass the output of the matched filter directly to the trellis or tree search algorithm, resulting in a class of receivers which we refer to as matched filter receivers. Matched filter receivers, however, are biased. In other words, their error performance is limited by untreated interference components. Some useful matched filter receivers are described in the following sections.

4.8.1 Matched filter receivers

An important type of matched filter DFSE (MF-DFSE) and matched filter M-algorithm (MF-MA) receivers have a front-end filter matched to the overall channel response followed by a reduced trellis or tree search algorithm with branch metric obtained by replacing $P^{-1} = R = I$, $Q = S$ in (4.38) and (4.22) respectively. The MF-DFSE receiver of this type was proposed in [7,50]. The MF-MA receiver of this type was considered in [48,51]. An upper bound on the first event error probability of the MF-DFSE(S) receiver was derived in [19,20]. Using $P^{-1} = R = I$, $Q = S$ in (4.51), note that the error event ε occurs in the MF-DFSE(S) receiver if

$$2\mathrm{Re}\{\underline{e}_k^H \underline{u}_k\} > \underline{e}_k^H S_k \underline{e}_k - 2\mathrm{Re}\{\underline{\xi}^H \dot{S}_{L-J}^H \dot{\underline{a}}_k\} \tag{4.78}$$

where $\dot{\underline{a}}_k = [a_k, \ldots, a_{k+L-J-1}]^T$, $\underline{\xi}$ is the tail of the error sequence $\underline{e}_k$ comprising the last $L - J$ non-zero components of $\underline{e}_k$, given by[11]

$$\underline{\xi} = [e_{k-L}, \ldots, e_{k-J-1}]^T \tag{4.79}$$

---

[11] In (4.79), $e_i = 0$ for $i < 0$.

and $\dot{S}$ is an $L \times L$ matrix given by

$$
\dot{S} = \begin{bmatrix} s(L) & \cdots & s(2) & s(1) \\ 0 & \ddots & & \vdots \\ \vdots & \ddots & s(L) & s(L-1) \\ 0 & \cdots & 0 & s(L) \end{bmatrix}. \tag{4.80}
$$

It then follows that the first event error probability can be upperbounded using the union bound as

$$
P_{FEE} \leq \sum_{\underline{e} \in E'} p_{\underline{e}} \mathrm{E}_{\underline{a}} \left[Q \left(\frac{\delta(\underline{e}) - \gamma(\underline{e}, \underline{a})}{2\sqrt{N_0}} \right) \right] \tag{4.81}
$$

where $\delta(\underline{e})$ is the error distance given by

$$
\delta(\underline{e}) = \sqrt{\underline{e}^H S_k \underline{e}} \tag{4.82}
$$

and $\gamma(\underline{e}, \underline{a})$ is the untreated interference given by

$$
\gamma(\underline{e}, \underline{a}) = 2\mathrm{Re}\{\underline{\xi}^H \dot{S}_{L-J}^H \underline{\dot{a}}_k\}/\delta(\underline{e}). \tag{4.83}
$$

McLane investigated truncated-state Viterbi detectors (TSVD) with standard matched filters in [32]. The difference between the TSVD algorithm of [32] and the MF-DFSE algorithm is that the MF-DFSE algorithm uses conditional tentative decisions to cancel the tail of the channel response while the TSVD algorithm simply ignores it. The error bounds obtained by McLane indicate the presence of untreated interference. However, the untreated interference in his bounds arises due to ignoring the tail of the channel response in the TSVD algorithm. Such an interference term does not appear in the bounds for DFSE as it is canceled by means of tentative conditional decisions in the DFSE algorithm. The untreated interference component that appears in the DFSE bound of (4.81) is, however, absent in McLane's bounds. The cause of this latter untreated interference component can be intuitively explained as follows. The matched filter statistics at the input of a reduced trellis search algorithm depend on L past and L future transmitted symbols (cf. (4.5)). The reduced trellis search algorithm (with memory order J) selects survivor paths extending up to time n on the basis of the metric accumulated up to time $n + J$. This premature elimination of candidate paths does not account for the interference arising from the $L - J$ future transmitted symbols. Clearly, this type of untreated interference affects both the

49

DFSE and TSVD algorithms. Hence, the bounds in [32] should be corrected to include this interference component.

A second type of matched filter receivers is obtained in the case where the front-end filter is matched to the transmit filer response. The reduced trellis and tree search algorithms of MF-DFSE(T) and MF-MA(T) receivers employ the branch metric given by (4.44) and (4.35) respectively with $P^{-1} = R' = I$, $Q' = \Phi$. Substituting these values in (A.2), we see that an upper bound on the first event error probability of the MF-DFSE(T) receiver is given by (4.81), where the error distance $\delta(\underline{e})$ is given by

$$\delta(\underline{e}) = \underline{e}^H C_k^H \Phi_k C_k \underline{e} \tag{4.84}$$

and the untreated interference $\gamma(\underline{e}, \underline{a})$ is given by

$$\gamma(\underline{e}, \underline{a}) = 2\mathrm{Re}\{\underline{\xi}^H (\ddot{C}_{L_d \times L - J})^H \ddot{\Phi} \ddot{C} \underline{\ddot{a}}_k\} / \delta(\underline{e}) \tag{4.85}$$

where $\underline{\ddot{a}}_k = [a_{k-L_c}, \ldots, a_k, \ldots, a_{k+L_d-1}]^T$ and $\ddot{C}$ and $\ddot{\Phi}$ are $L_d \times L$ and $L_d \times L_d$ matrices respectively, given by

$$\ddot{C} = \begin{bmatrix} c(L_c) & \cdots & c(1) & c(0) & 0 & \cdots & 0 \\ 0 & \ddots & & & \ddots & \ddots & \vdots \\ \vdots & \ddots & \ddots & & & \ddots & 0 \\ 0 & \cdots & 0 & c(L_c) & \cdots & c(1) & c(0) \end{bmatrix}, \tag{4.86}$$

$$\ddot{\Phi} = \begin{bmatrix} \phi(-L_d) & \cdots & \phi(-2) & \phi(-1) \\ 0 & \ddots & & \vdots \\ \vdots & \ddots & \phi(-L_d) & \phi(-L_d+1) \\ 0 & \cdots & 0 & \phi(-L_d) \end{bmatrix}. \tag{4.87}$$

The matrix $\ddot{C}_{L_d \times L - J}$ comprises the first $L - J$ columns of the matrix $\ddot{C}$. In the case of fractional sampling, the MF-DFSE(T) receiver corresponds to the fractional MLSE receiver of Section 3.5.

Note that for a given error sequence $\underline{e}$, the untreated interference $\gamma(\underline{e}, \underline{a})$ in (4.81) has zero mean in the case of i.i.d. transmitted symbols. The interference, thus, increases or decreases the error distance of the MF-DFSE receivers with equal probability. Due to the convexity of the $Q(\cdot)$ function, the error performance is, however, dominated by the

50

destructive effect of the untreated interference and is, thus, rather poor. Without giving an expression for the error probability of the MF-MA receivers, it can be noted that the MF-MA receivers also suffer from untreated interference.

4.9 Truncated memory MLSE receivers

Linear pre-filtering was proposed in [12,35] as a means to truncate the memory of the Viterbi algorithm in an MLSE receiver. In [12], the overall response of the channel/pre-filter combination is forced to a truncated and causal desired impulse response (DIR) of acceptably short span (say J symbols). Pre-filtering colors the noise in the output statistic. However, the Viterbi algorithm is used on the pre-filtered statistic as if the noise were white. An important difference between this approach and our generalized DFSE approach is that the receive filter in the case of DFSE is not specifically designed for a memory order. This allows one to vary the memory order of the trellis search algorithm without changing the receive filter. In the following, we look at the error performance of the pre-filtering method.

Let $\underline{x}$ be the statistic obtained after matched filtering/noise-whitening, i.e.

$$\underline{x} = F\underline{a} + \underline{w} \tag{4.88}$$

where $\underline{w}$ is a white Gaussian noise sequence with covariance $E[\underline{w}\underline{w}^H] = N_0 I$. Let G be an $N \times N$ lower-triangular banded Toeplitz matrix (with band width $J < L$) representing the DIR and H be the corresponding pre-filter matrix, given by $HF = G$. The statistic at the output of the pre-filter is given by

$$\underline{x}^p = G\underline{a} + \underline{w}^p \tag{4.89}$$

where $\underline{w}^p = H\underline{w}$ is the filtered noise.

Consider a path $\{\bar{a}_n\}$ in a truncated memory MLSE (TM-MLSE) receiver that diverges from the correct path $\{a_n\}$ at time 0 and remerges with it at a later time k. A first event error occurs at time 0 if $\{\bar{a}_n\}$ is picked as a survivor path. The error event occurs if the metric accumulated on the incorrect path is greater than the metric on the correct path, i.e.

$$-\|\underline{x}_k^p - G_k\underline{\bar{a}}_k\|^2 > -\|\underline{x}_k^p - G_k\underline{a}_k\|^2. \tag{4.90}$$

Using (4.89), we get

$$2\text{Re}\{\underline{e}_k^H G_k^H \underline{w}_k^p\} > \|G_k\underline{e}_k\|^2 \tag{4.91}$$

where $\underline{\epsilon}_k = \underline{\bar{a}}_k - \underline{a}_k$ is the error sequence. Note that H is a lower-triangular matrix. Therefore, $E[\underline{w}_k^p \underline{w}_k^{pH}] = N_0 H_k H_k^H$ and the probability of the error event ε: the sequence $\underline{a}_k$ is eliminated in favor of the sequence $\underline{a}_k + \underline{\epsilon}_k$, is given by

$$\Pr(\varepsilon) = Q\left(\frac{\delta(\underline{\epsilon})}{2\sqrt{N_0}}\right) \tag{4.92}$$

where $\delta(\underline{\epsilon})$ is the distance of the error sequence $\underline{\epsilon}$ (we drop the subscript k), given by

$$\delta(\underline{\epsilon}) = \frac{\|G_k \underline{\epsilon}\|^2}{\sqrt{\underline{\epsilon}^H G_k^H H_k H_k^H G_k \underline{\epsilon}}}. \tag{4.93}$$

4.10 Symbol error probability

Consider a path in the reduced-state trellis of a DFSE receiver that diverges from the correct path at time n_1 and remerges with it at a later time n_2. Due to feedback incorporated in the reduced trellis search algorithm, the event that the correct path is eliminated in favor of the incorrect path (an error event) depends on previous error events. The effect of the error propagation is, however, small in DFSE receivers as compared to simple decision feedback equalizers (DFE). This is because the decisions fed back in DFSE are conditioned on the state of the reduced trellis unlike the decisions in DFE. Moreover, the effect of error propagation is small at medium to high signal-to-noise ratio (SNR). This was shown to be the case for WF-DFSE receivers in [8,9]. Assuming no error propagation (i.e. a separation of more than $L - J$ correct decisions between error events), the probability that an error event occurs in a DFSE receiver can be upperbounded by the first event error probability [29]. The symbol error probability for unbiased DFSE receivers can then be upperbounded as [8,13]

$$P_s \leq \sum_{\underline{\epsilon} \in E'} w(\underline{\epsilon}) p_{\underline{\epsilon}} Q\left(\frac{\delta(\underline{\epsilon})}{2\sqrt{N_0}}\right) \tag{4.94}$$

where $w(\underline{\epsilon})$ is the number of symbol errors entailed by the error sequence $\underline{\epsilon}$, $\delta(\underline{\epsilon})$ is the distance of the error sequence and $p_{\underline{\epsilon}}$ is the probability that a transmitted sequence can have $\underline{\epsilon}$ as an error sequence. For i.i.d. transmitted sequences and input alphabet $\mathcal{A} = \{\pm 1, \pm 3, \ldots, \pm(|\mathcal{A}| - 1)\}$ (for $|\mathcal{A}|$ even), we have

$$p_{\underline{\epsilon}} = \prod_{n=0}^{k-1-J} \frac{|\mathcal{A}| - \frac{1}{2}|e_n|}{|\mathcal{A}|} \tag{4.95}$$

which reduces to

$$p_{\underline{\epsilon}} = 2^{-w(\underline{\epsilon})} \tag{4.96}$$

in the case of BPSK modulation. The error distance $\delta(\underline{e})$ is given by (4.74) and (4.75) for WF-DFSE receivers with the standard and transmit matched filters, respectively. The error distance for ZF-DFSE receivers given by (4.76) and (4.77), depends on the location and length of the error event. This is because the correlation in the noise samples given by S^{-1} varies over the length of the data sequence. However, note that the noise correlation is constant in the middle of a long sequence (i.e. S^{-1} is nearly Toeplitz except at the edges for $N \gg L$). In Appendix C, we obtain expressions for the error distance that assume the noise correlation to be constant. The error distance in the case of standard and transmit matched filtering is given by (C.5) and (C.6) respectively. The symbol error probability bound of (4.94) also holds for the truncated memory MLSE receiver of Section 4.9 with the error distance given by (4.93). In this case, it is a strict upper bound as there is no decision feedback and thus no error propagation.

For moderate SNRs, the upper bound given by (4.94) is dominated by the term

$$Q\left(\frac{\delta_{min}}{2\sqrt{N_0}}\right) \sum_{\underline{e} \in E'_{min}} w(\underline{e}) p_{\underline{e}} \tag{4.97}$$

where E'_{min} is the set of error sequences in E' that achieve the minimum distance (known as minimum distance sequences)

$$\delta_{min} = \min_{\underline{e} \in E'} \delta(\underline{e}). \tag{4.98}$$

The symbol error probability for MF-DFSE receivers can similarly be upperbounded as

$$P_s \leq \sum_{\underline{e} \in E'} w(\underline{e}) p_{\underline{e}} \mathrm{E}_{\underline{a}} \left[Q\left(\frac{\delta(\underline{e}) - \gamma(\underline{e}, \underline{a})}{2\sqrt{N_0}}\right) \right] \tag{4.99}$$

where the error distance $\delta(\underline{e})$ and the untreated interference $\gamma(\underline{e}, \underline{a})$ are given by (4.82) and (4.83) for the case of standard matched filtering and (4.84) and (4.85) for the case of transmit matched filtering respectively. Due to the presence of untreated interference, the upper bound in (4.99) is not dominated by the minimum distance error sequences only, unlike the bound for unbiased DFSE receivers. Higher distance error sequences should also be considered with worst case interference.

4.11 Error distance

The various DFSE receivers derived in the previous sections can be compared on the basis of their error distance. In the case of an unbiased DFSE receiver, the minimum error

53

distance squared per noise spectral density can be considered as its effective SNR [8]. For a given channel and memory order, the distance of a given error sequence depends on the type of the DFSE receiver. Specifically, it depends on the receive filter and the branch metric. In this section, we compare the error distance for various receivers.

Let $\underline{e} = [e_0, e_1, \ldots, e_{k-1-J}, 0, \ldots, 0]^T$ be an error sequence of length k belonging to the set E'_J (the set E' of allowable error sequences for a DFSE receiver with memory order $J < L$). Let $\underline{e}_+ = [\underline{e}^T, 0, \ldots, 0]^T$ (length $l = k + L - J$). Then, $\underline{e}_+ \in E'_L$, the set of allowable error sequences for an MLSE receiver. The distance of this sequence in the case of an MLSE receiver is given by

$$\delta(\underline{e}_+) = \underline{e}_+^H S_l \underline{e}_+ = \underline{e}^H S_k \underline{e} \tag{4.100}$$

which is equal to the distance of the corresponding error sequence in the case of a MF-DFSE receiver with the standard matched filter. Let E''_J be the set of all error sequences in E'_J appended by $L - J$ zeros $(L > J)$. Note that $E''_J \subsetneq E'_L$, i.e. the upper bounds given by (4.94) and (4.99) for DFSE receivers are determined using only a subset of the error sequences considered for an MLSE receiver[12]. Thus, if the untreated interference in the case of MF-DFSE(S) could be removed ideally with the aid of a genie, the upper bound for the receiver would be lower than MLSE. In fact, the error rate performance of the genie-aided receiver is generally better than MLSE in moderate SNRs where error propagation is negligible. For the other DFSE receivers, we will show that the error distance is smaller, in general, compared to the MF-DFSE(S) receiver (or an MLSE receiver).

4.11.1 WF-DFSE

Consider the case of WF-DFSE(S) receiver. Note that

$$\underline{e}_+^H S_l \underline{e}_+ = \underline{e}_N^H S \underline{e}_N = \|F\underline{e}_N\|^2 = \|F_l \underline{e}_+\|^2 = \|F_k \underline{e}\|^2 + \|\dot{\Psi}\underline{\xi}\|^2 \tag{4.101}$$

---

[12]The error sequences excluded have more than $J - 1$ consecutive zeros in the midst and hence cause a reduced trellis encoder with memory J to flush.

where $\underline{e}_N = [\underline{e}_+^T 0, \ldots, 0]^T$ (length N), $\underline{\xi}$ is given by (4.79) and $\dot{\Psi}$ is an $L - J \times L - J$ matrix given by

$$\dot{\Psi} = \begin{bmatrix} f(L) & \cdots & \cdots & f(J+1) \\ 0 & \ddots & & \vdots \\ \vdots & \ddots & f(L) & f(L-1) \\ 0 & \cdots & 0 & f(L) \end{bmatrix}. \qquad (4.102)$$

The matrix $\dot{\Psi}$ is illustrated in Fig. 4.6. The distance of a given error sequence is thus
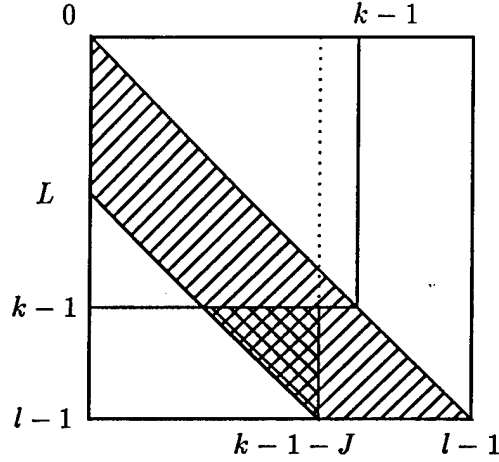
Figure 4.6: Illustration of $\dot{\Psi}$ within F_l.

smaller for WF-DFSE(S) as compared to MF-DFSE(S). The loss in squared distance is given by

$$\|\dot{\Psi}\underline{\xi}\|^2. \qquad (4.103)$$

Now consider the case of the WF-DFSE(T) receiver. Let

$$v(i,j) = \begin{cases} v(i-j) & 0 \le i - j \le L \\ 0 & \text{otherwise} \end{cases} \qquad (4.104)$$

be the coefficients of the lower-triangular Toepltiz matrix $V = F'C$. Then, similar to (4.101), we can write

$$\underline{e}_+^H S_l \underline{e}_+ = \|F_l'C_l\underline{e}_+\|^2 = \|F_k'C_k\underline{e}\|^2 + \|\ddot{\Psi}\underline{\xi}\|^2 \qquad (4.105)$$

where $\ddot{\Psi}$ is an $L - J \times L - J$ matrix given by

$$\ddot{\Psi} = \begin{bmatrix} v(L) & \cdots & \cdots & v(J+1) \\ 0 & \ddots & & \vdots \\ \vdots & \ddots & v(L) & v(L-1) \\ 0 & \cdots & 0 & v(L) \end{bmatrix}. \qquad (4.106)$$

The loss in squared distance in this case is given by

$$\|\ddot{\Psi}\underline{\xi}\|^2. \qquad (4.107)$$

Note that the matrix F of the whitened channel coefficients $\{f(n)\}$ (in the case of standard matched filtering), is invertible since $F(z)$, the z-transform of $\{f(n)\}$, is minimum-phase (has all roots inside the unit circle). Similarly, $F'(z)$, the z-transform of $\{f'(n)\}$, is minimum-phase. However, the z-transform $C(z)$ of the medium response coefficients $\{c(n)\}$ may be non-minimum phase. Therefore, $V(z) = F'(z)C(z)$, the z-transform of the coefficients of the whitened channel $\{v(n)\}$ (in the case of transmit matched filtering), is mixed-phase in general. The whitened channels in the two cases have the same magnitude response, as

$$F^*(z^{-1})F(z) = V^*(z^{-1})V(z) = S(z) \qquad (4.108)$$

where $S(z)$ is the z-transform of the sampled channel autocorrelation function $\{s(n)\}$. Note that channels with identical magnitude response but different phase responses have different energy distribution among tap coefficients. The minimum-phase channel has most of its energy contained in the leading tap coefficients, while the maximum-phase channel (with all roots outside the unit circle) has most of its energy contained in the lagging tap coefficients. As a result, the coefficients of the matrix $\dot{\Psi}$ (belonging to the minimum-phase channel F) have smaller magnitude, in general, than the coefficients of the matrix $\ddot{\Psi}$. Thus, the loss in squared distance compared to MLSE in the case of standard and transmit matched filtering given by (4.103) and (4.107) respectively is smaller in the first case.

4.11.2 ZF-DFSE

Next, consider ZF-DFSE receivers. In Appendix C, we show that the error distance for the case of ZF-DFSE(S) can be written as

$$\frac{\underline{e}^H S_k \underline{e}}{\sqrt{\underline{e}^H S_k (S^{-1})_k S_k \underline{e}}} = \frac{\underline{e}^H S_k \underline{e}}{\sqrt{\underline{e}^H S_k \underline{e} + \underline{\xi}^H \dot{S}_{L-J}^H (S_{22}^I)_L \dot{S}_{L-J} \underline{\xi}}} \qquad (4.109)$$

where $(S_{22}^I)_L$ is a submatrix of the matrix S^{-1} and is thus positive definite. Note that the second term in the denominator of the RHS of (4.109) is greater than zero as the matrix $\dot{S}$ is full rank (since $s(-L) \neq 0$). Thus, the error distance for ZF-DFSE(S) is less than MF-DFSE(S). Similarly, it can be shown that the error distance for ZF-DFSE(T) is smaller than that for MF-DFSE(T).

4.11.3 Optimum unbiased DFSE receivers

In this section, we show that WF-DFSE receivers are optimum in the sense that they minimize the first event error probability of unbiased DFSE receivers. Equivalently, we show that WF-DFSE receivers maximize the distance of a given error sequence in the class of DFSE receivers that satisfy the unbiasedness condition, i.e.

$$\frac{\underline{e}^H R_k Q_k \underline{e}}{\sqrt{\underline{e}^H R_k Q_k (S^{-1})_k R_k Q_k \underline{e}}} \leq \|F_k \underline{e}\| \tag{4.110}$$

with equality only if $Q_k = F_k$, where $(R, Q) = (I, S)$ or (F^H, F) and

$$\frac{\underline{e}^H C_k^H R_k' Q_k' C_k \underline{e}}{\sqrt{\underline{e}^H C_k^H R_k' Q_k' (\Phi^{-1})_k R_k' Q_k' C_k \underline{e}}} \leq \|F_k' C_k \underline{e}\| \tag{4.111}$$

with equality only if $Q_k' = F_k'$, where $(R', Q') = (I, \Phi)$ or (F'^H, F').

To prove Proposition (4.110), we note that

$$\begin{aligned} \underline{e}^H R_k Q_k \underline{e} &= \underline{e}^H (F_k)^H (F_k)^{-H} R_k Q_k \underline{e} \\ &\leq \|F_k \underline{e}\| \|(F_k)^{-H} R_k Q_k \underline{e}\| \\ &= \|F_k \underline{e}\| \sqrt{\underline{e}^H Q_k^H R_k^H (S^{-1})_k R_k Q_k \underline{e}} \end{aligned} \tag{4.112}$$

where the inequality in (4.112) is the Schwartz inequality which becomes an equality only if $R_k = Q_k^H = F_k^H$. The last equality in (4.112) follows from (4.72). Proposition (4.111) can be shown similarly.

Comparing the error distance of the WF-DFSE receiver with the truncated memory MLSE receiver of Section 4.9 (with the same memory order), we note that

$$\begin{aligned} \underline{e}^H G_k^H G_k \underline{e} &= \underline{e}^H G_k^H H_k F_k \underline{e} \\ &\leq \|H_k^H G_k \underline{e}\| \|F_k \underline{e}\| \end{aligned} \tag{4.113}$$

where $G_k = (HF)_k = H_k F_k$ follows from (4.73) as H is a lower-triangular matrix and we again use the Schwartz inequality. Thus, we get

$$\frac{\|G_k \underline{e}\|^2}{\sqrt{\underline{e}^H G_k^H H_k H_k^H G_k \underline{e}}} \leq \|F_k \underline{c}\|. \tag{4.114}$$

In conclusion, we see that the distance of a given error sequence for a DFSE receiver depends on the type of filtering and the branch metric. The distance for the MF-DFSE(S) receiver is the same as in the case of an MLSE receiver. For the unbiased DFSE receivers – WF-DFSE and ZF-DFSE, the distance is smaller. This is due to the fact that the standard matched filter collects all the energy of the pulse transmitted at a given time in the corresponding output sample (in other words, it maximizes the output SNR, given by $|s(0)|^2/N_0$). The noise-whitening filter spreads out the signal energy into $L + 1$ output samples in the process of whitening noise ($\sum_{i=0}^{L} |f(i)|^2 = |s(0)|^2$). The linear zero-forcing filter decorrelates all interfering signal components but enhances (and correlates) noise in the process. The reduced trellis-search algorithms that follow these filters recover part of the signal energy (or SNR) that is spread out but are unable to recover all of it. Thus, WF-DFSE and ZF-DFSE suffer from a loss of the effective SNR, while MF-DFSE(S) does not. Of course, the drawback with MF-DFSE is that the reduced trellis search algorithm is unable to resolve some anticausal interfering signal components. This problem is alleviated in BC-MF-DFSE where the untreated components are canceled using tentative decisions. If reliable tentative decisions can be obtained, the BC-MF-DFSE receiver presents an advantage over the unbiased DFSE receivers in terms of SNR.

The noise-whitening filter removes only the anti-causal signal components which is necessary for unbiasedness. The causal signal components forming the tail of the channel response are equalized using decision feedback which does not enhance noise. The zero-forcing filter on the other hand performs complete signal decorrelation. This leads to noise enhancement and a further loss of the error distance. Similarly, the use of pre-filtering to remove some of the causal signal components in a truncated memory MLSE receiver enhances noise. Thus, WF-DFSE has greater error distance than ZF-DFSE and truncated memory MLSE receivers with pre-filtering. Practically, error propagation slightly degrades DFSE performance at moderate SNRs. Error propagation, however, does not occur in a truncated memory MLSE receiver with pre-filtering as there is no decision feedback.

4.12 Bound evaluation

In this section, we describe a generating function method to evaluate the symbol error probability bounds given in Section 4.10 for unbiased DFSE receivers. Note that a generating function method has never been considered for the well-known WF-DFSE receiver. In [10] and [8], the minimum distance was used to approximate the symbol error probability. However, the approximation may not be very good depending on the system, even at high SNRs [39]. In [39], a stack algorithm was proposed to obtain a chosen number of the largest terms in the union upper bound of (4.94). It was stated in [39] that a generating function method can not be applied to the case of DFSE because unlike MLSE, branch distances in DFSE can not be uniquely determined from pairs of error states due to decision feedback incorporated in the branch metric calculation. We note that the problem with the approach in [39] is that the branch distance depends on $L + 1$ error symbols (where L is the channel memory) while the states in the error state diagram of [39] represent $J + 1$ error symbols (where $J < L$ is the memory order of DFSE). In the following, we show how an error state diagram used to obtain error distances in MLSE, can be modified in the case of DFSE.

An error state diagram (ESD) in the case of DFSE enumerates the distance $\delta(\underline{e})$, the number of symbol errors $w(\underline{e})$ and the *a priori* probability $p(\underline{e})$ of all error sequences $\underline{e}$ in the set of allowable sequences E'. Each path through the ESD corresponds to an error sequence in E'. For WF-DFSE, ZF-DFSE and MF-DFSE, the branch distance (defined later for each case) depends on $L + 1$ error symbols identified uniquely by a pair of error states, where an error state is defined as the value of L consecutive error symbols: $\{e_{j-L}, e_{j-L+1}, \ldots, e_{j-1}\}$. Since, an error symbol can take on any of $2|\mathcal{A}| - 1$ values (including zero), the diagram has $(2|\mathcal{A}| - 1)^L$ error states or nodes, as in MLSE [46]. The nodes are connected to each other through branches. Since an error sequence in the set E' can have no more than $J - 1$ consecutive zeros in the middle of the sequence, the nodes and branches that correspond to J or more consecutive zeros in the middle of the error path are expurgated. The modified error state diagram is shown in Fig. 4.7 for the case of a binary symbol alphabet, channel memory $L = 3$ and memory order $J = 1$. The error states or nodes are ternary L-tuples that take values in $\{0, +2, -2\}$. The pairs of error states that are negative of each other have been combined, as in [46]. This is because the branch distances for such error states are identical, as we will see later. Note that with $L = 3$, there should be $(3^3 - 1)/2 = 13$
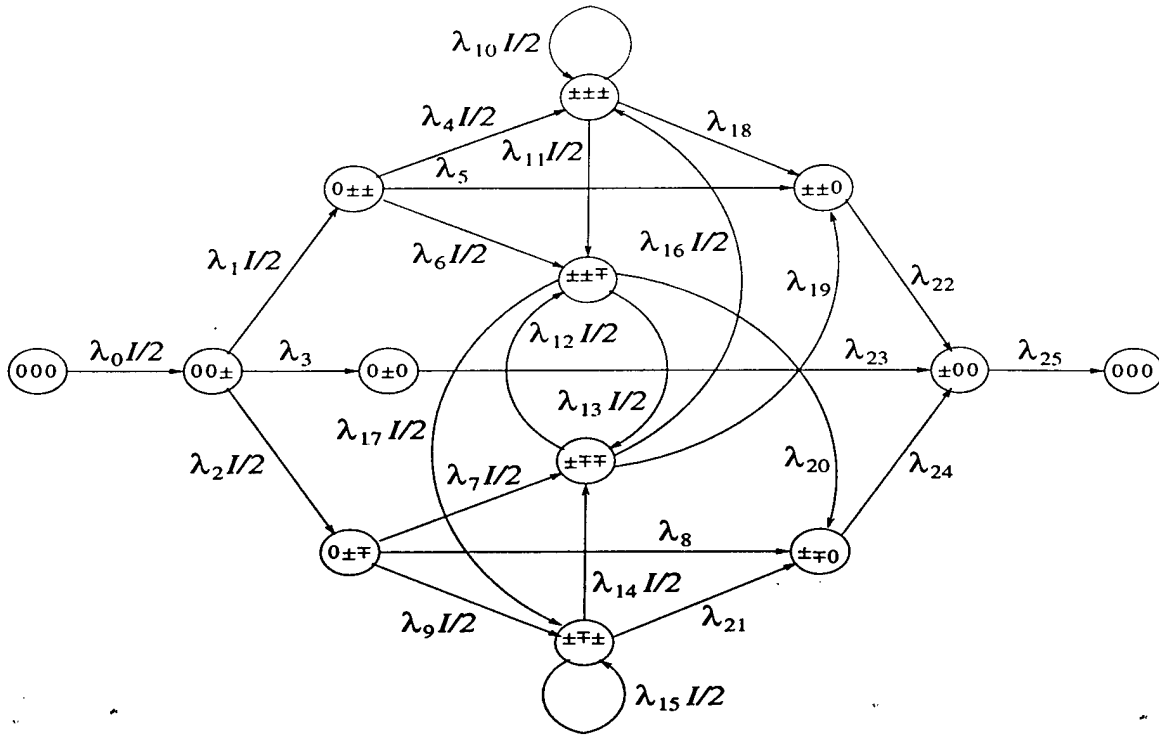
Figure 4.7: Error state diagram for DFSE ($L = 3, J = 1$).

non-zero error state pairs in the ESD. However, the nodes $\pm 0\pm$ and $\pm 0\mp$ do not appear in the ESD of Fig. 4.7. Moreover, the nodes 0 ± 0, $\pm \pm 0$, $\pm \mp 0$ and ± 00 have only one outgoing branch each. This is because the nodes and branches that correspond to a zero in the middle of the error path, have been eliminated because with $J = 1$, an allowable error sequences can not have any zeros in the middle of the sequence. The branches are labeled with the branch distance parameter λ and the number of symbol errors entailed by the transition as the exponent of dummy variable I. A factor of $1/2$ is used to account for the a-priori probability of error if the transition involves an error.

For the case of WF-DFSE, the error distance (squared) $\delta^2(\underline{e})$ is given by

$$\delta^2(\underline{e}) = \sum_{j=0}^{k-1+L-J} b_j \tag{4.115}$$

where k is the length of the error sequence $\underline{e} = \{e_0, e_1, \ldots, e_{k-1}\} \in E'_J$ and b_j is the branch

Table 4.1: Branch distance parameters for WF-DFSE ($L = 3, J = 1$)

$\lambda_0 = D^{4f(0)^2}$	$\lambda_1 = D^{4[f(0)+f(1)]^2}$
$\lambda_2 = D^{4[f(0)-f(1)]^2}$	$\lambda_3 = D^{4f(1)^2}$
$\lambda_4 = D^{4[f(0)+f(1)+f(2)]^2}$	$\lambda_5 = D^{4[f(1)+f(2)]^2}$
$\lambda_6 = D^{4[f(0)-f(1)-f(2)]^2}$	$\lambda_7 = D^{4[f(0)+f(1)-f(2)]^2}$
$\lambda_8 = D^{4[f(1)-f(2)]^2}$	$\lambda_9 = D^{4[f(0)-f(1)+f(2)]^2}$
$\lambda_{10} = D^{4[f(0)+f(1)+f(2)+f(3)]^2}$	$\lambda_{11} = D^{4[f(0)-f(1)-f(2)-f(3)]^2}$
$\lambda_{12} = D^{4[f(0)-f(1)-f(2)+f(3)]^2}$	$\lambda_{13} = D^{4[f(0)+f(1)-f(2)-f(3)]^2}$
$\lambda_{14} = D^{4[f(0)+f(1)-f(2)+f(3)]^2}$	$\lambda_{15} = D^{4[f(0)-f(1)+f(2)-f(3)]^2}$
$\lambda_{16} = D^{4[f(0)+f(1)+f(2)-f(3)]^2}$	$\lambda_{17} = D^{4[f(0)-f(1)+f(2)+f(3)]^2}$
$\lambda_{18} = D^{4[f(1)+f(2)+f(3)]^2}$	$\lambda_{19} = D^{4[f(1)+f(2)-f(3)]^2}$
$\lambda_{20} = D^{4[f(1)-f(2)-f(3)]^2}$	$\lambda_{21} = D^{4[f(1)-f(2)+f(3)]^2}$
$\lambda_{22} = \lambda_{23} = \lambda_{24} = \lambda_{25} = 1$	

distance given by[13]

$$
b_j = \begin{cases} \left(\sum_{i=0}^{L} f(i) e_{j-i} \right)^2 & j = 0, 1, \ldots, k-1 \\ 0 & \text{otherwise} \end{cases} \tag{4.116}
$$

Note that the segment of an error path $\underline{e}$ between the node $\{e_{k-L}, \ldots, e_{k-1-J}, 0, \ldots, 0\}$ ($e_{k-1-J} \neq 0$) and the all-zeros node corresponds to the tail of the error sequence $\underline{\xi}$. Note from (4.116) that the branches within this segment of an error path (which we refer to as tail branches) have distance zero. This is in accordance with (4.101) and (4.105), where the loss in squared distance (compared to MLSE) as given by $\|\dot{\Psi}\underline{\xi}\|^2$ and $\|\ddot{\Psi}\underline{\xi}\|^2$, respectively, occurs on the tail branches.

Table 4.1 lists the branch distance parameters λ_i for Fig. 4.7 for the case of WF-DFSE (also see footnote 13). The branch distance appears as the exponent of a dummy variable D. Let $T(D, I)$ be the generating function for the error paths for WF-DFSE, found by solving the state equations in the ESD of Fig. 4.7 simultaneously. The generating function

---

[13] In the case of transmit matched filtering, $f(i)$ should be replaced by $v(i)$.

61

can be expanded in a series as

$$\frac{\partial}{\partial I} T(D, I)\Big|_{I=1} = \sum_l N_l D^{\delta^2(l)} \tag{4.117}$$

where N_l is the number of error path pairs (negative of each other) with distance $\delta(l)$, per the number of symbol errors and the number of the corresponding input sequences. Then, the symbol error probability bound of (4.94) for WF-DFSE can be computed as[14]

$$P_s \le \sum_l 2N_l D^{\delta^2(l)}\Big|_{D^x = Q\left(\sqrt{x/2N_0}\right)}. \tag{4.118}$$

In the case of ZF-DFSE(S), the squared error distance is given by $\delta^2(\underline{e}) = b_n^2/b_d$, where

$$b_n = \sum_{j=0}^{k-1+L-J} b_{n,j} \tag{4.119}$$

is the numerator distance and

$$b_d = \sum_{j=0}^{k-1+L-J} b_{d,j} \tag{4.120}$$

is the denominator distance, and $b_{n,j}$ and $b_{d,j}$ are the corresponding branch distances which follow from (C.5) as

$$b_{n,j} = \text{Re}\left\{ e_j^* \left(s(0)e_j + 2\sum_{i=1}^{L} s(i)e_{j-i} \right) \right\} \tag{4.121}$$

$$b_{d,j} = \begin{cases} b_{n,j} & j = 0, 1, \ldots, k-1 \\ \underline{\xi}^H \dot{S}_{L-J}^H S_{L-J}' \dot{S}_{L-J} \underline{\xi} & j = k \\ 0 & \text{otherwise} \end{cases} \tag{4.122}$$

Note that the numerator and denominator branch distances differ only at the tail branches according to (C.5).

Table 4.2 lists the branch distance parameters λ_i for Fig. 4.7 in the case of ZF-DFSE(S). Dummy variables D_1 and D_2 are used to enumerate the numerator distance and the denominator distance, respectively. Let $T(D_1, D_2, I)$ be the generating function for the error paths in this case, which can be expanded in a series as

$$\frac{\partial}{\partial I} T(D_1, D_2, I)\Big|_{I=1} = \sum_l M_l D_1^{b_n(l)} D_2^{b_d(l)}. \tag{4.123}$$

where M_l is the number of error path pairs with numerator distance $b_n(l)$ and denominator distance $b_d(l)$, per the number of symbol errors and the number of the corresponding input

---

[14]Note that for real symbol alphabet, the noise is real with power spectral density $N_0/2$.

Table 4.2: Branch distance parameters for ZF-DFSE(S) ($L = 3, J = 1$)

$\lambda_i = D_1^{4\lambda_{1,i}} D_2^{4\lambda_{2,i}}$	
$\lambda_{1,0} = s(0)$	$\lambda_{1,1} = s(0) + 2s(1)$
$\lambda_{1,2} = s(0) - 2s(1)$	$\lambda_{1,4} = s(0) + 2s(1) + 2s(2)$
$\lambda_{1,6} = s(0) - 2s(1) - 2s(2)$	$\lambda_{1,7} = s(0) + 2s(1) - 2s(2)$
$\lambda_{1,9} = s(0) - 2s(1) + 2s(2)$	$\lambda_{1,10} = s(0) + 2s(1) + 2s(2) + 2s(3)$
$\lambda_{1,11} = s(0) - 2s(1) - 2s(2) - 2s(3)$	$\lambda_{1,12} = s(0) - 2s(1) - 2s(2) + 2s(3)$
$\lambda_{1,13} = s(0) + 2s(1) - 2s(2) - 2s(3)$	$\lambda_{1,14} = s(0) + 2s(1) - 2s(2) + 2s(3)$
$\lambda_{1,15} = s(0) - 2s(1) + 2s(2) - 2s(3)$	$\lambda_{1,16} = s(0) + 2s(1) + 2s(2) - 2s(3)$
$\lambda_{1,17} = s(0) - 2s(1) + 2s(2) + 2s(3)$	$\lambda_{1,3} = \lambda_{1,5} = \lambda_{1,8} = \lambda_{1,18-25} = 0$
$\lambda_{2,i} = \lambda_{1,i}$ for $i = 0, 1, \ldots, 21, 25$	
$\lambda_{2,22} = (s(2) + s(3))[s'(0)(s(2) + s(3)) + 2s'(1)s(3)] + s'(0)s(3)^2$	
$\lambda_{2,23} = s(2)[s'(0)s(2) + 2s'(1)s(3)] + s'(0)s(3)^2$	
$\lambda_{2,24} = (s(2) - s(3))[s'(0)(s(2) - s(3)) + 2s'(1)s(3)] + s'(0)s(3)^2$	

Figure 4.8: BER performance of various receivers in Example 1.

sequences. Then, the symbol error probability bound of (4.94) for ZF-DFSE(S) can be computed as

$$P_s \leq \sum_l 2M_l D_1^{b_n(l)} D_2^{b_d(l)} \Bigg|_{D_1^x D_2^y = Q\left(\sqrt{x^2/2N_0 y}\right)} . \tag{4.124}$$

A similar approach can be applied to evaluate the symbol error probability bound for ZF-DFSE(T). A generating function method for MF-DFSE(S) was described in [20].

4.13   Performance results

In this section, we compare the performance of the various receivers described in this chapter via simulation and analysis. We consider BPSK modulation and single-user static time-dispersive AWGN channels. We consider the cases of a symbol-spaced channel model (symbol-rate sampling) and a half symbol-spaced channel model (fractional sampling). The receiver is assumed to have perfect estimates of the symbol timing and the impulse response of the channel. Each simulation was run for a count of 600 errors.

The first example is taken from [39]. The overall channel response is given by symbol-

spaced tap coefficients[15] $f = (0.6335, 0.5456, 0.4479, 0.3167)$. The channel has memory $L = 3$ and is minimum-phase. Nyquist pulse-shaping is assumed. Fig. 4.8 shows the bit-error rate (BER) performance of various receivers for the channel in Example 1 with standard matched filtering. The memory order for the DFSE receivers is set to $J = 1$. With memory order one, the minimum distance in the DFSE receivers is achieved by the error sequences $\pm(2, -2, 0)$. For the MF-DFSE, WF-DFSE and ZF-DFSE receivers, the minimum distance as given by (4.82), (4.74) and (C.5) respectively, equals 0.7322, 0.6470 and 0.5936 respectively[16]. The minimum distance loss for WF-DFSE as compared to MLSE is about 1 dB while that for ZF-DFSE, it is 1.8 dB. Fig. 4.8 shows the upper bound (UB) on the symbol error probability given by (4.94) and the minimum distance bound (MB) given by (4.97) for WF-DFSE and ZF-DFSE. Note that the bounds were obtained assuming absence of error propagation. The simulated BER is marginally higher than the upper bound for both receivers. In the simulations, final decisions were obtained at a lag of 30 symbols. The minimum distance bound converges to the upper bound at high SNR as minimum distance sequences dominate the performance.

Also shown in Fig. 4.8 is the simulated performance of an optimum two-tap TM-MLSE receiver with desired impulse response $(0.7071, 0.7071)$ taken from [12]. Note that the WF-DFSE receiver performs better than the ZF-DFSE and TM-MLSE receivers at all SNRs as discussed in Section 4.11.3. Although the zero-forcing filter in the case of ZF-DFSE, performs more signal decorrelation (which results in noise enhancement) than the prefilter of TM-MLSE, ZF-DFSE performs better than TM-MLSE in this example. This is because, unlike the case of TM-MLSE, the trellis search algorithm in the case of ZF-DFSE takes into account the correlation in the noise samples and is thus able to recover some of the lost signal energy.

The MF-DFSE receiver achieves the maximum error distance equal to that of the MLSE receiver. However, it performs quite poorly due to the presence of untreated interference components. Also shown in Fig. 4.8 is a biased WF-DFSE receiver with the configuration $P^{-1} = F^H, Q = S, R = I$, considered in [37]. Again the effect of untreated interference is evident. The untreated interference arises due to a mismatch between the processing filter and the branch metric as discussed in Section 4.8.

---

[15]Normalized so that $\sum_{i=0}^{L} |f(i)|^2 = 1$.
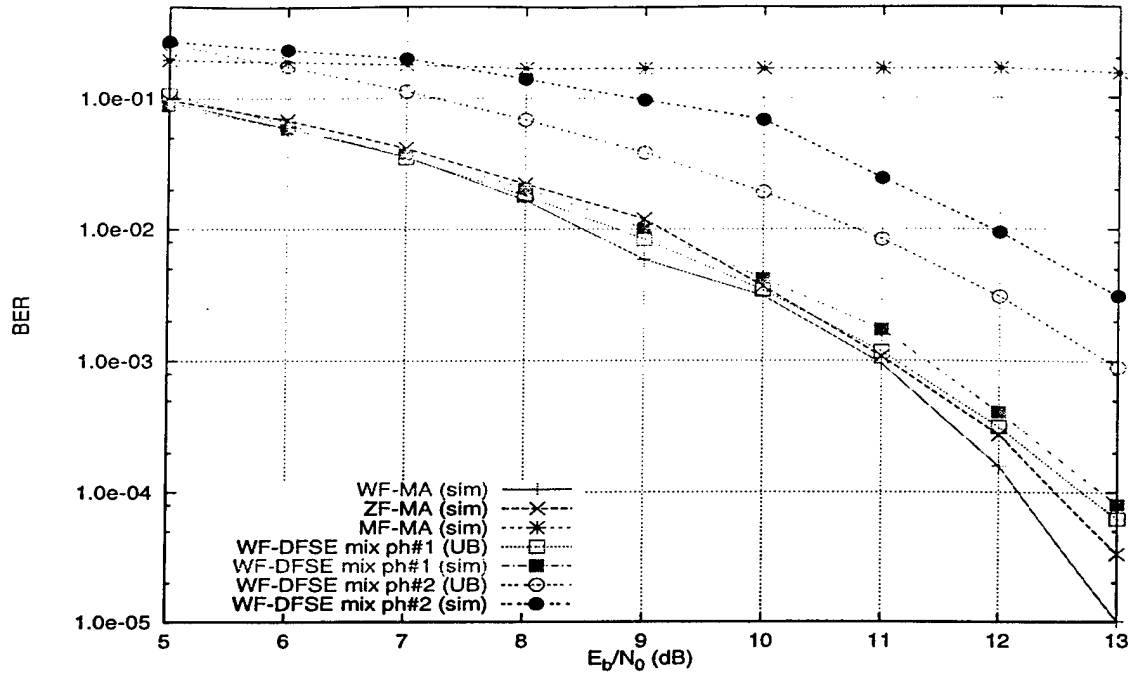
[16]After dividing by two.

65

Figure 4.9: BER performance of various receivers in Example 1.

Fig. 4.9 shows the simulated BER performance of the WF-MA, ZF-MA and MF-MA receivers for the channel in Example 1. The number of paths in the M-algorithm receivers is set to $M = 2$. The WF-MA receiver obtains the best performance. The MF-MA receiver exhibits a (high) error floor like the MF-DFSE and the biased WF-DFSE receivers, all of which belong to the class of biased receivers. Fig. 4.9 also shows the BER performance of WF-DFSE(T) receivers on mixed-phase channels with symbol-spaced medium responses $c = (0.4930, 0.6745, 0.3693, 0.4070)$ (#1) and $c = (0.4070, 0.3693, 0.6745, 0.4930)$ (#2). The channels have the same magnitude response as the channel in Example 1, which is minimum-phase. Note that the performance deteriorates as the channel phase increases. The deterioration in performance is due to two factors: the increase in the distance loss with the channel phase as discussed in Section 4.11 and the increase in error propagation. The latter effect is not captured in the upper bound, so the bound diverges as error propagation becomes significant. The loss in the minimum distance for mixed phase channels 1 and 2 as compared to MLSE is 1.6 dB and 3.1 dB as given by (4.103) and (4.107) respectively.

For our second example, the medium response is given by half-symbol spaced tap coefficients $c = (0.6335, 0.5456, 0.4479, 0.3167)$ (same as the minimum-phase channel of Ex-

66

ample 1 but with fractional spacing). The medium response memory is $L_c = 3$. We consider two different transmit filters specified by the sampled autocorrelation function $\varrho = (0.045, 0.0, 0.4053, 1.0, 0.4053, 0.0, 0.045)$ (T1) and $\phi = (0.33, 0.33, 0.33, 1.0, 0.33, 0.33, 0.33)$ (T2). The first one is a Nyquist-1 pulse (truncated to seven half-symbol samples) taken from [4, (5.5)] while the second one is arbitrarily chosen. The transmit filter memory is $L_d = 3$. The overall channel memory is thus $L = (L_c + L_d)/2 = 3$. The memory order is chosen as $J = 1$ for the DFSE receivers.

Fig. 4.10 shows the BER performance of various receivers for the two transmit filters (T1 and T2) with transmit matched filtering. In the case of T1, the WF-DFSE receiver achieves close to MLSE performance while the performance of MF-DFSE is less than a dB worse. ZF-DFSE is not shown for the case of T1 as its BER is very close to WF-DFSE at all SNRs. Note that the zero-forcing filter in ZF-DFSE(T) decorrelates only the transmit filter response, unlike ZF-DFSE(S) where the zero-forcing filter decorrelates the overall channel response. For the case of T2, we show upper bounds for WF-DFSE and ZF-DFSE which are marginally lower than the simulated results due to error propagation. Note that WF-DFSE performs better than ZF-DFSE at all SNRs as in Example 1. MF-DFSE in the case of T2 is much worse than MLSE as the sampled correlations in the case of T2 are more severe than T1.

4.14 Conclusions

We have presented a unified analysis of DFSE and M-algorithm receivers for channels with finite memory that examines the role of the receive filter and the branch metric. The analysis indicates that the error performance of certain receivers (called biased receivers) is affected by untreated interference components (bias) which arise due to a mismatch between the receive filter and the branch metric. We have shown that an unbiased receiver consists of a front-end filter (matched to the overall channel response or the transmit filter response) followed by the appropriate noise-whitening or zero-forcing filter and a reduced trellis or tree search algorithm. We have shown that the DFSE receivers with the noise-whitening filter (and the proper branch metric) are optimum among unbiased DFSE and truncated memory MLSE receivers (with pre-filtering) in the sense that they maximize the error distance. We have obtained novel receiver structures which employ transmit matched filtering and are

Figure 4.10: BER performance of various receivers in Example 2.

thus suitable for adaptive channel estimation in the presence of excess signal bandwidth. We have obtained upper bounds on the symbol error probability of the various DFSE receivers and described a generating function approach to evaluate the bounds. Simulation and analytical results were presented for the various receivers using a symbol-spaced channel model and a fractionally-spaced channel model. The bounds were found to be tight in each case.

CHAPTER 5

Bias-compensated matched-filter receivers

5.1 Introduction

In Chapter 4, we considered decision feedback sequence estimation (DFSE) and M-algorithm (MA) receivers that operate on matched filter statistics (MF-DFSE and MF-MA). These receivers are simple in that they do not require an additional processing filter like a noise-whitening or zero-forcing filter. Such a filter generally involves channel inversion and/or factorization operations which are not feasible in the case of time-varying, cyclo-stationary and bidirectional channels, as well as channels with deep spectral nulls. Applications that particularly involve such channels include multiuser detection for DS-CDMA systems, bidirectional equalization for the GSM system and fractional equalization for narrowband systems with excess signal bandwidth.

We showed in Chapter 4 that for each case of matched filtering – front-end filter matched to the overall channel response (standard) or transmit filter response (transmit), the MF-DFSE receivers have greater error distance than the corresponding whitening filter DFSE and zero-forcing filter DFSE receivers. In fact, the MF-DFSE receiver with the standard matched filter (MF-DFSE(S)) achieves the same error distance as an MLSE receiver. However, the high error distance of MF-DFSE receivers does not translate into good error-rate performance. This is because the MF-DFSE and MF-MA receivers belong to the class of biased receivers whose error-rate performance is affected by untreated interference components (bias). The bias, in fact, dominates the error-rate performance of these receivers as we saw in simulation examples given in Chapter 4.

The interference components that constitute the bias for the various matched filter

receivers were identified in Chapter 4 using an event error analysis. It was found that the interference arises due to a few anti-causal transmitted symbols. Thus, an intuitive solution to the problem of bias is to cancel it by means of tentative decision feedback. With reliable tentative decisions, the bias can be compensated effectively. As a result, the error-rate performance is no longer dominated by untreated interference components and is improved significantly for most channels of interest. A bias-compensated MF-DFSE (BC-MF-DFSE) receiver was proposed in [20][1] for the case of standard matched filtering. In this chapter, we describe this receiver and obtain a similar receiver for the case of transmit matched filtering. We also discuss an extension of this approach to the case of M-algorithm.

Tentative decisions needed for bias compensation can be obtained by employing a conventional symbol-by-symbol decision device. In a multistage scheme, the decisions obtained in the first stage can also be used to cancel bias in the next stage. On channels with severe intersymbol interference (ISI) or multiple-access interference (MAI), it is not possible to obtain reliable decisions by means of symbol-by-symbol detection. However, by using a minimum mean square error (MMSE) estimator (an optimal symbol-by-symbol soft decision), one can always reduce the mean square error after bias compensation no matter how severe the interference. In practice, we find that a MF-DFSE receiver with soft bias compensation (SBC-MF-DFSE) provides a significant gain over MF-DFSE for most channels of interest without much added complexity.

We analyze the performance of the MF-DFSE receiver for the case of standard matched filtering without and with bias compensation using hard as well as soft tentative decisions. In the case of hard tentative decisions, we obtain approximate semi-analytic upper bounds on the error probability by assuming independence between the main and tentative decision errors. In the case of soft linear tentative decisions, we apply a Chebyshev type technique to upper-bound the error probability in the presence of residual interference. We outline a generating function method to evaluate union bounds on the error probability of the various receivers. The bounds are relatively simple to compute when the memory order of the DFSE receiver and the channel memory is small. For channels with large memory, we use monte carlo simulations to compare the performance of the various receivers.

The chapter is organized as follows. In Sections 5.2 and 5.3, we describe the BC-MF-DFSE receiver for the case of standard (S) and transmit (T) matched filtering respectively.

---

[1]The algorithm is referred to as modified unwhitened DFSE (MUDFSE) in [20].

70

In Section 5.4, we briefly discuss bias compensation for matched-filter M-algorithm. In Section 5.5, we analyze the BC-MF-DFSE(S) receiver. In Section 5.6, we describe bias compensation using soft decisions and obtain various estimators. We analyze the SBC-MF-DFSE algorithm with linear soft decisions in Section 5.7. Simple Chebyshev type bounds for MF-DFSE and SBC-MF-DFSE are described in Section 5.8. In Section 5.9, we describe a generating function approach to evaluate the various bounds. The performance of the various receivers is compared via simulation and analysis in Section 5.10, where we give examples of equalization for ISI channels and multiuser detection for DS-CDMA channels.

5.2 The BC-MF-DFSE(S) receiver

The receiver consists of a front-end filter, which is matched to the overall channel impulse response, followed by a reduced trellis search algorithm. The trellis search algorithm computes path metrics as in MF-DFSE(S) i.e. using (4.37) and (4.38) with the formulation $P^{-1} = R = I$, $Q = S$. Conditional decisions are made (and the corresponding survivor paths are chosen) using the modified rule:

$$\hat{\alpha}_{n-J}(\beta_n) = \arg\max_{\alpha_{n-J}} \left[\mathcal{M}(\beta_n) + \Gamma(\alpha_n, \beta_n) - \text{bias}(\beta_n) \right], \tag{5.1}$$

where $\mathcal{M}(\beta_n)$ and $\Gamma(\alpha_n, \beta_n)$ are the accumulated metric and the branch metric of MF-DFSE(S) respectively and the bias term is given by

$$\text{bias}(\beta_n) = 2\text{Re}\left\{ \underline{\mu}_n^H \dot{S}_{L-J}^H \underline{\tilde{a}}_{n+1} \right\} \tag{5.2}$$

where $\underline{\mu}_n = [\hat{\alpha}_{n-L+1}(\beta_n), \ldots, \hat{\alpha}_{n-J-1}(\beta_n), \alpha_{n-J}]^T$ are the $L - J$ most recent symbols in the survivor path associated with state β_n, $\dot{S}_{L-J}$ is the principal submatrix of dimension $L - J$ of the matrix $\dot{S}$ given by (4.80) and $\underline{\tilde{a}}_{n+1} = [\tilde{a}_{n+1}, \ldots, \tilde{a}_{n+L-J}]^T$ are tentative decisions on $L - J$ future symbols obtained using conventional matched filter detection. In the case of antipodal transmitted symbols, the tentative decisions are obtained as

$$\tilde{a}_n = \text{sign}(z_n). \tag{5.3}$$

The algorithm is delayed by $L - J$ symbols as the statistic up to time $n + L - J$ is needed in the nth step to obtain tentative decisions. Note that the bias term follows from the expression for the untreated interference given by (4.83). The bias is used for survivor path selection only and does not contribute to the accumulated path metric. The bias

71

in (5.2) depends on the symbol α_{n-J} (which is falling out of the state) and the symbols $\alpha_{n-L+1}, \ldots, \alpha_{n-J-1}$ for which conditional decisions, taken from the survivor path history of state β_n, are used. The bias can be simplified to include the leading term only, which depends on α_{n-J}, as follows:

$$\text{bias}(\beta_n) \approx \text{bias}(\alpha_{n-J}) = \text{Re} \left\{ 2\alpha_{n-J}^* \sum_{i=J+1}^{L} s(-i)\tilde{a}_{n-J+i} \right\}. \tag{5.4}$$

Note that the approximate bias is independent of the state. It does not add significantly to the computational load and storage requirement of the MF-DFSE algorithm which is on the order of $(K - J)|\mathcal{A}|^J$, where K is the decision lag. This reduced-computation form of the algorithm was first proposed in [17].

5.2.1 Multistage BC-MF-DFSE(S)

The above algorithms can be run in a multistage configuration where decisions obtained at the output of the first stage are fed back to compute the bias in the second stage and so on, i.e.

$$(\tilde{a}_n)_1 = \text{sign}(z_n) \quad \text{and} \quad (\tilde{a}_n)_i = (\bar{a}_n)_{i-1}, \quad i > 1$$

where $\{(\bar{a}_n)_i\}$ are decisions obtained from the ith stage at lag K_i ($K_i \gg L$). Note that the decisions $\{(\bar{a}_n)_1\}$ are likely to be much more reliable than the tentative decisions $\{(\tilde{a}_n)_1\}$. The complexity and delay of an M-stage scheme is given by $\sum_{i=1}^{M}(K_i-J_i)M^{J_i}$ and $\sum_{i=1}^{M} K_i + L - J_1$ respectively.

5.3 The BC-MF-DFSE(T) receiver

A bias-compensated MF-DFSE receiver can also be obtained for the case of transmit matched filtering (BC-MF-DFSE(T)). In this case, the algorithm computes path metrics as in MF-DFSE(T) using (4.41). Conditional decisions are made using the modified rule:

$$\hat{\alpha}'_{n-J}(\beta_n) = \arg\max_{\alpha_{n-J}}[\mathcal{M}'(\beta_n) + \Gamma'(\alpha_n, \beta_n) - \text{bias}'(\beta_n)] \tag{5.5}$$

where $\mathcal{M}'(\beta_n)$ and $\Gamma'(\alpha_n, \beta_n)$ are the accumulated metric and the branch metric of MF-DFSE(T), respectively, and the bias term is given by

$$\text{bias}'(\beta_n) = 2\text{Re} \left\{ \underline{\mu}_n'^H (\ddot{C}_{L_d \times L-J})^H \ddot{\Phi} \ddot{C} \underline{\tilde{a}}'_{n+1} \right\} \tag{5.6}$$

where $\underline{\mu}'_n = [\eta'_{n-L+1}, \ldots, \eta'_{n-J-1}, \eta'_{n-J}]^T$ are the $L - J$ most recent symbols in the survivor path associated with state β_n and $\underline{\tilde{a}}'_{n+1} = [\eta'_{n-L_c+1}, \ldots, \eta'_n, \tilde{a}'_{n+1}, \ldots, \tilde{a}'_{n+L_d}]^T$, where $\{\tilde{a}'_n\}$ are tentative decisions obtained as $\tilde{a}'_n = \text{sign}(z'_n)$, in the case of antipodal transmitted symbols. The bias term follows from (4.85).

5.4 Bias compensation for M-algorithm

Note that a bias-compensated MF-MA can also be derived on the same principle as described above for BC-MF-DFSE i.e. using tentative decisions to cancel untreated interference components. The untreated interference in the case of MF-MA (with the standard matched filter) follows from (4.66) as $2\text{Re}\{\underline{\xi}(i)^H \dot{S}^H \underline{\hat{a}}_k\}/\delta(\underline{e}(i))$, where $\underline{\xi}(i) = [e_{k-L}(i), \ldots, e_{k-1}(i)]^T$ is the tail of the error sequence $\underline{e}(i)$ corresponding to the ith contender path and $\underline{\hat{a}}_k = [a_k, \ldots, a_{k+L-1}]^T$. The interference can be canceled by choosing survivor paths in the M-algorithm on the basis of the accumulated metric minus a bias term, computed using tentative decisions. Note that the bias term in this case depends on the last L symbols of the survivor path rather than the last $L - J$, as in the case of BC-MF-DFSE. This is because unlike DFSE, the M-algorithm is a tree search algorithm where contender paths are not constrained to merge. Since contender paths in DFSE always agree on the J most recent symbols, the bias term does not depend on them. However, this is not the case with the M-algorithm. Consequently, bias compensation requires more computation for MF-MA as compared to MF-DFSE. Moreover, as the number of interference components that need to be canceled is more in the case of MF-MA, the residual interference arising from tentative decision errors is more significant in the case of MF-MA. Thus, bias compensation does not look very attractive for MF-MA.

5.5 Analysis of BC-MF-DFSE(S)

Let $\{a_n\}$ be the sequence of symbols transmitted and $\{b_n\}$ be the sequence of states in the path of $\{a_n\}$ in the reduced trellis of the BC-MF-DFSE(S) receiver (with memory order J). Let $\{\bar{a}_n\}$ be a hypothetical sequence of symbols and $\{\bar{b}_n\}$ be the corresponding sequence of states in the reduced trellis that diverges from the correct sequence of states at time unit 0 and re-merges with it at a later time (say k). A first event error occurs at time 0 if the reduced trellis search algorithm picks $\{\bar{a}_n\}$ as the survivor sequence over $\{a_n\}$. It

follows from (5.1) that the error event occurs if

$$\sum_{n=0}^{k-1} \Gamma(\bar{a}_n, \bar{b}_n) - \text{bias}(\bar{b}_{k-1}) > \sum_{n=0}^{k-1} \Gamma(a_n, b_n) - \text{bias}(b_{k-1}) \tag{5.7}$$

where the bias term bias($\cdot$) is given by (5.2). Using (4.78) and (5.2), we see that the error event occurs if

$$2\text{Re}\{\underline{e}_k^H \underline{u}_k\} > \underline{e}_k^H S_k \underline{e}_k + 2\text{Re}\{\underline{\xi}^H \dot{S}_{L-J}^H \underline{t}_k\} \tag{5.8}$$

where $\underline{e}_k = \bar{a}_k - \underline{a}_k$ is the error sequence with the tail $\xi = (e_{k-L}, \ldots, e_{k-J-1})^H$ and $\underline{t}_k = \tilde{a}_k - \dot{a}_k$ are tentative decision errors in bias cancellation. To simplify analysis, we assume here that tentative decision errors are independent of main decision errors. This is not true in general because noise samples affecting the sampled statistic, obtained at the output of the matched filter, are correlated. However, independence can be assumed if the sampled channel correlations are small. Then, the probability of the error event ε: the sequence $\underline{a}_k$ is eliminated in favor of the sequence $\underline{a}_k + \underline{e}_k$ (for given $\underline{a}_k$ and $\underline{e}_k$), is approximated as

$$\text{Pr}(\varepsilon) \approx \text{E}_{\underline{t}} \left[Q \left(\frac{\underline{e}_k^H S_k \underline{e}_k + 2\text{Re}\{\underline{\xi}^H \dot{S}_{L-J}^H \underline{t}\}}{2\sqrt{N_0 \underline{e}_k^H S_k \underline{e}_k}} \right) \right] \tag{5.9}$$

where the expectation is taken over all possible values of the tentative decision error vector $\underline{t}$ having $L - J$ components. It follows that the first event error probability of the BC-MF-DFSE(S) receiver can be approximately upper-bounded as

$$P_{FEE} \overset{\sim}{\le} \sum_{\underline{e} \in E'} p_{\underline{e}} \text{E}_{\underline{t}} \left[Q \left(\frac{\delta(\underline{e}) + \gamma(\underline{e}, \underline{t})}{2\sqrt{N_0}} \right) \right] \tag{5.10}$$

where E' is the set of all error sequences $\underline{e} = e_0, e_1, \ldots, e_{l-1}, 0 \ldots, 0$ (of length $l + J$, $l > 0$, $e_{l-1} \ne 0$) with less than J consecutive zeros in the middle of the sequence and the last L components[2] equal to $(\underline{\xi}^T, 0, \ldots, 0)$. The quantity $\delta(\underline{e})$ is the distance of an error sequence $\underline{e} \in E'$ of length k, given by

$$\delta(\underline{e}) = \sqrt{\underline{e}^H S_k \underline{e}}, \tag{5.11}$$

$p_{\underline{e}}$ is the probability that a transmitted sequence can have $\underline{e}$ as an error sequence and $\gamma(\underline{e}, \underline{t})$ is the residual interference arising from tentative decision feedback, given by

$$\gamma(\underline{e}, \underline{t}) = 2\text{Re}\{\underline{\xi}^H \dot{S}_{L-J}^H \underline{t}\} / \delta(\underline{e}). \tag{5.12}$$

---

[2] $e_i = 0$, for $i < 0$.

The residual interference can be viewed as a normalized projection of the tentative decision error vector $\underline{t}$ onto the main decision error vector $\underline{\epsilon}$ as determined by the sampled channel autocorrelation spectrum S. The symbol error probability can be approximately upper-bounded using the union bound as

$$P_s \overset{\sim}{\leq} \sum_{\underline{e} \in E'} \text{w}(\underline{e}) p_{\underline{e}} \text{E}_{\underline{t}} \left[Q \left(\frac{\delta(\underline{e}) - \gamma(\underline{e}, \underline{t})}{2\sqrt{N_0}} \right) \right] \qquad (5.13)$$

where $\text{w}(\underline{e})$ is the number of symbol errors entailed by the error sequence $\underline{e}$. As discussed in Section 4.10, the above bound does not include the effect of error propagation.

In Appendix D, we derive expressions for the probability $\Pr(\varepsilon)$ for a two-stage BC-MF-DFSE receiver, with and without assuming independence between tentative and main decision errors.

5.5.1 Genie-aided MF-DFSE

Assume that perfect information is provided by a genie on the future inputs needed to compute the bias in BC-MF-DFSE i.e. $\underline{t}_k = \underline{0}$ w.p.1. The symbol error probability in this case is given by

$$P_s \leq \sum_{\underline{e} \in E'} \text{w}(\underline{e}) p_{\underline{e}} Q \left(\frac{\delta(\underline{e})}{2\sqrt{N_0}} \right). \qquad (5.14)$$

Note that the above expression for the symbol error probability of genie-aided MF-DFSE (GA-MF-DFSE) is the same as in the case of MLSE. The difference is that the ensemble average is taken over fewer error sequences for GA-MF-DFSE than for MLSE. The set E' does not contain error sequences with more than $J - 1$ but less than L consecutive zeros in the middle. However, these sequences are included in the case of MLSE. Thus, the upper-bound on the symbol probability of GA-MF-DFSE given by (5.14) is lower than MLSE. With the memory order J chosen as zero, all error sequences have length $k = 1$ symbol. This implies that the error distance squared is given by $\underline{e}^H S_k \underline{e} = |e|^2 s(0)$. In other words, zero-th order GA-MF-DFSE achieves the performance of the ISI-free channel. This makes sense since we assumed absence of error propagation from previous error events (by limiting ourself to first error events only) which accounts for all past interference in the case of zero memory order. In reality, zero-th order GA-MF-DFSE approaches ISI-free performance asymptotically at high signal-to-noise ratio for channels where the eye is not entirely closed, as error propagation becomes negligible.

5.6 Soft-input BC-MF-DFSE receivers

Instead of using hard tentative decisions to cancel bias in the BC-MF-DFSE receivers, soft tentative decisions can be employed to reduce the mean square error in the bias compensated output. Consider a memoryless AWGN channel, i.e.

$$z_n = \sqrt{E_b} a_n + w_n \tag{5.15}$$

where $\{w_n\}$ is an independent and identically distributed (i.i.d.) Gaussian random process with mean zero and variance σ_w^2 and $a_n \in \{\pm 1\}$. An optimum soft decision $\tilde{a}_n$ that minimizes the mean square error

$$\mathrm{MSE} = \mathrm{E}[(a_n - \tilde{a}_n)^2] \tag{5.16}$$

is given by [15]

$$\tilde{a}_n = \tanh(z_n \sqrt{E_b}/\sigma_w^2). \tag{5.17}$$

5.6.1 Optimum soft decision

Given the standard matched filter statistic z_n (4.4), the (one-shot) minimum mean square error (MMSE) estimator of a_n is given by [27]

$$\tilde{a}_n = \mathrm{E}[a_n | z_n]. \tag{5.18}$$

For a channel with memory as in (4.4), the above estimator does not turn out to be a simple function of the statistic as in (5.17). A simplified estimator can be obtained by invoking the central limit theorem [27] to approximate the sum of the post and pre-cursor interference components as Gaussian. For i.i.d. equiprobable and antipodal symbols a_n, assuming that $\sum_{i \neq 0} s(i) a_{n-i}$ is a Gaussian random variable with mean zero and variance $\sum_{i \neq 0} |s(i)|^2$, the following estimator is obtained[3]

$$\tilde{a}_n = \tanh\left(\frac{z_n}{\frac{N_0}{2} + \frac{1}{s(0)} \sum_{i \neq 0} |s(i)|^2}\right). \tag{5.19}$$

The above estimator replaces the hard decision of (5.3) in a Soft-input BC-MF-DFSE(S) (SBC-MF-DFSE(S)) receiver.

---

[3]Note that for real symbol alphabet, the noise is real with spectral density $N_0/2$ instead of N_0.

5.6.2 Optimum linear soft decision

Given the statistic z_n (4.4), we determine the (one-shot) linear minimum mean square error (MMSE) estimator of a_n, i.e. we find $\tilde{a}_n$ as a linear function of z_n such that the mean square error given by (5.16) is minimized. Assuming i.i.d., equiprobable antipodal symbols a_n, we get the linear MMSE estimator as

$$\tilde{a}_n = \frac{z_n}{\chi} \tag{5.20}$$

where χ is a normalization factor, given by

$$\chi = \frac{N_0}{2} + \frac{1}{s(0)} \sum_{i=-L}^{L} |s(i)|^2. \tag{5.21}$$

The mean square error of this estimator is given by

$$\mathrm{MSE} = 1 - \frac{s(0)}{\chi} \tag{5.22}$$

which is always less than 1. Thus, the estimator guarantees that the mean square error is reduced at the output of the estimator no matter how severe the interference components.

Note that the MMSE estimator of (5.19) is obtained by using a simplifying assumption, which may not be accurate especially for small channel memory L. However, the linear MMSE estimator of (5.20) is a true optimum estimator.

5.7 Analysis of SBC-MF-DFSE(S)

In this section, we examine the error performance of a SBC-MF-DFSE(S) receiver that employs the linear optimum soft decisions of (5.20) to cancel bias in the case of real antipodal signals. Following the development of (5.8), we see that a first event error, corresponding to the error sequence $\underline{e}_k$, occurs at time 0 in a SBC-MF-DFSE(S) receiver if

$$2\underline{e}_k^T \underline{u}_k > \underline{e}_k^T S_k \underline{e}_k + 2\underline{\xi}^T \dot{S}_{L-J}^T (\tilde{\underline{a}}_k - \dot{\underline{a}}_k) \tag{5.23}$$

where $\tilde{\underline{a}}_k = (\tilde{a}_k, \ldots, \tilde{a}_{k+L-J-1})^T$ are soft tentative decisions given by (5.20). Substituting (4.4) and (5.20) in (5.23), we get

$$2\underline{e}_k^T \underline{u}_k - 2\underline{\xi}^T \dot{S}_{L-J}^T \dot{\underline{u}}_k / \chi > \underline{e}_k^T S_k \underline{e}_k + 2\underline{\xi}^T \dot{S}_{L-J}^T \check{S} \check{\underline{a}}_k / \chi \tag{5.24}$$

where $\check{a}_k = (a_{k-L}, a_{k-L+1}, \ldots, a_{k+2L-J-1})^T$, $\check{u}_k = (u_k, \ldots, u_{k+L-J-1})^T$ and $\check{S}$ is an $(L-J) \times (3L-J)$ matrix given by

$$\check{S} = \begin{bmatrix} s(L) & \cdots & s(1) & (1-\chi)s(0) & s(-1) & \cdots & s(-L) & 0 & \cdots & 0 \\ 0 & s(L) & \cdots & s(1) & (1-\chi)s(0) & s(-1) & \cdots & s(-L) & \ddots & \vdots \\ \vdots & \ddots & \ddots & & & \ddots & & & \ddots & 0 \\ 0 & \cdots & 0 & s(L) & \cdots & s(1) & (1-\chi)s(0) & s(-1) & \cdots & s(-L) \end{bmatrix}.$$

(5.25)

Note that the quantity on the left-hand side of (5.24) is a Gaussian random variable with mean zero and variance given by

$$2N_0 \left(\underline{e}_k^T S_k \underline{e}_k - 2\|\dot{S}_{L-J}\underline{\xi}\|^2/\chi + \underline{\xi}^T \dot{S}_{L-J}^T S_{L-J} \dot{S}_{L-J}\underline{\xi}/\chi^2 \right),$$

(5.26)

where we use the fact that the last L components of $\underline{e}_k$ are $(\underline{\xi}^T, 0, \ldots, 0)$. Thus, the probability of the error event ε corresponding to the error sequence $\underline{e}_k$ of length k can be upper-bounded as

$$\Pr(\varepsilon) \leq \mathrm{E}_{\check{a}} \left[Q \left(\frac{\underline{e}_k^T S_k \underline{e}_k + 2\underline{\xi}^T \dot{S}_{L-J}^T \check{S}\check{a}/\chi}{\sqrt{2N_0 \left(\underline{e}_k^T S_k \underline{e}_k - 2\|\dot{S}_{L-J}\underline{\xi}\|^2/\chi + \underline{\xi}^T \dot{S}_{L-J}^T S_{L-J} \dot{S}_{L-J}\underline{\xi}/\chi^2 \right)}} \right) \right]$$

(5.27)

where the expectation is taken over the $3L-J$ components of $\check{a}$ independently of the error sequence $\underline{e}_k$. Since some of the first $L-J$ components of $\check{a}$ may be uniquely identified by specifying the error sequence $\underline{e}_k$, the expectation is taken over a slightly broader set than needed to obtain $\Pr(\varepsilon)$. Thus, (5.27) is an upper bound and not an exact expression. The symbol error probability can be upper-bounded using the union bound by assuming absence of error propagation from previous error events, as

$$P_s \leq \sum_{\underline{e} \in E'} \mathrm{w}(\underline{e}) p_{\underline{e}} \mathrm{E}_{\check{a}} \left[Q \left(\frac{\underline{e}^T S_k \underline{e} + 2\underline{\xi}^T \dot{S}_{L-J}^T \check{S}\check{a}/\chi}{\sqrt{2N_0 \left(\underline{e}^T S_k \underline{e} - 2\|\dot{S}_{L-J}\underline{\xi}\|^2/\chi + \underline{\xi}^T \dot{S}_{L-J}^T S_{L-J} \dot{S}_{L-J}\underline{\xi}/\chi^2 \right)}} \right) \right].$$

(5.28)

5.8 Simple upper bounds for MF-DFSE and SBC-MF-DFSE

The bounds of (4.99) and (5.28) for MF-DFSE and SBC-MF-DFSE receivers require ensemble averaging over the untreated interference components. In the case of the MF-DFSE(S) receiver, the expectation is taken over $L-J$ interference symbols while in the

case of the SBC-MF-DFSE(S) receiver with linear soft tentative decisions, the expectation is taken over $3L - J$ symbols. The latter is cumbersome to evaluate even for very short channel memory L. Simpler upper bounds can be obtained by extending the results of Glave [16] and Matthews [31] which upper and lower bound the probability of error of a thresholding detector in the presence of ISI. The Glave bound was also applied by Mclane [32] to upper bound the error probability of truncated-state Viterbi detectors. In the following, we apply the Glave bound to the case of MF-DFSE and SBC-MF-DFSE receivers.

Let w be a Gaussian random variable with mean zero and variance σ_w^2 and x be an arbitrary random variable subject to the constraints: $x \in [-I, I]$ almost surely and $E[x^2] \leq \sigma_x^2$. Glave showed in [16, theorem 3] that the probability $\Pr(|w + x| \geq K)$ can be upper-bounded as

$$\Pr(|w + x| \geq K) \leq \frac{\sigma_x^2}{I^2} \left[Q\left(\frac{K - I}{\sigma_w}\right) + Q\left(\frac{K + I}{\sigma_w}\right) \right] + 2\left(1 - \frac{\sigma_x^2}{I^2}\right) Q\left(\frac{K}{\sigma_w}\right) \qquad (5.29)$$

provided that $K - I \geq \sqrt{3}\sigma_w$. For a system with antipodal signals and symbol-by-symbol detection in the presence of ISI, I can be considered as the peak interference, K as the signal amplitude and $K - I$ as the eye opening.

Now we apply the above result to upper-bound the probability of a particular error event for the MF-DFSE(S) receiver obtained in Section 4.8.1. Given an error sequence $\underline{e} \in E'$ of length k with tail $\underline{\xi}$, the error probability given by

$$\Pr(\varepsilon) = E_{\underline{a}}\left[Q\left(\frac{\delta(\underline{e}) - \gamma(\underline{e}, \underline{a})}{\sqrt{2N_0}}\right) \right], \qquad (5.30)$$

for $a_n \in \{\pm 1\}$ (noise spectral density $N_0/2$), where $\gamma(\underline{e}, \underline{a})$ is given by (4.83), is upper-bounded as

$$\Pr(\varepsilon) \leq \frac{\sigma_1^2}{2I_1^2} \left[Q\left(\frac{\delta(\underline{e}) - I_1}{\sqrt{2N_0}}\right) + Q\left(\frac{\delta(\underline{e}) + I_1}{\sqrt{2N_0}}\right) \right] + \left(1 - \frac{\sigma_1^2}{I_1^2}\right) Q\left(\frac{\delta(\underline{e})}{\sqrt{2N_0}}\right) \qquad (5.31)$$

provided that

$$\delta(\underline{e}) - I_1 \geq \sqrt{6N_0}, \qquad (5.32)$$

where[4] $\delta(\underline{e}) = \sqrt{\underline{e}^T S_k \underline{e}}$, $I_1 = 2|\dot{S}_{L-J}\underline{\xi}|/\delta(\underline{e})$ and $\sigma_1^2 = 4\|\dot{S}_{L-J}\underline{\xi}\|^2/\delta^2(\underline{e})$. A similar bound can be obtained for the MF-DFSE(T) receiver.

---

[4] $|\underline{y}| \overset{\triangle}{=} \sum_i |y_i|$.

In the case of the SBC-MF-DFSE(S) receiver analyzed in Section 5.7, the error probability bound given by (5.27) can be further upper-bounded as

$$\Pr(\varepsilon) \leq \frac{\sigma_2^2}{2I_2^2} \left[Q\left(\frac{\delta^2(\underline{e}) - I_2}{\sqrt{2N_0\sigma_n^2}} \right) + Q\left(\frac{\delta^2(\underline{e}) + I_2}{\sqrt{2N_0\sigma_n^2}} \right) \right] + \left(1 - \frac{\sigma_2^2}{I_2^2} \right) Q\left(\frac{\delta^2(\underline{e})}{\sqrt{2N_0\sigma_n^2}} \right). \quad (5.33)$$

provided that

$$\delta^2(\underline{e}) - I_2 \geq \sqrt{6N_0\sigma_n^2}, \quad (5.34)$$

where $I_2 = 2|\check{S}^T \dot{S}_{L-J}\underline{\xi}|/\chi$, $\sigma_2^2 = 4\|\check{S}^T \dot{S}_{L-J}\underline{\xi}\|^2/\chi^2$ and $\sigma_n^2 = \delta^2(\underline{e}) - 2\|\dot{S}_{L-J}\underline{\xi}\|^2/\chi + \underline{\xi}^T \dot{S}_{L-J}^T S_{L-J} \dot{S}_{L-J}\underline{\xi}/\chi^2$.

Note that the matrix $\check{S}$ is given in terms of the sampled channel correlations and the normalization factor χ which depends on the noise spectral density $N_0/2$. The dependence on the noise spectral density means that the matrix $\check{S}$ has to be computed for each value of the signal-to-noise ratio (SNR). The extensive numerical computation can be avoided as the noise spectral density approaches zero. Thus, assuming high SNR, we use the approximation

$$\chi \approx \frac{1}{s(0)} \sum_{i=-L}^{L} |s(i)|^2. \quad (5.35)$$

The condition (5.34) is evaluated for the approximate value of χ although it does not guarantee that the condition is met for the actual value of χ. Using the approximate value of χ in the analysis, we, in fact, upper-bound the error probability for a SBC-MF-DFSE(S) receiver that employs the soft decision

$$\tilde{a}_n = \frac{z_n}{\frac{1}{s(0)} \sum_{i=-L}^{L} |s(i)|^2} \quad (5.36)$$

to cancel bias instead of the optimum linear soft decision (5.20).

In order to determine the union bound on the probability of symbol error, one must take an ensemble average over all possible error sequences $\underline{e} \in E'$ (4.99), (5.28). In order to apply the Glave bound, the corresponding conditions (5.32) and (5.34) must hold for all error sequences $\underline{e} \in E'$. Since the peak untreated interference I_1 and I_2 depend on the tail of the error sequence $\underline{\xi}$, it is not sufficient to check the conditions for the minimum distance sequences ($\underline{e}_{min} = \arg\min_{\underline{e} \in E'} \delta(\underline{e})$) only. In practice, the conditions have to be checked for a few of the higher distance sequences as well.

Glave's upper bound applies only at high SNR values and when the eye (due to the untreated interference) is open. Matthews [31] determined upper and lower bounds on the probability of error for a thresholding detector for the entire range of SNR. His bounds can also be applied to our case in a similar manner.

5.9 Bound evaluation

In this section, we describe a generating function method to evaluate the symbol error probability bounds for MF-DFSE, BC-MF-DFSE and SBC-MF-DFSE derived in Sections 4.10, 5.5 and 5.8, respectively for the case of standard matched filtering. Previously, the error probability of DFSE receivers was approximated by considering minimum distance error sequences and may be some higher distance sequences, which were found empirically. In Section 4.12, we described a generating function method that can be used for unbiased DFSE receivers. In [20], we proposed a generating function method to evaluate an approximate bound for the BC-MF-DFSE(S) receiver. This section includes treatment for the MF-DFSE(S), BC-MF-DFSE(S) and the SBC-MF-DFSE(S) receivers.

An error state diagram (ESD) enumerates the distance $\delta(\underline{e})$, the number of symbol errors $w(\underline{e})$ and the *a priori* probability $p(\underline{e})$ of all error sequences $\underline{e}$ in the set of allowable sequences E'. Each path through the ESD corresponds to an error sequence in E'. As in Section 4.12, an error state is defined as the value of L consecutive error symbols: $\{e_{j-L}, e_{j-L+1}, \ldots, e_{j-1}\}$. There are $(2|\mathcal{A}|-1)^L$ error states or nodes connected to each other through branches. The nodes and branches that correspond to J or more consecutive zeros in the middle of the error path are expurgated as in the case of unbiased DFSE receivers. The modified error state diagram is shown in Fig. 5.1 for the case of binary symbol alphabet, channel memory $L = 3$ and memory order $J = 1$. The pairs of error states that are negative of each other have been combined. Each branch is labeled with a branch distance parameter λ_i and the number of symbol errors entailed by the transition as the exponent of a dummy variable I.

For MF-DFSE(S), BC-MF-DFSE(S) and SBC-MF-DFSE(S), the distance squared of an error path through the ESD is given by (4.115), where the branch distance is given by

$$b_j = \text{Re}\left\{ e_j^* \left(s(0)e_j + 2\sum_{i=1}^{L} s(i)e_{j-i} \right) \right\} \tag{5.37}$$

which follows from (4.82). The branch distance parameters λ_i are listed in Table 5.1. The branch distance appears as the exponent of a dummy variable D.

Note that the difference between the ESD of Fig. 4.7 and that of Fig. 5.1 is that the tail branches (corresponding to the tail $\underline{\xi}$ (4.79) of an error sequence) have been expurgated in Fig. 5.1. This is because for biased and bias-compensated MF-DFSE receivers, the untreated and the residual interference components, respectively, depend on the tail of the error path.
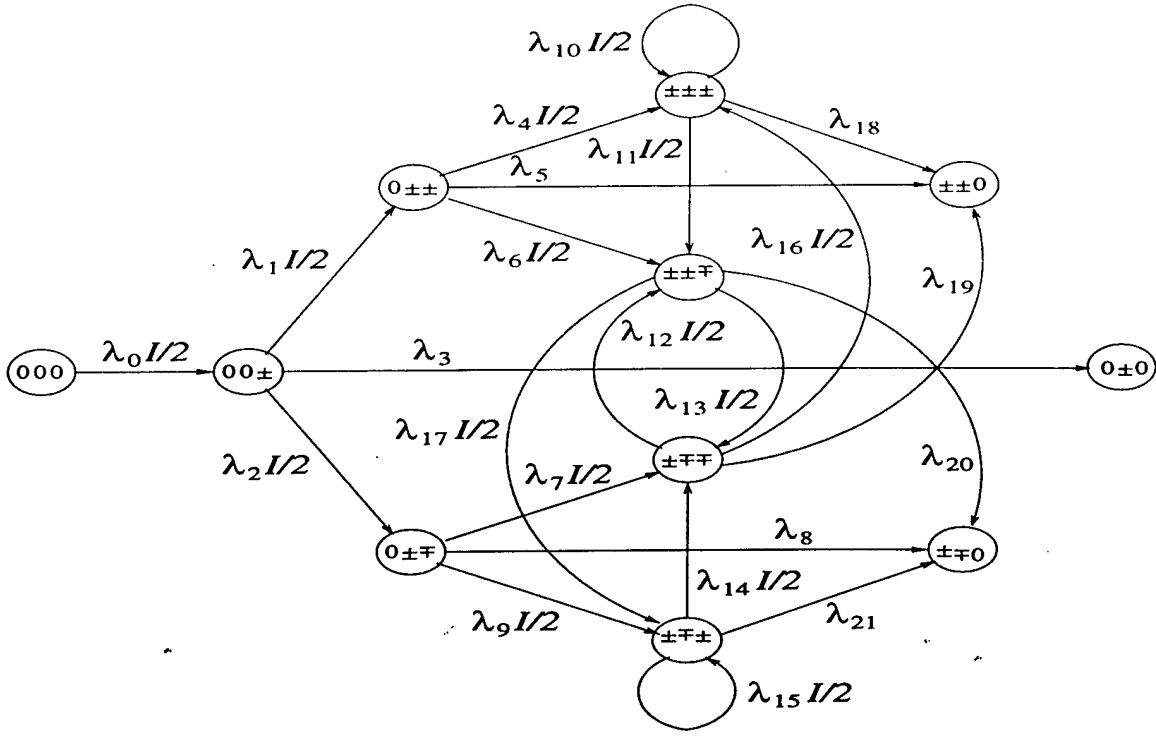
Figure 5.1: Error state diagram for MF-DFSE(S) ($L = 3, J = 1$).

Table 5.1: Branch distance parameters for MF-DFSE(S) ($L = 3, J = 1$)

$\lambda_0 = D^{4[s(0)]}$	$\lambda_1 = D^{4[s(0)+2s(1)]}$
$\lambda_2 = D^{4[s(0)-2s(1)]}$	$\lambda_4 = D^{4[s(0)+2s(1)+2s(2)]}$
$\lambda_6 = D^{4[s(0)-2s(1)-2s(2)]}$	$\lambda_7 = D^{4[s(0)+2s(1)-2s(2)]}$
$\lambda_9 = D^{4[s(0)-2s(1)+2s(2)]}$	$\lambda_{10} = D^{4[s(0)+2s(1)+2s(2)+2s(3)]}$
$\lambda_{11} = D^{4[s(0)-2s(1)-2s(2)-2s(3)]}$	$\lambda_{12} = D^{4[s(0)-2s(1)-2s(2)+2s(3)]}$
$\lambda_{13} = D^{4[s(0)+2s(1)-2s(2)-2s(3)]}$	$\lambda_{14} = D^{4[s(0)+2s(1)-2s(2)+2s(3)]}$
$\lambda_{15} = D^{4[s(0)-2s(1)+2s(2)-2s(3)]}$	$\lambda_{16} = D^{4[s(0)+2s(1)+2s(2)-2s(3)]}$
$\lambda_{17} = D^{4[s(0)-2s(1)+2s(2)+2s(3)]}$	$\lambda_3 = \lambda_5 = \lambda_8 = \lambda_{18-21} = 1$

In order to take an ensemble average over these components or apply the Glave bound, we have to enumerate the error paths that terminate in each tail sequence $\underline{\xi}$ separately. Noting that the interference term is insensitive to the sign of the tail sequence, we seek $(2|\mathcal{A}| - 1)^{L-J-1}$ generating functions ($J < L$), in general, corresponding to the error paths that terminate with a given tail $\underline{\xi}$ such that the last component of $\underline{\xi}$, $\epsilon_{k-1-J} \neq 0$.

Let $T_j(D, I)$ be the generating function for the error paths which terminate in the tail $\underline{\xi}_j$ ($j = 1, 2, \ldots, 3^{L-J-1}$) found by solving the state equations simultaneously. Each generating function can be expanded in a series as

$$\frac{\partial}{\partial I} T_j(D, I) \Big|_{I=1} = \sum_l N_{j,l} D^{\delta_j^2(l)} \tag{5.38}$$

where $N_{j,l}$ is the number of error sequence pairs with distance $\delta_j(l)$ that terminate in the tail $\underline{\xi}_j$, per the number of symbol errors and the number of the corresponding input sequences. Then, the symbol error probability bound of (4.99) for MF-DFSE(S) can be computed as

$$P_s \leq \frac{2}{|\mathcal{A}|^{L-J}} \sum_{j=1}^{3^{L-J-1}} \sum_l \sum_{\underline{a} \in \mathcal{A}^{L-J}} N_{j,l} Q\left(\frac{\delta_j(l) + \gamma\left(\underline{\xi}_j, \delta_j(l), \underline{\dot{a}}\right)}{\sqrt{2N_0}}\right) \tag{5.39}$$

where we use the fact that the untreated interference $\gamma(\underline{e}, \underline{a})$ given by (4.83) depends on the error sequence $\underline{e}$ only through the tail of the error sequence $\underline{\xi}$ and the distance of the error sequence $\delta(\underline{e})$. The input symbols are considered i.i.d. equiprobable and the interference is averaged for all possible values of $L - J$ input symbols. When L is relatively large and J is small, it leads to several terms in the summation. In this case, the Glave bound can be employed which requires averaging for only three values of interference. Note that the parameters I_1 and σ_1^2 as given in Section 5.8 depend on the error sequence only through its distance and the tail sequence. Thus, the Glave bound for MF-DFSE(S) can be evaluated as

$$\begin{aligned}
P_s \leq \ &\sum_{j=1}^{3^{L-J-1}} \sum_l N_{j,l} \left\{ \frac{\sigma_{1,j,l}^2}{I_{1,j,l}^2} \left[Q\left(\frac{\delta_j(l) - I_{1,j,l}}{\sqrt{2N_0}}\right) + Q\left(\frac{\delta_j(l) + I_{1,j,l}}{\sqrt{2N_0}}\right) \right] \right. \\
&+ \left. \frac{1}{2}\left(1 - \frac{\sigma_{1,j,l}^2}{I_{1,j,l}^2}\right) Q\left(\frac{\delta_j(l)}{\sqrt{2N_0}}\right) \right\}.
\end{aligned} \tag{5.40}$$

where the subscripts l and j are for the lth error sequence with the jth tail in the ESD.

Similarly, the Glave bound for the SBC-MF-DFSE(S) receiver described in Section 5.8 can be evaluated as

$$P_s \leq \sum_{j=1}^{3^{L-J-1}} \sum_l N_{j,l} \left\{ \frac{\sigma_{2,j,l}^2}{2I_{2,j,l}^2} \left[Q\left(\frac{\delta_j^2(l) - I_{2,j,l}}{\sqrt{2N_0 \sigma_{n,j,l}^2}}\right) + Q\left(\frac{\delta_j^2(l) + I_{2,j,l}}{\sqrt{2N_0 \sigma_{n,j,l}^2}}\right) \right] \right.$$

83

$$+ \left(1 - \frac{\sigma_{2,j,l}^2}{I_{2,j,l}^2}\right) Q \left(\frac{\delta_j^2(l)}{\sqrt{2N_0\sigma_{n,j,l}^2}}\right) \right\}. \tag{5.41}$$

The approximate symbol error probability expression for BC-MF-DFSE(S) given by (5.13) can be computed as

$$P_s \overset{\sim}{\leq} 2 \sum_{j=1}^{3^{L-J-1}} \sum_l \sum_{\underline{t}} N_{j,l} Q \left(\frac{\delta_j(l) + \gamma\left(\underline{\xi}_j, \delta_j(l), \underline{t}\right)}{\sqrt{2N_0}}\right) P_{\underline{t}} \tag{5.42}$$

where $\gamma\left(\underline{\xi}_j, \delta_j(l), \underline{t}\right)$ is the residual interference arising from tentative decision errors $\underline{t}$, given by (5.12). In order to compute (5.42), we assume that the sequence of tentative decision errors is an i.i.d. sequence which is independent of the sequence of main decision errors *unde* and has distribution

$$t_n = \begin{cases} 0 & 1-p \\ +1 & \frac{1}{2}p \\ -1 & \frac{1}{2}p \end{cases} \tag{5.43}$$

where p is the probability of tentative decision error which, in the case of a single-stage BC-MF-DFSE(S) receiver, is the symbol error probability of a conventional matched-filter (thresholding) detector.

As the noise is correlated, tentative decision errors are correlated with each other as well as with main decision errors. Our assumptions are thus optimistic because errors in the tentative detector will tend to occur in bursts, inducing errors in the main detector. Nevertheless, independence can be assumed in case noise correlations are small.

5.10 Performance results

In this section, we compare the performance of the various receivers described in this chapter and Chapter 4 via simulation and analysis. First, we we give some examples of equalization for BPSK modulated signaling on static time-dispersive AWGN channels. The receivers employ standard matched filtering and are assumed to have perfect knowledge of the symbol timing and the impulse response of the channel. Later, we give examples of multiuser detection for BPSK modulated signals on symbol-asynchronous DS-CDMA channels with AWGN. In the case of multiuser detection, the receiver has knowledge of the spreading codes, signal powers and the relative timing of all users.
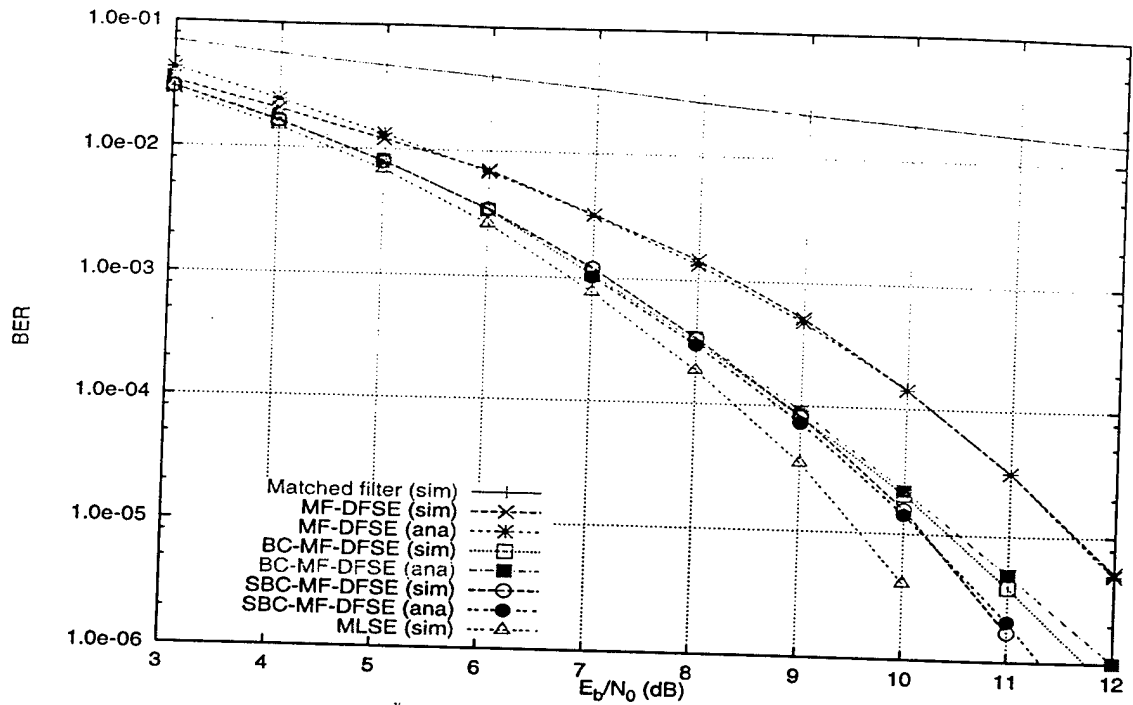
Figure 5.2: BER performance of various receivers in Example 1.

5.10.1 Equalization examples

We give four examples of equalization for a single user system. For our first example, we consider the symbol-spaced impulse response $f_1 = (0.9617, -0.2005, 0.1551, -0.1040)$. The channel has memory $L = 3$. Fig. 5.2 shows the bit-error rate (BER) of various receivers on channel 1. Each simulation was run for a count of 600 errors. The memory order J for the DFSE receivers is set to be one and final decisions are made at a lag G of 30 symbols. Note that the channel has much smaller ISI components than the channel in Fig. 4.8. As a result, the untreated interference in the case of MF-DFSE, given by (4.83), is small and the performance of MF-DFSE is not much worse than MLSE. Bias compensation using hard tentative decisions (BC-MF-DFSE) provides a gain of about a dB at moderate SNRs. Bias compensation using optimum linear soft tentative decisions (SBC-MF-DFSE) (5.20) shows improvement over compensation using hard tentative decisions at high SNR. This is because the mean square error after bias compensation is reduced and the effect is more significant as the noise diminishes.

The analytical results shown in Fig. 5.2 were obtained using the generating function method described in Section 5.9. The minimum error distance for the DFSE and MLSE
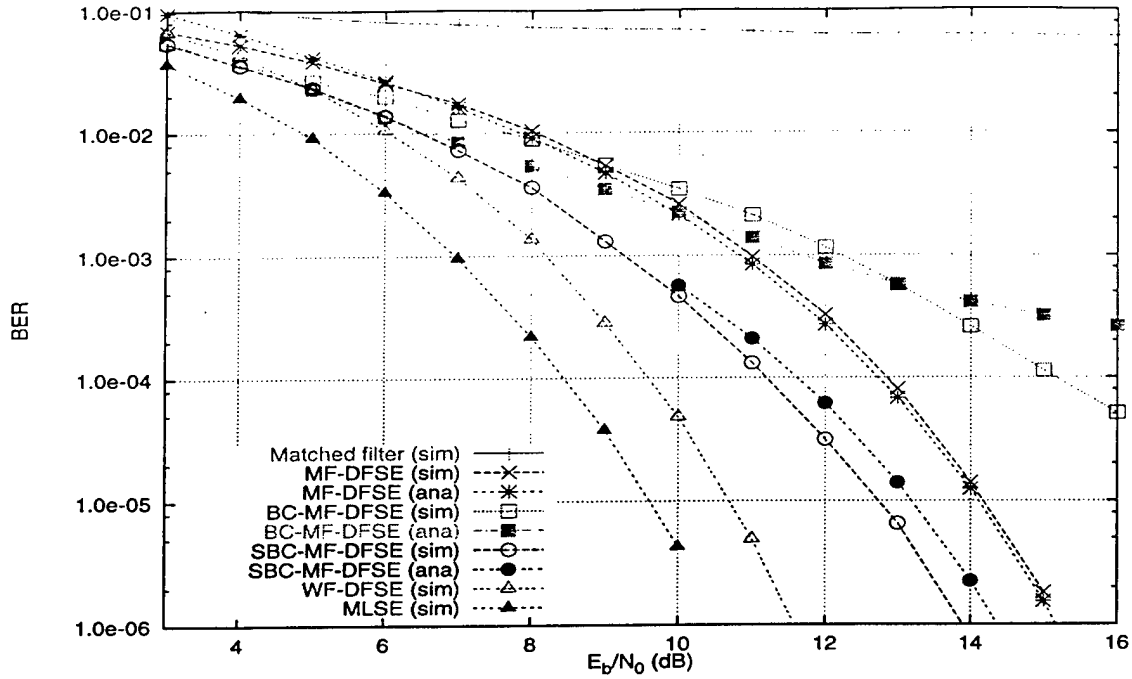
85

Figure 5.3: BER performance of various receivers in Example 2.

receivers in Fig. 5.2 is found to be one. For MF-DFSE, we evaluate the upper bound of (5.39), where we take ensemble average over the untreated interference components. For BC-MF-DFSE, we evaluate the semi-analytical bound of (5.42), where we assume independence between tentative and main decision errors and obtain the probability of tentative decision error, p in (5.43), from simulation (the matched filter detection curve in Fig. 5.2). For SBC-MF-DFSE, we evaluate the Glave bound of (5.41) using the approximate normalization factor of (5.35). For channel 1, the Glave bound holds for $E_b/N_0 > 6.6$ dB. All bounds in Fig. 5.2 are approximate in the sense that they do not consider error propagation inherent in DFSE receivers. However, error propagation is not significant for channels with moderate dispersion. All bounds are tight for the entire SNR range shown.

For our second example, the channel response is given by $f_2 = (0.84, -0.30, 0.40, 0.21)$. This channel also has memory $L = 3$ and the memory order for the DFSE receivers is chosen as one. The channel, is however, more dispersive than the channel in Example 1 (the sampled channel correlations s are larger in Example 2). The BER for various receivers is shown in Fig. 5.3. Bias compensation using hard tentative decisions (BC-MF-DFSE) actually deteriorates performance at moderate to high SNRs due to the lack of reliability of
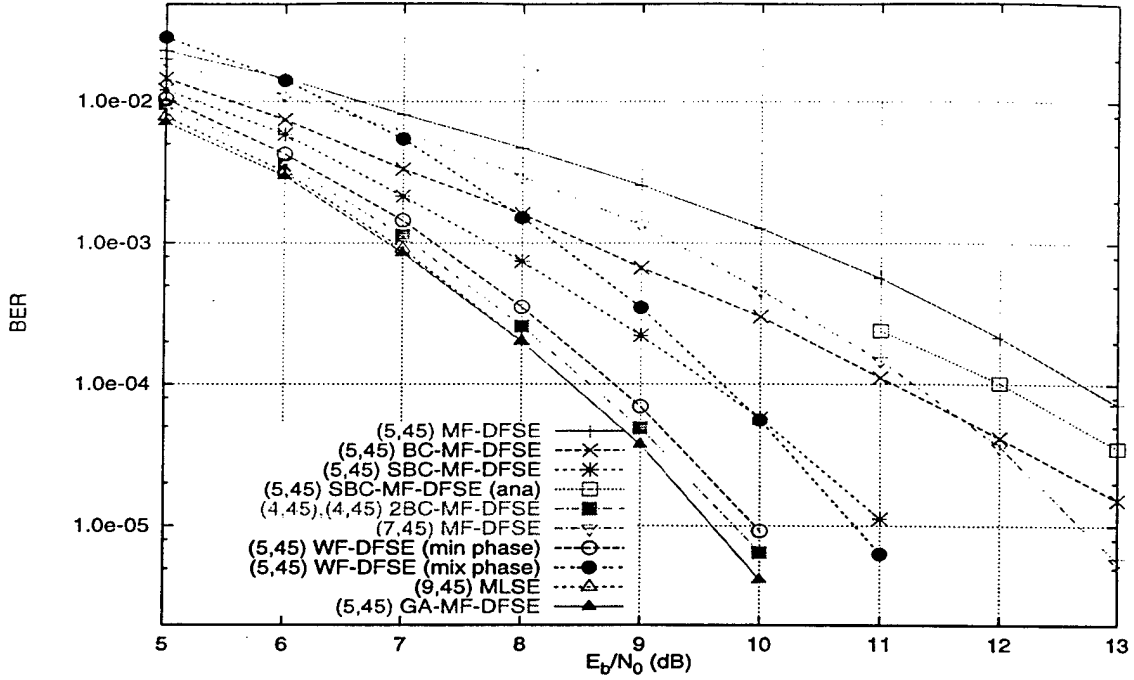
Figure 5.4: BER performance of various receivers in Example 3.

these decisions. However, by using optimum soft linear tentative decisions, SBC-MF-DFSE gains more than a dB over MF-DFSE. WF-DFSE, being an unbiased receiver, performs much better than the other DFSE receivers on the minimum phase channel as discussed in Chapter 4.

The analytical results shown in Fig. 5.3 were obtained in the same manner as described in Example 1. The Glave bound for SBC-MF-DFSE holds for $E_b/N_0 > 9.6$ dB for this channel. Notice that the semi-analytical approximate bound for BC-MF-DFSE does not seem to be consistent with the simulation curve. The simplifying assumptions used to obtain the semi-analytical expression are unrealistic when the sampled channel correlations are relatively large as in this case. The bounds for MF-DFSE and SBC-MF-DFSE are tight, the former being tighter as we performed ensemble averaging for the untreated interference components in the former case.

The channel for our third equalization example is a memory 9 minimum-phase channel with impulse response $f_{3,min} = (0.861, 0.258, -0.100, -0.274, 0.130, 0.100, -0.038, 0.112, -0.114, -0.228)$. A channel with the same magnitude response as $f_{3,min}$ but a mixed phase response is given by $f_{3,mix} = (0.5347, 0.6543, -0.1310, -0.2710, 0.0574, 0.0661, 0.1225, -0.1132,$

0.1566, −0.3679). Fig. 5.4 shows the BER performance of various detection schemes indexed with the memory order and the decision lag (J, G). Each simulation was run for a count of 1000 errors. Ideal noise whitening is assumed for WF-DFSE in the case of minimum-phase channel while transmit-matched filtering with Nyquist pulse-shaping at the transmitter is assumed in the case of mixed-phase channel.

Fig. 5.4 shows that BC-MF-DFSE (with hard tentative decisions) gains 1.0 − 1.5 dB over MF-DFSE with memory order 5 in the SNR range shown. With linear optimum soft decisions, SBC-MF-DFSE gains further over MF-DFSE and the gains increase with increasing SNR. The two-stage scheme 2BC-MF-DFSE described in Section 5.2.1 closely approaches MLSE performance and obtains a gain of 4 dB over MF-DFSE at an error rate of 10^{-4}. Note that the combined number of states in the two stages of 2BC-MF-DFSE is kept the same as in $(5, 45)$ MF-DFSE. The schemes with soft and two-stage bias compensation even perform better than $(7, 45)$ MF-DFSE (with higher memory order but no bias compensation) for this channel. The performance of WF-DFSE for the minimum-phase channel is close to MLSE. However, it's worse for the mixed-phase channel. The performance of MF-DFSE and other receivers that operate on matched filter statistics, is insensitive to channel phase. Note that the delay incurred from anti-causal noise-whitening needed to obtain a minimum-phase channel for WF-DFSE can be compared to the delay of a two-stage BC-MF-DFSE scheme.

Fig. 5.4 shows the simulated BER for $(5, 45)$ GA-MF-DFSE which is slightly lower than MLSE due to the reasons discussed in Section 5.5.1. Also shown in Fig. 5.4 is the Glave bound for single error sequences in SBC-MF-DFSE, which is good for $E_b/N_0 > 11$ dB. Since the performance on this channel is dominated by single error sequences, considering only single error sequences in the analysis is well justified. In spite of this, we find that the bound is very loose. This can be explained by noting that the channel has a large memory − 9. In the analysis in Section 5.8, the distribution of a linear combination of interference components that appear as an argument to the Q function in (5.27), is replaced by the worst case interference distribution concentrating at the three points of no interference, peak constructive interference and peak destructive interference (5.33). With the large number of significant interference components in this example: $3L − J = 22$, the worst-case distribution leads to quite pessimistic results.

For our last equalization example, the channel impulse response is taken from [12, Ex-
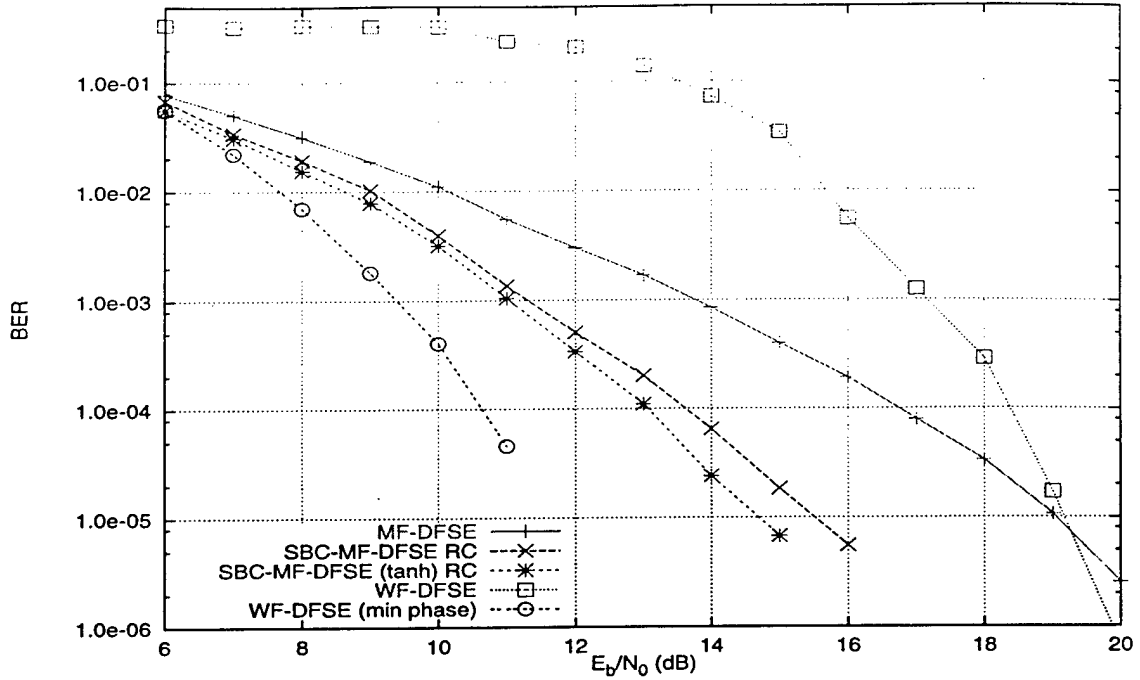
Figure 5.5: BER performance of various receivers in Example 4.

ample B]. The channel has memory 14 and is highly dispersive. Fig. 5.5 shows simulation results for various schemes with memory order 5 and decision lag 45 after a count of 600 errors. The performance of WF-DFSE is highly sensitive to channel phase. On this channel, symbol-by-symbol decisions are highly unreliable as the eye opening is −200%. Still, by using linear soft tentative decisions to cancel bias, significant performance improvement is obtained over MF-DFSE. Further improvement is obtained by using the following soft decision

$$\tilde{a}_n = \tanh\left(\frac{z_n}{\frac{N_0}{2} + \zeta s(0)}\right). \tag{5.44}$$

where ζ is a scale factor which is selected empirically. We found that the MMSE estimator of (5.19) which was obtained by assuming the interference as Gaussian, did not perform as well as the linear optimum estimator for any of the example channels considered in this section. In this example, $\zeta = 5.0$ while $\frac{1}{|s(0)|^2} \sum_{i \neq 0} |s(i)|^2 = 1.94$, which is the corresponding factor for the MMSE estimator of (5.19).

The bias compensation schemes shown in Fig. 5.5 use the reduced computation (RC) form of the bias term (5.4) which is independent of the state. In case of binary signaling, only two bias terms need to be computed at each recursion regardless of the trellis size. Thus,
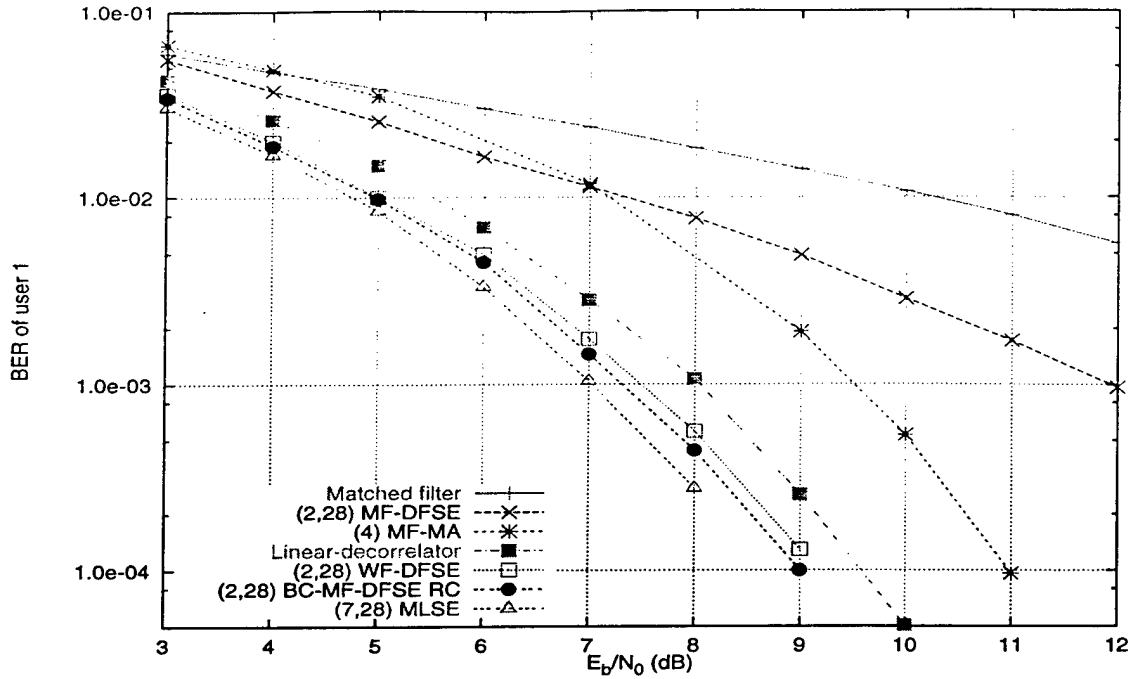
Figure 5.6: BER performance of various detection schemes for DS-CDMA channel 1.

the added complexity is very low for moderate trellis sizes. We found that the performance loss due to the approximation of the bias term was not more than a fraction of a dB for any of the channels considered in this section.

5.10.2 Multiuser detection examples

We simulate a BPSK modulated asynchronous DS-CDMA system on an AWGN channel with eight users whose signature waveforms are derived from Gold sequences of length 31. The spreading codes are short i.e. symbol-length. The relative delays of users are fixed for the simulation and are in an increasing order. All receivers have a bank of filters each of which is matched to the spreading code of a user followed by a synchronized symbol-rate sampler. The multiuser channel is static and has the spectrum

90

$$S(D) =$$

$$\frac{1}{31}\begin{bmatrix} 31 & 8-D & 7 & 6+D & -3+2D & -6+5D & -3+2D & -2+D \\ 8-D^{-1} & 31 & -D & 9-2D & -6-3D & -7-2D & -D & 9-2D \\ 7 & -D^{-1} & 31 & -D & -1 & -D & -1 & -2+D \\ 6+D^{-1} & 9-2D^{-1} & -D^{-1} & 31 & -D & -1 & -D & -1 \\ -3+2D^{-1} & -6-3D^{-1} & -1 & -D^{-1} & 31 & -D & -1 & -D \\ -6+5D^{-1} & -7-2D^{-1} & -D^{-1} & -1 & -D^{-1} & 31 & -D & -1 \\ -3+2D^{-1} & -D^{-1} & -1 & -D^{-1} & -1 & -D^{-1} & 31 & -D \\ -2+D^{-1} & 9-2D^{-1} & -2+D^{-1} & -1 & -D^{-1} & -1 & -D^{-1} & 31 \end{bmatrix}$$

Fig. 5.6 shows the BER of user 1 for various detection schemes when all users have identical SNR. Each simulation was run for a count of 500 errors. It is evident that even with ideal power control, the performance of the conventional matched filter detector that makes symbol-by-symbol decisions independently for all users, is significantly worse than optimum MLSE. With a four state trellis, MF-DFSE, that operates on the matched filter statistic of all users jointly, provides some improvement over the matched filter detector. The four-path MF-MA is $2-3$ dB worse than MLSE. The linear-decorrelator[5], that nulls out all multiple-access interference, loses about $0.5-1.0$ dB compared to MLSE due to noise enhancement. WF-DFSE that operates on the equivalent whitened minimum-phase channel obtains near MLSE performance. Not shown in Fig. 5.6, WF-MA with four survivor paths is also found to obtain near MLSE performance. However, WF-DFSE, WF-MA and the linear-decorrelator require multiuser channel inversion and/or factorization which has complexity quadratic in the number of users. The M-algorithm receivers require sorting of survivor paths at each recursion which is not needed by the DFSE schemes as they are trellis based.

The single-stage BC-MF-DFSE receiver which employs hard tentative decisions to cancel bias, obtains the best performance on this channel (next to MLSE). With four states only, BC-MF-DFSE closely approaches the performance of MLSE which requires 128 states in the Viterbi algorithm. Bias approximation in this case does not result in any appreciable loss of performance.

Fig. 5.7 shows the BER of user 1 versus the SNR of the rest of the users. The SNR of

---

[5]The linear-decorrelator comprises a zero-forcing filter followed by a thresholding device.
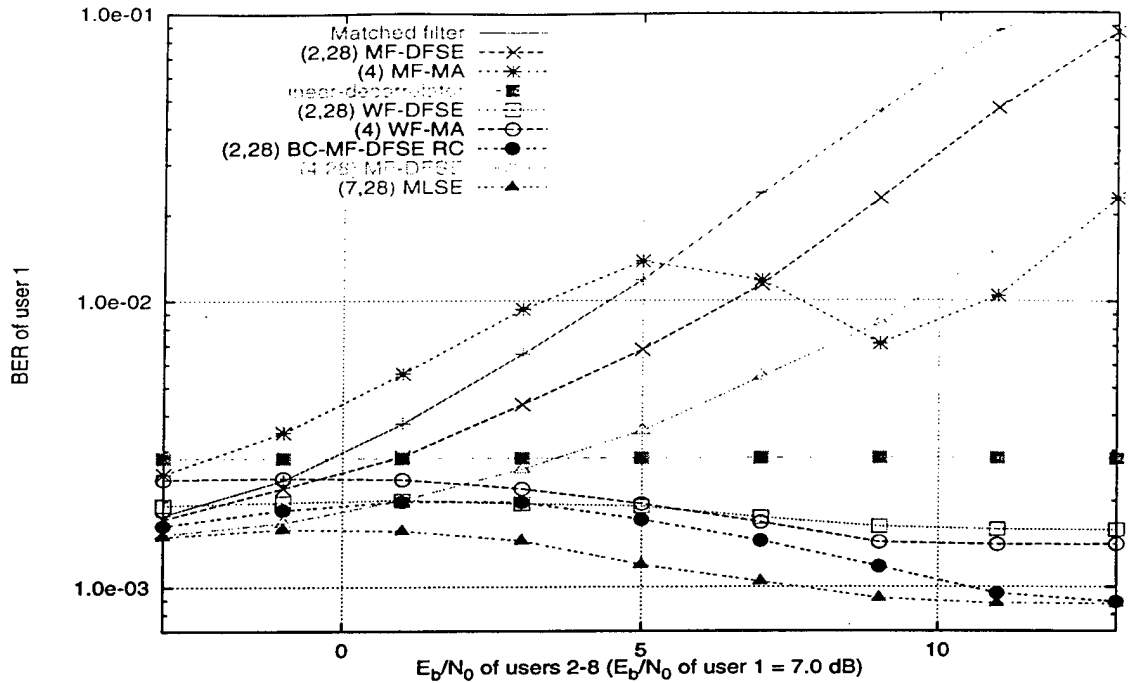
Figure 5.7: Near-far performance of various detection schemes for DS-CDMA channel 1.

user 1 is held constant at 7.0 dB. It can be seen that the matched filter detector, MF-DFSE and MF-MA do not perform well in a near-far situation. Such a situation occurs as an example when interfering users are closer to the base station than the desired user in the uplink and can thus get most of their signal power through to the base station in the absence of a (good) power control algorithm. In this case, the untreated interference dominates the performance of the sub-optimal matched filter type receivers as the ratio of the interference-to-desired signal power increases. However, WF-DFSE, WF-MA and the linear-decorrelator perform well as they do not suffer from untreated interference components.

Note that although the symbols of the desired user are not detected reliably by the matched filter detector, the symbols of the interfering users are detected quite reliably as their SNR increases. Thus, even in the severe near-far situation, the untreated interference (that affects MF-DFSE) is removed reliably by means of hard tentative decisions. As a result, BC-MF-DFSE outperforms all other methods, including MF-DFSE with higher memory order, and converges to MLSE in high SNR of interfering users, for this system.

For our second multiuser detection example, we consider another eight-user BPSK-modulated DS-CDMA system with short Gold spreading codes of length 31. The multiuser
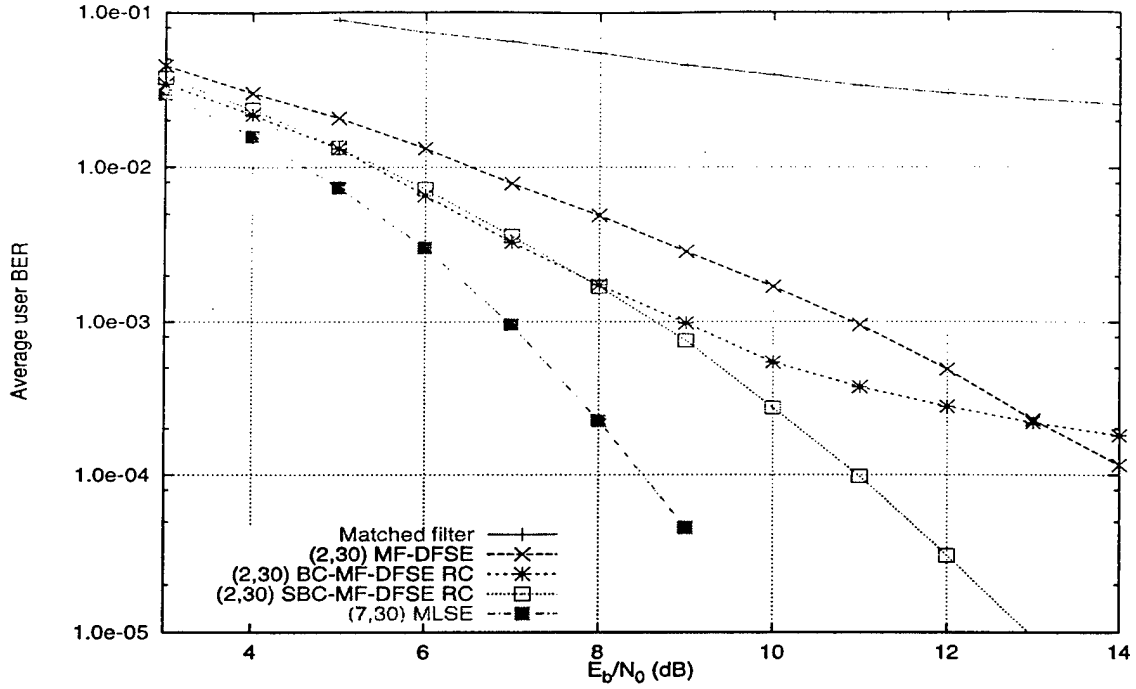
92

Figure 5.8: BER performance of various detection schemes for DS-CDMA channel 2.

channel spectrum is given by

$$S(D) =$$

$$\frac{1}{31}\begin{bmatrix} 31 & -D & -9 & 6+D & 5-6D & 4+3D & -5+4D & -2+D \\ -D^{-1} & 31 & -D & 3+4D & -6-3D & -1 & 10-3D & 1-2D \\ -9 & -D^{-1} & 31 & -2+D & -1 & -D & 7 & -2+D \\ 6+D^{-1} & 3+4D^{-1} & -2+D^{-1} & 31 & -D & -7-2D & 6+D & -5-4D \\ 5-6D^{-1} & -6-3D^{-1} & -1 & -D^{-1} & 31 & -10+D & -3+2D & -6-3D \\ 4+3D^{-1} & -1 & -D^{-1} & -7-2D^{-1} & -10+D^{-1} & 31 & -D & 3+4D \\ -5+4D^{-1} & 10-3D^{-1} & 7 & 6+D^{-1} & -3+2D^{-1} & -D^{-1} & 31 & 8-D \\ -2+D^{-1} & 1-2D^{-1} & -2+D^{-1} & -5-4D^{-1} & -6-3D^{-1} & 3+4D^{-1} & 8-D^{-1} & 31 \end{bmatrix}$$

Fig. 5.8 shows the average simulated BER of users for various detection schemes when all users have identical SNR. Note that the spreading codes in this system have higher partial correlations than the system in Example 1. The conventional matched filter detector does not perform very well. As a result, bias compensation using hard tentative decisions provides

93

some gain at moderate SNR, but causes a loss at high SNR. By using linear MMSE estimates for bias compensation in SBC-MF-DFSE, the loss can be converted to a significant gain at high SNR.

The multiuser detection results presented in this section were obtained for DS-CDMA systems with short (symbol-length) spreading codes. In current DS-CDMA systems, long spreading codes are generally employed which have periods much longer than the symbol interval. Long codes are preferable over short codes as they have better autocorrelation and cross-correlation properties. However, long codes are difficult to deal with for multiuser detection schemes that perform some kind of linear filtering like zero-forcing or noise-whitening. This is because the multiuser channel changes every symbol interval in the presence of long codes. Even with short codes, the multiuser channel changes with user arrival and departure. These variations in the channel are difficult, if not impossible, to track for a linear filter. Symbol-asynchronism also poses a problem. However, it is quite easy to generate user code partial correlations at the base station by means of a bank of on-line correlators that are properly synchronized to each user's code. The tracking of the medium responses of users has become a standard for Rake receivers used in conventional DS-CDMA receivers. These are the only requirements for a multiuser receiver like MF-DFSE that operates on joint matched filter statistics. Thus, MF-DFSE with hard or soft bias compensation is quite attractive for asynchronous DS-CDMA systems with short or long spreading codes.

5.11   Conclusions

In this chapter, we considered bias compensation (cancellation of untreated interference components) for reduced trellis and tree search algorithms that operate on matched filter statistics. Our main emphasis was on bias-compensated matched-filter decision feedback sequence estimation (BC-MF-DFSE) receivers with standard matched filters. Cancellation of future interfering components is performed by using tentative decision feedback. We considered using hard and soft tentative decisions for this purpose as well as multistage schemes. As soft tentative decisions, we considered optimum symbol-by-symbol linear and non-linear MMSE estimates of symbols.

We examined the error-rate performance of MF-DFSE with and without bias compen-

94

CHAPTER 6

Soft-output algorithms

6.1 Introduction

The various algorithms considered in the previous chapters generate hard decisions at the output. Such algorithms äre fine as long as one is interested in minimizing the error rate for a single system. For concatenated systems with memory, however, the performance of the outer system can be significantly enhanced by providing it with soft decisions in the form of likelihoods, symbol *a-posteriori* probabilities (APP) or erasures. One example of such a system is error control coding for intersymbol interference (ISI) channels. Another example is multiuser demodulation for a direct-sequence CDMA (DS-CDMA) system with error control coding and interleaving. In order to make the most of the code, the demodulator must provide soft information to the decoders. Unfortunately, most multiuser detection algorithms ignore the possibility of generating this reliability information and concentrate instead on minimizing the demodulated error rate.

Recently, a considerable amount of work has been done in symbol-by-symbol detection techniques for channels with ISI [1,3,21,23,25,28]. Li *et al.* [28] showed that optimum soft-output equalization can be performed with a forward-only recursion with complexity that grows exponentially with the channel memory. An earlier algorithm proposed by Abend *et al.* [1] requires complexity which is exponential in the decision lag, which is generally chosed to be much larger than the channel memory. The optimum soft-output algorithm (OSA) of Li *et al.* operates on discrete-time statistics containing white noise. On the other hand, the optimal symbol-by-symbol detection (OSSD) algorithm of Hayes *et al.* [23] operates on standard matched filter statistics. They and other authors, however, over-

estimate the complexity of this algorithm. We derive a forward-recursive matched-filter optimum soft-output algorithm (MF-OSA) following their development. The complexity of this algorithm is at par with the OSA. The MF-OSA can be reduced to add-compare-select operations mostly like the sub-optimum soft-output algorithm (SSA) of [28], resulting in the MF-SSA.

The OSA can be applied to the problem of multiuser estimation, but this requires noise whitening. Despite the strides made in the noise-whitening technique [47], it requires sizable complexity and is not very suitable for long spreading sequences and dynamic channels. The algorithm of Verdú [42] operates on standard matched-filter statistics like the MF-OSA. However, it has high latency as it requires a backward-forward recursion like the BCJR algorithm [3]. The MF-OSA is, thus, attractive in this case. It is an optimum demodulator for a coded multiuser DS-CDMA system with ideal interleaving, in the sense that without exploiting any information about coding in the demodulation process, it supplies each individual decoder with as much information as possible about the sequence of modulator-input symbols for the corresponding user while suppressing the irrelevant information about other user's sequences. This is called user-separating demodulation in [36].

Bayesian Conditional Decision Feedback Estimation (BCDFE) proposed in [25] for ISI channels is a reduced-complexity symbol-by-symbol estimation technique that employs an efficient method for trellis memory reduction like the DFSE algorithm. The scheme is designed to produce symbol APP estimates to enhance outer decoding. However, we note that while the scheme is capable of providing good hard decisions on symbols, it fails to deliver reliable estimates of symbol APPs. Fortunately, this can be fixed by a modification of the algorithm. The modified BCDFE algorithm recursively updates conditional symbol APP estimates (conditioned on the reduced state) and averages them over the state at a smoothing lag to obtain reliable symbol APP estimates.

The chapter is organized as follows. Sections 6.2 and 6.3 describe the MF-OSA and MF-SSA respectively. The modified BCDFE algorithm is derived in Section 6.4. We compare the complexity of the various algorithms in Section 6.5. The algorithms are considered for soft-output multiuser estimation with error control coding in Section 6.6. Simulation is undertaken to compare the performance of the various algorithms with the soft-output Viterbi algorithm (SOVA) [21] for a DS-CDMA system with four asynchronous users. Simulation results are presented in Section 6.7.

6.2 A matched-filter optimum soft-output algorithm

In this section, we derive an optimal forward-recursive soft-output algorithm that operates on standard matched filter statistics. We consider the system model of Section 2.2. The baseband received signal is given by (2.3). The algorithm finds the set of symbol *a-posteriori* probabilities (APP) $\{p(\alpha_n|y(t))\}_{n=0}^{N-1}$, for $\alpha_n \in \mathcal{A}$. From the log-likelihood function given by (2.6), it follows that

$$p(\underline{\alpha}_N, y(t)) = C \exp\left[-\frac{1}{2N_0} \int_{t \in I} \left|y(t) - \sum_{n=0}^{N-1} \alpha_n h(t - nT; t)\right|^2 dt\right] p(\underline{\alpha}_N) \qquad (6.1)$$

where $\underline{\alpha}_N = [\alpha_0, \alpha_1, \ldots, \alpha_{N-1}]^T$ is a sequence of hypothesized symbols which is assumed to be independent and identically distributed with probability $p(\underline{\alpha}_N) = \prod_{n=0}^{N-1} \alpha_n$ and C is a constant independent of the sequence hypothesis. From (2.6), (2.11) and (2.18), it follows that

$$p(\underline{\alpha}_N, y(t)) = C_1 \exp\left[\Lambda(\underline{z}_N, \underline{\alpha}_N)/2N_0\right] p(\underline{\alpha}_N) \qquad (6.2)$$

where $\underline{z}_N = [z_0, z_1, \ldots, z_{N-1}]^T$ is the sequence of standard matched statistics given by (2.14) and C_1 is another constant independent of the sequence hypothesis. The log-likelihood metric[1] $\Lambda(\underline{z}_N, \underline{\alpha}_N)$ is given by

$$\Lambda(\underline{z}_N, \underline{\alpha}_N) = \sum_{n=0}^{N-1} \Gamma_n(z_n, \alpha_n, \sigma_n) \qquad (6.3)$$

where the branch metric $\Gamma_n(z_n, \alpha_n, \sigma_n)$ corresponding to the state $\sigma_n : \alpha_{n-1}, \alpha_{n-2}, \ldots, \alpha_{n-L}$ and the input symbol α_n is given by

$$\Gamma_n(z_n, \alpha_n, \sigma_n) = \text{Re}\left\{\alpha_n^* \left[2z(n) - s(0; n)\alpha_n - 2\sum_{l=1}^{L} s(l; n)\alpha_{n-l}\right]\right\}. \qquad (6.4)$$

For $n = 0, 1, \ldots, N - 1$, $0 \le i \le n - L - 1$ and $\alpha \in \mathcal{A}$, define

$$\Omega(\underline{z}_n, \sigma_n) \stackrel{\triangle}{=} \sum_{\underline{\alpha}_{n-L}} \exp\left[\Lambda(\underline{z}_n, \underline{\alpha}_n)/2N_0\right] p(\underline{\alpha}_n), \qquad (6.5)$$

$$\Omega_i(\underline{z}_n, \sigma_n, \alpha) \stackrel{\triangle}{=} \sum_{\underline{\alpha}_{n-L}|\alpha_i=\alpha} \exp\left[\Lambda(\underline{z}_n, \underline{\alpha}_n)/2N_0\right] p(\underline{\alpha}_n), \qquad (6.6)$$

where[2] $\underline{x}_n = [x_0, x_1, \ldots, x_{n-1}]^T$. Then, for $0 \le i \le n - L$, we have

$$\Omega_i(\underline{z}_{n+1}, \sigma_{n+1}, \alpha) = \sum_{\underline{\alpha}_{n-L+1}|\alpha_i=\alpha} \exp\left[\frac{\Lambda(\underline{z}_n, \underline{\alpha}_n) + \Gamma_n(z_n, \alpha_n, \sigma_n)}{2N_0}\right] p(\underline{\alpha}_{n+1})$$

---

[1]The notation is modified slightly to indicate the functional dependencies.
[2]The notation single bar | means 'given'.

$$= \sum_{\alpha_{n-L}|\alpha_i=\alpha} \exp\left[\frac{\Gamma_n(z_n,\alpha_n,\sigma_n)}{2N_0}\right] p(\alpha_n) \sum_{\alpha_{n-L}|\alpha_i=\alpha} \exp\left[\frac{\Lambda(z_n,\alpha_n)}{2N_0}\right] p(\alpha_n)$$

$$= \sum_{\alpha_{n-L}|\alpha_i=\alpha} \exp\left[\Gamma_n(z_n,\alpha_n,\sigma_n)/2N_0\right] p(\alpha_n)\Omega_i(z_n,\sigma_n,\alpha) \tag{6.7}$$

where the first equality follows from (6.3) and the second equality follows from the fact that the branch metric $\Gamma_n(z_n,\alpha_n,\sigma_n)$ is independent of the hypothetical symbols α_{n-L}. In (6.7), it is understood that $\Omega_{n-L}(z_n,\sigma_n,\alpha) = \Omega(z_n,\tilde{\sigma}_n)$, where $\tilde{\sigma}_n = \sigma_n|\alpha_{n-L} = \alpha$. Similarly, it can be shown that

$$\Omega(z_{n+1},\sigma_{n+1}) = \sum_{\alpha_{n-L}} \exp\left[\Gamma_n(z_n,\alpha_n,\sigma_n)/2N_0\right] p(\alpha_n)\Omega(z_n,\sigma_n). \tag{6.8}$$

By substituting (6.5) and (6.6) in (6.2), note that

$$p(\sigma_N, y(t)) = \sum_{\alpha_{N-L}} p(\alpha_N, y(t)) = C_1\Omega(z_N,\sigma_N) \tag{6.9}$$

and for $0 \le i \le N - L - 1$,

$$p(\sigma_N, a_i = \alpha, y(t)) = \sum_{\alpha_{N-L}|\alpha_i=\alpha} p(\alpha_N, y(t)) = C_1\Omega_i(z_N,\sigma_N,\alpha). \tag{6.10}$$

Thus, for $0 \le i \le N - L - 1$, we get the symbol APPs as

$$p(a_i = \alpha|y(t)) = \frac{\sum_{\sigma_N} \Omega_i(z_N,\sigma_N,\alpha)}{\sum_{\sigma_N} \Omega(z_N,\sigma_N)}. \tag{6.11}$$

The last L symbols are assumed known at the receiver. Equations (6.8), (6.7) and (6.11) complete the recursion of the matched-filter optimal soft-output algorithm (MF-OSA) with forward-only recursion. The algorithm was first derived in [18] for soft-output multiuser detection using a bank of matched filters. In [18], the algorithm is referred to as optimal soft-output multiuser estimation (OSOME).

It is not necessary to observe the entire signal in order to obtain close to optimum estimates of symbol APPs. In general, good estimates can be obtained at a sufficient decision lag as in the case of an MLSE algorithm. For a decision lag $G \ge L$, the MF-OSA(G) algorithm consists of the following steps. For each time $n = 0, 1, \ldots, N - 1$, compute and store the state metrics given by (6.8). For each $n \ge L$, $i = n - G, \ldots, n - L$ and[3] $\alpha \in \mathcal{A}'$, compute and store the symbol metrics given by (6.7). For each $n \ge G$ and $\alpha \in \mathcal{A}'$, estimate symbol APPs as

$$p(a_{n-G} = \alpha|y(t)) = \frac{\sum_{\sigma_{n+1}} \Omega_{n-G}(z_{n+1},\sigma_{n+1},\alpha)}{\sum_{\sigma_{n+1}} \Omega(z_{n+1},\sigma_{n+1})}. \tag{6.12}$$

---

[3] $\mathcal{A}'$ is the set of all but one symbol (say α') in the alphabet $\mathcal{A}$.

$$p(a_{n-G} = \alpha'|y(t)) = 1 - \sum_{\alpha \in \mathcal{A}'} p(a_{n-G} = \alpha|y(t)). \tag{6.13}$$

Note that the symbol *a priori* probabilities $p(\alpha_n)$ can be dropped from all computations if the symbols are equally likely *a priori*.

6.3 A matched-filter sub-optimum soft-output algorithm

The MF-OSA algorithm described in the previous section requires a large number of multiplication and exponentiation operations which lead to high implementation complexity. In this section, we simplify the MF-OSA algorithm so that it requires mostly add-compare-select operations, like an MLSE algorithm. For this purpose, we define

$$\Omega'(\underline{z}_n, \sigma_n) \triangleq \max_{\underline{\alpha}_{n-L}} [\Lambda(\underline{z}_n, \underline{\alpha}_n)/2N_0 + \log(p(\underline{\alpha}_n))], \tag{6.14}$$

$$\Omega'_i(\underline{z}_n, \sigma_n, \alpha) \triangleq \max_{\underline{\alpha}_{n-L}|\alpha_i=\alpha} [\Lambda(\underline{z}_n, \underline{\alpha}_n)/2N_0 + \log(p(\underline{\alpha}_n))]. \tag{6.15}$$

A derivation similar to (6.7) can be used to show that for $0 \le i \le n - L$,

$$\Omega'_i(\underline{z}_{n+1}, \sigma_{n+1}, \alpha) = \max_{\alpha_{n-L}|\alpha_i=\alpha} [\Gamma_n(z_n, \alpha_n, \sigma_n)/2N_0 + \Omega'_i(\underline{z}_n, \sigma_n, \alpha)] + \log(p(\alpha_n)) \tag{6.16}$$

and

$$\Omega'(\underline{z}_{n+1}, \sigma_{n+1}) = \max_{\alpha_{n-L}} [\Gamma_n(z_n, \alpha_n, \sigma_n)/2N_0 + \Omega'(\underline{z}_n, \sigma_n)] + \log(p(\alpha_n)). \tag{6.17}$$

Note that (6.17) is similar to the recursion of the MLSE receiver of Section 2.4. By substituting (6.14) in (6.2), we see that

$$\max_{\underline{\alpha}_{N-L}|\alpha_i=\alpha} p(\underline{\alpha}_N, y(t)) = C_1 \exp [\Omega'_i(\underline{z}_N, \sigma_N, \alpha)]. \tag{6.18}$$

Comparing the above equation with (6.10), note that the sum of exponentials of positive quantities is dominated by the term with the largest exponent. Thus, symbol APPs can be approximated as

$$p(a_i = \alpha|y(t)) \approx \frac{\sum_{\sigma_N} \exp [\Omega'_i(\underline{z}_N, \sigma_N, \alpha)]}{\sum_{\sigma_N, x \in \mathcal{A}} \exp [\Omega'_i(\underline{z}_N, \sigma_N, x)]}. \tag{6.19}$$

For a decision lag $G \ge L$, the matched-filter sub-optimal soft-output algorithm MF-SSA(G) consists of the following steps. For each time $n = 0, 1, \ldots, N - 1$, recursively compute and store the state metrics given by (6.17). For each $n \ge L$, keep the history of the best surviving path $\hat{\alpha}_{n-G}(\sigma_n), \ldots, \hat{\alpha}_{n-L}(\sigma_n)$ leading to each state σ_n, as in the Viterbi algorithm. For each

100

$n \geq L$, $i = n - G, \ldots, n - L$ and $\alpha \neq \hat{a}_i(\sigma_n)$, compute and store the symbol metrics given by (6.16) (note that $\Omega'_i(\underline{z}_n, \sigma_n, \hat{a}_i(\sigma_n)) = \Omega'(\underline{z}_n, \sigma_n)$, so there is no need to compute and store it separately). For each $n \geq G$ and $\alpha \in \mathcal{A}$, estimate symbol APPs as

$$p(a_{n-G} = \alpha | y(t)) \approx \frac{\sum_{\sigma_{n+1}} \exp\left[\Omega'_{n-G}(\underline{z}_{n+1}, \sigma_{n+1}, \alpha)\right]}{\sum_{\sigma_{n+1}, x \in \mathcal{A}} \exp\left[\Omega'_{n-G}(\underline{z}_{n+1}, \sigma_{n+1}, x)\right]}. \tag{6.20}$$

Note that the above algorithm avoids the multiplication operations of the MF-OSA(G) algorithm of Section 6.2. Exponentiation operations are needed, however, in the last step. The algorithm was proposed in [18] for multiuser detection, where we refer to it to as sub-optimal soft-output multiuser estimation (SSOME). A variation of the above algorithm estimates symbol APPs as

$$p(a_{n-G} = \alpha | y(t)) \approx \frac{\exp\left[\Omega'_{n-G}(\underline{z}_{n+1}, \sigma^*_{n+1}, \alpha)\right]}{\sum_{x \in \mathcal{A}} \exp\left[\Omega'_{n-G}(\underline{z}_{n+1}, \sigma^*_{n+1}, x)\right]}. \tag{6.21}$$

where $\sigma^*_n = \arg \max_{\Omega'(\underline{z}_n, \sigma_n)}$. This algorithm requires only two exponentiation operations in the last step. The algorithm is referred to as SSOME1 in [18]. It is similar in construction to the sub-optimal soft-output algorithm (SSA) of [28].

6.4 A reduced-state soft-output algorithm

In this section, we describe a forward-recursive reduced-state soft-output algorithm which operates on whitened-matched filter statistics. The algorithm can be considered as a reduced-complexity alternative to the optimal soft-output algorithm (OSA) of Li *et al.* [28]. It was obtained by modifying the algorithm of Lee *et al.* [25], which is referred to as Bayesian conditional decision feedback equalization (BCDFE). The BCDFE algorithm does not produce good soft outputs. The modified algorithm derived here was first proposed in [18] where we refer to it as modified BCDFE (MBCDFE).

The algorithm operates on whitened-matched filter statistics which may be obtained by applying the noise-whitening filter to the discrete-time matched filter statistics $\underline{z}_N$. The equivalent whitened discrete-time system model is given by

$$y_n = \sum_{i=0}^{L} f(i; n) a_{n-i} + w_n \tag{6.22}$$

where w_n is a sample of a complex white Gaussian noise process with mean zero and variance N_0 and $f(i; n)$ are whitened channel coefficients (possibly time-varying in index n).

Let (J, G) be the memory order and the decision lag for the algorithm. respectively chosen arbitrarily in the range $0 \leq J \leq L \leq G$. Let $\underline{y}_n = [y_0. y_1, \ldots, y_{n-1}]^T$ be the sequence of statistics received up to time $n - 1$ and $\beta_n : a_{n-1}. a_{n-2}, \ldots, a_{n-J}$ represent the reduced state at time n. The algorithm recursively estimates the probabilities $p(\beta_n | \underline{y}_n)$ and $p(a_{n-i} = \alpha | \underline{y}_n, \beta_n)$ for $J + 1 \leq i \leq G$ and $\alpha \in \mathcal{A}$. For this it employs the recursive relations:

$$p(\beta_{n+1} | \underline{y}_{n+1}) = \frac{\sum_{\alpha_{n-J}} p(\beta_{n+1}, \alpha_{n-J}, y_n | \underline{y}_n)}{\sum_{\alpha_{n-J}, \beta_{n+1}} p(\beta_{n+1}, \alpha_{n-J}, y_n | \underline{y}_n)}, \qquad (6.23)$$

$$p(a_{n-J} = \alpha | \underline{y}_{n+1}, \beta_{n+1}) = \frac{p(\beta_{n+1}, a_{n-J} = \alpha, y_n | \underline{y}_n)}{\sum_{\alpha_{n-J}} p(\beta_{n+1}, \alpha_{n-J}, y_n | \underline{y}_n)} \qquad (6.24)$$

and

$$\begin{aligned} p(a_{n-i} = \alpha | \underline{y}_{n+1}, \beta_{n+1}) &= \sum_{\alpha_{n-J}} p(a_{n-i} = \alpha | \underline{y}_{n+1}, \beta_{n+1}, \alpha_{n-J}) p(\alpha_{n-J} | \underline{y}_{n+1}, \beta_{n+1}) \\ &\approx \sum_{\alpha_{n-J}} p(a_{n-i} = \alpha | \underline{y}_n, \beta_n) p(\alpha_{n-J} | \underline{y}_{n+1}, \beta_{n+1}) \end{aligned} \qquad (6.25)$$

for $J + 1 \leq i \leq G$, where in (6.25) we assume that given $\underline{y}_n$ and β_n, the symbols a_{n-i} $(J + 1 \leq i \leq G)$ are conditionally independent of the statistic y_n and the input symbol a_n. The assumption is true for $J = L$, i.e., a full-state algorithm. The probability $p(\beta_{n+1}, \alpha_{n-J}, y_n | \underline{y}_n)$ is given by

$$p(\beta_{n+1}, \alpha_{n-J}, y_n | \underline{y}_n) = p(y_n | \underline{y}_n, \alpha_n, \beta_n) p(\beta_n | \underline{y}_n) p(\alpha_n) \qquad (6.26)$$

where using the assumption following (6.25), the probability $p(y_n | \underline{y}_n, \alpha_n, \beta_n)$ is given by

$$p(y_n | \underline{y}_n, \alpha_n, \beta_n) = \sum_{\{\alpha_{n-i}\}_{i=J+1}^L} p\left(y_n \Big| \alpha_n, \beta_n, \{\alpha_{n-i}\}_{i=J+1}^L\right) p\left(\{\alpha_{n-i}\}_{i=J+1}^L \Big| \underline{y}_n, \beta_n\right) \qquad (6.27)$$

which is approximated by the Gaussian density

$$p(y_n | \underline{y}_n, \alpha_n, \beta_n) \approx p\left(y_n \Big| \alpha_n, \beta_n, \{\hat{a}_{n-i}(\beta_n)\}_{i=J+1}^L\right) \qquad (6.28)$$

where $\{\hat{a}_{n-i}(\beta_n)\}_{i=J+1}^L$ are conditional decisions (conditioned on state β_n) obtained as

$$\hat{a}_{n-i}(\beta_n) = \arg\max_{\alpha_{n-i}} p(\alpha_{n-i} | \underline{y}_n, \beta_n). \qquad (6.29)$$

The modified BCDFE (J, G) algorithm consists of the following steps. For each time $n = 0, 1, \ldots, N - 1$, compute and store the state probabilities for each reduced state β_n using (6.23), (6.26) and (6.28). For each $n \geq J$, $J + 1 \leq i \leq G$ and $\alpha \in \mathcal{A}$, compute and

Algorithm	Compare	Add	Multiply	Divide	Exp	Storage
MF-OSA	1	$2^L(2A_\Gamma + G - L + 3)$	$2^{L+1}(G - L + 1)$	1	2^{L+1}	$2^L[f + f(G - L)]$
MF-SSA	$2^L(G - L + 1)$	$2^L(2A_\Gamma + 2G - 2L + 4)$	0	1	2^{L+1}	$2^L[f + (f + 1)(G - L)]$
MF-SSA1	$2^L(G - L + 2)$	$2^L(2A_\Gamma + 2G - 2L + 2)$	0	1	1	$2^L[f + (f + 1)(G - L)]$
SOVA	$2^L(G - L + 2)$	$2^L(2A_\Gamma + 3e + 4)$	$2^{L+1}(e)$	2^L	2^L	$2^L[f + (f + 1)(G - L)]$
BCDFE	$2^{J+1}(G - J) + 1$	$2^J(2A_\Gamma + 4)$	$2^J(3)$	2^{J+1}	2^{J+1}	$2^J(f + G - J)$
MBCDFE	$2^J(L - J) + 1$	$2^J(2A_\Gamma + G - J + 4)$	$2^J(2G - 2J + 3)$	2^{J+1}	2^{J+1}	$2^J[f(G - J + 1) + L - J]$

Table 6.1: Complexity in number of operations per iteration ($f = \#$bits required to store a floating point number, $e = \#$places where the hypothesized symbols of two merging paths differ.)

store the conditional symbol APPs using (6.24), (6.25), (6.26) and (6.28). For each $n \geq J$ and $J \leq i \leq L - 1$, obtain and store conditional decisions using

$$\hat{a}_{n-i}(\beta_{n+1}) = \arg\max_{\alpha_{n-i}} p(\alpha_{n-i}|\underline{y}_{n+1}, \beta_{n+1}). \tag{6.30}$$

Note that these decisions will be used in (6.28) in the next recursion. Finally, for each $n \geq G$, estimate symbol APPs using

$$p(a_{n-G} = \alpha|\underline{y}_{n+1}) = \sum_{\beta_{n+1}} p(a_{n-G} = \alpha|\underline{y}_{n+1}, \beta_{n+1}) p(\beta_{n+1}|\underline{y}_{n+1}). \tag{6.31}$$

The number of multiplication and exponentiation operations required in the above algorithm can be cut drastically by operating in the log domain as in the algorithm described in Section 6.3.

Note that the BCDFE algorithm proposed in [25] recursively obtains conditional hard decisions instead of conditional symbol APPs in the modified algorithm (6.25). This results in a significant loss of the soft information. The modified algorithm uses conditional hard decisions in (6.28) only to truncate the state, in the same manner as in DFSE. This does not have much effect on the quality of soft decisions as we observe from simulation.

6.5 Complexity comparison

Table 6.1 compares the complexity of the various algorithms discussed in this chapter for binary symbol alphabet. It is assumed that A_Γ add operations are needed to compute the branch metric $\Gamma_n(.)$ in (6.8) (or the Gaussian density (6.28) for the BCDFE algorithms).
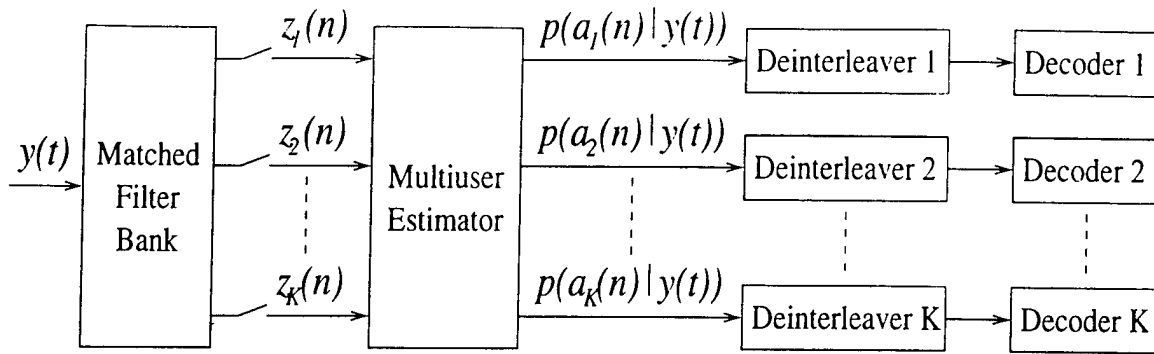
Figure 6.1: Multiuser receiver for a coded DS-CDMA system.

Note that the complexity of MF-OSA(G), where G is the decision lag, is on the order of $2^L(G-L)$. MF-SSA does not require any multiplication operations. However exponentiation operations are needed for soft-output generation. MF-SSA1 avoids most of the exponentiation operations as well. The complexity of MBCDFE(J,G), where J is the memory order chosen, is on the order of $2^J(G-J)$. The modified algorithm requires some extra storage and computational complexity as compared to the original algorithm.

6.6 Application to multiuser estimation

The algorithms described in this chapter are considered for multiuser estimation with error control coding. Fig. 6.1 shows a multiuser receiver for a coded asynchronous DS-CDMA system. The multiuser estimator operates on the discrete-time matched-filter statistics of all users jointly and produces *a-posteriori* probabilities for the coded symbols of all users at the output. These soft outputs are de-interleaved for each user and then fed into the soft-decision decoder for each user separately. The original and modified BCDFE algorithms operate on whitened-matched filter statistics. The corresponding receiver is similar to the receiver of Fig. 6.1 except that it includes a noise-whitening filter which follows the matched filter bank.

6.7 Simulation results

We simulated an asynchronous DS-CDMA system with four users that employ BPSK modulation and rate $\frac{1}{2}$, memory 4 convolutional encoding over an AWGN channel. Code
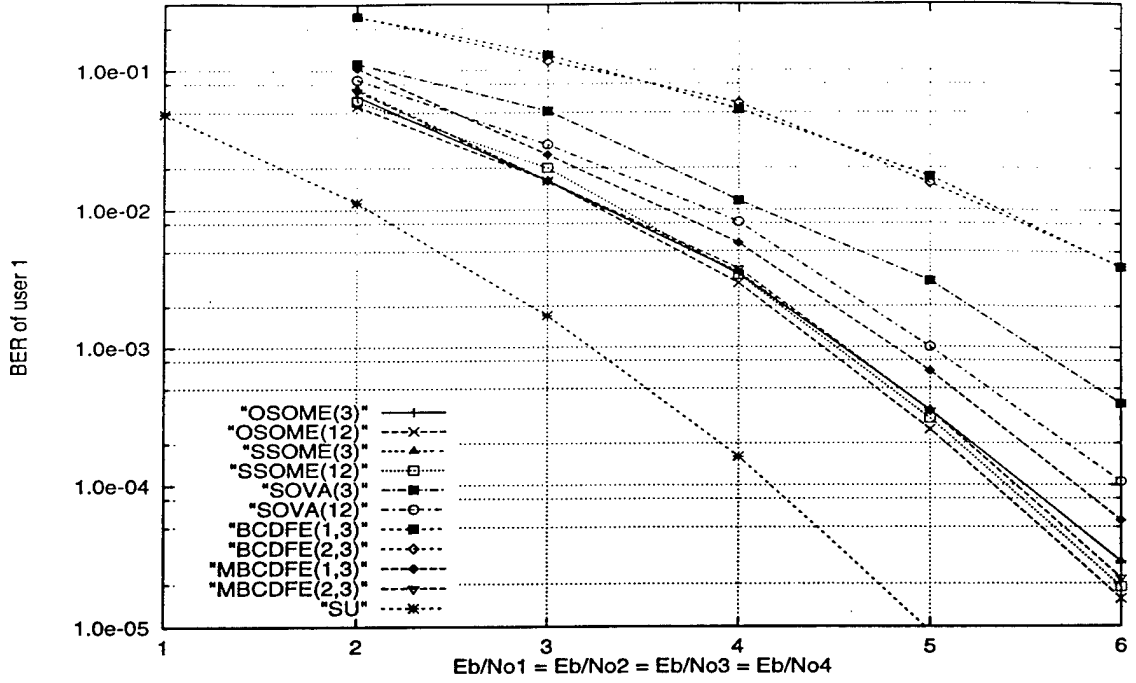
Figure 6.2: BER performance of various algorithms in ideal power control.

symbol sequences of all users are interleaved by a 30 × 30 interleaver. Each user is assigned a short Gold spreading sequence with 7 chips/coded symbol. The relative delays of users are arbitrarily chosen in an increasing order and are fixed for the simulation. The multiuser channel has the spectrum

$$
S(D) = \frac{1}{7}
\begin{bmatrix}
7 & -4 - D & 1 + 2D & -D \\
-4 - D^{-1} & 7 & -4 - D & 3 \\
1 + 2D^{-1} & -4 - D^{-1} & 7 & -2 + D \\
-D^{-1} & 3 & -2 + D^{-1} & 7
\end{bmatrix}
\tag{6.32}
$$

Fig. 6.2 shows the BER of user 1 versus the signal-to-noise ratio (E_b/N_0) in perfect power control. Each simulation was run for a count of 500 errors. It can be seen that the BER curves of OSOME(3), OSOME(12), SSOME(3), SSOME(12) and MBCDFE(2,3) lie in a band of width 0.2 dB. The OSOME(12) algorithm loses about 1.2 dB over coded single user performance. SSOME(3) achieves a 0.4 − 0.5 dB gain over SOVA(12) in the range 3 − 6 dB. Note that SSOME(3) requires only state metrics (and no symbol metrics) to be computed. We have not plotted the BER performance for SSOME1 because SSOME1(3)
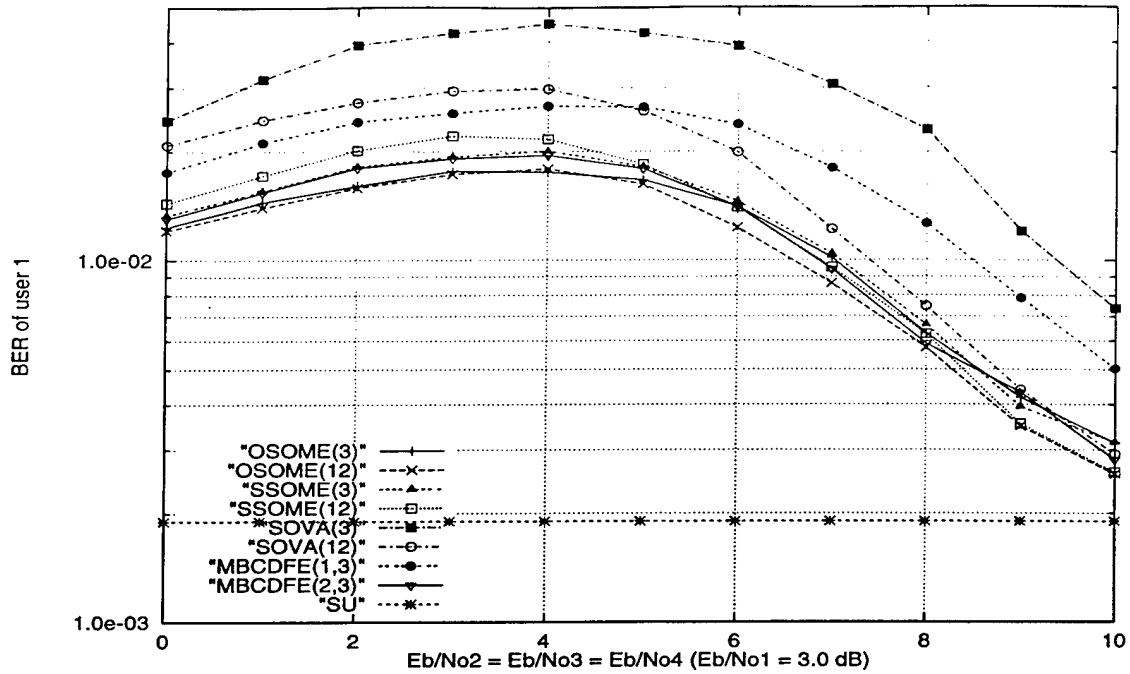
Figure 6.3: BER performance of various algorithms in near-far situation.

(the case of no symbol metrics) is identical to SOVA(3) and SSOME1(12) approaches the performance of SSOME(12). This shows that for small smoothing lags, it is beneficial to average the output symbol soft information over the states in the trellis, as in the case of SSOME. However, for large lags, it is sufficient to obtain the soft information from the most likely state in the trellis, as in SSOME1. The modified BCDFE algorithm with reduced-state trellises gains $1.0 - 2.0$ dB over the original BCDFE algorithm because the soft outputs of the later are no better than hard decisions.

Fig. 6.3 shows the BER of user 1 versus E_b/N_0 of interfering users (with E_b/N_0 of user 1 fixed at 3.0 dB). 10^5 data symbols were used for each simulation. The BER curves of all schemes tend to single user performance under extreme conditions of multiple-access interference. Thus, Fig. 6.2 depicts almost worst case performance for user 1 given its E_b/N_0. Note that MBCDFE(1,3) outperforms SOVA(12) under power control in moderate E_b/N_0. Although the application of MBCDFE requires noise-whitening, its performance/complexity tradeoff is highly desirable.

6.8 Conclusions

In this chapter, we derived soft-output algorithms for channels with memory which operate on standard matched-filter statistics. The new optimum and sub-optimum soft-output algorithms (MF-OSA and MF-SSA respectively) are similar in structure and complexity to the OSA and the SSA proposed earlier for whitened statistics. The algorithms have low latency as they employ a forward-only recursion. They were considered for multiuser detection in the presence of error control coding. The algorithms are especially suitable for asynchronous DS-CDMA systems with long spreading sequences. Adaptive complexity reduction techniques like the T-algorithm and T-algorithm with soft-limiting, can be applied to reduce the exponential complexity of these algorithms.

We also derived a reduced-state forward-recursive soft-output algorithm that operates on whitened matched-filter statistics. The algorithm generates good quality soft information with reduced complexity. It is obtained by modifying an algorithm proposed earlier which fails to generate good soft information.

CHAPTER 7

Conclusions

In this thesis, we have considered optimal and reduced-complexity techniques for equalization and multiuser detection. New techniques were developed, motivated by analysis of existing techniques and spurred by practical applications. One problem that was tackled was optimal[1] equalization for a wireless communication system with excess signal bandwidth and a fast time-varying medium. A new receiver was proposed which comprises a filter matched to the transmit pulse-shaping filter followed by a fractional-rate sampler and an adaptive Viterbi algorithm. The front-end filter is non-adaptive which is desirable for implementation. The receiver is insensitive to sampler timing phase due to fractional sampling. The Viterbi algorithm exploits the knowledge of the pulse-shaping filter to account for the correlation in the sampled statistics and requires only one-step prediction for medium-response coefficients.

We have presented a unified analysis of decision feedback sequence estimation (DFSE) and M-algorithm receivers for systems with finite memory that examines the effect of the receive filter and the branch metric of the reduced trellis or tree search algorithm. We considered receivers with a front-end filter matched to the overall channel response (standard matched filter) or the transmit filter response (transmit matched filter) and a symbol or fractional-rate sampler. An event error analysis indicates that interference components (bias) arise if there is a mismatch between the receive filter and the branch metric. These components can not be resolved by the trellis or tree search algorithm in a biased receiver and severely limit its error-rate performance. We have shown that an unbiased receiver consists of a standard or transmit matched filter followed by the appropriate noise-whitening

---

[1]Optimal in the sense of a known time-varying channel.

or zero-forcing filter and a reduced trellis or tree search algorithm with the appropriate metric.

We have compared various trellis-based techniques on the basis of the distance of a given error sequence which characterizes the probability of the associated error event. Our definition of the error distance includes the effect of noise enhancement which is inherent in trellis-based techniques operating on statistics containing non-white noise. This allowed us to compare trellis-based techniques with various receive filters on a fair basis. We showed that whitening filter DFSE (WF-DFSE) has higher error distance than zero-forcing filter DFSE (ZF-DFSE) and truncated-memory MLSE (TM-MLSE) with pre-filtering. Matched filter DFSE (MF-DFSE), in the case of standard matched filtering, achieves the same error distance as an MLSE receiver. Unfortunately, matched-filter type receivers belong to the class of biased receivers. Thus, their error-rate performance is dominated by untreated interference components for most channels in spite of their excellent error distance. After identifying the anti-causal interference components affecting MF-DFSE, we proposed several schemes that utilize tentative decisions to cancel these components. For this purpose, we considered hard and soft tentative decisions obtained in a symbol-by-symbol fashion as well as a multistage configuration.

We have obtained union bounds on the symbol error probability of the various receivers assuming no error propagation. In the case of MF-DFSE, with and without linear soft-input bias-compensation, we applied a Chebyshev technique for upperbounding the error probability in the presence of untreated or residual interference. We have outlined modified generating function methods to evaluate the union bounds. Simulation and analytical results were presented for equalization of inter-symbol interference and multiuser detection for direct-sequence code-division multiple-access (DS-CDMA) systems. The bounds were found to be tight in general for channels with relatively small memory. It was found that soft bias compensation enhances the performance of MF-DFSE for all channels of practical interest. Compensation of just the dominant bias term for MF-DFSE, obtains most of the gain without increasing complexity significantly. The scheme does not require any processing filters like the noise-whitening or zero-forcing filter and is insensitive to channel phase. These attributes make it attractive for multiuser detection for asynchronous DS-CDMA systems and bidirectional equalization for the GSM system.

We have derived soft-output algorithms for channels with memory which operate on

standard matched-filter statistics. The new optimum and sub-optimum algorithms employ a forward-only recursion and have complexity which is exponential in the channel memory only. These algorithms are suitable for soft-output demodulation for a coded multiuser DS-CDMA system. We have also derived a reduced-state soft-output algorithm which operates on whitened statistics. The algorithm provides reliable soft decisions with an adjustable performance/complexity tradeoff. It was obtained by modifying the BCDFE algorithm which fails to provide reliable soft decisions, as we find by means of simulation of a coded DS-CDMA system.

APPENDICES

APPENDIX A

Analysis of the alternative DFSE receiver

Consider the DFSE receiver of Fig. 4.4. Following the treatment given in Section 4.6.1, we see that a first event error occurs at time 0 in the reduced trellis search algorithm of Fig. 4.4 if

$$2\text{Re}\{\bar{\underline{a}}_k^H C_k^H (P^{-1})_k \underline{x}_k'\} - \bar{\underline{a}}_k^H C_k^H R_k' Q_k' C_k \bar{\underline{a}}_k > 2\text{Re}\{\underline{a}_k^H C_k^H (P^{-1})_k \underline{x}_k'\} - \underline{a}_k^H C_k^H R_k' Q_k' C_k \underline{a}_k$$

(A.1)

where $\underline{x}_k' = [x'(0), x'(1), \ldots, x'(k-1)]^T$ and the matrices C_k, R_k' and Q_k' are principal submatrices of dimension k of the matrices C, R' and Q' respectively. Using (4.28), (A.1) can equivalently be written as

$$2\text{Re}\{\underline{e}_k^H C_k^H (P^{-1})_k P_{k \times N} \underline{u}'\} > \underline{e}_k^H C_k^H R_k' Q_k' C_k \underline{e}_k + 2\text{Re}\{\underline{e}_k^H C_k^H R_k' Q_k' C_k \underline{a}_k\}$$

$$- 2\text{Re}\{\underline{e}_k^H C_k^H (P^{-1})_k P_{k \times N} \Phi C \underline{a}\}$$

(A.2)

which is the condition for the error event ε defined in Section 4.6.1. The unbiasedness condition for this receiver can then be written as

$$C_k^H (P^{-1})_k P_{k \times N} \Phi C = C_k^H R_k' Q_k' C_k [I_k | O_{k \times N-k}] \quad \forall \, 1 \leq k < N$$

(A.3)

or equivalently using the fact that $R_k' Q_k' = Q_k'^H R_k'^H$:

$$(P^{-1})_k P_{k \times N} = Q_k'^H (Q'^{-H})_{k \times N} \quad \forall \, 1 \leq k < N$$

(A.4)

where the matrix $(Q'^{-H})_{k \times N}$ comprises the top k rows of the matrix Q'^{-H}. It follows from (A.2) and (A.3) that the probability of the error event ε for an unbiased DFSE receiver with the front-end filter matched to the transmit filter response, is given by

$$\text{Pr}(\varepsilon) = Q\left(\frac{\underline{e}_k^H C_k^H R_k' Q_k' C_k \underline{e}_k}{2\sqrt{N_0 \underline{e}_k^H C_k^H R_k' Q_k' (\Phi^{-1})_k R_k' Q_k' C_k \underline{e}_k}}\right).$$

(A.5)

112

An upper bound on the first event error probability is given by (4.62) with the error distance $\delta(\underline{e})$ in this case defined as

$$\delta(\underline{e}) \triangleq \frac{\underline{e}_k^H C_k^H R_k' Q_k' C_k \underline{e}_k}{\sqrt{\underline{e}_k^H C_k^H R_k' Q_k' (\Phi^{-1})_k R_k' Q_k' C_k \underline{e}_k}}. \qquad (A.6)$$

APPENDIX B

Filters that satisfy unbiasedness

Let Y be an $N \times N$ Toeplitz matrix with elements

$$
y(i,j) = \begin{cases} 1 & i = j \\ y(i-j) & 0 < |i-j| \leq L_y \\ 0 & \text{otherwise} \end{cases} \tag{B.1}
$$

Let P^{-1} be the $N \times N$ Toeplitz matrix defined in (4.19) with the diagonal element $p'(0)$ set to 1. Assume that the inverses of the submatrices Y_k and $(P^{-1})_k$ exist for all $k \leq N$.

Proposition B.0.1 *Let* $\max(L_y, l_f, l_p) + 1 < N < \infty$. *If*

$$
(P^{-1})_k P_{k \times N} = Y_k (Y^{-1})_{k \times N} \quad \forall \, k = 1, 2, \ldots, N-1 \tag{B.2}
$$

then

$$
P = Y^{-1}. \tag{B.3}
$$

In order to prove the above proposition, we make use of the following lemma [5]:

Lemma B.0.1 *Let* T *be an* $m \times m$ *invertible Toeplitz matrix subdivided into* $k \times k$, $k \times (m-k)$, $(m-k) \times k$ *and* $(m-k) \times (m-k)$ *submatrices* T_{11}, T_{12}, T_{21} *and* T_{22} *as shown below. Then* $S = T^{-1}$ *is partitioned similarly into* S_{11}, S_{12}, S_{21} *and* S_{22}:

$$
T = \begin{bmatrix} T_{11} & T_{12} \\ T_{21} & T_{22} \end{bmatrix}, \quad S = \begin{bmatrix} S_{11} & S_{12} \\ S_{21} & S_{22} \end{bmatrix},
$$

where, assuming T_{11} is invertible.

$$S_{11} = T_{11}^{-1} + T_{11}^{-1}T_{12}(T_{22} - T_{21}T_{11}^{-1}T_{12})^{-1}T_{21}T_{11}^{-1}.$$

$$S_{12} = -T_{11}^{-1}T_{12}(T_{22} - T_{21}T_{11}^{-1}T_{12})^{-1}.$$

$$S_{21} = -(T_{22} - T_{21}T_{11}^{-1}T_{12})^{-1}T_{21}T_{11}^{-1},$$

$$S_{22} = (T_{22} - T_{21}T_{11}^{-1}T_{12})^{-1}.$$

Let the matrices P^{-1} and Y be subdivided into $k \times k$, $k \times (N - k)$, $(N - k) \times k$ and $(N - k) \times (N - k)$ submatrices P'_{11}, P'_{12}, P'_{21} and P'_{22} and Y_{11}, Y_{12}, Y_{21} and Y_{22} respectively as shown below

$$P^{-1} = \begin{bmatrix} P'_{11} & P'_{12} \\ P'_{21} & P'_{22} \end{bmatrix}, \quad Y = \begin{bmatrix} Y_{11} & Y_{12} \\ Y_{21} & Y_{22} \end{bmatrix}, \tag{B.4}$$

for $k = 1, 2, \ldots, N - 1$. Then, using Lemma B.0.1, (B.2) can be broken into two equations concerning the first k and the last $N - k$ columns of the $k \times N$ matrices on either side of (B.2), given by

$$P'_{11}[P_{11}'^{-1} + P_{11}'^{-1}P'_{12}(P'_{22} - P'_{21}P_{11}'^{-1}P'_{12})^{-1}P'_{21}P_{11}'^{-1}] =$$
$$Y_{11}[Y_{11}^{-1} + Y_{11}^{-1}Y_{12}(Y_{22} - Y_{21}Y_{11}^{-1}Y_{12})^{-1}Y_{21}Y_{11}^{-1}] \tag{B.5}$$

and

$$P'_{11}[-P_{11}'^{-1}P'_{12}(P'_{22} - P'_{21}P_{11}'^{-1}P'_{12})^{-1}] = Y_{11}[-Y_{11}^{-1}Y_{12}(Y_{22} - Y_{21}Y_{11}^{-1}Y_{12})^{-1}] \tag{B.6}$$

respectively for $k = 1, 2, \ldots, N - 1$. Substituting (B.6) into (B.5) and simplifying, we get

$$P'_{21}P_{11}'^{-1} = Y_{21}Y_{11}^{-1}. \tag{B.7}$$

Let $k = 1$, then $P'_{11} = Y_{11} = 1$ and (B.7) implies that the first column of the matrix P^{-1} is equal to the first column of the matrix Y. Since P^{-1} and Y are Toepltiz matrices, all elements in the lower triangle of P^{-1} are equal to the corresponding elements of Y, i.e. $P'_{21} = Y_{21}$ for all $k = 1, 2, \ldots, N - 1$. Thus, (B.7) implies that

$$P'_{11} = Y_{11} \tag{B.8}$$

for all $k = 1, 2, \ldots, N - 1$. Since $N > \max(L_y, l_f, l_p) + 1$, (B.8) involves all non-zero elements of the matrices P^{-1} and Y. Thus,

$$P = Y^{-1}. \tag{B.9}$$

Note that the diagonal elements of the matrices P^{-1} and Y were set to 1 to factor out a scaling factor. In general, we have

$$P = cY'^{-1} \qquad (B.10)$$

where c is a constant scaling factor.

APPENDIX C

Error distance for ZF-DFSE

Let the matrices S and S^{-1} be subdivided into $k \times k$, $k \times (N-k)$, $(N-k) \times k$ and $(N-k) \times (N-k)$ submatrices S_{11}, S_{12}, S_{21} and S_{22} and S_{11}^I, S_{12}^I, S_{21}^I and S_{22}^I respectively as shown below

$$S = \begin{bmatrix} S_{11} & S_{12} \\ S_{21} & S_{22} \end{bmatrix}, \quad S^{-1} = \begin{bmatrix} S_{11}^I & S_{12}^I \\ S_{21}^I & S_{22}^I \end{bmatrix}. \tag{C.1}$$

Then, using Lemma B.0.1, we get

$$\begin{aligned} S_k(S^{-1})_k S_k &= S_k + S_{12}(S_{22} - S_{21}S_{11}^{-1}S_{12})^{-1}S_{21} \\ &= S_k + S_{12}S_{22}^I S_{21}. \end{aligned} \tag{C.2}$$

For $k \geq L$, we have

$$S_k(S^{-1})_k S_k = S_k + \begin{bmatrix} 0_{k-L} & 0 \\ 0 & \dot{S}^H (S_{22}^I)_L \dot{S} \end{bmatrix}. \tag{C.3}$$

Note that for $N \gg L$, S^{-1} is near Toeplitz in the middle of the matrix. Thus, we can replace the matrix $(S_{22}^I)_L$ in (C.3) by the principal submatrix S_L' of an $N \times N$ Toeplitz matrix S' with elements $s'(i,j) = s'(i-j)$, given by the inverse z-transform of $1/S(z)$. Thus, for an error sequence $\underline{e} \in E'$ with tail $\underline{\xi}$ as defined in (4.79), we have

$$\underline{e}^H S_k(S^{-1})_k S_k \underline{e} \approx \underline{e}^H S_k \underline{e} + \underline{\xi}^H \dot{S}_{L-J}^H S_{L-J}' \dot{S}_{L-J} \underline{\xi}. \tag{C.4}$$

The error distance for ZF-DFSE(S) given by (4.76) can then be approximated as

$$\delta(\underline{e}) \approx \frac{\underline{e}^H S_k \underline{e}}{\sqrt{\underline{e}^H S_k \underline{e} + \underline{\xi}^H \dot{S}_{L-J}^H S_{L-J}' \dot{S}_{L-J} \underline{\xi}}}. \tag{C.5}$$

The above expression is approximate for error events occurring near the edges of the data burst where the noise correlation is not the same as in the middle, while it is exact for short error events occurring toward the middle of the burst.

Similarly, it can be shown that the error distance for ZF-DFSE(T) given by (4.77) can be approximated as

$$\delta(\underline{e}) \approx \frac{\underline{e}^H C_k^H \Phi_k C_k \underline{e}}{\sqrt{\underline{e}^H C_k^H \Phi_k C_k \underline{e} + \underline{\xi}^H (\ddot{C}_{L_d \times L - J})^H \ddot{\Phi}^H (\Phi')_{L_d} \ddot{\Phi} \ddot{C}_{L_d \times L - J} \underline{\xi}}} \tag{C.6}$$

where Φ' is an $N \times N$ Toeplitz matrix with elements $\phi'(i,j) = \phi'(i-j)$ obtained from the inverse z-transform of $1/\Phi(z)$ (where $\Phi(z)$ is the z-transform of $\{\phi(i)\}$).

APPENDIX D

Error probability of two-stage BC-MF-DFSE(S)

In this appendix, we derive expressions for the probability of a particular error event in a two-stage BC-MF-DFSE receiver with standard matched filtering. The first stage of the receiver is MF-DFSE(S) with memory order J_1 and the second stage is BC-MF-DFSE(S) with memory order J_2. The second stage uses the final decisions of the first stage to cancel bias. A valid error sequence in the first (second) stage does not have J_1 (J_2) consecutive zeros in the middle of the sequence and has J_1 (J_2) consecutive zeros at the end of the sequence. Let E_1 (E_2) be the set of all valid error sequences in the first (second) stage.

It follows from (4.78) that an error event beginning at time l_1 and ending at time l_2 (corresponding to the error sequence $\underline{t} = [t_{l_1}, t_{l_1+1}, \ldots, t_{l_2-1}]^T \in E_1$, $l = l_2 - l_1$) occurs in the first stage (assuming no error propagation from previous error events) if

$$2\text{Re}\{\underline{t}^H \underline{u}'\} > \underline{t}^H S_l \underline{t} - 2\text{Re}\{\underline{t}'^H \dot{S}_{L-J}^H \underline{a}'\} \tag{D.1}$$

where $\underline{u}' = [u_{l_1}, \ldots, u_{l_2-1}]^T$, $\underline{t}' = [t_{l_2-L}, \ldots, t_{l_2-J_1-1}]^T$ and $\underline{a}' = [a_{l_2}, \ldots, a_{l_2+L-J_1-1}]^T$. Given errors $\underline{t}'' = [t_k, \ldots, t_{k+L-J_2-1}]^T$ in the first stage, an error event occurs between times 0 and k (corresponding to the error sequence $\underline{e} = [e_0, e_1, \ldots, e_{k-1}]^T \in E_2$) in the second stage if

$$2\text{Re}\{\underline{e}^H \underline{u}''\} > \underline{e}^H S_k \underline{e} + 2\text{Re}\{\underline{e}''^H \dot{S}_{L-J}^H \underline{t}''\}. \tag{D.2}$$

where $\underline{u}'' = [u_0, \ldots, u_{k-1}]^T$ and $\underline{e}'' = [e_{k-L}, \ldots, e_{k-J_2-1}]^T$. Note that the sequence of tentative decision errors $\underline{t}''$ can be the result of several contiguous error events[1] in the first stage. We assume that $\underline{t}''$ can result from at most one error event in the first stage. This assumption is actually true for $J_1 \geq L - J_2 - 1$.

---

[1] Error events in the first stage are separated by at least J_1 consecutive correct decisions.

Let T be the set of all error sequences $\underline{t} \in E_1$ that include $\underline{t}''$ as a subsequence. Let $X = 2\text{Re}\{\underline{c}^H \underline{u}''\}$ and $Y = 2\text{Re}\{\underline{t}^H \underline{u}'\}$. Given $\underline{c} \in E_2$, $\underline{t} \in T$ and $\underline{a}' \in \mathcal{A}^{L-J_1}$, X and Y are jointly Gaussian random variables with means zero, variances $\sigma_X^2 = 4N_0\underline{c}^H S_k \underline{c}$ and $\sigma_Y^2 = 4N_0\underline{t}^H S_l \underline{t}$ respectively, and covariance

$$E[XY^*] = \sum_{n=0}^{k-1} \sum_{m=l_1}^{l_2-1} 4N_0\text{Re}\{e_n^* s(n-m)t_m\}. \tag{D.3}$$

The joint probability of occurrence of $\underline{e} \in E_2$ and $\underline{t} \in T$ is given by

$$\Pr(\underline{e}, \underline{t}) = \sum_{\underline{a}' \in \mathcal{A}^{L-J_1}} \left[\int_{x_1}^{\infty} \int_{y_1}^{\infty} f_{XY}(x, y) dx \, dy \right] P_{\underline{a}'} \tag{D.4}$$

where $x_1 = \underline{e}^H S_k \underline{e} + 2\text{Re}\{\underline{e}''^H \dot{S}_{L-J}^H \underline{t}''\}$ and $y_1 = \underline{t}^H S_l \underline{t} - 2\text{Re}\{\underline{t}'^H \dot{S}_{L-J}^H \underline{a}'\}$. The probability that the error event ε: $\underline{e} \in E_2$ occurs in the second stage is thus given by

$$\Pr(\varepsilon) = Q\left(\frac{1}{2}\sqrt{\frac{\underline{e}^H S_k \underline{e}}{N_0}}\right) \Pr(\underline{t}'' = \underline{0}) + \sum_{\underline{t} \in T'} \Pr(\underline{e}, \underline{t}) \tag{D.5}$$

where T' is a subset of the set T which includes all error sequences in T except those for which $\underline{t}'' = \underline{0}$. Note that $\Pr(\underline{t}'' = \underline{0})$ can be over-bounded by 1[2]. Thus, we get

$$\Pr(\varepsilon) \leq Q\left(\frac{1}{2}\sqrt{\frac{\underline{e}^H S_k \underline{e}}{N_0}}\right) + \sum_{\underline{t} \in T'} \Pr(\underline{e}, \underline{t}). \tag{D.6}$$

Assuming independence between errors occurring in the two stages (i.e. independent X and Y), we get

$$\Pr(\varepsilon) \overset{\sim}{\leq} Q\left(\frac{1}{2}\sqrt{\frac{\underline{e}^H S_k \underline{e}}{N_0}}\right) + \sum_{\underline{t} \in T'} \sum_{\underline{a}' \in \mathcal{A}^{L-J_1}} Q\left(\frac{\underline{e}^H S_k \underline{e} + 2\text{Re}\{\underline{e}''^H \dot{S}_{L-J}^H \underline{t}''\}}{2\sqrt{N_0 \underline{e}^H S_k \underline{e}}}\right)$$
$$Q\left(\frac{\underline{t}^H S_l \underline{t} - 2\text{Re}\{\underline{t}'^H \dot{S}_{L-J}^H \underline{a}'\}}{2\sqrt{N_0 \underline{t}^H S_l \underline{t}}}\right) P_{\underline{a}'}. \tag{D.7}$$

---

[2] The bound becomes asymptotically tight at high signal-to-noise ratio.

BIBLIOGRAPHY

BIBLIOGRAPHY

[1] K. Abend and B. D. Fritchman, "Statistical detection for communication channels with intersymbol interference," *Proceedings of the IEEE*, vol. 58, no. 5, pp. 778–795, May 1970.

[2] J. B. Anderson and S. Mohan, "Sequential coding algorithms: A survey cost analysis," *IEEE Transactions on Communications*, vol. 32, pp. 169–176, February 1984.

[3] L. Bahl, J. Cocke, F. Jelinek, and J. Raviv, "Optimal decoding of linear codes for minimizing symbol error rate," *IEEE Transactions on Information Theory*, vol. IT-20, no. 3, pp. 284–287, March 1974.

[4] J. W. M. Bergmans, *Digital Baseband Transmission and Recording*, Boston: Kluwer Academic Publishers, 1996.

[5] A. Bjorck, *Large Scale Matrix Problems*, New York: Elsevier North Holland, 1981.

[6] G. E. Bottomley and S. Chennakeshu, "Unification of MLSE receivers and extension to time-varying channels," *IEEE Transactions on Communications*, vol. 46, no. 4, pp. 464–472, April 1998.

[7] A. Duel and C. Heegard, "Delayed decision feedback sequence estimation for QAM and trellis coded systems," *Conference on Information Siences and Systems*, vol. 20, pp. 367–372, March 1986.

[8] A. Duel and C. Heegard, "Delayed decision-feedback sequence estimation," *IEEE Transactions on Communications*, vol. 37, no. 5, pp. 428–436, May 1989.

[9] A. Duel-Hallen, *Detection algorithms for Intersymbol Interfence Channels*, PhD thesis, Cornell University, August 1987.

[10] V. M. Eyuboglu and S. U. H. Qureshi, "Reduced-state sequence estimation with set partitioning and decision feedback," *IEEE Transactions on Communications*, vol. 36, no. 1, pp. 13–20, January 1988.

[11] V. M. Eyuboglu and S. U. H. Qureshi, "Reduced-state sequence estimation for coded modulation on intersymbol interference channels," *IEEE Journal on Selected Areas in Communications*, vol. 7, no. 6, pp. 989–995, August 1989.

[12] D. D. Falconer and F. R. Magee Jr., "Adaptive channel memory truncation for maximum likelihood sequence estimation," *Bell Systems Technical Journal*, vol. 52, pp. 1541–1562, November 1973.

[13] G. D. Forney, "Maximum-likelihood sequence estimation of digital sequences in the presence of intersymbol interference," *IEEE Transactions on Information Theory*, vol. IT-18, no. 3, pp. 363-378, May 1972.

[14] G. J. Foschini, "A reduced state variant of maximum likelihood sequence detection attaining optimum performance for high signal-to-noise ratios." *IEEE Transactions on Information Theory*, vol. 23, pp. 605-609, September 1977.

[15] T. Frey and M. Reinhardt, "Signal estimation for interference cancellation and decision feeedback equalization," *IEEE Vehicular Technology Conference*, pp. 155-159, 1997.

[16] F. E. Glave, "An upper bound on the probability of error due to intersymbol interference for correlated digital signals," *IEEE Transactions on Information Theory*, vol. IT-18, pp. 356-363, May 1972.

[17] A. Hafeez and W. E. Stark, "Decision feedback sequence estimation for unwhitened ISI channels," *Annual Allerton Conference on Communication, Control and Computing*, vol. 35, pp. 493-502, September 1997.

[18] A. Hafeez and W. E. Stark, "Soft-output multiuser estimation for asynchronous CDMA channels," *IEEE Vehicular Technology Conference*, vol. 47, pp. 465-469, May 1997.

[19] A. Hafeez and W. E. Stark, "Decision feedback sequence estimation for unwhitened ISI and multiuser CDMA channels," *IEEE Vehicular Technology Conference*, pp. 424-429, May 1998.

[20] A. Hafeez and W. E. Stark, "Decision feedback sequence estimation for unwhitened ISI channels with applications to multiuser detection," *IEEE Journal on Selected Areas in Communications*, vol. 16, no. 9, pp. 1785-1795, December 1998.

[21] J. Hagenauer and P. Hoeher, "A Viterbi algorithm with soft-decision outputs and its applications," *Proceedings of Globecom*, vol. 3, pp. 47.1.1-47.1.7, November 1989.

[22] K. Hamied and G. L. Stuber, "A fractionally spaced MLSE receiver," *IEEE International Conference on Communication*, pp. 7-11, 1995.

[23] J. F. Hayes, T. M. Cover, and J. B. Riera, "Optimal sequence detection and optimal symbol-by-symbol detection: Similar algorithms," *IEEE Transactions on Communications*, vol. COM-30, no. 1, pp. 152-157, January 1982.

[24] H. Kubo, K. Murakami, and T. Fujino, "An adaptive maximum-likelihood sequence estimator for fast time-varying intersymbol interference channels," *IEEE Transactions on Communications*, vol. 42, pp. 1872-1880, Feb./Mrach/April 1994.

[25] G. Lee, S. B. Gelfand, and M. P. Fitz, "Bayesian decision feedback techniques for deconvolution," *IEEE Journal on Selected Areas in Communications*, vol. 13, no. 1, pp. 155-165, January 1995.

[26] W. U. Lee and F. S. Hill Jr., "A maximum likelihood sequence estimator with decision feedback equalization," *IEEE Transactions on Communications*, vol. COM-25, pp. 971-980, September 1977.

[27] A. Leon-Garcia. *Probability and Random Processes for Electrical Engineering*. Reading: Addison-Wesley, 2nd edition, 1994.

[28] Y. Li, B. Vucetic, and Y. Sato. "Optimum soft-output detection for channels with intersymbol interference," *IEEE Transactions on Information Theory*, vol. IT-41, no. 3, pp. 85–96, May 1995.

[29] S. Lin and D. J. Costello Jr., *Error Control Coding: Fundamentals and Applications*, New Jersey: Prentice-Hall, 1983.

[30] Q. Liu and Y. Wan, "A unified MLSE detection technique for TDMA digital cellular radio," *IEEE Vehicular Technology Conference*, pp. 265–268, 1993.

[31] J. W. Matthews, "Sharp error bounds for intersymbol interference," *IEEE Transactions on Information Theory*, vol. IT-19, pp. 440–447, July 1973.

[32] P. J. McLane, "A residual interference error bound for truncated-state Viterbi detectors," *IEEE Transactions on Information Theory*, vol. IT-26, pp. 549–553, September 1980.

[33] K. Okanoue, A. Ushirokawa, H. Tomita, and Y. Furuya, "New MLSE receiver free from sample timing and input level controls," *IEEE Vehicular Technology Conference*, pp. 408–411, 1993.

[34] S. U. H. Qureshi, "Adaptive equalization," *Proceedings of the IEEE*, vol. 73, no. 9, pp. 1349–1387, September 1985.

[35] S. U. H. Qureshi and E. E. Newhall, "An adaptive receiver for data transmission over time-dispersive channels," *IEEE Transactions on Information Theory*, vol. IT-19, pp. 448–457, July 1973.

[36] M. Rupf, F. Turkoy, and J. L. Massey, "User-separating demodulation for code-division multiple-access systems," *IEEE Journal on Selected Areas in Communications*, vol. 12, no. 5, pp. 786–795, June 1994.

[37] C. Schlegel, "The receiver filter influence on reduced-state trellis decoding on channels with ISI," *IEEE Transactions on Vehicular Technology*, 1995. Under revision.

[38] N. Seshadri, "Joint data and channel estimation using blind trellis search algorithms," *IEEE Transactions on Communications*, vol. 42, pp. 1000–1011, Feb./Mrach/April 1994.

[39] W. Sheen and G. L. Stuber, "Error probability for reduced-state sequence estimation," *IEEE Journal on Selected Areas in Communications*, vol. 10, no. 3, pp. 571–578, April 1992.

[40] G. Ungerboeck, "Adaptive maximum-likelihood receiver for carrier-modulated data-transmission systems," *IEEE Transactions on Communication Technology*, vol. COM-22, no. 5, pp. 624–636, May 1974.

[41] H. L. VanTrees, *Detection, Estimation and Modulation Theory Part III: Radar-Sonar Signal Processing and Gaussian Signals in Noise*, New York: John Wiley & Sons, 1968.

[42] S. Verdú. *Optimum multiuser signal detection*. PhD thesis. University of Illinois at Urbana-Champaign. August 1984.

[43] S. Verdú, "Minimum probability of error for asynchronous gaussian multiple-access channels," *IEEE Transactions on Information Theory*. vol. IT-32, no. 1, pp. 85–96. January 1986.

[44] S. Verdú, *Multiuser Detection*, New York: Cambridge University Press, 1998.

[45] F. L. Vermeulen and M. E. Hellman, "Reduced state Viterbi decoders for channels with intersymbol interference," *IEEE International Conference on Communication*, pp. 37B-1–37B-4, 1974.

[46] A. Viterbi and J. K. Omura, *Principles of Digital Communication and Coding*, McGraw-Hill, 1979.

[47] L. Wei and L. K. Rasmussen, "A near ideal noise whitening filter for an asynchronous time-varying CDMA system," *IEEE Transactions on Communications*, vol. 44, no. 10, pp. 1355–1361, October 1996.

[48] L. Wei, L. K. Rasmussen, and R. Wyrwas, "Near optimum tree-search detection schemes for bit-synchronous multiuser CDMA systems over gaussian and two-path rayleigh-fading channels," *IEEE Transactions on Communications*, vol. 45, no. 6, pp. 691–700, June 1997.

[49] K. Wesolowski, "An efficient DFE & ML suboptimum receiver for data transmission over dispersive channels using two-dimensional signal constellations," *IEEE International Symposium on Information Theory*, pp. 23–28, June 1985.

[50] K. Wesolowski, R. Krenz, and K. Das, "Efficient receiver structure for GSM mobile radio," *International Journal on Wireless Information Networks*, vol. 3, no. 2, pp. 117–122, 1996.

[51] Z. Xie, C. Rushforth, R. Short, and T. K. Moon, "Joint signal detecetion and parameter estimation in multiuser communications," *IEEE Transactions on Communications*, vol. 41, pp. 1208–1215, August 1993.